UNCLASSIFIED

## AD NUMBER

AD052144

## NEW LIMITATION CHANGE

TO

Approved for public release, distribution unlimited

FROM

Distribution authorized to U.S. Gov't. agencies and their contractors; Specific Authority; 28 Mar 2000. Other requests shall be referred to Office of Naval Research, Washington, DC.

## AUTHORITY

ONR ltr dtd 7 Mar 2000

THIS PAGE IS UNCLASSIFIED

# ...s Technical Information Agenc

# 12144

NOTICE: ...MENT OR OTHER DRAWINGS, SPECIFICATIONS OR OTHER DATA ARE USED FOR ...PURPOSE OTHER THAN IN CONNECTION WITH A DEFINITELY RELATED GOVERNMENT ...MENT OPERATION, THE U. S. GOVERNMENT THEREBY INCURS NO RESPONSIBILITY ...NOR ANY OBLIGATION WHATSOEVER; AND THE FACT THAT THE GOVERNMENT ...HAVE FORMULATED, FURNISHED, OR IN ANY WAY SUPPLIED THE ...SPECIFICATIONS, OR OTHER DATA IS NOT TO BE REGARDED BY ...OTHERWISE AS IN ANY MANNER LICENSING THE HOLDER OR ANY OTHER ...PERSON, OR CONVEYING ANY RIGHTS OR PERMISSION TO MANUFACTURE ...PATENTED INVENTION THAT MAY IN ANY WAY BE RELATED THERETO.

Reproduced by

...UMENT SERVICE CENTER

...OTC BUILDING, DAYTON 2, OHIO

UNCLASSIFIED

# DISCLAIMER NOTICE

THIS DOCUMENT IS BEST QUALITY PRACTICABLE. THE COPY FURNISHED TO DTIC CONTAINED A SIGNIFICANT NUMBER OF PAGES WHICH DO NOT REPRODUCE LEGIBLY.

Preprint
AD No. 52 [illegible]
ASTIA FILE COPY

# Second ONR SYMPOSIUM on DETONATION

February 9, 10, 11, 1955

Washington, D. C.

OFFICE OF NAVAL RESEARCH
DEPARTMENT OF THE NAVY
Washington, D. C.

preprints

# Second ONR SYMPOSIUM on DETONATION

February 9 and 10, 1955
NATIONAL ACADEMY OF SCIENCES
Washington, D. C.

February 11, 1955
U. S. NAVAL ORDNANCE LABORATORY
White Oak, Maryland

Sponsored by
OFFICE OF NAVAL RESEARCH
DEPARTMENT OF THE NAVY

## FOREWORD

These papers are to be presented at the Second Symposium on Detonation being sponsored by this Office on 9, 10, and 11 February 1955. Two volumes are being issued, one containing the unclassified and the other the classified papers. Inasmuch as these preprints are receiving a limited distribution they are not to be considered as a substitute for publication in appropriate scientific journals.

The object of this symposium is to bring together scientists from government, university and industry to discuss recent advances in theory, experiment and application in this field of theoretical physics.

This Office is of the opinion that the symposium at which these papers will be discussed will stimulate new research in this complex field. The relationship of advances in the knowledge of detonation phenomena to the effectiveness of the use of molecular explosives makes this aspect of science of importance to the Department of the Navy and the Department of Defense.

To all those who are contributing papers and plan to attend this symposium, the Office of Naval Research expresses its appreciation.

F. R. FURTH
Rear Admiral, USN
Chief of Naval Research

CONTENTS


1. CHARGE PREPARATION FOR PRECISE DETONATION VELOCITY STUDIES . . 1
Edward James, Jr.
Los Alamos Scientific Laboratory

2. TECHNIQUE FOR THE MEASUREMENT OF DETONATION VELOCITY . . . . . 15
A. H. Campbell, M. E. Malin, T. J. Boyd, Jr., and J. A. Hull
Los Alamos Scientific Laboratory

3. A MICROWAVE TECHNIQUE FOR MEASURING DETONATION VELOCITY . . . 33
T. J. Boyd, Jr., and P. Fagan
Los Alamos Scientific Laboratory

4. MEASUREMENT OF DETONATION TEMPERATURES . . . . . 39
F.C. Gibson, M. Bowser, C. R. Summers, F. Scott,
J. C. Cooper, and C. M. Mason
U. S. Bureau of Mines

5. A NEW CINE MICROSCOPE AND ITS APPLICATION TO DETONATION PHENOMENA . . . . . 50
J. S. Courtney-Pratt
University of Cambridge

6. THE MEASUREMENT OF DENSITY CHANGES IN GASEOUS DETONATIONS . . 69
G. B. Kistiakowsky and P. H. Kydd
Harvard University

7. THE ATTAINMENT OF THERMODYNAMIC EQUILIBRIUM IN DETONATION WAVES . . . . . 80
G. B. Kistiakowsky and Walter G. Zinman
Harvard University

8. ON THE STRUCTURE OF A DETONATION FRONT . . . . . 98
W. R. Gilkerson and Norman Davidson
California Institute of Technology

9. HIGH TEMPERATURE THERMODYNAMICS AND GASEOUS DETONATIONS IN MIXTURES OF CYANOGEN, OXYGEN, AND NITROGEN . . . . . 113
M. M. Peek and R. G. Thrap
Los Alamos Scientific Laboratory

10. DETONATION IN GASES AT LOW PRESSURE . . . . . 133
Arthur L. Bennett and Henry W. Wedaa
U. S. Naval Ordnance Test Station

11. MEASUREMENTS ON GASEOUS DETONATION WAVES . . . . . 146
J. A. Nicholls, R. B. Morrison, and R. E. Cullen
University of Michigan

12. STUDIES ON GASEOUS DETONATION . . . . . 163
B. Greifer, F. C. Gibson, and C. M. Mason
U.S. Bureau of Mines

13. CONDENSATION SHOCKS AND WEAK DETONATIONS . . . . . 177
S. G. Reed, Jr., and W. H. Heybey
U.S. Naval Ordnance Laboratory

14. THE STRUCTURE OF A STEADY-STATE PLANE DETONATION WAVE WITH FINITE REACTION RATE . . . . . 194
John G. Kirkwood, Yale University
William W. Wood, Los Alamos Scientific Laboratory

15. THE MEASUREMENT OF CHAPMAN-JOUGUET PRESSURE FOR EXPLOSIVES . . . . . 209
W. E. Deal, Jr.
Los Alamos Scientific Laboratory

16. MEASUREMENT OF THE CHAPMAN-JOUGUET PRESSURE AND REACTION ZONE LENGTH IN A DETONATING HIGH EXPLOSIVE . . . . . 225
Russell E. Duff and Edwin Houston
Los Alamos Scientific Laboratory

17. THE DETONATION ZONE IN CONDENSED EXPLOSIVES . . . . . 240
H. Dean Mallory and S. J. Jacobs
U.S. Naval Ordnance Laboratory

18. CALCULATION OF THE DETONATION PROPERTIES OF SOLID EXPLOSIVES WITH THE KISTIAKOWSKY-WILSON EQUATION OF STATE . 265
W. Fickett and R. D. Cowan
Los Alamos Scientific Laboratory

19. A SOLID-STATE MODEL FOR DETONATIONS . . . . . 286
R. B. Parlin and J. C. Giddings
University of Utah

20. DIAMETER EFFECT IN CONDENSED EXPLOSIVES. THE RELATION BETWEEN VELOCITY AND RADIUS OF CURVATURE OF THE DETONATION WAVE . . . . . 306
William W. Wood, Los Alamos Scientific Laboratory
John G. Kirkwood, Yale University

21. THE DETONATION BEHAVIOR OF LIQUID TNT . . . . . 321
E. A. Igel and L. B. Seely, Jr.
Los Alamos Scientific Laboratory

22. DETONATION IN HOMOGENEOUS EXPLOSIVES . . . . . 336
A. W. Campbell, M. E. Malin, and T. E. Holland
Los Alamos Scientific Laboratory

23. PARTICLE SIZE EFFECTS IN ONE- AND TWO-COMPONENT EXPLOSIVES . . . . . 360
M. E. Malin, A. W. Campbell, and C. W. Mautz
Los Alamos Scientific Laboratory

24. DETONATION WAVE FRONTS IN IDEAL AND NON-IDEAL DETONATION . . 382
Melvin A. Cook
University of Utah

25. DETERMINATION OF REACTION RATE OF SODIUM NITRATE AND THE EQUATION OF STATE OF 50/50 TNT-$NaNO_3$ . . . . . 401
Melvin A. Cook and Wayne O. Ursenbach
University of Utah

26. THE DECOMPOSITION OF ALPHA-LEAD AZIDE . . . . . 411
J. M. Groocock
C.S.A.R., Ministry of Supply, Great Britain

27. THE DETONATION OF AZIDES BY LIGHT . . . . . 425
J. S. Courtney-Pratt and G. T. Rogers
University of Cambridge

28. DETONATION IN AZIDES WHEN THE DIMENSIONS ARE COMPARABLE WITH THE LENGTH OF THE REACTION ZONE . . . . . 443
F. P. Bowden and A. C. McLaren
University of Cambridge

29. ORIGIN OF LUMINOSITY IN DETONATION FLAMES . . . . . 453
Elwyn Jones
Imperial Chemical Industries Limited, Scotland

30. THE ROLE OF GAS POCKETS IN THE PROPAGATION OF LOW VELOCITY DETONATION . . . . . 464
Owen A. J. Gurton
Imperial Chemical Industries Limited, Scotland

31. SENSITIVENESS TO DETONATION . . . . . 483
Elwyn Jones and Ian G. Cumming
Imperial Chemical Industries Limited, Scotland

32. INITIATION OF MILITARY EXPLOSIVES BY PROJECTILE IMPACT . . . 494
J. M. Dewey
Aberdeen Proving Ground

INDEX TO AUTHORS . . . . . 502

# CHARGE PREPARATION FOR PRECISE DETONATION VELOCITY STUDIES

Edward James, Jr.
Los Alamos Scientific Laboratory
Los Alamos, New Mexico

## INTRODUCTION

High precision determination of detonation velocity in solid explosives presents special difficulties not associated with liquid and gaseous explosives. In particular, the problem of homogeniety with respect to density and composition is peculiar to solids. Particle size distribution also has an effect on detonation velocity which, of course, is not encountered in homogenous explosives. These factors especially must be rigorously controlled in order to achieve the desired confidence intervals in our detonation velocity studies.

To accomplish our aim of the highest degree of homogeneity obtainable, a great deal of development work has been done in the past few years. The various development phases, to mention only a few, have included design engineering, instrumentation, rheological studies, casting techniques, pressing techniques, analytical methods, and data analysis. Obviously, all of this work cannot be treated within the scope of this paper; therefore, this discussion is limited to casting, pressing, machining and inspection techniques.

Some detonation velocity data are presented to show the degree of precision obtained.

## CASTING

A complete description of the casting techniques used on the various explosives studied here at Los Alamos Scientific Laboratory would be needlessly long. I have, therefore, selected "Grade V New Composition B" produced by Holston Defense Corporation as being representative of a typical ordnance explosive and will describe the experimental methods and techniques related to detonation velocity studies on this material in some detail. Other common cast explosive

have been just as thoroughly studied but the techniques involved generally differ only in detail, not in principle.

Melt Preparation

We use 30- or 50-gallon vacuum melt kettles to melt our explosive. For most precise detonation velocity work, smaller kettles introduce an undesirable variability because several melts may be required to prepare enough material to complete an experiment.

Our kettles are equipped with two agitators, each with a variable speed control. One of the agitators, a large anchor-type, conforms to the hemispherical contour of the jacketed kettle bottom and the blades are pitched so as to impart an upward movement to the melt. The second agitator, a smaller turbine-type, is offset and at an angle from center. This turbine stirs in opposition to the anchor.

The temperature of the melt is controlled by a sensitive hot- and cold-water proportioning system supplying circulating water to the jacket and capable of holding the temperature of the melt to ± 1°C. During the melting operation the temperature differential between the jacket and melt is kept to a minimum to prevent local overheating.

A vacuum system is used which can maintain the kettle at pressures as low as 25 mm Hg. Figure 1 is a simplified illustration of a melt kettle.

We conduct a series of experiments to determine the optimum melting procedure and, for any subsequent experiment, the different steps and conditions are exactly specified. Attention is paid to the effect of variations in time, temperature and speeds of agitation since they undoubtedly affect the rheology of the melt in a complex fashion. It is known for instance that the particle size distribution of RDX in Composition B and the attendant apparent viscosity is sensitive to the melt procedure. Long periods of unduly high-temperature stirring tend to eliminate the finer RDX crystals, presumably through preferential solubility in the liquid TNT phase and then redeposition on the larger RDX crystals.

Our procedure for melting a 275-lb batch of Composition B in a 30-gallon kettle allows one hour melting time and subsequently 30 minutes of stirring at 25 mm absolute pressure. Jacket temperature is at a maximum of 110°C when melting is started and automatically reduces to 83° by the time melting is completed. The anchor agitator operates at 30 rpm and the turbine at 100 rpm.

Casting

Efforts to cast cylindrical charges of the desired diameter for rate sticks, even with long riser sections, have been abandoned. Our molds are designed with the idea of achieving minimum composition and density spreads within a region of the casting large enough to include a number of rate sticks. The casting is sawed into sections,

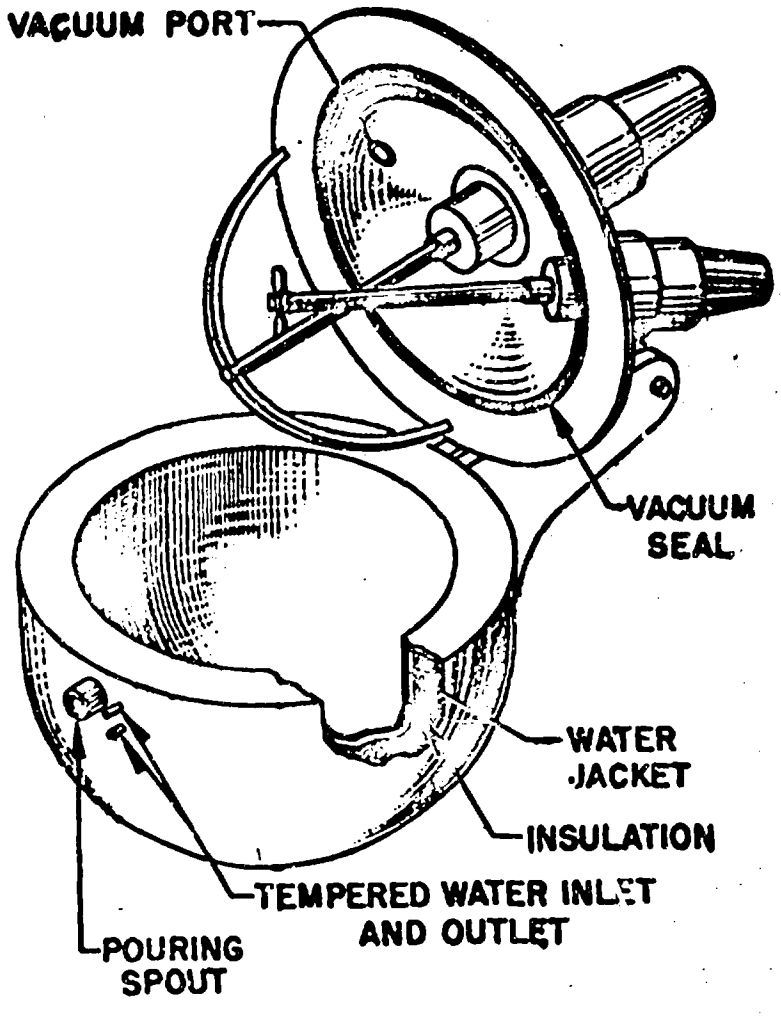


Figure 1 Melt Kettle, Y-3 Design

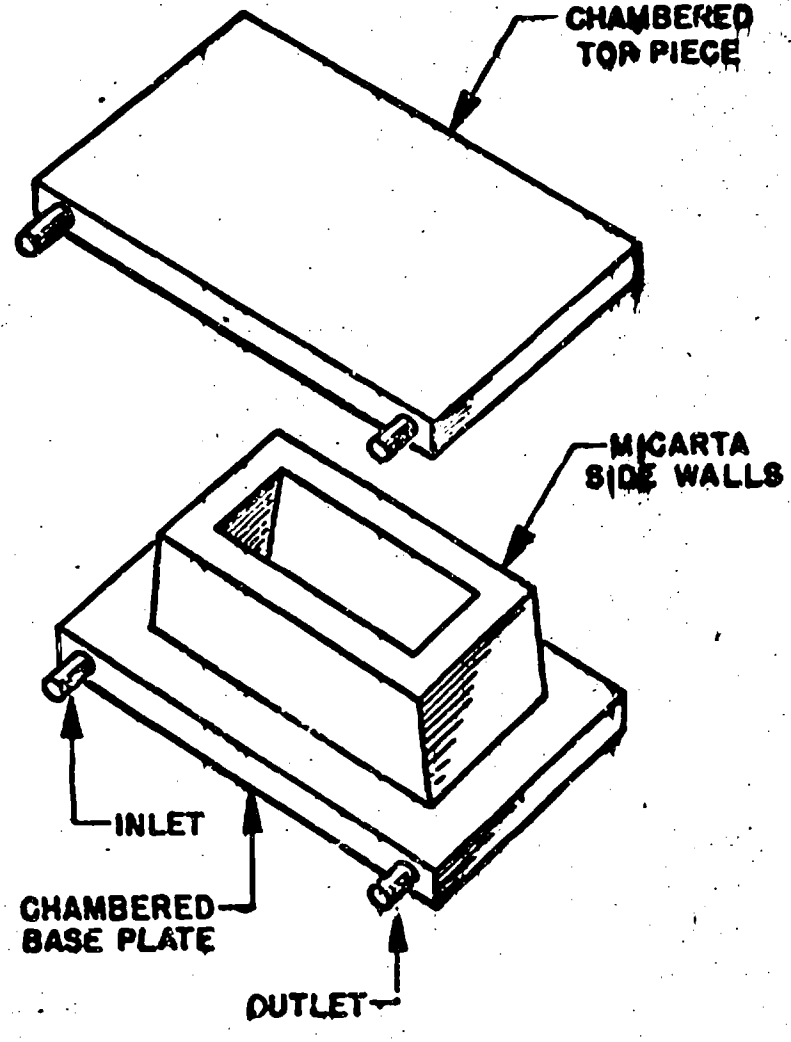


Figure 2 Slab Mold

the poorest sections discarded, and the rods sticks machined out of the high-quality pieces.

The mold used to produce the castings for most of our experiments is illustrated in Figure 2. This mold makes a slab approximately 8-inches high and 12 x 16 inches on a side. Both the top and bottom heat transfer section of the mold are supplied with individually program-controlled circulating water. Temperatures are maintained within ± 2°C and cycle timing controlled within ± 5 minutes. The side walls are made of a laminated cloth impregnated with phenolic resin (Micarta) which serve more or less as an insulator and prevent freezing from the sides inward. The rest of the mold is made of 24ST dural.

In our procedure for Composition B we preheat the mold to 90°C (at least two hours are required for the Micarta side walls). Pouring is done at 83°C and care is taken to insure that little or no air is entrapped. The melt is allowed to settle in the mold for two hours with the top plate at 85°C and bottom plate at 90°C. During this time the RDX settles to its equilibrium packing arrangement in the fluid TNT. At the end of the two-hour settling period, temperature in the bottom plate is reduced to 50°C and freezing from the bottom started. Two hours later temperature in the bottom plate is further reduced to 30°C and held for an additional six hours. During this ten hours the top plate remains at 85°C. Next, the top plate is lowered to 80°C and the two plates held at their respective temperatures for six hours more, at which time the tempered water supply to the top plate is cut off. Temperature of the bottom plate is maintained at 30°C for six additional hours and finally turned off. Three hours later the mold is disassembled, the casting removed, placed in an insulated box and allowed to remain for at least twelve additional hours. The top half of the slab is then sawed off and discarded. The remainder of the slab is now ready for the sawing and machining.

This rather involved procedure is the result of a development program in which various time and temperature cycles were tested and the optimum procedure selected on the basis of the radiographic inspection as well as the results of a statistical analysis of composition and density spreads. Sample plugs were removed from representative castings and subjected to a submersion density check and a chemical composition analysis. Thus we determined that the casting procedure described in the preceding paragraph has a 95% certainty of producing, over the lower four-in. thickness, a casting with maximum density spreads of 0.010 gm/cc and composition spreads of 2.3% RDX.

The procedure described is for Composition B containing 0.1% of an additive which is a 50/50 weight mixture of o-nitrotoluene and p-nitrotoluene. These additives form a eutetic with TNT which apparently contributes a great deal toward making strain-free castings. Similar casting procedures have been worked out without any additive but they are much more time-consuming.

The Micarta side walls play, we believe, a role in making a more or less strain-free casting. Their low heat conductivity allows the liquid/solid interface to move as a plane from the bottom of the casting mold upward during the freezing process. At least this is true for the first four inches. After the first four inches are frozen, we are not much concerned with the upper region except that the upper region, if frozen too fast, can induce strain in the lower section. We deduce this freezing pattern by observing the orientation of the TNT crystals at various levels of the casting. We also observe that when freezing is deliberately induced from the sides inward, a strained casting results. Numerous cracks are invariably present and if the casting is subjected to even minor temperature variations there is a tendency for it to warp.

Our concern with strain-free castings has to do with a desire to produce charges with little or no tendency to develop cracks between the time they are fabricated and fired. It is clear that, should cracks develop after dimensional inspection, the inspection results are no longer the true measure of the dimensions of the test charge.

PRESSING

At Los Alamos Scientific Laboratory we have studied a number of formulations similar to Composition A but with a variety of other binders. Those with a relatively high softening point seem preferable when the purpose is to produce charges of maximum quality.

Most of these explosives are made by a slurry process similar in principle to the process used in the manufacture of Composition A. When very high melting point binders are used it is convenient to dissolve the binder in a suitable solvent. The solution is then added to a violently agitated aqueous dispersion of RDX. The solvent is then stripped from the slurry by distillation. Subsequently the slurry is filtered and then dried. This process, if properly controlled for the specific wax, produces more or less spherical granules about 1 mm in diameter.

Such explosives are most conveniently fabricated by compression molding in an evacuated die. Certain of the inherent difficulties of cast explosives, such as the settling problem and attendant composition inhomogeniety, either do not exist or are of a much smaller degree in pressed explosives. In fact, we have seldom been able to demonstrate compositional variation within a single pressing. Usually, analytical differences are of the same order of magnitude as the errors of analysis, and statistical tests show no significance in the compositional spreads reported.

The story of density spreads is somewhat different. Large density spreads are observed if pressing is done without evacuating the mold cavity. A considerable amount of development work has gone into various techniques of molding and we have concluded that only vacuum molding will produce the charges of sufficiently high quality

for precision detonation velocity work.

Figure 3 illustrates one of two types of vacuum molds in use here for charge preparation in detonation velocity studies. The molding process is quite similar to conventional compression molding used in the plastics industry, the principal difference being in the additional vacuum feature.

The mold is constructed of 4340 steel except for the punches and the metal immediately surrounding the die cavity. These are made of "Crocar", a high alloy oil-hardening tool steel. The "Crocar" is hardened to Rockwell 57 ± 2C. The mold surfaces are polished to a mirror finish. This high polish contributes to easy ejection. The mold is chambered to permit water circulation through both the top and bottom punch as well as around the die cavity. Vacuum sealing is done with the "O" rings illustrated. Clearances between punches and die are of the order of one mil per inch diameter.

The heat transfer system is similar to the one used in casting and capable of equally precise temperature control. It operates, however, at an input pressure of 95 psia and a suction pressure of 55 psi; therefore, temperatures up to 150°C are attainable.

The mold is installed on an Elmes 300-ton compression-molding press equipped with a semi-automatic control circuit. After loading the mold with molding powder the operator has only to start the cycle. The rest of the operation is automatically controlled by a series of relays and time clocks. In this way, absolute uniformity of timing is insured.

Heating explosives powder in the mold is rather wasteful since the mold is more efficiently utilized in actual pressing. Therefore, we preheat our powder in trays to a temperature depending on the formulation in a steam-heated forced-draft oven. When a fairly rigid binder is used, temperatures as high as 115°C may be necessary. The powder is transferred to the mold at the same temperature and the remotely-controlled pressing cycle begun. The press ram carrying the lower punch and the die advances to a prepress position, thereby compacting the powder slightly. After five seconds, the ram retracts to evacuation position. A poppet valve in the upper punch opens and evacuation begins at a slow rate through a throttled vacuum line. The prepressing and throttling are both intended to minimize entrainment of molding powder. At the end of 15 seconds, the density of the residual air being pumped out is sufficiently low so that entrainment ceases to be a problem. At this time, full vacuum is applied and at the end of one minute total evacuation time, the absolute pressure in the mold cavity has been reduced to less than 1 mm Hg. The press now goes on compression stroke simultaneously with the closing of the vacuum valve. Pressure applied is usually around 13,000 psi. Fifteen seconds are required to completely close the press. The leak rate of the mold at 1 mm Hg is about 0.1 mm Hg per minute, so during the fifteen seconds elapsing after the vacuum is cut off and full

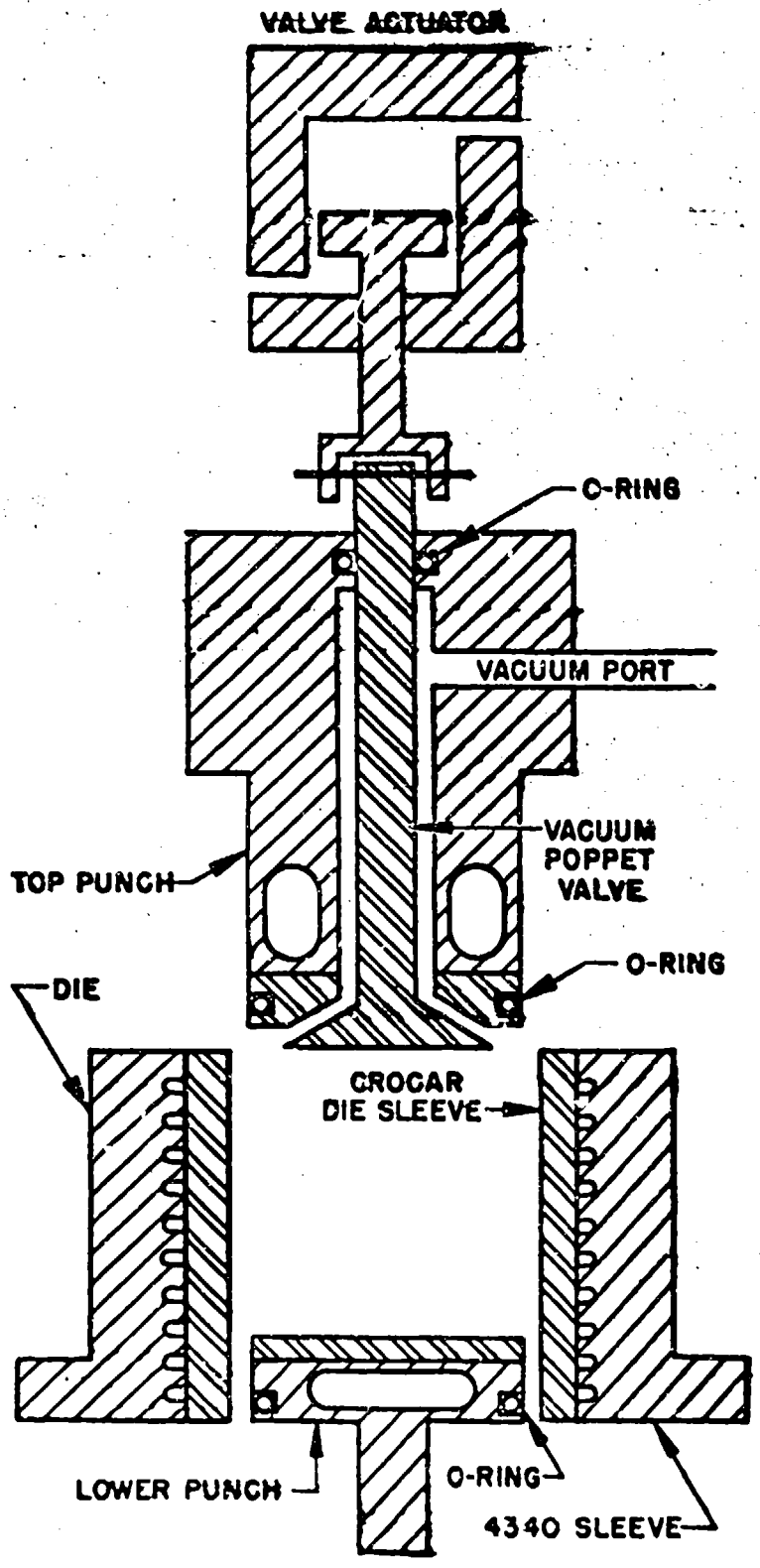


Figure 3 Vacuum Mold

compression occurs, the pressure rise is insignificant. The pressure dwell lasts 20 seconds. At the end of the cycle, the press ram retracts and the molded charge is automatically ejected. If an appropriate minimum molding temperature has been selected the charge is, of course, still at this temperature, but sufficiently rigid to be handled. It is then cooled slowly, either by wrapping in an insulating blanket or placing in an insulated box. Cooling usually takes 12 hours or so. This slow cooling is necessary only when large changes are pressed. Certain compositions are less sensitive than others to thermal shock and therefore even the largest charges do not require any special handling during cooling.

Just as with cast charges, we require that a usable pressed charge shall be free of cracks.

The procedure described above is quite general for most formulations. For example, Composition A with wax of the usual melting point is pressed by exactly the same procedure except the temperature need not be above 70°C and indeed densities of 1.63 gm/cc are readily attained by pressing Composition A at room temperature.

We have had more success in pressing high-quality TNT than we have had with casting. We are able, routinely, to press to a density of 1.62 gm/cc and for us to obtain an equivalent density with cast TNT has been a matter of occasional rare luck. The pressing procedure for TNT is identical to the one outlined above except that we use a 70°C preheat and 70°C mold temperature. In the case of TNT, temperatures must not exceed 75°C or some local melting will occur.

The specific procedure described is by no means the only one which can be used to make high-quality charges. The procedure merely happens to suit our particular equipment and in the interests of reproducibility it is rigorously observed. The procedure works well on very large pressings and has been successfully used on 12-in. dia. x 8-in. high charges.

We do not attempt to use explosives as they come from the pressing operation, but rather we consider our pressings to be machining stock. The various rate sticks are machined from the pressings just as we do with cast explosives; the only difference being that with pressed explosives we have no riser section nor non-uniform region which must be discarded.

Extensive density-spread analyses on individual pressings show typically maximum spreads of 0.005 gm/cc in the six-inch diameter pressings and standard deviation of density about the mean of the sampling-plug density is 0.0023 gm/cc. Between-piece population standard deviation of density runs in the neighborhood of 0.0015 gm/cc. Composition variations within a single pressing and between pressings from the same lot of raw material are less than 0.2%. As stated before, composition analyses usually give spreads which are

statistically indistinguishable from the analytical error.

## MACHINING

Both the rough castings and the pressed blanks are machined to the final dimension. No very special techniques not already familiar to the machine-tool industry are employed, but certain additional safety precautions are observed. For example, before explosives are submitted for routine machining, a high-speed machining test is done on a remotely-controlled drill press with a face milling tool. Speeds as high as 1400 rpm and feeds of 0.045 in. per revolution are employed. On a six-in. dia. charge the linear cutting rate is as high as 2200 ft. per min. at the edge. When a test explosive survives this test without any evidence of decomposition it is considered safe to machine with flat-edged milling tools or the pointed tools common to lathe work at rates up to 200 ft. per min. Cut-off tools and drills are an exceptional case because effective cooling of the cutting edge is difficult. This latter type of machining operation is considered hazardous, and the drilling of small-diameter deep holes especially is avoided.

Most rate sticks are cylindrical. The operation of cutting the cylinder to the correct diameter is usually done first. The cylinder is then sawed to an appropriate length and finished dimension obtained either by milling or facing off on a lathe. Rectangular sticks are prepared by milling alone.

Whenever possible, machining is done while flooding with water. Water-soluble and porous explosives are machined dry. Dry machining, we feel, is justified insofar as the high-speed test is done without water.

The fragility of certain explosives, in particular cast materials, poses a special problem not often encountered in normal machining practice. Securing the piece to be machined on the lathe or mill requires that special vacuum chucks be used with large pieces. Small pieces do not have sufficient area for vacuum chucks to work so we use "Lucite" collets since ordinary metal collets cause excess breakage.

## INSPECTION

### Radiographic

Before machining, all charges are subject to radiographic inspection. In this manner cavities and cracks are detected. Should any defects exist the charge is rejected.

### Dimensional

Diameter and length measurements are made with conventional measuring devices such as micrometers, dial indicator gauges and, on occasion, a cathetometer is used for cross-checking.

Temperature control during inspection is essential because the explosives under investigation all exhibit the high linear coefficients of expansion characteristic of organic compounds. The value of the coefficient of thermal expansion almost invariably lies in the range of $7 \pm 2 \times 10^{-5}$ in./in./°C.

Most cast explosive charges containing appreciable amounts of TNT exhibit an irreversible growth when subjected to temperature cycling. This phenomenon is believed due to certain impurities in TNT; e.g., DNT. The net result is that Composition B and TNT charges, when stored in a magazine for any length of time, will show considerable growth and reinspection is therefore necessary. In order to avoid excessive growth we also make an effort to fire the charges with a minimum delay once they are machined. Also they are protected against excessive temperature variations.

Some explosives may show slight shrinkage on aging. Once the shrinkage has taken place the pieces are dimensionally stable. We therefore allow such sticks to age some time after machining before the final dimensional inspection is made.

Density

A density determination is made on every charge intended for velocity work. The method used depends somewhat on the geometry and size of the piece. The density of small-diameter charges is most easily and perhaps most accurately determined by measuring the volume by the submersion method. We compute the volume of all larger charges from the dimensional inspection data and obtain the density from the volume and weight. We compare the values obtained by each method on a selected intermediate size. Charges are classed according to the density determination and, in the case of pressed charges, only those within $\pm$ 0.001 gm/cc of the average density are accepted for detonation velocity work. Cast charges for obvious practical reasons cannot be held to this tight a density selection specification; however, a $\pm$ 0.003 gm/cc tolerance is considered acceptable.

Although each of the density methods give standard deviations which are of the order of 0.0003 gm/cc, when an individual sample is checked a number of times there is some question of the absolute accuracy of the average. For example, the average density of a lot of one-half-inch diameter charges whose density is determined by displacement, is as much as 0.002 gm/cc higher than the density calculated from dimensional data. Just which method gives the more nearly correct answer is not known. The submersion method suffers the disadvantage that when complete wetting is obtained the results may be spurious due to some capillary penetration. On the other hand, insufficient wetting would cause the apparent volume to be too large, just the opposite effect of penetration. The density computed from dimensional inspection data obtained on small charges is undoubtedly in error to some degree since the surfaces are not truly smooth because of tool marks. Density values by each method for pieces of one inch in diameter and larger

check within 0.0005 gm/cc. For a given lot of pieces machined from a single charge we assume that the small-diameter rate sticks (less than 0.500 in.) have the same absolute density as the density determined for the larger pieces cut from the same charge. The standard deviation of the density we ascribe to the series of small-diameter rate sticks is, however, taken from the displacement volume measurement data. We justify this reasoning by the fact that we believe the submersion method gives relatively high precision, even though we suspect its absolute accuracy.

Composition

Composition analyses on Composition B are done in the usual manner.(1) Our data indicate that the analytical procedure described in the JAN specification produces a standard error of about 0.1%.

Every cast rate stick increment of a composite explosive is sectioned in such a manner that a sample plug is cut from the regions just beyond each end of the stick. By proper arrangement of the sampling pattern, additional data on the composition adjacent to the central region is obtained. Selected charges from the slab are accepted for detonation velocity measurements only if composition spread inferred from the composition analysis adjacent to the specific charge is no more than 0.5 percent RDX. Composition spread analyses are not done on vacuum-pressed charges because of their inherent uniformity; however, lot analyses are performed routinely on the molding powder itself.

Methods of analysis of explosives mixtures vary somewhat with the type of formulation. Except for the use of a solvent picked for the specific components of the explosive, the procedure is similar to the one used for Composition B. Analytical precision of the order of 0.1% is obtained for most mixtures involving RDX.

Detonation velocity measurements are usually corrected to a common density and composition. The velocity correction factor we use for Composition B with respect to density is 3400 m/sec/gm/cc and for composition is 10 m/sec/%RDX. Several other values are used by workers in the field but the exact values are not highly important for small corrections.(2)

Particle Size

Pressed explosives such as TNT present a problem in describing their particle size distribution. It is a simple matter by conventional wet-screening methods to obtain a distribution characteristic of the molding powder. Whether or not this distribution has any real meaning after the explosive has been highly compressed to almost crystal density is not known. At any rate, we have followed the line of least resistance and we characterize the particle size distribution of a simple pressed explosive by the numbers obtained from the screen analysis on the powder before pressing.

The situation with respect to composite cast explosives is more confusing. In Composition B, solution and recrystallization of RDX during melt preparation as well as during the manufacturing process alters the original distribution, especially of the finer fractions. Extracting TNT from samples of the finished casting and determining the new particle size distribution is perhaps the best approach but the extraction procedure itself also suffers from the same inherent difficulty of probably causing some change in particle size.

The situation in Composition A is not quite as complex as observed for cast explosives. The RDX is relatively insoluble in the wax phase and for those compositions employing a solvent for the wax the process time during which the RDX is subjected to solvent action is quite short compared to the time involved in the Composition B system. Therefore, a determination of particle size distribution of the RDX used in preparation of the mixture is a fair indication of the final particle size in a pressed piece. Some crushing of the RDX particles must occur during pressing but it is to be remembered that the wax probably contributes a cushioning effect.

Some of our formulations include a fine fraction which passes through a 325 mesh screen. The distribution of this fraction is determined by a photometric method.

Particle size distribution of the explosive powder aggregate as distinguished from the particle size of the RDX itself is not believed to have any influence on the detonation process and therefore is only considered insofar as it is related to the practical aspects of pressing.

## DETONATION VELOCITY OF MODIFIED COMP. A.

A special formulation similar to Comp. A, but with a somewhat higher-melting wax was used to press 6-in. dia. by 4-in. high cylinders in our vacuum mold according to the procedure given in the section on pressing. Composition analysis before pressing indicated an RDX content of 91.8 ± 0.1 percent. Particle size distribution of the RDX used in the composition is approximately that given in the table below. Five cut of a total of twenty-five of the 6-in. x 4-in. cylinders were sectioned for density spread. The extreme variation found in any one cylinder was 0.004 gm/cc. Average maximum variation was 0.0032 gm/cc.

Two-inch long cylinders of 1 in., 1/2 in., 1/3 in., 1/5 in., and 1/6 in. diameter were machined from the molded blanks. Those pieces falling within the density limit of 1.6874 ± 0.0010 gm/cc were selected for the detonation velocity determination. This density is approximately 99% of crystal density.

PARTICLE SIZE OF RDX

| Particle Size Range | Percent in Range | |
|---|---|---|
| Above 300 μ | 6.6 | Sieve Analysis |
| Between 300 - 250 μ | 6.6 | |
| " 250 - 210 μ | 2.8 | |
| " 210 - 177 μ | 7.6 | |
| " 177 - 149 μ | 9.7 | |
| " 149 - 125 μ | 15.7 | |
| " 125 - 105 μ | 8.6 | |
| " 105 - 88 μ | 6.8 | |
| " 88 - 74 μ | 3.6 | |
| " 74 - 62 μ | 3.8 | |
| " 62 - 53 μ | 1.4 | |
| " 53 - 44 μ | 4.2 | |
| " 44 - 35 μ | 3.2 | |
| " 35 - 30 μ | 1.1 | Centrifuge |
| " 30 - 25 μ | 5.3 | |
| " 25 - 20 μ | 7.9 | |
| " 20 - 15 μ | 9.6 | |
| " 15 - 10 μ | 4.6 | |
| " 10 - 7.5 μ | 1.7 | |
| Less than 7.5 μ | 0.2 | |
| | 98.7 | |

The velocity data on these rate sticks were obtained by Group GMX-8 using the techniques described by Campbell, Kalia, Boyd and Bull.(3) In Table I the data are summarized. The temperature of the rate sticks was observed at the time of firing and corrections made for length and density whenever firing temperature differed by more than 5°C from inspection temperature. The linear coefficient of expansion used in computing the correction was $6.7 \times 10^{-5}$ in./in./°C. An energy correction was also made assuming that the heat capacity of the material was 0.35 cal/gm/°C and assuming that $D \propto [0.35\ (T-25) + 1100]^{1/2}$ where T is in °C. The heat of explosion of RDX at 25°C is taken as 1100 cal/gm. The net detonation velocity correction for temperature for all temperature effects is thus estimated to be -0.35 m/sec/°C.

An average velocity and the associated 95% confidence limit of the average was computed at each diameter. In Figure 4 these averages and their 95% confidence limits are plotted as a function of reciprocal diameter.

The data were fitted by the least squares method to an equation of the form

$$D = a_0 + a_1\ (1/d) + a_2\ (1/d)^2$$

Each average was weighted according to the reciprocal of the square of its confidence limit.

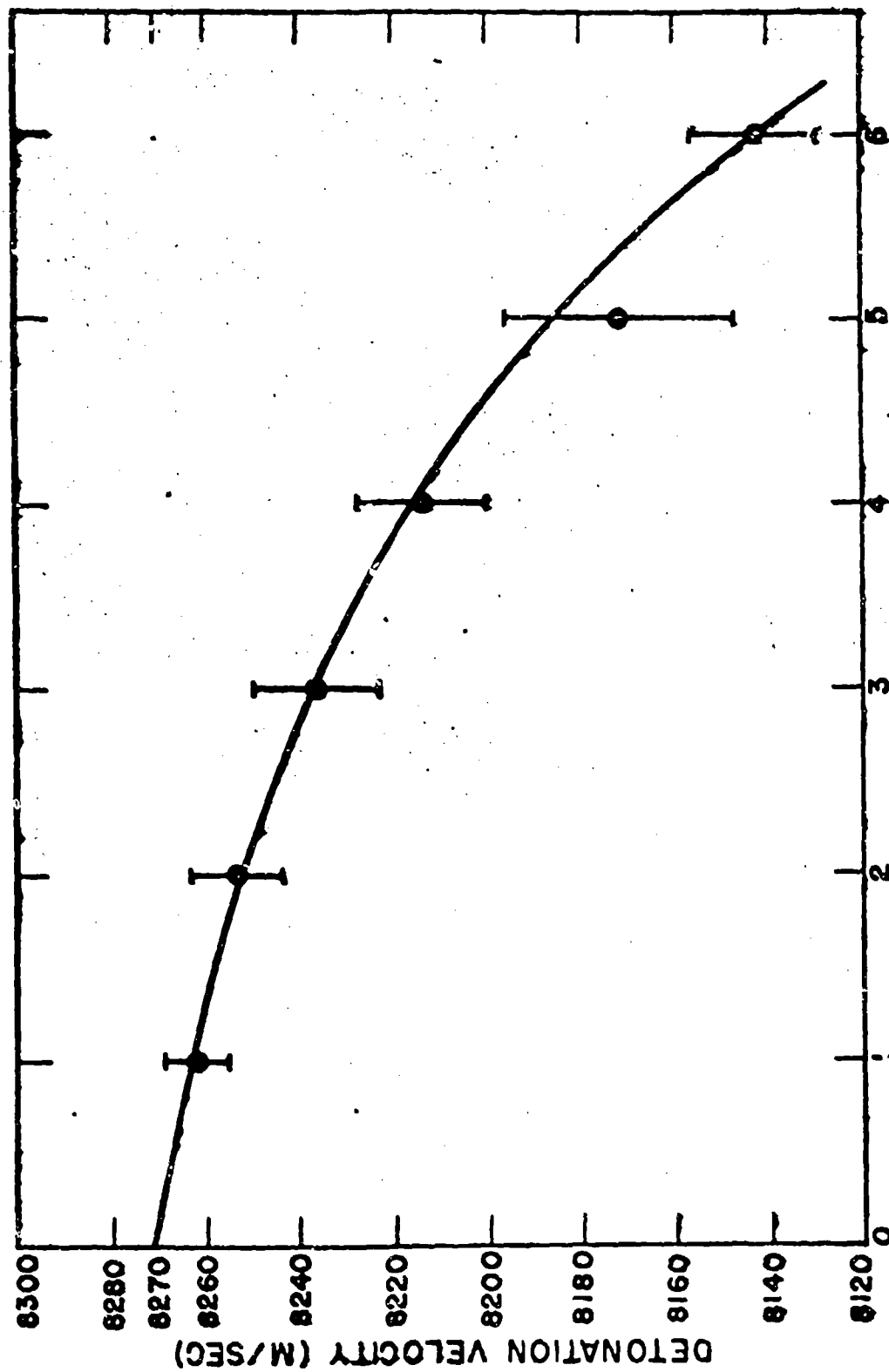


Figure 4. Detonation Velocity of Modified Comp. A as a Function of Diameter, $\rho = 1.687$ gm/cc, $T = 25°C$

## TABLE I

### DETONATION VELOCITY - DIAMETER STUDY

MODIFIED COMPOSITION A $\rho$ = 1.687 ± 0.001 gm/cc (corrected to 25°C)

| DIA (in.) | D (m/sec) | $\bar{D}$ | $\sigma$ | $\pm L_{95}$ |
|---|---|---|---|---|
| 0.999 | 8253.7<br>8267.1<br>8260.3<br>8261.7<br>8283.8<br>8266.3 | 8261.8* | 5.4 | 6.7 |
| 0.500 | 8259.5<br>8235.0<br>8263.3<br>8259.1<br>8251.5<br>8251.5 | 8253.7 | 11.3 | 14.0 |
| 0.333 | 8218.8<br>8234.2<br>8230.8<br>8231.4<br>8255.6<br>8245.7 | 8236.1 | 12.9 | 13.5 |
| 0.250 | 8223.5<br>8198.3<br>8226.6<br>8227.0<br>8201.8<br>8203.1 | 8213.4 | 13.5 | 14.2 |
| 0.200 | 8195.1<br>8205.8<br>8162.7<br>8161.7<br>8139.9<br>8164.4 | 8171.6 | 24.3 | 25.5 |
| 0.167 | 8140.4<br>8145.7<br>8157.4<br>8127.4<br>8127.4<br>8159.2 | 8142.9 | 13.9 | 14.7 |

* Fifth increment omitted from calculation of average.

The standard errors of the coefficients were computed according to an extension of the method described by Birge.(4) Birge's treatment is limited to equally-spaced arguments and if one is desirous of weighing their data the method is inadequate. Members of Group T-8, LASL, however, have extended the method to use points weighed according to the inverse of the square of the confidence limit attached to any one point.

The values for the coefficients so obtained and their standard errors are:

$$a_0 = 8269.8 \pm 1.231$$

$$a_1 = -1.082 \pm 0.885$$

$$a_2 = 3.385 \pm 0.129$$

The standard deviation of the weighted average points about the fitted curve is 2.165 m/sec.

A simple linear fit was also made and the following values obtained:

$$a_0 = 8296.9 \pm 2.949$$

$$a_1 = -23.72 \pm 0.855$$

The standard deviation of the data about the fitted line in the linear case is 9.463 m/sec.

The two D axis intercepts are 8296.9 and 8269.8 m/sec for the linear and quadratic fits respectively. The quadratic fit is significantly, at the 95% confidence level, better than the linear fit and so, on a purely statistical basis, extrapolation of the quadratic fit may be expected to give a value more nearly correct for the steady state plane wave velocity at infinite diameter. The 95% confidence limit associated with this intercept is 2.5 m/sec.

## ACKNOWLEDGMENT

The author wishes to make it clear that the techniques described in this paper are only in a small part results of his efforts. The combined work of a large number of people over a period of several years has gone into the refinements of techniques described in this paper. The discussion concerning casting is primarily the result of the efforts of Group GMX-3 of the Laboratory. Vacuum-pressing developments have been carried out in Groups GMX-2 and GMX-3. Detonation velocity measurements on the finished rate sticks have all been done by Group GMX-8. Radiographic inspection development is the result of the efforts of Group GMX-1. Valuable assistance has also been received from the Engineering Department of the Laboratory, and the

machine computations for curve fitting and data analysis have been done by Group T-1.

## REFERENCES


1 JAN-C-401, September 25, 1946, par. F-4a (1).

2 OSRD Report No. 5611, M. D. Hurwitz et al., "Rate of Detonation of Various Explosive Compounds and Mixtures".

3 Campbell, Kalin, Boyd and Hull, "Techniques for the Measurement of Detonation Velocity."

4 R. T. Birge, Review of Modern Physics, 19, 4 - 298

# TECHNIQUE FOR THE MEASUREMENT OF DETONATION VELOCITY

A. W. Campbell, M. E. Malin, T. J. Boyd, Jr., and J. A. Hull
Los Alamos Scientific Laboratory
Los Alamos, New Mexico

## INTRODUCTION

Until the last few years most of the measurements of detonation rates have been made with the use of streak cameras, the method of Dautriche, or with the Mettegang recorder. It is the purpose of this paper to describe an electronic method capable of very high precision in the measurement of detonation rates. Commonly referred to as the "pin method", it has been in use at Los Alamos from approximately the year 1944 to date. Recently, Gibson[1] reported a similar technique.

While at first glance the pin method may appear to resemble the Mettegang recorder method, there is a basic difference. The latter depends upon the interruption of the primary circuit of a high voltage transformer to produce a spark which registers on a strip of carbonized paper carried on a revolving drum; the technique to be described here relies upon the conductivity of the detonation wave to discharge a capacitor, forming a pulse which is presented on an oscilloscope trace and photographed.

The pin method offers several advantages over other available methods. Chief among these is that of increased time resolution. In contrast to the Mettegang recorder, the pin technique provides a record of the pulse shape and thus gives evidence of the strength of the detonation wave, i.e., whether the detonation wave may be dying out or is comparatively strong. The pin method also provides a means of observing directly the progress of the wave in the interior of an irregularly shaped piece of explosive; by way of contrast, optical methods for detonation velocity measurement must make observations on the exterior surface of the piece and infer the velocity of the wave from geometrical considerations.

## INSTRUMENTATION

The pin method makes use of electronic circuitry, which may

be divided conveniently into three parts: beginning at the explosive, these include ionization-operated or shock-operated switches, which are inserted into the explosive; a signal mixer circuit and transmission line; and a cathode-ray chronograph, commonly referred to as a "pin machine", which presents the signals on a calibrated time base. For the sake of clarity, these will be discussed in the reverse order.

Chronograph. Many different circuits have been developed by various workers for use with explosives. These have employed a variety of time base presentations including circular sweeps, spiral, linear and raster sweeps, and zigzag sweeps. This discussion will

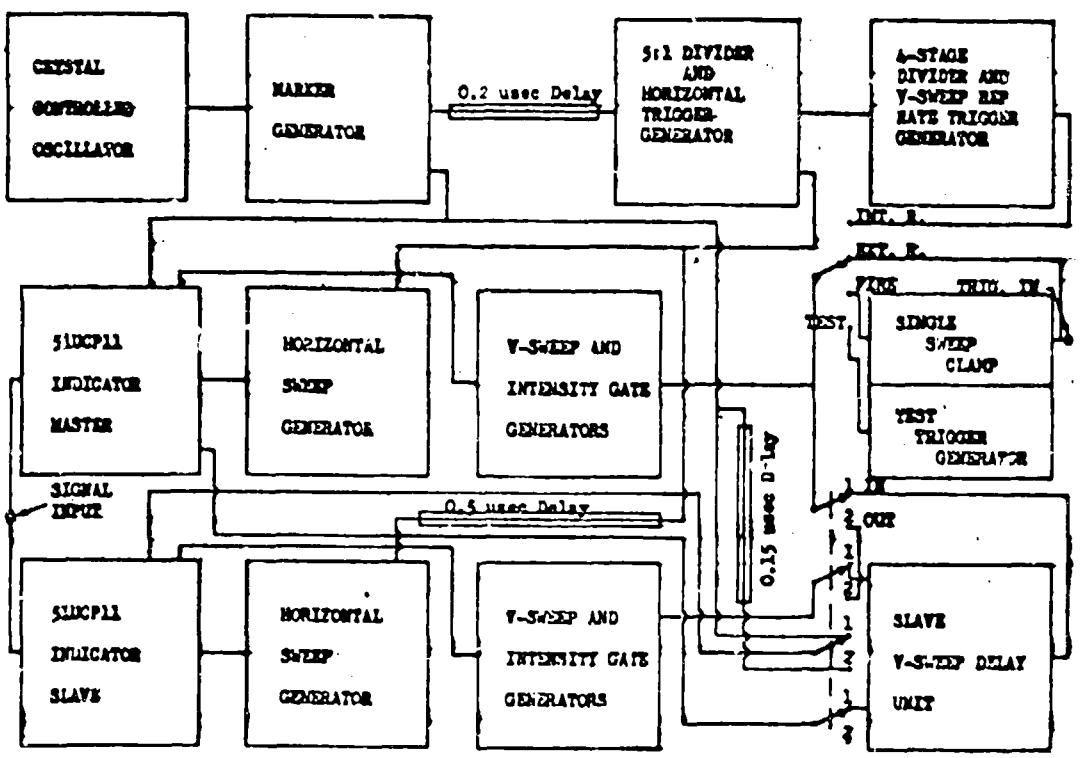


Fig. 1. Block diagram of chronograph circuit.

be limited to a circuit providing a raster presentation, because the authors have found such a circuit to be preferable on the bases of time coverage, attainable precision and ease of maintenance.

The raster chronograph is shown in block diagram in Fig. 1. A typical record from this chronograph is shown in Fig. 2. This apparatus provides two sweep presentations, with a maximum sweep time of 150 μsec. These may be operated in parallel to provide duplicate records and thus increase the precision of observation, or may be operated in tandem to increase the time coverage.

While a detailed discussion of the circuit would be out of place here, a brief description of the functioning of the circuit will be given. Referring to Fig. 1, the output from the crystal-controlled oscillator is shaped by the marker generator to provide

1/2-μsec, square-wave timing marks for the indicators. The master indicator, or sweep circuit, receives the timing marks directly. The slave indicator receives the timing marks after they have passed through a 0.15 μsec delay line, when the indicators are operated in parallel, or receives them directly when the indicators are operated in tandem.

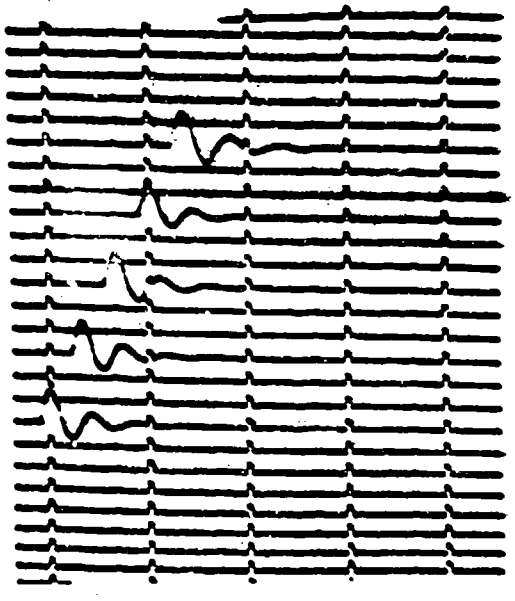

Fig. 2. Sample chronograph record. Pin switch signals are equally spaced at intervals of 7.33 μsec.

The marker generator also supplies 1/2-μsec pulses through a 0.2 μsec delay line to a 5:1 frequency divider which, in turn, drives the horizontal trigger generator. The master horizontal sweep generator receives these trigger pulses at 2.5-μsec intervals. The slave horizontal trigger generator receives the same pulses after being delayed by one marker interval. By delaying the slave sweep by one marker interval, and by delaying the slave time markers by 0.15 μsec as noted in the previous paragraph, it is made impossible for a signal common to both master and slave records to be adversely affected on both because of coincidence with a marker or with a back-sweep.

The 400 kc horizontal repetition rate pulses are divided by the 4-stage divider to provide an internal, vertical repetition rate of approximately 200 sweeps per sec. By repeating the complete pattern so rapidly, it is made to appear as a steady pattern to the eye to aid in adjustment of the pattern. The vertical sweep and intensity gate generators may be triggered from the internal repetition rate pulses, an external source of repetitive pulses, the single sweep clamp circuit, or the manual test trigger.

The precision which is attainable with these chronographs is derived from close control on the frequency of the crystal controlled oscillator and on the linearity of the horizontal sweeps. The oscillator is a crystal-controlled free-running Miller oscillator having a frequency of 2 Mc ± 50 cps. While this may seem to be greater precision than is necessary, it is easily attained and, for all practical purposes, eliminates the time calibration marks as a source of experimental error.

Sweep linearity is controlled to 1% between adjacent calibration marks (1/2-μsec). This is accomplished by selecting the 5LUCP11 cathode-ray tubes for linearity of deflection as a function of the deflection voltage, and by adjusting the sweep circuit linearity controls. The standard error of measurement, resulting from errors in sweep calibration, linearity, and judgement of the film reader is found to be $3 \times 10^{-9}$ sec for transit times of 25 μsec or less.

Mixer Circuits. The mixer circuit is a network of capacitors and resistors which form and send to the chronograph the electrical pulses which mark the passage of the detonation wave through the explosive charge. In Fig. 3 is shown a diagram of the circuit used with most solid explosives. The condensers, C, are charged through isolation resistors, R. When the detonation wave closes a pin switch, one side of the capacitor is shorted to ground. The other side then discharges into the RG 21-412 signal cable, producing a signal pulse. $R_1$ prevents recharging of the condenser during the shot either by other condensers in the mixer, or by the power supply. The characteristic impedance, $R_4$, prevents reflection of the signals back down the RG 63/U cable. If pulses are reflected to the left by a faulty connection or other defect, they are absorbed by either $R_3$-$R_4$ or $R_2$. Because the 5LUCP11 display tube has four vertical deflection plates, it is possible to put the signal pulses on a plate separate from that used for calibration pulses and for the vertical sweep. This eliminates the problem of a mixer circuit at this point.

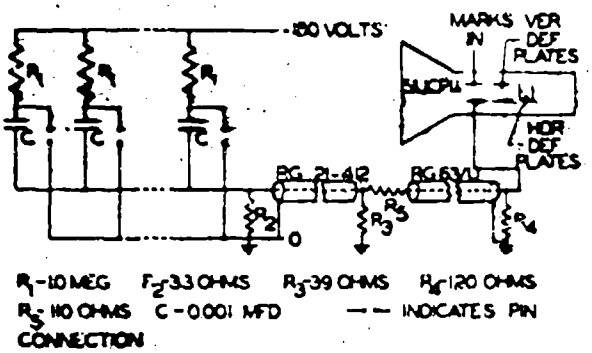


Fig. 3. Mixer circuit.

When pin switches must be closely spaced in the charge, the mixer circuit is modified as shown in Fig. 4. With close spacing, the conductivity of the detonation wave and of the shock wave serves to connect the discharging capacitor with those which have been discharged. The result is that the signal rise is affected adversely. To prevent reverse current flow into the discharged capacitors, diodes are inserted as shown. These act practically as rectifiers, permitting current flow in the desired direction only.

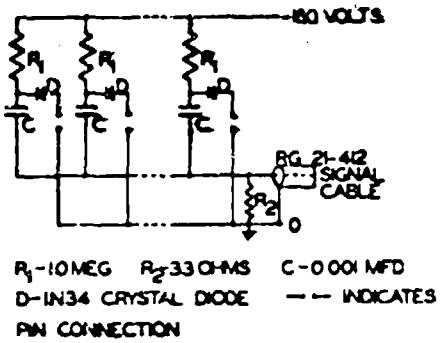


Fig. 4. Mixer circuit for use with closely spaced pin switches.

A second modification is necessary when the undetonated explosive is moderately conducting. As shown in Fig. 5, the isolation resistors, R, are replaced with diodes. This permits increased charging current to the leaking pin switches, but prevents the discharged capacitors from drawing current from those still charged via the charging connection. In addition, it is sometimes necessary to increase the discharge time of the capacitors.

For best results all mixers are constructed with shortest leads possible. Parts are staked together, and the finished mixer is mounted close to the charge. When the latter is detonated, both mixer and the section of RG 21-1/2 coaxial cable are destroyed by blast. All pin switch leads must be of the same length to within a few inches, or the transit time of electric pulses in the leads must be taken into account for precision work.

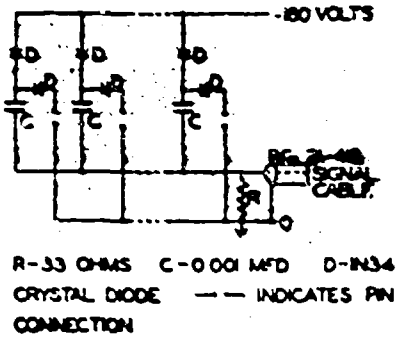


Fig. 5. Mixer circuit modified for use with moderately conducting explosive.

Switches. The most commonly used type of pin switch is the one depending upon ionization for closure. Usually, this is arranged as shown in Fig. 6, although other arrangements will be discussed later under the section on charge preparation. The switch is made with the thinnest metal foils which have at the same time sufficient mechanical strength to withstand the necessary manipulation in preparing the switch. The most commonly used foils are silver, aluminum and copper in 1/8-inch widths and in thicknesses ranging from 0.2 mil to 1.5 mil. Occasionally, gold leaf is used. This has a thickness of approximately 0.01 mil. However, it is difficult to use because of its lack of mechanical strength, and because it tends to stick to most objects brought near it as a result of electrostatic attraction.

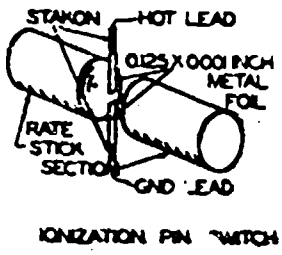


Fig. 6. Pin switch construction.

The voltage on the pin switch is dictated by the sensitivity of the indicator circuit. When no signal amplification is required, and when it is unnecessary to mix signals at the indicator by means of cathode followers, a suitable value of the pin voltage is 180 volts.

The gap width on the pin switch is usually held to about 1 mm to 3 mm. For two-component cast explosives or for pressed explosives, the detonation front has been found to be quite irregular, the irregularities being comparable in size to the grains of explosive. Therefore, it is desirable to have the dimensions of the

pin switch gap many times that of the largest grains of explosive, to improve the statistics of switch closure.

Occasionally, the ionization switch is found to be inadequate. One example of such an instance is encountered in the very weak initiation of a solid explosive. Here, the detonation wave may proceed without sufficient ionization to operate the switch described above. In this event, a switch involving mechanical closure may be used. Such a switch is shown schematically in Fig. 7.

The mechanical closure is effected by the motion of a thin metal foil, which is accelerated by the pressure of the detonation wave. In order to keep the closing delay as small as possible the metal foil and the insulating foil should be kept very thin, usually less than 1 mil. Typical insulating materials include mica and Mylar or Nylon plastics. Closure times of $10^{-8}$ seconds are easily attained.

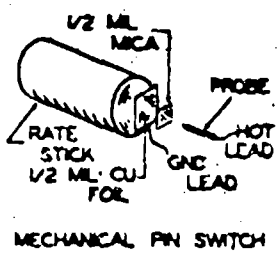


Fig. 7. Pin switch construction.

## ELECTRICAL EFFECTS

Before discussing the method of preparing charges for velocity measurement by the pin technique, it will be well to consider three electrical effects which have been observed to be associated with the detonation of an explosive charge.

The first of these is a difference between the potential of the detonation wave and ground potential resulting from the voltage pulse used to fire the electric detonator. If this potential difference is allowed to persist until the detonation wave reaches the first pin switch, it will be recorded as electrical noise on the chronograph trace. By grounding the detonation wave near the point of initiation, this potential difference can be eliminated.

The second and most important electrical effect, insofar as the pin technique is concerned, is the appearance of a potential difference between the detonation wave and ground, as a result of the detonation process.

This potential difference may be observed by use of the circuit diagrammed in Fig. 8. An uncharged copper wire is placed so as to contact the detonation wave. This wire is connected to ground via a co-axial cable and its termination, $R_1$. The electrical circuit is believed to be closed by capacitive coupling between ground and the detonation products. While the probe is in contact with a detonation wave or a conducting shock wave, a potential difference is observed between the terminals of $R_1$. This potential is commonly of the order of a few hundred volts, but may exceed 1000 volts under some circumstances.

In Fig. 9 are shown sample oscillograph records taken with the explosive and circuit arrangement shown in Fig. 8. These records show the effect of changing the gas surrounding the explosive. The signal probe was inserted in the explosive to a depth of one inch. When the detonation wave struck the probe a positive signal (downward deflection) was recorded, which seems to be proportional to the temperature of the shock wave in the surrounding atmosphere. When the shock wave from the end of the stick reached the plastic insulation on the probe, the major signal pulse began. This ended with the decay of the shock wave.

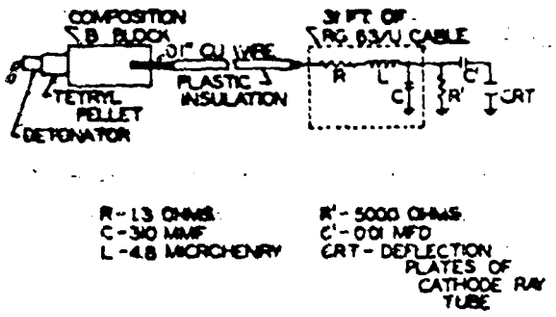


Fig. 8. Experimental arrangement for observing charge separation in detonation wave.

It is also important to note that insulation of the pin switch leads from the detonation wave is impossible by ordinary means. Figure 10 shows the signals obtained in an atmosphere of air when the conductor was insulated with plastic, rubber and glass.

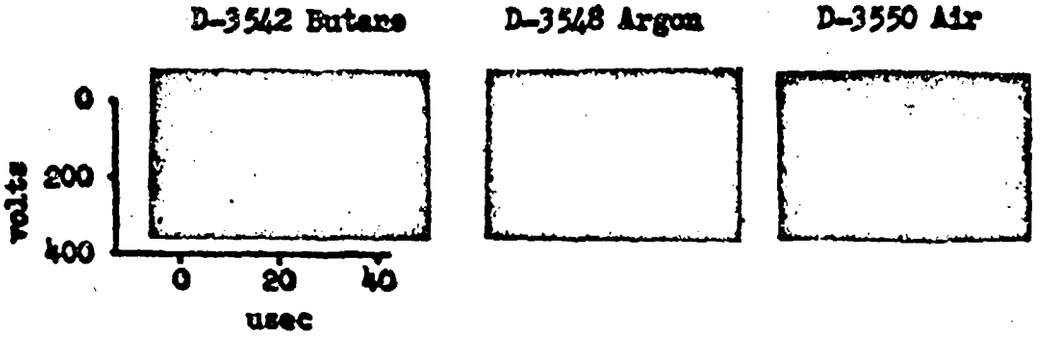


Fig. 9. Effect of atmosphere on voltage recorded by circuit of Fig. 8 using bare copper probe. Time scale: 1.75 μsec/cm.

For the purpose of reference, a signal obtained with an uninsulated probe is included. In order to keep the signals within the limits of the oscillograph screen, the signals shown in Fig. 10 were attenuated by a factor of five relative to those shown in Fig. 9.

Perhaps the most plausible explanation of the potential difference between the detonation wave and ground is that involving charge separation. It is postulated that, because of greater mobility, more electrons than positive ions escape from the reaction zone, leaving the latter positive, a condition in agreement with experimental observation. It is further postulated that electrons escaping in the forward direction are soon captured. The presence of the resulting negative region in front of the detonation wave is observed when suitable amplification and time resolution are used in the signal

circuit.

Finally, the charge-separation hypothesis requires that, while a potential difference must exist between the detonation wave and the product gases, the system as a whole must not develope a net charge. Experimentally, no net charge is observed on explosive fired in a Faraday cage.

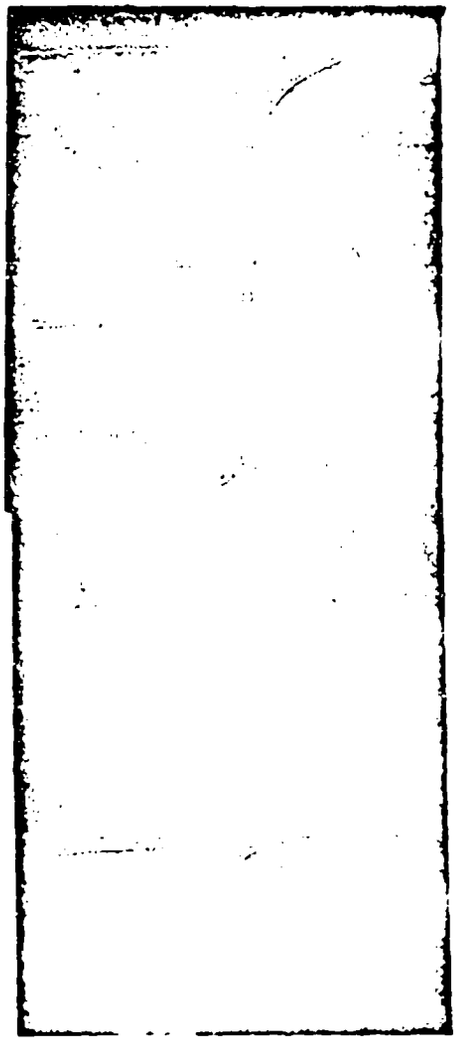

D-3368 30 mil conductor, 35 mil plastic coating

D-3369 150 mil conductor, 90 mil rubber coating

D-3374 100 mil conductor, no coating

D-3376 30 mil conductor, 15 mil glass coating

Fig. 10. Effect of probe insulation on voltage recorded by circuit in Fig. 8. The record from a bare probe, showing a 400-volt deflection, is shown for reference, D-3374.

Whether or not the above explanation of the second electrical effect is correct, it is important in using the pin technique to be aware of the phenomenon. Failure to properly ground the detonation wave in the vicinity of a pin switch results in electrical noise intruding on the chronograph record. In Fig. 11 is shown a record on which this has occurred. One pin signal appears at the right end of line 10 measuring from the top of the pattern. In the next section,

methods of grounding the detonation wave so as to eliminate electrical noise will be discussed.

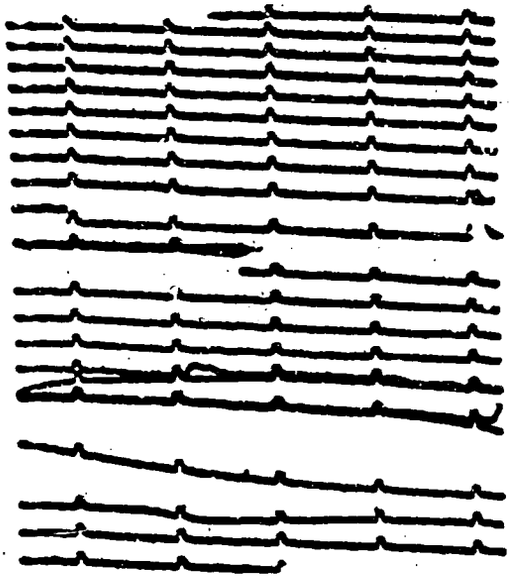

Fig. 11. Sample raster record showing electrical noise on detonation wave.

The third type of electrical effect observed when explosive is detonated is a radiation signal, which may be similar to that observed by Kolsky[2]. This radiation does not interfere with the signal circuits described here for use with the pin technique, but is discussed briefly for the sake of completeness. It results from the charge separation mentioned above and/or from the fact that when a piece of explosive is detonated in air, the surrounding shock wave constitutes an expanding, conducting envelope. In the presence of an electric or a magnetic field, e.g., the earth's, this envelope becomes polarized and its surface charge produces effects in external space equivalent to those of a dipole. It has been experimentally demonstrated that the electrical effects of this dipole can be adequately described by means of quasi-stationary field theory.

If the explosive being detonated is particularly deficient in oxygen, e.g., Torpex, the radiation signal exhibits two maxima: the first is attributed, as mentioned above, to the conducting shock wave, the second to the flame produced by oxidation of the detonation products after mixing with air.

## CHARGE PREPARATION

The pin technique for measuring detonation velocities, as mentioned above, is capable of very high precision. The standard error of observation can be reduced to better than 0.1% of the rate for charges a few inches in length. Expressed in terms of time, the standard error is, for most experiments, independent of the total time covered, amounting to approximately $3 \times 10^{-9}$ sec. This precision is useless, however, unless every precaution is taken in the preparation of charges for rate measurements. Some of the precautions to be discussed here result from the nature of the pin technique, others are necessary to any precise method of measuring detonation

velocity.

Assuming that uniform explosive is at hand and that density and composition are known, the first problem in charge preparation is the insertion of pin switches. In the case of liquid explosives, charged probes may be inserted as shown in Fig. 12. The spacing of the probes can be measured with a cathetometer to a precision of about 1 mil. By means of the common ground, the detonation wave is maintained at ground potential. The discharge of the pin mixer capacitors takes place via the spaced probes and the detonation wave to ground.

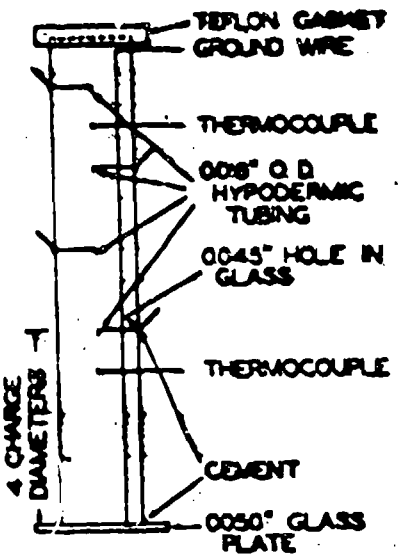


Fig. 12. Pin switch arrangement for liquid explosives.

For granular explosives at low loading densities the arrangement used is shown in Fig. 13. Each switch is composed of a pair of fine copper wires stretched taut by means of a clamp on the outside of the containing tube. The spacing between wires is regulated to a few multiples of the maximum grain size. In order to avoid premature operation of the switch by means of photoionization, enameled wires are used. Axial spacing of the wires is controlled by boring the holes for them with a milling machine.

In high density pressings and in castings, thin metal foils are used to form pin switches as explained earlier. The position of the end of each charged foil relative to the center of the rate stick is kept constant, otherwise the curved detonation front will not short all switches in exactly the same manner. To avoid the use of a layer of glue to hold the foils in place the latter are moistened with water. An alternative method of forming pin switches is to use a common ground on the outside of the charge such as is used for liquids, and to use a single charged foil extending in to the center of the stick.

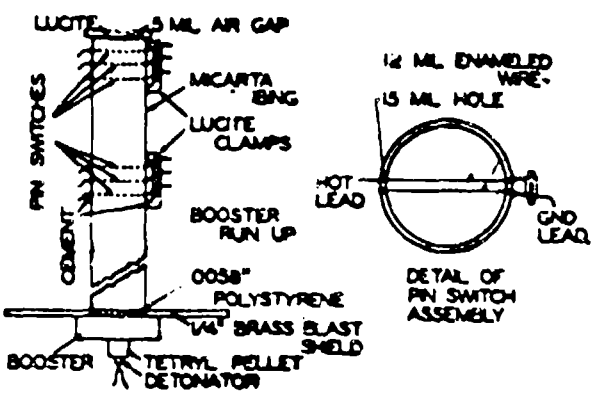


Fig. 13. Pin switch arrangement for granular explosives.

After the method of switch insertion has been decided, in the case of the cast or pressed explosives, some method of assembling the ag-

ments must be devised. The simplest method is to tape them together using a pressure sensitive tape. The use of cellophane tape has, unfortunately, several disadvantages, chief among which is the danger of jetting if the tape is applied loosely. When a small space exists between the lateral surface of the charge and tape, a gas "jet" may be formed. This jet may precede the detonation wave by several tenths of a microsecond and discharge the pin switch prematurely.

A preferred method of charge assembly is that of clamping as shown in Fig. 14. This leaves the sides of the charge free and provides positive contact between charge segments. It is well to point out here again that only the thinnest possible foils are used between segments so as to keep the gap between segments as small as possible. This is necessary because an air gap results in a momentary slowing of the detonation wave, perhaps by dissipating the von Neuman "spike". Quantitatively, a small gap is believed to increase the transit time of a piece of explosive by about $10^{-8}$ sec per mil thickness of the gap. Thus, in a two-inch segment of explosive having a detonation velocity of 8000 m/sec, a booster gap of 1 mil would result in a velocity error of approximately 10 m/sec.

Fig. 14. Method of charge assembly using clamping.

In boostering the charge, a single detonator or a plane wave generator is used, followed with 2 to 6 diameters of booster identical with the charge over which rate measurements are to be taken. When using high-energy boosters on rate sticks with low detonation rates, it has been found necessary to impede the expansion of the booster gases by means of a coating of putty or sand, since in some cases the booster gases have preceeded the detonation front in the stick, closing the pin switches prematurely.

In making velocity measurement on low energy explosives or on sticks of large diameter it is frequently advisable to provide grounding in addition to that furnished by the grounded side of the pin switch. This results from the resistance of the detonation wave and explosion products—the grounded side of the pin switch fails to ground the wave near the lead from the pin mixer. As a result, the latter begins to respond to the generation of charge on the shock front, introducing noise on the chronograph record to the extent that the latter may not be assessable. It is the practice in such instances to run a ground lead paralleling each charged probe and extending beyond the limits attained by the shock wave during the observation.

A final precaution which must be taken if high precision is to be maintained is the control of firing temperature. The detonation velocity of Nitromethane, for example, has been found to vary with the initial temperature at the rate of -3.7 m/sec/°C[3]. In the

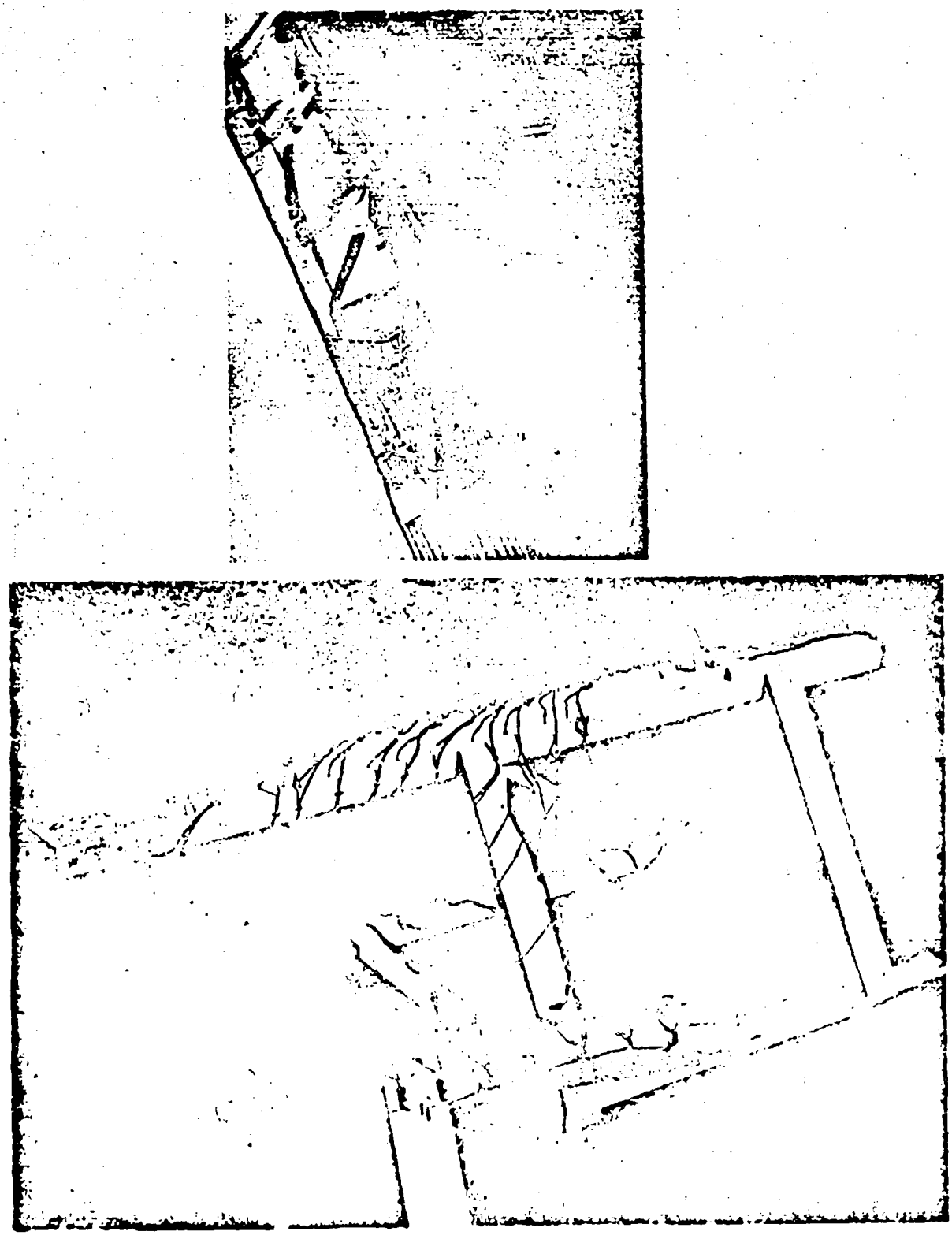

Fig. 15. Above: detail of assembly of 0.500 in. diameter charge on V-notched blocks. Below: fully assembled. Mixer in foreground.

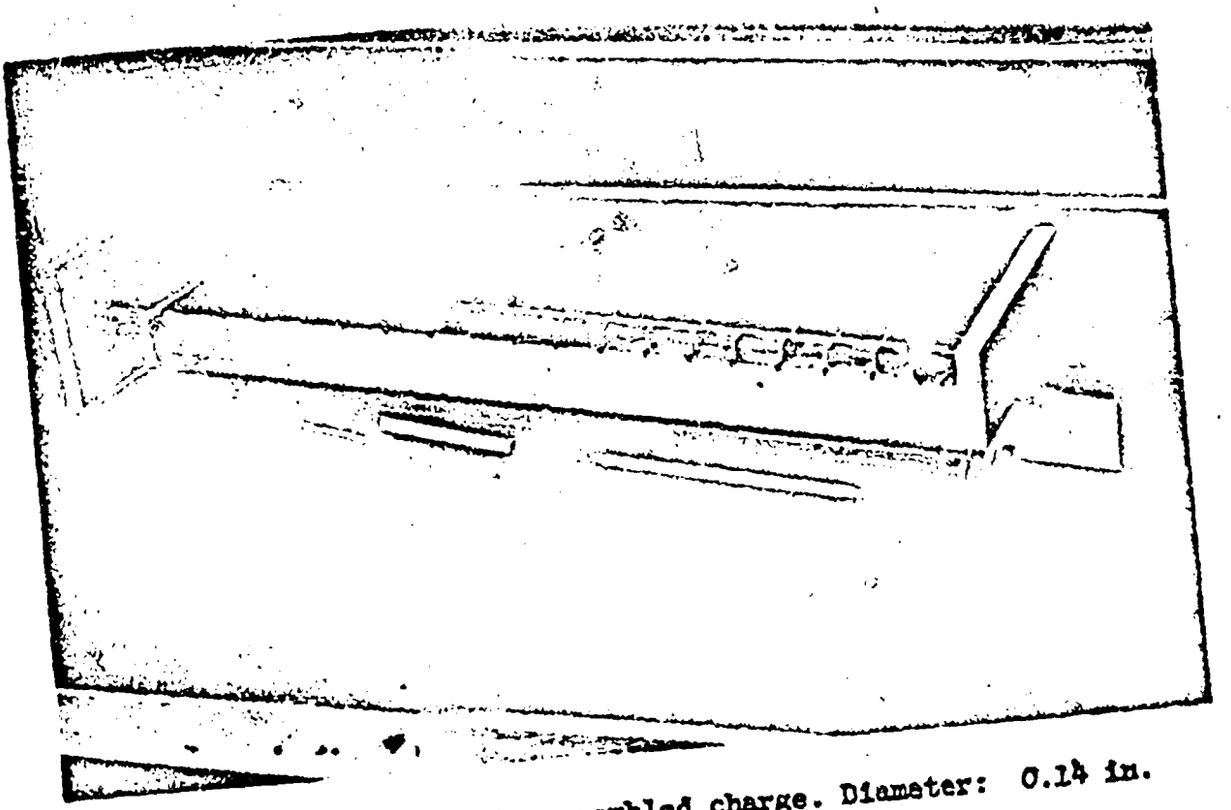

Fig. 16. View of partially assembled charge. Diameter: 0.14 in.

case of Composition B, Mauta[4] has found the transit time to vary inversely with the temperature at the rate of 1% per 100°C. Taking the linear coefficient of thermal expansion to be $5 \times 10^{-5}$/°C the velocity variation would be 0.5 m/°C.

It is therefore evident that precision rate sticks may not be exposed to direct sunlight nor fired without suitable thermal insulation if precise data are desired.

## SAMPLE DATA

In Tables I and II are shown sample data taken with the electronic technique. In taking such data, it is common practice to operate several sweeps in parallel to produce replicate records. This may be done to guard against the failure of a single circuit to operate properly, or several results may be averaged to further reduce the error of analysis.

TABLE I

Sample transit time data for pressed TNT. The charge consisted of six sections 1/2 inch in diameter arranged in a column. Transit time data were taken over the last four sections.

| Density g/cc | Transit time, μsec* sweep-3 | sweep-4 | sweep-5 | average | Detonation velocity m/sec |
|---|---|---|---|---|---|
| 1.642 | 7.338 | 7.330 | 7.333 | 7.333 | 6925 |
| 1.642 | 7.338 | 7.339 | 7.336 | 7.336 | 6921 |
| 1.641 | 7.337 | 7.321 | 7.334 | 7.334 | 6928 |
| 1.641 | 7.338 | 7.334 | 7.333 | 7.333 | 6929 |

*The record from sweep-7 is shown in Fig. 3. Shot No. B3243.

TABLE II

Sample transit time data for Nitromethane. The explosive was contained in a glass tube 2.570 inches in diameter and 30 inches long. Pin switches were arranged as shown in Fig. 12.

| Switch interval mm | Transit time, μsec sweep-2 | sweep-4 | sweep-5 | average | Detonation velocity m/sec |
|---|---|---|---|---|---|
| 126.27 | 19.903 | 19.893 | 19.896 | 19.897 | 6346 |
| 134.99 | 21.252 | 21.272 | 21.274 | 21.266 | 6348 |
| 129 415 | 20.388 | 20.385 | 20.379 | 20.384 | 6349 |

Additional data taken with this technique are presented in other papers given at this conference including: Detonation in

Homogeneous Explosives and Particle Size Effects in One-and-Two-Component Explosives.

## CONCLUSION

A technique has been developed for measuring transit times in explosives charges which is capable of higher precision than are the methods heretofore used. While it can be used in conjunction with the streak camera, it is not subject to the limitations of the latter. Distortion of the detonation wave at the charge boundaries are not detrimental, nor does confinement of the charge in metal or other opaque materials hamper the measurement of detonation rate. If full advantage is to be taken of the precision afforded by the pin method, great care must be taken in preparing each charge and in controlling the firing conditions.

## ACKNOWLEDGEMENT

Because so many workers have contributed to the development of the circuitry and the technique of charge preparation, it is impossible to give appropriate credit to each. Recognition should be made here, however, of the important contributions of James L. Tuck and Roy W. Goranson, both of whom were active in introducing variations of the pin method to this laboratory.

---

(1) F. C. Gibson, Rev. Sci. Instr. 25, 226-31(1954) Mar.
(2) H. Kolsky, Nature 173, 76, (1954).
(3) A. W. Campbell, M. E. Malin, T. E. Holland, Detonation in Homogeneous Explosives. (This Conference).
(4) C. W. Mauer, Unpublished Report, Los Alamos Scientific Laboratory.

# A MICROWAVE TECHNIQUE FOR MEASURING DETONATION VELOCITIES 3

T. J. Boyd, Jr. and Peter Fugan
Los Alamos Scientific Laboratory
Los Alamos, New Mexico

The measurement of detonation velocities at the Los Alamos Scientific Laboratory is usually accomplished by a pin technique[1]. However, this technique often proves unwieldy when applied to nonsteady state studies where the detonation velocity varies with time. In such cases, it has been found practical to employ a microwave technique for measuring these nonsteady velocities. This technique is based on the reflection of microwaves from the ionized detonation front and yields a sequence of detonation velocities which are averages over equal and adjacent intervals along the length of the explosive being studied. In a measurement of the detonation velocity where the pin technique could be employed, the microwave technique would be less accurate and more complicated. There were, however, a sufficient number of nonsteady state studies where the pin technique was impractical to warrant the development of the microwave technique for routine use.

Before the actual microwave system is explained, the basic technique will be illustrated by considering the simplified version shown in Fig. 1. A microwave oscillator is connected to a lossless waveguide section which is terminated by a perfectly conducting, movable piston. In order to isolate the oscillator from any load changes caused by the piston movement, an attenuator is inserted between the piston and the oscillator. A probe is inserted to sample the electric field in the guide. If it is assumed that only one mode, or field configuration, exists in the waveguide, the electromagnetic field in the waveguide can be represented as the sum of an incident and a reflected wave. In the lossless case considered, the sum of the waves is a pure standing wave. The transverse electric field intensity is zero at the piston and at distances which are an integral number of half guide-wavelengths from the piston. As the piston is moved, a periodic signal is recorded by the probe and detector. One cycle of the recorded signal will correspond to a piston displacement of one-half the wavelength in the guide. If the guide wavelength and the initial position of the piston are known, then the position of the piston as a function of time can be determined.

The above analysis assumes the presence of only one mode in the guide. It is possible to choose the dimensions of the guide such

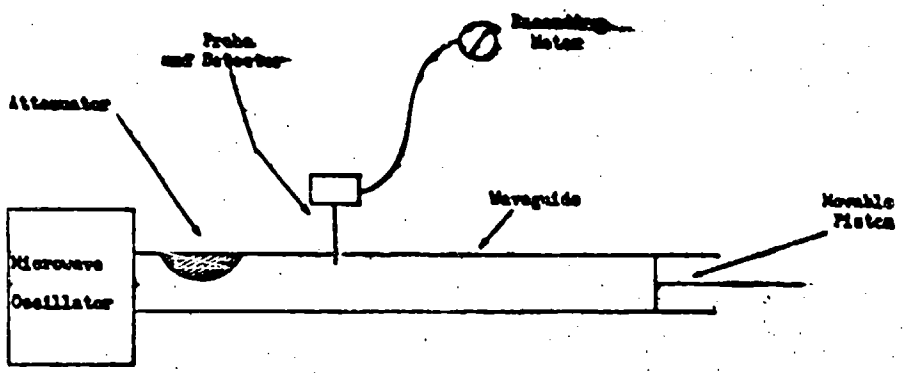


Figure 1

that only one mode, the so-called dominant mode, can exist in the guide. For a waveguide of circular cross section of radius r, the condition for the existence of only the dominant mode is given by the expression.

$$\lambda/3.412 \leq r \leq \lambda/2.613$$

where $\lambda$ is the wavelength of a plane electromagnetic wave in an unbounded volume of the dielectric in the waveguide. The wavelength, $\lambda$, can be related to the operating frequency, f, of the oscillator by the expression

$$\lambda = \frac{c_o}{f} \frac{1}{(\epsilon_1 \mu_1)^{1/2}}$$

where $C_o$ is the velocity of light in free space, and $\epsilon_1$ and $\mu_1$ are the dielectric constant and magnetic permeability, respectively, of the medium in the waveguide. When the dimensions of the guide and the operating frequency have been chosen, the guide wavelength, $\lambda g$, can be computed from the expression

$$\lambda_g = \frac{\lambda}{\left[1-(\lambda/\lambda_c)^2\right]^{1/2}}$$

where the critical wavelength, $\lambda_c$, for the dominant mode in a guide of circular cross section is given by

$\lambda_c = 3.412\ r$

This simplified version can now be compared with the practical circuit shown in Fig. 2. The piston is replaced by the detonation front and the probe by a waveguide crystal detector mount. A

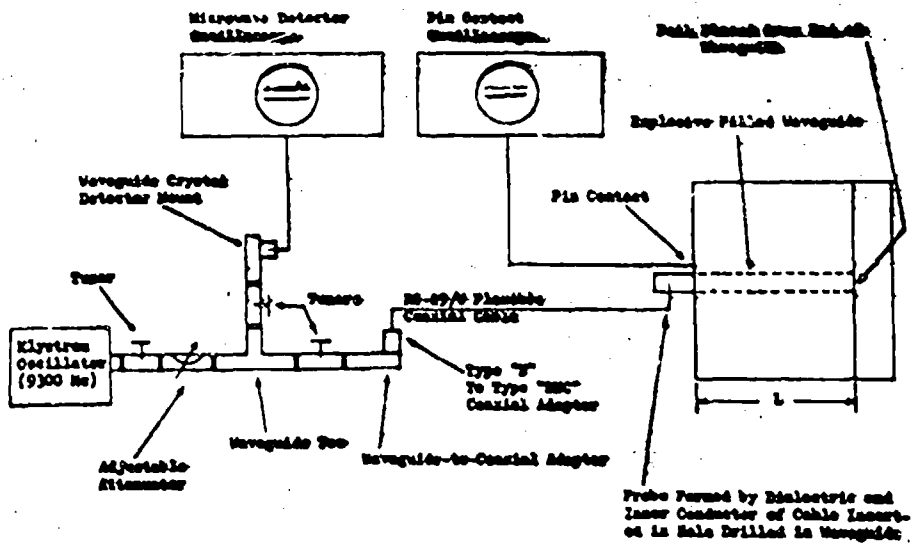


Figure 2

short length of flexible coaxial cable couples the crystal detector to an explosive-filled waveguide which is inserted in the explosive to be studied. This cable permits isolation of the electronic gear from the explosive system, thus minimizing the equipment expenditure per shot. As in the simple model, the signal at the detector should be periodic with a movement of $\lambda_g/2$ of the detonation front, where $\lambda_g$ is the guide wavelength in the explosive-filled guide.

Some of the functional details of the circuit shown in Fig. 2 should be explained. The klystron operates at a frequency of 9300 megacycles per second. The tuner adjacent to the klystron is adjusted for maximum power output from the klystron, and the attenuator isolates the klystron from load changes. The detector, together with its tuner is mounted on the side arm of either an E- or H-plane tee. Both the detector and the waveguide-to-coaxial adaptor are matched to the waveguide before assembly in order to obtain a larger and more reproducible signal amplitude. Since the impedance of the crystal mount may depend upon its power level and external load, it should be matched at its maximum expected power level and normal operating load impedance. The waveguide-to-coaxial adaptor is matched with a long length of the relatively lossy cable, which simulates an infinite length of line attached to the adaptor. The cable is then cut to the desired length (up to 6' lengths have been used and longer lengths may be used if the attenuation of the cable is not objectionable) and the braid at the cut end is folded back over the outer covering of the cable, exposing a short length of dielectric and inner conductor. This short length

of dielectric and inner conductor forms a probe, which is inserted in the explosive-filled waveguide.

The explosive-filled waveguide is prepared by machining a stick of explosive, wrapping it with a thin layer of aluminum foil, and drilling a hole near one end for insertion of the probe. The diameter of the stick is chosen to allow propagation of only the dominant, or $TE_{11}$ mode. For example, at an operating frequency of 9300 megacycles, the stick diameter for Composition B is approximately one-half inch. For this size stick of Composition B at an operating frequency of 9300 megacycles, $\lambda g$ is approximately 3 centimeters. The stick is made longer than the explosive to be tested to permit insertion of the probe. The hole for the probe is drilled perpendicular to the axis of the stick. This orientation of the probe permits efficient excitation of the dominant mode. The depth of the hole and the distance of the center of the hole from one end of the stick is approximately $\lambda g/4$. The stick is wrapped with two layers of 0.5 mil aluminum foil. This wall thickness is sufficient to confine the electromagnetic fields to the interior of the waveguide but does not measurably affect the detonation in the explosive. Experiments using the smear camera technique have shown that wall thickness of 15 mils could be tolerated.

If air spaces exist between the explosive stick and the foil, jetting will occur with resultant distortion of the recorded signal. These air spaces can be eliminated by coating the stick with a thin layer of silicone grease prior to wrapping.

The explosive-filled waveguide is inserted in a hole drilled in the piece of explosive under test. Silicone grease is used again to exclude air spaces between the waveguide and the surrounding explosive. Both the stick and the piece of explosive being tested should be of the same composition and density.

Noise originating in the explosive or in the mechanism used to detonate the explosive[1] can obscure the signal trace received from the detector. It was found that this noise could be effectively eliminated by avoiding any electrical connections between the detonated explosive and the waveguide or external circuits. In particular, when the probe is inserted in the waveguide, the braid of the coaxial cable is separated by a layer of cement from the foil wrapped around the explosive-filled waveguide.

A circular disk of aluminum, 0.2 mils thick, placed over the end of the waveguide shields the microwave circuit from events occuring prior to the time when the detonation reaches the waveguide. The start of the signal trace records the time when the detonation front has reached the waveguide. The arrival of the detonation front at the end of the explosive being tested is detected by a pin contact time. This pin time is necessary since the record does not end until the detonation front arrives at the probe. The microwave detector signal and the pin signal are recorded on separate oscilloscopes. The two displays are correlated in time by a common reference pulse placed on both.

Representative signal traces are shown in Fig. 3. Each signal trace is accompanied by a time calibration trace. These traces, together with a knowledge of the length of the explosive being tested, provide sufficient information to determine the times when the detona-

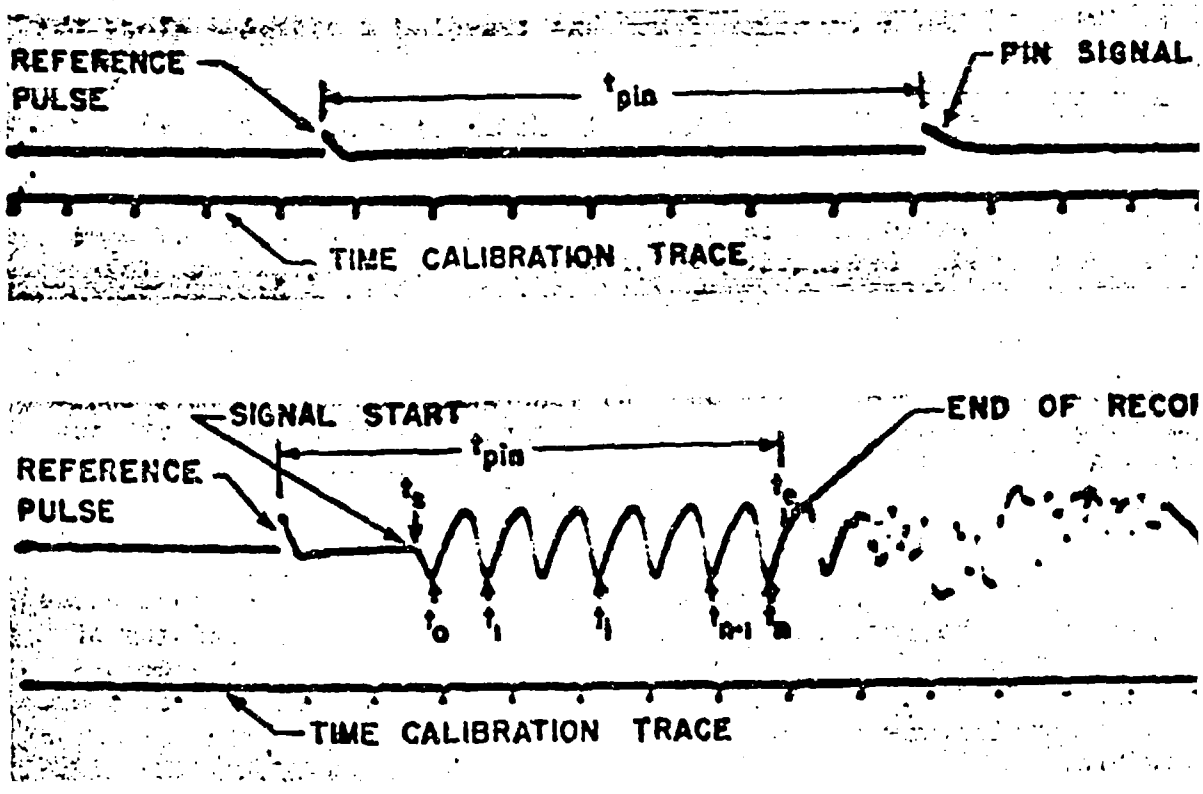


Figure 3.

tion front has reached a sequence of positions in the explosive. Since the detonation front has moved a distance of $\lambda_g/2$ during the time interval between common reference points on any two adjacent cycles of the record, the half-guide wavelength can be found by dividing the length of the explosive by the total number of cycles in the record. Usually, greater accuracy can be achieved by reading the peaks or troughs, of the record, rather than an arbitrary reference point each cycle. The incomplete end intervals of the record must be assigned fractions of a cycle. Unless there is additional information on the detonation rate of the explosive, it is assumed that the end intervals have the same periods as their adjacent intervals. With this assumption, the half-guide wavelength for the record shown in Fig. 3 is given by

$$\lambda_g/2 = L \Big/ \left[ \frac{t_o - t_s}{t_1 - t_o} + n + \frac{t_e - t_n}{t_n - t_{n-1}} \right]$$

where L is the length of the explosive being studied, $t_s$ is the time when the microwave signal starts, $t_e$ is the pin contact time, n is number of complete cycles, and $t_o$, $t_1$, ... $t_{n-1}$, $t_n$ are the times of the peaks (or troughs), $t_o$ being the time for the first peak and $t_n$ the time for the last peak before the pin contact time. At time

$t = \tau_i$ (Fig. 3) the detonation front has traveled a distance along the waveguide given by

$$d = \left(\frac{t_o - t_x}{t_1 - t_o}\right) \frac{\lambda_g}{2} + 2 \frac{\lambda_g}{2} \quad (i = 0, 1, 2 \ldots n).$$

Therefore the position of the detonation front as a function of time can be determined. Detonation velocities can be obtained from this information.

It should be emphasized that the microwave techniques should not be used where the pin technique may be employed. The accuracy of the pin technique is 0.1%,(1) and the accuracy of the microwave technique is of the order of one or two percent. The microwave technique is more complicated because of the greater difficulty in fabricating the explosive charge, adjusting the measuring equipment, and interpreting the signal records. In addition, the microwave technique is limited to those explosives which have good dielectric properties. When applicable, the microwave technique provides an almost continuous measurement of the position of the detonation front as a function of time without measurably affecting the detonations. Since the cross-sectional area of the waveguide is small, signal distortion due to side blasts and variations in the waveform of the detonation front is almost negligible.

In the preceding paragraphs, a method involving microwaves has been described for observing the velocity of a detonation wave in the interior of an explosive charge. Circuits for generating and detecting the microwaves together with the display and reduction of the resultant signal have been discussed. The described system is presently being used at the Los Alamos Scientific Laboratory on a routine basis.

---

(1) "Techniques for the Measurement of Detonation Velocity", A. W. Campbell, et. al. (This conference).

# MEASUREMENT OF DETONATION TEMPERATURES

F. C. Gibson, M. Bowser, C. R. Summers,
F. Scott, J. C. Cooper, and C. M. Mason
U. S. Bureau of Mines
Pittsburgh, Pennsylvania

## Introduction

The temperature in the detonation front is, at the present time, one of the parameters most urgently needed in the field of solid explosives. Recent surveys (1, 2) show that although the measurement of this parameter has been a matter of active interest for some time, the experimental determination of definitive temperatures has not been very successful. At the last conference, studies (3, 4) were reported on the luminosity emitted from the exterior of charges detonated in air, in water, and in a partial vacuum. The luminosity records obtained at that time were difficult to interpret owing to a multiplicity of peaks, and it now appears that true amplitudes were not observed due to the integrating effect of the field slit. The method described in the present paper, although introducing a foreign material into the explosive powder, provides an interval of time conducive to sampling by one-megacycle circuitry and views the detonation radiation at the core of the charge in solid explosives. It is hoped that temperature data obtained by this method will be of sufficient accuracy to permit its use in developing a single suitable equation of state.

## Theory

The two-color method currently employed is based on Wien's radiation equation which assumes that the radiation is black or grey body. From the equation

$$E_\lambda = c_1 \lambda^{-5} e^{-c_2/\lambda T}$$

it follows that the curve obtained by plotting the logarithm of the ratio of the radiation densities for two wavelengths, $\lambda_1$ and $\lambda_2$, against the reciprocal of the absolute temperature will be a straight line. The slope of the line depends on the frequencies of

the band pass filters, and its intercept is determined by the relative sensitivities of the electrical equipment which make up each channel.

To determine the nature of the available radiation, spectrograms of detonating tetryl were taken by superimposing the radiation from the axial cavities of twelve charges. It was hoped that radiation from the tetryl charge could be compared with the radiation from the explosive pellets used in the temperature work. However, as the radiation from the former required twelve shots to give a weak spectrum, it has not proved practical to obtain spectra from the charges used for temperature determination. A full investigation of this will be made as time permits. The spectrum obtained is a continuum extending through and well above and below the region of the spectral pass bands of the two interference filters employed.

## Method

The novel feature of this method for sampling the radiation which is to be evaluated for quality is the use of a transparent plastic rod imbedded axially in the explosive charge during fabrication of the pellet. This rod (methyl methacrylate) protrudes from the end of the cylinder opposite to the initiated end. In this way, the radiation at the core of the explosive is transmitted along the plastic rod by internal reflection to the aperture of the sensing equipment. The charge confines itself, and the explosion pressures essential to high-order complete detonations are maintained at the zone of measurement as the plastic is completely surrounded by high explosive. The rod is inserted into the charge for a distance of about 2 cm. providing a detonation front transit time of 3 or more microseconds, depending on the velocity of detonation. This interval, which is relatively long with respect to the response times of electronic equipment, permits the temperature to be evaluated after equilibrium conditions have been attained in the system. In addition, refinement of the system may give temperature gradients along the rod due to non-homogeneity in the pellet density, a result of wall friction effects of both the fabricating die and the plastic rod during pressing. A cross sectional view of the charge is shown in figure 1. The end of the rod is pointed to allow powder flow in pressing, thus preventing the pile-up of powder on the end of the rod. Such pile-up would result in undesirable density gradients and rod fracture.

Typical luminosity-time records for TNT are shown in figure 2. Figure 2(a) is the single-channel trace of a TNT charge fired in ambient air. The waveform is analyzed for temperature at points, (a) through (e), each point, except (c), being a maximum or minimum so that the amplitudes of the two channels can be compared accurately at that instant. However, this method makes no allowance for response times of the equipment which may impair the accuracy. Therefore in subsequent analyses, another method was used which is

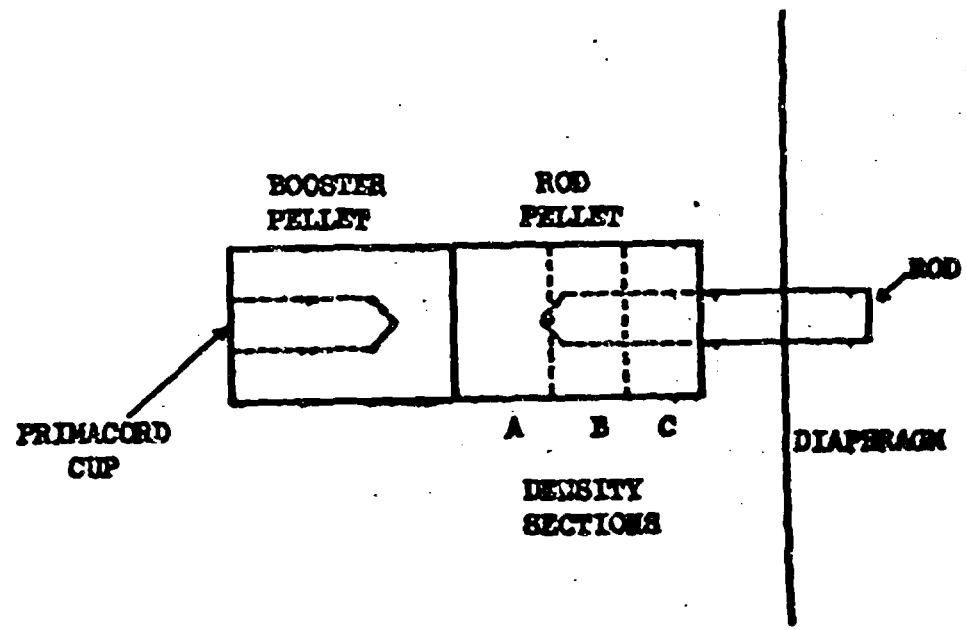


Fig. 1.--Drawing of a test charge (scale size). Density determinations were made by dissection of rod pellets into segments A, B, and C. Diaphragm is to exclude charge-side radiation from the system during period of passage of the detonation along the rod within the charge.



Unclassified

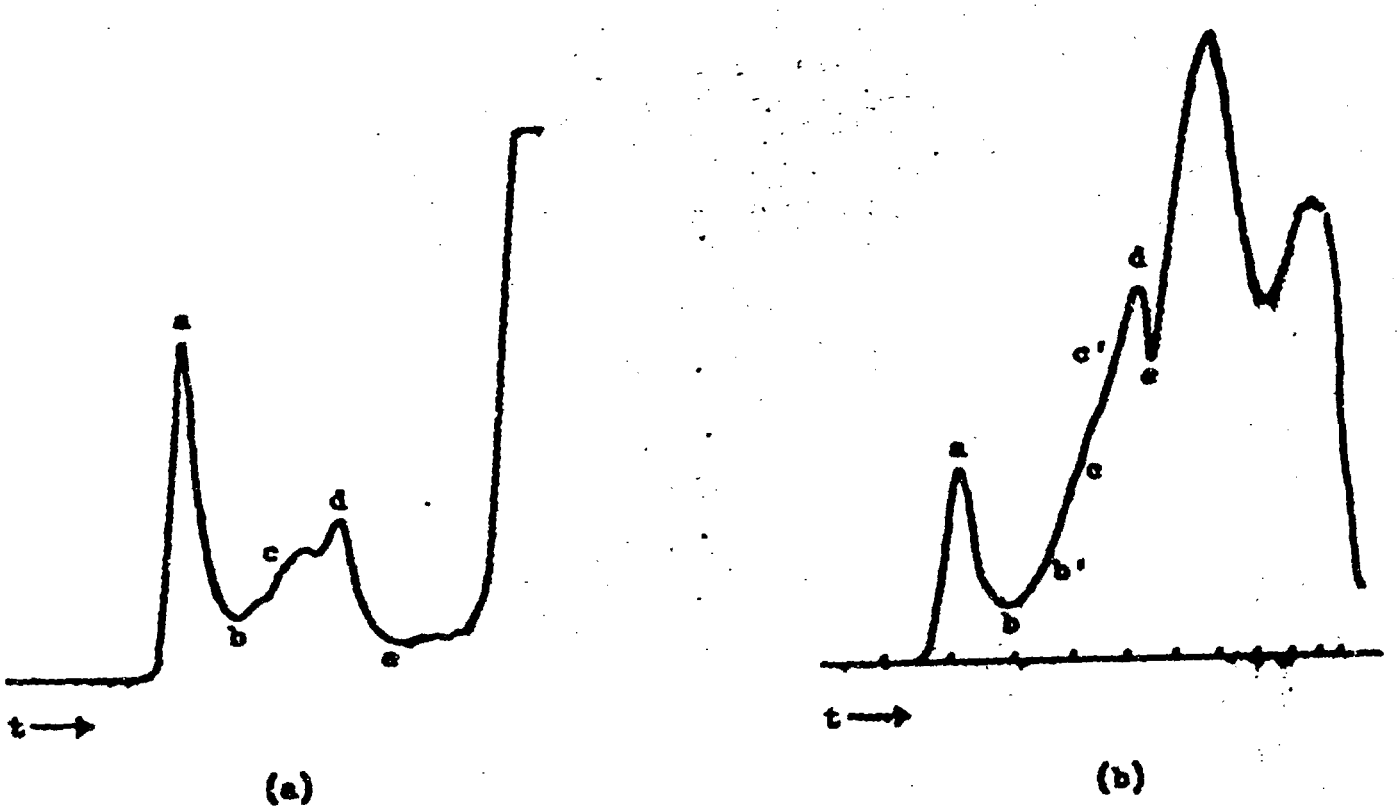


Fig. 2.--(a) Time-luminosity curve for TNT fired in ambient air.
(b) Time-luminosity curve for propane impregnated TNT fired in ambient propane. The time scale is in microseconds.

illustrated by the waveform of a propane-impregnated TNT charge (figure 2(b)) fired in ambient propane. In this method, the radiation is sampled after an equilibrium condition has been attained, taking points b', c, and c', at finite times after the first appearance of luminosity from the rod. The points b' and c' were chosen so as to represent the temperatures at the instant when the detonation wave was in the density segments shown in the charge drawing in figure 1. The initial pip, a, may be due to the increased area effect at the rod end as well as to additional luminosity from the shock wave upon impact on the end of the rod. It is believed that the phenomena of opacity due to shock pressure noted by other researchers in plastics of this type may occur here. However this cannot be verified unless charges with detonation velocities lower than the shock velocity in the plastic are tested. The opaque diaphragm shown in figure 1 prevents extraneous radiation from entering the system until after the detonation has passed the charge end and traveled across the gap between it and the baffle diaphragm. Of general interest may be the fact that in this system there is about ten times more radiation from the rod than from a 1.5 kv carbon arc lamp, and that the air-shock radiation amplitude is about ten times as great as that from the rod.

Studies of the pellets were made with the image-converter camera described elsewhere (5), modified to provide streak photography. These tests were conducted to establish the radiation luminosity dependence on the presence of air, propane, and the plastic rod. In air, streak photographs of charges from which the rods had been withdrawn showed strong shock reinforcement due to shock collision within the axial cavity. The same charge fired in ambient propane showed only radiation at the cavity bottom and along the explosive-cavity interface. The luminous zone in this case can be visualized as a doughnut of light traveling at detonation velocity down the cavity wall. Exposures also were made with the rod in place and fired in ambient propane after the charges had been carefully vacuum-impregnated with propane. Here the light was greatly reduced when the detonation reached the charge end, indicating that most of the radiation was not due to shock action on or in the plastic rod but to the explosive material, intergranular voids, or the small space between the rod and the explosive. The actual source of this radiation is still unknown; however the agreement between the experimental results and theory strongly suggests that the radiation is from the detonation zone.

## Apparatus

A diagram of the apparatus is given in figure 3. The explosive charge is positioned as shown in the drawing and during calibration the standard source is placed in the same position as the charge. Accurate positioning is achieved by projecting an image of the hole in the aperture plate through the window into the bombproof. The size of the hole in the plate is such that when it

is enlarged by the field lens it appears slightly larger than the end of the plastic rod (about 3/8 inches). The motor-driven disc acts as a light chopper and is used during calibration to provide a.c. signals from a steady radiation source. A slit on the periphery has a width of about 0.020 inch and scans the aperture hole in about fifty microseconds. The pulse width on the calibration trace can be adjusted by varying either the slit width (a step slit is available) and/or the motor speed (the diameter of the disc is fixed at 16 inches). A lamp-photomultiplier combination, the direct output of which can be switched into the trigger generator or into the oscillographs, allows either single or repetitive sweep operation and is controllable in time by displacing the lamp-phototube assembly with respect to a circular aperture in the disc that has a fixed relationship to the slit. The trigger generator is a simple thyratron circuit which allows single-sweep operation of the oscillograph from either the ionic conductivity probes in the charge or the disc as mentioned. A secondary lens forms a defocused image of the end of the rod on the photomultipliers which are 1-1/2" end-on types so that the entire photocathode surface is employed. At the cross-over point an adjustable slit is used for vernier control of the radiation entering the phototubes. Coarse attenuation is provided by the use of grid attenuators placed to the rear of the field lens and adjacent to it. A half-silvered mirror separates the light into two beams. A transmission filter of the interference type is located in front of each phototube so that the only radiation entering the tube housing is through the filter. The band pass of each is 70 to 100 angstroms at half amplitude.

The electrical circuitry comprises a video amplifier-cathode follower combination and a high-speed oscillograph for each channel yielding a signal proportional to the energy density. Operating levels of the electrical equipment are adjusted by varying the photomultiplier dynode voltages to provide optimum signal-to-noise ratio, and a degree of balance that allows a signal ratio of unity to occur near 4000°K, as the desired temperature for calibration and explosive used lies between 2000°K and 6000°K. As previously mentioned, the light level is adjusted so as not to exceed a maximum amplitude on either oscillograph. This avoids nonlinearity difficulties that otherwise would be encountered since the utilized radiation varies over a factor of several hundred.

The film records (photographic negatives for the explosives tests; Polaroid-Land for the longer sweep calibration traces) are analyzed by means of an optical comparator with the amplitude-time selection as previously described. The time base is furnished by a crystal-controlled oscillator operating at a frequency of 1,2 or 2.5 megacycles.

## Results

Most of the work to date has been devoted to recognition

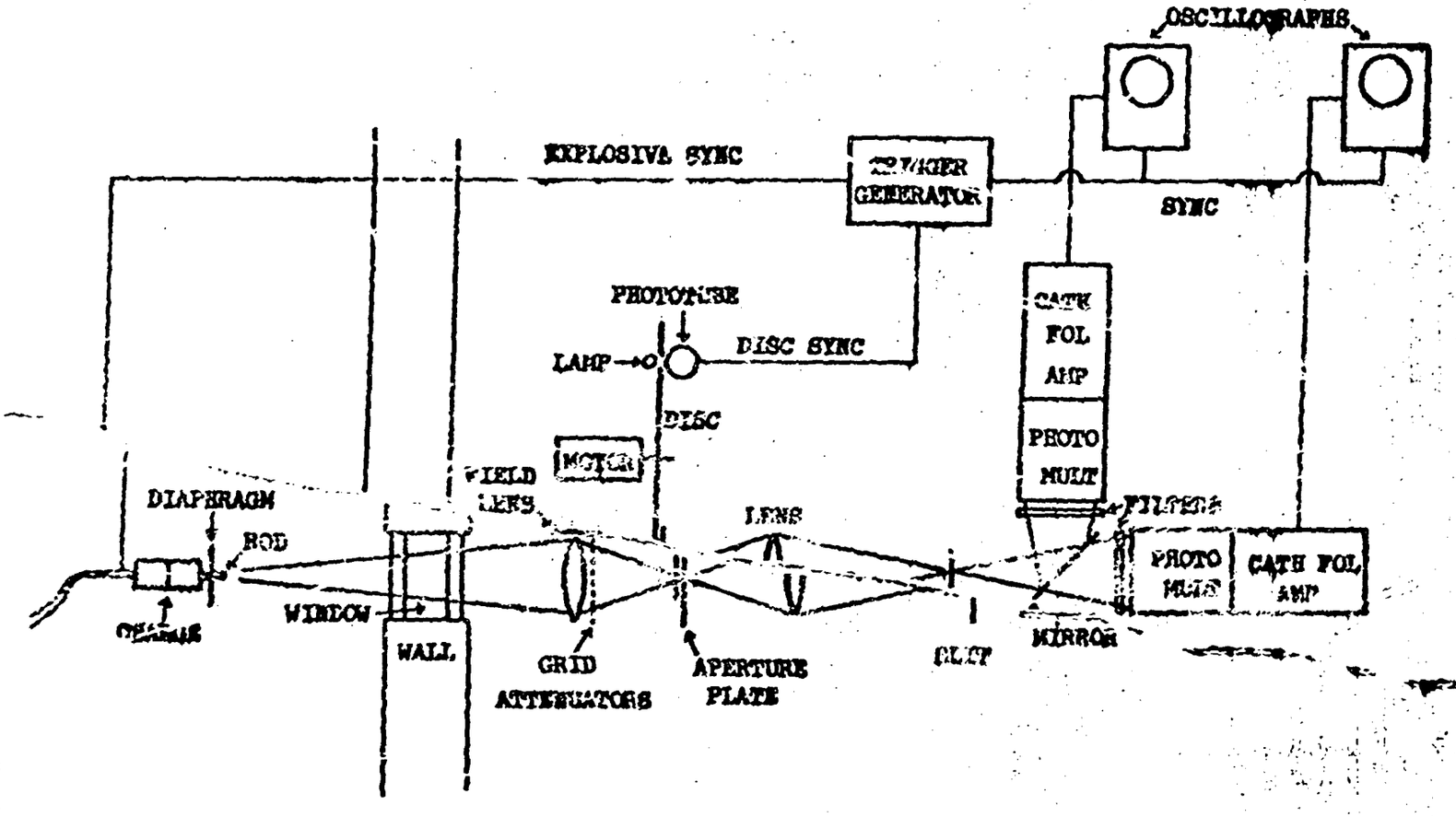


Fig. 3.--Diagram of the apparatus for detonation temperature determination.

Unclassified

Unclassified
Gibson

of the idiosyncrasies and deficiencies of the system. Preliminary testing of the equipment with rod pellets has been made for tetryl and TNT in both air and propane. The data are considered preliminary, pending complete calibration of the system. Tentative detonation temperature data for tetryl and TNT charges fired in ambient air are given in table 1. The temperature of the TNT is higher because of the influence of the shock temperatures in the air both around the rod and in the intergranular voids. In the tetryl, which has a higher density, air-shock luminosities are minimized. This effect is substantiated when the data are compared with that given in table 2 for similar charges which had been propane-impregnated and fired in a propane surround. Densities of representative pellets of each explosive were determined on three segments (see figure 1). The temperature at b' is considered to be representative of the B segment and being nearer the center of the charge is probably the desirable zone for temperature analysis. The propane effectively reduced the air-shock components in the temperature obtained at point e after the detonation had passed out of the charge. Temperatures of the air shock obtained at point c and given in table 1 may be considered reasonably accurate if detonation spectrograms recently obtained, indicating a continuum for the composite charge radiation, are correct.

These results appear of a reasonable order of magnitude when compared with the theoretical detonation temperatures shown in figure 4 (6, 7, and 8).

Further refinements are being made and it is anticipated that additional data will be available which will support or invalidate these preliminary data.

## ACKNOWLEDGEMENTS

This work was supported by the Office of Ordnance Research, Department of the Army, Army Project 599-01-004, Ordnance Project TB2-0001.

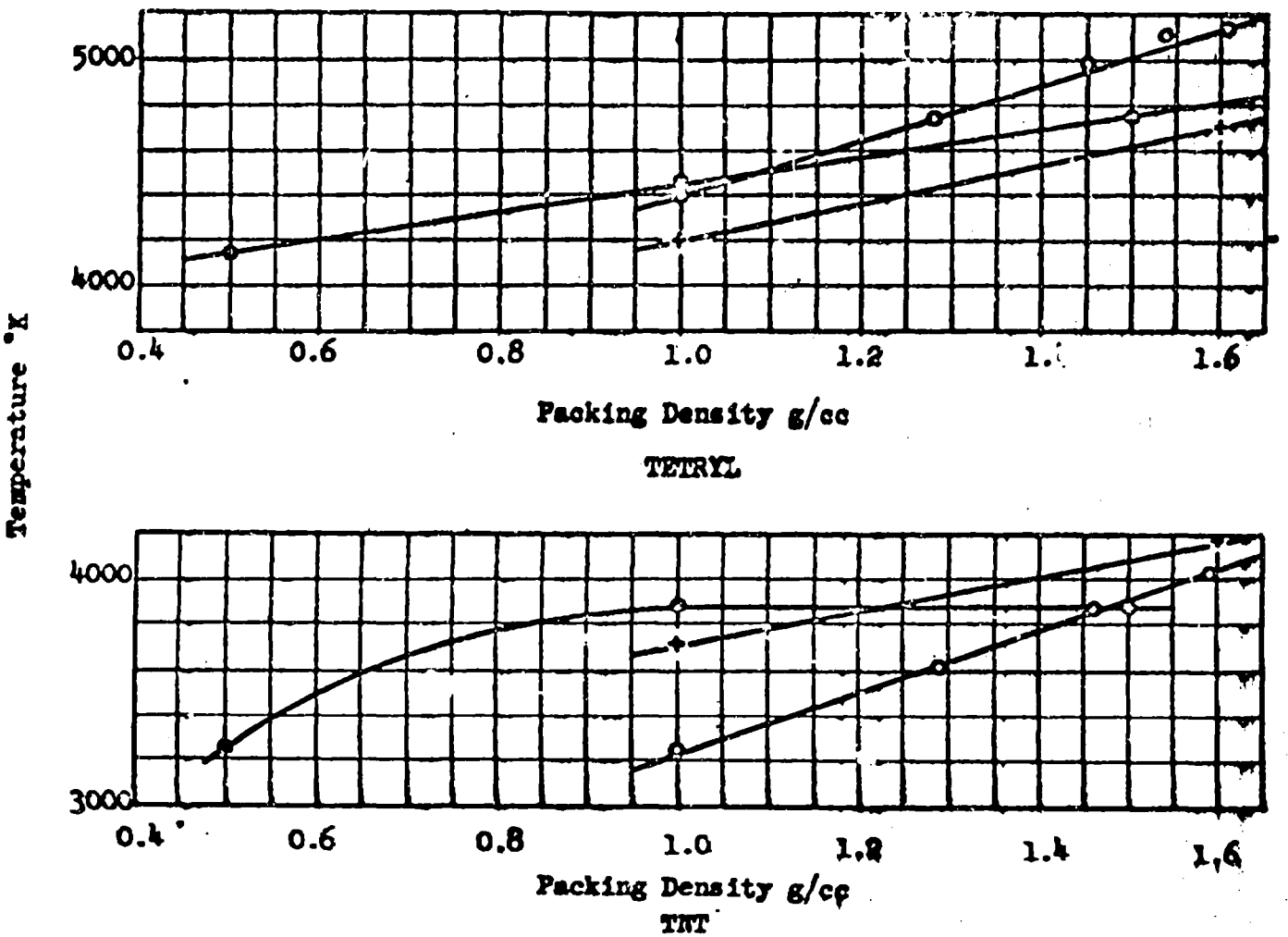


Fig. 4.--Theoretical detonation temperatures of TNT and Tetryl

Table 1.--Tentative data on detonation temperatures for two explosives fired in ambient air

| Explosive | Representative density g/cm$^3$ (Average) | Temperature-time profile K° * | | | | |
|---|---|---|---|---|---|---|
| | | a | b | c | d | e |
| Tetryl | 1.64 | - | 4700 | - | 5200 | 9300 |
| TNT | 1.44 | 6300 | 5300 | - | 5700 | 14000 |

* This profile is measured at various points along the time-luminosity curve shown in figure 2(a).

Table 2.--Tentative data on detonation temperatures for two propane-impregnated explosives fired in ambient propane

| Explosive | Representative density segment g/cm$^3$ | | | Temperature-time profile K° * | | | | | | |
|---|---|---|---|---|---|---|---|---|---|---|
| | A | B | C | a | b | b' | c | c' | d | e |
| Tetryl | 1.61 | 1.68 | 1.63 | 4800 | 5100 | 5000 | 5600 | 5300 | 5400 | 4200 |
| TNT | 1.39 | 1.46 | 1.47 | 5400 | 4400 | 3900 | 4500 | 4300 | 3800 | 3800 |

* This profile is measured at various points along the time-luminosity curve shown in figure 2(b) with points b', c, and c' taken at finite times with respect to the first appearance of luminosity in the rod.

## LIST OF REFERENCES

(1) Technical Memorandum, Institute for the Study of Rate Processes, University of Utah, "The Measurement of Temperature in Explosives", August 31, 1953, Contract Number N7onr-45107, Project Number 357 239 (Salt Lake City).

(2) A Study of Techniques for the Measurement of Detonation Spectra and Temperatures by J. H. Hett and J. B. Gilstein. Final Report from Research Division, New York University, May 14, 1953, Contract DA-30-069-ORD-945, Department of the Army (Restricted).

(3) Boyer, R. L., "Determination of Detonation Temperatures in High Explosives", Phy. Rev., 74, 1221 (1948).

(4) U. S. Bureau of Mines Progress Reports, "The Physics and Chemistry of Explosive Phenomena", January 1947 to June 30, 1950, Contract NAonr 29-48, NR 053 047.

(5) F. C. Gibson, M. L. Bowser, C. W. Ramsley, and F. H. Scott, "Image-Converter Camera for Studies of Explosive Phenomena", Review of Scientific Instruments, 25, No. 2, 173-176, February 1954.

(6) P. Caldirola, J. Chem. Phys. 14, 738 (1946). See also S. M. Brinkley, Jr., ibid. 15, 113 (1947).

(7) M. A. Cook, ibid. 15, 518 (1947). See also S. Patterson, ibid. 16, 159 (1948).

(8) S. Patterson, Research 1, 221 (1948).

# A NEW CINE MICROSCOPE AND ITS APPLICATION TO DETONATION PHENOMENA

J.S. Courtney-Pratt, B.E., Ph.D.,
Research Laboratory for the Physics & Chemistry of Surfaces,
Department of Physical Chemistry
University of Cambridge

Abstract

A Microscope has been built using the principle of image dissection that has been applied recently to the optical systems of cameras, so that series of photographs can be recorded at high speed, without complex equipment. (J.S. Courtney-Pratt, J.Phot.Sci.,1953,1,21) A plate embossed with a large number of small lenses is used to dissect the picture into small elements. These are all recorded simultaneously on a plate, but each element is separated from its neighbours by a distance that is large compared with the size of the element. Many successive pictures may be similarly dissected and recorded on the same plate interlaced with the others. The displacement of successive images with respect to the plate need only be as great as the width of a single picture element. In some cameras the displacement was produced by altering the direction in which light fell on to the lenticular plate. In the new microscope the displacement is produced by traversing the photographic plate. The phenomenon may be studied in transmission or reflection and very simple light sources are adequate.

The microscope has been used to take series of 200 pictures at 25,000 per second at magnifications of several hundred X. Higher magnifications are possible but at reduced speeds. Any smaller magnification can be achieved at the same or slower speeds, by simple substitution of longer focal length objectives, and the apparatus may even be used for high speed photography of distant objects. It has also been used to take series of shadowgraphs.

The quality of the pictures is limited by the number of lenslets across the lenticular plate - at present 320 lines across the field - but there is no reason why larger plates might not be used with corresponding improvement of picture quality up to the point at which the resolution is limited by the objective.

The microscope can be used to unscramble the composite record for slow motion viewing and for conventional printing of individual pictures. Separate unscrambling apparatus can easily be made.

The microscope is being used to study the earliest stages of detonation phenomena.

The speed, the range of magnifications, and the simplicity of the apparatus make it suitable for the study of many physical problems.

Introduction In the Research Laboratory for the Physics and Chemistry of Surfaces we have been studying fast reactions (1), and have developed a number of new photographic techniques (2-10). One branch of this work has been a study of the application of the principle of image dissection to cameras (6-9). This makes it possible to record a series of photographs at high speed without complex equipment.

The basic optical layout is shown in Figure 1. The main lens L forms a real image I of the object O on the front surface of a plate embossed with a large number of small lenslets. Consider the rays that pass through a small aperture at the centre of the main lens. These rays fall on the lenticular plate and each of its lenslets focusses the light that falls on it to a small element on its principal axis. The photographic emulsion is placed in the focal plane of the lenticular plate, and the picture recorded by the emulsion is thus made up of a large number of small dots. In practice this is not a serious disadvantage. Most printed illustrations are similarly made up of dots. Provided the total number of dots is sufficiently large any given amount of information or picture quality can be reproduced. The large number of dots that go to make up a picture are all recorded simultaneously on the photographic plate, but each element is separated from its neighbours by a distance that is large compared with the size of the element. Many successive pictures may be similarly dissected and recorded on the same plate interlaced with the others. The displacement of successive images with respect to the plate need only be as great as the width of a single picture element. The displacement may be produced by altering the direction in which light falls on the lenticular plate or by traversing the photographic plate or the lenticular plate.

In one of the simplest sorts of camera, use was made of the first arrangement - altering the direction in which light falls on the lenticular plate. Consider again in Figure 1 the rays that pass through a small aperture near the outer edge of the main lens L. These rays form a real image I of the object O in the same place as before. Again each of the lenslets of the lenticular plate focusses the light that falls on it to a small element in the focal plane of the lenticular plate. However, these rays now fall obliquely on the lenslets so that the picture elements are no longer on the principal axes of the lenslets but are in a displaced peripheral position.

A convenient way of moving an aperture across a suitable lens is to cut the aperture in a disc mounted to run in the iris plane of a camera lens. As the disc rotates the aperture moves across. It is not necessary to restrict the movement of the aperture to a single line, and it is possible to move a series of apertures across different parts of the lens by disposing the apertures as a spiral array around

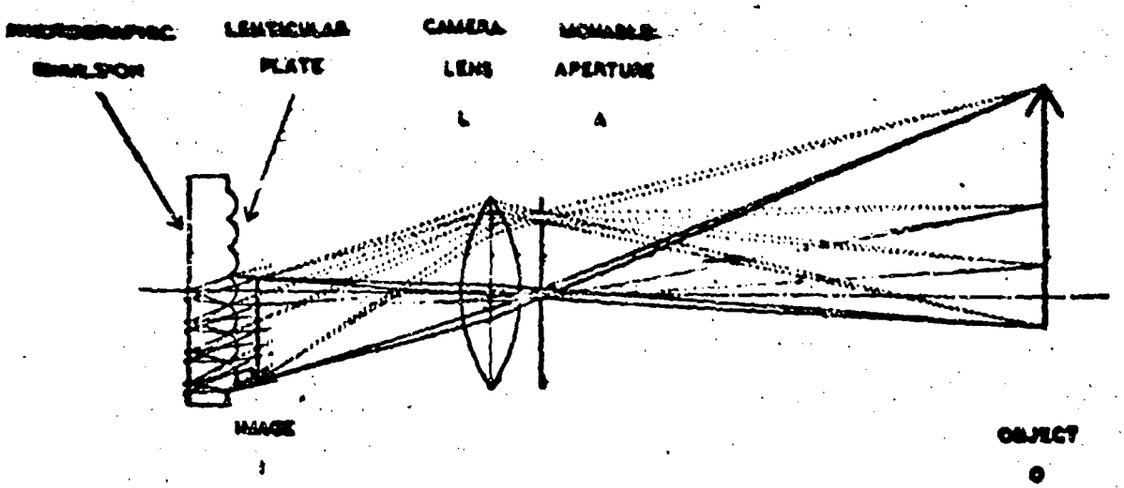


Figure 1: Diagram of the basic optical layout for image dissection multiple frame photography. The camera lens L forms a real image I of the object O on the lenticular plate which dissects the picture into a large number of elements each separated from its neighbours by distances large compared with its size, so that considerable numbers of independent pictures can be recorded on the one plate. The displacement of the picture elements for successive pictures can be achieved either by altering the direction in which light falls on the lenticular plate, and this can be achieved by movement of the aperture across the lens; or by traversing the lenticular plate or the photographic plate. Solid lines indicate the light paths when the aperture is in a central position. Dotted lines indicate light paths if the aperture is moved to a peripheral position.

the dia-

A number of cameras of this kind have been built in the P.C.S. Laboratory, and more recently commercial manufacture has been commenced by J. Langham Thompson Ltd.* The cameras are able to take series of 200 pictures at rates up to 125,000 per second. None of the mechanical tolerances of manufacture are at all stringent in these cameras. Their overall effective aperture is about F6.3 and their resolution, in different examples, 100, 200 or 300 lines across the field in both dimensions. They can be used equally well for self-luminous objects or for objects that are illuminated in reflection or in silhouette. They can be used conveniently for the photography of objects that are relatively distant, that is at magnifications from 1:∞ to approximately 1:1: and with some complexity the magnifications can be increased a little beyond this. At magnifications much greater than unity the distance between the lenticular plate and the camera lens is much larger than the focal length of the lens and it is impossible to obtain enough scanning distance across the aperture of the lens to make full use of the photographic emulsion.

The Cine-Microscope It seemed that some of the difficulties of working at high magnification might be overcome if the sequential recording were effected by traversing the photographic plate instead of by moving an aperture across the camera lens. The major disadvantage that had to be faced was that the mechanical tolerances of movement of the photographic plate and of subsequent replacement of the plate after development, and removement were very much more stringent than in the earlier cameras. Figure 2 is a diagram of the optical layout for a simple microscope. Just as before, the main lens forms a real image of the object on the lenticular plate. Each of the lenslets of the plate forms a point image of the aperture of the main lens. As the photographic plate is traversed the bright elements each trace out a line on the photographic emulsion. If the direction of movement of the photographic plate were parallel to either of the axes of the lenticular plate, then after a distance of movement equal to the pitch spacing of the lenslets of the plate the traces drawn out by adjacent elements would begin to overlap. If the direction of traverse is inclined at an angle of, say, 1 in 10 to either axis of the lenticular plate, then the traverse distance can be equal to 10 times the pitch spacing of the lenslets before there is any overlapping of traces. In practice, the size of the image element is less than 1/20 of the pitch spacing and this means that it is possible to record on the photographic plate, traces for each lenslet that could contain 200 separate points. If the illumination is intermittent, these will be discrete points. If the phenomenon being photographed is of slowly varying intensity then there will be a continuous line but of modulated density.

If the distance between the lenticular plate and the microscope objective is large, the geometrical size of each image element is automatically kept suitably small as the angle subtended at the

*J. Langham Thompson Ltd., Springland Laboratories, Bushey Heath, Herts.

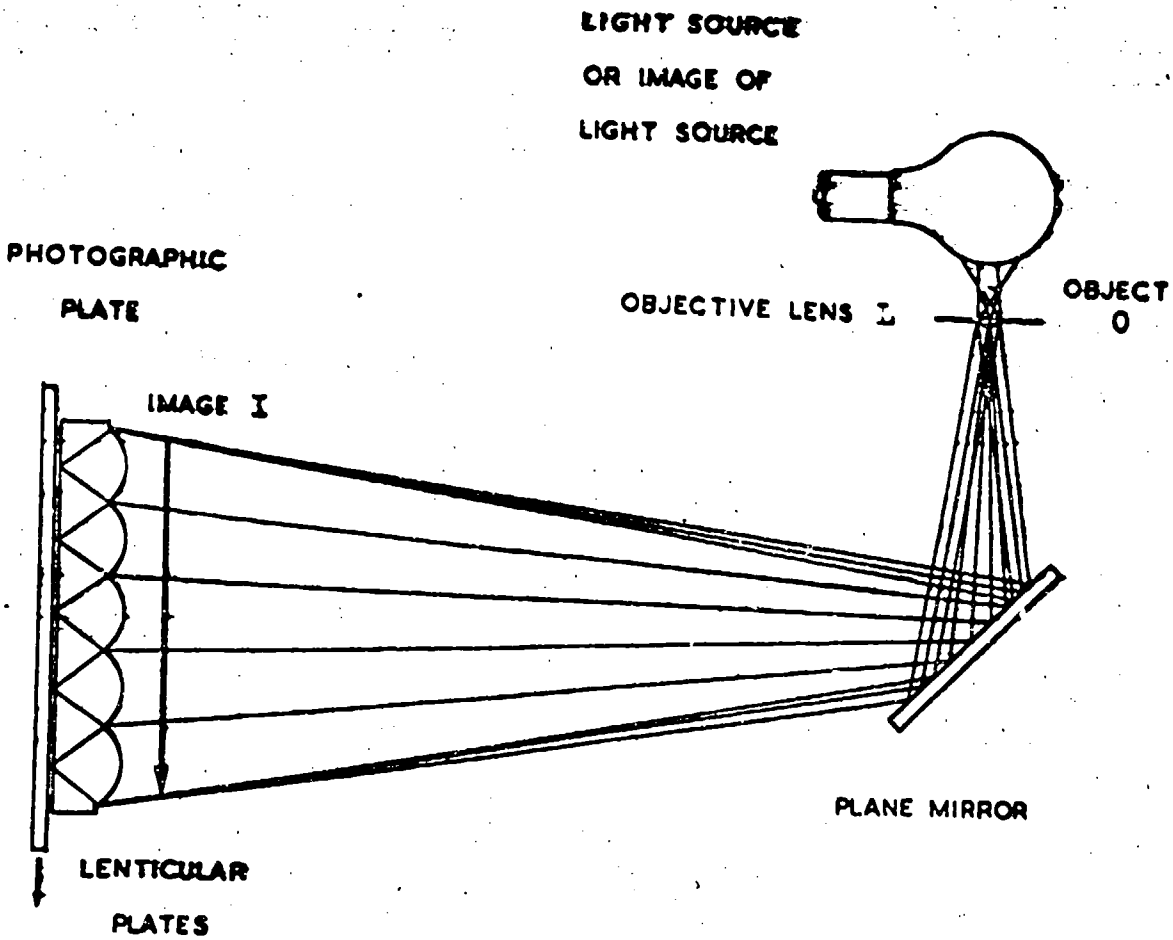


Figure 2: Diagram of the optical layout for multiple frame photography in a simple microscope. The lens L forms a real image I of the object O on the lenticular plate. Each lenslet of the lenticular plate forms an image on the photographic emulsion of the aperture of the microscope objective. Sequential recording is effected by traversing the photographic plate.

lenticular plate by the microscope objective aperture is very small. This means that the objective aperture need not be artificially restricted. This is of great importance as full use may then be made of all the light-gathering power that is available with modern microscope objectives.

Again, if the distance between the lenticular plate and the microscope objective is large it is possible to make use of a large lenticular plate and still keep within the field angle of conventional microscope objectives. The resolution of the picture depends on the number of lenslets across the plate and with the plates that we use there are 25 lenslets per cm. The larger the plate the higher can be the picture quality.

The number of pictures that can be recorded in a series depends on the size of the image elements. More strictly the number is proportional to $p^2/\epsilon^2$ where p is the pitch spacing of the lenslets and $\epsilon$ is the width of an image element. The success of the method is thus critically dependant on the qual' - of the lenticular plates, and I would like to express my thanks for the assistance and co-operation of M.R. Marilhat whose firm* has supplied all the lenticular plates that I have used. They were developed primarily for stereoscopic photography by the Bonnet process[11]. A thin sheet of plastic bonded to a sheet of glass is embossed by a die or matrix cut in fine-grained metal with an array of cylindrical lenses. If two such cylindrical lenticular plates are placed together with their embossed faces just touching, the combination acts as though the plate has been embossed with an array of spherical lenses[12]. A parallel beam of light is brought to a corresponding array of point foci and the resolution is surprisingly good. The width at half intensity of such point foci is less than p/100. In practice the size of the image element is increased above this because of the grain of the photographic emulsion, and the physical size of the objective aperture. Moreover, image elements to be clearly resolved must be further apart than their widths at half intensity as otherwise there is some interference and ghosting. However, with present apparatus an image width of p/20 can easily be achieved using process plates, and about twice this with fast emulsions.

Figure 3 is a photograph of a microscope made to try out these ideas. A number of pieces from a Vickers projection microscope‡ have been incorporated. It is possible to use any of the objectives, eye-pieces, illuminators, condensors and any of the attachments to the mechanical stage that are currently available. The box-like structure to which these pieces of the projection microscope are attached simply ensures that the microscope objective (and the projection eye-piece, if one is used) are a long distance from the lenticular plate.

A framework has been built from drawn steel angle to contain the lenticular plate, the photographic plate and the traverse mechanism. This frame is kinematically mounted on the end of the main frame of the

* "La Reliephographie" 152 Av. des Champs Elysees, Paris.
‡ Manufactured by Cooke, Troughton & Simms Ltd., Haxby Rd., York.

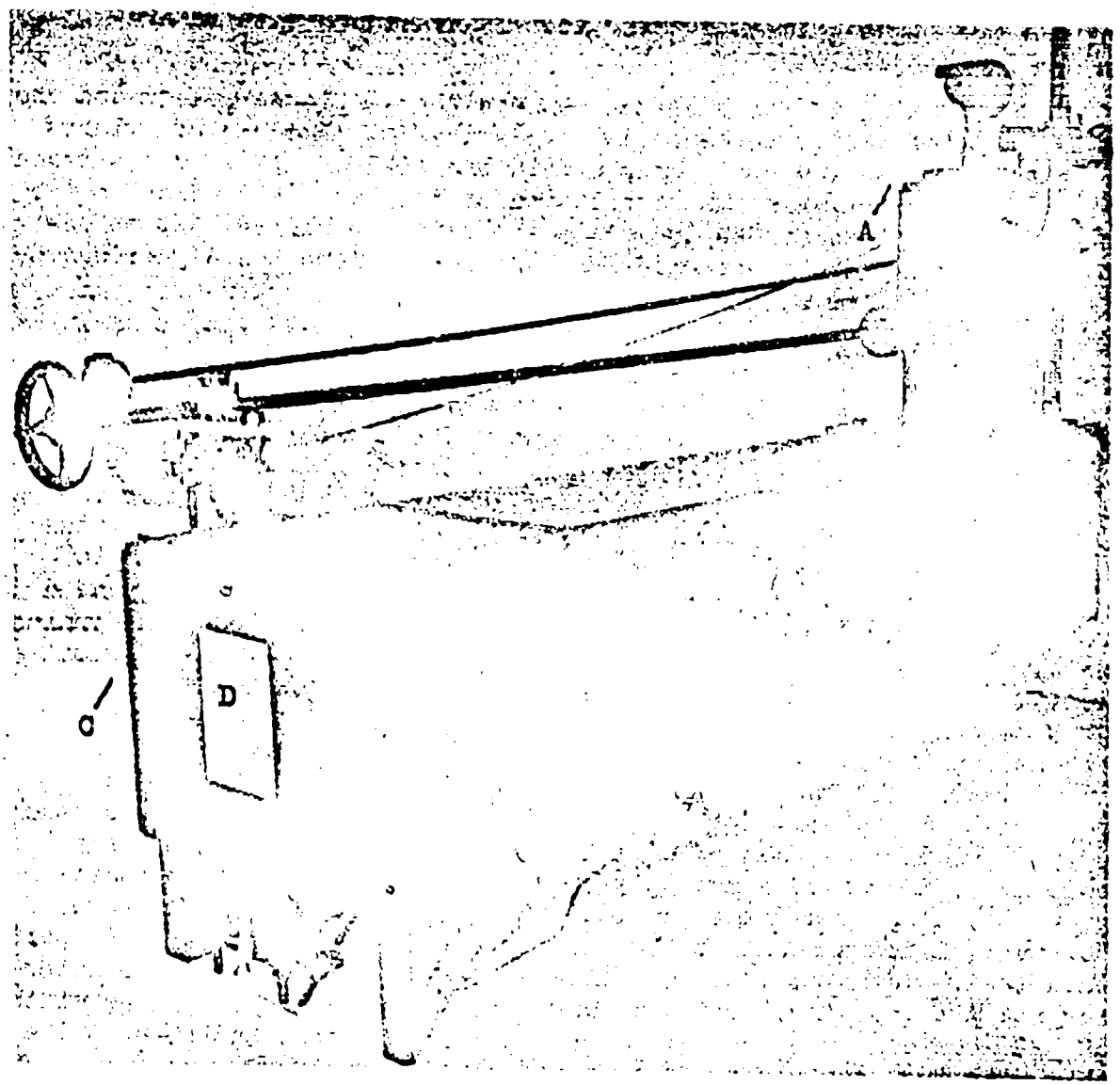


Figure 3: Photograph of the cine-microscope - A. Parts of a Vickers Projection Microscope. B. Main Frame. C. Detachable camera back holding lenticular plate, photographic plate, and traverse mechanism. D. Traversing frame to hold photographic plate. E. Detachable micrometer traverse for unscrambling the composite record.

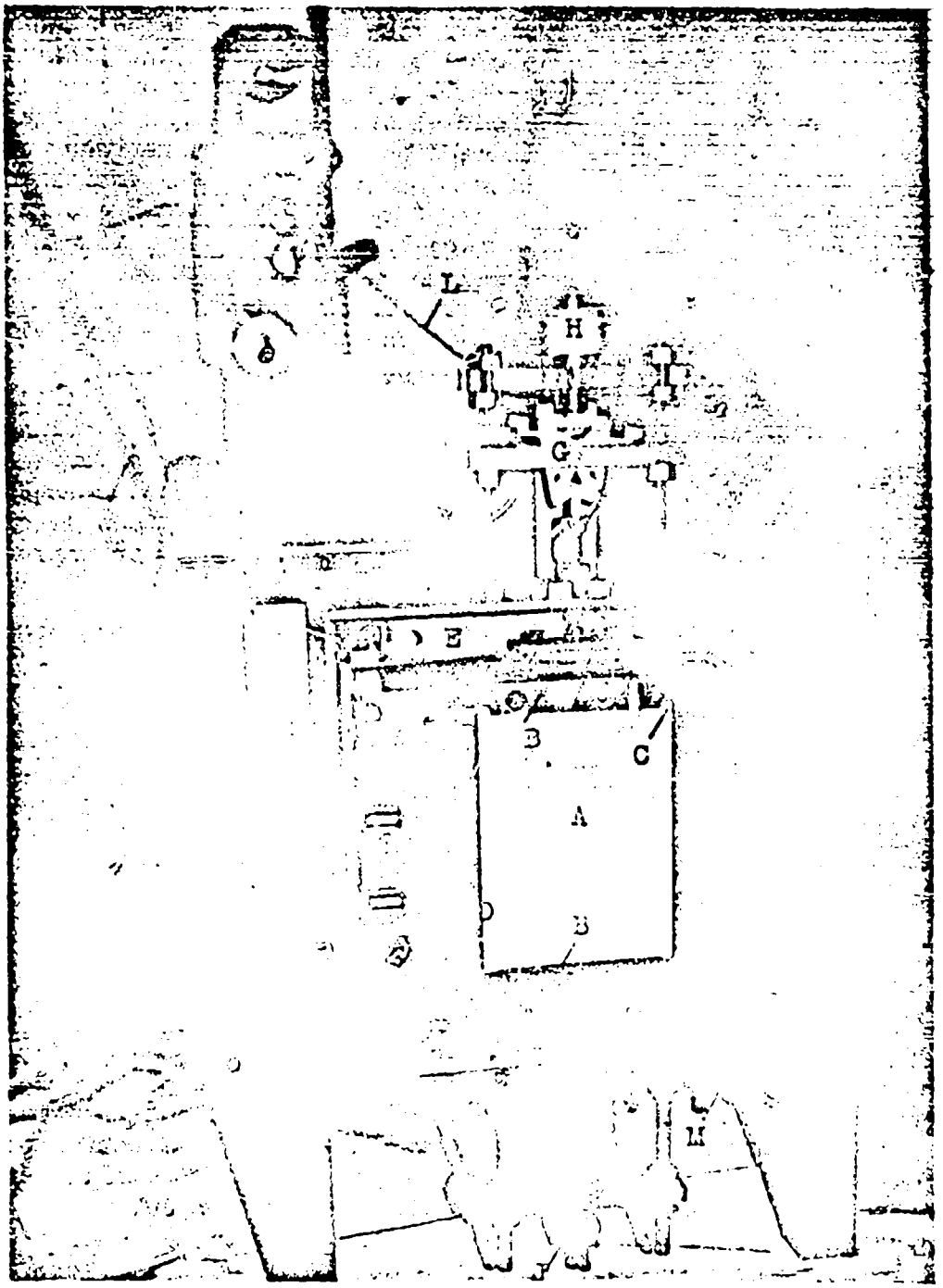


Figure 4: Enlarged view showing traverse mechanism of the cine-microscope. A-The photographic plate. B - clamps. C-Kinematic stops. D-traversing frame to hold plate. E-Elastic steel links. F-Stiff cantilever springs. G-Toggle catch mechanism. H-Release solenoid. J-Accelerator springs and buffers. K-Bell crank. L-Steel tape to operate capping shutter. M-Adjustable synchronising contacts. N- Timing Wheel, 200 teeth, 50 r.p.m. The photographic plate A in the plateholder D can move up and down. The lenticular plate, not visible in this figure, is immediately in front of the photographic plate, and is fixed with respect to the axis of the microscope.

microscope. Figure 4 shows a closer view of the traverse mechanism. The photographic plate A is fastened by clamps B against kinematic stops C in a steel frame D. To avoid any possibility of back lash, this steel frame is mounted on four elastic steel links E. These form an elastic parallelogram linkage but if their outer ends were rigidly fixed they would not allow movement without extension of the links. Accordingly, the outer ends of the steel links E are fastened to four very stiff cantilever springs F. The photographic plate and steel frame D can then be traversed up and down about one centimetre for a force of 15 kilogrammes. A similar force applied in either direction in a horizontal plane produces a deflection which is less than 0.005 cm. As the cross forces need never be greater than a fraction of a kilogramme it is easy to maintain reproducibility of the traverse to a very high order. The variation of force with displacement in the traverse direction is non-linear. The force for small displacements is very small: the force for larger displacements rises very steeply. If the frame D is displaced and then allowed to spring back, the initial acceleration is very high but it traverses the centre section at nearly constant velocity.

At the top of Figure 4 can be seen a toggle catch mechanism G. It is possible with this to hold the frame displaced and then to release it either mechanically, or electrically by cutting off the current in the solenoid H. At the bottom of this Figure can be seen a system of accelerator springs and buffers J which can increase the working velocity of the plate a factor of $2\frac{1}{2}$ - from 30 cms/second to 75 cms/second.

Figure 5 is an enlarged view of a small section of a composite plate on which are recorded some 200 pictures of a rotating slotted wheel. Behind each lenslet of the lenticular plate is a track which is alternately dark and light depending on whether or not there was an image of a tooth or a space falling at that moment on that lenslet. It can be seen that the tracks are distinct and separate, and are inclined at an angle of about one in thirteen to the array of lenslets. Figure 6 is an enlargement of a small section of the same composite plate on which fell an image of a second rotating wheel. In this case the small wheel was driven by a synchronous motor at 3000 r.p.m. and had cut in its periphery 200 small teeth. The alternate teeth were cut twice as deep and other sub-multiple numbers of teeth were cut at greater depths. Again, as each slot passed in front of any given lenslet a dot was recorded, and it can be seen that discrete dots have been recorded at $10^4$/second. On occasions on which the additional springs were used to accelerate the plate these timing dots were spaced $2\frac{1}{2}$ times further apart so that even at the most conservative estimate it is possible to record pictures at 25,000 per second. This speed could easily be increased a further factor of 3 even using the present elastic suspension system and accelerator springs, if a plate holder of similar design to the present one, but made of light alloy, were substituted for the steel plate holder.

Viewing the Record On some occasions it is valuable to study the

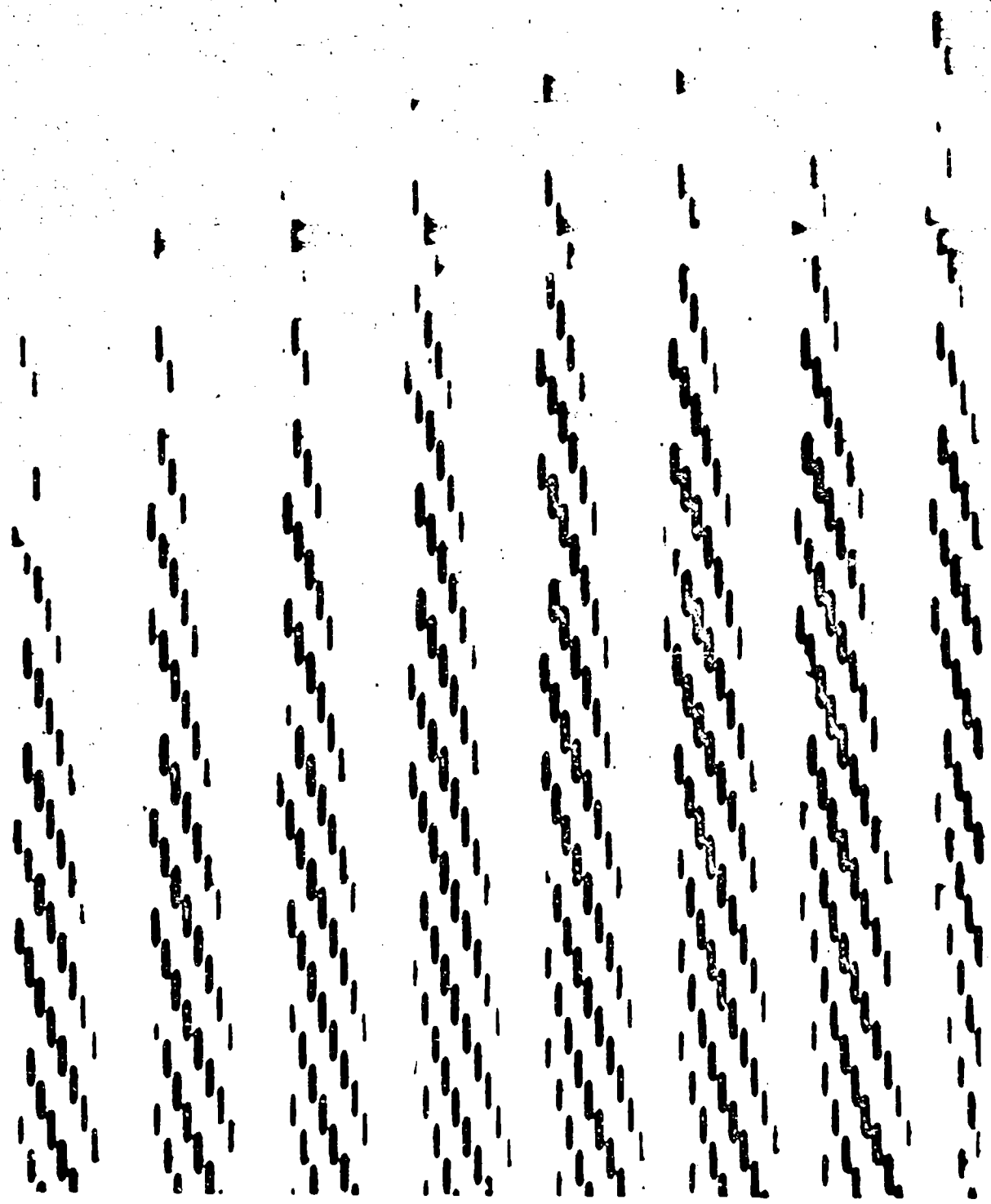

Figure 5: An enlargement at 50X of part of the composite plate on which was recorded a series of 200 pictures at $10^4$/sec. of the rotation of a slotted wheel. The trace behind each lenslet is alternately dark and light depending on whether or not there was falling on it the image of a spoke or a slot of the rotor.

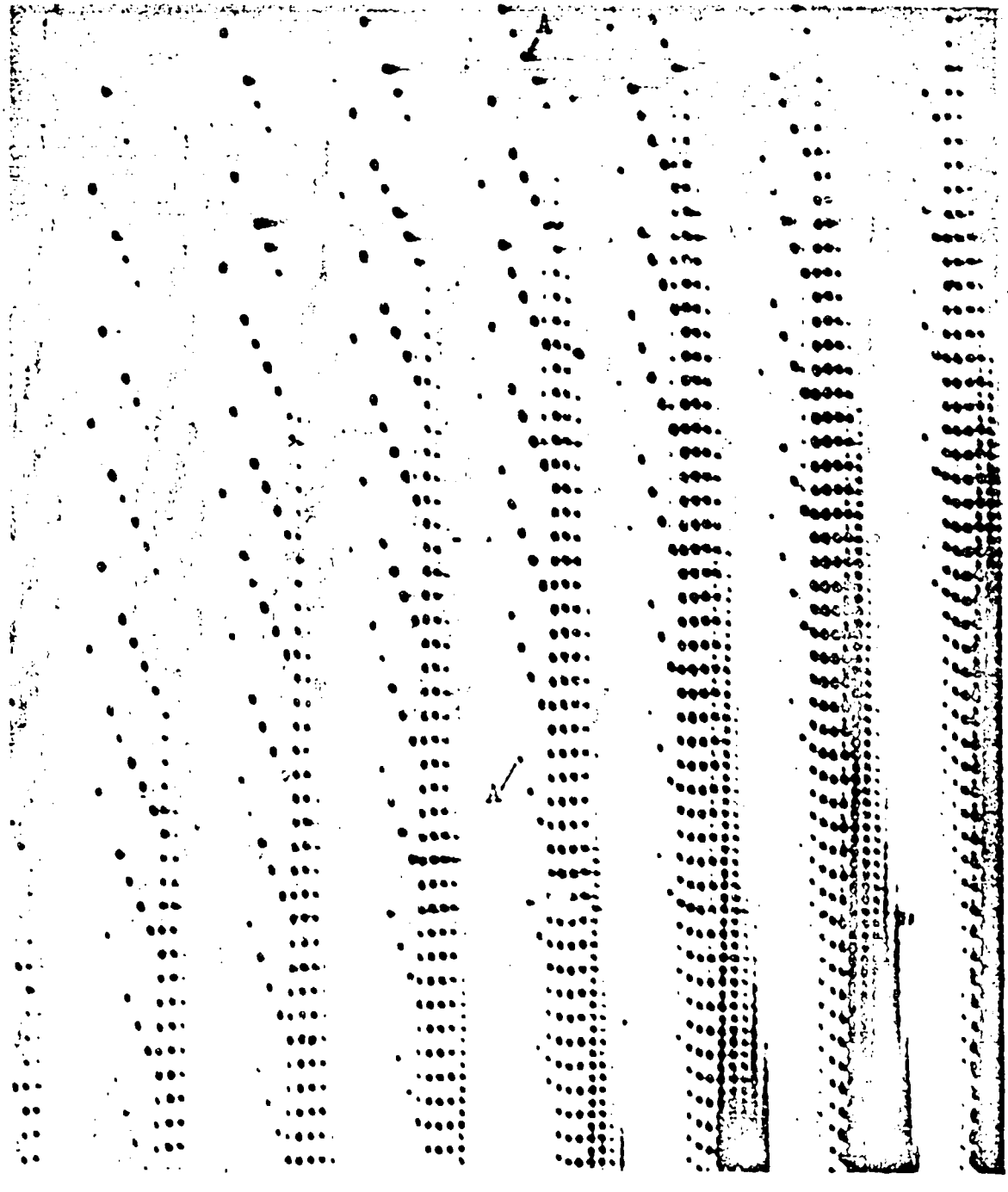


Figure 6: An enlargement at 50X of part of the composite plate on which was recorded a series of 200 pictures at $10^4$/sec. of the rotation of a toothed wheel revolving at 50 r.p.s. In the periphery of the wheel are 200 slots. Alternate slots are twice as deep and other submultiple numbers are deeper still. This wheel silhouetted on each composite plate provides a useful time reference as the dots for the shortest teeth occur at $10^4$/sec. - those seen on the right of the Fig. Other lenslets draw out a series of dots at 1/2, 1/10, 1/20, 1/100 of this frequency - e.g. at AA the dots occur at $10^3$/ sec.

composite plate directly. For example, from these last two enlargements it would be possible to determine the rate of rotation of the slotted rotor. More usually, one wishes to examine individual pictures or frames – that is, to unscramble the composite record. There are various ways of doing this. The simplest is to replace the composite plate after processing in the plate holder D, and to illuminate the microscope objective with a steady light source. Light will pass through the apparatus just as during recording and each lenslet of the lenticular plate will concentrate light on to that particular part of the track that was recorded when the photographic plate was in that identical position. The light that falls on any lenslet is focussed to a small dot on the photographic plate. Some of this light is absorbed, depending on the density of the plate at that point, and the remainder passes through the photographic plate and spreads out so that at a distance behind the emulsion about equal to the focal length, f, of the lenslet the light fills an area about equal to the aperture of the lenslet $p^2$. Thus, in a plane distant f behind the emulsion there is a picture of smoother toning but otherwise identical to the single frame made up of the tiny distinct dots that were all recorded simultaneously. This picture can be viewed directly or it can be allowed to fall on a diffusing screen so that it can be more easily seen when looked at obliquely, or alternatively, a photographic printing paper can be placed at this plane for obtaining a direct or 'contact' print.

If the photographic plate is slowly traversed by a micrometer, such as that shown in Figure 3, at E, just below the plate holder D, the phenomenon recorded can be viewed in slow motion. It is possible to copy this slow motion presentation with an ordinary cine-camera for later projection through conventional apparatus. In another method of unscrambling, the direction of the light rays can be reversed. That is, the photographic plate is illuminated from behind and the record can be viewed by placing the eye at the position of the microscope objective or recorded by placing there the lens of a copying camera.

Figure 7 shows four contact prints taken from the same plate, enlargements of parts of which are shown in Figures 5 and 6. These prints were each taken simply by holding a printing paper against the back of the photographic plate when it was placed in some one of its traverse positions and a light placed over the microscope objective. The second of the prints is similar to the first except that the plate has been traversed forward by .0025 cm. a distance corresponding to $10^{-4}$ of a second. It can be seen that the timing wheel has travelled forward one tooth in this interval. The third and fourth prints are similar frames but recorded at later intervals. These prints give some idea of the resolution and fidelity of the record.

Applications of the Apparatus The microscope has been used to study a number of things such as the vibration of fibres, the formation of droplets, and the operation of relay contacts.

There is no necessity to restrict the use of this apparatus to photography at enlargement. The whole of the recording mechanism can be used in any camera to take pictures at the same speeds as

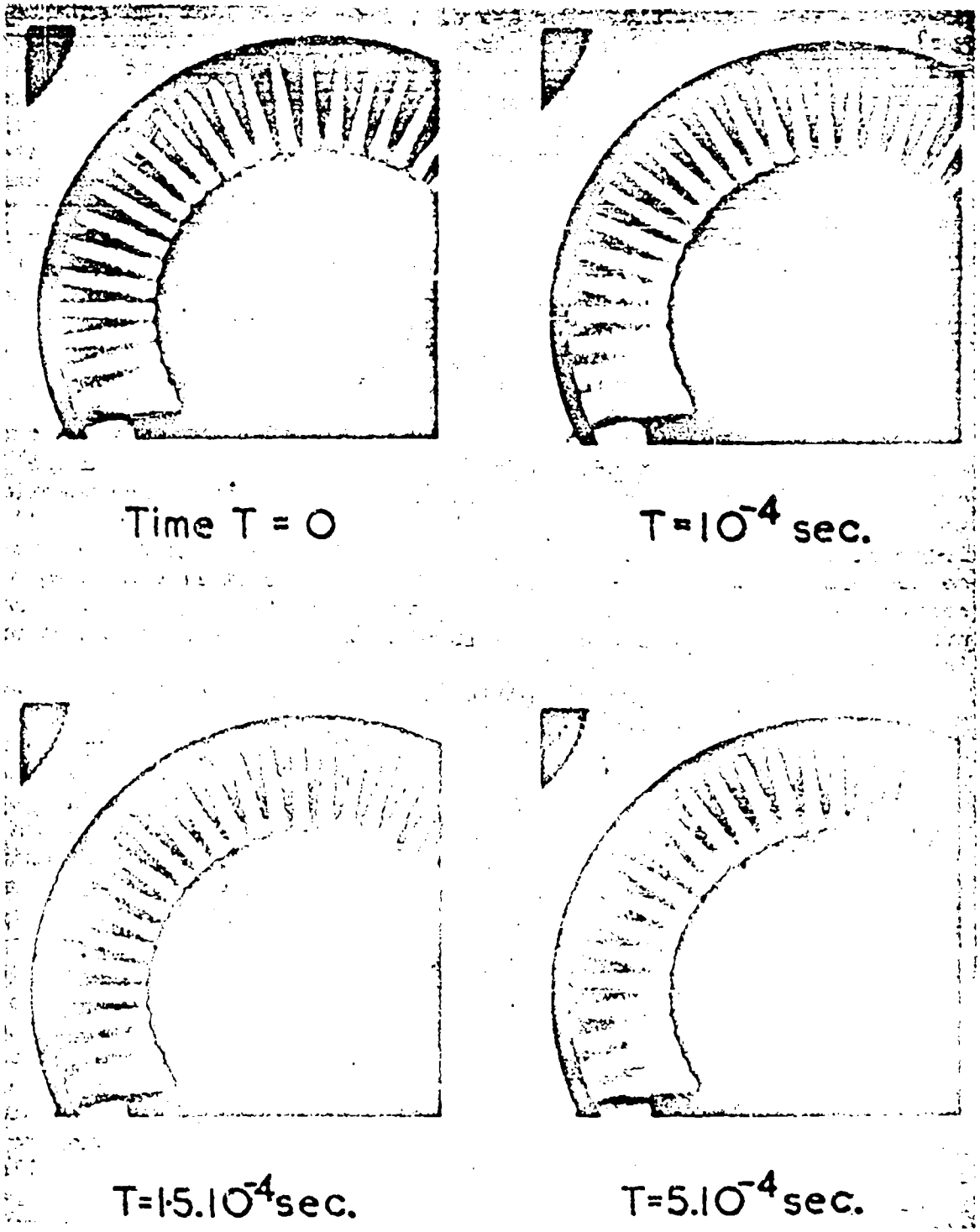


Figure 7: Four prints unscrambled on the microscope from the series of 200 recorded on the composite plate from which Figures 5 and 6 have been enlarged. The slotted rotor and the timing wheel can both be seen to rotate. The measured interval between the first two prints is $10^{-4}$ sec., between the second two is half of this, while the last is somewhat later. Both the slotted rotor and the timing wheel have been recorded as shadowgraphs at unity magnification.

Unclassified

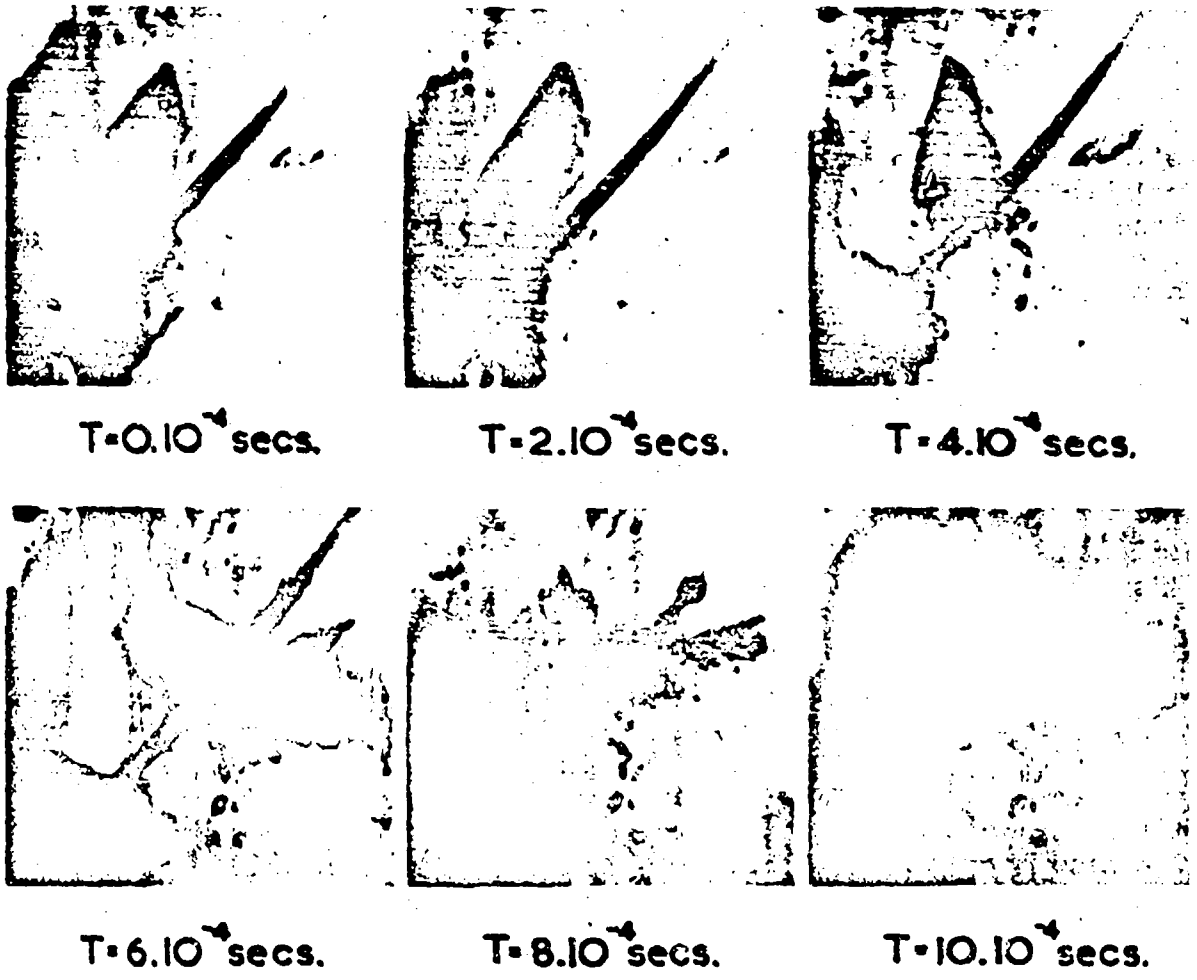


Figure 8: A selection of 6 pictures from the series of 200 recorded at an enlargement of 65X of the ignition of a small crystal of mercury fulminate by a wire heated by a sudden pulse of current. (i) T=0 Two crystals and Platinum Rhodium wire of diameter 0.003" before ignition. (ii) $T=2.10^{-4}$ sec. The larger crystal is ignited at the lower left where it is in contact with the wire. (ii) $T=4.10^{-4}$sec. The crystal begins to move bodily under the reaction from the expansion of the gaseous products of decomposition. The decomposition has formed a crater in the side of the crystal. (iv) $T=6.10^{-4}$sec. The crystal has moved further across the field of view and has turned through 90°. Small fragments have broken away from the crystal and are left behind. These fragments do not decrease in size, nor does the crater increase, and presumably reaction has ceased. (v) $T=8.10^{-4}$sec. The wire has melted and has formed into droplets thinly joined by molten filaments. Severe block cracking of the crystal is evident. (vi) $T=10.10^{-4}$sec. Some of the droplets of the melted wire have coalesced and are at this stage oscillating vigorously. It will be noted that the fragments broken from the large crystal are not consumed, and the smaller crystal has remained unaffected throughout.

before (i.e. up to 25,000 frames/second). Simply by the substitution of suitable lenses the apparatus can be used at low magnification - or for the photography of remote objects. These objects, too, can be either self-luminous or separately illuminated. On one occasion, for example, the microscope objective was replaced by a spectacle lens of focal length 1 metre, and an iris fitted to stop it down to an aperture of 1.2 cms. The camera was then used to photograph the cutter of a milling machine running at 600 r.p.m. from a distance of 2½ metres.

However, the main field of work in which we are using the microscope is the study of the earliest stages of explosive reactions. There are many problems in the mechanism of the ignition of crystals of explosives - How do the crystals burn? Do they break up into blocks? Does detonation proceed uniformly through a crystal? How is the reaction transferred from one crystal to another? Why, sometimes, does a detonation fade? In some cases reaction has been initiated by an intense flash of light, in others azides and fulminates have been ignited by direct contact with a heated wire.

I would like to express my thanks to Dr. A. Yoffe, for the series of six pictures which are shown in Figure 8. These are a selection from the 200 recorded at a magnification of 65X. The illumination was provided by a Philips' Photo-flash bulb, type PF 60E, and an ordinary condenser system was used. The photographic plate was Ilford process type N40, developed in ID 11 for 2 to 3 minutes. The slow motion record shows the ignition of the crystal of mercury fulminate at one edge by contact with the platinum rhodium wire (dia. 0.003") when it was heated by a sudden 5 amp current pulse. The rapid evolution of gas propels the crystal bodily across the field of view, the part of the crystal that has been decomposed can be clearly seen, and when the crystal has travelled some distance a fragment near this crater breaks off and is left behind, probably because of thermal stresses or due to the evolution of gas within the crystal material. While the crystal is moving across the field of view, the heating wire melts, forms into small droplets, and some of these later coalesce. In the slow motion play-back of the record, the droplets after they coalesce can be seen to oscillate rapidly. It is interesting to note that a second crystal that was originally near the first remained stationary throughout the record, and had not been ignited, although a burning crystal was in close proximity. Indeed it would appear that the first crystal, though it burnt vigorously near the point at which it was heated, did not continue to react at the same rate, and may even have ceased to decompose.

Light Sources and Accessories As mentioned earlier it is possible to make use of the whole of the light gathering power of the microscope objective. Furthermore, all the light which falls on any lenslet of the plate is concentrated to a small picture element which may well be 1/400 of the size of the lenslet. The brilliance of the points that are actually imaged on the emulsion is thus much greater than would be the case in a conventional microscope. Because of this intensifying effect of a lenticular plate[12] and because it is possible to use large numerical aperture objectives, it is possible to take

pictures at high magnification with short exposure times even using comparatively weak sources. A limit to the magnification and speed that is possible with a given photographic emulsion is set by the specific brilliance of the source, provided, of course, that the source is above a certain minimum size. It is possible to use arc lamps, but by far the most convenient sources and, in fact, the ones that I have used for all the illustrations in this paper, are ordinary photo-flash bulbs (magnesium-oxygen). The specific brilliance of these bulbs is of the order of $10^5$ candles/cm$^2$, and is comparable with the brilliance of the crater of a carbon arc. The duration of the flash varies with the different types of bulb, but for the brighter bulbs it is above half intensity for more than 1/100 sec. and usually has a long low-intensity afterglow. The flash from one of these bulbs is sufficient to allow a recording of the whole series of 200 pictures on the one photographic plate, even a process plate, at magnifications up to 500X and more.

It was desirable to reduce the fogging of the film from stray light or from the afterglow from photo-flash bulbs, and a capping shutter has been incorporated in the microscope. A small bell crank K is operated as the plate holder D, Figure 4, moves down and this draws a steel tape L through a slot just below the microscope objective. An aperture cut in the steel tape registers with the microscope objective aperture and allows exposure of the photographic plate for the correct traverse distance, when the plate is in mid-traverse and moving with nearly constant velocity. I would like to express my thanks to G.R.R. Bray for suggestions which, with minor modification, led to the development of this form of capping shutter. Adjustable contacts M have been provided for synchronising light sources or features of the event from movement of the plate holder.

The specific brilliance of flash discharge sources can be higher than that of a carbon arc and some work has been undertaken with D.P.C. Thackeray to produce suitable discharge lamps for use with this cine-microscope. Some of these are described briefly in a paper presented at the recent Conference in Paris on High Speed Photography(10). It was found that enough light could be produced to record pictures at $10^4$ frames/second if a current somewhere between 10 and 100 amps was passed between the electrodes in a short gap flash tube. The current could be provided by using a simple contacter on a high-tension supply, or with some difficulty by the use of a number of condensers and chokes arranged as a lumped delay line. Repetitive flashing of the source was also tried, using a rotary brush switch.

The specific brilliance of the spot on the screen of a cathode ray tube is also comparable with the brilliance of the crater of an arc lamp and a good deal of work has been done in the P.C.S. Laboratory on the development of gear for making use of the cathode ray tube as a source of light in high-speed photography(10).

Now in all the uses of the apparatus described above the light that comes through the objective falls directly on the lenticular plate and the physical size of the aperture of the

objective is quite small and fairly distant from the lenticular plate. If any object were placed between the objective and the lenticular plate it would cast a shadow on the plate. The apparatus could thus be used to record a series of shadowgraphs. In fact, use has been made of this for adding a time scale to all of the plates by means of the toothed wheel M, Figure 6, as described earlier; and Figures 5,6 and 7 all relate to a shadowgraph recording of the rotation of a slotted rotor and this timing wheel.

As explained earlier, it is possible to unscramble the composite record by replacing the composite plate, after processing, in the plate holder. It would be difficult to make lenticular plates sufficiently nearly identical to be able to unscramble in one apparatus a record made in another. It is, however, often convenient to have a separate means for unscrambling a record and this can be done quite simply:- A graticule plate, such as the Kodak MR plate, is placed behind the lenticular plate and a static picture taken. When this is developed there are small black dots in a clear field. A contact print of this is taken on another graticule plate and when this is developed there are small clear dots in a black field. This array of dots is identical with the array of foci of the crossed pair of lenticular plates. If now a composite plate is aligned on top of this and the two together viewed in transmission, only one of the recorded frames from the composite plate will be visible at a time. By traversing one plate relative to the other it is possible to obtain slow-motion viewing. This provides a much more graphic presentation of an event than the individual examination of successive discrete frames.

Summary A microscope has been built using the principles of image dissection. Without elaborate gear it has proved possible to take series of 200 pictures at 25,000 per second at magnifications as high as 500X, using process plates, and providing the illumination for the whole of each series from one magnesium-oxygen photo-flash bulb. Micrographs have been taken in transmission and in reflection. The resolution of the pictures is 320 lines across the field in each dimension - comparable, that is, with the quality that can be obtained on a standard 16 mm. cine-frame.

It has been shown that, by the simple substitution of long focus lenses, the apparatus can be used equally well for the photography of remote objects at the same high rates. It has also been used for recording fast series of shadowgraphs.

Much higher magnifications (up to 5000X) are possible but at reduced rates. As at these high magnifications the limitation on maximum recording rate is one of light level and plate speed, it is possible to obtain considerable improvement by the use of fast emulsions, but this can only be done at some expense in the number of separate pictures that can be resolved in a series.

It is to be expected that the maximum rate of taking pictures for magnifications lower than 500X, where the limitation is imposed by considerations of mechanical inertia, could be increased by substitution of light alloy components and some attention to design

detail by a factor of 4 at least, so that pictures could be taken at rates in excess of $10^5$/second without increasing the delay between release and full running speed beyond the present figure of $10^{-2}$ second. This comparatively long delay is a drawback and means that for the photography of many phenomena synchronisation must be from the camera to the event.

The apparatus can be used to unscramble its own record for slow motion viewing or for taking prints of particular pictures. Separate unscrambling apparatus has also been made.

Studies have been made of the initiation and the early stages of reaction in small crystals of explosives, such as azides and fulminates. Records have also been taken of the initiation of reaction by high intensity light flashes.

Timing reference marks at $10^4$/sec. are recorded on the composite plate. Synchronising contacts and a synchronised capping shutter are incorporated.

The speed, the range of magnifications, and the simplicity of the apparatus make it suitable for the study of many physical problems.

## Acknowledgements

The broad principles upon which this cine-microscope and particularly the last design of unscrambler have been built bear considerable resemblance to those embodied in apparatus developed by Fordyce Tuttle (13,14) and by Morton Sultanoff (15,16,17), and I would like to acknowledge the help that I have received from them in discussion and from their papers. I would like to express my thanks to Dr. F.P. Bowden, F.R.S., for his continued advice and encouragement, and to thank the other members of our laboratory for their assistance. I also wish to express my thanks for the support given by the Ministry of Supply (Air), the Royal Society, and Vauxhall Motors Limited.

## References

(1) F.P. Bowden and A.D. Yoffe, Initiation and Growth of Explosion in Liquids and Solids, Cambridge University Press 1952.
(2) J.S. Courtney-Pratt, Research 2, 287, 1949.
(3) J.S. Courtney-Pratt, Proc. Roy. Soc. A204, 27, 1950.
(4) J.S. Courtney-Pratt, Phot.J., 92B, 137, 1952.
(5) J.S. Courtney-Pratt, Brit. Pat.No. 662,065.
(6) J.S. Courtney-Pratt, J. Phot.Sci., 1, 21, 1953
(7) J.S. Courtney-Pratt, Fourth Symposium (International) on Combustion, M.I.T., The Williams & Wilkins Company, Baltimore, pp.508-526, 1953.
(8) J.S. Courtney-Pratt, Brit. Pat. No. 712,997.
(9) J.S. Courtney-Pratt, A High Speed Cine Microscope, International Symposium on High Speed Photography, Paris, September, 1954.
(10) J.S. Courtney-Pratt, and D.P.C. Thackeray, Fast Multiple Frame Photography by Cathode Ray Tube Illumination, International

Symposium on High Speed Photography, Paris, September, 1954.
(11) La Reliephographie, Societe pour l'Exploitation des Procedes de Photographie en Relief. Maurice Bonnet. Brit. Pat.No.615,629. No. 619,948. No. 622,917, No. 638,551. Brit.Prov.Pat.No,26923/45.
(12) La Reliephographie, Society pour l'Exploitation des Procedes de Photographie en Relief. Maurice Bonnet. Brit. Prov. Pat. No. 29577/45, No. 29578/45. French Pat. No. 745/942.
(13) Fordyce E. Tuttle, J. Soc. Mot. Piot.Engrs., 53, 451, 1949
(14) Fordyce E. Tuttle, J. Soc. Mot. Piot.Engrs., 53, 462, 1949
(15) M. Sultanoff, Rev.Sci.Ins., 21,653,1950
(16) M. Sultanoff, J. Soc. Mot. Pict. Engrs., 55, 158, 1950
(17) M. Sultanoff. Soc. Mot. Piot. Engrs. Convention, October 1952.

# THE MEASUREMENT OF DENSITY CHANGES IN GASEOUS DETONATIONS 6

G. B. Kistiakowsky and P. H. Kydd
Harvard University
Cambridge, Massachusetts

## Abstract

An apparatus is described for determining rapid density changes in gaseous detonation waves. Its time resolutions is better than 1/2 μsec; quantitative measurements of density changes are possible to about 15%, with an absorbing path of 10 cm and gas densities in the range of 1 g/liter.

Experiments with several explosive mixtures at an initial pressure of one atmosphere have failed to reveal reaction zones (v. Neumann spikes) in detonation waves. Upon resorting to xenon as the X-ray absorbing component, it became possible to study gas density changes in detonation waves produced in mixtures at a small fraction of one atmosphere pressure. Using stoichiometric hydrogen oxygen mixtures with added xenon, the first indications of the spike were obtained at 1/8 Atm. initial pressure. The spike lasted about 3 μsec at 0.1 Atm. and was broadened to 20 μsec at 0.025 Atm. Replacement of xenon with a much higher partial pressure of argon repressed the spike.

---

Studies of the variation of gas density as a detonation wave passes through an explosive medium should offer a confirmation of the well-known Zeldovich-von Neumann theory of the detonation reaction zone, and yield at least qualitative information on the kinetics of the reactions occurring. The theory predicts a discontinuous rise in density at the wave front to the value expected for a pure shock wave moving at the detonation velocity. The non-isentropic heating of the gas by the shock initiates vigorous chemical reaction, which causes the temperature to rise and the density to fall until chemical equilibrium is reached in the Chapman-Jouguet state (1). One should therefore observe a sharp density peak, whose shape and duration are related to the rate of attainment of equilibrium. In a

typical case the density of shocked but unreacted gas is about five times the initial density, and it decreases to less than twice this amount in the C-J state. The technique of gas density determination by X-ray absorption is particularly well suited to this problem, as it offers instantaneous and continuous measurement of density, and is independent of chemical change or visible light associated with the detonation reaction. An apparatus of this type has been developed (2), and the latest modification of it will be described.

An X-ray absorption photometer with oscillograph recording and suitable calibration equipment has been incorporated into a 10 cm I.D. detonation tube in such a way as to obtain a continuous record of the average gas density along one diameter within the tube. As a detonation wave moves past the photometer slits in a direction normal to this diameter, the changes in gas density in the wave front are displayed on the oscillograph and photographed.

The chief difficulty encountered in the use of this method has been the low signal to statistical noise ratio obtainable with conventional X-ray equipment in the short time intervals of interest. There are two ways of alleviating this; first, to increase the intensity of the primary X-ray beam, since the signal to noise ratio increases as the square root of the total intensity; second, to increase the absorption by using soft X-rays and adding a strongly absorbing component to the explosive mixture.

The most satisfactory type commercial X-ray tube for this application is one with a copper target and beryllium window producing a high intensity of low energy X-rays. The tube in use at present is a Machlett model AEG-50-A. This tube has a grounded water-cooled anode with a focal spot 1.5 mm wide and has been operated at 22 KV DC, 32 ma, supplied by a G.E. XRD X-ray diffraction apparatus transformer and rectifier. The high voltage is filtered by a 1/2 microfarad condenser; the filament current of approximately 4 amps AC is supplied by the same transformer. To increase the intensity without damage to the tube, an automatic switch has been incorporated in the tube filament supply to increase the emission current to 32 ma, somewhat higher than is recommended for continuous operation, for a period of three seconds during which the detonation takes place.

Since the usual explosive mixtures studied do not absorb even soft X-rays to a sufficient extent, it has been found necessary to increase the absorption coefficient by adding a component of high atomic number. Argon and later Xenon have been used successfully, the latter giving sufficient absorption at partial pressures as low as 7 mm.

The X-ray beam is allowed to pass through the 10 cm I.D. detonation tube by two opposing beryllium windows resting on flats milled in the tube wall, see Figure 1. Slits, 3/32" wide in the direction of the wave travel, were milled in the wall under the

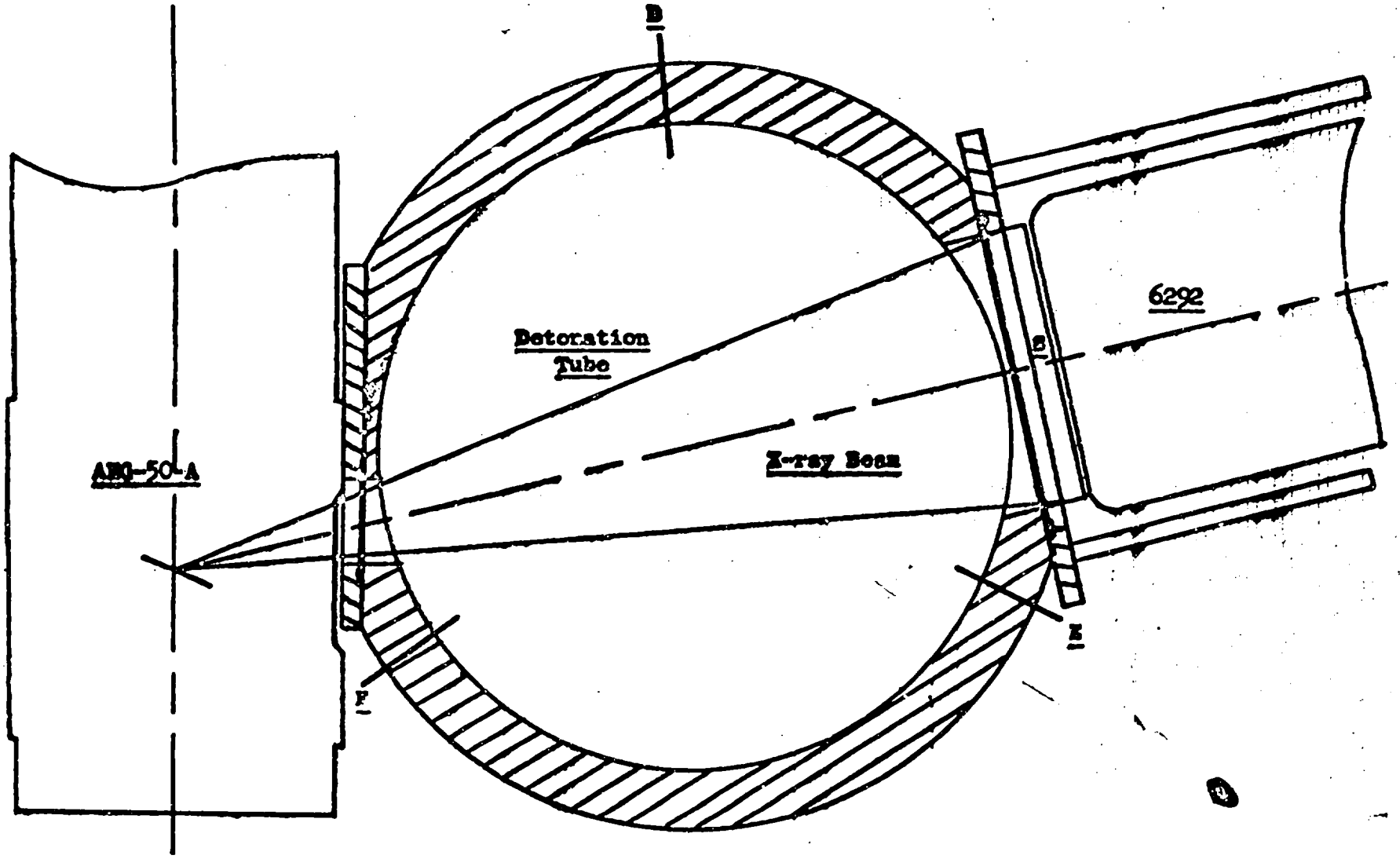


Figure 1. Cross-section of the Detonation Tube at the X-ray Windows. Beryllium windows indicated by heavy lines between flats on tube wall and cover plates; D, E, F, positions of ionization gages to measure tilt of wave; S, thallium activated sodium iodide scintillation crystal.

windows defining a 17° wedge of radiation. The windows are .010" think, supported by 1/3" steel cover plates which carry 1/16" wide defining slits and rubber gaskets to seal the windows. This arrangement leaves the windows free to be removed, and yet is strong and vacuum tight.

The cover plate over the exit window also carries the photomultiplier detector. This is a DuMont type 6292 end-window tube with a photocathode diameter of 1-11/16", coupled with a 1-3/4" diameter, thallium activated, sodium iodide scintillation crystal. The potential divider for the dynode supply voltages and a cathode follower to match the output to the input of the signal amplifier are mounted in a small chassis attached to the tube socket. The tube and socket slip into a brass tube soldered at right angles to the cover plate which provides shielding from light and electrical interference as well as support. The signal amplifier is a Browning video type with a constant and adjustable gain of as much as 650 from 7 CPS to 4 Mc. The amplifier is connected to the vertical plates of an Atomic Instrument Co. single sweep oscilloscope with an adjustable horizontal sweep duration, which can be accurately timed by 20 microsecond pips. The X-ray intensity vs. time traces obtained when the oscilloscope is tripped are photographed.

To relate the vertical displacements of the CRO traces to gas density changes requires two separate operations. The first of these is to determine the change in output of the photomultiplier as a function of the gas density for a given set of operating conditions of the X-ray tube. The output is read directly on the microammeter shown in Figure 2. This corresponds to the observed X-ray intensity, I, and is plotted against gas density as the natural logarithm of the ratio of I to $I_o$, the output with the detonation tube evacuated. The slope of this plot is the mass absorption coefficient times the (constant) path length in the absorption equation

$$\ln \frac{I}{I_o} = -\alpha$$

The absorption coefficients determined in this manner are not constants due to the non-monochromatic nature of the radiation and are dependent on the X-ray tube voltage and emmission current.

To the accuracy of the present measurements, the slight effects of chemical change on X-ray absorption are negligible. Therefore, the calibration is carried out with a non-explosive gas mixture at room temperature chosen so that the ratio of atomic species is identical to that of the explosive mixture to be used later. The calibration curve determined for this mixture is then taken to be that of the explosive mixture before, during, and after the explosive reaction.

The second step is to relate the vertical displacements on the CRO records of each experiment to changes of X-ray intensity and thus, through the above calibration curve, to changes in density. To accomplish this the X-ray intensity is observed on the microammeter immediately before each experiment. Because of the AC amplifier used, this corresponds to a horizontal line of zero vertical deflection on the oscilloscope record. Immediately after the experiment the photomultiplier supply voltage is turned off. A circuit shown in Figure 7 is connected to the detector chassis which substitutes for the photomultiplier and produces step function traces on a separate film, corresponding to known changes in X-ray intensity from the initial value. The mode of operation is as follows. After the calibration circuit is connected, the initial intensity adjustment is set to reproduce the initial observed current on the microammeter. Then the step intensity selector is set to the first position and the thyratron switch triggered by shorting the grid to the cathode. This raises the potential at A, causing less current to flow through the initial intensity adjustment resistor, i.e. simulating a reduced X-ray intensity in a stepwise manner. The single sweep oscilloscope is triggered at the same instant and the result is a horizontal trace corresponding to a decreased intensity as might have been caused by a sudden increase in gas density. This decreased intensity is then read on the meter. The thyratron switch is turned off, by breaking the grid-cathode short circuit and breaking the connection in the step intensity selector; the next selector setting is chosen and the process repeated. This is continued until the desired lines are drawn, and a base line corresponding to $I_i$ added by triggering the oscillioscope manually, with the thyratron switch open. By matching the baselines corresponding to $I_i$ in this record and the density record obtained in the detonation experiment, it is possible to read the intensity at any point by interpolation between the calibration lines.

To convert the intensity values to gas density, $I_o$ must first be determined by using $I_i$, the known initial density, and the calibration curve. Then values of $\ln \frac{I}{I_o}$ can be referred back to the calibration curve and the density determined at any point.

Random errors are introduced during this procedure by the static calibration and the reading of the two films. The total error from these sources is estimated to be 10%. Further random error occurs due to the statistical fluctuations of X-ray intensity. It has proved possible to compensate for this to a large extent by making a number of duplicate runs and averaging the results at each time of interest.

The systematic errors are more difficult to estimate as well as more serious. Despite the fact that low output currents were drawn from the previously employed 1P21 photomultiplier tube during the static calibration, serious fatigue was encountered, which

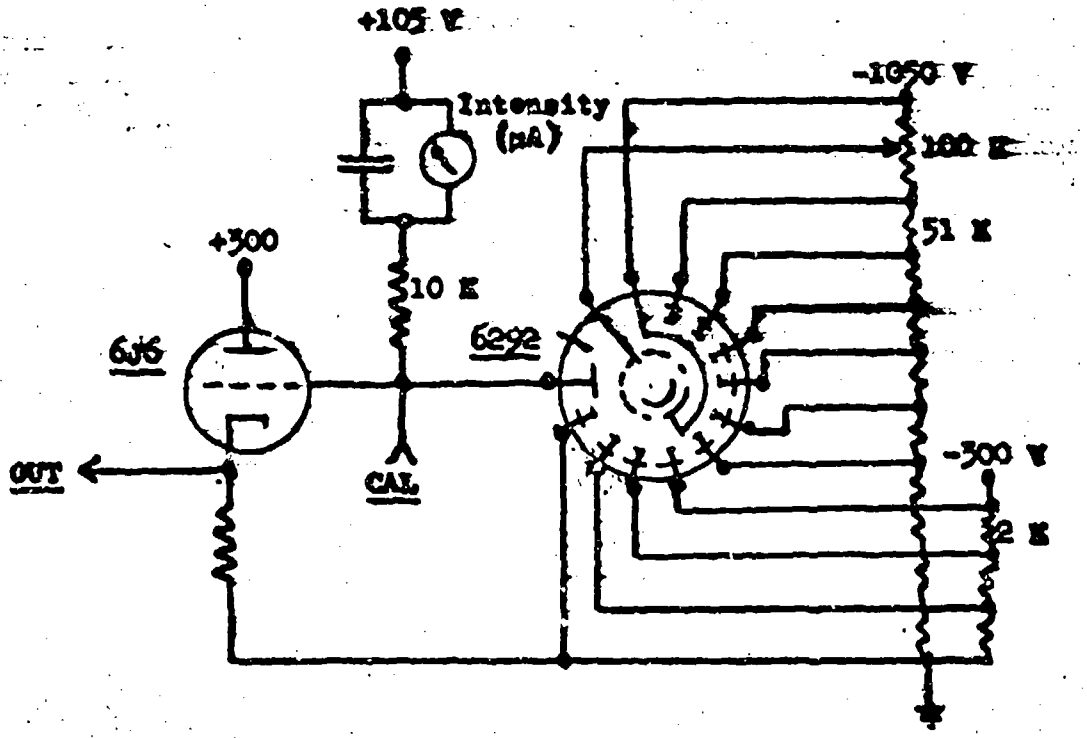


Figure 2. Photomultiplier Detector Circuit.

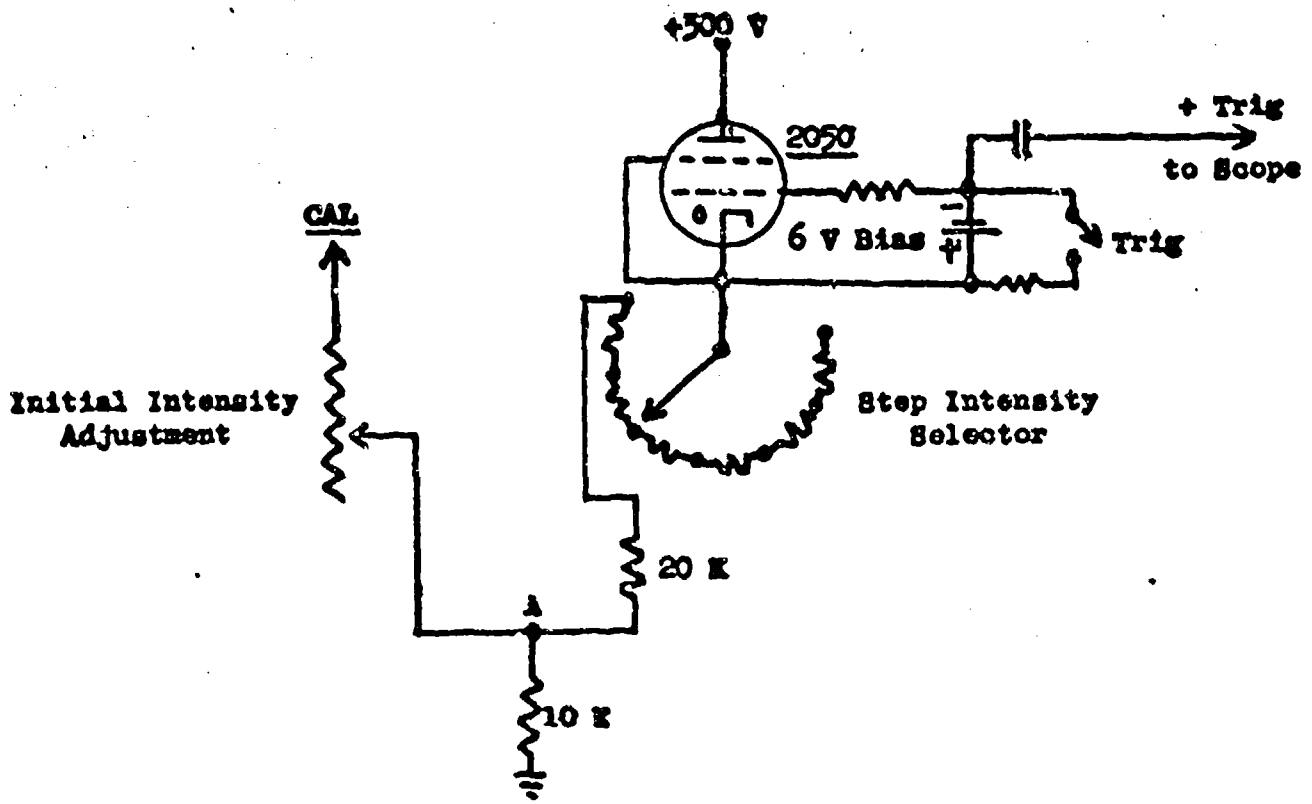


Figure 3. Calibration Circuit.

necessitated corrections. Any change in the characteristics of the oscilloscope and amplifier between the experiment and the calibration could aggravate this. The agreement between theory and experiment to date has been within 15%.

The detonation tube is made up of sections of 10 cm ID steel and brass pipe equipped with flanges and O ring grooves at the ends and bolted together to make up any desired length. A 50 cm length at the initiation end is separated from the remainder by a thin plastic diaphragm and filled with equimolar acetylene-oxygen. This when ignited by spark very rapidly forms a stable plane detonation wave which is transferred through the diaphragm to the experimental mixture. In addition to the X-ray apparatus, the remainder of the tube is equipped with ionisation gages (3), which produce small electrical signals when struck by the detonation wave front. The signals can be displayed directly on a time calibrated oscilloscope sweep and photographed, but more accurate reading is possible by inserting the amplifier-pulse shaper described in (8). Twelve gages are spaced at 10 cm intervals along the top of the tube. The first and ninth serve to trigger the velocity recording scope and the density recording scope respectively, and the other nine determine the velocity. At the tenth and eleventh positions, two additional gages, at the same distance along the tube but at 120 degrees to the first, indicate the tilt of the wave front. The signals from these gages are delayed by 2 and 4 microseconds respectively to distinguish them from the first. The end wall of the tube contains three more gages on a diameter to detect non-planarity of the wave; the signals are delayed in the same manner as the tilt signals. It has been found that at low experimental pressures favorable to X-ray investigation plane and normal waves could only be obtained in relatively long tubes and a length of 3.5 meters from diaphragm to slit system has proved satisfactory. In addition the ionization gages were found to be insensitive to low pressure detonation waves in $H_2$-$O_2$. However, by using higher voltage on the ionization gap electrodes with very small signal condensers of 15-30 μμf to prevent multiple signals, and especially by using steel wires protruding 1/4" into the tube as the electrodes, this difficulty was overcome down to experimental pressures of 15 mm.

## Results

The experiments so far performed have been made with an earlier modification of the apparatus herein described which differed only in detail A number of experiments were made to detect the reaction zone in detonations of both hydrogen-oxygen and acetylene-oxygen mixtures at one atmosphere initial pressure. Under these conditions the reaction zone was undiscoverable within the resolving time of the apparatus of less than 1/2 microsecond. Nothing of interest was determined in this phase of the investigation, and the apparatus was used to verify the hydrodynamic predictions for the

density distribution in the rarefaction region behind the steady state zone (4). This was done for equimolar acetylene-oxygen with 20% added argon at a point 69 cm from initiation. It was found that the manner of initiation was important for the rapid establishment of a normal detonation, and that simultaneous sparks distributed evenly over the initiation end wall gave very satisfactory results. This initiation system has been used since in all experiments. The results were in agreement with the hydrodynamic prediction of an isentropic expansion wave following the detonation wave front, with the gas expanding until its forward motion ceased and then remaining at rest at constant density.

At the completion of this work hydrogen-oxygen mixtures were again studied, this time at reduced pressure with xenon as the absorbing additive. Due to the pressure dependence of the reaction rates, it was now possible to identify the reaction zone and vary its duration by varying the pressure. The highest pressure at which concrete evidence of the reaction zone was obtained was 95 mm of 70% $H_2$-30% $O_2$ with 15mm Xe added, with which a sharp density spike was observed in one experiment. At 85 mm reactant pressure, the reaction zone was observed consistently and five experiments were performed so that the results could be averaged and the statistical fluctuations reduced, as shown in Figure 4. The density does not reach the full shock value by a large margin though measurements were carried out to within 1/2 microsecond of the wave front. This is partly due to finite time resolution of the equipment and perhaps to errors in the static calibration curve. However, since the same behavior was noticed in experiments at lower pressures in which the reaction zone is much longer and in which the C-J density is reproduced accurately, it appears that, contrary to expectation, the reaction starts practically instantaneously at a very high rate which decays rapidly as equilibrium is approached.

Experiments at 65 mm show somewhat longer reaction times and a closer approach to the theoretical density at the wave front but still show no evidence of an induction period.

It was found that detonations would propagate in a normal fashion at reactant pressures as low as 15 mm with 11 mm Xe added, though at a very low velocity of close to 1200 m/sec. At these low pressures the reaction zone is approximately 20 microseconds long, Figure 5, and though the initial portion is often marred by non-planarity of the wave front, it still shows the steady fall of density from the extreme front of the wave to the C-J state.

This is not enough evidence as yet to clearly specify the dependence of the reaction zone length on reactant pressure, but a preliminary estimate is that the duration of the reaction increases as the inverse square of the pressure.

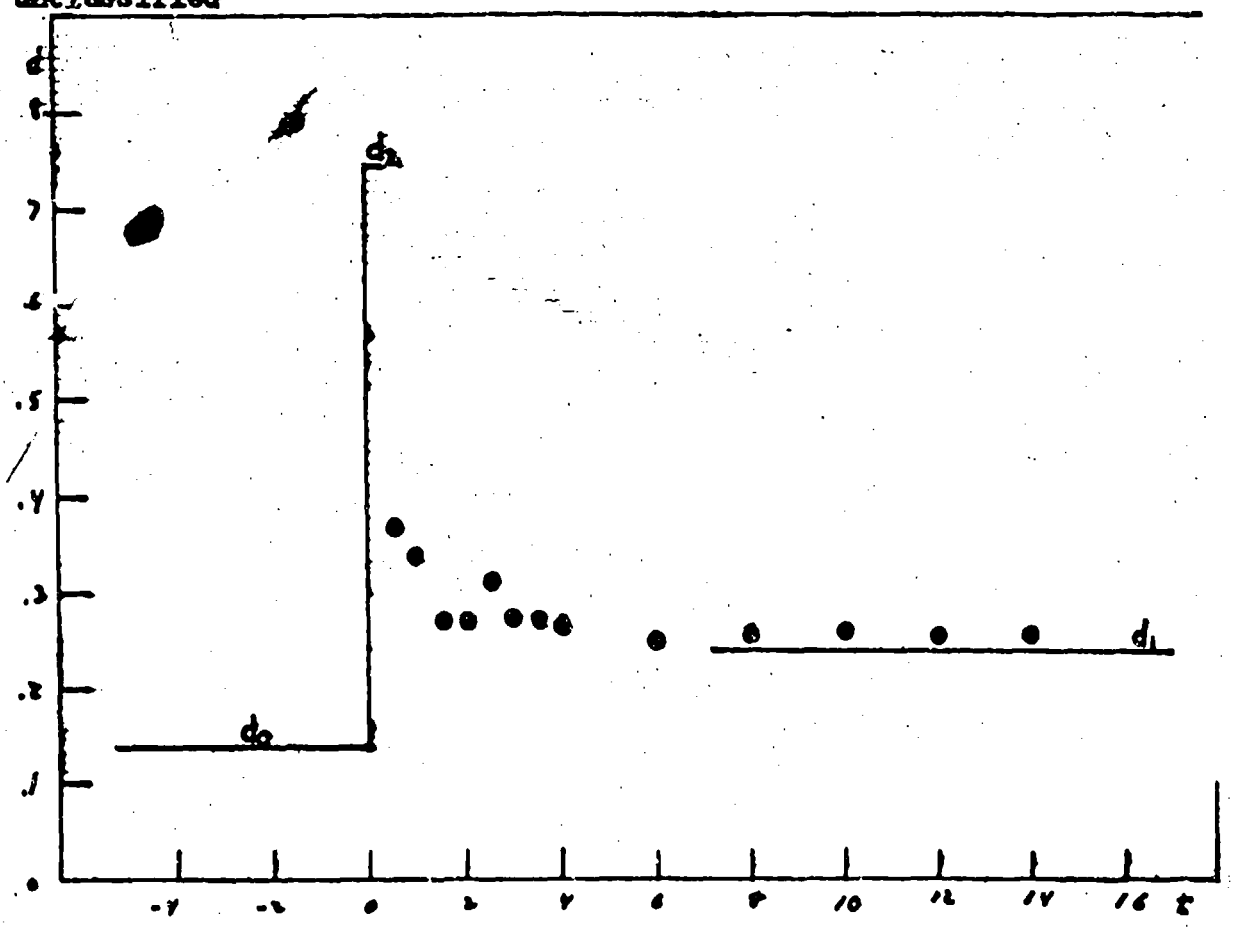


Figure 4. The Reaction Zone in Hydrogen-Oxygen Mixture at 85 mm Total Pressure; Average Density Values for 5 Experiments.

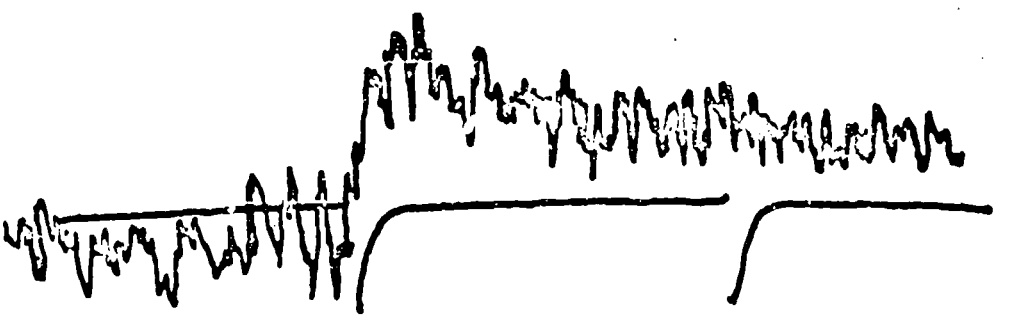

Figure 5. The Reaction Zone in Hydrogen-Oxygen Mixture at 15 mm Total Pressure. Density (Ordinate) vs. Time (Abscissae), Distance Between Negative Timing Markers 20 μsec.

The observed duration of the reaction zone is not identical with the time that a gas volume element spends in passing from the shock front to the C-J state, i.e. with the duraction of chemical reactions in this volume element. Considerations of the reaction zone as a stationary wave form moving by the observer with the detonation velocity lead to the expression:

$$\tau_r = \frac{\int_0^l \rho\, dl}{D\,\rho_0} = \tau_0 \frac{\int_0^l \rho\, dl}{l\,\rho_0} = \tau_0 \frac{\rho_{av.}}{\rho_0}$$

where $\tau_0$ is the observed duration of the reaction zone, $\tau_r$ is the true duration of chemical reactions in a volume element; $\rho_0$ is the initial gas density, $l$ is the observed length of the reaction zone ($l = \tau_0/D$), $\rho$ is the instantaneous density of gas in the reaction zone. If the latter is replaced by the average gas density in the reaction zone, $\rho_{av}$, the last form of the equation results which is particularly instructive. Since the actual densities observed average from 2 to 2.5 times the initial density, the actual reaction times appear to be 2 to 2-1/2 times the observed ones. This ratio does not significantly depend on the initial pressure in the above described experiments.

The effect of inert gas is of interest. When a mixture of 13 parts argon and three parts stoichiometric $H_2+O_2$ was detonated at a total pressure of 1/2 atm., i.e. a pressure of $H_2-O_2$ of 71 mm at which the reaction zone would certainly have been observed had the argon not been present, no trace of a density peak was discernable in two identical experiments. This indicates that added rare gas increases the reaction rate even though it lowers the temperature in the shock wave.

It is a pleasure to acknowledge the support of this research by the Office of Naval Research under Contract N5ori-076, T.O. XIX, NR-053-094, with Harvard University; also the gift of Xenon by the Linde Air Products Co. Some of the electronic equipment described was constructed by Mr. Roger Humberger.

## Bibliography

1. J. G. Kirkwood and W. W. Wood, J. Chem. Phys. (in press)

2. G. B. Kistiakowsky, J. Chem. Phys. 19, 1611 (1951)

3. H. T. Knight and R. E. Duff, Rev. Sci. Inst. (in press)

4. G. B. Kistiakowsky and P. W. Kydd, J. Chem. Phys. (in press)

# THE ATTAINMENT OF THERMODYNAMIC EQUILIBRIUM IN DETONATION WAVES 7

G. B. Kistiakowsky and Walter G. Zinman
Harvard University
Cambridge, Massachusetts

## Abstract

Detonation velocities were accurately measured in lean acetylene-oxygen mixtures in which unreacted oxygen may be delayed reaching equilibrium in regard to its vibrational heat capacity and dissociation into atoms. Comparison with calculated velocities proves that with all mixtures containing from 50 to 5% acetylene the observed velocities agree with equilibrium calculations. The degree of agreement is such that equilibrium temperatures are determined to better than 1%.

Observed detonation velocities in mixtures containing 53 and 55% acetylene are inconsistent with equilibrium calculations, provided the heat of sublimation of carbon is taken to be 141 Kcal. They agree excellently with similar calculations assuming 170 Kcal as the heat of sublimation. This is regarded as strong evidence for the latter value.

Up to 71% acetylene the observed velocities agree with calculations assuming that no solid carbon is formed in the Chapman-Jouguet state, although total equilibrium demands its presence. With 71% acetylene two velocities are observed in the same experiment. First a slow wave, whose velocity agrees with a calculation not allowing for solid carbon. Then, after an almost discontinuous transition, a faster wave whose velocities is fairly close to a velocity calculated under the assumption of total equilibrium including solid carbon. With still more acetylene only the faster type of wave is observed.

The nature of the transition at 71% acetylene is discussed on the basis of ideas advanced by Doering and by Kirkwood and Wood.

The effect of tube diameter on detonation velocity has been measured in several mixtures and has been found to be of a small constant magnitude.

## Introduction

Whether or not thermodynamic equilibrium is attained in the Chapman-Jouguet (C-J) state of stationary detonation waves, has been repeatedly considered from the experimental and the theoretical point of view. In more recent times Lewis and Friauf (1) demonstrated that the velocities in hydrogen-oxygen mixtures agreed far better with calculations in which complete thermodynamic equilibrium was assumed to exist among the reaction products in the C-J state, than with those assuming quantitative reaction. Zeldovich (2) came to the same conclusion. The detonation velocities obtained in this laboratory (3) for cyanogen-oxygen mixtures containing at least 50% oxygen agreed within experimental error with the velocities calculated assuming thermodynamic equilibrium in the C-J state. The high value for the heat of dissociation of nitrogen which had been used in these calculations has now been confirmed (4), and the high value for the heat of dissociation of carbon monoxide which had also been used in these calculations seems probable (5). Also in the case of acetylene-oxygen mixtures containing from 25 to 50% oxygen (6) and of the approximately stoichiometric mixture of carbon monoxide and oxygen (7), excellent agreement with equilibrium calculations had been obtained.

From the theoretical point of view, the attainment of equilibrium in the C-J plane is not a necessary requirement. Zeldovich (2) pointed out that an endothermic reaction lagging behind the exothermic processes responsible for the detonation will not be included in the C-J state and will occur, therefore, in the rarefaction wave where it has no effect on the detonation wave parameters.

The rigorous analytical treatment of the problem by Kirkwood and Wood (8) has defined the conditions under which equilibrium may not be attained. The C-J state corresponds to the condition

$$[1] \qquad \sum_j \sigma^j r^j = 0$$

where the $r^j$ are the chemical rate functions of the j reactions, presumed to be involved in the detonation process, while the $\sigma^j$ describe the effect of each reaction on the pressure of the system, caused by the enthalpy and mole number change. As they point out, the normal case is for the left side of [1] to become zero when all $r^j$ vanish, because equilibrium has been attained. However, when some $\sigma^j$ ha egative values (i.e. when reactions occur which are either endothermic or are accompanied by a large volume decrease, or both), equation [1] may be satisfied prior to establishment of equilibrium. In this event those residual reactions which occur after the summation in [1] has become negative, occur behind the C-J state and have no effect on the detonation parameters. The authors are unable to decide, on the basis of their steady state considerations, what happens if the summation in [1] becomes positive again after having been negative for some time. A less defined case of a fast and slow exothermic reaction has been qualitatively discussed by Doering (9).

He suggests that while the detonation wave is still "young" and therefore its rarefaction wave is steep, the slow exothermic reaction must occur in the rarefaction wave. With the progress of the detonation wave, the rarefaction becomes less steep and the delayed reaction develops a shock which must eventually overtake the C-J plane. Thereupon, the slow reaction contributes to the parameters of the wave. In the language of Kirkwood and Wood, Doering's proposal means that in the early stages of a detonation wave its parameters are determined by that thermodynamic state of the system which corresponds to the earliest vanishing of the left side of [1]. With the aging of the detonation, the wave parameters suffer a discontinuous change and become determined by that subsequent state of the system in which eq. [1] is satisfied again.

The experimental evidence on deviations from equilibrium is rather inconclusive, except for one instance. The evidence cited by Zeldovich (2) on the pressure dependence of detonations in hydrogen-chlorine mixtures is open to other interpretation. In the light of subsequent experience in this Laboratory on overdrive and the diameter effect, the suggestion (10) that significant deviations from equilibrium were observed in the hydrogen-oxygen mixtures does not seem tenable. In cyanogen-oxygen mixtures containing excess cyanogen (3), the observed velocities are appreciably higher than calculated, but the calculations involve simplifying assumptions about the thermodynamic functions of the cyanogen molecule and the experimental data are not altogether trustworthy, as was noted at the time. A few velocities measured in lean acetylene-oxygen mixtures (6) are significantly higher than calculated. The most striking deviation is that observed in acetylene-oxygen mixtures containing between 55 and 70% acetylene (6). The velocities of these mixtures are lower and decrease faster with rising acetylene concentration than is predicted on the basis of calculations performed, assuming that the thermodynamically required amount of solid carbon is formed before the C-J state is reached. Moreover, the velocity was observed to increase from 70 to 80% acetylene to values which are in fair agreement with the complete equilibrium calculations. It was suggested, therefore, that delays in nucleation of solid carbon particles prevent this reaction from occurring within the reaction zone leading to the C-J state until, owing to decreasing temperature and increasing unburned acetylene concentration, the degree of supersaturation becomes great enough to insure adequately fast precipitation of carbon.

The present paper deals with the last two instances of deviations from complete equilibration, since they appeared to be best authenticated by previous work.

## Experimental Details

In general, the equipment and experimental procedures were similar to those described previously (3). The following points of difference should be noted.

In addition to piezoelectric velocity gages previously described, also the ionization gages (11) were used occasionally. They appeared to function at least as well as the others.

In the light of previous experience, it was clear that emphasis should be placed on tests of stability and constancy of detonation velocities. Therefore, seven to eight equidistant gages (10 - 12 cm apart) were mounted in the experimental sections of each of the detonation tubes. Only those runs in which at least six of these gages gave pips on the CRO record were used for velocity calculations. The velocities were obtained by the method of least squares from the time intervals between gage signals. The standard deviations of the velocities so calculated ranged between 3 and 8 m/sec. Once in a great while a gage signal appeared many microseconds too soon or too late. Such signals were not used in the calculations, as they were traced to solid deposits on the gage bodies.

In the course of these experiments the gas mixing and storage system underwent several modifications and, because of explosion hazards, was eventually converted to an all-metal system, with an O-ring sealed piston pump providing for the mixing and the transfer of gases from stainless steel storage tanks. Airco oxygen containing 0.5-0.6% argon and 0.0-0.1% nitrogen and standard grade Linde argon containing 0.4% nitrogen were used without further purification. Acetylene from a Prestolite tank was passed through Dry Ice traps to eliminate acetone and other high-boiling impurities. It was then analyzed mass spectrometrically and found to be 99.8% pure, the impurity being very largely methane.

## The Results and Conclusions

The results obtained fall into two categories, those dealing with the lean and those dealing with the rich acetylene-oxygen mixtures. They are considered here in that order.

It has been pointed out by Zeldovich (2) that in branching chain reactions--and most if not all high temperature oxidation reactions are of this type--the last event chronologically is the recombination of free radical intermediates which are first produced in concentrations exceeding thermodynamic equilibrium. As such recombinations, because of large enthalpy decrease, have positive $\sigma$, the summation on the left of [1] should vanish only when equilibrium is attained. The situation is different when a large excess of an inert diatomic gas is added to the system. As it does not participate in the reaction chains, the excitation of its vibrational heat

capacity and its dissociation into atoms might occur largely through random processes of thermal energy exchange. Since the temperature rises monotonically to the C-J state, these processes might be the last to be completed; having negative $\sigma$, they will recede behind the C-J state, according to the Kirkwood-Wood argument. Unfortunately, the inclusion of a large molefraction of an inert gas leads to instability of detonation waves and so to failure of experiments to test the proposition. But mixtures of a large excess of oxygen with a little acetylene may come close to the above condition because here most of the oxygen does not take part in the reaction and yet they support steady detonation waves. The detonations were initiated in an equimolar acetylene-oxygen mixture, which was separated from the mixture being studied by a thin plastic diaphragm. The detonation in the equimolar mixture ruptured the diaphragm and started a detonation in the mixture being observed. With this technique, it was found that mixtures containing less than 5% of acetylene gave distinctly non-steady waves. No detailed measurements were made on these mixtures. The main source of difficulty with other mixtures has been the overdrive from the initiator compartment. It showed itself as a decreasing velocity in the experimental mixtures. To insure against the results being falsified on this score, interval velocities obtained between gages spaced 10-12 cm apart in the experimental sections of the tubes were analyzed by the usual statistical procedures for significant trends and only those runs accepted which gave no evidence thereof. The following Table 1 gives an example of an acceptable run and of one wherein the wave was overdriven. Further tests were made by using the initiator mixture at different initial pressures, so as to vary the shock pressure acting on the experimental mixture. As the following Table 2 shows, there exists a range of initiator strengths within which the same detonation velocity is obtained in the experimental mixture, which is therefore considered to be the steady velocity.

The magnitude of random errors involved in the present measurements is seen from the following. The standard deviation of measured velocities within 44 pairs of runs made under identical conditions was 4 m/sec. The standard deviation within 7 pairs of runs, identical in all respects except that a separately prepared gas mixture was used for each of the runs comprising a pair, was 7 m/sec. The compositions included in this analysis range from the leanest to the richest studied. Systematic errors due to the time standard used, impurities of gases, their deviations from ideality, not allowed for in making up the mixtures, etc. involve together an error certainly less than 0.2% in detonation velocity. Altogether, it would seem that a probable error of 0.3 to 0.4% in each velocity determination is a conservative estimate.

Earlier work from this Laboratory indicated (3,6) that detonation velocities depend on the tube diameter to such an extent that the extrapolation (3) from the widest diameter used (10 cm) to the velocity of the infinite plane wave adds a significant increment. Quite limited measurements suggested also that this correction is

Table 1. A comparison of steady and overdriven waves.

Run A: A steady run made with a 7.5% acetylene-92.5% oxygen mixture at an initial pressure of one atmosphere in the 5 cm tube.

Run B: An overdriven run made with a 6.0% acetylene-94% oxygen mixture at an initial pressure of one atmosphere in the same tube.

| Distance from Diaphragm to Start of Interval (cm) | Gage to Gate Interval Velocity (m/sec) Run A | Run B |
|---|---|---|
| 68.6 | 1764 | 1714 |
| 80.1 | 1763 | 1693 |
| 91.5 | 1755 | 1713 |
| 102.9 | 1760 | 1679 |
| 114.3 | 1761 | 1679 |
| 125.8 | 1758 | 1671 |
| 137.2 | 1769 | 1683 |
| Least Squares Velocity | 1762 | |

Table 2. Initiation experiments made with a mixture of 8.2% acetylene and 91.8% oxygen at an initial pressure of one atmosphere in the 5 cm tube.

| Pressure of Initiator Mixture (Atmospheres) | Velocity (m/sec) in the Experimental Mixture. |
|---|---|
| 3/8 | 1796 |
| 1/2 | 1793 |
| 5/8 | 1792 |
| 3/3 | 1790 |
| 7/8 | 1791 |
| 1 | 1792 |

very sensitive to the composition of the mixture. Considerable effort was concentrated therefore now on determining the diameter effect for variously composed mixtures. Figure 1 shows the results for all those mixtures with which experiments were made in three or four different tubes. The data obtained with the smallest (1.3 cm) tube are of doubtful significance because of experimental imperfections but they suggest an only limited validity of the linear relation between velocity and inverse tube diameter. The other data shown give an extrapolation to infinite diameter of about 7 m/sec, which agrees well with the previously determined (6) diameter effect of 9 m/sec for equimolar mixtures. However, the new data show that within the experimental error the diameter effect is independent of composition except possibly for the 75 - 25% mixture. Velocity data in two tubes of different diameters were obtained for several other mixtures. They confirm the independence of the diameter effect from composition, shown by Figure 1. The velocities measured by Guenoche and Manson (12) were obtained in tubes of rather small diameters. Hence extrapolations to infinite diameter are quite uncertain, but the magnitude of the correction appears to be even less on the basis of their data than the 7 m/sec suggested above. In any case, it is certain that this correction is almost within the experimental error of the present measurements.

To compare the experimental extrapolated velocities with those calculated by the thermo-hydrodynamic procedure, it is necessary to make a correction for gas non-ideality in the C-J state. If the Schmidt equation (13) is used for this purpose, as seems entirely legitimate, the correction amounts to ca. -0.15% (14) and thus just about cancels the increase in velocity on extrapolating to infinite diameter. Hence velocities obtained in the 10 cm tube are directly compared below with theoretical velocities.

The hydrodynamic velocity calculations on lean mixtures were kindly performed by Dr. R. E. Duff of the Los Alamos Laboratory, using IBM computing machines. Aside from the uncertainties in the thermodynamic functions used, all taken from the NBS tables (15) or extrapolated therefrom to higher temperatures by standard procedures, the calculations are accurate to better than 0.1% in the composition and temperature of the C-J state. They were obtained by a method of successive approximations, analogous to that employed in manual calculations but adapted for machine operation. The following species were allowed for: $CO_2$, CO, $H_2O$, OH, $H_2$, H, $O_2$, O. The concentrations of carbon vapor, $H_2O_2$ and $O_3$ are too small to affect the calculations; the chemical potential of the radical $HO_2$ is not known, but, by analogy with ozone, it may be safely omitted as of no importance in equilibrium calculations. In computing the detonation velocities from the parameters of the C-J state, Dr. Duff assumed that the sound velocity involved in this calculation is that corresponding to mobile equilibrium. Brinkley and Richardson (16) concluded, however, that the velocity corresponding to frozen equilibrium is correct and

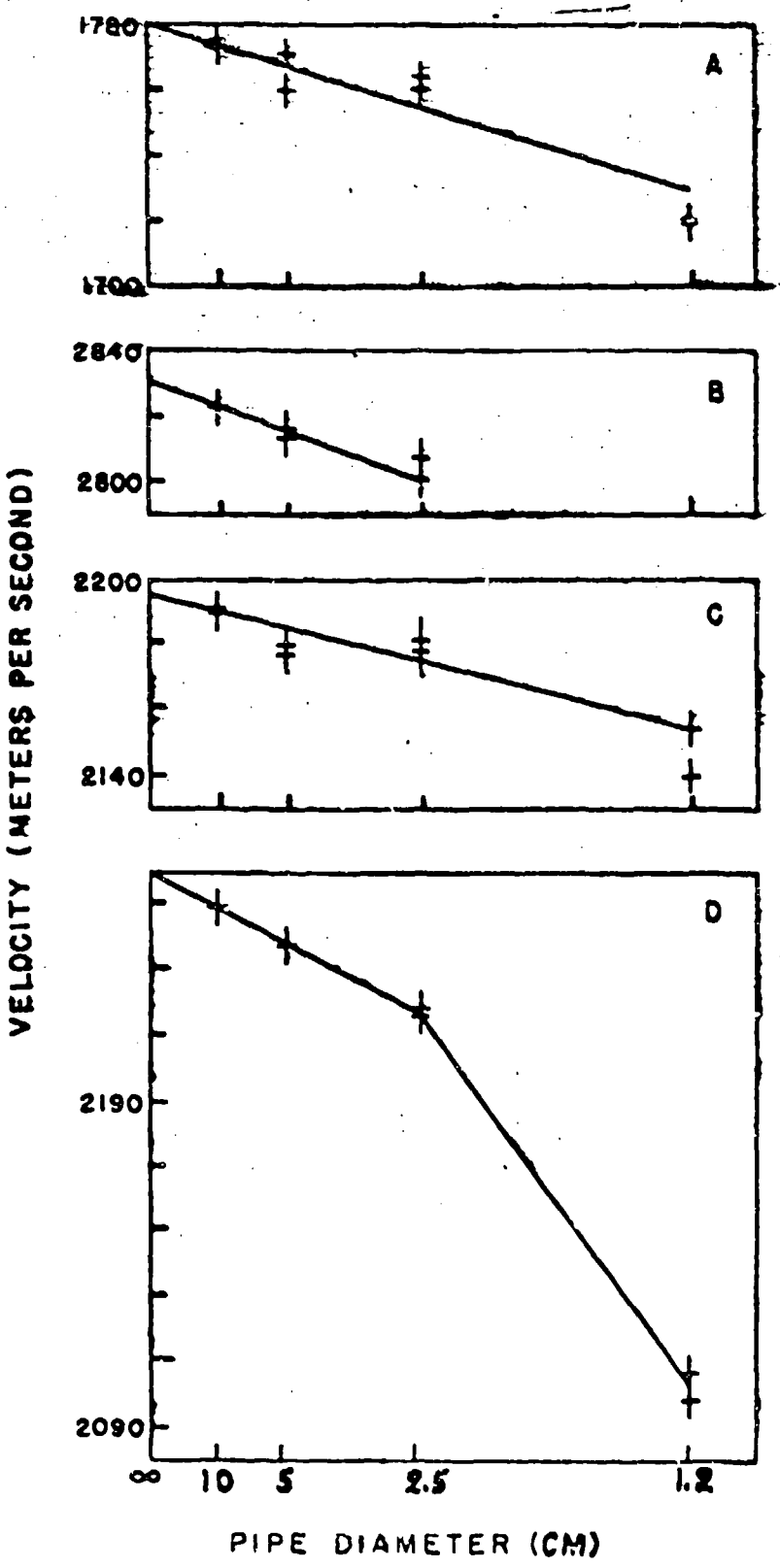


**Figure 1.** Detonation velocity in acetylene-oxygen mixtures in tubes of different diameter plotted against inverse tube diameter. Graph A: 7.5% acetylene; Graph B: 53% acetylene; Graph C: 70% acetylene; Graph D: 75% Acetylene.

Kirkwood and Wood (8) now confirm this deduction. The corresponding correction to Dr. Duff's velocities amounts, however, to only +4 m/sec in the mixture containing 25% acetylene and is less in leaner mixtures. His values, therefore, were used without correction.

The problem of calculating non-equilibrium detonation velocities has, of course, no single answer because so many alternative assumptions may be made and each suffers from artificiality. At our request, Dr. Duff calculated also non-equilibrium velocities assuming that the vibrational heat capacity of unreacted oxygen was not excited ($C_v = 5/2$ R) but that its degree of dissociation into atoms was the same as if it has the normal chemical potential. This assumption changed the other equilibria only insofar as it changed the C-J temperature of the reaction products. Rather rough estimates carried out by us indicate that the supression of oxygen dissociation should double deviations from equilibrium velocities, compared with calculations of Dr. Duff.

In Figure 2 the lower curve shows the equilibrium velocities, while the upper curve shows velocities with vibrationally non-excited oxygen. The experimental data are shown by circles. Their position on the diagram is such as to reject definitely the possibility of non-attainment of equilibrium in these mixtures. The earlier results (6) obtained in this composition range undoubtedly were too high because of overdrive, not sufficiently guarded against at the time. We also obtained such high velocities, but they invariably showed downward trends. The earlier results (6) on richer mixtures (with which ours agree at 25% acetylene) have shown that between 50 to 25% acetylene there exists perfect agreement between experiments and equilibrium calculations. Now this agreement has been extended down to 5% acetylene. This is instructive because in mixtures containing nearly 50% acetylene the major dissociation equilibrium is that of hydrogen. In the very lean mixtures, on the other hand, the dissociations of oxygen and water vapor are thermodynamically of greater importance. The kinetic mechanisms by which these dissociations tend to equilibrium are undoubtedly different and yet, as the measurements show conclusively, they all reach equilibrium in the C-J state. It might be noted in this connection that in comparison with the other methods of studying gaseous equilibria at very high temperatures, the technique of detonation velocities is extremely precise. Thus if the entire residual discrepancy between the experiments and calculations is regarded as an experimental error in temperature estimation, the measurements on these acetylene-oxygen mixtures permit the determination of temperatures to better than 1% accuracy in the range from 3000 to 4500° K.

Mixtures of acetylene and oxygen containing excess acetylene are of interest in two respects. In those containing but a small excess of acetylene, the temperature of the C-J state is so high that unburned acetylene must be substantially dissociated into hydrogen and gaseous carbon if the heat of sublimation of the latter is only 141 Kcal (17). Since the alternate value, 170 Kcal, is not as yet

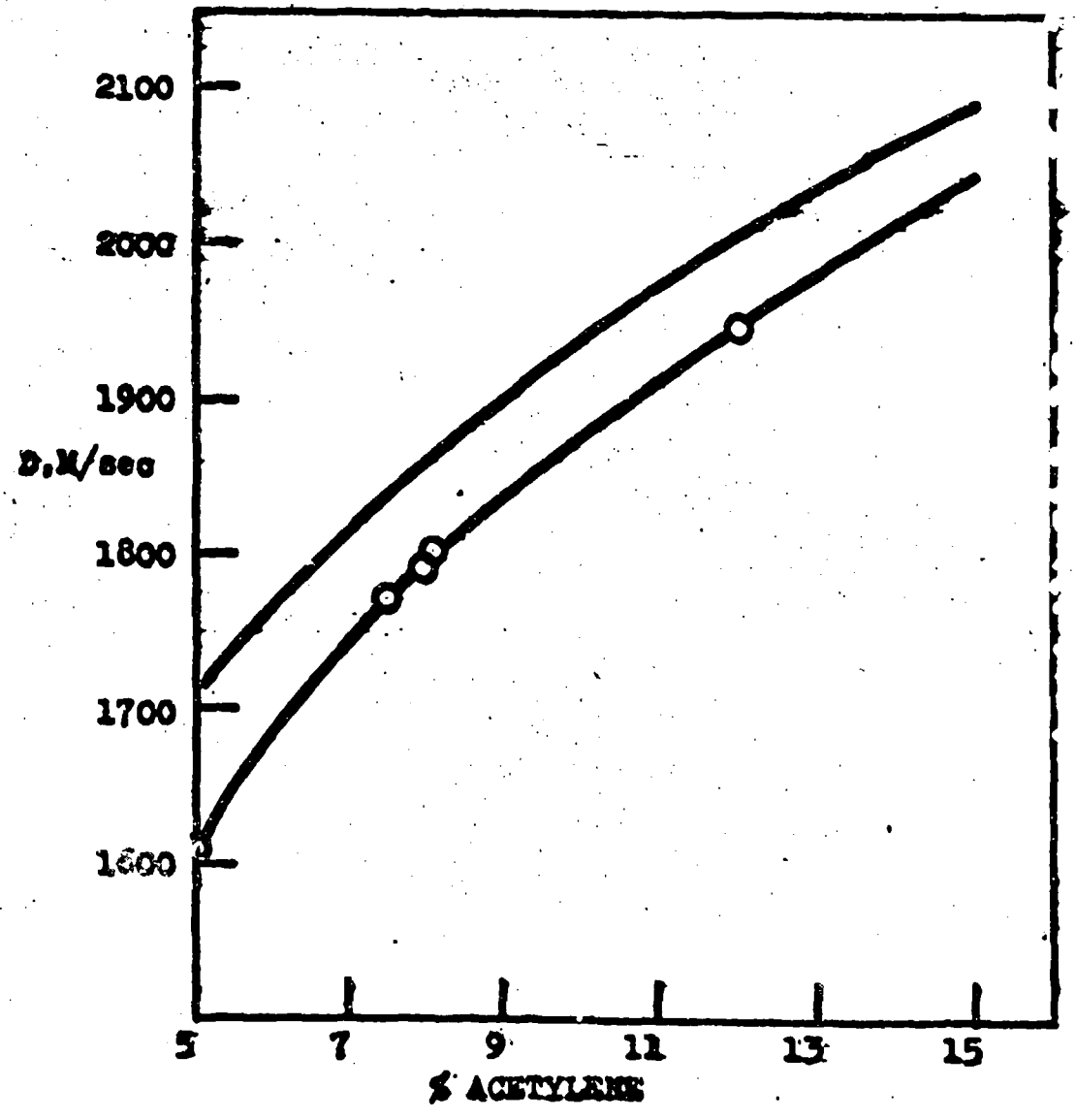


Figure 2. Observed and calculated detonation velocities in lean acetylene-oxygen mixtures. Circles: averages of at least two runs each in the 10 cm tube at 1 Atm. pressure. Lower curve: calculated velocities under the assumption of complete equilibrium. Upper curve: excess molecular oxygen assumed to be non-vibrating but in equilibrium with oxygen atoms.

proven beyond further doubt (5), contributory evidence obtained in the present investigation is of some interest. The experimentally observed velocity in a mixture containing 53% acetylene at 1 atm. initial pressure (cf Figure 1) is 2822 meters, which value should be within 10 m/sec of the true velocity of an infinite plane wave in ideal gases. The calculation of the theoretical velocity was carried out by previously described (3) manual techniques. Thermodynamic functions were the same as previously used (6). Allowance was made in the calculations for the following species: $C_2H_2$, CH, CO, $C_2$, $H_2$, H. Having thus determined the equilibrium composition, pressure and temperature of the C-J state, it was found upon their substitution into the appropriate equilibrium equations that the concentrations of the following specie were too small to alter the results of the calculation, had they been allowed for: $O_2$, $CO_2$, $H_2O$, $CH_4$, $C_2H_4$. The equilibrium concentrations of $C_2$ etc. are not known, but if the assumptions of Glockler (18) are accepted, these carbon specie affect significantly the calculated velocity, by lowering it a few tenths of a percent, only if the heat of sublimation is 141 Kcal. Without allowing for them, this heat of sublimation leads to a calculated velocity of 2750 m/sec. With the 170 Kcal value, the result is 2819 m/sec. If acetylene is assumed to be vibrationally excited, but not dissociated, the result is 2830 m/sec. Were it not vibrationally excited, the result would be sufficiently higher to be in significant disagreement with the experimental figure. Finally, if hydrogen left behind when acetylene is oxidized to carbon monoxide is also assumed not to be dissociated, although vibrationally excited, the velocity is raised to ca. 2900 m/sec. The experimental value is consistent only with the equilibrium calculation assuming 170 Kcal as the heat of sublimation and with the non-equilibrium calculation which excludes the dissociation of acetylene but includes that of hydrogen. The second alternative makes it impossible to assert that the high heat of sublimation has been proven. However, in the context of the previously discussed results on lean mixtures, the supposition that hydrogen is dissociated but acetylene (which plays now a role similar to that of excess oxygen in lean mixtures) while vibrationally excited is not dissociated is so improbable that strong evidence for the high heat of sublimation is believed to have been adduced.

With 55% acetylene, the experimental velocity is 2745 m/sec while the equilibrium calculation, with 170 Kcal as the heat of sublimation, gives 2741 m/sec.

Our early experiments with these and richer acetylene-oxygen mixtures suffered from considerable lack of reproducibility, a fact noted also by other investigators. The cause was eventually traced to loose carbon black which remained in the tube from run to run, was stirred into the fresh admitted gases, and slowed down the detonation wave by the inertia of carbon particles. After the procedure was adopted of removing all loose carbon before each run, entirely consistent data were obtained up to 80% acetylene. At

still higher concentrations, wave instability was regularly observed, presumably indicative of incipient spin which is strong in pure acetylene (19).

In Figure 3 are shown the results on rich acetylene-oxygen mixtures, obtained at 1 Atm. initial pressure in tubes of 10 cm diameter. Within the experimental error, the velocities shown in Figure 3 are identical with extrapolated and corrected velocities. Lines A and B in this figure are interpolations between calculated velocities, the first for the homogenous equilibrium not involving solid carbon, the other for complete equilibrium. Had the heat of sublimation of carbon been assumed to be 141 Kcal, the calculated velocity curve would have started at the same value as curve A for the equimolar mixture, dropped about 70 m/sec lower than the curve shown for the mixture containing 53% acetylene, and then drawn closer again, to become experimentally indistinguishable from it when more than 60% acetylene is present.

In the composition range of 50 to 71% acetylene, the experimental points lie quite close to the calculated curve A. The deviations are undoubtedly within the combined experimental and calculational errors because in richer mixtures, in which the C-J temperature is low and much unoxidized acetylene is present, the calculations which allow only for its dissociations into the CH radicals and into $H_2$ + 2 C (both of which are then entirely insignificant) become rather inadequate, in view of other possible constituents of homogenous equilibrium ($CH_4$, $C_2H_4$, $H_2CO$, etc.) and of uncertainties in the thermodynamic functions of acetylene. Figure 3 shows that at 71% acetylene a discontinuous rise in velocity is observed. This we shall consider in some detail later. Above 71% acetylene the experimental points are far from curve A, but still do not fall on curve B. This discrepancy, however, is not a convincing evidence that complete equilibrium is not established in the C-J state. Firstly, the calculations, as noted above, are quite uncertain in this region. Secondly, the calculations assume that graphite is the solid product. Actually formed is extremely finely divided active carbon, whose chemical potential is probably well above that of graphite, so that less energy is released for wave propagation by its formation, as was noted already in the earlier publication (6).

Figure 4 shows the interval (gage to gage) velocities for mixtures containing close to 71% acetylene. Each point is the average of two or more runs. With 70% acetylene a normal velocity is observed all along the tube. The initial velocity with 71% is lower (and hence close to curve A of Figure 3), but some distance down the tube the velocity undergoes a nearly discontinuous change, followed by a more gradual rise. With 72% acetylene only the high velocity is observed. There appears to be a substantial upward trend in velocity which is statistically just significant. The same is true of the upward trend observed with the 75% acetylene mixture.

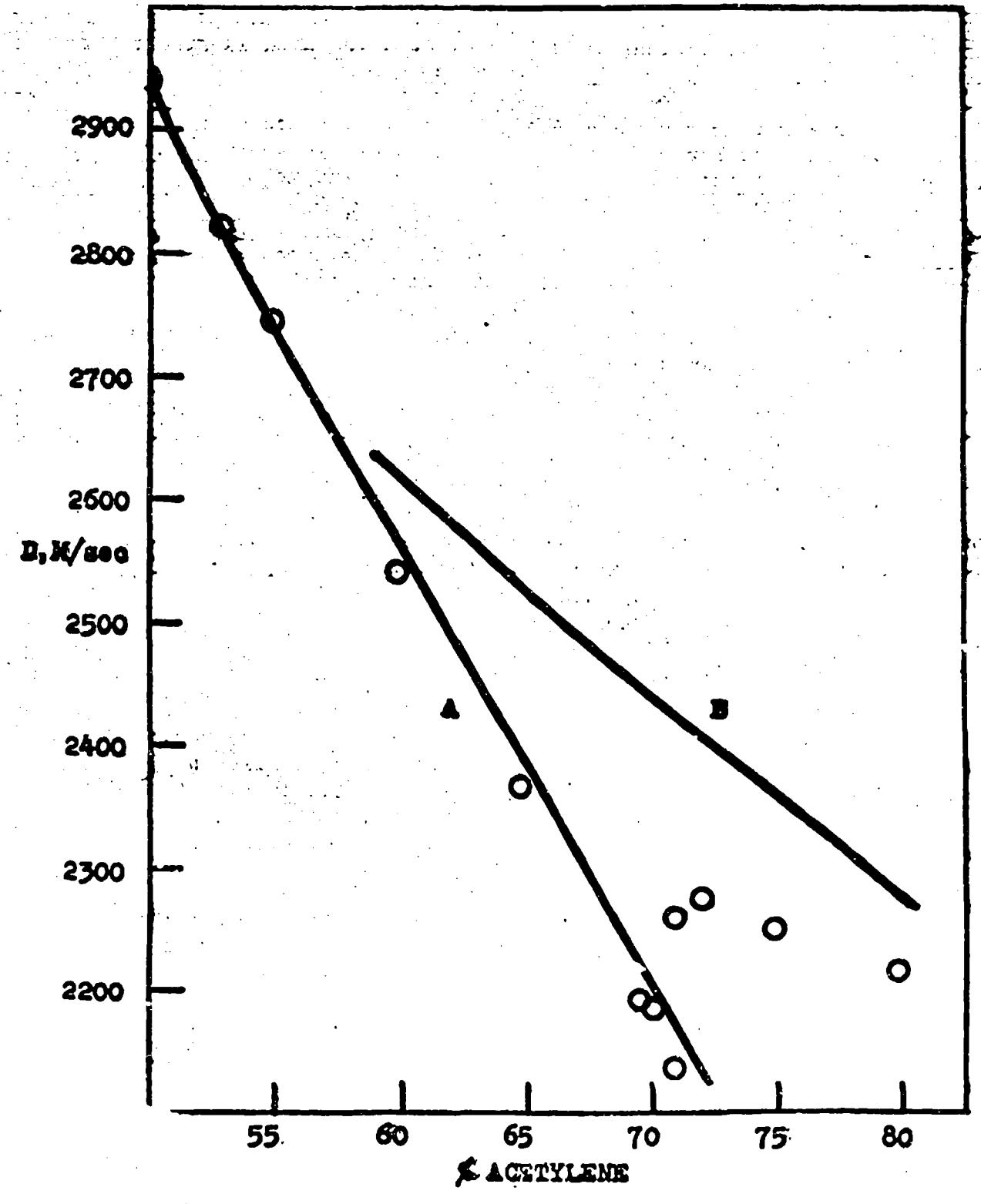


Figure 3. Observed and calculated detonation velocities in rich acetylene-oxygen mixtures. Circles: averages of experimental data except for velocities at 50% and 80% acetylene which are taken from reference (6). Lower curve calculated on the assumption of homogenous equilibrium only. Upper curve includes solid carbon among reaction products.

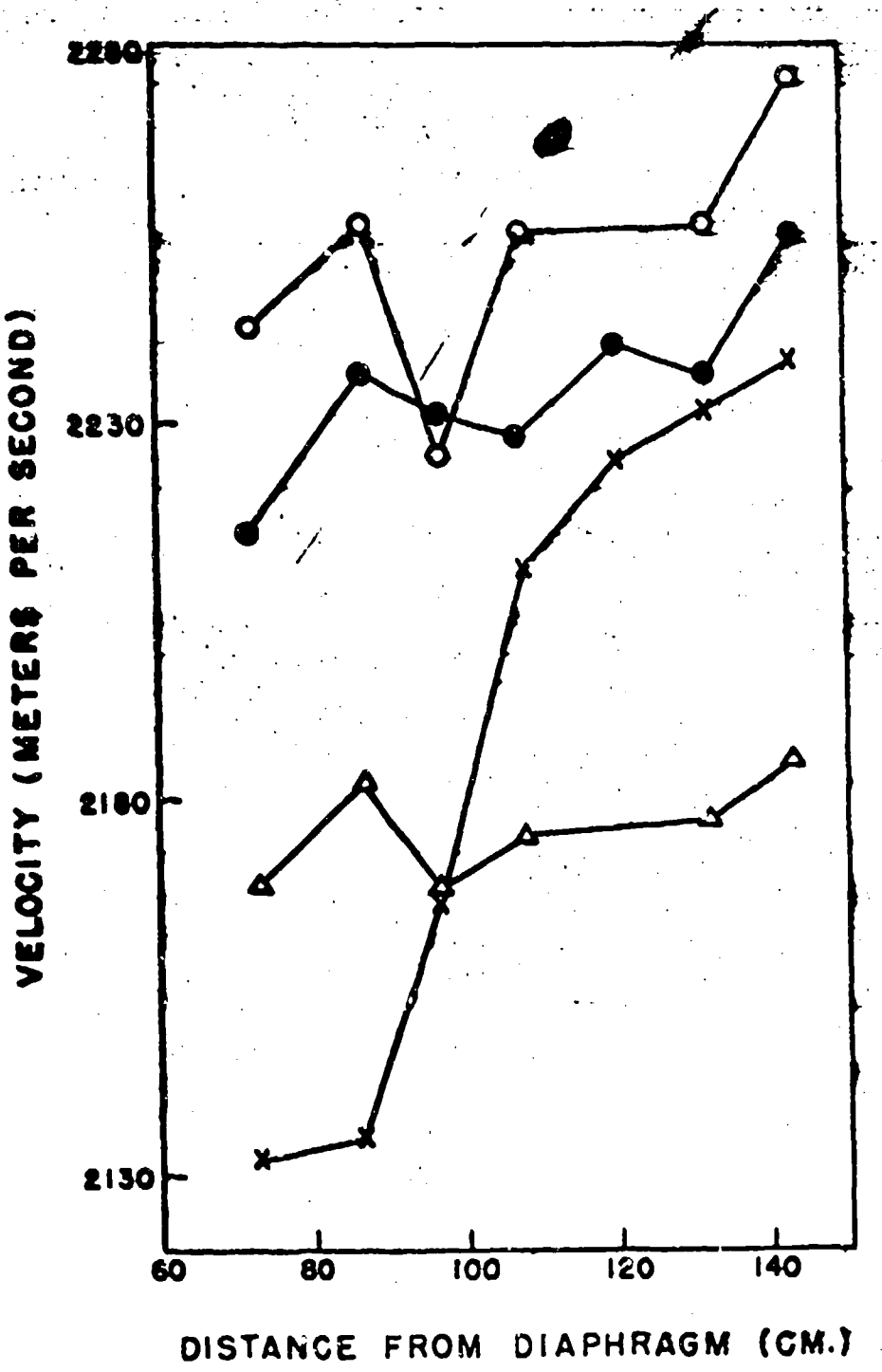


Figure 4. Detonation velocity as a function of distance from the plane of initiation. Triangles; 70% acetylene; crosses; 71% acetylene; dots; 72% acetylene; circles; 75% acetylene.

Thus the limiting steady velocities in these mixtures are probably higher than shown in Figure 3 and lie therefore closer to the theoretical curve.

We believe that these observations represent the first experimental examination of the situation envisaged by Doering and more precisely by Kirkwood and Wood, that equation [1] is satisfied for two consecutive states of the system, with an intervening period of negative values of the function involved. In our case, the function might go negative, after the homogenous equilibrium has been established, because of energy losses to the walls. This is suggested by the observed difference in the behavior of the waves in the 5 and 2.5 cm tubes. In the latter the transition to high velocities occurs much farther from the point of initiation than in the 5 cm tube.

In accord with Doering's general concept, we believe that the condensation of carbon starts a substantial distance behind the shock front because of delays in nucleation, and so it occurs in the rarefaction wave following the homogenous reaction. As the rarefaction wave comes less steep with the progress of the wave down the tube (20), the energy released in the carbon condensation reaction develops a finite pressure wave, which is able to advance toward the C-J state because of its locally supersonic velocity. At some instant it reaches the C-J state, and from this time on the energy released by the carbon precipitation commences to contribute to the wave propagation because, within the entire region from the primary shock to the carbon precipitation zone, the gas is now moving with subsonic velocity relative to the shock front. If the new stationary state is established instantly, the change in the detonation velocity should be discontinuous, but the observed upward trends after the initial rapid change suggests that the transition takes some time. In fact, the velocity trends noted in the 72% and 75% mixtures may be due to similar transitions having taken place too near the diaphragm to be observed. On the other hand, had we had available very long tubes, we might have observed, much farther from the diaphragm, transitions in leaner mixtures.

When the transition to the new C-J plane has been completed and the wave has again attained a stationary character, the structure of its steady state region is probably as follows. Behind the shock front there is a zone of oxidation reactions (von Neumann spike), probably of quite short duration. Thereupon follows a region of substantially constant pressure, in which no rapid reactions take place; finally comes the region of carbon precipitation from residual acetylene with a further drop of pressure, ending in the C-J state. Such structure would be quite analogous to that reported recently for non-spinning detonation waves in pure acetylene by Duff, Knight and Wright (19), except that there the initial reaction zone is absent because of lack of oxygen.

The existence of the second reaction zone and its motion relative to the front of the detonation wave should be observable optically because of probable accompanying changes in luminosity. Experiments with a smear camera are now underway to demonstrate its existence.

It remains to describe some experiments which are perhaps inconsistent with the interpretation advanced above. If one uses identical partial pressures of acetylene and oxygen as in the previously described experiments, but adds some argon, the effect should be first of all a lowering of temperature in the C-J state and therefore an increase in the degree of supersaturation with respect to solid carbon. Therefore, we expected that in such triple mixtures the transition to higher velocities would occur at substantially lower acetylene:oxygen ratios. Upon adding 114 mm Argon to 1 Atm. of acetylene-oxygen mixtures, the discontinuous transition was indeed observed with the acetylene-oxygen ratio varying from 69:31 to 71:29. But the addition of 190 mm of argon did not shift the transition to still lower acetylene concentrations. The experiments were not very reproducible and are inconclusive. Smear camera investigation, now underway, may provide better information on the internal structure of these complex detonation waves and perhaps serve as a technique for a quantitative study of the kinetics of condensation of carbon.

It is a pleasure to acknowledge the support of this research by the Office of Naval Research under Contract N5ori-076, T.O. XIX, NR-053-094, with Harvard University.

## Bibliography

1. B. Lewis and J. B. Friauf. J.A.C.S. 52, 3905 (1930)

2. Y. B. Zeldovich, Theory of Combustion and Detonation of Gases (translated from Russian), Technical Report No. F-TS-1226-IA (GDAM A9-T-45), Air Material Command, Dayton, Ohio

3. G. B. Kistiakowsky, H. T. Knight, and M. E. Malin, J. Chem. Phys. 20, 876 (1952)

4. J. M. Hendrie, J. Chem. Phys. 22, 1503 (1954)

5. W. A. Chupka and M. G. Inghram, J. Chem. Phys. 22, 1472 (1954)

6. G. B. Kistiakowsky, H. T. Knight, and M. E. Malin, J. Chem. Phys. 20, 884 (1952)

7. G. B. Kistiakowsky, H. T. Knight, and M. E. Malin, J. Chem. Phys. 20, 994 (1952)

8. J. G. Kirkwood and W. W. Wood, J. Chem. Phys. (in press)

9. W. Doering, Ann. phys. 43, 421 (1943)

10. D. J. Beretta, E. F. Greene, and G. B. Kistiakowsky, J.A.C.S. 72, 1080 (1950)

11. R. E. Duff and H. T. Knight, Rev. Sci. Inst. (in press)

12. H. Guenoche and N. Manson, Rev. de l'Inst. Francais du Petrole et Annales des Combustibles Liquides 9, 214 (1954)

13. H. Eyring, R. E. Powell, G. H. Duffey, and R. B. Parlin, Chem. Rev. 45, 69 (1949)

14. In reference 3, through an arithmatical error pointed out to us by Dr. R. E. Duff, this correction was estimated to be ca. 0.4%.

15. National Bureau of Standards, Selected Values of Thermodynamic Functions (1945, 1947, 1949)

16. S. R. Brinkley, Jr., and J. M. Richardson, Fourth Symposium (International) on Combustion (Williams and Wilkins Company, Baltimore, 1953), page 450

17. Th. Doehaerd, P. Goldfinger, and F. Waelbroeck, Bull Soc. Chim. Belg. 62, 498 (1953)

18. G. Glockler, J. Chem. Phys. 22, 159 (1954)

19. R. E. Duff, H. T. Knight, and H. R. Wright, J. Chem. Phys. 22, 1618 (1954)

20. G. B. Kistiakowsky and P. H. Kydd, J. Chem. Phys. (in press)

# ON THE STRUCTURE OF A DETONATION FRONT*,** 8

W. R.Gilkerson*** and Norman Davidson
Gates and Crellin Laboratories of Chemistry
California Institute of Technology
Pasadena, California

## ABSTRACT

An effort was made to observe the structure of the reaction zone for a detonation in a gas. Detonations in a 50%$H_2$:50%$O_2$ mixture at 0.035 atm. pressure containing 1% $I_2$ were initiated by shock waves in a shock tube. Because of ignition delays and the short length of tube available, the detonations did not settle down to a steady state and were of unexpectedly high velocity. The iodine served as a colorimetric indicator for the shock front. The light output of the detonation is a step function of time with a front coincident with the shock front within 2-3 $\mu$ sec. The experiment indicates that the reaction zone is less than $10^4$ collisions thick. A crude theoretical estimate of the reaction zone thickness of 1000-4000 collisions is made. Possible chain initiating steps are also considered.

*Research supported by the O.N.R., Project NR 051-248.
**This paper has been submitted for publication to the Journal of Chemical Physics.
***Present address: Department of Chemistry, University of South Carolina, Columbia, S. C.

The v. Neumann theory of detonation (1) assumes that the front consists of a shock wave which compresses and heats the unburned gas, thereby initiating combustion, and a reaction zone in which the temperature rises and the density falls as the combustion proceeds. The plane behind the reaction zone where the high temperature equilibrium essentially obtains is called the Chapman-Jouget (CJ) plane for an ordinary detonation.

The experiment described herein is an attempt to observe the thickness of the reaction zone for a detonation in a hydrogen-oxygen gas mixture in a glass tube. It has been successful only in establishing an upper limit for the thickness of this zone under certain special conditions. Kistiakowsky (2) has observed the density profile for a detonation in a mixture of oxygen, acetylene, and methyl bromide, presumably at 1 atm. initial pressure, by x-ray absorption, and reports that in this system the reaction zone is less than 1 mm thick.

The basic idea of the experiment is to observe a detonation in a $H_2$-$O_2$ mixture containing a small amount of $I_2$. Light absorption provides information about the concentration of iodine and therefore about the shock front. This can be compared with the position of the combustion zone as manifested by light emission by the reacting mixture.

The experiment was carried out in a shock tube, and some of its features may be described by reference to figure 1a. When the membrane breaks, the expansion of the high pressure gas, hydrogen, into the low pressure reaction mixture results in a strong shock wave which initiates combustion. We call the resulting detonation a supported detonation because the "push" by the high pressure driving gas prevents the formation of a rarefaction wave behind the CJ plane, as is characteristic of an ordinary detonation. For the actual pressure ratios used, the detonation is somewhat stronger than is a free detonation. This subject is discussed in detail below.

## EXPERIMENTAL

The shock tube and our general techniques have been described previously (3). The driving section is a 180 cm length of 15 cm diameter steel pipe. The shock wave section is a 140 cm length of 15 cm aluminum pipe and a 150 cm length of 15 cm Pyrex pipe. Cellulose acetate membranes are clamped between the steel and aluminum sections. The shock wave chamber could be evacuated to 0.5 $\mu$ pressure and degassed or leaked at a rate less than 0.1 $\mu$ $min.^{-1}$. Tank hydrogen and oxygen (Linde) were passed over Drierite and through flow-meters, mixed, and then passed through the pressure reducing, iodine saturating system described previously (3). After the tube was filled, a sample of the mixture was withdrawn into a one liter bulb and ignited by a hot platinum wire. The water produced was

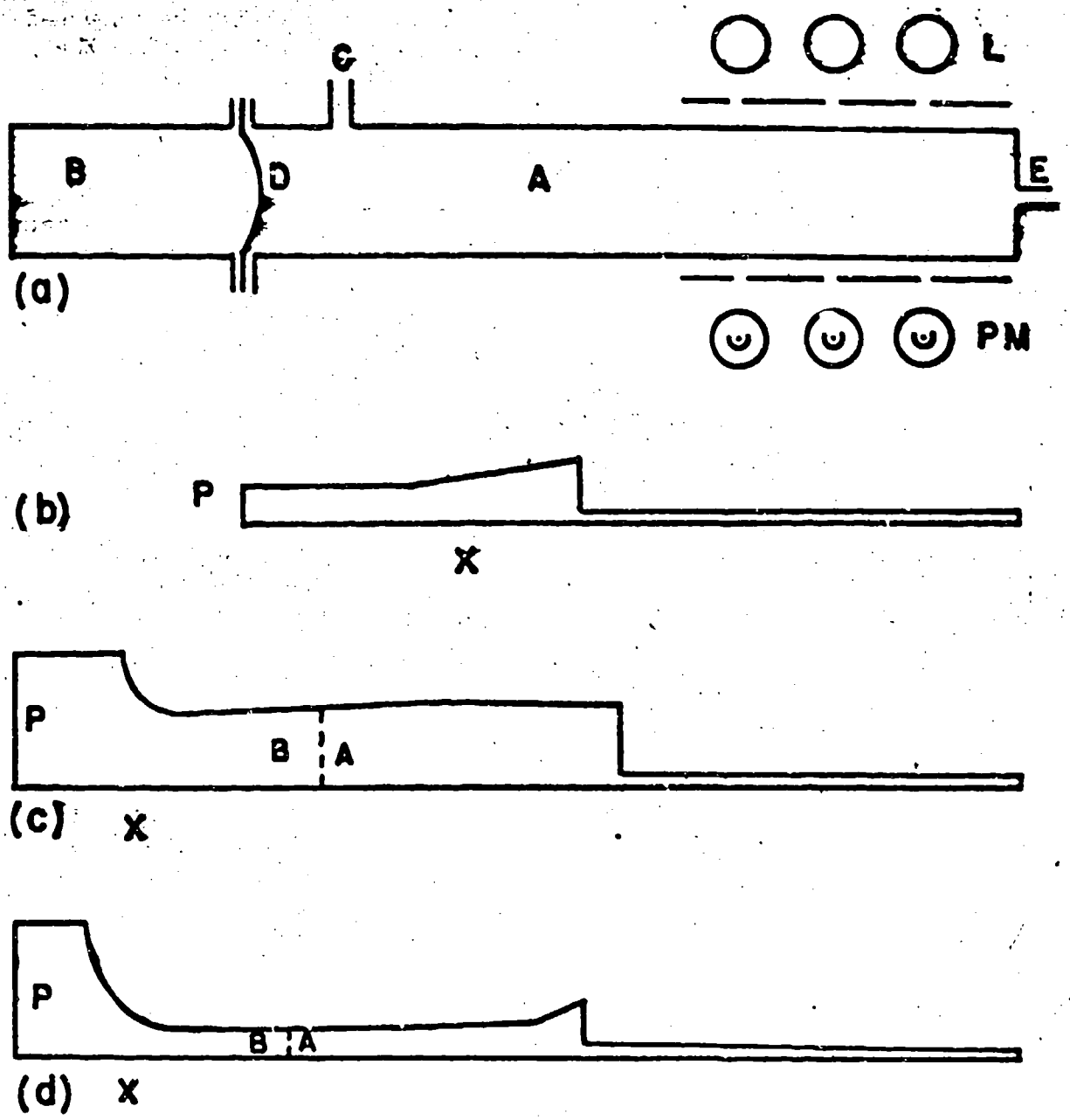


*Fig.* 1. (a) Schematic diagram of apparatus. B, driving gas ($H_2$); D, diaphragm; A, driven gas ($H_2$,$O_2$); L, lights; PM, photomultipliers; C, tc vacuum line; E, gas inlet; (b,c,d) Pressure, P, as a function of distance, x, at sometime after the bursting of the diphragm or the beginning of detonation for a free detonation (b); a supported detonation (c); and an insufficiently supported detonation (d). The dotted lines in (c) and (d) indicate the contact surface between expanded, cold driving gas and shocked, combusted, driven gas.

taken up by Drierite. From the pressure before and after combustion, the ratio of oxygen to hydrogen, $L$ (table II) was computed. This analysis was reproducible and accurate to $\pm$ 0.6%.

## "SUPPORTED" DETONATION

The symbols to be used in this discussion are: $P$ = pressure, $M$ = mean molecular weight of unreacted gas, $V$ = volume per $W$ grams of gas, $H$ = enthalpy per $W$ grams, $S$ = shock velocity, $S_f$ = velocity of a free detonation calculated using the Chapman-Jouget condition, $y$ = material velocity of gas in laboratory system. Subscripts 1 and 2 refer to unshocked and shocked gas at chemical equilibrium respectively.

As is well known, the P,V behavior of a fluid subject to shock compression is defined by the Rankine-Hugoniot (RH) equation, $(P_2 - P_1)(V_2 + V_1) = 2(H_2 - H_1)$. This with the perfect gas law and the thermodynamic conditions for chemical equilibrium between the various components can be used to define the behavior of a detonating mixture, and the RH curve so calculated for $50H_2:50O_2$ at an initial pressure of 0.035 atm. is illustrated in Fig. 2. Useful numerical results are given in Table I. The velocity of any particular shock is $S^2 = V_1^2 (P_2 - P_1)/(V_1 - V_2)$. The tangent illustrated in Fig. 2 defines the slowest shock possible for the mixture provided it reacts to chemical equilibrium. We refer to this wave as a free detonation; the gas at the CJ plane has a material velocity $y$ and a temperature such that

$$S - y = V_2 (P_2 - P_1)^{1/2} (V_1 - V_2)^{-1/2}$$

is the local sound velocity. For a shock proceeding to point A of Fig. 2, the velocity is greater than that for a free detonation, the temperature is higher, and $S - y$ is locally subsonic. For a shock proceeding to point B, the velocity $S$ is greater than that for a free detonation, the temperature is lower, and $S - y$ is supersonic.

Fig. 1b,c,d illustrates pressure profiles for several possible experiments. Fig. 1b is for a free detonation originating at the closed end of a tube. A rarefaction originates at the same end and follows the detonation. In a shock tube configuration with a sufficiently large bursting pressure ratio, the pressure profile will be that of Fig. 1c. The push by the driving gas is sufficient to suppress the rarefaction and give a step function shape to the pressure wave. If the bursting pressure ratio is insufficient for the expanding gas from the driving chamber to reach the velocity $y$ at the pressure $P_2$ which obtains at the CJ plane for a supported detonation, then the situation is as depicted in Fig. 1d. There is a rarefaction behind the detonation front and the velocity of the front is the same as that for a free detonation.

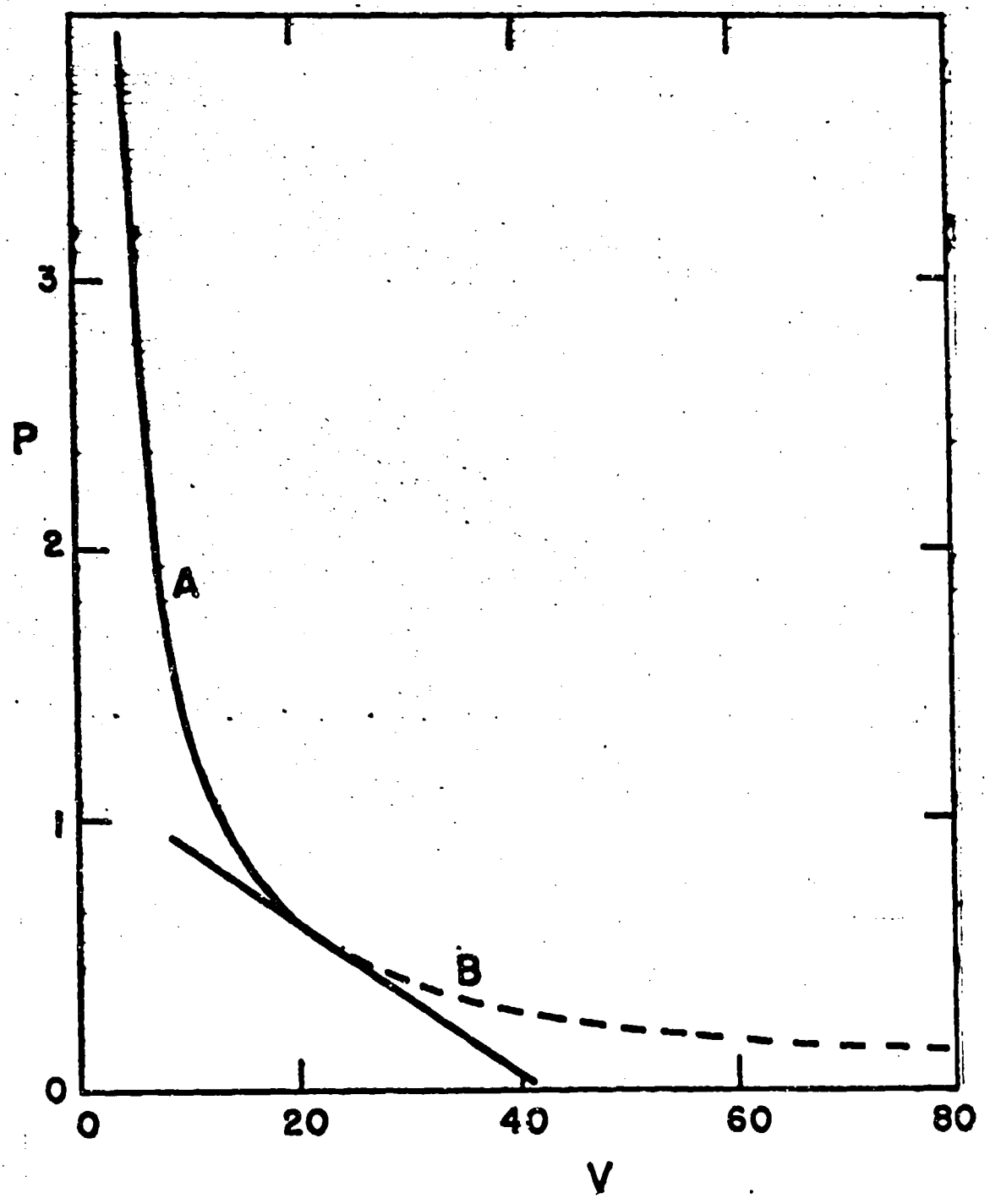


Fig. 2. Rankine-Hugoniat curve for a detonation in 50%$H_2$:50%$O_2$; initial conditions, 0.035 atm., 300°K, $\underline{V}$ = 41.4 liter gram$^{-1}$; $\underline{P}$ in atm., $\underline{V}$ is specific volume, liter gram$^{-1}$

## Table I

### Calculated Properties in 50%$H_2$:50%$O_2$ Detonations

| $P_2/P_1$ | $V_1/V_2$ | $T_2$ °K | S cm/sec x $10^{-5}$ | OH | H | O | $H_2$ | $O_2$ | $H_2O$ |
|---|---|---|---|---|---|---|---|---|---|
| | | | | mol fractions | | | | | |
| 112 | 8.90 | 3750 | 3.62 | 0.179 | 0.133 | 0.205 | 0.0760 | 0.209 | 0.199 |
| 75.3 | 6.94 | 3500 | 3.57 | .168 | .0915 | .153 | .0670 | .244 | .276 |
| 16.0 | 1.84 | 3000 | 2.20 | .124 | .0492 | .0811 | .0545 | .256 | .435 |
| 9.50 | 1.15 | 2900 | 3.09 | .114 | .0441 | .0736 | .0505 | .262 | .456 |
| 3.46 | 0.444 | 2750 | — | .104 | .0430 | .0702 | .0485 | .268 | .467 |

(initial conditions, 0.035 atm., 300°K, thermodynamic data from "Selected Values of Chemical Thermodynamic Properties," National Bureau of Standards, Series III, 1950).

The equation relating the velocity ($v_4$) and pressure ($P_4$) of the gas from the driving chamber expanding from the pressure $P_3$, if the initial velocity of sound be $a_3$ is

$$v_4 = (2a_3/\gamma - 1)\left[1 - (P_3/P_4)^{(\gamma-1)/2\gamma}\right].$$

By matching $v_4$ and $P_4$ to $v_2$ and $P_2$, the shock velocity vs. bursting pressure graph in Fig. 3 is obtained. The upper arm of the curve is the predicted steady state detonation velocity as a function of bursting pressure for an ideal shock tube. The lower dotted arm of the curve represents computed velocities for a transition to the dotted arm of the RH curve, Fig. 2. Gas on this arm of the RH curve is in an unstable condition in that the velocity $S - y$ is supersonic and a shock transition to the upper arm of the RH curve is possible. The transition to the dotted arm of the curve is impossible in the v. Neumann description of a detonation in which combustion is preceded by a shock wave. It is conceivable if the combustion is initiated by the diffusion of free radicals ahead of the shock zone and takes place in the few mean free paths that constitute the shock zone. Very high velocities for rather low bursting pressures are possible for this hypothetical case.

The computed free detonation velocity for $50\%H_2:50\%O_2$ at 0.035 atm. is $2.20 \times 10^5$ cm/sec. The velocity at an initial pressure of 1 atm. is $2.33 \times 10^5$ cm/sec.[1]; at the lower pressure, more enthalpy is absorbed in dissociation processes.

The experimental results are not suitable for quantitative comparison with Fig. 3. It should be remarked however that the effect of a small amount of iodine on the calculated curve would be quite small.

## RESULTS AND DISCUSSION

Successful detonations occurred with bursting pressure ratios of 87 or greater, but did not occur with bursting pressure ratios (B) below 80. The theoretical B to just support a free detonation is 35, and shock tube experience indicates that a pressure ca. 10% higher might actually be required. Presumably the failure to obtain detonations at low B is because the shock wave resulting when the membrane breaks is too weak to initiate combustion. The calculated temperature for B = 85 for a pure shock tube experiment with no combustion is 1140°K. It may be recalled that Fay (4) observed the surprisingly low shock ignition temperature for stoichiometric $H_2:O_2$ of 400°K. It is not possible to say which of the many differences between the two experiments is responsible for the striking difference

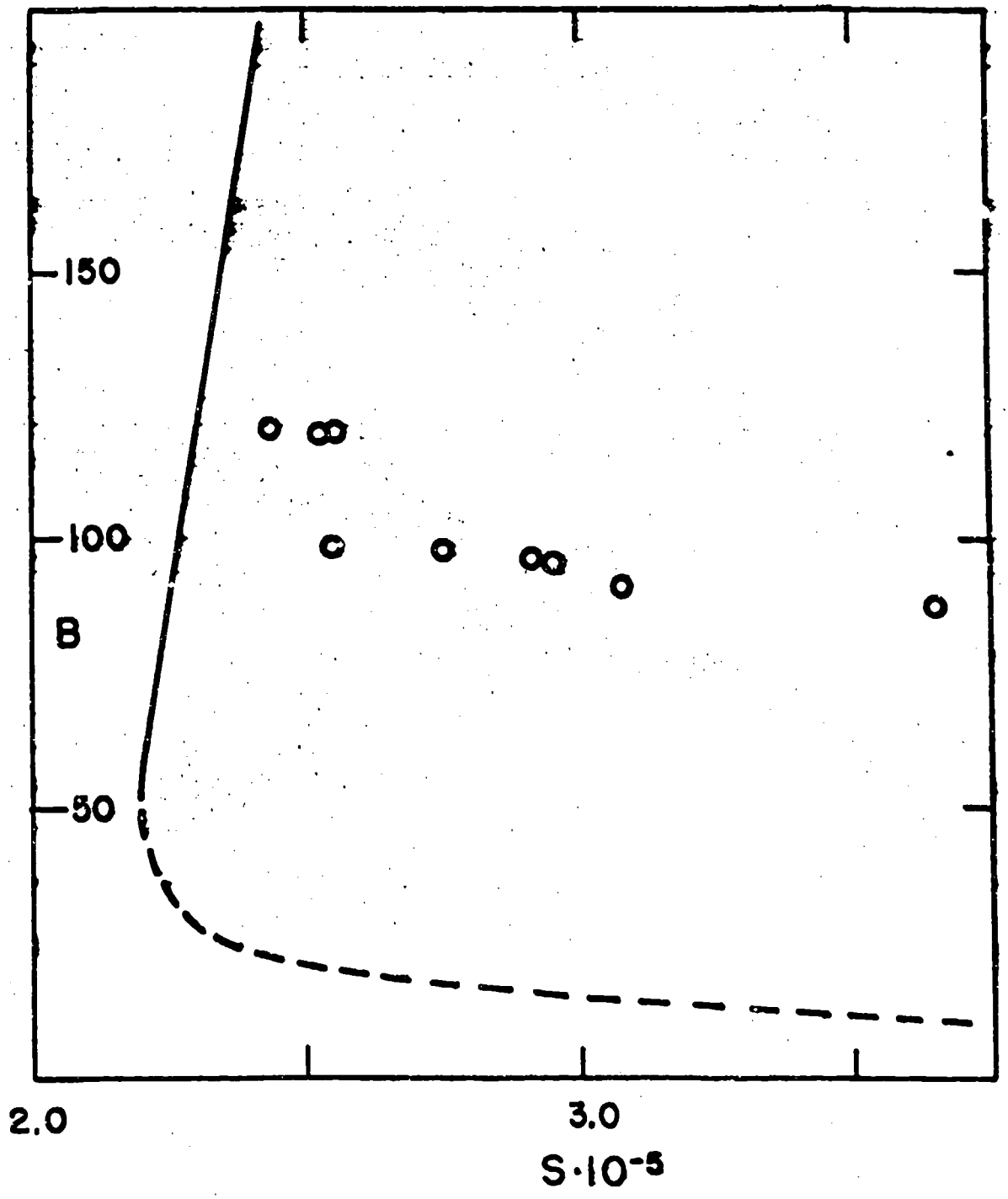


Fig. 3. The bursting pressure ratio, B, vs. velocity, S, cm sec$^{-1}$; ——, calculated for the solid arm of the RH curve, Fig. 2; - - - -, calculated for the dotted (unstable) arm of the RH curve, Fig. 2; O, experimental points, stations 1-3, Table II.

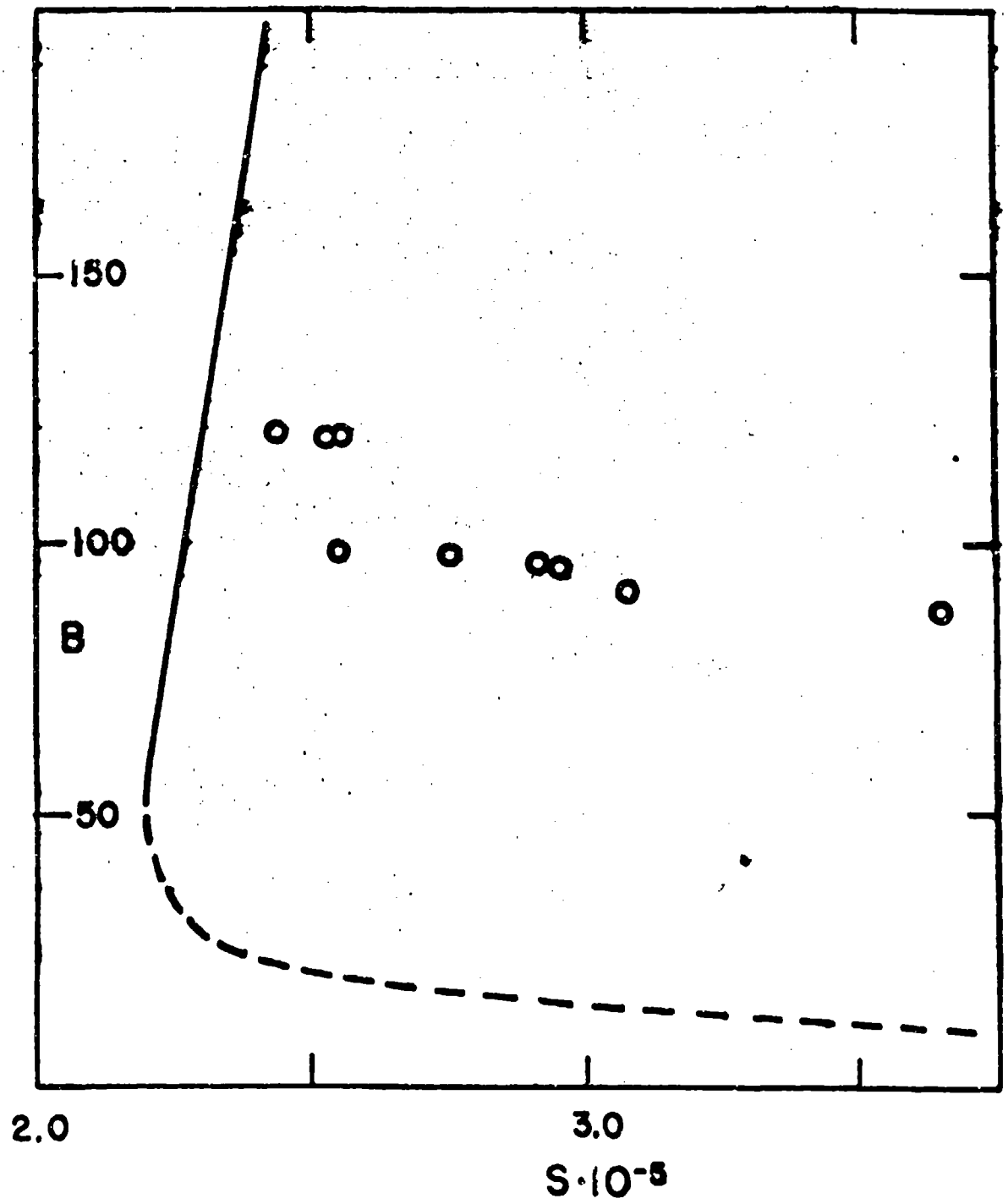


Fig. 3. The bursting pressure ratio, B, vs. velocity, S, cm sec$^{-1}$; ——, calculated for the solid arm of the RH curve, Fig. 2; - - - -, calculated for the dotted (unstable) arm of the RH curve, Fig. 2; O, experimental points, stations 1-3, Table II.

in results. One important possibility is that iodine added in our experiments inhibits ignition.

It is the general belief that it is difficult to maintain stable free detonations at low pressures. Mooradian and Gordon (5) report stable free detonations initiated by shock waves in a 1" pipe for an initial pressure of 0.125 atm. They also report stable detonations in 1:10 Knallgas:argon at 1 atm. pressure. The low pressure (0.035 atm. initial pressure) detonations achieved here are presumably due to the fact that the detonations were supported, and indeed overdriven, so that quenching by the rarefaction wave is absent, and due to the large tube diameter, which deemphasizes attenuation by the walls.

Photoelectric measurements were obtained at three stations 240 cm (16 tube diameters), 260, and 280 cm from the membrane. Observations were made with light beams defined by 2.5 cm by 1 mm slits. The collimation was such that for perfect alignment of the slits and tube, a 3 mm length of the tube was observed by the photomultiplier for light absorption, and a 5 mm length for light emission. A signal due to absorption of blue green light at station 1 was used for triggering the oscilloscope sweeps. Light absorption measurements were made at station two with blue green light from a projection lamp passed through an interference filter with a maximum at 487 mμ and a half-width of 8 mμ, and a transmission of the order of 1/2 - 1% through the rest of the spectrum. In some experiments a sharp cut Corning filter (No. 3385) opaque for wavelengths less than 480 mμ was also used. In others, this cutoff filter was omitted and the light emission by the detonation, which is principally blue light, was superimposed on the light absorption changes. Light output of blue light (Corning filter No. 5562) was observed at station 3. Time intervals between the several stations were measured on the oscilloscope traces. In some runs, the time interval between the first and third stations was also measured with a Potter 1.6 Megacycle Counter Chronograph; these results agreed with the oscilloscope measurements.

Table XI shows quantitative data for most of the experiments. The photoelectric signals of transmission of blue green light (Fig. 4) at station 2 show that (a) for typical experiments, there is no observed compression of the iodine, but that it disappears directly at the shock front; (b) the light output of the detonation is coincident with the shock front within the rise time of either signal (2 - 3 μsec.). The calculated shock temperatures before combustion ($T_s$, Table II) are sufficiently high so that the thermal dissociation of iodine (3) is sufficiently fast to account for (a), without invoking an increased rate of removal of iodine by the combustion process or by an increased rate of thermal dissociation due to combustion.

Observation (b) is, we believe, the most important result of this investigation. The reaction zone is less than 2 - 3 μsec. or 4-6 mm. thick.

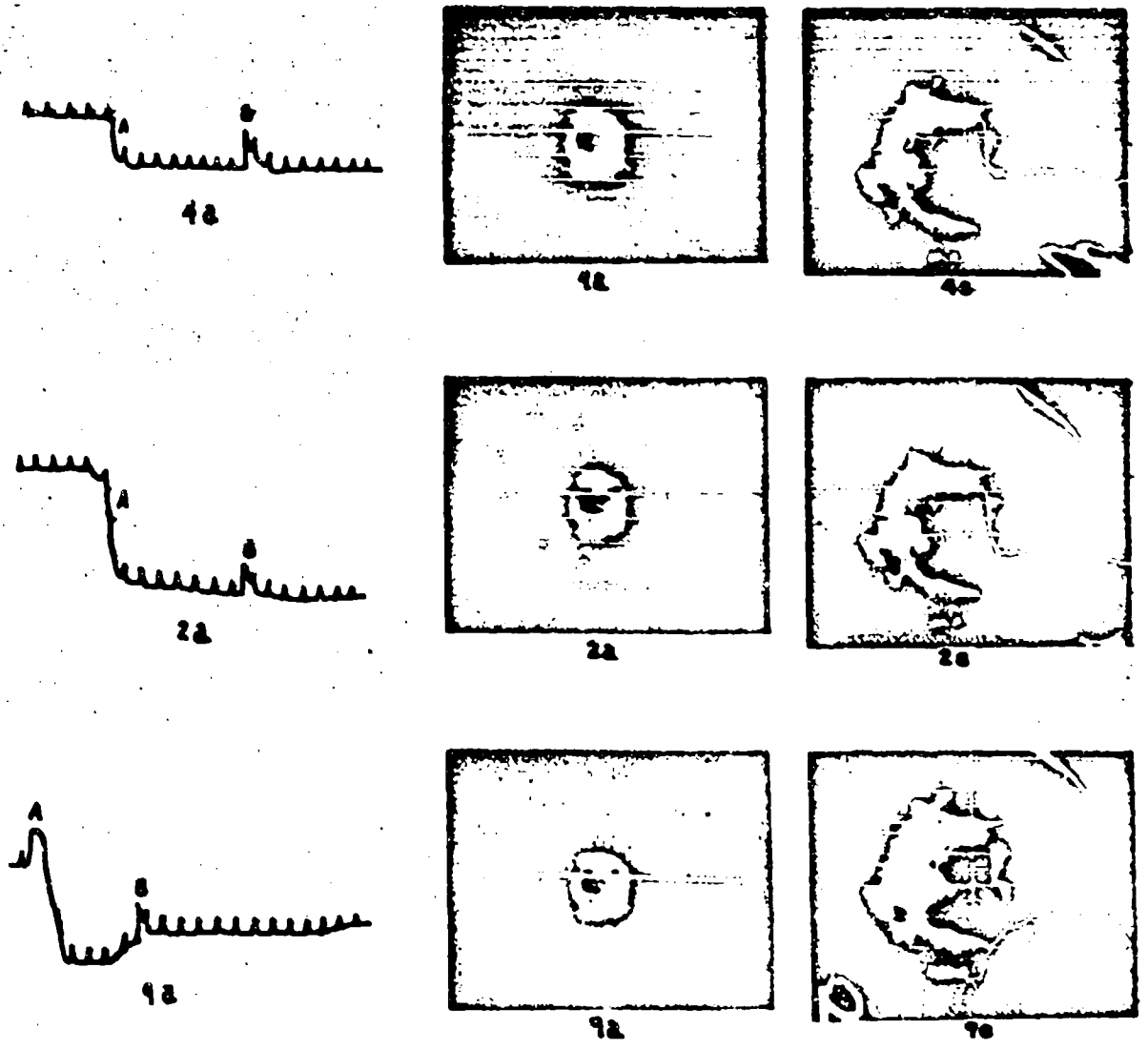


Fig. 4. Oscillograph records of photocurrent for some experiments. 4a, 2a, 9a are principally light absorption records at station 2 for expts. 4, 2, 9 of Table II. A, increase (or decrease (9a)) of light upon passage of the shock front. B, timing pulse from trigger circuit when shock passed station 3. The smudges are cathode glow on the CRO screen and are not significant. The small dips are 10 usec timing markers. The smooth horizontal traces are either voltage calibrations or the cm rulings on the CRO screen. In 4a, the light filter was the 487 mμ interference filter plus the 3385 Corning cut-off filter. The increase in light at the shock front is 1.7 times that expected for complete dissociation of the $I_2$, the additional amount being due to light emission. In 2a, the cut-off filter was omitted, permitting more transmission of blue light. The increase in transmission is 3.7 times that expected for complete dissociation of the $I_2$. 4e, 2e, 9e are light emission records at station 3 through a Corning 5562 blue filter (360-500 mμ). The slit geometry at the two stations was about the same, but the photoelectric sensitivity at station 3 was adjusted to be 1/120 that at station 2.

Table II

Observed Velocities of Supported Detonations

| Experiment No. | B | $S_{1,3}$ (cm/sec x $10^{-3}$) | $S_{2,3}$ (cm/sec x $10^{-3}$) | $T_s$ °K | exp(-17,000/RT) | L |
|---|---|---|---|---|---|---|
| 1 | 121 | 2.43 | 2.50 | 2060 | 1/62 | 0.982 |
| 2 | 120.5 | 2.55 | 2.69 | 2130 | 1/54 | 0.877 |
| 3 | 120 | 2.52 | 2.71 | | | 0.989 |
| 4 | 98.9 | 2.54 | 2.72 | | | 0.902 |
| 5 | 98.0 | 2.75 | 3.46 | | | 0.958 |
| 6 | 96.7 | 2.91 | 2.89 | 2680 | 1/24 | 0.993 |
| 7 | 96.2 | 2.95 | 3.06 | 2760 | 1/22 | 0.967 |
| 8 | 91.4 | 3.07 | 3.56 | | | 0.967 |
| 9 | 87.5 | 3.65 | 3.71 | | | 0.881 |

B = bursting pressure ratio; $S_{i,j}$ = velocity between stations i and j; $T_s$ = computed temperature behind shock for velocity $S_{1,2}$, assuming no combustion, and that $C_p$ = 7/2 R, L = mole ratio of $O_2$ to $H_2$.

* Professor G. B. Kistiakowsky, while refereeing this manuscript, has very generously transmitted the following communication to us. "Using the X-ray absorption technique, we have now observed reaction zones (as zones of high initial density) in $2H_2$-$O_2$ mixtures at pressures from 85 to 20 mm (with some Xe added to increase X-ray absorption). The waves were not overdriven but steady and of normal velocity; the duration of the reaction zone varies from a couple of microseconds at the highest to 20 μsec at the lowest pressure, changing roughly as $1/P^2$. There seems to be no induction period . . . . I suspect that the overdrive and the presence of iodine must have somehow reduced the duration of the zone in the present experiments; or that the light emission starts as soon as reaction starts, not when it essentially ends, and then continues." These results predict that the time of passage of the reaction zone at the pressure used by us would be 11 μsec. for a free detonation. The approximate calculations presented further on in the present paper predict a difference of a factor of about three between a free detonation and the overdriven detonations studied here, so that the time of passage of the reaction zone would be 3-4 μsec., which is only slightly larger than the upper limit estimated by us. The possible explanations proffered by GBK for any such differences are eminently reasonable.

The light emission, as observed at station 3, consists principally of blue light and is a step function of time. There is no build-up of the luminosity nor is there a peak due to chemiluminescence of the reaction zone.

Fig. 4c is an atypical record that was obtained only once. One sees compression of the iodine followed by a long delay with very little dissociation (temperature below 1200°K) followed by a detonation front which is luminous and where the iodine rapidly disappears. We believe that this is due to delayed ignition of the gas behind the shock, so that the pure shock (no combustion) has reached the second light station before the detonation catches up with and merges with the shock. (The recorded velocities for this experiment are not significant because of uncertainties as to the optical signal at station 1 which triggered the various timing circuits.)

In typical experiments Table II shows that the shocks are accelerating as they proceed downstream; although for pure shock waves, the velocities are quite steady (3). Furthermore, the velocities are much higher than the theoretically expected value. Unusually high unsteady velocities at the inception of detonation are commonly observed (6,7). Probably in all of our experiments, combustion did not begin immediately when the membrane broke, but was delayed until the shock propagated some distance downstream. When combustion starts, an unsteady very fast detonation moves up and merges with the shock. A longer tube than was available for the present investigation would be required in order for the steady state behavior of the system to be established.

Assuming that the average no. of collisions per sec. per molecule at room temperature at 1 atm. pressure is $10^{10}$, an average compression factor of 3.5 for the reaction zone to the CJ plane, and an average temperature of ca. 2700°, the observation that the reaction zone is less than 5 mm thick means that the reaction is complete in less than $9 \times 10^3$ collisions. Without attempting a complete solution of the flame equations (8), it is possible to make a rough estimate of the time for complete combustion as follows.

Assume the divergent chain reaction scheme,

| | | $\Delta E$ (kcal) |
|---|---|---|
| $H + O_2 \xrightarrow{k_1}$ | $OH + O$ | 17.0 |
| $O + H_2 \longrightarrow$ | $OH + H$ | 3.0 |
| $OH + H_2 \longrightarrow$ | $HOH + H$ | -15.5 |

At the temperature of a detonation, the conventional low temperature chain breaking step, $H + O_2 \longrightarrow HO_2$, is not of great importance because of the instability of $HO_2$. Three body chain terminations like $H + H + M \longrightarrow H_2 + M$ have k's of the order (3) of $10^{-32}$ $atom^{-2}$ $cc^2$ $sec^{-1}$; even if all of the gas were dissociated into atoms or radicals, their concentration would be ca. $2 \times 10^{18}$ $cc^{-1}$, and the half time for recombination of the order of $10^{32}/(4 \times 10^{36}) = 2.5 \times 10^{-5}$ sec. or $2.5 \times 10^4$ collisions and this type of termination would not affect the reaction kinetics very much.

Reaction (1) is probably the slow step in the divergent chain. One can therefore treat OH and O as intermediates present at low concentration to which the steady state approximation applies and consider the time rate of change of the hydrogen atom concentration. The resulting equation is $d(H)/dt = 2 k_1(O_2)$, and the solution for constant $k_1(O_2)$ is $(H) = (H)_0 e^{2k_1(O_2)t}$. Each chain cycle creates two H atoms and two HOH molecules. In the final mixture, there are ca. $10^{18}$ molecules/cc. If $(H)_0 = 1$ atom/cc, the time required for complete reaction is $18 \times 2.3/(2k_1(O_2)) = 20$ chain cycles.

Baldwin and Walsh (9) have argued that at 520°C, $k_1 = 10^{-14}$ $atom^{-1}$ cc $sec^{-1}$, although Lewis and Von Elbe (10) recommend $k_1 = 10^{-17}$.

The value $10^{-14}$ equated to $PZ \exp(-17{,}000/RT)$ gives P approximately unity. Referring to the initial temperature of the shocked gas (Table II), the Boltzmann factor for $k_1$, at 2060° is 1/62, at 2700° it is 1/22, and at the equilibrium temperature of ca. 3400° it is 1/10. At 1580°, the temperature of the shocked, uncombusted gas in a free detonation, the Boltzmann factor is 1/200. The initial rate of the reaction will always be the slowest and we may

estimate therefore a thickness of the reaction zone of the order of 20 x 200 = 4000 collisions with $O_2$ molecules for a free detonation and 20 x 60 = 1200 collisions for some of the supported detonations of Table II. These estimates are consistent with the experimental observation that the reaction zone is less than $10^4$ total collisions thick. If P, the steric factor for reaction (1) were 0.01 or less, the reaction zone would probably be thick enough to be observed in our experiment. Indeed, the arguments presented above indicate that if a decrease by a factor of ten in the number of collisions to be resolved could be achieved, the structure of the reaction zone could be observed, at least coarsely.

The activation energy of 17 kcal for the rate determining step (1) means that this reaction occurs at only a small fraction of the pertinent collisions even at ca. 2000°K and excludes the possibility mentioned previously of the reaction occurring ahead of the shock wave leading to a transition to the lower arm of the HH curve.

It is of interest to make some equally crude calculations about the chain initiating step. Assume that it is $H_2 + O_2 = 2OH$. Using the approximate rule for reactions of this type that the activation energy in the exothermic direction is 0.25 times the sum of the bond energies, $E_{ACT} = D_{H_2} + D_{O_2} - (1/2)D_{OH} = 70$ kcal. Assuming a steric factor of 0.1 and a rate constant $10^{-11}$ exp (-70,000/RT) $atom^{-1}$ cc $sec^{-1}$ and $(H_2) = (O_2) = 10^{18}$, the initial rate of production of OH radicals is $10^{18}$ $cc^{-1}$ $sec^{-1}$ at 2000° and $10^{16}$ $cc^{-1}$ $sec^{-1}$ at 1580; in each case the rate is ample to initiate the divergent chain.

The relative importance of chain initiation by diffusion of radicals into unreacted gas may be estimated as follows. Let $\ell$ be the thickness of the reaction zone and $c_o$ the concentration of H atoms (the most diffusible species) at equilibrium, and $D$ their diffusion coefficient. In a system of coordinates sitting on the shock wave, the number of H atoms diffusing upstream across any plane into unreacted gas is $D\, c_o/\ell$. The volume of gas flowing across the same plane is $S(V_2/V_1)$, ($V_1/V_2$ is the compression factor) so that the volume rate of production of H atoms by diffusion is $(D\, c_o\, \ell/S)\,(V_1/V_2)$. For $D = 5$ $cm^2$ $sec^{-1}$, which is reasonable for our experiment, $c_o = 10^{17}$ atom/cc, and $\ell = 10^{-1}$ cm, this is $10^{11}$ atom $cc^{-1}$ $sec^{-1}$, $10^{-7}$ - $10^{-5}$ less than the estimated rate of initiation by chemical reaction.

ACKNOWLEDGMENT

We are grateful to Dr. Arthur Bennett and Professor G. B. Kistiakowsky for stimulating advice and discussion.

## LITERATURE CITED


1 Referred to, for example, by Berets, Greene, and Kistiakowsky, J. Am. Chem. Soc., 72, 1080 (1950).

2 G. B. Kistiakowsky, J. Chem. Phys., 19, 1611 (1951).

3 Britton, Davidson and Schott, Disc. of the Faraday Soc., in press.

4 J. Fay, "Fourth Symposium on Combustion," Williams and Wilkins Co., Baltimore (1953), p. 501.

5 A. J. Mooradian, W. E. Gordon, "Gaseous Detonation III. Detonation Limits in Hydrogen-Oxygen Mixtures" ONR report on Contract N7onr-292. Task Order I, with the University of Missouri (1950). See also Ph. D. Thesis by A. J. M.

6 Berets, Greene and Kistiakowsky, J. Am. Chem. Soc., 72, 1086 (1950).

7 A. J. Mooradian, W. E. Gordon, J. Chem. Phys., 19, 1166 (1951).

8 Hirschfelder, Curtiss and Campbell, "Fourth Symposium on Combustion," Williams and Wilkins Co., Baltimore (1953), p. 190.

9 R. R. Baldwin and A. D. Walsh, Discussions of the Faraday Soc., in press.

10 B. Lewis and G. von Elbe, "Combustion, Flames and Explosions of Gases," Academic Press, New York (1951), p. 59.

# HIGH TEMPERATURE THERMODYNAMICS AND GASEOUS DETONATIONS IN MIXTURES OF CYANOGEN, OXYGEN, AND NITROGEN



H.M. Peek and R.G. Thrap
Los Alamos Scientific Laboratory
Los Alamos, New Mexico

## INTRODUCTION

This paper is a report of experiments concerning the validity of the Chapman-Jouguet theory (1,2,3,4,5,6) in the case of mixtures of cyanogen, oxygen, and nitrogen. There are several reports in the literature of similar experiments (6,7), but due to experimental errors and lack of sufficient calculated results in most of them, the only effective investigation of the experimental and theoretical problems involved is that of Kistiakowsky, Knight, and Malin (KKM) (7). The methods used here are essentially the same as those used by KKM, but these experiments cover a wider range of compositions and the calculations are considerably more extensive than theirs.

The detonation velocities have been measured in tubes of two, three, and four in. i.d. for gaseous mixtures of cyanogen and oxygen in the composition range 30 to 55 mole % cyanogen and for a gaseous mixture of cyanogen, oxygen, and nitrogen of composition 40 mole % cyanogen, 40 mole % oxygen, and 20 mole % nitrogen. The results for mixtures of greater than 50 mole % cyanogen were not reproducible and are not further discussed in this paper.

These experimental results are compared with Chapman-Jouguet values computed on an International Business Machines Type-701 digital computer for which the problem was coded by one of the authors (RGT) using standard methods developed at this Laboratory.(8)

## EXPERIMENTAL DETAILS

### A. Preparation of Mixtures

Oxygen and nitrogen were obtained from commercial cylinders after passage through Drierite to remove water. Mass spectrometric analyses of the dried gases were made and the results were used to determine the

final mixture composition. Typical analytical results are as follows: Oxygen tank - 99.8 mole % $O_2$, 0.2 mole % A; Nitrogen tank - 99.7 mole % $N_2$, 0.2 mole % $O_2$, and 0.1 mole % A.

Cyanogen was prepared by the reaction of $Cu^{++}$ with $CN^-$ in concentrated aqueous solution at about 50°C and 0.5 atm. The gaseous products from this reaction were first passed through a trap at 0°C to condense some of the water vapor, then through a silver nitrate bubbler to remove HCN, through a second 0°C trap to remove more water, and finally through a three-ft. long column of Drierite to remove the rest of the water before being condensed in a vessel at liquid nitrogen temperature. The crude product was twice distilled and collected at dry-ice temperature prior to the final distillation and collection at liquid nitrogen temperature in a metal storage vessel equipped with a high-pressure, vacuum-tight valve and pressure gauge. Periodic mass spectrometric analyses indicated run-to-run purities of 99.8 to 99.9 mole % $C_2N_2$. The remaining constituents were HCN and a small amount of water. The water was removed prior to making a mixture by passage through a Drierite column. No attempt was made to remove the small amount of HCN present. The effects of this impurity are discussed below.

Mixtures of the gases were prepared in a vacuum-tight system of valves and copper tubing which connected together a vessel of constant but unknown volume; a constant-displacement, variable-speed, reciprocating pump; and a mercury capillary manometer. In preparing a mixture, cyanogen was admitted to the mixing vessel of volume $V_C$ until pressure $P_A$ was reached. Then by manipulation of appropriate valves, oxygen was admitted to a pressure $P_{A+B}$ under conditions that insured no mass flow out of the system. If there was to be a third component, it was added in a similar manner. All pressures were determined to ± 0.05 mm Hg by cathetometer readings of the capillary manometer. When all the gases had been admitted, the mixing pump was turned on and the gases were mixed by circulation through a closed loop.

The composition of the mixture was determined by solving the following equations for $n_A$ and $n_{A+B}$, modified as necessary if there were three components:

$$P_A V_C = n_A(RT + B_A P_A) \tag{1}$$

and

$$P_{A+B} V_C = n_{A+B}(RT + B_{A+B} P_{A+B}), \tag{2}$$

where $n_A$ is the number of moles of cyanogen in the volume $V_C$ at pressure $P_A$ and temperature T, $n_{A+B}$ is the total moles of gas admitted to the system at pressure $P_{A+B}$, and $B_A$ and $B_{A+B}$ are second virial coefficients appropriate to cyanogen and the cyanogen-oxygen mixture, respectively. The condition of no mass flow out of the system when introducing the gases means that $n_A + n_B = n_{A+B}$, but note that $P_A + P_B \neq P_{A+B}$; i.e., this is the effect of gaseous imperfection of the mixture. The $n_A$ and $n_B$ lead to mole fractions which are then corrected for the deviations from 100% purity according to the mass

spectrometric analyses.

In all of this work the values for $B_A$ and $B_{A+B}$ were calculated from data compiled by Hirschfelder, et al.(9)

B. Detonation Tubes, Velocity Measurement, and Initiators

Detonation tubes of 2.00, 3.00, and 4.00 in. i.d. (± 0.01 in.) were constructed from steel tubing of 1/2 in. wall thickness. The tubes consisted of two flanged sections bolted together and made vacuum-tight by using Neoprene "O" rings. The initiator was located at one end of a 3-1/2 ft-long section and the other 3 ft-long section was used as the velocity measuring section. The detonation tubes could be evacuated and filled by means of copper tubing and appropriate valves attached at the initiator end. The tubes were filled by means of the pump used in making the gas mixture. The final pressure was adjusted by manipulation of appropriate valves, the pressure being determined by cathetometer reading of the capillary manometer.

The detonation tubes were located in a building equipped with heating and ventilation controls such that the tube temperatures were maintained within two or three degrees of 25°C. The time between shots in any given tube was always of sufficient duration to allow the tubes to cool to ambient temperature.

The detonation velocities were measured by ionization gauges and associated electronic equipment similar to that described in detail by Knight and Duff.(10) A gauge consists of two copper wires, 0.020 in. i.d., inserted into a Teflon plug at a separation of 0.125 in., so that the ends of the wires are flush with the end of the plug. The Teflon plugs were machined and drilled, using an appropriate jig to ensure constant plug dimensions and location of gauge wires.

The gauges, seven per tube, were first mounted in modified Amphenol connectors having an appropriate tongue which fixed the orientation of the Teflon plug in the connector. The mounted gauges were inserted into holes in the wall of the measuring section of the tube; the gauges were flush with the inner tube wall and were made vacuum-tight by the use of "O" rings. The gauge-locating holes were carefully machined to ensure a snug fit of the plugs. The great care taken in machining the gauges, inserting the wires, and locating the gauge holes results in a very small error in the determination of gauge distances. As a result of several measurements using a micrometer and standard dowel pins, the gauge distances are known to ± 0.0003 in. The gauge distances were checked from time to time as the tubes were used in making shots.

Across each gauge there is a potential difference of about 200 v which charges a condenser in each gauge circuit; this condenser discharges as the detonation wave passes the gauge. The signal from the gauge nearest the initiating end is used to trigger a Raster-type

oscilloscope on which the remaining six signals are displayed after amplification and shaping. The signals as displayed on the oscilloscope are photographically recorded on Kodak Single Coated X-Ray film which is processed according to the manufacturer's recommendations. The times at which gauges "fired" are determined by reading these records. The average detonation velocity is then computed as the slope of the least squares straight line through the time-distance points. For a given mixture and initial pressure the average detonation velocities from each tube are then used to compute the infinite-diameter velocity required for comparison with the theoretical value. This is done by making a least squares straight line calculation of the velocity as a function of the reciprocal of the tube diameter.

The probable error in the average detonation velocity for any shot was easily determined from the results of the least squares calculation.(11) If this probable error exceeded five or six m/sec, the shot was repeated using a different initiator. It was found, in this way, that the nearly equimolar cyanogen-oxygen mixtures were adequately initiated by a small exploding wire. As the initial cyanogen concentration decreased, it was necessary to use small amounts of PETN; and for the weakest shots, including the mixture with added nitrogen, it was necessary to add a few grams of tetryl.

## EXPERIMENTAL RESULTS

Table I summarizes the results obtained for the cyanogen-oxygen mixtures. Table II contains the results for the mixture containing added nitrogen. The error quoted is the probable error in the slope of the least squares straight line through the time-distance points. In computing the infinite-diameter velocities for one atm initial pressure, as shown in Table III, small variations in initial pressure and composition have been ignored. All shots were made at an initial temperature of 25°C.

There are several sources of error contributing to the uncertainties in the infinite-diameter velocities. First, there is the error of 0.001 in the cyanogen mole fraction due to the HCN impurity. Second, there is the effect of record-reading errors; this is probably the largest experimental error. It is, however, less than four m/sec, since the records could be read to at least $\pm$ 0.2 $\mu$sec. Next, there is an effect of no more than $\pm$ 0.2 m/sec in individual velocities due to gauge distance errors. Finally, the velocity-reciprocal tube diameter points do not lie exactly on a straight line as assumed in making the extrapolation to the infinite-diameter velocity. This leads to errors which are smaller for some mixtures than for others since in some cases several shots of the same mixture were fired at the same tube diameter. The combined effect of all these errors is an uncertainty of about five m/sec in the velocities given in Table III.

TABLE I. Experimental Detonation Velocities in Cyanogen-Oxygen Mixtur

| Composition[a] | | | | D, m/sec | | |
|---|---|---|---|---|---|---|
| $X^0_{C_2N_2}$ | $X^0_{O_2}$ | $X^0_I$ | $P_0$ atm | 4 in. | 3 in. | 2 in. |
| 0.496 | 0.503 | 0.001 | 1.045 | 2758.3±0.5 | | |
| 0.496 | 0.503 | 0.001 | 1.026 | 2759.6±1.6 | | |
| 0.500 | 0.499 | 0.001 | 1.0011 | 2746.9±1.2 | 2752.3±2.8 | |
| 0.498 | 0.501 | 0.001 | 1.0005 | 2753.4±2.4 | 2748.3±1.4 | |
| 0.499 | 0.500 | 0.001 | 1.0011 | | 2745.8±1.3 | |
| 0.499 | 0.500 | 0.001 | 1.0003 | | | 2740.3±1. |
| 0.499 | 0.500 | 0.001 | 1.0000 | | | 2742.7±1. |
| 0.499 | 0.500 | 0.001 | 0.9985 | | | 2743.1±1. |
| 0.499 | 0.500 | 0.001 | I.0007 | | | 2742.3±1. |
| 0.499 | 0.500 | 0.001 | 0.5046 | | | 2703.6±2. |
| 0.499 | 0.500 | 0.001 | 0.5040 | | | 2703.7±1. |
| 0.484 | 0.515 | 0.001 | 0.9964 | 2754.3±5.0 | | 2733.6±4. |
| 0.478 | 0.521 | 0.001 | 1.0049 | 2752.8±0.6 | 2751.4±0.8 | |
| 0.451 | 0.548 | 0.001 | 1.0001 | 2687.9±2.1 | 2680.1±0.8 | |
| 0.448 | 0.551 | 0.001 | 1.0044 | 2679.8±0.1 | | |
| 0.448 | 0.551 | 0.001 | 1.0005 | | 2676.3±0.0 | 2668.0±1. |
| 0.401 | 0.598 | 0.001 | 1.0008 | 2496.1±0.3 | 2492.0±0.3 | 2482.0±0. |
| 0.352 | 0.647 | 0.001 | 1.0002 | 2368.2±0.2 | 2361.1±0.3 | 2356.3±0. |
| 0.301 | 0.697 | 0.002 | 1.0008 | 2251.6± | 2249.6±0.1 | 2241.5±0. |
| 0.300 | 0.698 | 0.002 | 1.0004 | 2254.7±0.0 | 2251.2±0.0 | 2241.9±0. |

[a] Superscript zero refers always to the initial mixture composition.

TABLE II.
Experimental Detonation Velocities in a Cyanogen-Oxygen-Nitrogen Mixture

| $X^{\circ}_{C_2N_2}$ | $X^{\circ}_{O_2}$ | $X^{\circ}_{N_2}$ | $X^{\circ}_{A}$ | $P_{o}$, atm | D, m/sec | | |
|---|---|---|---|---|---|---|---|
| | | | | | 4 in. | 3 in. | 2 in. |
| 0.401 | 0.400 | 0.198 | 0.001 | 0.9968 | 2641.9±0.4 | 2635.8±0.4 | 2631.8±0.3 |

TABLE III. Infinite-Diameter Detonation Velocities

| $X^{\circ}_{C_2N_2}$ | $X^{\circ}_{O_2}$ | $X^{\circ}_{A}$ | D, m/sec |
|---|---|---|---|
| 0.499 | 0.500 | 0.001 | 2768 |
| 0.449 | 0.550 | 0.001 | 2694 |
| 0.401 | 0.598 | 0.001 | 2511 |
| 0.352 | 0.647 | 0.001 | 2378 |
| 0.301 | 0.698 | 0.001 | 2263 |
| 0.401[a] | 0.400 | 0.001 | 2650 |

[a] This entry refers to the mixture with added nitrogen; refer to Table II for composition and initial pressure.

The final result for the equimolar mixture is in excellent agreement with the corresponding data of KKM. However, at other compositions the agreement is not very good, the present results being higher. These experiments also show that the detonation velocity is a maximum for a mixture containing about 49 mole % $C_2N_2$ rather than for a 50% mixture as previously supposed.[6,7] The data of Table I also show, in disagreement with the results of KKM[7], that the effect of tube diameter on the detonation velocity is practically independent of the composition.

## THEORETICAL DETAILS

In calculating the theoretical results the product gases are assumed to be ideal. With this assumption the Chapman-Jouguet condition (7) and the Hugoniot equation can be written as follows:

$$F \equiv (1+\gamma) + \left\{(1+\gamma)^2 - \frac{4T_o \Sigma n^{\circ}}{\gamma T \Sigma n_i}\right\}^{1/2} - 2\frac{V_o}{V} = 0 \qquad (3)$$

and

$$G \equiv 1 + \frac{\bar{C}_p(T)}{\bar{C}_p(T_o)}\left[\frac{R_1(P-P_o)(V_o+V)}{2R_2 T_o \bar{C}_p(T)} - \frac{I}{T_o} + \frac{\Delta H_f^\circ(T_o)_{exp} - \sum n_i \Delta H_f^\circ(T_o)_i}{T_o \bar{C}_p(T)}\right] = 0 \quad , \tag{4}$$

in which F and G are dimensionless functions useful in calculations for numerical convenience. In these equations the subscript zero refers to the initial state of the unreacted explosive mixture, lack of subscript refers to the products in the Chapman-Jouguet state, V is specific volume, T is temperature, P is pressure, $\gamma$ is the ratio of the constant-pressure to constant-volume heat capacities of the product mixture, $\sum n^\circ$ is the total moles per gram of reactant, $\sum n_i$ is the total moles per gram for the products, $R_1$ and $R_2$ are the gas constant in units of cal/mole/deg and cc atm/mole/deg, respectively, $\Delta H_f^\circ(T_o)_{exp}$ is the heat of formation in units of cal/g for the explosive mixture at temperature $T_o$, $\Delta H_f^\circ(T_o)_i$ is the heat of formation in units of cal/mole for product component i at temperature $T_o$, and the $\bar{C}_p$'s are average constant-pressure specific heats for the mixture between temperature T or $T_o$ and 0°K. The equation for the Chapman-Jouguet detonation velocity, D, can be conveniently rewritten in dimensionless form

$$\frac{D^2}{P_o V_o} = \frac{(P/P_o - 1)}{(1 - V/V_o)} \quad . \tag{5}$$

Except for argon, which is treated as an inert, the $n_i$ are to be determined by solution of the various equilibrium conditions and mass balance relations among the assumed product components. Then, if the temperature variations of enthalpy and heat capacity are known for these components, Equations (3) and (4) can be solved, using the assumed ideal equation of state of the product mixture, to give the values of T, P, and V at the Chapman-Jouguet plane. The detonation velocity is then computed from Equation (5).

The velocity computed under the assumption of an ideal product mixture must be corrected for non-ideality. The correction used here is that indicated by Schmidt.(12) The Abel "co-volumes" for these mixtures are approximated from the empirically-determined Lennard-Jones "12-6" potential parameters discussed by Beattie and Stockmayer.(13)

In these calculations a total of eleven product components is considered. The most important equilibria are as follows:

$$1/2\ N_2 \rightleftharpoons N \qquad (6)$$

$$C(s) + 1/2\ O_2 \rightleftharpoons CO \qquad (7)$$

$$C(s) + 1/2\ N_2 \rightleftharpoons CN \qquad (8)$$

$$1/2\ O_2 \rightleftharpoons O \qquad (9)$$

$$1/2\ N_2 + 1/2\ O_2 \rightleftharpoons NO \qquad (10)$$

$$C(s) + O_2 \rightleftharpoons CO_2 \qquad (11)$$

$$2C(s) + N_2 \rightleftharpoons C_2N_2 \qquad (12)$$

It is not inconceivable that other reactions involving more complicated molecules may be of importance. However, the only reaction that seemed reasonable, i.e., one involving $C_2N$, could not be included due to a lack of the necessary thermodynamic data.

For these mixtures the equilibrium problem can be reduced to obtaining the solution of two non-linear equations in two variables; this description is also appropriate to Equations (3) and (4). The method used here was suggested to the authors by W. W. Wood[14] of this Laboratory and is described briefly in the Appendix.

## Thermodynamic Data

Enthalpy data are from the National Bureau of Standards' tables[15] except for CN and $C_2N_2$. Data for CN are from the results of Johnston, et al.[16] Data for $C_2N_2$ were computed by the authors using the harmonic-oscillator, rigid-rotator approximation* and spectroscopic data summarized by Herzberg.[17] Since the data of the NBS tables[15] do not extend beyond 5000°K, the data from 3000° to 5000°K were used to make least squares quintic fits, i.e.,

$$\bar{C}_p(T)_i = \frac{(H^\circ - H_o^\circ)_i}{T} = a + bT + cT^2 + dT^3 + eT^4 + fT^5 \qquad (13)$$

and these fits were extrapolated to the desired temperature where necessary. Similar fits were made for CN and $C_2N_2$ using the data mentioned which were available from 3000° to 6000°K. The validity of the fits and extrapolations was checked by comparing selected values with the high temperature values calculated by Pickett and Cowan.[18] The errors were never greater than 0.1%.

* Errors due to the harmonic-oscillator, rigid-rotator approximation in calculating the data for $C_2N_2$ turn out to be negligible since, for the mixture studied, there is essentially no $C_2N_2$ in the product mixture.

Heat capacities were computed for all components by means of the equation

$$C_p^\circ(T)_i = \overline{C}_p(T)_i + T \frac{d}{dT} \overline{C}_p(T)_i \qquad (14)$$

using the quintic fits for $\overline{C}_p(T)_i$. Equation (14) is exact if $\overline{C}_p(T)_i$ and its temperature derivative are known exactly at the temperature of interest. Since the $\overline{C}_p(T)_i$ fits were quite good, it seemed justifiable to compute the temperature derivative from these fits by direct differentiation. Such a procedure has the added advantage of requiring only one fit to compute two quantities.

This method of calculating $C_p^\circ(T)_i$ was checked as follows: (1) For C, O, and N, values from Equation (14) were compared with data computed by the authors at a few temperatures using standard procedures and spectroscopic data summarized by the National Bureau of Standards(19); (2) For $O_2$, $N_2$, and CO, values from Equation (14) were compared with data computed at a few temperatures by Pickett and Cowan(20), and Wood(21); (3) For CN, values from Equation (14) were compared with the data of Johnston, et al.(16) In every case the disagreement was less than 0.3%, the largest errors being confined to the components present only in small amounts.

Free energy functions, $-(F^\circ - H_0^\circ)/T$, for CN are taken from the data of Johnston, et al.(16); data for C, O, N, and $C_2N_2$ were computed by the authors from spectroscopic data.(17,19) For all other components the data of the NBS tables (15) were used to make cubic fits in ln (T/3000) and these fits were extrapolated to the desired temperature. The extrapolations were checked by comparison with the results of Pickett and Cowan(18) and were found to be very good.

$\Delta H_0^\circ$ data for CN and $C_2H_2$ are from Brewer, et al.(22), and Knowlton and Prosen(23), respectively; data for N and O were computed from dissociation energies, $D_0^\circ$, compiled by Herzberg.(24) All other $\Delta H_0^\circ$ values are computed from the data listed in the NBS tables.(15)

Equilibrium constants are computed from $\Delta H_0^\circ$ and free energy data in the usual way. For computing convenience the equilibrium constants were then fitted as cubics in T, a separate fit being used for each 1000° interval in the temperature range 3000° to 7000°K.

The thermodynamic functions computed by the authors are given in Table IV. Physical constants are taken from Herzberg.(24)

## THEORETICAL RESULTS

Calculations were made for cyanogen-oxygen mixtures in the composition range 10 to 52 mole % cyanogen and for a mixture of cyanogen, oxygen, and nitrogen containing 40 mole % cyanogen, 40 mole % oxygen, and 20 mole % nitrogen. Table V shows the computed detonation properties for the mixtures, the detonation velocities having been

TABLE IV. Computed Thermodynamic Functions*

| T °K | $\frac{(H^\circ-H_0^\circ)}{T}$ | $-\frac{(F^\circ-H_0^\circ)}{T}$ | T °K | $-\frac{(F^\circ-H_0^\circ)}{T}$ | | |
|---|---|---|---|---|---|---|
| | $C_2H_2$ | $C_2H_2$ | | C(g) | H | C |
| 298.16 | 10.213 | 47.444 | 3000 | 44.249 | 43.117 | 45.052 |
| 3000 | 18.059 | 80.472 | 3250 | 44.653 | 43.515 | 45.456 |
| 3200 | 18.210 | 81.642 | 3750 | 45.377 | 44.228 | 46.177 |
| 3400 | 18.346 | 82.750 | 4000 | 45.705 | 44.550 | 46.502 |
| 3600 | 18.469 | 83.802 | 4250 | 46.015 | 44.854 | 46.808 |
| 3800 | 18.581 | 84.804 | 4750 | 46.585 | 45.414 | 47.370 |
| 4000 | 18.682 | 85.759 | 5000 | 46.849 | 45.674 | 47.630 |
| 4200 | 18.776 | 86.673 | 5250 | 47.101 | 45.923 | 47.877 |
| 4400 | 18.861 | 87.549 | 5750 | 47.573 | 46.391 | 48.339 |
| 4600 | 18.940 | 88.389 | 6000 | 47.784 | 46.612 | 48.556 |
| 4800 | 19.013 | 89.197 | 6250 | 48.008 | 46.825 | 48.764 |
| 5000 | 19.081 | 89.974 | 6750 | 48.411 | 47.232 | 49.158 |
| 5200 | 19.144 | 90.724 | 7000 | 48.602 | 47.427 | 49.345 |
| 5600 | 19.258 | 92.147 | | | | |
| 5800 | 19.309 | 92.823 | | | | |
| 6000 | 19.357 | 93.479 | | | | |
| 6200 | 19.402 | 94.114 | | | | |
| 6400 | 19.445 | 94.731 | | | | |
| 6600 | 19.486 | 95.330 | | | | |
| 6800 | 19.523 | 95.912 | | | | |
| 7000 | 19.560 | 96.479 | | | | |

* Units are cal/mole/deg.

TABLE V. "Standard" Calculated Detonation Properties.[a]

| $x^{o}_{C_2H_2}$ [b] | $V_o$, cc/g | V, cc/g | P, atm | T, °K | D, m/sec |
|---|---|---|---|---|---|
| 0.5195 | 572.7 | 323.9 | 54.80 | 5930 | 2685 |
| 0.4995 | 578.3 | 327.4 | 56.80 | 6181 | 2750 |
| 0.4795 | 584.0 | 331.2 | 56.15 | 6133 | 2750 |
| 0.4395 | 595.8 | 339.4 | 50.31 | 5535 | 2634 |
| 0.3995 | 608.1 | 347.0 | 44.06 | 4958 | 2490 |
| 0.3595 | 620.8 | 354.0 | 39.66 | 4627 | 2383 |
| 0.3296 | 630.7 | 359.2 | 37.00 | 4454 | 2316 |
| 0.2996 | 640.9 | 364.6 | 34.61 | 4310 | 2253 |
| 0.1997 | 677.5 | 383.6 | 27.52 | 3883 | 2052 |
| 0.1497 | 697.3 | 394.5 | 24.05 | 3631 | 1938 |
| 0.0998 | 718.3 | 407.1 | 20.19 | 3263 | 1798 |

| $x^{o}_{C_2H_2}$ | $x^{o}_{O_2}$ | $x^{o}_{N_2}$ [c] | $V_o$, cc/g | V, cc/g | P, atm | T, °K | D, m/sec |
|---|---|---|---|---|---|---|---|
| 0.401 | 0.400 | 0.198 | 619.9 | 351.2 | 48.84 | 5771 | 2637 |

a. $P_o = 1.000$ atm., $T_o = 298.16°K$

b. $x^{o}_{O_2} = 0.998\ (1-x^{o}_{C_2H_2})$: $x^{o}_{A} = 1-x^{o}_{O_2}-x^{o}_{C_2H_2}$

c. $x^{o}_{A} = 1-x^{o}_{C_2H_2}-x^{o}_{O_2}-x^{o}_{N_2}$

corrected for gaseous imperfection of the products. For convenience, these results are called "standard" results. This designation will mean results obtained in which $D_0^0$ for $N_2$ is 9.756 ev, $\Delta H_f^0(25°C)$ for CN is 94.8 kcal/mole, and $\Delta H_f^0(25°C)$ for $C_2H_2$ is 73.84 kcal/mole. The computed equilibrium compositions of the "standard" product mixtures are given in Table VI. Table VII compares some of the "standard" velocities with values calculated by changing $\Delta H_f^0(25°C)$ for $C_2H_2$ from 73.84 to 75.84 kcal/mole and $\Delta H_f^0(25°C)$ for CN from 94.8 to 95.8 kcal/mole.

The only known error in the calculated results, aside from the small errors in thermodynamic data and the imperfection correction, is one due to failure to account for HCN in the experimental mixture; i.e., in the calculations HCN is assumed to be $C_2H_2$. Approximate calculations show that the effect on detonation velocity due to this assumption is to decrease the calculated value by at most 0.2 m/sec; therefore, the calculated results are quoted to only four significant figures.

These results do not agree with the data calculated by KKM (7) for similar mixtures. There seem to be several reasons for the discrepancies. Probably the most important one is failure to allow for excited electronic levels and anharmonicity in computing their thermodynamic data for C, O, N, and CN at temperatures above 5000°K. Their results also contain errors associated with failure to attain convergence of the numerical iterations to better than 0.2% of the temperature; the present calculations were carried out to a convergence of better than 0.01%. Finally, their results seem to have the small errors almost always made when doing such complicated numerical calculations on a desk-type calculator.

## DISCUSSION

In Table IX and Figure I the "standard" velocities are compared with the experimental results. In some cases the calculated result has been computed from a four or five point Lagrangian interpolation of the results given in Table V.

The most important question to be considered is whether a comparison of experimental and theoretical results demonstrates the validity of the Chapman-Jouguet theory. According to a recently developed theory of the detailed structure of the detonation wave(25), it is necessary to consider the kinetic details of the detonation reaction in order to show that the Chapman-Jouguet state is the state of thermodynamic equilibrium. There are no experimental data on reaction kinetics at these detonation temperatures, and for reactions which might be important in these cases there seems to be a dearth of data from which to make ever order of magnitude approximations. Consequently, it does not seem possible at the present time to demonstrate conclusively that thermodynamic equilibrium is attained in these mixtures.

**TABLE VI, "Standard" Product Gas Compositions.**

| $x^{\circ}_{C_2N_2}$ [a] | $x_{CO}$ | $x_{N_2}$ | $x_{O_2}$ | $x_O$ | $x_N$ | $x_C$ | $x_{CO_2}$ | $x_{NO}$ | $x_{CN}$ | $x_{C_2N_2}$ | $x_A$ |
|---|---|---|---|---|---|---|---|---|---|---|---|
| 0.5195 | 0.6141 | 0.3070 | 0.315(-5)[b] | 0.464(-2) | 0.157(-1) | 0.161(-1) | 0.129(-3) | 0,681(-3) | 0.409(-1) | 0.225(-4) | 0,620(-3) |
| 0.4995 | 0.6227 | 0.3028 | 0.480(-4) | 0.220(-1) | 0.230(-1) | 0.828(-2) | 0.423(-3) | 0,882(-2) | 0.170(-1) | 0.258(-5) | 0,649(-3) |
| 0.4795 | 0.6135 | 0.2948 | 0.292(-3) | 0.526(-1) | 0.212(-1) | 0.294(-2) | 0.106(-2) | 0,679(-2) | 0.612(-2) | 0.359(-6) | 0,676(-3) |
| 0.4395 | 0.5664 | 0.2721 | 0.421(-2) | 0.122 | 0.758(-2) | 0.123(-3) | 0.598(-2) | 0,208(-1) | 0.424(-3) | 0.486(-8) | 0,729(-3) |
| 0.3995 | 0.5087 | 0.2458 | 0.233(-1) | 0.1591 | 0.223(-2) | 0.577(-5) | 0.226(-1) | 0,375(-1) | 0.362(-4) | --- | 0,797(-3) |
| 0.3595 | 0.4487 | 0.2230 | 0.592(-1) | 0.1711 | 0.961(-3) | 0.771(-6) | 0.472(-1) | 0,490(-1) | 0.714(-5) | --- | 0,882(-3) |
| 0.3296 | 0.4022 | 0.2071 | 0.945(-1) | 0.1728 | 0.587(-3) | 0.241(-6) | 0.672(-1) | 0,546(-1) | 0.277(-5) | --- | 0,953(-3) |
| 0.2996 | 0.3546 | 0.1915 | 0.1366 | 0.1703 | 0.376(-3) | 0.850(-7) | 0.872(-1) | 0,584(-1) | 0.117(-5) | --- | 0,104(-2) |
| 0.1997 | 0,1889 | 0.1379 | 0.3320 | 0.1353 | 0.7 (-14) | 0.2 (-8) | 0.1457 | 0,588(-1) | 0.6 (-7) | --- | 0,134(-2) |
| 0,1497 | 0.1067 | 0.1036 | 0.4703 | 0.995(-1) | --- | --- | 0.1620 | 0,514(-1) | --- | --- | 0,152(-2) |
| 0,0998 | 0.0351 | 0.0775 | 0.6443 | 0.489(-1) | --- | --- | 0.1561 | 0,363(-1) | --- | --- | 0,172(-2) |
| 0,401[c] | 0.5466 | 0.4073 | 0.223(-4) | 0.113(-1) | 0.146(-1) | 0.356(-2) | 0.332(-3) | 0,199(-2) | 0.115(-1) | 0.214(-5) | 0,703(-3) |

a. The remaining initial mole fractions, $P_o$, and $T_o$ are the same as indicated in Table V.

b. The number in parentheses is the power of 10 by which the entry is to be multiplied.

c. This row gives results for the mixture with added nitrogen; mole fractions of initial mixture listed in Table V.

TABLE VII. Detonation Velocity vs Dissociation Energy of $N_2$.

| $X^o_{C_2N_2}$ | Detonation Velocity, m/sec | |
|---|---|---|
| 0.4995 | 2750[a] | 2670[b] |
| 0.4795 | 2750 | 2653 |
| 0.4495 | 2634 | — |
| 0.3995 | 2490 | 2455 |
| 0.2996 | 2253 | 2246 |
| 0.1997 | 2052 | 2050 |

[a] $D^o_0$ of $N_2$ = 9.756 ev

[b] $D^o_0$ of $N_2$ = 7.373 ev, all other data same as "standard" results

TABLE VIII. Calculated Velocities for Various Heats of Formation.

| $X^o_{C_2N_2}$ | Detonation Velocity, m/sec | | |
|---|---|---|---|
| 0.499 | 2750[a] | 2760[b] | 2763[c] |
| 0.449 | 2671 | 2684 | 2684 |
| 0.401 | 2494 | 2507 | 2506 |
| 0.352 | 2366 | 2374 | 2374 |
| 0.301 | 2256 | 2263 | 2263 |
| 0.401[d] | 2637 | 2648 | 2646 |

[a] "Standard" results in this column.

[b] "Standard" except $\Delta H^o_f(25°C)$ for $C_2N_2$ = 75.84 kcal/mole.

[c] "Standard" except $\Delta H^o_f(25°C)$ for $C_2N_2$ = 75.84 kcal/mole and $\Delta H^o_f(25°C)$ for CN = 95.8 kcal/mole.

[d] This row refers to the mixture with added nitrogen.

TABLE IX. Experimental vs "Standard" Calculated Velocities.

| $X^o_{C_2N_2}$ | $D_{exp}$, m/sec | $D_{calc}$, m/sec | Disagreement[a] |
|---|---|---|---|
| 0.499 | 2768 | 2750 | -0.6% |
| 0.449 | 2694 | 2671 | -0.8% |
| 0.401 | 2511 | 2494 | -0.7% |
| 0.352 | 2378 | 2369 | -0.5% |
| 0.301 | 2263 | 2256 | -0.3% |
| 0.401[b] | 2650 | 2637 | -0.5% |

[a] This column computed as $\frac{100(D_{calc} - D_{exp})}{D_{exp}}$

[b] This row refers to the mixture containing added nitrogen.

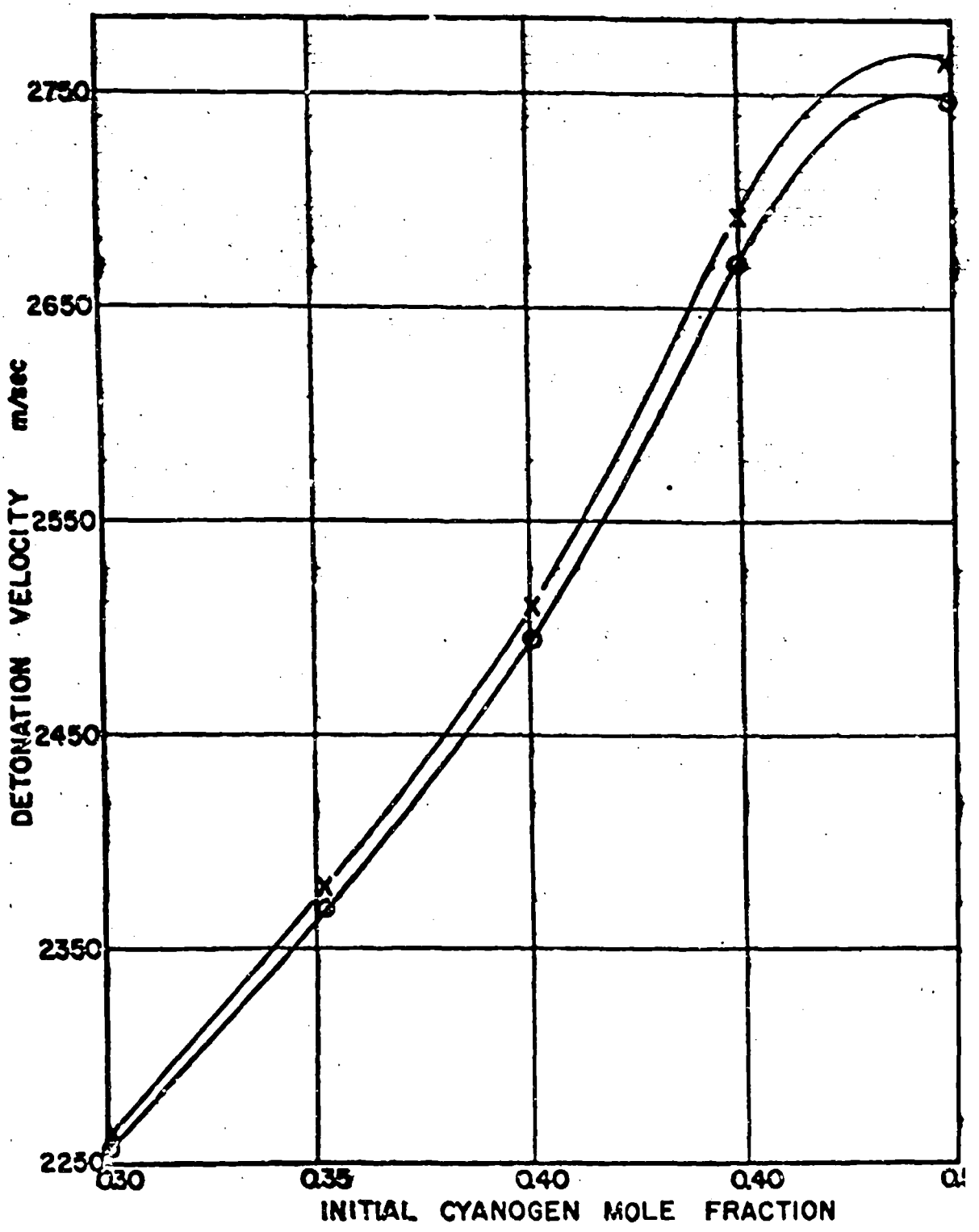


FIGURE 1

EXPERIMENTAL vs STANDARD CALCULATED VELOCITIES

X = EXPERIMENTAL  O = CALCULATED

However, it is possible to make at least one intuitive argument. This argument was suggested by Kistiakowsky (26) and goes somewhat as follows. Within a very short time after the onset of reaction in any region of interest there are relatively large concentrations of free radicals formed.(6) In the case of the nearly equimolar mixtures of cyanogen and oxygen the latter stages of the over-all reaction would involve the exothermic recombination of these free radicals, resulting in a certain distribution of, say, oxygen molecules among the possible energy states. If thermodynamic equilibrium were not attained, a different distribution among available states would be expected when there is "excess" oxygen present, as in the case of mixtures containing appreciably less than 50 mole % cyanogen. In this case the latter stages of the over-all reaction would be composed of processes involving the endothermic heating and dissociation of the "excess" oxygen ("excess" denoting the difference in concentrations of oxygen and cyanogen). Similar arguments should apply to the question of thermodynamic equilibrium in the case of the mixture containing added nitrogen. If the values calculated by assuming thermodynamic equilibrium are the same, or very nearly the same, as the experimental velocities over a fairly wide range of composition, this is evidence that thermodynamic equilibrium is attained.

On the basis of the above argument and the agreement demonstrated in Table IX it seems reasonable to assume thermodynamic equilibrium was attained in the mixtures studied. It then follows that the thermodynamic data used in the computations are very nearly correct, and it is of interest to inquire if better agreement can be attained by changing some of the more uncertain data.

There are two types of change which may be made. The first is to change thermodynamic data for the reactants and the second is to change the data for a particular product component(s). Changes of the former type would produce an effect for all the mixtures with the magnitude of the effect depending on the composition, but changes of the latter type would affect only those mixtures in which there is an appreciable concentration of the particular component in the product mixture.

With regard to changes in reactant thermodynamic data the only datum subject to change, which also produces an effect of the desired magnitude when changed, is $\Delta E_f^\circ(25^\circ C)$ for $C_2N_2$. There are three quantities in doubt in the case of data for the products; namely, $D_0^\circ$ for $N_2$ and CO, and $\Delta E_f^\circ(25^\circ C)$ of CN. Of these four quantities the dissociation energies are limited by spectroscopic evidence (24,28) to certain well-determined, but widely separated, values, while the heats of formation are subject to possible errors of only a few kcal/mole.

The results of Table VII clearly show that $D_0^\circ$ for $N_2$ is 9.756 ev rather than 7.373 ev. Although there is still some controversy over the value of $D_0^\circ$ for CO(24), only one of the disputed values, 11.108 ev, was used extensively in these calculations. However, in a few cases calculations were made using the value

9.605 ev. In these cases the calculated velocity was lowered by about the same order of magnitude as when $D_0^0$ for $N_2$ was lowered to 7.373 ev. Consequently, $D_0^0$ for CO is 11.108 ev.

The results in the third velocity column of Table VIII are compared with the experimental results in Figure II. Clearly, the agreement between calculation and experiment is better in this case than when the experimental results are compared with the "standard" calculated values. This better agreement is an indication that $\Delta H_f^0(25°C)$ of CN(22) and $C_2N_2$(23) are perhaps slightly higher than previously supposed.

In summary, the authors believe that these experiments have demonstrated the validity of the Chapman-Jouguet theory for gaseous mixtures of cyanogen, oxygen, and nitrogen. On this basis the agreement between calculated and experimental detonation velocities shows that $D_0^0$ for $N_2$ is 9.756 ev and $D_0^0$ for CO is 11.108 ev. There is also some evidence indicating that $\Delta H_f^0(25°C)$ of CN and $C_2N_2$ are perhaps higher than previously supposed.

## APPENDIX

Let the two non-linear equations in two variables be written as:

$$f = f(\alpha,\beta) = 0 \qquad \text{and} \qquad g = g(\alpha,\beta) = 0,$$

and suppose that these equations may be inverted to the form:

$$\alpha = F(f,g) \qquad \text{and} \qquad \beta = G(f,g).$$

Let the solution of the former equations be $(\alpha_0,\beta_0)$ and expand F and G in a Taylor's series about that point. The result is approximately,

$$\alpha = \alpha_0 + af + bg, \tag{15}$$

and

$$\beta = \beta_0 + a'f + b'g, \tag{16}$$

where a, a', b, and b' denote the partial derivatives of F and G with respect to $\alpha$ and $\beta$. Equations (15) and (16) are equations of planes, the constants of which can be determined by computing the values of f and g for each of three values of $\alpha$ and $\beta$. The only constant of interest in this case is $\alpha_0$ or $\beta_0$, since these constants can then be used to compute a new f and g and this process can be repeated until the equations have been solved to the desired precision. No proofs of conditions for convergence of this iteration are known to the authors, but Milne(27) cites possible cases to be avoided in a somewhat similar method for one non-linear equation.

Practical experience with this method shows that the three initial guesses for $\alpha$ and $\beta$ should be triangularly spaced about the solution. It turns out that if good initial guesses are made the computation of the detonation properties of any given mixture can be

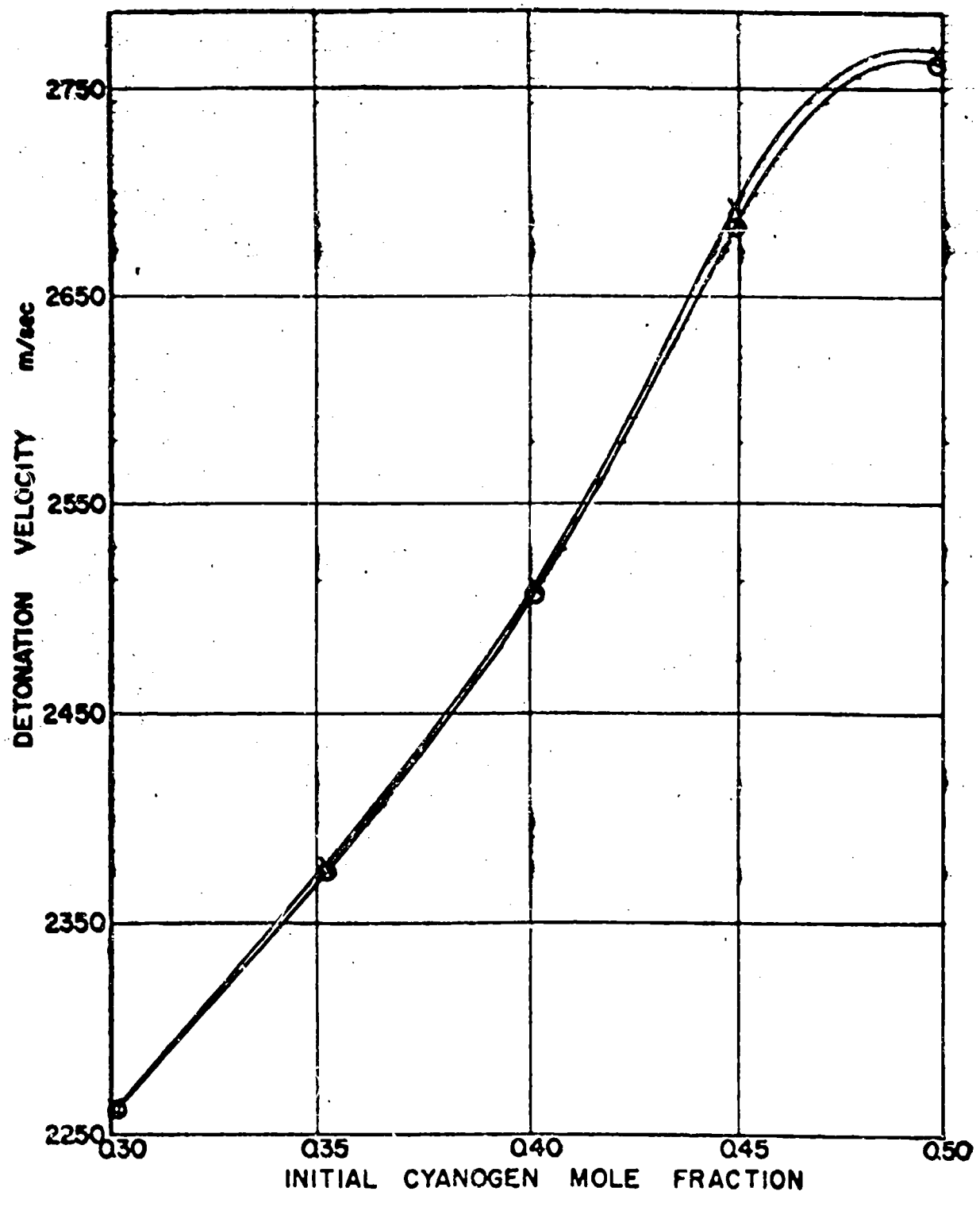


FIGURE II

EXPERIMENTAL vs ADJUSTED CALCULATED VELOCITIES

X = EXPERIMENTAL O = CALCULATED

completed on the IBM Type-701 computer in 20 to 30 seconds. At the worst, a complete calculation might take 45 seconds.

## ACKNOWLEDGMENTS

The authors wish to acknowledge interest and very helpful discussion on the part of many of their colleagues; in particular, W. W. Wood, W. Fickett, R. E. Duff, H. T. Knight, L. [illegible]. Smith, and, especially, Professor G. B. Kistiakowsky. They also acknowledge the assistance of Patricia Fain, W. H. Rogers, and R. J. Riedel who performed the mass spectrometric analyses.

## BIBLIOGRAPHY

1. D. L. Chapman, Phil. Mag. 47, 90(1899).
2. E. Jouguet, J. Mathematique, 347(1905), 6(1906).
3. W. J. M. Rankine, Phil. Trans. 160, 277(1870).
4. H. Hugoniot, J. de l'Ecole Polytech. 57, 3(1887), 58, 1(1888).
5. R. Becker, Z. Physik. 8, 321(1922); Z. Elektrochem. 42, 457(1936).
6. B. Lewis and G. von Elbe, Combustion, Flames, and Explosions of Gases, Academic Press, Inc., New York, 1951.
7. G. B. Kistiakowsky, H. T. Knight, and M. E. Malin, J. Chem. Phys. 20, 876(1952).
8. S. Schlesinger, Los Alamos Scientific Laboratory, Report LA-1573, 1953.
9. J. O. Hirschfelder, C. F. Curtiss, and R. B. Bird, Molecular Theor of Gases and Liquids, John Wiley and Sons, Inc., New York, 1954.
10. H. T. Knight and R. E. Duff, Rev. Sci. Instr., in press.
11. H. Margenau and G. M. Murphy, Mathematics of Physics and Chemistry D. Van Nostrand Company, Inc., New York, 1943.
12. A. Schmidt, Z. ges. Schiess-u-Sprengstoffw. 30, 364(1935).
13. J. A. Beattie and W. H. Stockmayer, A Treatise on Physical Chemistry, Chapter II, Volume II, Edited by H. S. Taylor and S. Glasstone, D. Van Nostrand Company, Inc., New York, 1951.
14. W. W. Wood, private communication.
15. Selected Values of Thermodynamic Properties, Series III, National Bureau of Standards, U. S. Government Printing Office, Washington, D. C., 1947.
16. H. L. Johnston, J. Belzer, and L. Savedoff, Cryogenic Laboratory of Ohio State University, Technical Report TR 316-7, May, 1953.
17. G. Herzberg, Infrared and Raman Spectra, D. Van Nostrand Company, Inc., New York, 1945.
18. W. Fickett and R. D. Cowan, to be published.
19. National Bureau of Standards, Atomic Energy Levels, Circular 467, U. S. Government Printing Office, Washington, D. C., 1948.
20. W. Fickett and R. D. Cowan, private communication.
21. W. W. Wood, private communication.
22. L. Brewer, L. K. Templeton, and F. A. Jenkins, J. Am. Chem. Soc., 1462(1951).

23. J. W. Knowlton and E. J. Prosen, J. Research National Bureau of Standards, 46, 489(1951).
24. G. Herzberg, Spectra of Diatomic Molecules, D. Van Nostrand Company, Inc., Second Edition, New York, 1950.
25. W. W. Wood and J. G. Kirkwood, J. Chem. Phys., to be published.
26. G. B. Kistiakowsky, private communication.
27. W. E. Milne, Numerical Calculus, Princeton University Press, 1949.
28. J. M. Hendrie, J. Chem. Phys. 22, 1503(1954). This determination of $D_0^0$ for $N_2$ was published during preparation of this paper and constitutes definite evidence for the higher value.

# DETONATION IN GASES AT LOW PRESSURE

Arthur L. Bennett and Henry W. Wedke
U. S. Naval Ordnance Test Station
China Lake, California

Preliminary results of an investigation of detonation in gases were reported previously (1). The 2.5 cm square tube used then was not long enough to insure stable detonation nor was it feasible to provide adequate velocity measurement. A new tube of aluminum has been constructed and instrumented. The behavior of detonation in acetylene-oxygen and in stoichiometric hydrogen-oxygen at initial pressures down to 10 mm Hg is reported herein.

The driver section of the tube is 97 cm long and 12 cm in diameter. A diaphragm is normally used to isolate this section from the remainder of the tube. The first part of the experimental section is 215 cm long and 12 cm in diameter. A transition section 46 cm long provides a smooth transition to the final 10-cm square section 183 cm long. This section has a number of 2.5-cm windows flush with the interior surface. The run from the diaphragm to the window used for photoelectric measurements is 398 cm or 33 tube diameters. The run in the square section alone is 137 cm or 13.7 times the tube height.

Valves in both the driver section and experimental section lead to a diffusion pump for evacuation. Storage tanks are used for premixing the various gases. The mixture ratio is established by the pressure increment of each component. The mixture is allowed to stand at least 12 hours for diffusion. Control of the mixture ratio is run on the mass spectrometer.

The position of the detonation is determined by eleven ionization probes along the top of the tube at 36 to 50 cm intervals. The probe design and circuit used at Los Alamos (2) has been modified to suit the recording equipment. The probe consists of a 1.5 mm nichrome wire surrounded by Teflon 4 mm in diameter. The Teflon and wire are pressed tightly into a hole in a tube wall and then smoothed off flush with the interior surface. The signal pulse created by the discharge through the ionized gas of a 100-μμf capacitor charged to a potential from 22 to 450 volts (depending on the pressure) is

transmitted through a germanium diode to the coaxial cable connecting all probes to the input of the Time Interval Recorder. The time constant of the circuit depends on the conductivity of the gas and varies from 0.1 us for higher initial pressures to 10 μs for the lowest.

The time scale of the Time Interval Recorder (TIR) is provided by a Tektronix Time Mark Generator (TMG) controlled by a 1-megacycle crystal oscillator which furnishes pulses from 1 μs to 1 second spacing. The duration of the record is 2000 μs at 1.5 mm/μ sec. Two Tektronix type 511 oscilloscopes, each with a 35 mm still camera, are used. The scopes are triggered alternately at 50 μs intervals by pulses from the TMG. The scopes are sweeping alternately, but dark, until the first probe signal is received by the control equipment. This signal brightens the beam of the active scope wherever the beam is at that instant and this scope continues to write for a full sweep of about 60 μs. At 50 μs on the TMG the second scope also begins to sweep providing an overlap in the recording.

Both scopes record three signals mixed in the TIR and fed to the vertical deflection: (a) the probe signals (positive); (b) TMG pulses at 1- and 5-μs intervals (negative); and (c) a sawtooth signal of 2000-μs duration which provides a vertical displacement of about 4 mm between successive lines. The relative times of the probe signals are read by interpolation between the 1-μs markers.

An "ionization profile" is obtained with an auxiliary oscilloscope. The positive side of a 23-volt battery is connected to the probe through a 10 K resistor, the other terminal being grounded to the tube. The probe is connected through coaxial cable to the input of the scope. The zero of the scope is set at the top line of the graticule and the sensitivity adjusted so that shorting the probe gives a deflection of 2 or 4 cm according to the linear range of the scope. Deflection of 1/4 the preset deflection corresponds to an internal resistance of 30,000 ohms, 1/2 to 10,000, and 3/4 to 3333.

A "light profile" is recorded with a separate oscilloscope. Two 0.65-mm slits 2.5 cm high separated 17.5 cm are aligned perpendicular to the axis of the tube in line with one of the windows. The slits exclude all direct light from the tube beyond a width of 1.2 mm at the distant wall of the tube, and hence the time resolution is 0.5 μsec for the slowest detonation recorded. Behind the second slit a 10-stage, end-on, S4 photomultiplier type 6199 at 90 v/stage, battery powered, is used. The anode resistor of 1000 ohms with a short, low-capacity coaxial cable gives a time resolution of 0.1 μs and a good signal-to-noise ratio. The slit lengths were adjusted to limit the maximum current to 4 mA.

The standard operating procedure is to clean the tube of any diaphragm debris, put in a new diaphragm, and pump a vacuum below 25 microns Hg. A leak rate of 10 microns a minute is considered satisfactory. The two sections of the tube are filled in turn, the

pressure being read on a dial manometer accurate to 0.2 mm Hg. Prior to this the oscilloscopes have been readied so that the tube is fired within 1 to 2 minutes of the completion of filling.

## EXPERIMENTAL RESULTS

The location of the probes relative to the diaphragm is given in Table 1. The measured detonation velocities for acetylene-oxygen are presented in Tables 2 and 3. Only the measurements over the latter part of the tube are given to indicate the degree of uniformity of the velocity. Some runs in Table 2 were made with red zip tape 0.002-inch thick, 0.003-inch acetate film and 0.002-inch copper foil as indicated. No appreciable effect on the velocity is evident at the usual working distance from the diaphragm. It was noted that at 50 mm initial pressure the velocity at the probes near the location of the diaphragm would be above 3200 m/sec without the diaphragm and then would settle down to uniform velocity. With the zip-tape diaphragm, however, the run-up to detonation was smooth and the final uniform velocity was present at the first interval.

The measurements in Table 3 were made to investigate the effect of the transition from round to square section. The ignition spark plug was placed at the end of the square section, 9.3 cm from probe 11, and the velocity was measured in the upstream direction. There appears to be no significant difference. The uniformity of the velocity at high pressure indicates that the measured distances and the timing are highly accurate.

The detonation velocities for stoichiometric hydrogen-oxygen are given in Tables 4 and 5. The mean velocities are plotted in Figure 1. The velocity computed by Hooradian and Gordon (3) is shown for comparison. Good agreement of the observed velocities down

TABLE 1

DIMENSIONS OF THE TUBE

| Element | Distance (Cm) | Element | Distance (Cm) |
|---|---|---|---|
| Diaphragm | 0 | 7 | 288.69 |
| Probe 1 | 22.50 | 8 | 325.25 |
| 2 | 60.58 | 9 | 361.81 |
| 3 | 98.63 | 10 | 398.31 |
| 4 | 136.78 | 11 | 434.82 |
| 5 | 187.46 | End | 444.10 |
| 6 | 238.14 | | |

to 100 mm initial pressure is evident. The velocity of the one run at 10 mm is high relative to the velocities for 30 to 20 mm. In this case the driver initial pressure, 40 mm $C_2H_2+O_2$, is high enough so that the pressure behind the detonation in $2H_2+O_2$ may well exceed the Chapman-Jouget pressure.

Figure 2 (a) is the light profile for 400 mm $2H_2+O_2$ taken at the side of the tube at the same distance from the diaphragm as Probe 10. Figure 2 (b) is taken at the same location at a side probe centered in the slits of the photomultiplier. A considerable degree of correlation is noted, even though the probe measures the conductivity of at most a few millimeters of the gas adjacent to the wall, whereas the photomultiplier receives light from the full 10-cm depth of the tube. The local nature of the probe measurement is indicated by the wider fluctuation of the record.

The light and probe profiles at 50 mm initial pressure of $2H_2+O_2$, driven by the detonation of 50 mm of $C_2H_2+O_2$, Figure 3 (a) and 3 (b), respectively, show a similarity to those of higher pressure. It is to be noted, however, that, following the initial peak and a plateau of 30 μsec, there is a progressive increase in intensity, which continues for the whole 150 μsec recorded, to a value equal to or exceeding the initial peak.

At 20 mm initial pressure of $2H_2+O_2$ driven by 35 mm $C_2H_2+O_2$, illustrated by Figure 4, there is some fluctuation in intensity over about 50 μsec in the five records obtained. In each, however, the increase in intensity beginning about 15 μsec after the start of emission leads to a value greater than the initial peak, 150 to 170 μsec.

Figure 5 is the record obtained at 10 mm initial pressure of $2H_2+O_2$ driven by 40 mm of $C_2H_2+O_2$. The increase in light after the first peak is striking in this case.

Light profiles of longer duration have not as yet been taken. The many ionization profiles taken at slower recording speed indicate that the maximum conductivity occurs in a rather broad maximum at about 200 μsec after the first signal. No marked dependence on pressure of the interval to maximum conductivity is evident at the location of the window near the end of the tube.

Examination of the light profiles shows that the duration of the rise of intensity to the first peak becomes progressively longer as the pressure is lowered. The mean values of the time of rise are: for 400 mm, less than 1 μsec (1 run); 50 mm, 3 μsec (2); 20 mm, 5 μsec (5); and 10 mm, 7 μsec (1).

## DISCUSSION

The observed increase in the time taken to reach the first maximum could be interpreted to be the duration of the reaction zone.

This interpretation must be qualified, however, by the continuing increase in emission lasting some 200 μsec. Even if the radiation is purely thermal, the increase in intensity following the first peak indicates an increase in temperature, contrary to the Chapman-Jouget model of the detonation phenomena, unless one accepts the interpretation that the reaction zone is upwards of 200 μsec or some 50 cm in extent.

Our present interpretation of these data is that, even after a run of more than 30 tube diameters, stable detonation has not been achieved. Even though the detonation velocities show little variation over the last three measured intervals, the marked irregularity of the ionization profiles suggest that the detonation is not a single shock followed by chemical reaction, but rather a series of shocks or pressure pulses overtaking the leading shock from the rear. As Brinkley and Richardson (4) have shown, energy released in the rarefaction wave is not lost, but will be delivered, at least in part, upstream. The average velocity will, therefore, be reasonably constant even though the arrival of the pulses must result in fluctuations of short duration.

Is the observed turbulence at low pressure a general phenomenon or is it peculiar to the geometry of the tube used? One should expect the transition from circular section to square section to produce lateral shocks, mild because the maximum angle of the wall relative to the axis is about one degree. A number of runs have been made to investigate this point. Figure 6 is a typical record: (a) is the ionization profile at probe 5, 29 cm upstream from the beginning of the transition section. Figure 6 (b) is the profile at probe 7, 28 cm downstream from the end of the transition. Figure 6 (c) is the profile at the usual measuring location, probe 10. This run was 100 mm $2H_2+O_2$, driven by 150 mm $C_2H_2+O_2$. Our interpretation of the group of records is that the irregularities smooth out in the course of the run through the tube without regard to the geometry. The indication is, therefore, that the turbulence is not peculair to this tube, but that detonation initiated by the technique used here will require a run of considerably more than 30 tube diameters to become stable.

REFERENCES

(1) Detonation in Gases, Bulletin A.P.S., Vol. 27, No. 6, Dec. 1952.

(2) Precision Measurement of Detonation and Strong Shock Velocity in Gases. Knight and Duff, Bulletin of the APS, Vol. 29, No. 1, January 1954.

(3) ONR Contract N7 onr-292. MS provided through the courtesy of ONR.

(4) Fourth Symposium (International) on Combustion, 1952, p. 450

TABLE 2

DETONATION VELOCITY OF 0.5 ACETYLENE, 0.5 OXYGEN (m/sec)

| Run No. | 189 | 193 | 196 | 194 | 205 | 143 | 176 | 178 | 195 | 177 | 179 | 180 | 197 |
|---|---|---|---|---|---|---|---|---|---|---|---|---|---|
| Pressure (mm Hg) | 100 | 100 | 100 | 100 | 100 | 50 | 50 | 50 | 50 | 50 | 50 | 50 | 50 |
| Diaphragm | - | - | - | zip | zip | - | - | - | - | zip | .003 acetate | .002 Cu | zip |
| Probe 6-8 | | | 2793 | | 2799 | | | | | | | | |
| 7-8 | 2793 | 2793 | | 2799 | | 2736 | 2763 | 2759 | 2763 | 2765 | 2761 | 2765 | 2761 |
| 8-9 | | | 2790 | | 2794 | 2745 | 2757 | 2763 | | 2754 | 2763 | 2755 | 2767 |
| 8-10 | 2804 | 2797 | | 2791 | | | | | 2757 | | | | |
| 9-10 | | | 2788 | | 2803 | 2765 | 2767 | 2781 | | 2765 | 2758 | 2764 | 2763 |
| 10-11 | 2797 | 2791 | 2806 | 2795 | 2797 | 2768 | 2761 | 2764 | 2755 | 2759 | 2685 | 2745 | 2767 |
| Mean 8-11 | 2801 | 2794 | 2794 | 2792 | 2798 | 2759 | 2762 | 2769 | 2756 | 2759 | 2769 | 2755 | 2766 |
| Component | | | | | | | | | | | | | |
| $C_2H_2$ (%) | | | | | | | 49.57 | 49.42 | 50.17 | 49.57 | 49.42 | 49.42 | 50.87 |
| Acetone (%) | | | | | | | .60 | .60 | 1.10 | .60 | .60 | .60 | .74 |
| $O_2$ (%) | | | | | | | 49.66 | 49.78 | 48.57 | 49.66 | 49.78 | 49.78 | 48.20 |
| A (%) | | | | | | | .17 | .20 | .16 | .17 | .20 | .20 | .19 |

TABLE 3

DETONATION VELOCITY OF 0.5 ACETYLENE, 0.5 OXYGEN (m/sec)

| Run No. | 141 | 171 | 173 | 174 | 175 |
|---|---|---|---|---|---|
| Pressure (mm Hg) | 250 | 100 | 100 | 50 | 50 |
| Diaphragm | - | - | - | - | - |
| Probe 8-7 | 2856 | 2797 | | | |
| 7-6 | 2847 | 2799 | | | |
| 6-5 | 2855 | 2803 | 2798 | | |
| 5-4 | 2851 | 2803 | 2797 | 2766 | 2766 |
| 4-3 | | | 2801 | 2762 | 2764 |
| 3-2 | | | 2789 | 2761 | 2759 |
| 2-1 | | | | 2763 | 2761 |
| Mean (last 3 int.) | 2851 | 2802 | 2796 | 2762 | 2761 |
| Component | | | | | |
| $C_2H_2$ (%) | | 51.48 | | | 49.57 |
| Acetone (%) | | .03 | | | .60 |
| $O_2$ (%) | | 48.31 | | | 49.66 |
| A (%) | | .18 | | | .17 |

TABLE 4

DETONATION VELOCITY OF STOICHIOMETRIC HYDROGEN-OXYGEN

| Run No. | 139 | 232 | 233 | 200 | 201 | 202 | 203 | 204 | 206 | 209 | 210 |
|---|---|---|---|---|---|---|---|---|---|---|---|
| Pressure (mm Hg) | | | | | | | | | | | |
| Driver $C_2H_2+O_2$ | 200 | 170 | 170 | 100 | 100 | 85 | 85 | 85 | 150 | 125 | 100 |
| Exper. $2H_2+O_2$ | 400 | 400 | 400 | 200 | 200 | 200 | 200 | 200 | 100 | 100 | 100 |
| Probe 6-8 | | 2813 | | 2765 | 2767 | 2766 | 2769 | 2777 | 2713 | 2718 | 2724 |
| 8-9 | 2819 | 2812 | 2797 | 2761 | 2752 | 2769 | 2769 | 2773 | 2708 | 2728 | 2708 |
| 9-10 | 2829 | 2827 | 2816 | 2767 | 2782 | 2760 | 2786 | 2765 | 2729 | 2723 | 2723 |
| 10-11 | 2829 | 2810 | 2814 | 2761 | 2769 | 2769 | 2765 | 2786 | 2718 | 2714 | 2724 |
| Mean 8-11 | 2826 | 2816 | 2809 | 2763 | 2768 | 2766 | 2773 | 2775 | 2718 | 2722 | 2722 |
| Component | | | | | | | | | | | |
| $H_2$ (%) | | | | 67.39 | 67.16 | 67.16 | 67.16 | | | | |
| $O_2$ (%) | | | | 31.51 | 32.29 | 32.39 | 32.39 | | | | |
| A (%) | | | | 0.11 | 0.09 | 0.09 | 0.09 | | | | |
| $N_2$ (%) | | | | 0.99 | 0.36 | 0.36 | 0.36 | | | | |

TABLE 5

DETONATION VELOCITY OF STOICHIOMETRIC HYDROGEN-OXYGEN

| Run No. | 213 | 224 | 225 | 228 | 216 | 185 | 186 | 187 | 217 | 219 | 220 | 221 | 230 | 223 |
|---|---|---|---|---|---|---|---|---|---|---|---|---|---|---|
| Pressure (mm Hg) | | | | | | | | | | | | | | |
| Driver $C_2H_2+O_2$ | 50 | 50 | 50 | 50 | 35 | 50 | 50 | 50 | 35 | 50 | 35 | 35 | 40 | 40 |
| Exper. $2H_2+O_2$ | 50 | 50 | 50 | 50 | 50 | 30 | 30 | 30 | 25 | 20 | 20 | 20 | 20 | 10 |
| Probe 6-8 | 2647 | 2647 | 2647 | 2631 | 2660 | | | | 2569 | 2562 | 2600 | 2569 | 2627 | 2739 |
| 7-8 | | | | | | 2661 | 2630 | 2593 | | | | | | |
| 8-9 | 2668 | 2668 | 2656 | 2649 | 2603 | 2539 | 2557 | 2574 | 2556 | 2521 | 2486 | 2538 | 2486 | 2611 |
| 9-10 | 2641 | 2644 | 2656 | 2664 | 2697 | 2517 | 2552 | 2570 | 2588 | 2543 | 2532 | 2683 | 2534 | 2570 |
| 10-11 | 2567 | 2645 | 2653 | 2664 | 2613 | 2571 | 2470 | 2589 | 2570 | 2535 | 2609 | 2570 | 2535 | 2552 |
| Mean 6-11 | 2631 | 2651 | 2653 | 2652 | 2643 | 2572 | 2552 | 2581 | 2571 | 2540 | 2557 | 2590 | 2546 | 2618 |
| " 8-11 | 2625 | 2652 | 2655 | 2659 | 2633 | 2548 | 2526 | 2578 | 2571 | 2533 | 2542 | 2597 | 2518 | 2578 |

| Component | |
|---|---|
| $H_2$ (%) | 65.85 |
| $O_2$ (%) | 33.71 |
| A (%) | .10 |
| $N_2$ (%) | .34 |

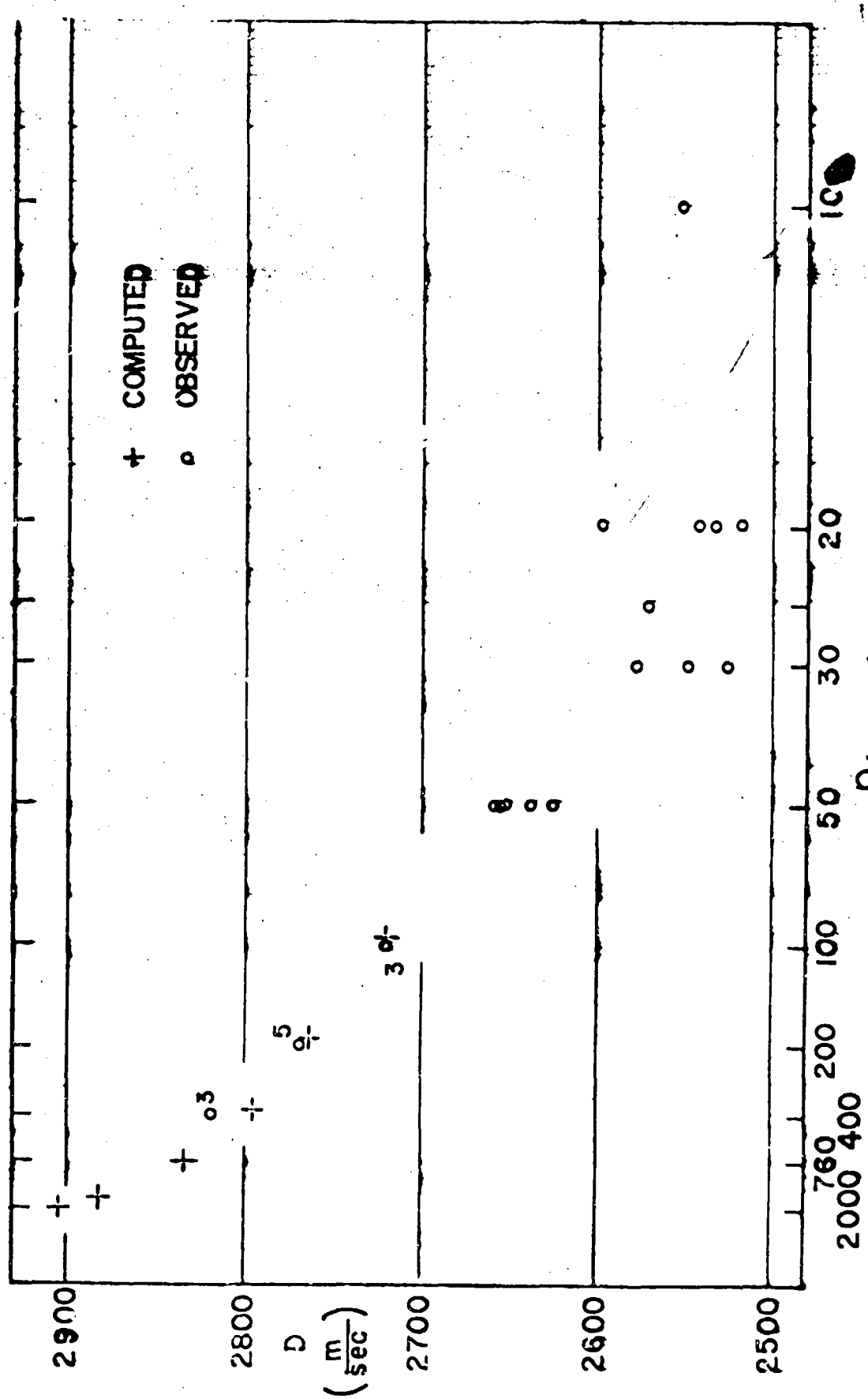


Fig. 1 - Detonation velocity of $2H_2+O_2$ vs p.

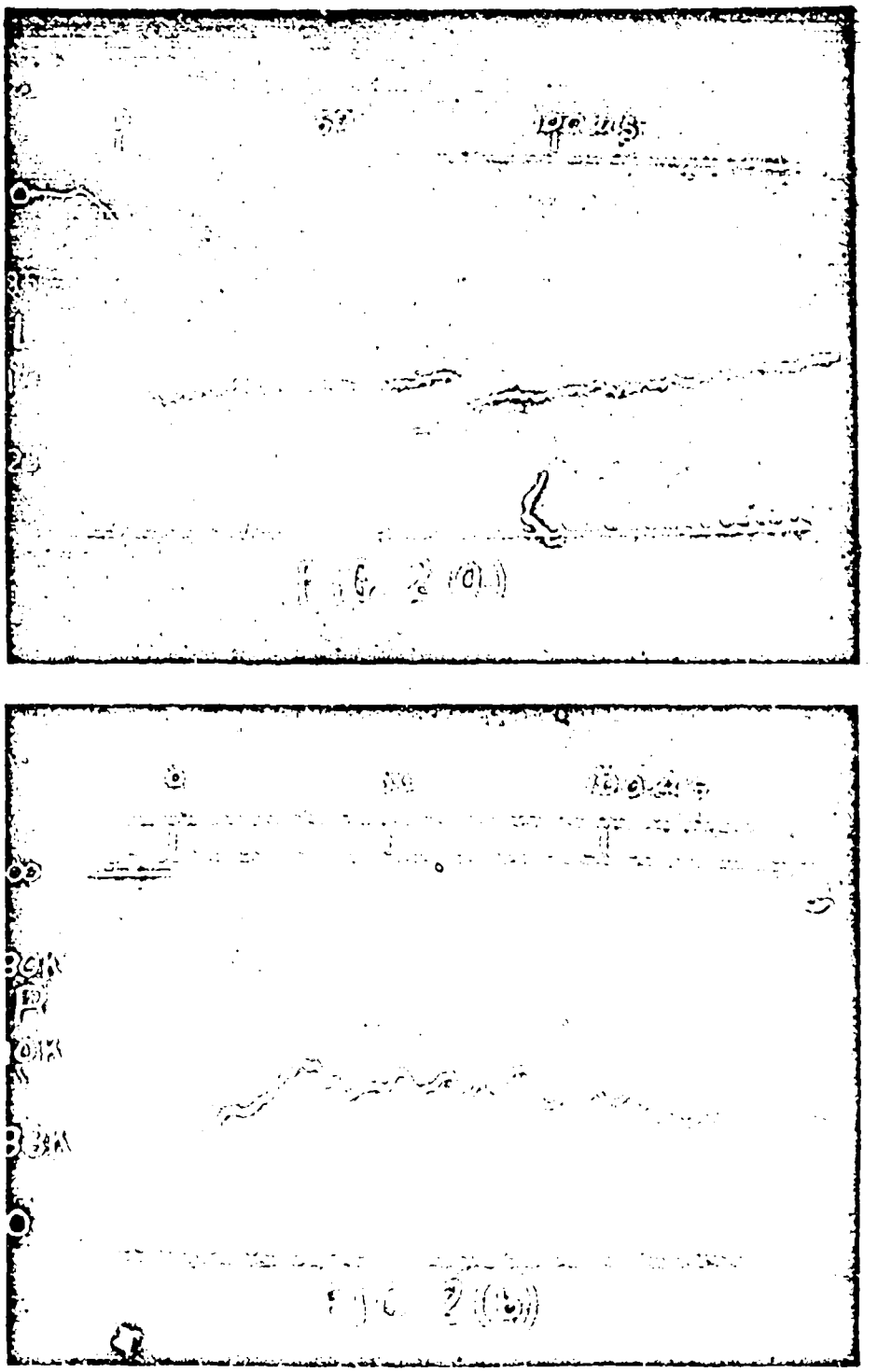

Fig. 2 - (a) Light profile, (b) Ionization profile. 400 mm Hg initia
pressure of $2H_2+O_2$ detonated by 170 mm Hg of $C_2H_2+O_2$.

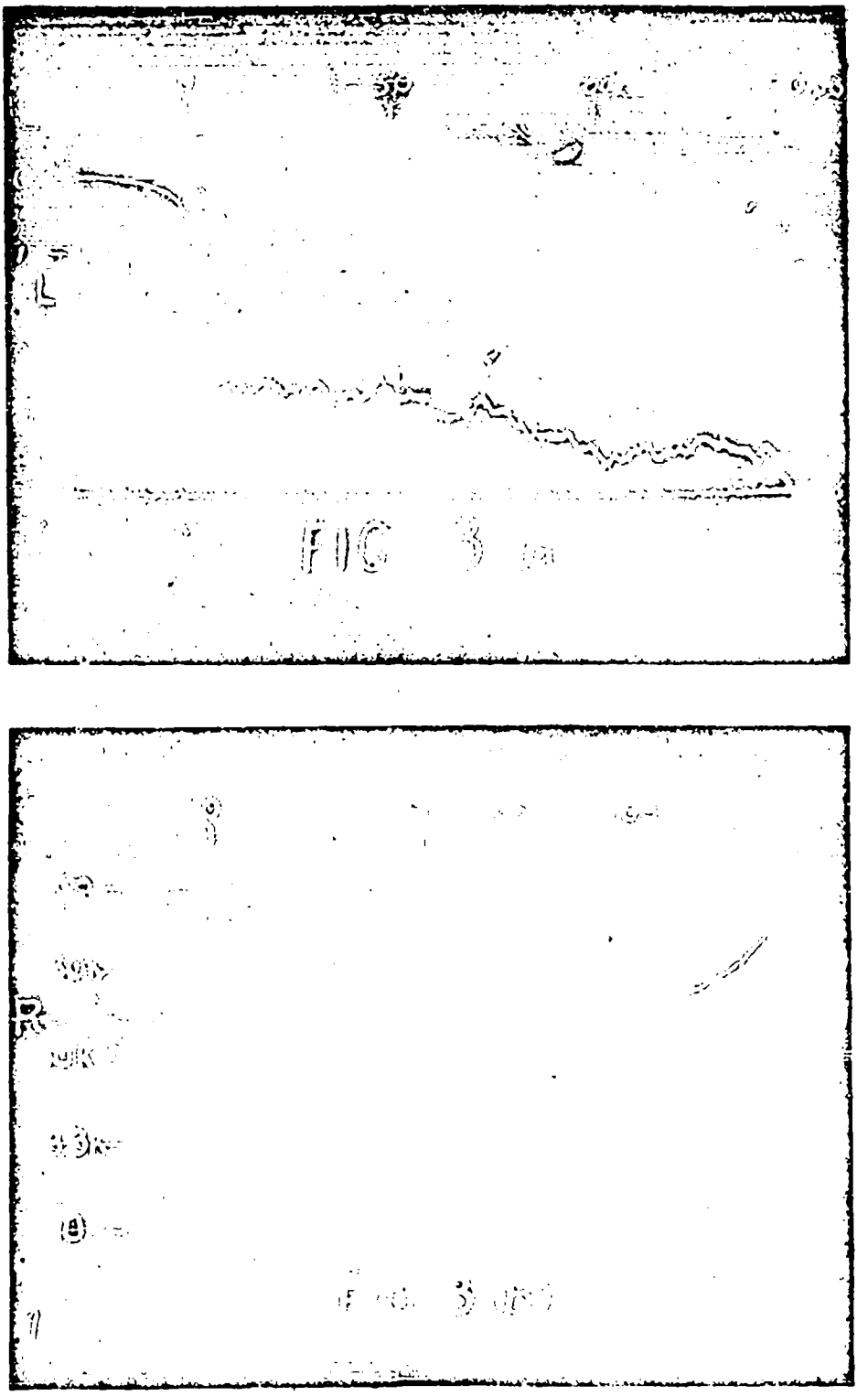

Fig. 3 - (a) Light profile, (b) Ionization profile. 50 mm Hg initial pressure of $2H_2+O_2$ detonated by 50 mm Hg of $C_2H_2+O_2$.

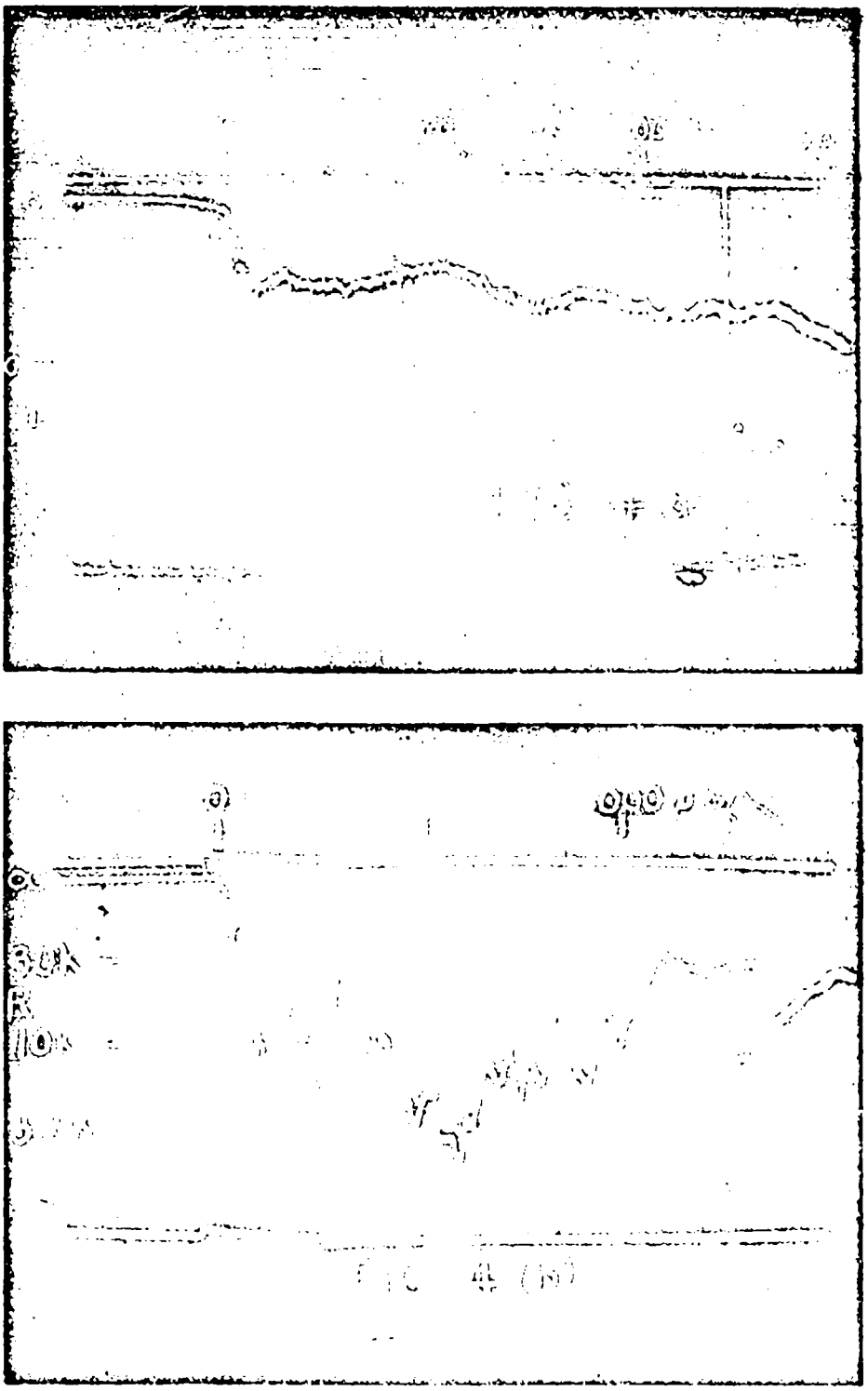

Fig. 4 - (a) Light profile, (b) Ionization profile. 20 mm Hg initial pressure of $2H_2+O_2$ detonated by 35 mm Hg of $C_2H_2+O_2$.

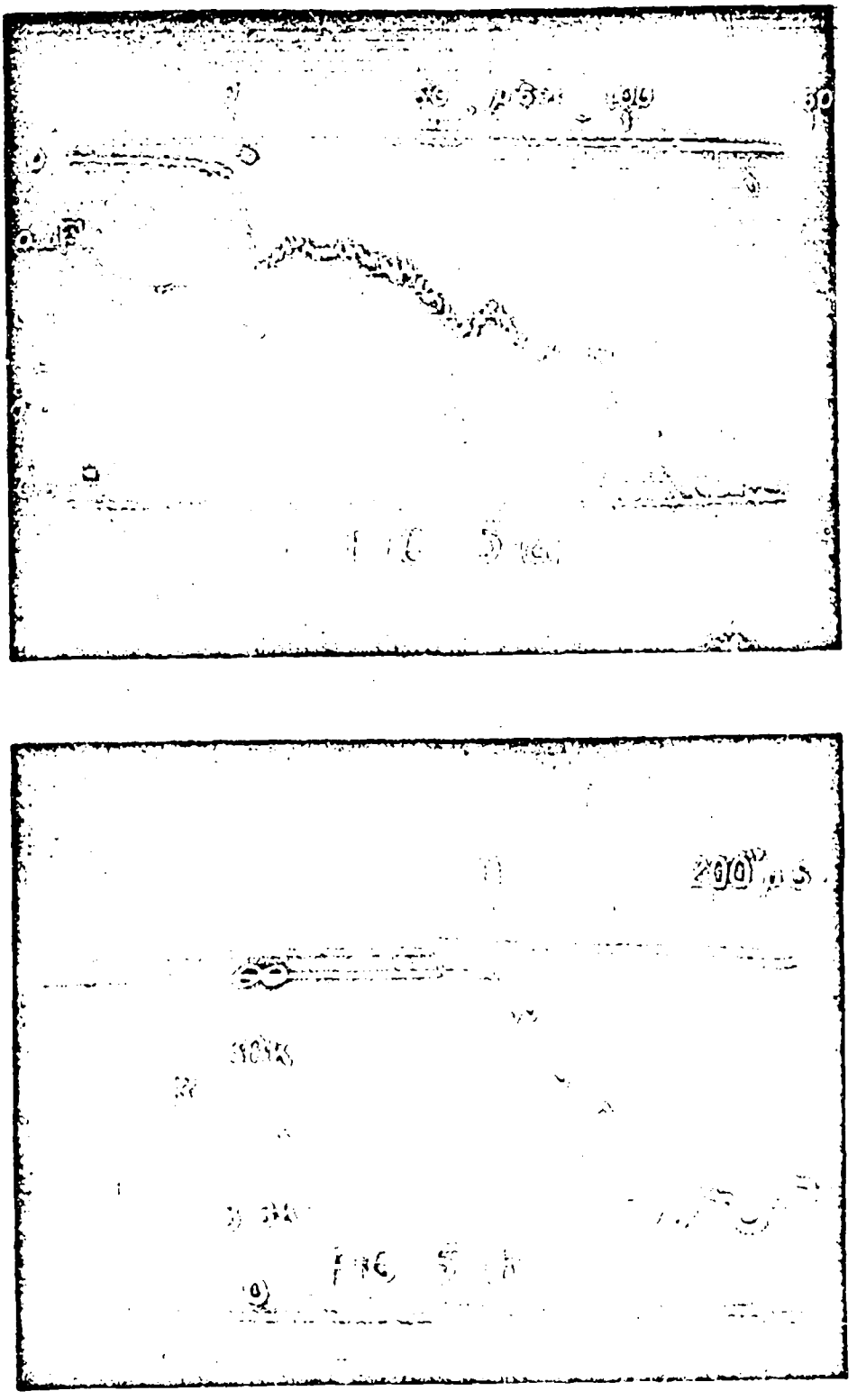

Fig. 5 - (a) Light profile, (b) Ionization profile. 10 mm Hg initial pressure of $2H_2+O_2$ detonated by 40 mm Hg of $C_2H_2+O_2$.

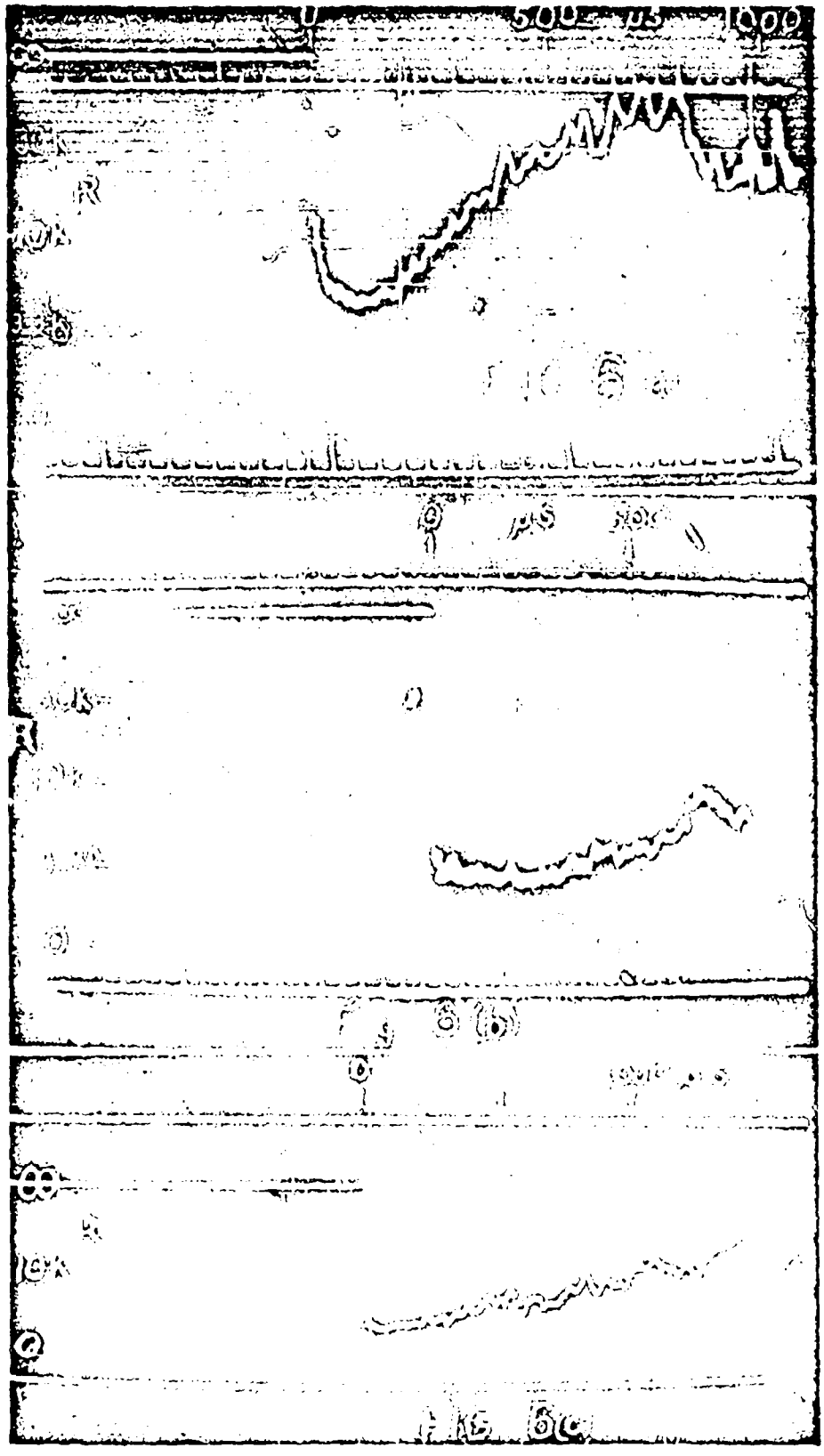

Fig. 6 - Ionization profile development along the tube.
100 mm Hg $2H_2+O_2$ detonated by 150 mm Hg $C_2H_2+O_2$. (a) Probe 5 at 187 cm from diaphragm, (b) Probe 7 at 289 cm, (c) Side probe at 398 cm from diaphragm.

# MEASUREMENTS ON GASEOUS DETONATION WAVES II

J. A. Nicholls, R. B. Morrison, R. E. Cullen
Aircraft Propulsion Laboratory
Engineering Research Institute
University of Michigan
Ann Arbor, Michigan

Most analyses of detonation describe the phenomenon in terms of the change in state conditions across the wave wherein Hugoniot curves are utilized (1). Such an approach is of great utility but tends to obscure the dynamic properties of velocity and heat release. Accordingly, it is enlightening to analyze the equations from the latter point of view and then to trace the various possible processes. Despite a number of simplifying assumptions which are necessary to do this readily, the analysis has a very definite qualitative value.

The system to be considered is as shown in Figure 1. The detonation wave is treated as a standing wave so that the unburned mixture is flowing into the wave front at velocity, $U_1$, and the burned products recede from the front at velocity, $U_2$. Assuming lean fuel-air mixtures

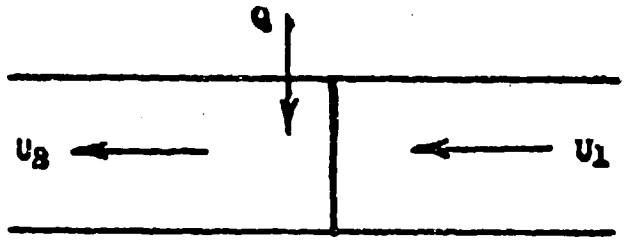


Figure 1. Heat Addition in a Constant Area Duct

so that the process may be treated as an air cycle, the following equations for steady one dimensional flow in a constant area tube may be written:

Conservation of Mass:

$$\rho_1 U_1 = \rho_2 U_2 \qquad (1)$$

Conservation of Momentum:

$$P_1 + \rho_1 U_1^2 = P_2 + \rho_2 U_2^2 \qquad (2)$$

Conservation of Energy:

$$h_1 + \tfrac{1}{2}U_1^2 + Q = h_2 + \tfrac{1}{2}U_2^2 \qquad (3)$$

Equation of State:

$$P = \rho RT \qquad (4)$$

where:

P = static pressure

$\rho$ = density

U = velocity

h = enthalpy

Q = heat addition

T = static temperature

R = gas constant for air

The equations of mass, momentum and state may then be combined to yield an expression for the final temperature. That is:

$$T_2 = \frac{\frac{U_2}{U_1}(RT_1 + U_1^2) - U_2^2}{R} \qquad (5)$$

Assuming a perfect gas so that the enthalpies depend on temperature alone, equation (5) along with the energy equation is sufficient to yield a plot of the final state of the mixture as a function of the initial conditions. This curve is shown in Figure 2 where heat release is plotted against velocity with temperature as a parameter.

The path lines, denoted by $T_p$, represent the transient condition of the stream as heat is added. There are, of course, a number of these path lines but for purposes of discussion only two are shown.

There are also a number of static temperature lines but only one is shown. The line of Q = 0 represents the loci of all points of sonic velocity as heat cannot be added to a sonic stream without a readjustment of the flow. For any path line, such as the ones shown in Figure 2, conditions to the left of points g or h are of subsonic velocity and those to the right are supersonic. The initial conditions of temperature and velocity establish the process on a path line. As heat is added the process follows this path line and whether the velocity be subsonic or supersonic, the heat addition will force the process towards sonic velocity.

## DETONATIVE PROCESSES

The heat release - velocity curves are instructive in describing the various types of detonation possible (2). Consider a combustible mixture at an initial temperature, $T_1$, and of velocity, $U_1$. This establishes the process on a path line, say at point a in Figure 2. If a shock wave occurs, the process jumps adiabatically to point b, the subsonic branch of the same path line. Suppose that chemical reaction takes place which yields an amount of heat, $Q_R$. The process then advances along the path line to point c where $Q_b - Q_c$ is equal to $Q_R$ and $U_c$ is subsonic. Such a process is entirely possible and is ordinarily classified as a strong detonation.

If, in the above case, $Q_R$, is just equal to $Q_b$, the process will terminate at point g, that is the combustion products will be moving at a Mach number of one relative to the front. This is the Chapman-Jouguet type of detonation and is ordinarily the type observed.

The third possibility for this shock process is that where $Q_R$ is greater than $Q_b$, say equal to $Q_e$. The implication of heat addition to a sonic stream requires that there be a readjustment of the flow and hence an unsteady condition exists. Since no solution can exist below $Q_b$, the intersection of the lines $Q = Q_b$ and $T = T_1$ represents the minimum velocity detonation which will satisfy the hydrodynamic equations. This advances the process from point a to point e and then to f and h which is again the Chapman-Jouguet type of detonation.

The third type of detonation, classified on the Hugoniot Curve as weak detonation, is described as a supersonic combustion wave with the combustion products also moving supersonic relative to the front. A process of this type could be visualized as one with an initial state of a and a final state of d. Now there are two possible mechanisms by which this final condition could be attained. First there could be a shock to point b, heat addition to c, and an adiabatic jump to d. This latter path, that from b to c to d is known as a strong deflagration. However, it can be shown that such a path involves a decrease in entropy under adiabatic conditions and is thus

impossible. The remaining possibility is to proceed directly to point 4 with the stream remaining supersonic throughout the heat addition. In view of the present knowledge of flame propagation it seems very unlikely that this mechanism could ever occur though it may be possible under other forms of energy addition. It appears then, that two types of detonation are possible; that of the Chapman-Jouguet type or a strong detonation. The latter has been evidently experienced but only as a transient phenomenon.

The above discussion is premised on conditions of one dimensional steady flow. Accordingly, it cannot serve to explain such wave structures as shown in Figure 5 (taken from reference 3). The pictures shown are of two separate lean hydrogen-oxygen detonations propagating to the right in a ½ inch by 3/8 inch tube. Assuming that the waves developed identically, it can be seen from the similarity of the two photographs that they are about 180° out of phase. Very possibly this is a case of spinning detonation and calculation of the pitch agrees quite well with the theory of J. A. Fay (4). Also, the pitch is about identical to the perimeter of the tube. From the photographs it is apparent that the assumption of one dimensional steady flow is not entirely valid and the instabilities are time dependent. Needless to say, the chemical kinetics will be altered by such instabilities and it becomes hard to separate the chemical aspects from the hydrodynamics.

## CORRELATION OF DETONATION VELOCITIES

The heat addition - velocity curve has proved valuable in studying qualitatively the phenomenon of detonative combustion. However, its use has been restricted to an air cycle and consequently does not allow for any change in molecular weight across the combustion front. A more rigorous treatment of the equations with appropriate simplifications points to two non-dimensional parameters; namely, $\frac{m_1 Q}{m_2 c_{p1} T_1}$ and $M_D$, where $m_1$ and $m_2$ are the molecular weights before and after combustion respectively, $c_{p1}$ is the specific heat at constant pressure for the initial mixture, and $M_D$ is the Mach number of detonation. Such an analysis has been described in an earlier paper (5) and shall not be repeated here. Q is the actual energy added and should, of course, allow for the effects of dissociation.

The detonation velocities of a number of gaseous mixtures have been measured at the Aircraft Propulsion Laboratory and reported earlier (2). These data were reduced to the parameters mentioned above and the results are shown in Figure 4. Simplifications on the chemical aspects were made so as to permit ready calculation. It can be seen that the data correlate very well although the slope differs from that of the theory. A few points at the lower Mach numbers are

seem to fall off of the curve. These points correspond to those near the limits of detonation and it is highly probable that the flow was unstable when the velocity measurements were effected.

## SPARK SCHLIEREN PHOTOGRAPHS

A number of spark schlieren photographs of detonation waves have been obtained. For the most part these waves were initiated by a spark in a rectangular tube of ½ inch by 3/8 inch internal dimensions.

The first series of pictures, Figure 5, represent a time sequence in the initiation of detonation in a 50% (by volume) acetylene-oxygen mixture. Each photograph is for a different detonation, but taken at a different time interval from the energization of the initiating spark. In Figures 5a, 5b, and 5c, the flame front with the preceding shock wave can be seen propagating along the tube. In Figures 5d and 5e the shock front has evidently initiated combustion directly behind it and is now propagating to the right as a detonation. The generated retonation wave has evidently passed through the original flame front and has reflected from the closed end of the tube as a shock wave. It is believed that the inclined shock waves behind the detonation front can be attributed to the spark ignition as numerous photographs of shock initiated detonations do not seem to show this phenomenon. Another spark ignited detonation is shown in Figure 6. This is of a 50% hydrogen-oxygen detonation and was effected with a rectangular tube of 2-½ inches by 3-½ inches. Again, the trailing inclined shocks are apparent.

A second series of pictures were taken of a 50% hydrogen-oxygen detonation passing over an inclined wedge. The wedge was mounted in the 2-½ inch by 3-½ inch tube such that the bottom surface was parallel to and ½ inch above the lower wall of the tube. In this way part of the detonation could traverse the lower channel and serve as a time reference to clock the portion of the wave passing over the upper surface of the wedge. This, of course, assumes no influence of the collision with the wedge on the characteristic Chapman-Jouguet velocity of detonation for that mixture. The first picture of this time sequence is shown in Figure 7. The wave is moving to the right and it appears as though the upper portion has already accelerated. The curved shock which interacts with the detonation front to form a triple point is originally generated from the apex of the wedge. The rectangular shape near the leading edge of the wedge and the fuzziness along the inclined surface are due to marks on the glass sides of the tube. At later times, Figures 8 and 9, the upper portions of the detonation wave are seen to be definitely accelerating away from the lower Chapman-Jouguet condition. The influence of the bubble undoubtedly accounts for the excess Chapman-Jouguet velocity of that portion of the detonation front which is perpendicular to the wedge. However, it is difficult to understand why the other portion has been accelerated as it has theoretically been unaffected by the

presence of the wedge. Other photographs, along with those shown, have enabled the variation of velocity of the components of the detonation front with time to be determined. This information is plotted in Figure 10.

Spark schlieren photographs of various hydrogen-oxygen detonations have been obtained and are shown in Figure 11. The volumetric mixture ratio is indicated under each photograph. In the case of 19.5% detonation the initial front has passed out of the picture to the right and the combustion lags considerably behind, as much as 4 to 5 inches. As the mixture is enriched this combustion lag is noticably shortened until the combustion is evidently initiated immediately in the shock front as shown in Figure 11-d.

All of the schlieren photographs shown to this point have been limited to one per detonation. This makes it extremely difficult to detect any unsteadiness in the propagation. Accordingly, two spark gaps were designed and fabricated to serve as light sources for two separate schlieren systems. In addition an adjustable time delay was incorporated between the two spark gaps. In order to utilize very small time delays, it was necessary to overlap the two schlieren fields of view. Hence, the two optical paths crossed at the test section of the tube with an included angle of about 7 degrees. This leads to some slight discrepancy between two pictures of the same wave. A few of these dual spark photographs were obtained on lean hydrogen-oxygen detonations and are shown in Figures 12, 13, and 14. The time delays between photographs in the figures are 7.0, 7.5 and 8.0 microseconds respectively. Apparently there is a rotation or oscillation taking place. The marked difference between these figures suggests that insufficient tube length was used to insure that Chapman-Jouguet detonation was established. It is planned to investigate this aspect further.

## ACKNOWLEDGEMENT

Sincere appreciation is extended to Project Squid which has sponsored a large part of the work and the formulation of this paper. Some of the data presented was obtained and reported under an earlier Air Force contract (References 2 and 3).

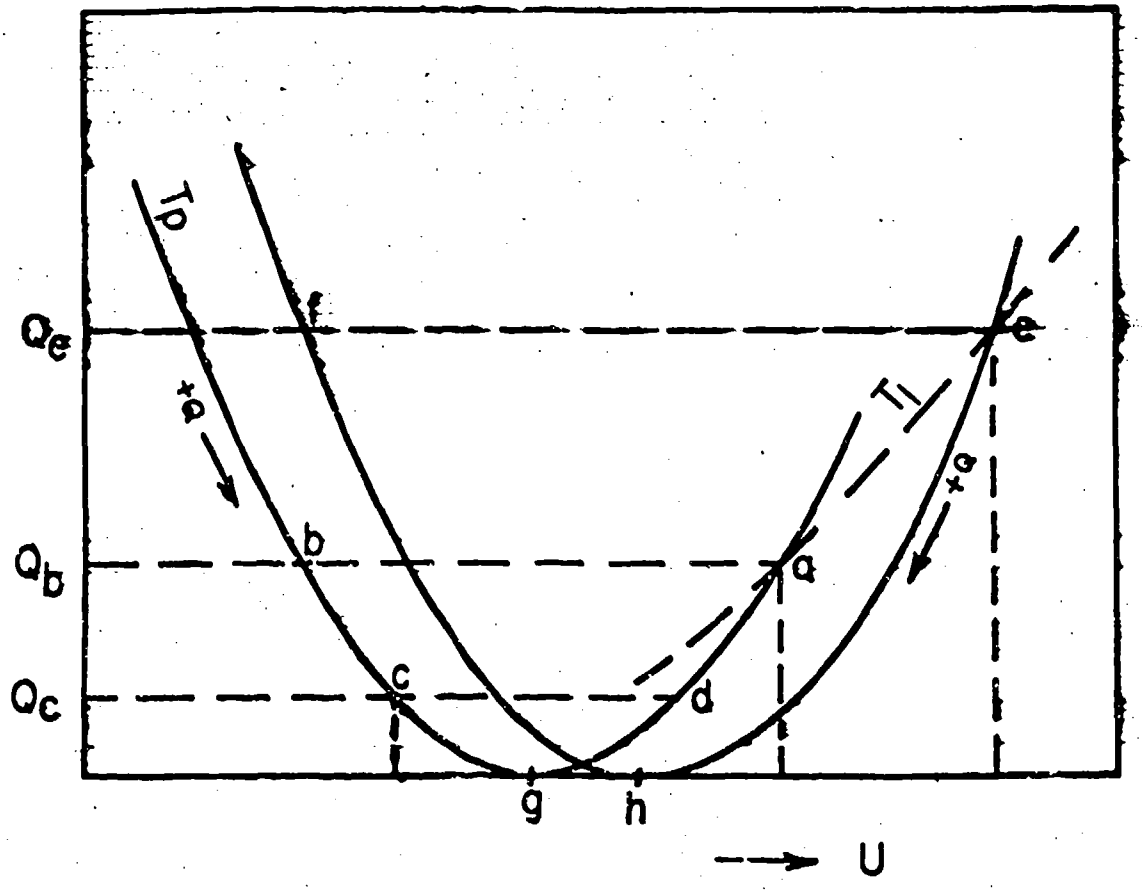


Figure 2 - Heat Release vs. Velocity

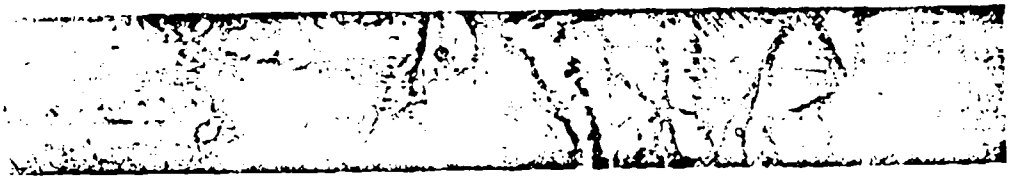

(a)

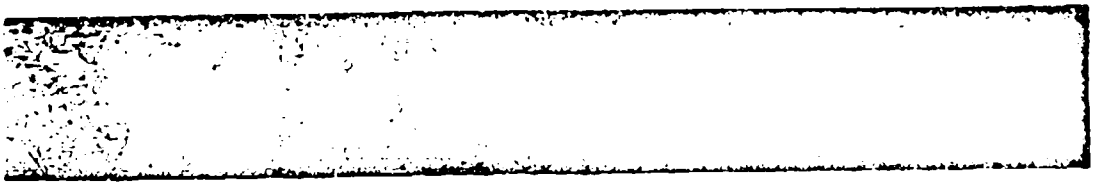

(b)

Figure 3 - 24% Hydrogen-Oxygen Detonations

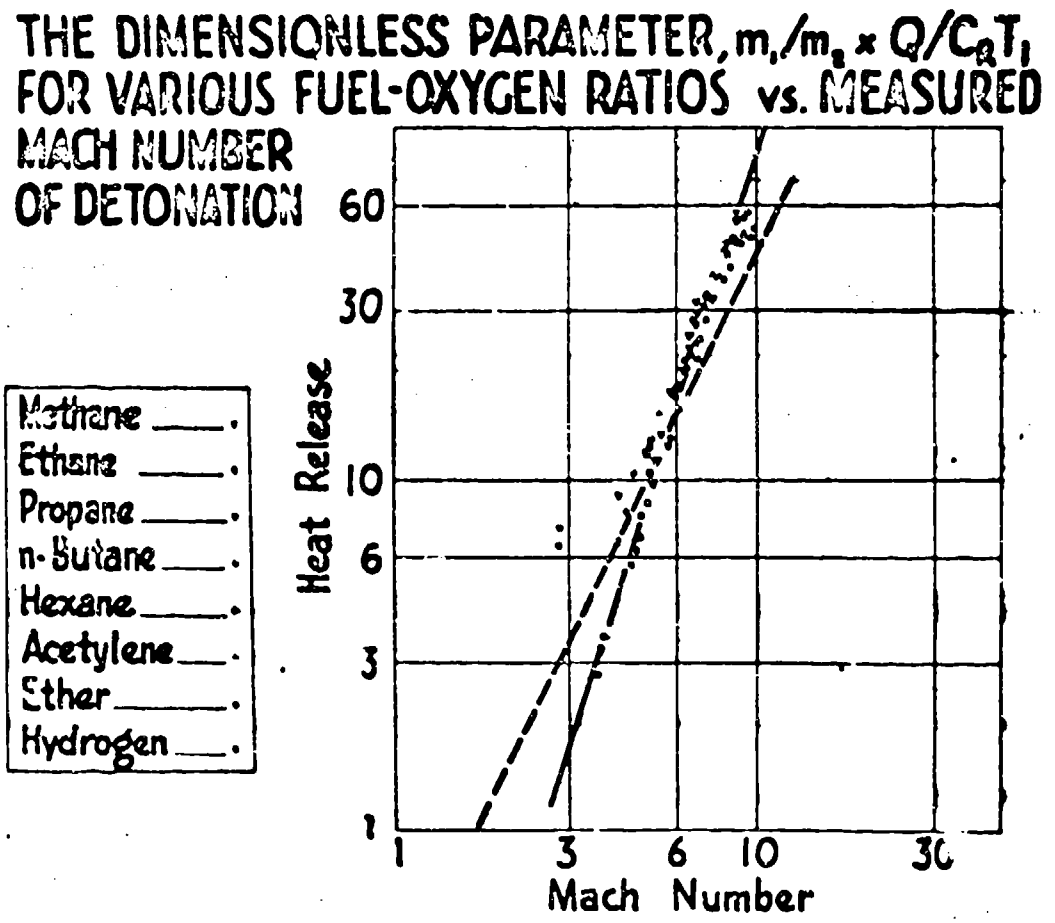


Figure 4 - Correlation of Detonation Velocities

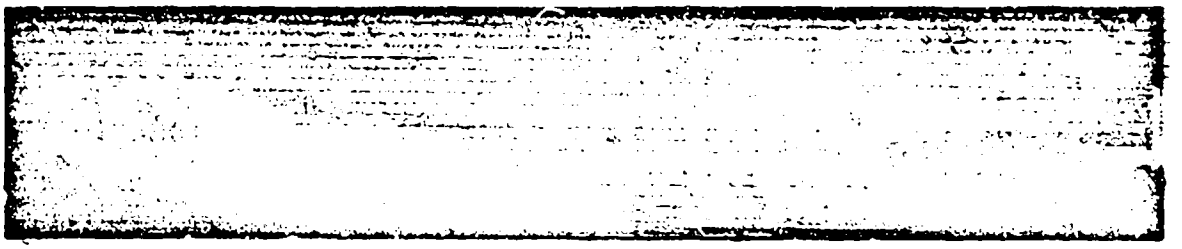

(a)

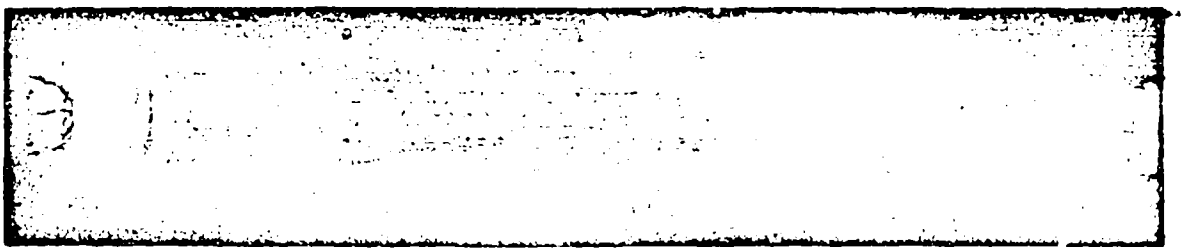

(b)

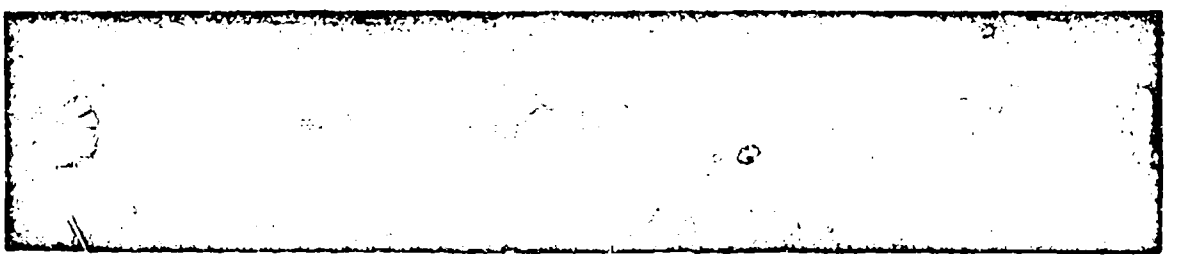

(c)

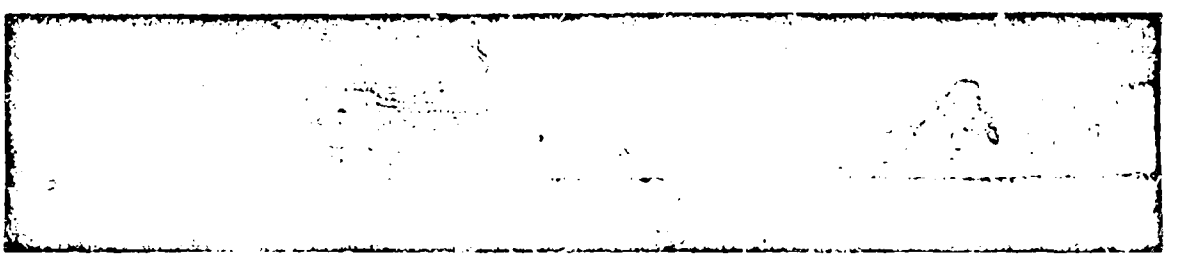

(d)

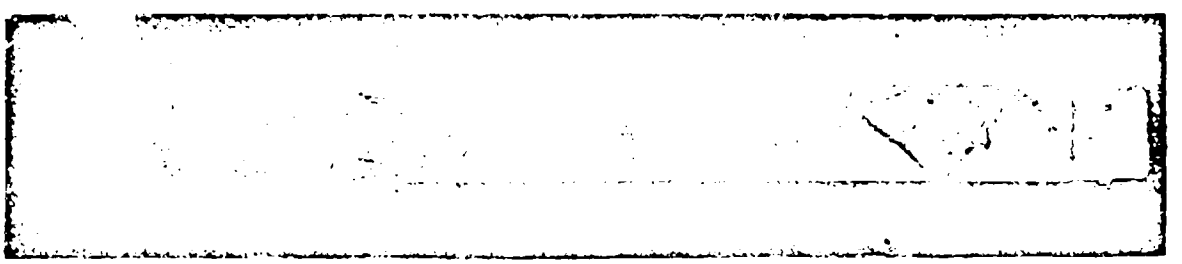

(e)

Figure 5 - Spark Initiation of Acetylene-Oxygen Detonation

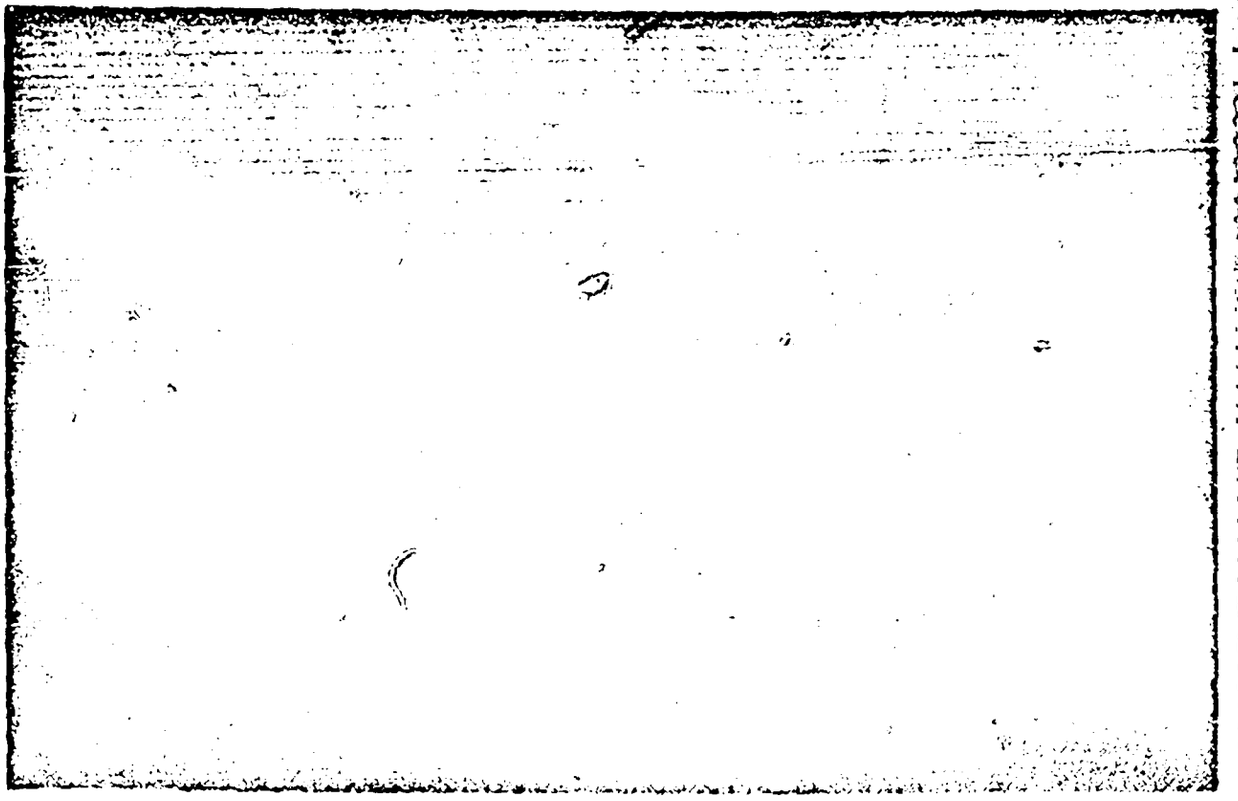

Figure 6 - 50% Hydrogen-Oxygen Detonation

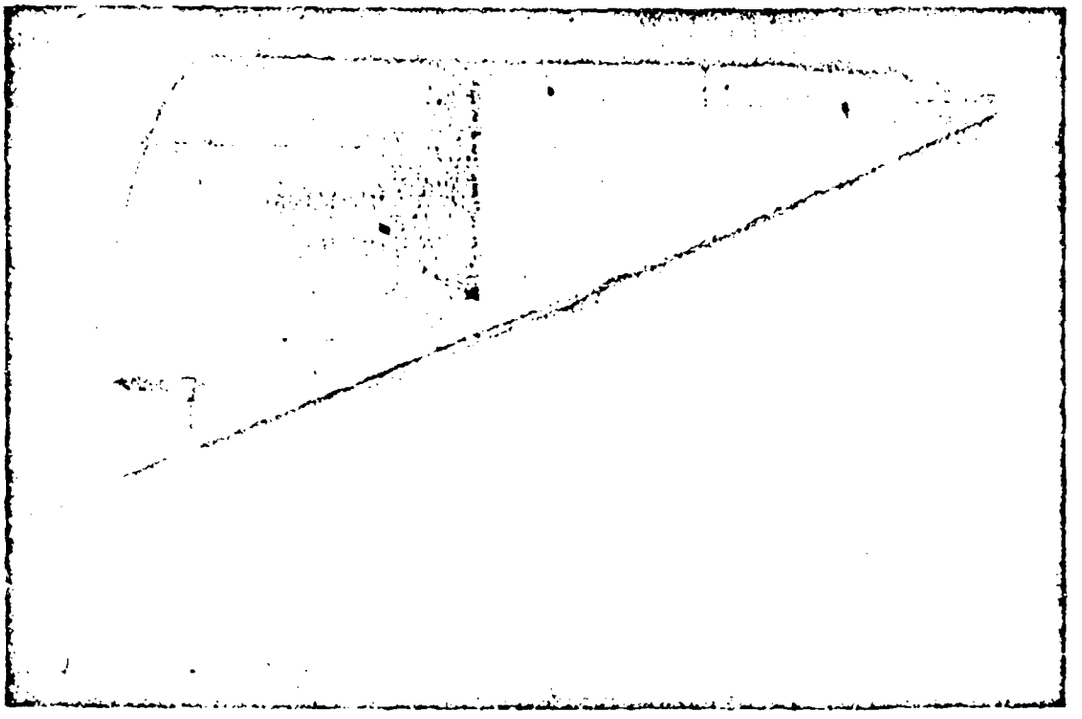

Figure 7 - Detonation Wave over a Wedge

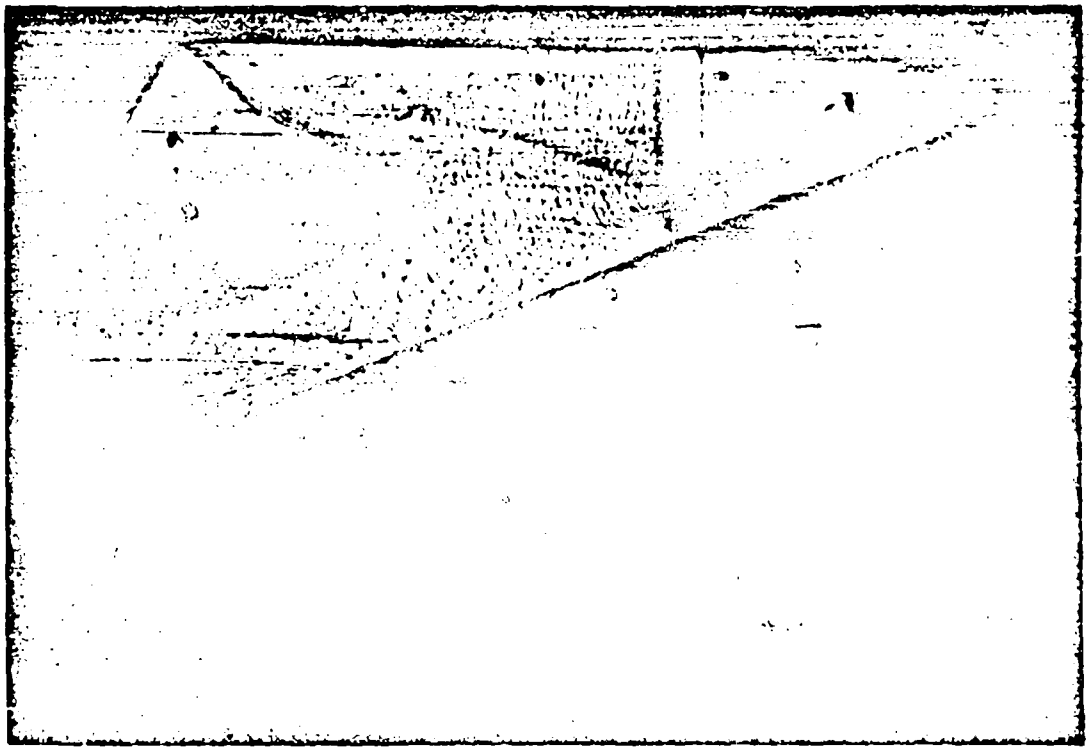

Figure 8 - Detonation Wave over a Wedge

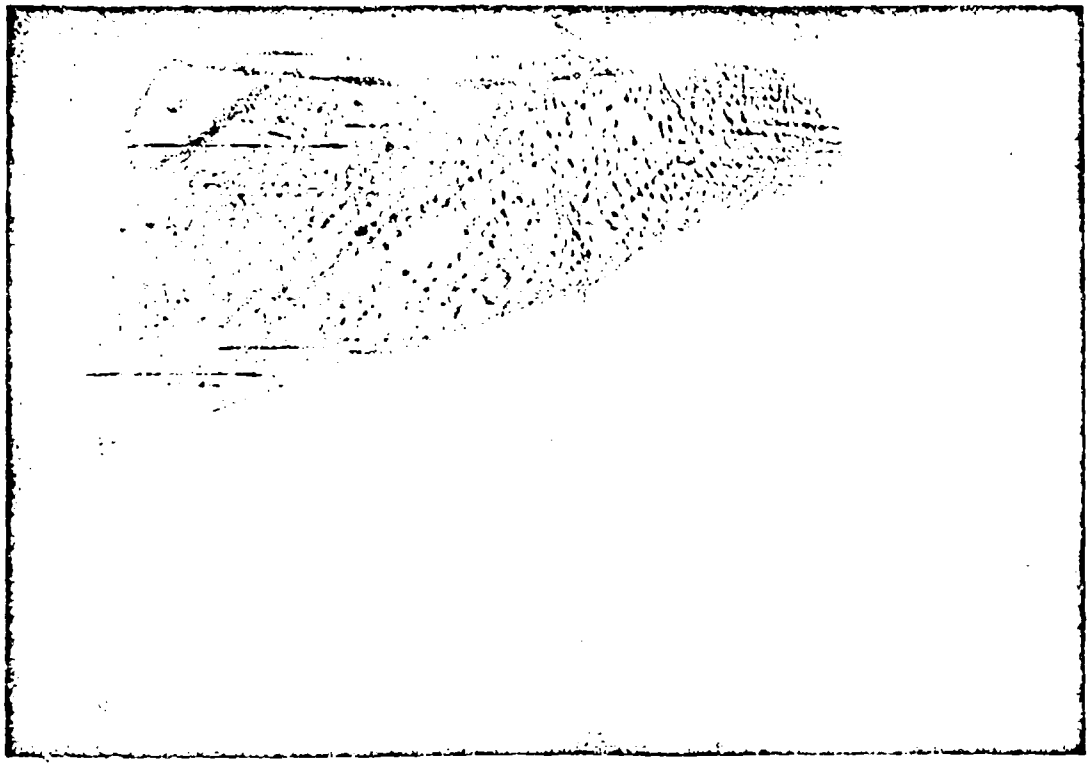

Figure 9 - Detonation Wave over a Wedge

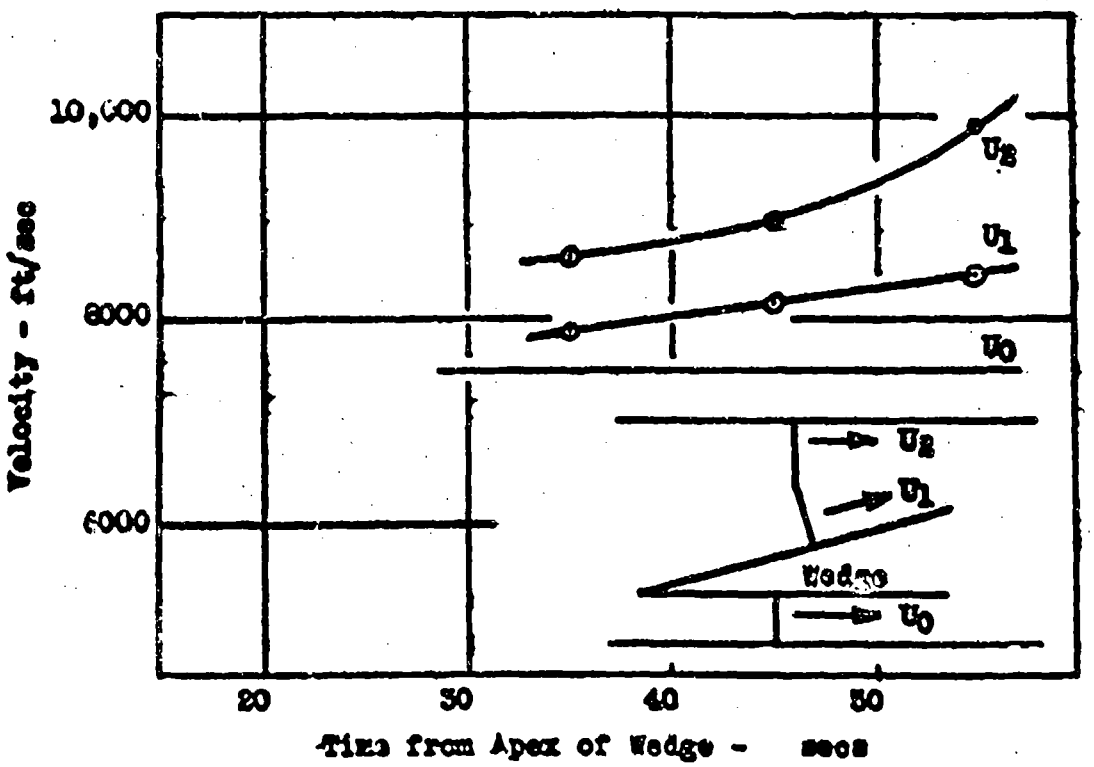


Figure 10 - Results of Wedge Experiment

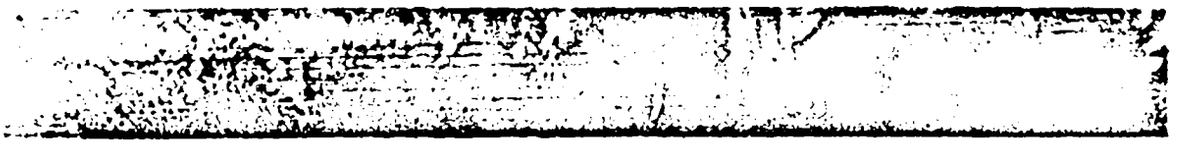

(a) 19.5% Hydrogen-Oxygen

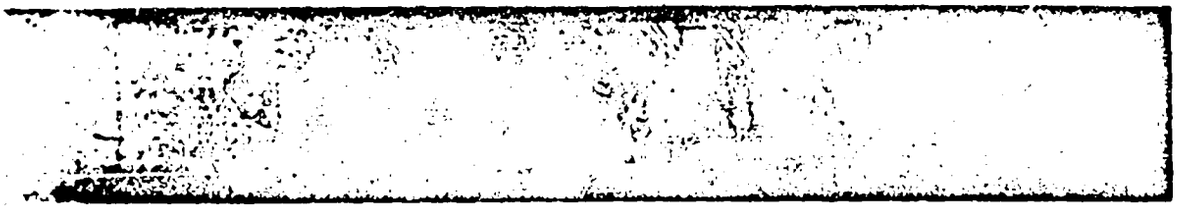

(b) 40% Hydrogen-Oxygen

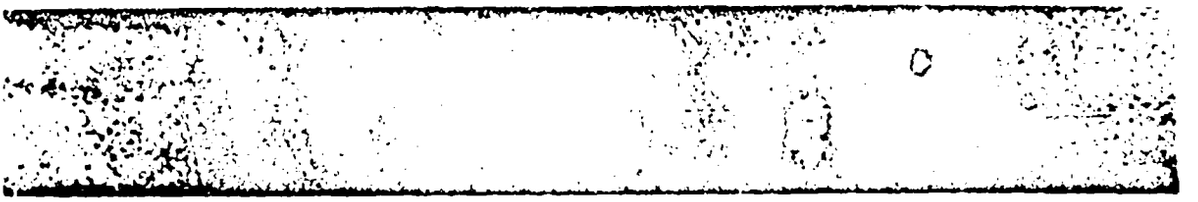

(c) 50% Hydrogen-Oxygen

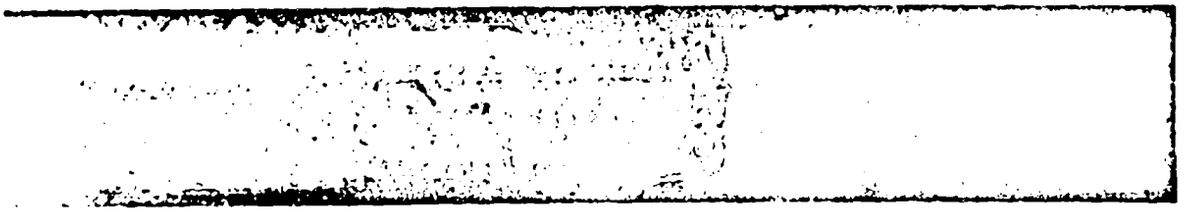

(d) 72% Hydrogen-Oxygen

Figure 11 - Hydrogen-Oxygen Detonations

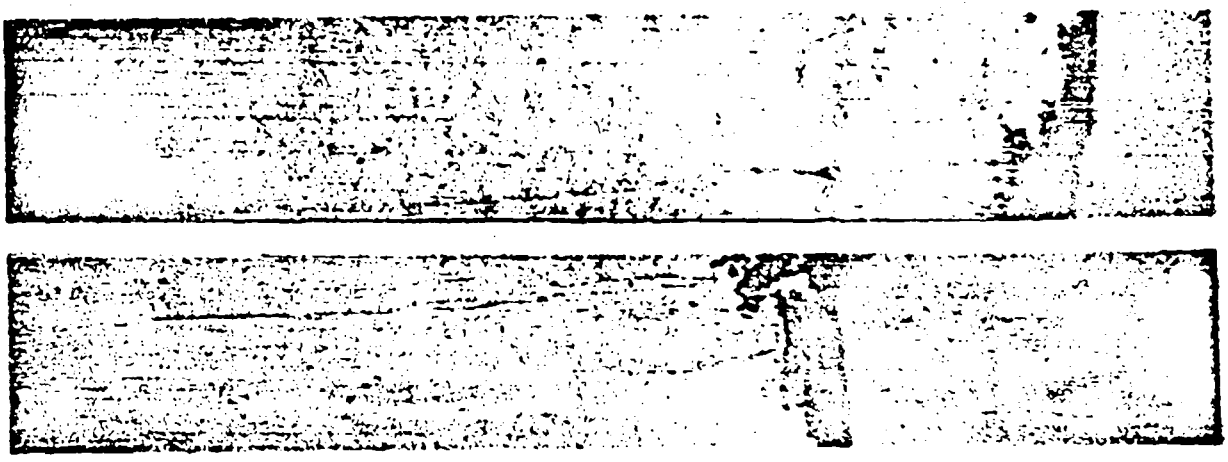

Figure 12 - Hydrogen-Oxygen Detonation,
7 secs Delay

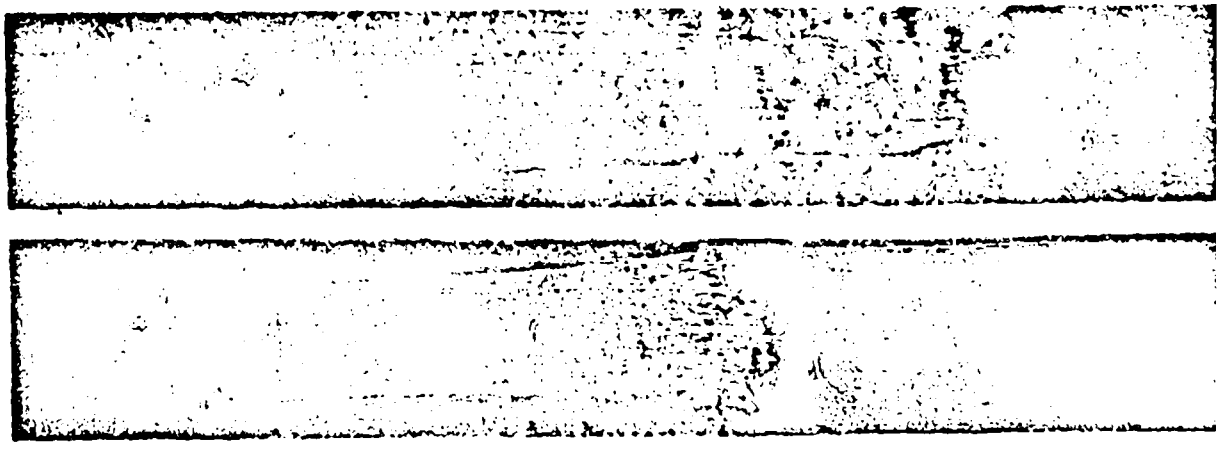

Figure 13 - Hydrogen-Oxygen Detonation,
7.5 secs Delay

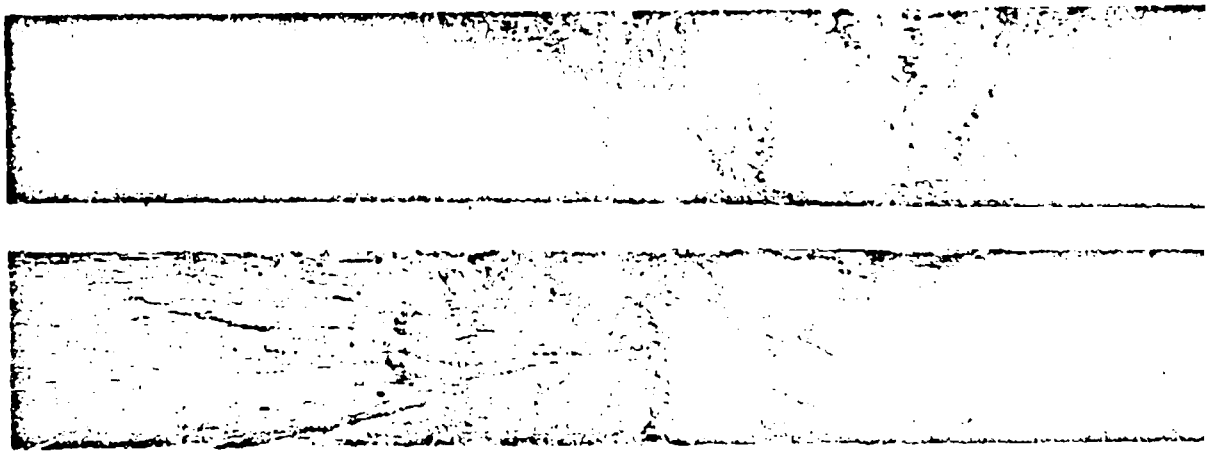

Figure 14 - Hydrogen-Oxygen Detonation,
8.0 secs Delay.

## REFERENCES

1. Courant, R. and Friedricks, K. O., "Supersonic Flow and Shock Waves," Interscience Publishers, Inc., New York, 1948.

2. Morrison, R. B., "A Shock Tube Investigation of Detonative Combustion," University of Michigan, UMM-97, 1952.

3. Nicholls, J. A., Morrison, R. B., Reid, F. A., Ong, R., "Final Report on Detonative Combustion," University of Michigan, Engineering Research Institute, August 1953.

4. Fay, J. A., J. Chem. Phys., 20, No. 6, 942-950, June 1952.

5. Morrison, R. B., "A Study of Detonative Phenomena in Gaseous Mixtures by the Use of Shock Tube Techniques," ASME Paper No. 52-SA-20.

# STUDIES ON GASEOUS DETONATION

12

B. Greifer, F. C. Gibson and C. M. Mason
U. S. Bureau of Mines
Pittsburgh, Pennsylvania

## Introduction

A photographic investigation of combustion waves in gases was undertaken to observe experimentally the constitution of deflagrations and detonations. Although the principles of the techniques applied were not new, the careful use of precision optical components produced exceptionally detailed and revealing pictures. Photographs obtained for various mixtures of oxygen with hydrogen and/or carbon monoxide support many of the concepts on the mechanism of detonation presented in the literature and permit a choice among several theories of detonation wave structure.

## Experimental Procedure

A diagram of the laboratory set-up is shown in figure 1. The explosions occurred in a steel tube of rectangular cross section with suitable observation ports and were photographed by the schlieren technique. The essential components of the optical system for schlieren photography were a matched pair of parabolic reflectors of 16 inches diameter and 126 inches focal length, a point source of light at the focus of one mirror, a field slit at the detonation tube, a knife edge at the focus of the other mirror, and a rotating-mirror camera immediately behind the knife edge. With this optical system, density gradients were observed readily in the detonation tube placed in the light path between the two mirrors.

As the resolution, i.e. the ability to separate the fine detail in the photographs, depends upon the degree of optical perfection, the fabrication and mounting of the mirrors were subject to rigid specifications. The mirrors were set into heavy cast iron mounts which rested on concrete pillars that passed through the laboratory floor into the ground beneath the building. These mounts were massive enough to assure vibrationless support for the mirrors,

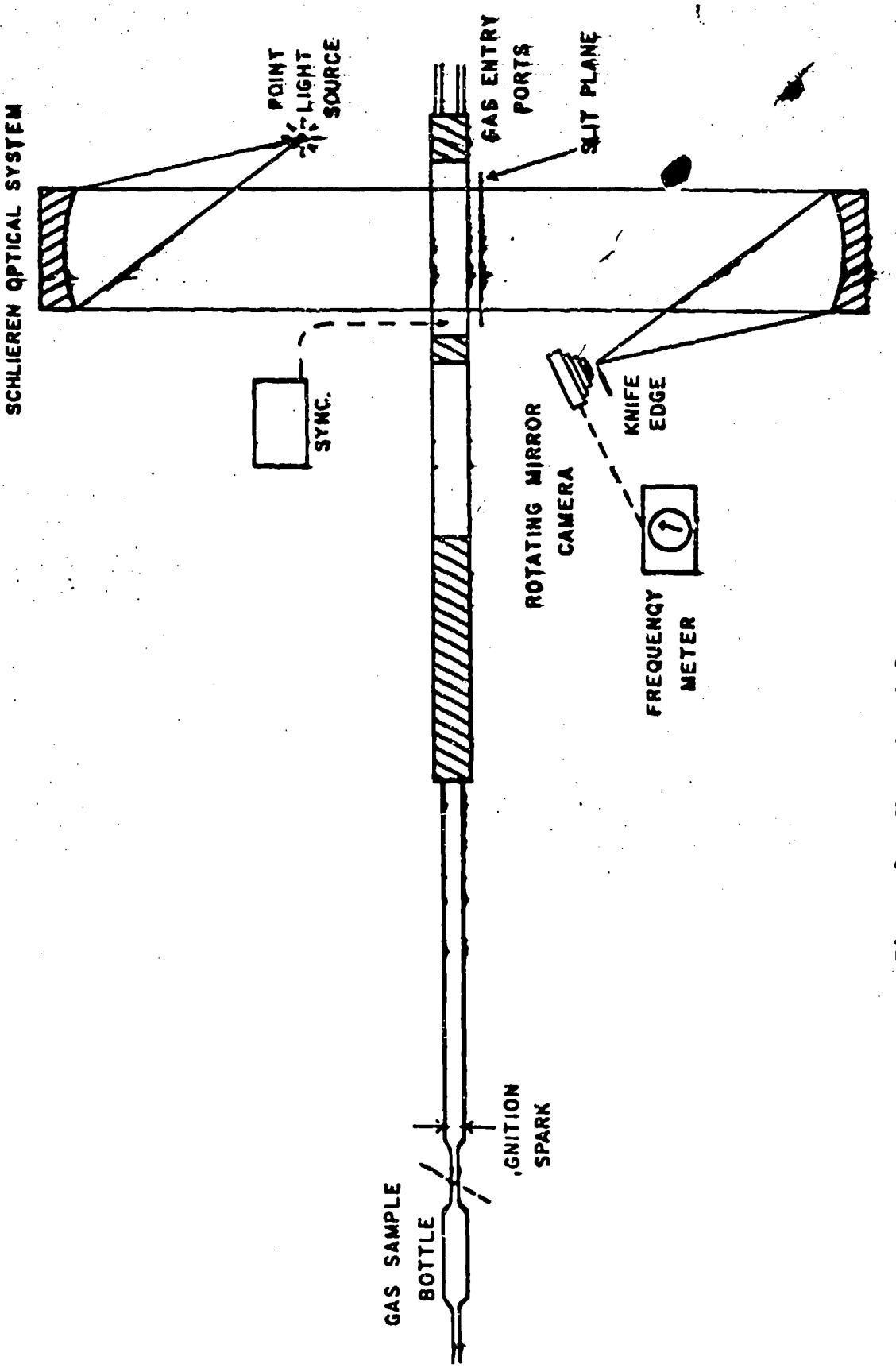


Figure 1 - Experimental arrangement.

yet were precise enough to provide delicate micrometer adjustment in three planes, for focusing and aligning the optical system.

The rotating-mirror camera was simple in design and could be constructed readily from commercially available materials. It has been described in detail elsewhere (1). A steel tube of rectangular cross section, one inch high by 3/4 inches wide and 7 feet long, was used for the hydrogen-oxygen work. To obtain detonation with carbon monoxide, it was necessary subsequently to add enough half-inch copper tubing to increase the over-all length to 55 feet. This change of size and shape is not believed to have any significant effect on the transition from deflagration to detonation, because this transition did not occur until the combustion had progressed well into the rectangular section.

In each experiment, the tube was filled with a gas mixture of known composition which was ignited at the open end of the tube by means of an electric spark. Electronic synchronization activated the schlieren light source while the combustion was in the field of view of the camera. Each print was mounted within a coordinate grid and the various structural features were measured directly.

## Hydrogen-Oxygen Explosions

Figure 2 is representative of the photographs obtained for stoichiometric mixtures of hydrogen and oxygen. It shows a detonation wave traveling across the field of view from left to right and a reflection from a corner of the observation window which projected slightly into the path of the combustion. The group of parallel lines behind the shock front is due to strains in the glass windows. Note that the group is reflected elastically, the speed remaining constant at 3140 m/s. This is to be compared with the reflected shock in the gas which has decelerated from 3140 m/s to 1350 m/s.

An important feature which may be observed in this hydrogen-oxygen photograph (figure 2) is the appearance of striations with a positive slope. These striations indicate the presence of a disturbance traveling 600 m/s in a direction opposite to the movement of the detonation and will be referred to as "retrograde striations". It has been suggested (2) that these retrograde striations are evidence of periodic velocity change of the detonation front or of spinning detonation. This appears to be the first time that such a phenomenon has been observed for stoichiometric mixtures of hydrogen and oxygen (3). The period of occurrence of the retrograde striations in hydrogen-oxygen detonations is 0.4 microsecond, corresponding to a recurrence frequency of 2.5 megacycles.

## Carbon Monoxide-Oxygen Explosions

In the case of carbon monoxide-oxygen mixtures, it was possible to adjust the experimental conditions so as to obtain

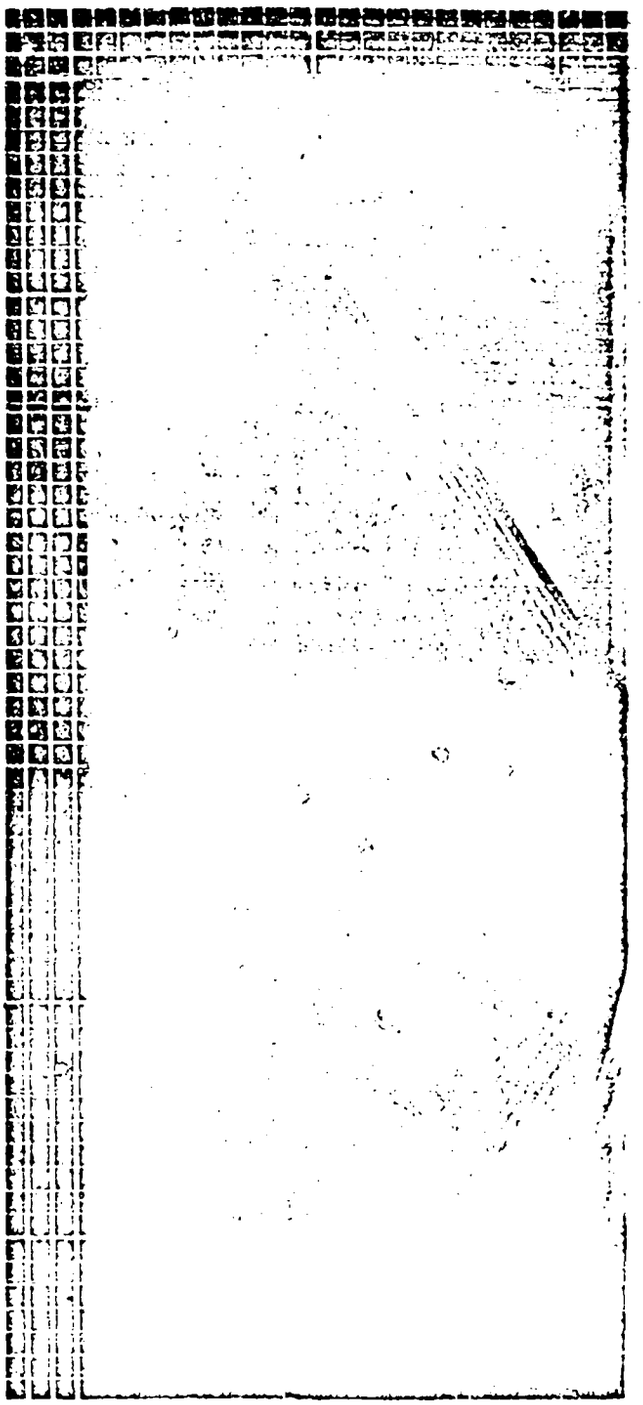

Figure 2 - Streak Schlieren Photograph of Detonation in a Mixture of 70% Hydrogen, 28% Oxygen, 2% Inert Gas. Observe the retrograde striae, the strains in the glass windows of the detonation tube, and the reflections off the end of the observation section. Each horizontal scale division equals 7.06 mm, and each vertical division 1.41 microseconds.

photographs of deflagration and detonation and, in a few cases, of the actual transition from one to the other. Figure 3 is a photograph of a carbon monoxide-oxygen deflagration and figure 4 shows a similar deflagration just before the transition to detonation. Figure 5 is a line drawing of the features of a deflagration to be compared with figures 3 and 4. The transition from deflagration to detonation is photographed in figure 6 and shown diagramatically in figure 7.

One feature of considerable interest is the pronounced hooks or "cusps" shown in figure 5. These are prominent in figure 3, discernible by careful scrutiny in figure 4, and visible in the deflagration region of figure 6. These cusps are located immediately behind the shock wave, well inside the reaction zone. The peaks of the cusps fall 4 to 7 mm. behind the shock wave in the tube. This distance may be compared with the thickness of the shock (0.8 mm.) and the 25-to-50 mm. average thickness of the entire reaction zone. It is possible that the peaks of these cusps represent sites of energy release in the chemical reactions which trail the shock wave. Such sites of energy release would form a cusp-shaped pattern on a streak photograph. It has been predicted (4) that a flame front might be overtaken from the rear by weak compression waves and thus be accelerated discontinuously. Sighting along the line of the shock front in figure 4, we see that wherever such a pressure wave strikes the shock front from behind there is such an increase of flame velocity. This is pictorial confirmation of the above prediction.

Figures 6 and 7 show a deflagration becoming a detonation. The deflagration wave changes suddenly to a detonation at point T, the transition point, and a rearward-traveling wave, the retonation wave, marks the sudden release of energy. The fact that point T (figure 7) is not on a linear extension of the deflagration shock front may be due to the initiation of detonation above or below the slit and off center in the tube. Other photographs have located T right in line with S. The close resemblance between the shape of T and the shape of the cusps is to be noted.

Figure 8 is a photograph of detonation in carbon monoxide and oxygen immediately after the transition point T; figure 9 shows a detonation at a somewhat later time. The co-linearity of the shock front in the luminous and schlieren photographs may be noted (figure 8), although the significance of this co-linearity is dimmed somewhat by the consideration that there is a definite parallax between a two-mirror system (schlieren) and a one-mirror simple reflection (luminosity).

The arcs between the detonation and retonation waves in figure 8 are due to multiple reflections of pressure waves from the walls of the detonation tube. The last of these arcs are still visible in figure 9. These pressure waves originate at the moment

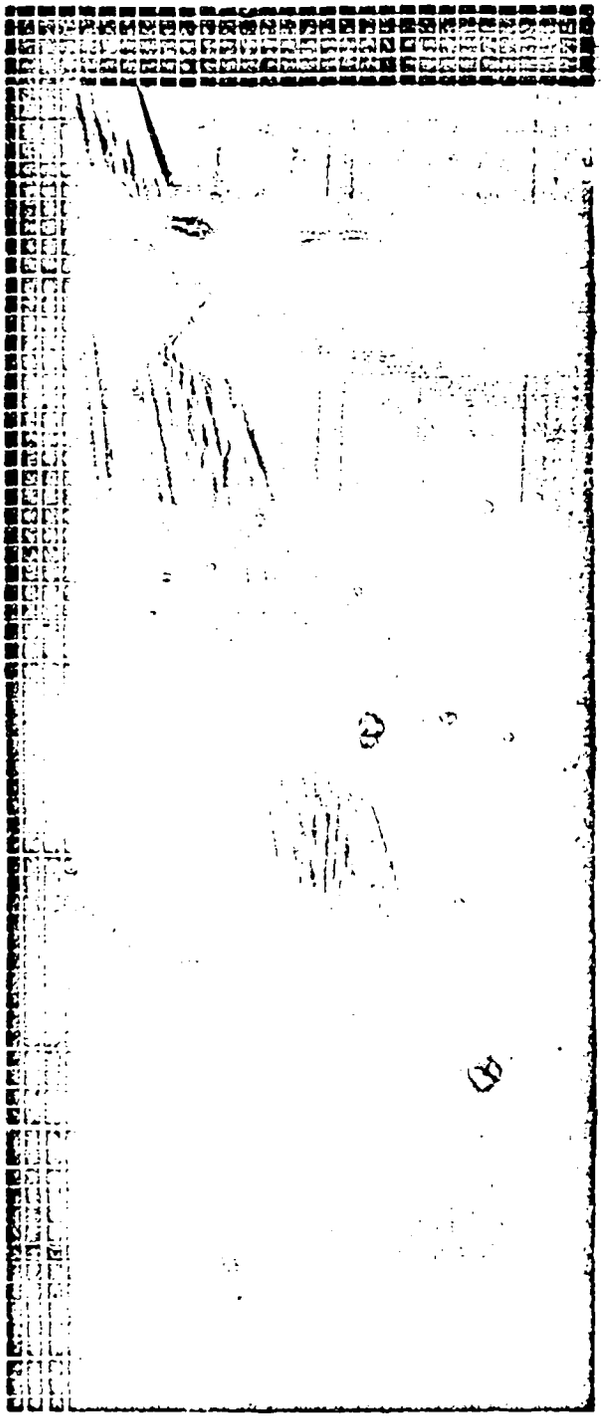

Figure 3 - Streak Schlieren Photograph of Deflagration in a Mixture of: 64.1% Carbon Monoxide, 30.5% Oxygen, 2.2% Hydrogen, 3.2% Moisture and Inert Gases. Note cusps immediately behind the shock. Each horizontal scale division equals 7.06 millimeters, and each vertical division is 2.82 microseconds.

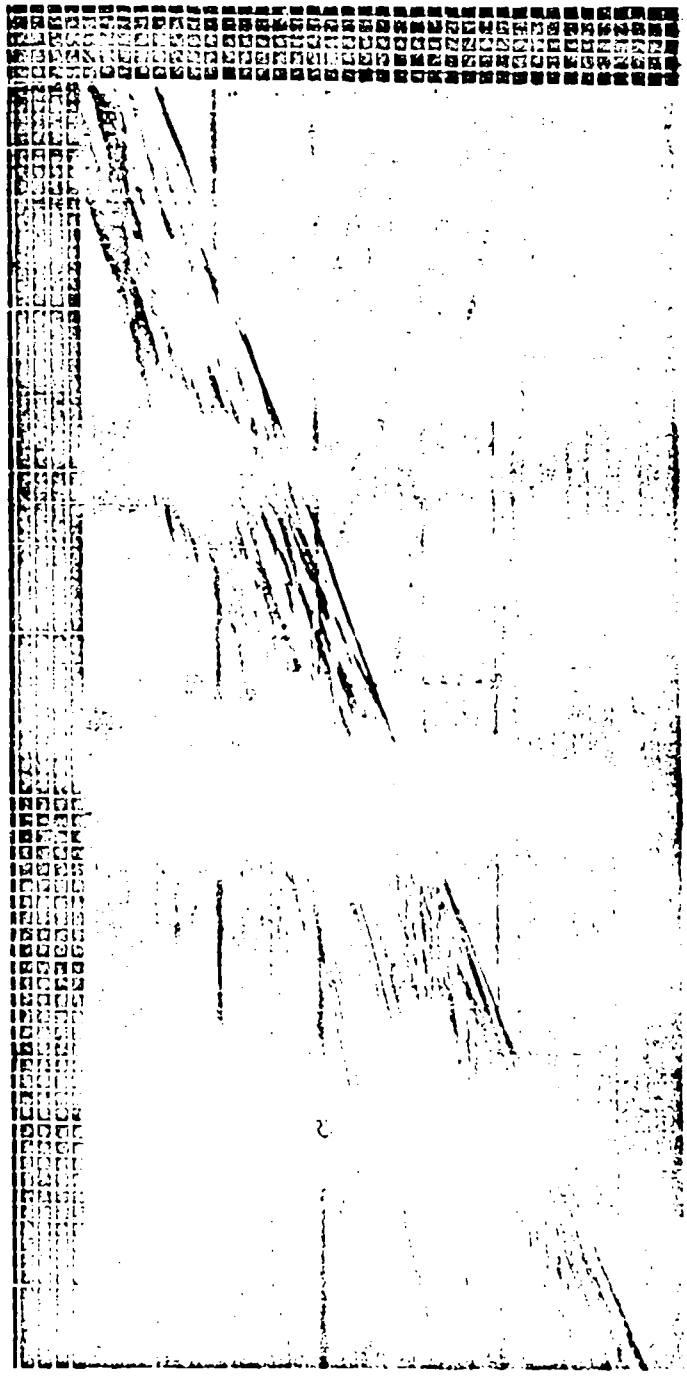

Figure 4 - Streak Schlieren Photograph of Deflagration in a Mixture of: 47.4% Carbon Monoxide, 49.1% Oxygen, 1.1% Hydrogen, 2.4% Moisture and Inert Gases. Note acceleration of shock front by support of pressure waves from behind. Each scale division is 7.06 millimeters horizontally, and 2.82 microseconds vertically.

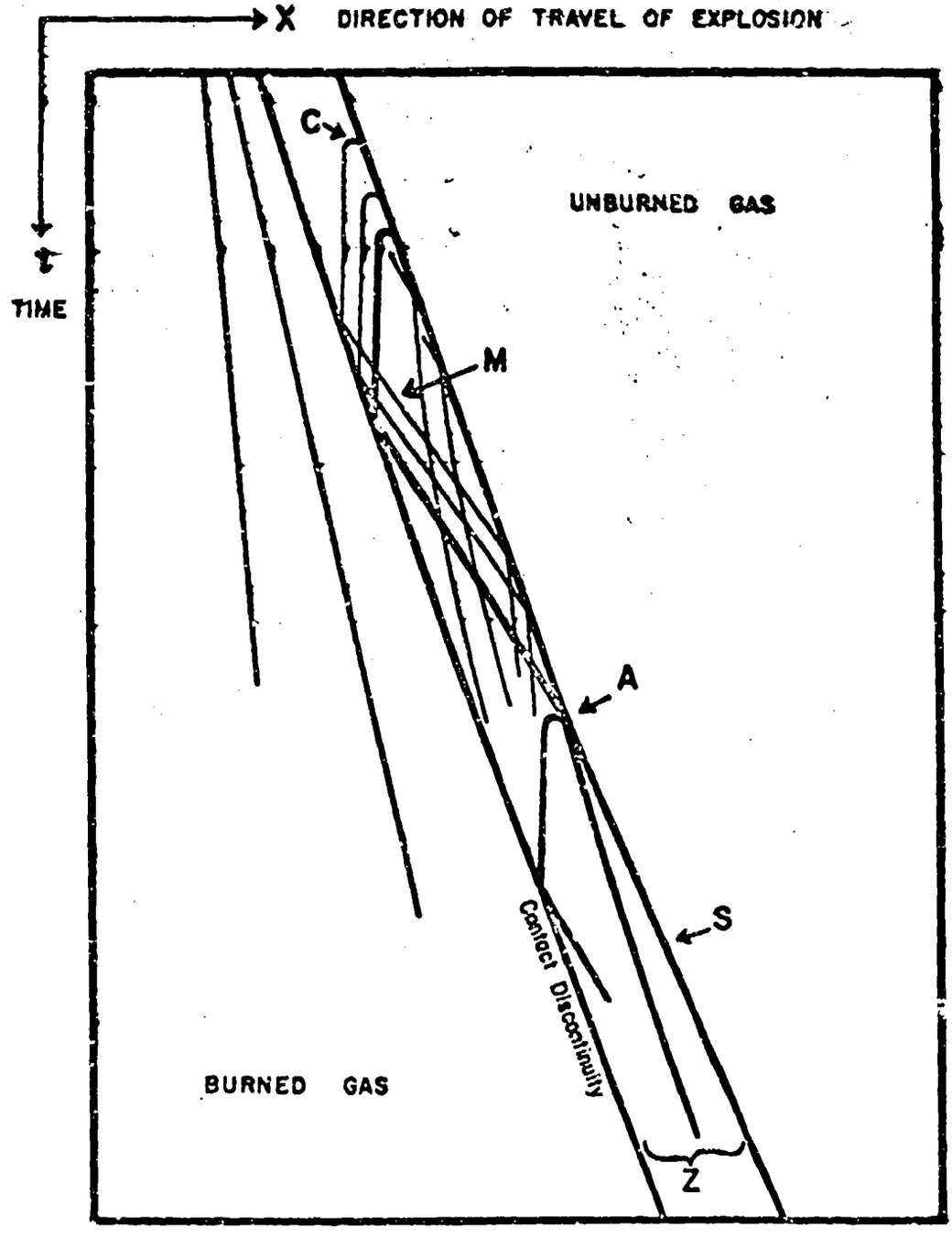


Figure 5 - Deflagration in a $CO-O_2$ Explosion.

C - Cusp
M - Multiple reflections of compression waves
A - Acceleration of shock front at this point
Z - Reaction Zone
S - Shock front

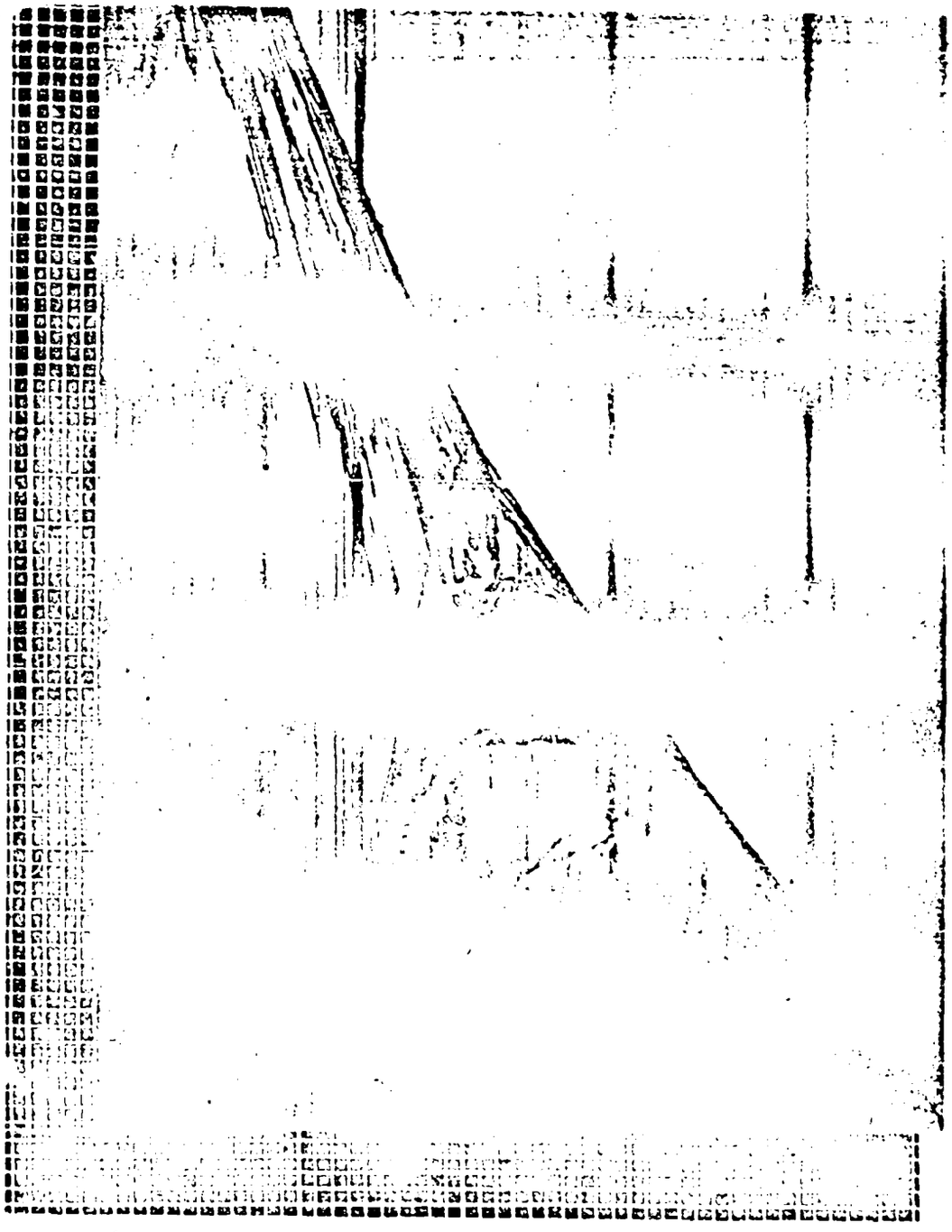

Figure 6 - Streak Schlieren Photograph of the Transition from Deflagration to Detonation in a Mixture Containing 64.5% Carbon Monoxide, 31.6% Oxygen, 1.6% Hydrogen, 2.3% Moisture and Inert Gases. Each horizontal scale division equals 7.06 mm, and each vertical scale division 2.82 microseconds.

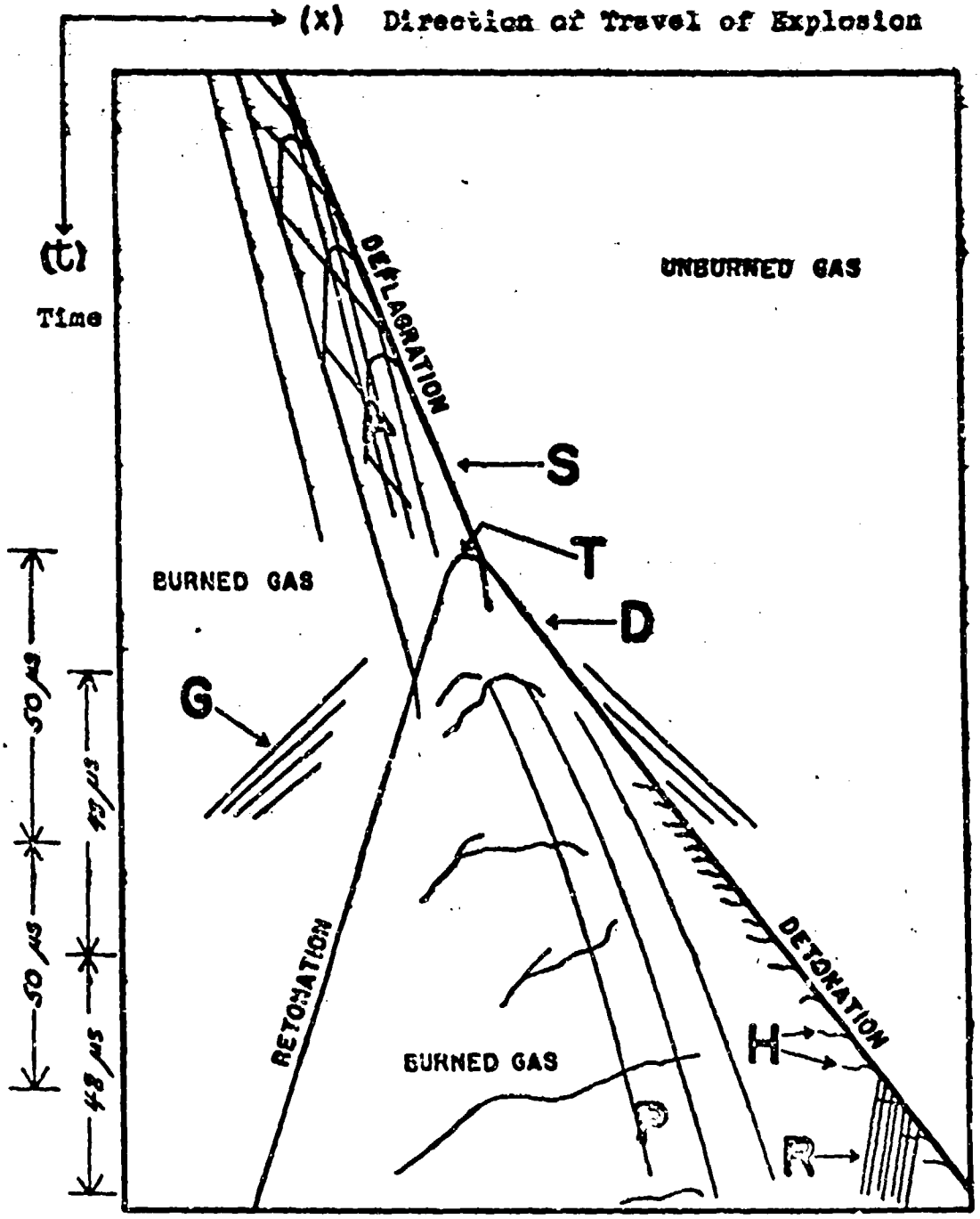


Figure 7 - Initiation of Detonation in a $CO-O_2$ Explosion

A - Combustion wave reaction zone
C - Shocks in glass windows
T - Transition point
P - Particle paths
S - Shock in gas
D - Detonation front (shock front)
H - Horizontal striae
R - Retrograde striae

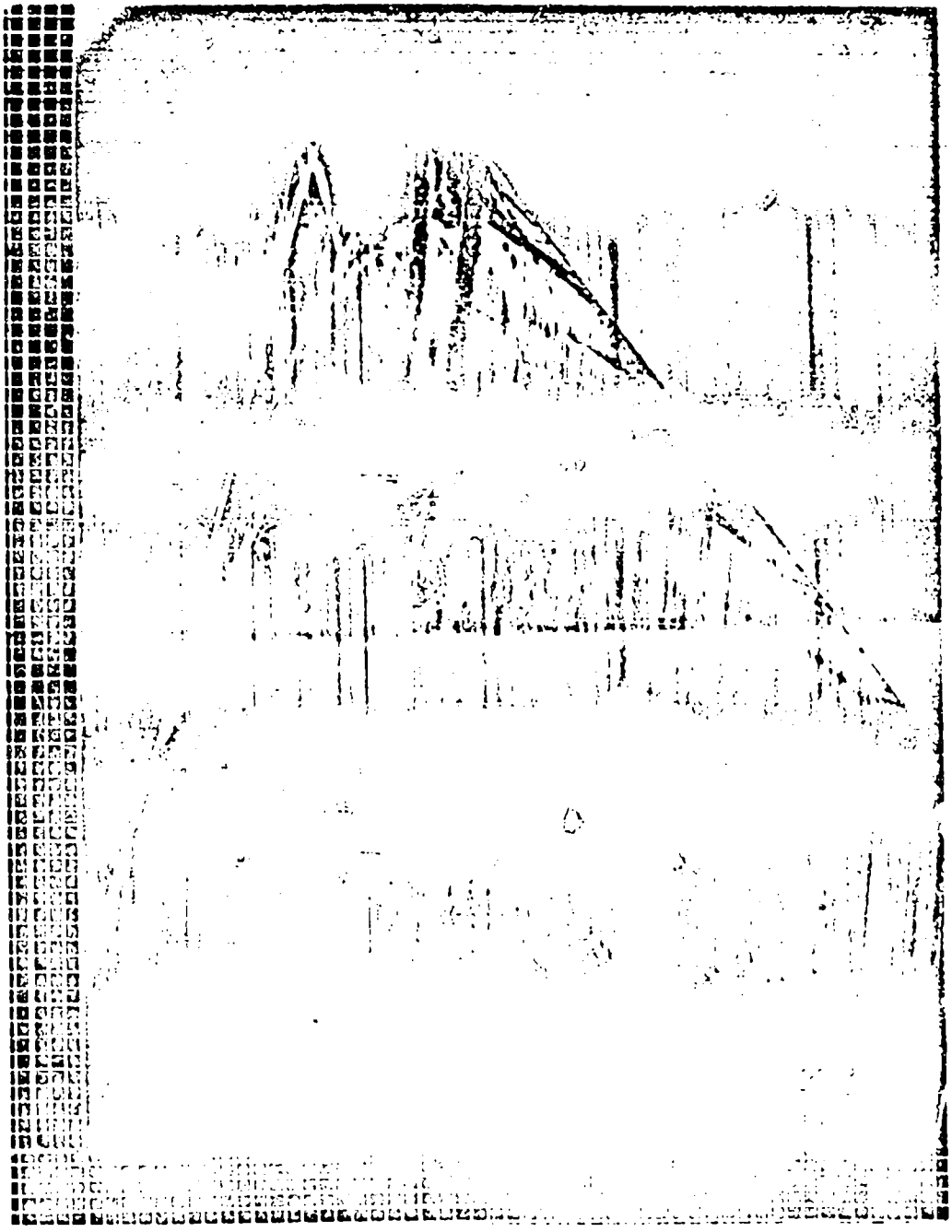

Figure 8 - Streak Schlieren Photograph of Initiation of Detonation in a Mixture Containing 72.2% Carbon Monoxide, 21.6% Oxygen, 1.1% Hydrogen, 5.1% Moisture and Inert Gases. Note retonation wave, retrograde striae, particle paths, and arc-shaped foci caused by multiple reflection of the pressure waves inside the detonation tube. Each scale division equals 7.06 mm horizontally, 2.82 microseconds vertically.

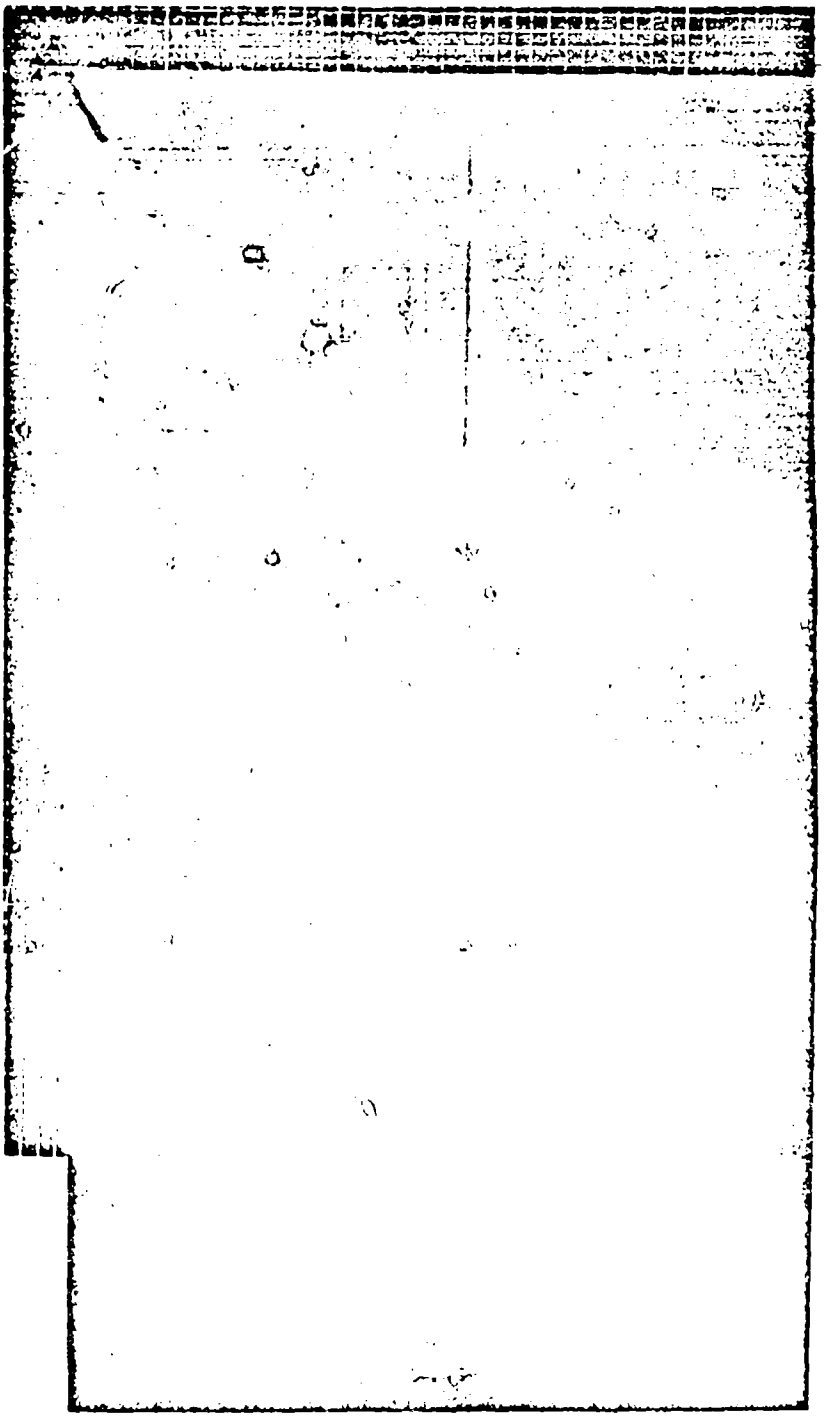

Figure 9 - Streak Schlieren Photograph of Detonation in a Mixture Containing 69.8% Carbon Monoxide, 25.8% Oxygen, 1.9% Hydrogen, 2.5% Moisture and Inert Gases. Note horizontal striae, retrograde striae, periodic velocity change of flame front, and foci due to multiple reflections of pressure waves inside the detonation tube. Each horizontal scale division equals 7.06 millimeters, each vertical division 2.82 microseconds.

of transition T (figure 7) and the frequency of the reverberation as shown on the photographs is sonic and relates to the physical dimensions of the tube.

The retrograde striations are clearly visible in all the carbon monoxide-oxygen photographs. They are indicated by R in figure 7 and are easily seen in figures 8 and 9.

A detailed examination of figure 9 shows that the detonation front consists of a smooth featureless black line--the shock--followed closely by a zone of optical gradients which approaches and recedes cyclically from this shock. One retrograde striation is formed during each cycle and direct measurements on the photographs indicate a recurrence frequency of the order of one megacycle. This frequency seems too high for any kind of mechanical spinning phenomenon in the gases, suggesting that the concept of periodic velocity change developed by Becker (5) and Lewis and von Elbe (6) may apply here.

It is planned in the near future to supplement the present photographs by end-on pictures of detonations to be used in determining whether the analysis developed by Smith and Sprenger (7) for rocket combustion is applicable to the gaseous systems considered here.

## ACKNOWLEDGEMENTS

This work was supported by the Office of Ordnance Research, Department of the Army, Army Project 599-01-004, Ordnance Project TB2-0001.

## LIST OF REFERENCES

(1) U. S. Bureau of Mines Summary Technical Report No. 3376. Studies on Detonation Phenomena in Gases. I. Rotating Mirror Camera. B. Greifer, March 31, 1953.

(2) von Elbe, G. Private communication.

(3) U. S. Bureau of Mines Progress Report No. 1, "Detonation and Explosives Phenomena", July 1 to September 30, 1953, Army Project 599-01-004, Ordnance Project TB2-0001.

(4) B. Lewis and G. von Elbe, "Combustion, Flames and Explosions of Gases", Academic Press Inc., New York, 1951, p. 614.

(5) R. Becker, Z. Elektrochem. 42, 457 (1936).

(6) B. Lewis and G. von Elbe, ibid., p. 624.

(7) R. P. Smith and D. F. Sprenger, Combustion Instability in Solid-Propellant Rockets, Fourth Symposium (International) on Combustion, Sept. 1-5, 1952, Cambridge.

S. G. Reed, Jr. and W. H. Heybey
U. S. Naval Ordnance Laboratory
White Oak, Silver Spring, Maryland

## INTRODUCTION

Rapid condensation of gas constituents in supersonic nozzle flow leads to shock-like phenomena which have been known for some time (1,9) and have been discussed by various authors. The exothermic character of these processes places them in close relation to flow processes involving chemical reactions. This relationship has been stated speculatively by J. M. Burgers (2) and has been touched on more recently by K. Oswatitisch (3); however, a detailed treatment of these rapid condensation phenomena from this standpoint has not appeared in the literature. Some steps towards such a treatment are taken in the present paper by describing the place the irreversible condensations occupy within the general framework of flow discontinuities induced by exothermic processes. Such a place exists because the laws of conservation of mass, momentum, and energy are the foundation of the treatment of all these flow discontinuities. It then becomes apparent that irreversible condensation processes in supersonic flow are formally identical with weak detonations and may be viewed as examples of such. We call them here "weak condensation detonations."

Chemical weak detonation fronts have never been definitely observed (4). Theoretically, this gap in available experience is commonly linked to the initiation process (5,13). More recently, however, the possible existence of three-dimensional weak detonations has been demonstrated by G. I. Taylor (6) and of one-dimensional detonations by K. O. Friedrichs (7). Taylor gives no hint as to the physical conditions under which his solution might be realized; Friedrichs, however, does discuss the existence problem, linking it with the behavior of chemical reaction rates.

In the following we present, first, a discussion of the normal condensation shocks in a steady supersonic air stream containing

a small portion of water vapor. This enables a comparison to be made with the standard treatment of steady detonation theory. Next, the case of rapid condensation of a pure substance, e.g., steam, in steady nozzle flow is presented. Both of these examples show that these condensation processes are, in fact, weak detonations. A discussion of the kinematical features of such a process in one-dimensional unsteady flow is then given and compared with shock tube experiments. Finally, the relationship of these processes to the theoretical weak detonation solutions of K. O. Friedrichs is discussed briefly.

## STEADY CONDENSATION SHOCKS IN AIR INDUCED BY SUDDEN CONDENSATION OF A SMALL FRACTION OF WATER VAPOR

If a small amount of water vapor condenses in an air stream, the ensuing changes of the mass flow, of the gas constant, and of the ratio of specific heats can be neglected. The simple theory (10) considers the condensation merely as a heat source and deals with the changes wrought upon a uniform air stream by steady injection of heat energy, say of g calories per unit mass, at a fixed station. This addition instantaneously raises the original stagnation enthalpy (from $h_0$ to $h_0 + g$ calories per unit mass) and, consequently, the sound speed at a fictitious throat from $a^*$ to $a^{*1}$. The discontinuous change of state is governed by the three conservation laws (of mass, momentum, and energy) which permit a complete description of the transition. In what follows the states immediately in front of and behind the shock will be designated by the subscripts 1 and 2, respectively. The dimensionless flow speeds $v_1 = u_1/a^*$ and $v_2 = u_2/a^{*1}$ are related by the conservation laws which yield

$$2Qv_1v_2 = (1 + v_1^2) \pm \left|\sqrt{(1 + v_1^2)^2 - 4Q^2v_1^2}\right| \qquad (1)$$

where

$$Q^2 = 1 + g/h_0 = (a^{*1}/a^*)^2$$

It is seen that the velocity $v_2$ is not determined by $v_1$ alone; the quantity g must also be known. Its numerical value is probably connected with the speed with which, at temperature $T_1$, undercooled water vapor is condensing. This condensation rate cannot be determined from gas dynamical relations alone, although there is a connection, as we shall see in discussing Friedrich's work at the end of this paper. Thus, the quantity g will be taken here as an indeterminate parameter. In order for $v_2$ to be real, however, g obviously cannot be larger than

$$g_{max} = h_0 \frac{(v_1^2 - 1)^2}{4v_1^2} \qquad (2)$$

This condition is imposed by the three conservation laws.

The ambiguity in sign appearing in equation (1) can be removed. Since normal condensation shocks have been observed in supersonic flow only, we first take it that $v_1 > 1$. Secondly, no change of state can occur in the uniform air stream if no liquid is formed at all, so that $v_2 = v_1$ if $Q = 1$. These conditions require the upper sign in equation (1). Once the velocity $v_2$ is thus established as a unique function of $v_1$ and $g$, a simple analysis, omitted here, shows that a normal condensation shock transforms supersonic velocity at the front side into a (smaller) supersonic velocity at the back side, at the same time raising pressure and density. It thus provides for the same change of state as would a one-dimensional weak detonation front separating unburnt gas from burnt gas in a chemical reaction process (5). The part of the air stream containing liquid water obviously corresponds to the burnt gas flow.

## RELATIONSHIP WITH WEAK DETONATIONS

For a mathematical treatment in terms of a Hugoniot diagram, one will first observe that the internal energy, $e$, per unit mass of air, assumed to be a perfect gas, is the same function of specific volume, $\tau$, and pressure, $p$, before and behind the front:

$$e = \frac{1}{\gamma - 1} p\tau$$

The equation of the Hugoniot curves then becomes

$$\frac{\gamma + 1}{\gamma - 1} (p_1 \tau_1 - p\tau) + \tau_1 p - p_1 \tau + 2g = 0 \qquad (3)$$

It is seen that for parametric values of $g$ the curves here are non-intersecting hyperbolas with common asymptotic lines

$$p = - \frac{\gamma - 1}{\gamma + 1} p_1 \quad , \quad \tau = \frac{\gamma - 1}{\gamma + 1} \tau_1$$

Adopting now the pattern used in conventional theory to exclude weak detonations (3,14), we replace the ideally sharp shock discontinuity by a narrow reaction zone within which the heat is liberated gradually. In other words, the agglomeration of water molecules into droplets is not supposed to occur instantaneously, since it requires a small but finite time to be completed. It thus extends across a narrow slab, which in turn is subdivided into individual layers, each characterized by the amount of heat liberated up to that layer. The Hugoniot curve, equation (3), with $g = g_i$ gives the possible $p - \tau$ relationship in that layer; the values actually prevailing are obtained by the intersection with the Rayleigh line,

$$\frac{p - p_1}{\tau - \tau_1} = - \rho_1^2 u_1^2 = - \gamma \frac{p_1}{\tau_1} M_1^2$$

where $\rho_1$ denotes the density forward of the shock and $M_1$ is the supersonic Mach number at which condensation sets in.

## HUGONIOT CURVES AND RAYLEIGH LINE FOR A CONDENSATION PROCESS

The slope of the Hugoniot hyperbola at $P_1$, according to equation (3), is $-\gamma p_1/\tau_1$. Since $M_1 > 1$, it follows that at $P_1$ the inclination of the Rayleigh line is steeper than that of the Hugoniot curve. Hence, the intersection points on Figure 1 will, in chemical reaction processes, correspond to detonations. We denote by $g_f$ the final amount of heat liberated by the condensation process, thus assigning a definite value to the parameter g. It is geometrically clear that $g_f$ cannot be larger (for a given Rayleigh line) than a certain amount $g_{max}$ (which is given analytically by equation (2)). The Hugoniot hyperbola $g = g_{max}$ will have a point of contact with the Rayleigh line on Figure 1. With detonations this point describes a Chapman-Jouguet process (5,14) for which the velocity is sonic in the burnt gas, and behind a condensation shock the velocity $u_2$ is known to be sonic if the maximum amount of heat is liberated (10).

The successive states within the narrow reaction zone are given by a sequence of points on the Rayleigh line. This sequence starts out at $P_1$ and comprises all the intersection points with the Hugoniot curves for $g = g_i$, until the point $T_2$ on the hyperbola $g = g_f$ is reached. With chemical reactions all these points would characterize the momentary state within a weak detonation zone. Beyond $T_2$ the sequence cannot be continued, because this would call for layers where more than the final amount of heat is liberated. In particular, the strong detonation point $T_2'$ cannot be reached. This reasoning evidently is parallel to that commonly used in excluding strong deflagrations (5) and, therefore, weak detonations, since these are visualized as initiated by a shock setting off a strong deflagration. It appears that this mechanism cannot be upheld for weak condensation detonations; since they are real, they cannot begin with a shock. Measurements by P. Wegener (8) reveal that, although on Schlieren pictures the water condensation in supersonic air flow may have a shock-like appearance, the actual reaction zone, as indicated by non-isentropic gradual pressure variation, can be quite wide (order of magnitude 1 cm). It should also be noted that K. O. Friedrichs (7), in establishing the existence of weak detonations, never makes use of a shock transition in the unburnt gas. The Chapman-Jouguet process appears as a limiting case of weak detonations. One can adapt the arguments usually given (5) for the "stability" of the Chapman-Jouguet point when approached from the "strong" side along a fixed Rayleigh line to show that this point has also an analogous stability when approached from the weak detonation side. A weak detonation cannot proceed past the Chapman-Jouguet point.

It can be fairly objected that the discussion just presented is artificial in the sense that g or $g_f$ cannot be arbitrarily fixed.

To answer this objection theoretically would require proof of the existance, uniqueness, and stability of the process at hand. Friedrichs (7) has shown the existence and uniqueness, but not the stability, of possible weak detonations. A practical answer is provided by the experimental fact that stable condensation shocks do occur, for fixed starting conditions, at a fixed Mach number.

CASE OF SUDDEN CONDENSATION OF A SINGLE COMPONENT GAS

There is, of course, only one Hugoniot curve for the final equilibrium state that can be attained in a steady, adiabatic process starting from a given initial state. This can be shown for the case of the mixture of water vapor and air discussed above; for simplicity we give here the Hugoniot diagram for pure water vapor. Using thermodynamic data for steam, Hugoniot diagrams can be drawn for equilibrium conditions downstream of any given point. Figure 2 illustrates the type of result obtained. AA' represents the coexistence line, below which two-phase equilibrium prevails. The dotted curve is a dry-steam isentrope, continued metastably into the shaded coexistence region to the condition $Z_1$. The Hugoniot curve H, corresponding to $Z_1$ and to equilibrium conditions downstream, can be shown to be convex and to exhibit a sharp rise in the absolute value of its slope at its point of intersection with the coexistence line. The Rayleigh line through $Z_1$ intersects H in the two points $Z_2$ and $Z_2'$; $Z_2$ is the weak detonation solution and is the one that corresponds to the mixture of droplets and vapor observed experimentally. If the expansion continues downstream of $Z_2$, it does so along a mixed phase adiabatic; and if equilibrium of the two phases is maintained, the adiabatic is reversible. To our knowledge, no direct observation has been made that the flow downstream of $Z_2$ is supersonic in the case of steam; in the case of the irreversible condensation of a small amount of water vapor in air, or of air itself, this has been confirmed by observation of Mach lines (9,11). One can, however, calculate sound speed at $Z_2$ for steam with available thermodynamic data, obtain flow speed from the Hugoniot diagram (knowing the speed at $Z_2$), and establish that the flow is indeed supersonic.* Jouguet's rule (5) is thus verified. A Chapman-Jouguet process would occur in the special case in which the Rayleigh line was tangent to H at $Z_2$.

Figure 3 shows schematically a one-parameter family of Hugoniot curves representing idealized progressive stages of condensation advancing from the "dry" Hugoniot $H(\epsilon = 0)$ towards the equilibrium Hugoniot curve $H(\epsilon = 1)$. It is taken for granted that a single significant parameter $\epsilon$ may be found corresponding to a given mixture of growing molecular clusters (size larger than

*This can be verified for the experiments reviewed by Ruedy (reference (12)). The method of obtaining the sound speed is given in reference (11).

critical) and single molecules. Here the family of Hugoniot curves is a pencil coalescing at the point C because of the single-phase condition above the coexistence line $AA'$.

This diagram suggests that the sequence of weak detonation from $Z_1$ to $Z_2$, followed by a normal shock from $Z_2$ to $Z_2'$, will give the same end result as a "dry" normal shock leading directly from $Z_1$ to $Z_2'$. It can be verified easily that this "transitive" relation of the shock solution holds in general.

## CONDENSATION SHOCKS IN ONE-DIMENSIONAL UNSTEADY FLOW

In two-dimensional steady nozzle flow, normal condensation shocks have been observed only within a limited domain of Mach numbers; in the majority of cases the shocks are X-shaped. There is, however, no reason why, in strictly one-dimensional flow, normal shocks could not arise at any supersonic Mach number. In the following, some considerations are offered to support this view. In order to obtain a variation of Mach number, we deal with unsteady flow as may be produced, e.g., by a piston receding with uniform velocity, U, from a semi-infinite air chamber. The air is first taken as dry; its initial state is denoted by the subscript o. In an x - t diagram the flow process is characterized by a pencil of straight rarefaction lines (Figure (4)), along each of which the flow state is constant. This centered simple wave will be defined by the condition

$$u + \sigma = \sigma_0 = \text{const.}$$

where u is the local particle velocity and $\sigma$ is the Riemann function which, in the case considered here of an ideal gas, is known to be proportional to the local velocity of sound,

$$\sigma = \frac{2}{\gamma - 1}\, a$$

The equation of any rarefaction (characteristic) line is then given as

$$\frac{x}{t} = u - a = k$$

where $1/k$ is the slope of the line in the x - t diagram.

Abandoning now the assumption of dry air, we stipulate the presence of a certain amount of water vapor, which may not yet be saturated at stagnation conditions, and thus partakes in the expansion process. Suppose that at $T_1 \leq T_o$ the vapor is saturated. In general, condensation will not occur at that temperature, since the change of state in the expanding gas column is not infinitely slow. A gas layer that became saturated with water vapor at time $t_1$

will continue to expand at constant entropy until, at some later time $t_1$ it attains a temperature $T < T_1$ at which condensation takes place. According to a recent investigation by Kantrowitz (16)*, the elapsed time and the condensation delay $T_{sat} - T$ are connected by the approximate relation

$$t - t_1 = \frac{B}{(T_{sat} - T)^4} \tag{4}$$

where the constant B is of order $10^3$ (degree$^4$ x sec). Here $T_{sat}$ denotes the saturation temperature at the pressure prevailing at temperature T; $T_{sat}$ must not be confused with the temperature $T_1$, where the vapor is saturated at the higher pressure $p_1$. Obviously, $T < T_{sat} < T_1$.

The location taken by the gas layer when it reaches the temperature T evidently indicates the momentary shock location. The ordinate is known to be given by

$$\frac{t}{t_1} = \left(\frac{T_1}{T}\right)^{\frac{1}{2}\frac{\gamma+1}{\gamma-1}} \tag{5}$$

whereas the abscissa follows from

$$\frac{x}{t} = u - a = \sigma_0\left(1 - \frac{\gamma+1}{2}\sqrt{\frac{T}{T_0}}\right) \tag{6}$$

since this is the equation of the characteristic line along which the temperature T prevails.

The Kantrowitz relation can now serve to set up the equation of the shock path. Every individual gas layer is characterized by the time, $t_1$, at which the air in it becomes saturated. On eliminating $t_1$ from equations (4) and (5) we obtain

$$t = \frac{B}{(T_{sat} - T)^4\left[1 - \left(\frac{T}{T_1}\right)^{\frac{1}{2}\frac{\gamma+1}{\gamma-1}}\right]} \tag{7}$$

This is the ordinate of the shock path in terms of the parameter T which, in the x - t diagram, determines the individual characteristic lines. The abscissa is given by equation (6).**

---

* Much of our discussion is independent of this explicit relation due to Kantrowitz. See also Oswatitisch (17).

** In the presence of the shock the dashed parts of the originally straight rarefaction lines (Figure 4) will alter their course.

It is seen that the shock never can be found to the left of the characteristic line $T = T_1$ (since t would become negative if $T > T_1$); indeed, as $t \to \infty$, if $T \to T_1$, the shock path, coming from the right, approaches asymptotically the "saturation characteristic" $T = T_1$. Moreover, it can intersect but once with any characteristic line, since equation (4) is a unique function of T. As a consequence, the shock path, at any point P within the fan, will make a larger angle with the positive x-axis than does the rarefaction line through P. Hence, the shock velocity relative to the tube wall, V, satisfies

$$V < k = u - a$$

at P, as is readily verified from the fact that the slopes of the intersecting lines are $1/v$ and $1/k$, respectively. The Mach number relative to the shock is

$$M = \frac{u - v}{a} > 1$$

If we now follow the shock curve as it approaches the asymptotic line, the difference between V and $k = u - a$ becomes increasingly smaller. It is thus seen that normal condensation shocks can occur theoretically at supersonic Mach numbers as low as we may choose.

Presumably the highest Mach number will be found at the intersection of the shock with the last characteristic line on which any quantity will be given the subscript 2. The particle velocity here is equal to the piston velocity

$$u_2 = U$$

The sound speed can be obtained from the simple-wave condition

$$\sigma_0 = U + \sigma_2$$

It follows that

$$a_2 = \frac{\gamma - 1}{2} \sigma_2 = \frac{\gamma - 1}{2} (\sigma_0 - U)$$

The shock velocity $V_2$ could be computed from the shock path equations (6) and (7). One would have to introduce the explicit dependence on T of $T_{sat}$ with the use of the Clapeyron-Clausius relationship of saturation pressure and temperature. It was found that, in order to arrive at a closed formula, several simplifying assumptions had to be made and that, even then, the expressions became rather unwieldy. With more ease the velocity $V_2$ can be obtained from the shock path within the zone of constant state extending between the piston path and the last characteristic line.

In this zone the Kantrowitz relation gives

$$t - t_1 = \frac{B}{(T_{sat} - T_2)^4} = t' = \text{const.}$$

In the idealized expansion process considered here the gas layer immediately adjacent to the piston is saturated at time $t_1 = 0$; $t'$ then denotes the time at which condensation occurs in that layer.* The condensation shock makes its first appearance at $t = t'$, $x = Ut'$, which is a point on the piston path.

It is not hard to deduce that the path in the constant-state zone of a gas layer that was saturated at $t = t_1 \neq 0$ is the straight line

$$Ut - x = a_2 t_1 \left(\frac{T_1}{T_2}\right)^{\frac{1}{2}\frac{\gamma+1}{\gamma-1}}$$

On eliminating $t_1$ from this equation and the Kantrowitz relation the shock path in that zone is found to be

$$Ut - x = a_2 (t - t') \left(\frac{T_1}{T_2}\right)^{\frac{1}{2}\frac{\gamma+1}{\gamma-1}}$$

This again is a straight line. Its reciprocal slope is

$$\frac{dx}{dt} = V_2 = U - a_2 \left(\frac{T_1}{T_2}\right)^{\frac{1}{2}\frac{\gamma+1}{\gamma-1}}$$

Hence, the Mach number relative to the shock in the constant-state zone (which includes the last characteristic line) becomes

$$M_2 = \frac{u_2 - V_2}{a_2} = \left(\frac{T_1}{T_2}\right)^{\frac{1}{2}\frac{\gamma+1}{\gamma-1}} = \left(\frac{\sigma_1}{\sigma_o - U}\right)^{\frac{\gamma+1}{\gamma-1}}$$

$\sigma_1$ and $\sigma_o$ are given quantities. It is seen that the Mach number $M_2$ becomes large if the piston velocity approaches the velocity

$$\sigma_o = \frac{2}{\gamma - 1} a_o$$

The results of these considerations indicate that the apparent restriction of normal condensation shocks to a limited region of Mach numbers, as suggested by available experimental evidence in two-dimensional nozzle flow, is probably not founded in the nature of the irreversible condensation process.

---

* Relations such as Kantrowitz' cannot be expected to hold for very small times $t'$. Gilmore (21) has estimated these induction times; for conditions of interest here they are of the order $10^{-8}$ sec.

Condensation shocks in unsteady one-dimensional flow have been obtained in shock tube experiments made at the University of Toronto.* Figure 5 gives an example. That the condensation shock should appear as a straight line even within the expansion fan is explained by the fact that the entire path corresponds to a time interval of about 1/2 milliseconds during which the condensation shock velocity is not likely to change noticeably save in extreme cases.

In the experiment from which Figure 5 was obtained the air was saturated initially. Figure 5 seems to raise a difficulty because, from our discussion, the condensation shock should approach, asymptotically, the saturated state, which would be the first rarefaction line in Figure 5. The observed condensation shock seems to diverge from the rarefaction line. The experiments of C. T. R. Wilson (18) may throw some light on a possible explanation. Wilson found that for an expansion which is very slow, as it is in the later stages of an expansion such as Figure 5, and for saturated air relatively free of condensation nuclei, a minimum expansion ratio was required before the onset of rapid condensation. The line $T = T_0$ then can never be reached. The characteristic asymptotically approached by the condensation shock in Figure 4 may be relabeled the "Wilson line". One can show that, for the time interval in Figure 5, the shock line should be fairly straight and close to the Wilson line if the expansion were an ideal, centered, simple wave. In fact, it is not a centered, simple wave and, although velocity measurements can be made in these experiments, one cannot determine the thermodynamic states because the path of the contact surface is not determinable from the picture.**

It is interesting to remark that T. Lee (20) has observed three-dimensional unsteady condensation shocks due to jet formation when a diaphragm is burst in a shock tube. These would correspond to the weak detonation solution indicated by G. I. Taylor (6).

## DISCUSSION

A more detailed description of the weak condensation detonation processes discussed above may help to clarify their relation to more familiar types of chemical detonation processes.

If one tries to describe the processes occurring in the detonation front itself, the theory of steady detonation waves (see, e.g., von Neumann (14)) gives some support to the notion that

---

* The authors are indebted to Dr. G. N. Patterson and Dr. I. Glass of the Institute of Aerophysics, University of Toronto, for doing these experiments at our request, and for permission to publish one of the resulting wave-speed camera photographs.

** Possibly modification of these experiments is possible in which the gas is allowed to push a piston, the path of which could be measured (11). With this the condensation history from time zero could be observed.

ordinary chemical detonations start from a situation in the neighborhood of a normal shock solution of the conservation equation for the unburned gas and proceed along a sequence of (local) steady states to the Chapman-Jouguet point.

In the case of the weak condensation detonations, we have seen that the analogous sequence of states starts in the neighborhood of the "weak" disturbance solution and remains there.*

For both sorts of detonation the equilibrium of molecular species or phases is reached in a kinetic balance of forward and reverse reactions. In the usual chemical process, both forward and reverse reaction rates increase with the temperature. In the case of condensation processes the forward reaction rate (the condensation) decreases with increasing temperature while the reverse reaction rate (evaporation) increases. The process may cut itself off (i.e., equilibrium may be established) even if some of the vapor is not yet condensed.

In order to obtain the weak condensation detonation, an unstable condition is brought on by means of a fast adiabatic expansion. Two basic mechanisms are at work in such a condensation process. The first stage, as is well known, depends on the build-up of "critical" nuclei; once these are present in sufficient quantity the rapid stage of condensation commences. The first stage is "hidden" insofar as it is not made manifest by any appreciable alteration of thermodynamic properties. The evaporation (reverse) process depends on the presence of droplets and on the heat release due to their fast initial growth.

This description prepares the way for a comparison with the weak detonation solution found by Friedrichs (7). Friedrichs has treated the one-dimensional model detonation process as governed by a differential equation involving macroscopic viscosity, heat conduction, and a reaction rate. He has shown the possibility of weak detonation solutions of these equations and has shown that these will have an eigenvalue of locally steady propagation velocity for given boundary conditions ahead of the wave and for a given form of the reaction rate. In this these solutions have formal similarity to flame solutions. Assuming a reaction rate increasing with temperature, the weak detonation solutions are characterized as being associated with a reaction rate which he terms "extremely fast". Much of his discussion is independent of this assumption. What is essential to the matter is the behavior of the solutions of his

---

*The fact that the disturbance is small in the condensation case indicates that one might compute eigenvalues of the propagation velocity by an appropriate modification of a procedure used for flames (14); inversely, the pattern of solution fields for different assumptions as to the reaction rate indicates more closely what conditions might have to be met to have a chemical weak detonation.

model equations in the $(\xi, \theta, \tau)$ space, where $\xi$ is the fraction of burnt gas, $\theta$ = a reduced temperature, and $\tau$ = specific volume. To have a weak detonation solution, Friedrichs finds, in accordance with physical expectation, that the transition between the planes $\xi = 0$ to $\xi = 1$ must be effected without departing far from the plane $\theta = \theta_1$, where $\theta_1$ is the reduced temperature ahead of the reaction front. This is the reason for the requirement that the reaction rate be fast at a relatively low temperature.

It is known from experience that the weak condensation detonations satisfy the condition of transition from $\xi=0$ to $\xi = 1$ without marked increase in temperature. The reaction rate has two fast stages: rapid growth on nuclei, and the reverse reaction of evaporation moderating the growth of droplets. A second type of weak detonation solution found by Friedrichs involves a shock transition in the neighborhood of the plane $\xi = 1$, i.e., in the burnt gas. This cannot occur in the condensation case because of the stabilizing conditions of the reaction rate.

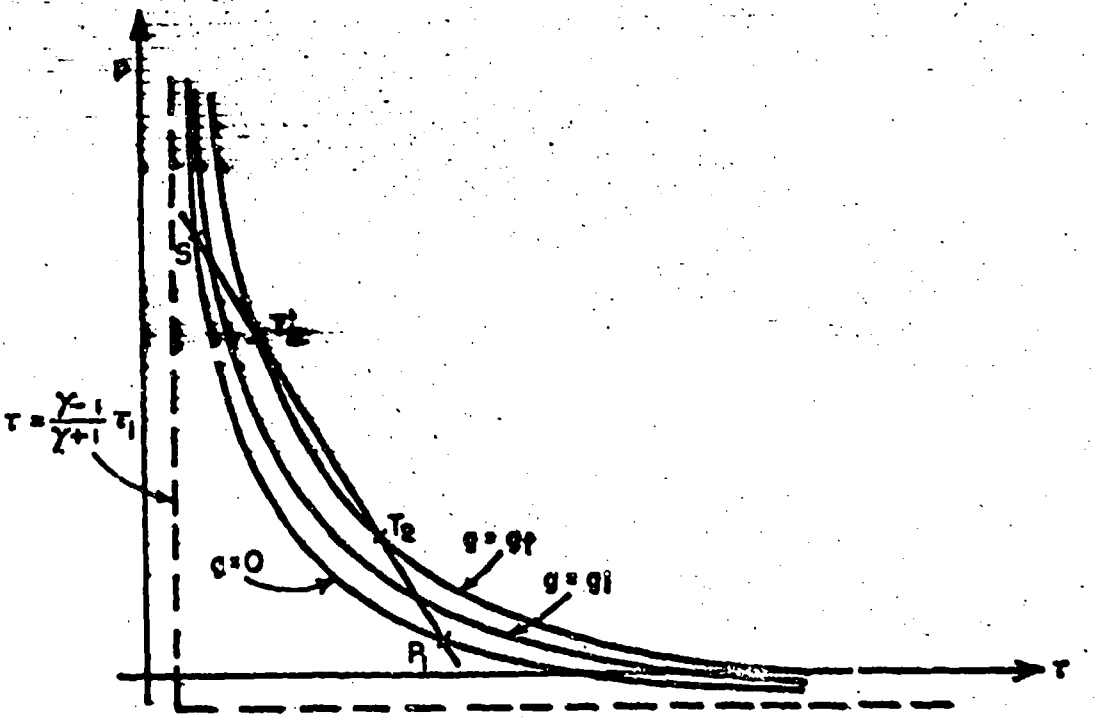


Figure 1 - Hugoniot curves and Rayleigh line for condensation of a fraction of water vapor.

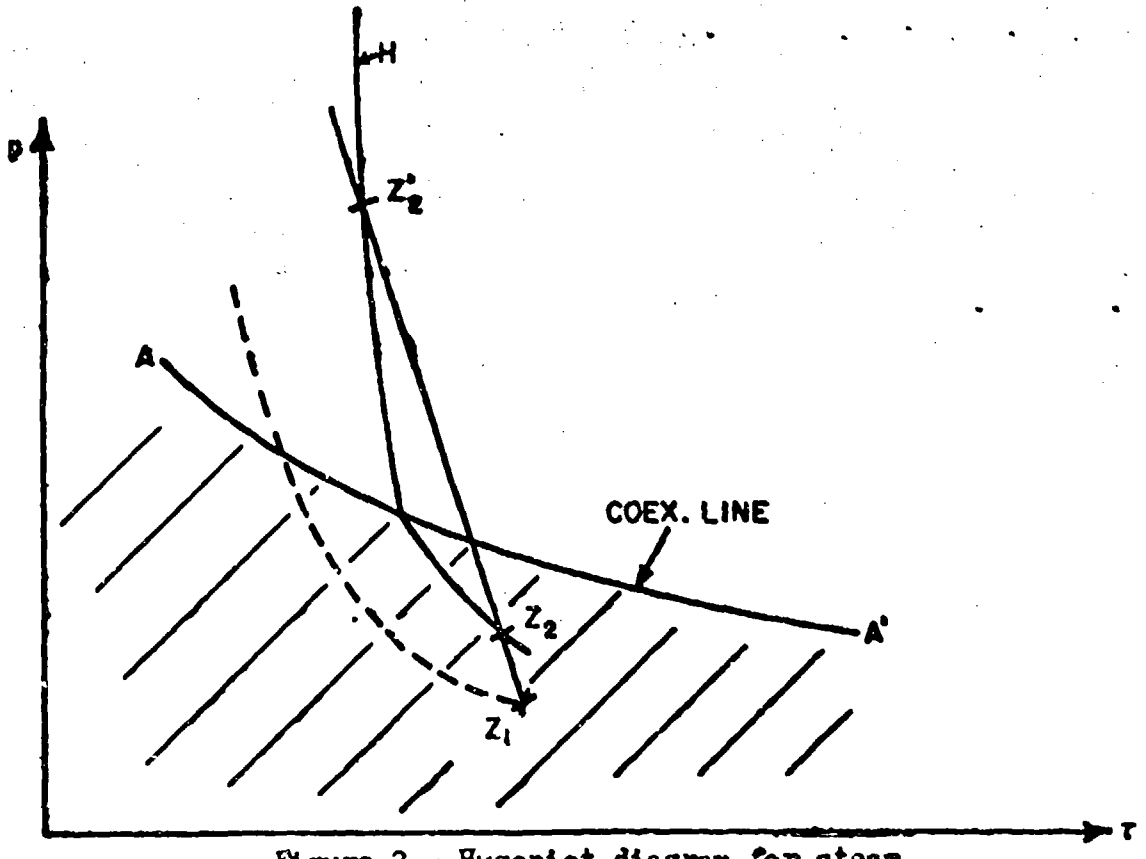


Figure 2 - Hugoniot diagram for steam.

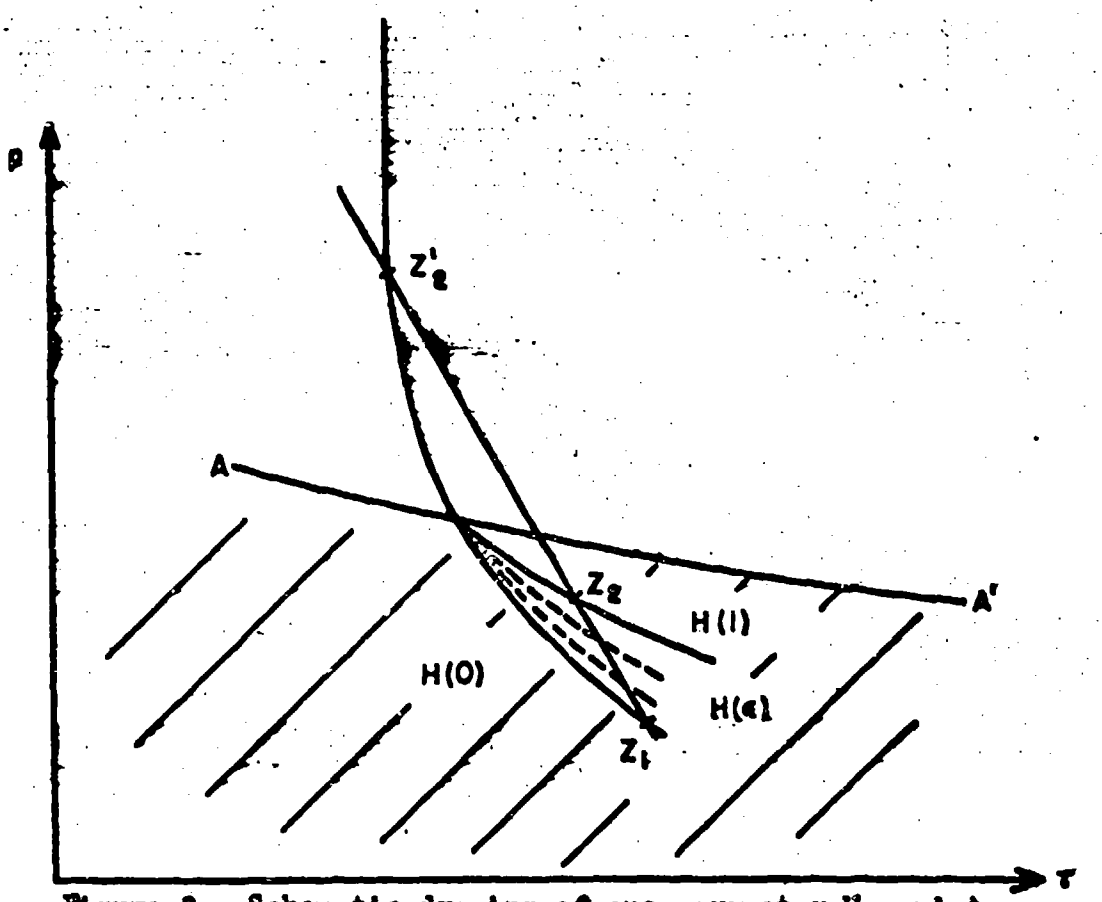


Figure 3 - Schematic drawing of one-parameter Hugoniot curves for steam.

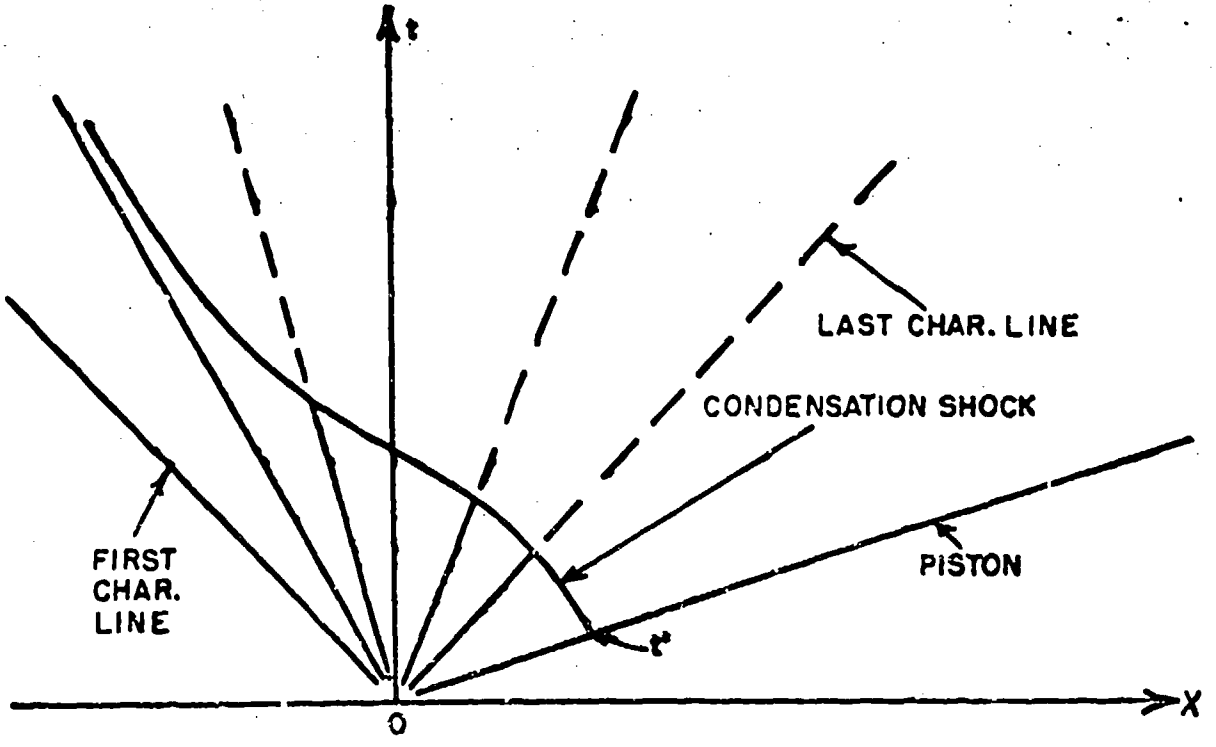


Figure 4 - Condensation shock in a centered simple wave expansion.

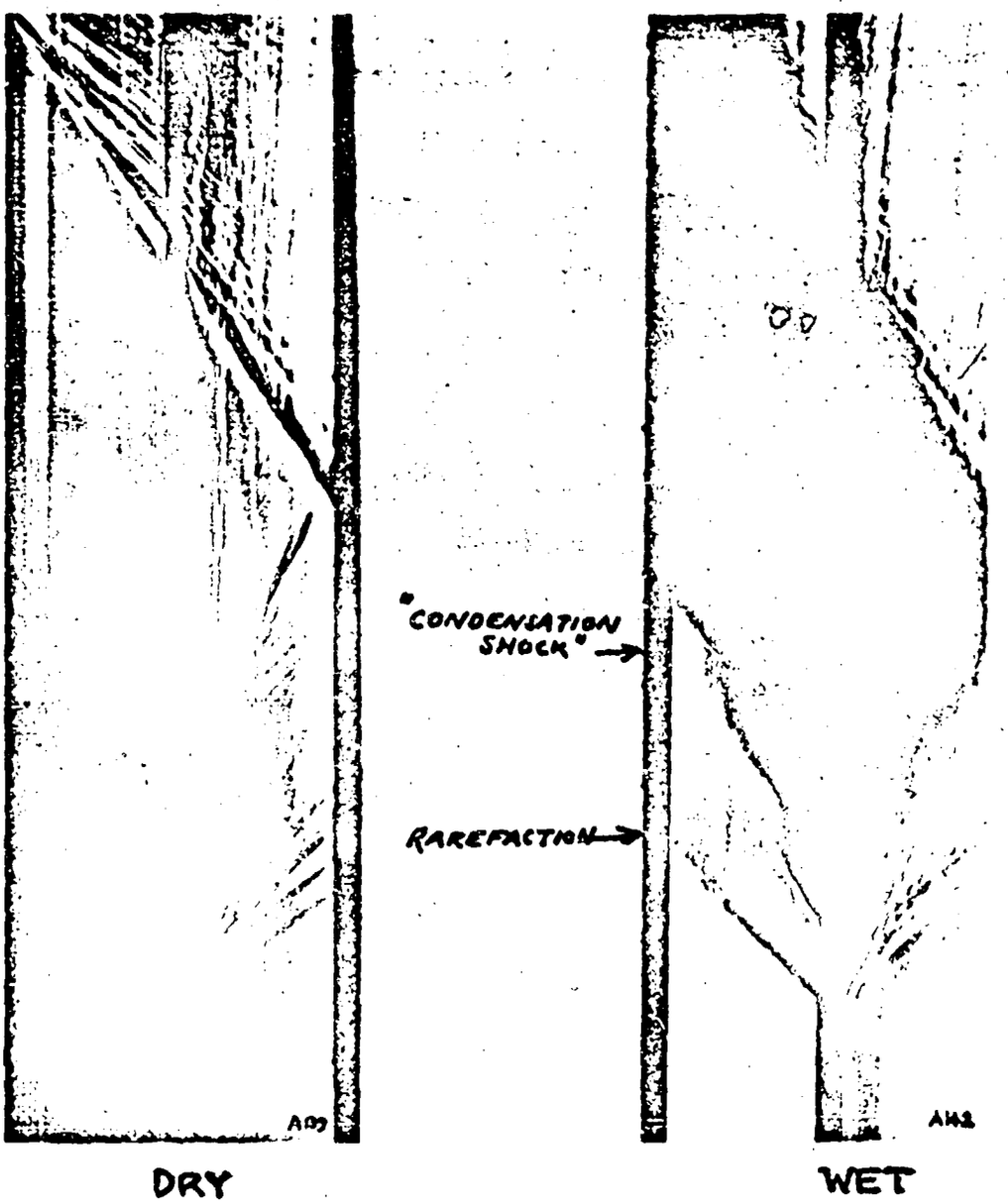


Figure 5 - Wave speed camera photographs of unsteady expansions in dry and moist (wet) air.

## BIBLIOGRAPHY


(1) C. Weiselsberger and L. Prandtl, Proc. Volta Conference, Rome 1935 (water vapor in air); C. Robb, Can. J. Research A19, p. 87, 167 (1941) (pure steam).

(2) J. M. Burgers, Address at the dedication of the Naval Ordnance Laboratory Aeroballistic Research Facilities 1949. (NOLR 1130).

(3) K. Oswatitisch, Gasdynamik (Springer, Wien 1951) p. 59, 65.

(4) A. R. Ubbelohde, Proc. Roy. Soc. A204 (1950); Proc IV International Conference on Combustion and Detonation (1952) (Williams and Wilkins Co., Balt., Md.).

(5) R. Courant and K. O. Friedrichs, Supersonic Flow and Shock Waves, (N. Y.; Interscience 1948); Y. B. Zeldowich, "Theory of Combustion and Detonation of Gases" (Acad. Sci. USSR 1944).

(6) G. I. Taylor, Proc. Roy. Soc. A200 (1950) p. 235.

(7) K. O. Friedrichs, NAVORD Report 79-46.

(8) P. P. Wegener, To appear in J. Appl. Physics.

(9) R. Hermann, Luftfahrtforschung, 19, p. 201 (1942).

(10) W. Heybey NACA TN 1174 (1947).

(11) D. Coles, Guggenheim, Aero. Lab., Cal. Inst. of Technology, Private Communication (1951).

(12) S. G. Reed, Jr., J. Chem. Phys. 20, p. 539 (1952).

(13) R. Ruedy, Can. J. Research A22, p. 77 (1944).

(14) J. Von Neumann, OSRD Report 549 (1942).

(15) D. Layzer, J. Chem. Phys. 22, p. 222 (1954).

(16) A. Kantrowitz, J. Chem. Phys. 19, p. 1097 (1951).

(17) K. Oswatitisch, ZAMM 22, p. 1 (1942).

(18) C. T. R. Wilson. Proc. Roy. Soc. A61, p. 240; Phil. Mag. 189, p. 281 (1897).

(19) Michels, Slawsky, and Jacobs, Physica XX, p. 223 (1954).

(20) T. Lee, Dissertation, U. of Toronto (1950).

(21) F. R. Gilmore, Thesis, Cal. Inst. of Tech. (1951).

# THE STRUCTURE OF A STEADY-STATE PLANE DETONATION WAVE WITH FINITE REACTION RATE

14

John G. Kirkwood
Sterling Chemical Laboratory
Yale University
New Haven, Connecticut

and

William W. Wood
Los Alamos Scientific Laboratory
Los Alamos, New Mexico

## ABSTRACT

An analytical elaboration of von Neumann's model of the detonation wave is presented. A hydrodynamic argument for the well-known Chapman-Jouguet condition is advanced, and the sound speed to be used therein is identified as that obtained with frozen chemical equilibrium, in agreement with a recent result of Brinkley and Richardson. Possible situations in which the classical Chapman-Jouguet hypothesis might be incorrect are very briefly discussed.

## I

The propagation of a plane detonation wave through a semi-infinite explosive medium has been discussed theoretically by a number of investigators[1-12], beginning with Chapman[1] and Jouguet[2]. The central problem is the selection of a unique detonation process from a one-dimensional continuum of processes all of which satisfy the usual conservation laws for mass, momentum, and energy. The rule by which this selection is made is known as the Chapman-Jouguet (denoted in the following by C-J) hypothesis, after these early investigators. The chemical reaction responsible for the detonation process has been treated as an instantaneous transformation in many of these discussions[1-5, 9, 11]. In particular, Brinkley

and Kirkwood have studied the stability of the C-J detonation under this assumption.

Chemical reaction rates are of course finite, and as a consequence the region in which the chemical transformation takes place must be of non-vanishing dimensions. Certain well known properties of detonation waves in finite geometry afford experimental verification of this, and in fact considerable interest is attached to the determination of such parameters as the reaction time, etc. The classical paper in the discussion of the influence of finite reaction rates on the detonation process is that of von Neumann[7]. The present work is essentially an analytical elaboration of his geometrical discussion, which we hope will clarify several points. Brinkley and Richardson[10] have also recently considered this question, and our Section IV is similar in certain respects to their work.

## II

Our model is that of a fluid undergoing one-dimensional, compressible, non-dissipative, adiabatic, reactive flow.* Shocks are treated as mathematical jump

---

*See ref. 12 for a discussion in which dissipative and diffusion processes are considered.

---

discontinuities in certain of the hydrodynamic-thermodynamic variables. Among the variables specifying the state of the system are certain composition variables $\lambda^j$, $j = 1, 2, \cdots r$, corresponding to certain independent chemical reactions, r in number, involving the n components of the fluid, which reactions are denoted by

$$\sum_{\alpha=1}^{n} \nu_\alpha^j X_\alpha = 0, \quad j = 1, 2, \cdots r \qquad (1$$

The $\nu_\alpha^j$ are stoichiometric coefficients, positive for products, negative for reactants, and so chosen that (1 expresses the transformation of unit mass of reactants to products; $X_\alpha$ denotes unit mass of component $\alpha$. The $\lambda^j$ are progress variables, specifying the increase in mass of the various components within a fluid element of total

mass m due to the r chemical reactions:

$$dm_\alpha = m \sum_{j=1}^{r} \nu_\alpha^j \, d\lambda^j, \quad \alpha = 1, 2, \ldots, n. \tag{2}$$

We assume throughout this discussion the existence of local thermodynamic quasi-equilibrium, such as to permit the definition of local temperature, etc., and to permit the assumption that the various thermodynamic quantities may be regarded as functions of a suitable set of independent thermodynamic variables. We also suppose the Lagrangian time derivatives of the progress variables to be given by

$$\frac{d\lambda^j}{dt} = r^j, \tag{3a}$$

$$r^j = r_f^j - r_b^j, \quad j = 1, 2, \ldots, r. \tag{3b}$$

where $r_f^j$ and $r_b^j$ are chemical rate functions for the forward and back directions of reaction j, given as functions of the local thermodynamic state.

In regions of space-time in which shocks are absent the flow is governed under our assumptions by the usual hydrodynamic equations

$$\frac{d\rho}{dt} + \rho \frac{\partial u}{\partial x} = 0, \tag{4a}$$

$$\frac{du}{dt} + v \frac{\partial p}{\partial x} = 0, \tag{4b}$$

$$\frac{d\varepsilon}{dt} + p \frac{dv}{dt} = 0, \tag{4c}$$

$$\frac{d}{dt} = \frac{\partial}{\partial t} + u \frac{\partial}{\partial x} \tag{4a}$$

$$\frac{\partial}{\partial t} = \left(\frac{\partial}{\partial t}\right)_x, \quad \frac{\partial}{\partial x} = \left(\frac{\partial}{\partial x}\right)_t.$$

We use $\rho$ to denote matter density; $u$ the mass velocity in a coordinate system with x as space variable, t as time variable; p the fluid pressure; v the specific volume equal to $1/\rho$; E the specific internal energy, assumed to be a known function of the local thermodynamic state, say the variables $\lambda$, $\rho$, S, where $\lambda$ denotes the set of variables $\lambda^j$; S the specific entropy. The equation of state is also assumed, giving p as a function of $\lambda$, $\rho$, and S.

From the alternative form of the first law

$$\frac{dE}{dt} = T\frac{dS}{dt} - p\frac{dv}{dt} + \frac{1}{m}\sum_\alpha \mu_\alpha \frac{dm_\alpha}{dt}, \tag{5}$$

in which $\mu_\alpha$ denotes the specific chemical potential, we obtain the entropy transport due to chemical reaction:

$$\frac{dS}{dt} = \sum_j \frac{\Delta^j F}{T} \frac{d\lambda^j}{dt}, \tag{6a}$$

$$\Delta^j F = \sum_\alpha \nu_\alpha^j \mu_\alpha \tag{6b}$$

Corresponding to the classical Riemann analysis of the hydrodynamic equations in the non-reactive case, we now utilize the equation of state, and the entropy transport equation as well, to establish the relation between the substantive derivatives of p, $\rho$, and $\lambda$. The usual rule for differentiation gives

$$\frac{dp}{dt} = \left(\frac{\partial p}{\partial \rho}\right)_{S,\lambda} \frac{d\rho}{dt} + \left(\frac{\partial p}{\partial S}\right)_{\rho,\lambda} \frac{dS}{dt} + \sum_j \left(\frac{\partial p}{\partial \lambda^j}\right)_{S,\rho} \frac{d\lambda^j}{dt}. \tag{7}$$

With the definitions

$$c_e^0 = \left(\frac{\partial E}{\partial \varrho}\right)_{S,\lambda} , \tag{8a}$$

$$\beta_0 = \left(\frac{\partial V}{\partial T}\right)_{p,\lambda} , \tag{8b}$$

$$c_p^0 = \left(\frac{\partial H}{\partial T}\right)_{p,\lambda} , \tag{8c}$$

we obtain after some manipulation the relation

$$\frac{d\varrho}{dt} = \frac{1}{c_e^2}\frac{dp}{dt} - \varrho \sum_j \sigma^j \frac{d\lambda^j}{dt} , \tag{9}$$

where

$$\sigma^j = \frac{\varrho\beta_0 T}{c_p^0}\left(\frac{c_p^0}{\beta_0}\Delta^j v - \Delta^j H\right) = \frac{1}{\varrho c_e^2}\left(\frac{\partial p}{\partial \lambda^j}\right)_{E,\varrho} \tag{10a}$$

$$= -\frac{\varrho\beta_0}{c_p^0}\left(\frac{\partial E}{\partial \lambda^j}\right)_{p,V} ;$$

$$\Delta^j H = \sum_\alpha \nu_\alpha^j \bar{H}_\alpha = \left(\frac{\partial m H}{\partial N}\right)_{T,p} ; \tag{10b}$$

$$\Delta^j V = \sum_\alpha \nu_\alpha^j \bar{V}_\alpha = \left(\frac{\partial m V}{\partial \lambda^j}\right)_{T,P}, \tag{10c}$$

here H denotes the specific enthalpy, $\bar{H}_\alpha$ and $\bar{V}_\alpha$ respectively the usual thermodynamic partial specific enthalpy and volume of component $\alpha$. It will be noted that the quantities $C_s$, $\beta_s$, and $C_p^\circ$ are the sound speed, volume expansion coefficient, and constant pressure heat capacity evaluated with the composition frozen at its instantaneous value. The parameters $\sigma^j$ are thermodynamic variables which, as we shall see, determine in conjunction with the rate functions $r^j$ the explosive behavior of the medium.

Use of (9 permits the elimination of the derivatives of the density from the hydrodynamic equations:

$$\rho \frac{\partial u}{\partial x} + \frac{1}{C_s^2} \frac{dp}{dt} = \rho \sum_j \sigma^j r^j, \tag{11a}$$

$$\rho \frac{du}{dt} + \frac{\partial p}{\partial x} = 0, \tag{11b}$$

$$\frac{d\lambda^j}{dt} = r^j, \quad j = 1, \ldots, r. \tag{11c}$$

We note that these equations are similar to the well-known equations for non-reactive flow, the frozen sound speed appearing in the expected place, but with a non-vanishing right hand side in the first equation. We also note that when our reactive system is at chemical equilibrium, the right hand side vanishes, since $r^j$ becomes zero when the forward and backward rates become equal. The appearance of the frozen sound speed is of some interest.

The differential equations (11 hold in regions of the flow which are free from shocks. Treating the latter as mathematical discontinuities, they are governed by the

well-known Rankine-Hugoniot conditions,

$$\rho_2 (U - u_2) = \rho_1 (U - u_1), \tag{12a}$$

$$p_2 - p_1 = \rho_1 (U - u_1)(u_2 - u_1), \tag{12b}$$

$$E_2 - E_1 = \tfrac{1}{2} (p_2 + p_1)(v_2 - v_1), \tag{12c}$$

in which $U$ denotes the shock velocity and the other symbols have their usual meaning with the subscripts distinguishing the values on the two sides of the shock. These relations across discontinuities, and the differential equations in regions free from them, supplemented by suitable boundary conditions, determine the flow of our one-dimensional, reactive fluid.

We now apply them to the propagation of a steady-state plane detonation wave through a semi-infinite explosive medium in a direction perpendicular to the plane surface. We suppose the detonation to have been initiated at this surface at zero time, and suppose the boundary condition to be imposed at this rear surface by a prescribed motion of an infinite piston (see, e.g. refs. 7 and 11). We will consider only the steady-state detonation assumed to be approached eventually, at least for some modes of initiation. Here we adopt the model of the detonation wave used by von Neumann, in which the reaction is initiated by a shock wave in the unreacted medium preceding the reaction zone. (The reaction rates $r^j$ are assumed to vanish in the medium in front of the shock wave.) We denote by D the velocity at which this shock propagates along the x-axis (taken as perpendicular to the rear surface and pointing into the explosive), the unreacted, unshocked medium being stationary in this coordinate system. During the approach to steady state, D may depend on t, but is assumed to approach a constant value as t increases. In addition to this assumption, the notion of a steady state also includes the supposition that there exists immediately following the shock a region of constant length in which the various hydrodynamic variables are independent of time when viewed from a coordinate system moving with the velocity D. This

steady-zone is followed by a flow region whose character is determined by the rear boundary condition. In certain simplified cases it may have approximately the form of a centered-rarefaction wave, reducing the pressure and mass velocity from their values at the boundary between this region and the steady zone to their values at the rear surface. We now proceed to discuss these two flow regions separately, beginning with the steady zone.

## III

We introduce the moving coordinate system mentioned above.. For convenience we take as space variable the distance measured backwards from the shock front. The transformation is

$$\xi = \int_{t_0}^{t} D(t')\,dt' - x, \qquad t = t. \tag{15}$$

With this change of independent variable the differential equations (11 become

$$-\rho c_0^2 u_\xi + (D-u)p_\xi + p_t = \rho c_0^2 \sum_j \sigma^j r^j, \tag{14a}$$

$$\rho(D-u)u_\xi - p_\xi + \rho u_t = 0, \tag{14b}$$

$$(D-u)\lambda^j_\xi + \lambda^j_t = r^j_\xi \quad j = 1, 2 \cdots\cdots r, \tag{14c}$$

$$u_\xi = \left(\frac{\partial u}{\partial \xi}\right)_t, \text{ etc.}; \quad u_t \left(\frac{\partial u}{\partial t}\right)_\xi, \text{ etc.}$$

Solving the first two equations for $u_s$ and $p_s$, we obtain

$$u_s = -\frac{1}{\eta}\left[\sum_j \sigma^j r^j - \frac{1}{\rho c_0^2} p_t - \frac{D-u}{c_0^2} u_t\right], \quad (15a$$

$$p_s = -\frac{1}{\eta}\left[\rho(D-u)\left(\sum_j \sigma^j r^j - \frac{1}{\rho c_0^2} p_t\right) - \rho u_t\right], \quad (15b$$

$$\eta = 1 - \frac{(D-u)^2}{c_0^2}. \quad (15c$$

If we assume a region of steady state behavior, the time derivatives vanish, and the equations reduce to

$$u_s = -\frac{1}{\eta}\sum_j \sigma^j r^j, \quad (16a$$

$$p_s = -\frac{\rho(D-u)}{\eta}\sum_j \sigma^j r^j, \quad (16b$$

$$\lambda^j_s = \frac{1}{D-u} r^j, \; j = 1 \cdots n \quad (16c$$

It is easily seen from these equations that the state variables in the steady zone satisfy the Rankine-Hugoniot relations (12, with states 1 and 2 being any points in the steady zone. Since the steady zone point just to the rear of the shock is connected to the medium ahead by these same relations it is clear that we may write

$$\rho(D-u) = \rho_0 D, \quad (17a$$

$$p - p_0 = \rho_0 D u, \tag{17b}$$

$$E - E_0 = \frac{1}{2}(p + p_0)(v_0 - v), \tag{17c}$$

the zero subscripts denote values of the quantities in the medium ahead; unsubscripted quantities are at any point in the steady zone. Equations (17, coupled with any one of the differential equations (16, determine the state variables as functions of the distance behind the leading shock, for any assumed value of D. The latter is not yet determined.

We note that we will encounter difficulty in integrating (16a or (16b if $\eta$ becomes zero. Since the flow back of a plane shock relative to the shock front is always subsonic, $\eta$ will be positive at $\xi = 0$.

## IV

Corresponding to the classical Riemann analysis for the case of non-reactive flow, we anticipate that, for piston motions opposite in direction to that of the motion of the detonation wave, there will be a rarefaction wave of non-steady character reducing the pressure from its value at the end of the steady zone to a lower value, possibly zero, at the piston surface. Consequently we devote this section to a brief discussion of the characteristic curves of the set of differential equations (11. Without reproducing all the steps, we state the results as follows. The set of equations (11 is always hyperbolic. The characteristics in the x - t plane, r + 2 in number, are given by the following equations:

$$\left(\frac{dx}{dt}\right)_{r+1,\, r+2} = u \pm c_0, \tag{18a}$$

$$\left(\frac{dx}{dt}\right)_j = u, \quad j = 1, 2 \cdots\cdots r. \tag{18b}$$

The first two characteristics may be thought of as giving the paths of "sound waves" through a given point in the x - t plane. The other characteristics are degenerate, all coinciding with the streamline through the point.

These results are similar to the well-known results for non-reactive flow, $c_o$ appearing in the place of the ordinary non-reactive sound speed. There is, however, an important difference; equations (11 are not homogeneous, and therefore not reducible, contrary to the case with the non-reactive equations. Thus part of the usual theory of hyperbolic flow fails to carry over into the reactive case. However, certain general properties of hyperbolic equations remain, among them the following: the boundary between two space-time regions in which the flows are of different type (for example, a region in which the flow is steady adjacent to a region in which the flow is non-steady) must be a characteristic. In the next section we make an important application of this principle.

## V

We now proceed to draw certain conclusions concerning the detonation process from the analyses of the preceding two sections. As noted at the end of the last section, the boundary between our steady region and the succeeding flow must be a characteristic curve, assuming that the differential equations remain valid across the boundary - i.e. assuming the boundary is not a shock. It then follows that the flow variables are continuous (not necessarily their derivatives); hence the flow variables are constant along the boundary, and it follows from (18 that the boundary characteristic is straight. Since it is clear that it cannot be a streamline, and since in our coordinate system the wave is forward facing, it must be a $u + c_o$ characteristic. Still further, in order for the x dimension of the steady zone to be constant in time, it is necessary that the slope of this characteristic in the x - t plane be the same as that of the leading shock locus. We obtain as a necessary condition at the end of the steady zone

$$D = u + c_o , \qquad (19$$

a result which has also been obtained by Brinkley and Richardson[10].

Returning to relations (16 for the steady zone, we

note that the preceding result makes $\eta$, the denominator of the expressions for $A_{ij}$ and $B_{ij}$, vanish. In order to avoid singularities in these space derivatives the numerators must also vanish, which requires as an additional condition at the end of the steady zone

$$\sum_j \sigma^{ij} \nu_j = 0 . \qquad (20$$

These two equations, (18 and (20 may be taken as a generalized statement of the C-J condition. That the indeterminacy of (16 is as it should be is readily appreciated from the fact that (16 holds for the space derivatives in both directions at the end of the steady zone. The indeterminacy thus permits these derivatives to be discontinuous at the end of the steady zone, and in particular allows the derivatives on the non-steady side to be time dependent.

Clearly (20 is satisfied if all the rate functions vanish,

$$r^j = 0, \quad j = 1, \ldots, r, \qquad (21$$

corresponding to instantaneous chemical equilibrium. This, coupled with (18 corresponds to von Neumann's normal C-J condition. It is the one in common use; see, e.g. Lewis and Friauf[13], papers by Kistiakowsky and co-workers[14].*

---

*It may be noted that the C-J condition used by these investigators actually implies the use of $c_0$, although it has apparently been regarded as an approximation to a sound speed defined by $\left(\frac{\partial p}{\partial \varrho}\right)_{s, \sum \nu_\alpha \mu_\alpha = 0}$.

---

We note that (16, (19, and (21, with the equation of state taken as $E = E(\lambda, p, V)$, constitute $r + 4$ equations for the $r + 4$ unknowns D, p, v, u, and $\lambda$. Thus we may expect to be able to solve them for D and the state variables at the end of the steady-zone. Of course, in actual practice, rather than (21 one uses the ordinary relations for chemical equilibrium

$$\sum_\alpha \nu_\alpha^j \mu_\alpha = 0, \quad j = 1, 2 \ldots r. \qquad (22$$

It is also possible for $\sum_j \sigma_j r^j$ to vanish with some or all $r^j$ non-vanishing, due to some of the $\sigma_j$ becoming negative (or conceivably some of the $r^j$); this corresponds to von Neumann's pathological case. In this case we obtain a sufficient number of equations to determine D and the C-J values of the state variables by eliminating $\xi$ from (16c, obtaining r - 1 equations

$$\frac{d\lambda^j}{d\lambda^1} = \frac{r^j}{r^1} \quad , \quad j = 2, 3 \cdots r. \qquad (23$$

These may be integrated by use of the initial conditions at the shock front; with (17, (23, (19, and (20 we then obtain r + 4 equations. In general such a calculation requires explicit knowledge of the rate functions $r^j$, in addition to the usual thermodynamic data; this is to be contrasted with the normal case, where the latter information suffices. There might even be multiple zeros of $\sum \sigma_j r^j$, in which case the C-J condition is ambiguous.

For the special case of a single reaction the analysis can be carried a little further: the particular case in which $\sigma$ might become negative while $\eta$ is positive, $\sigma$ thereafter remaining negative, so that the C-J point would have to correspond to r = o, can be eliminated. It is possible to show under reasonable assumptions concerning the finiteness of certain thermodynamic variables, that it is impossible for $\eta$ to vanish under these conditions.

Also, for the case of a single reaction, the relation of our treatment to von Neumann's discussion of the pathological case, in terms of the envelope to the family of partial Hugoniot curves with parameter $\lambda$, is readily seen from the third of the equivalent expressions for $\sigma$ given in (10a. In this case also, the calculations of detonation velocity can be performed in the pathological case in the absence of detailed knowledge of the rate function, since (20 reduces to $\sigma$ = o, which is a purely thermodynamic relation. It is, of course, necessary to know what reaction is involved.

No example of a pathological detonation is definitely known. From (10a it is clear that a negative $\sigma$ requires either a volume decrement or an endothermic reaction under the local conditions. Thus the possibility of pathological

behavior may arise, for instance, in gaseous detonations not too strongly exothermic involving an over-all mole decrement, or in detonations in which an exothermic reaction is succeeded by an endothermic one, possibly involving a mole decrement. In condensed explosives the situation is considerably obscured by uncertainties in our present knowledge of equations of state, not to mention kinetics. A possible example might occur in the case of aluminized explosives.

## REFERENCES


1. D. L. Chapman, Phil. Mag. 47, 90 (1889).

2. E. Jouguet, Compt. rend. 132, 573 (190), 144, 415 (1907).

3. R. Becker, Z. Elektrochem. 23, 40, 304 (1917); Z. Physik 8, 321 (1922).

4. W. Jost, Z. Elektrochem. 41, 183 (1935); Z. Physik Chem. 42, 136 (1939).

5. R. L. Scorah, J. Chem. Phys. 3, 425 (1935).

6. Y. B. Zeldovitch, J. Exptl. Theor. Phys. (USSR) 10, 542 (1940).

7. J. von Neumann, OSRD 549 (1942); see also W. Doering, Ann. der Physik 43, 421 (1943).

8. H. Eyring, R. E. Powell, G. H. Duffy, and R. B. Parlin, Chem. Revs. 45, 69 (1949).

9. S. R. Brinkley, Jr. and J. G. Kirkwood, Third Symposium on Combustion, Flame, and Explosion Phenomena (Williams and Wilkins Company, Baltimore, 1949), page 586.

10. S. R. Brinkley, Jr. and J. M. Richardson, Fourth Symposium (International) on Combustion, Williams and Wilkins Company, Baltimore, 1953), page 450.

11. R. Courant and K. O. Friedrichs, Supersonic Flow and Shock Waves, (Interscience Publishers, Inc., New York), page 204.

12. C. F. Curtiss, J. O. Hirschfelder, and D. E. Campbell, The Theory of Flame Propagation and Detonation, CM-690, University of Wisconsin (1952).

13. B. Lewis and J. B. Friauf, J. Am. Chem. Soc. 52, 3905 (1930).

14. G. B. Kistiakowsky, H. T. Knight, and M. E. Malin, J. Chem. Phys. 20, 884 (1952); other papers by Kistiakowsky and co-workers.

W. E. Deal, Jr.
Los Alamos Scientific Laboratory
Los Alamos, New Mexico

## BASIC PRINCIPLES

A steady-state plane detonation wave has been shown by von Neumann (1) to consist of a shock followed by a reaction zone of decreasing pressure terminating at the Chapman-Jouguet (C-J) plane. The unsteady flow behind this plane of complete reaction has been described by Taylor (2); such flow is essentially a rarefaction wave centered at the rear of the explosive. The generally accepted picture of the pressure profile of a detonation wave is thus much like that of Figure 1.

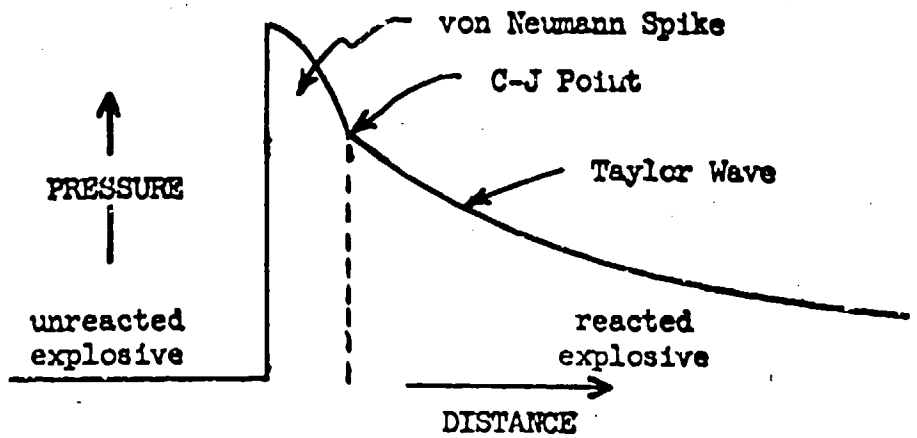


Figure 1 - Pressure Profile of a Detonation Wave

When such a wave impinges upon an inert material in contact with the explosive, the wave transmitted is a shock followed closely by a steep rarefaction which is in turn followed by a more gradual rarefaction. As this wave travels thru the material, the steep rare-

faction overtakes and destroys that portion of the wave corresponding to the von Neumann spike. Then in further travel thru the material the rarefaction corresponding to the Taylor wave gradually reduces the pressure of the remaining shock front. Also, a shock or rarefaction is reflected back into the explosive. If the pressure of the shock front in the inert material is plotted as a function of material thickness, a curve such as Figure 2 results. $P_m$ of this figure corresponds to the pressure at the end of the reaction zone in the explosive (the C-J pressure). Since in these experiments the effects of the von Neumann spike will have become attenuated, we can limit theoretical consideration to a simple wave rising only to the Chapman-Jouguet pressure. If pressure and particle velocities are equated across the interface one obtains the equation:

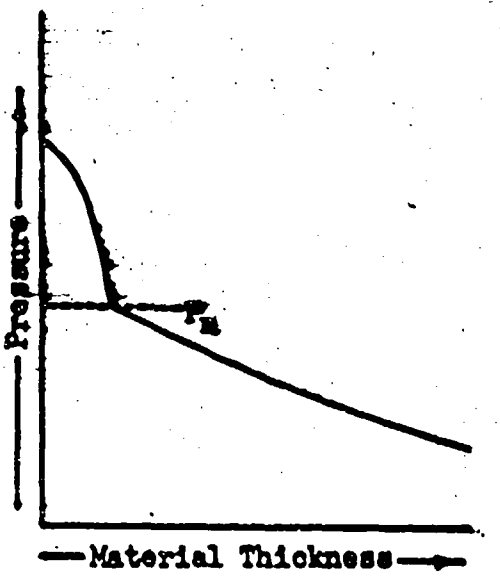


Figure 2 - Shock Front Pressure as a Function of Material Thickness

$$\frac{P_m}{P_{c-j}} = \frac{\rho_t^\circ D_t}{\rho_i^\circ D_i} \qquad \frac{\rho_i^\circ D_i + \rho_r^\circ D_r}{\rho_t^\circ D_t + \rho_r^\circ D_r}$$

Here,

$P_{c-j}$ is the Chapman-Jouguet pressure in the detonation,

$P_m$ is the pressure induced in the inert material.

The $\rho$'s are densities, and

the D's are shock (or detonation) velocities which are particularized by the subscripts:

i referring to conditions behind the incident front

r referring to conditions behind the reflected front

t referring to conditions behind the transmitted front.

Conditions in front of these waves are referred to by a superscript zero accompanied by the appropriate subscript. All velocities are measured relative to the fluid in front of them.

If the further approximation $\rho_r^\circ D_r = \rho_i^\circ D_i$ is made (3), the interface equation can be written:

$$P_{c-j} = P_m \frac{\rho_t^o D_t + \rho_i^o D_i}{2\rho_i^o D_t}$$

The C-J pressure is then determined since $\rho_t^o$ and $\rho_i^o$ are the simply measurable initial densities of the material and explosive, $D_i$ is the readily measurable detonation velocity (4), and $D_t$ and $P_m$ are available from equation of state data if one hydrodynamic variable of the C-J state is measured (5). The quantity established in these experiments was the free-surface velocity corresponding to $P_m$ in Figure 2.

An alternative method which also ignores the presence of the spike, but tends to minimize the effect of the reflected wave into the explosive is to establish $P_m$ and the corresponding particle velocity for each of several materials of different shock impedance. These define a curve in the pressure-particle velocity plane. This curve must pass thru the C-J point since it is really the locus of all possible shocked and rarefied states (for one direction of wave travel) for the reacted explosive. From the conservation equations one can write:

$$\frac{P_d}{V_o - V_d} = (\rho_o D)^2$$

where V is specific volume and the subscripts d and o refer to initial conditions and conditions immediately behind the detonation front, respectively. Thus, as shown by von Neumann (1) and illustrated in Figure 3, $(\rho_o D)^2$ is the slope in

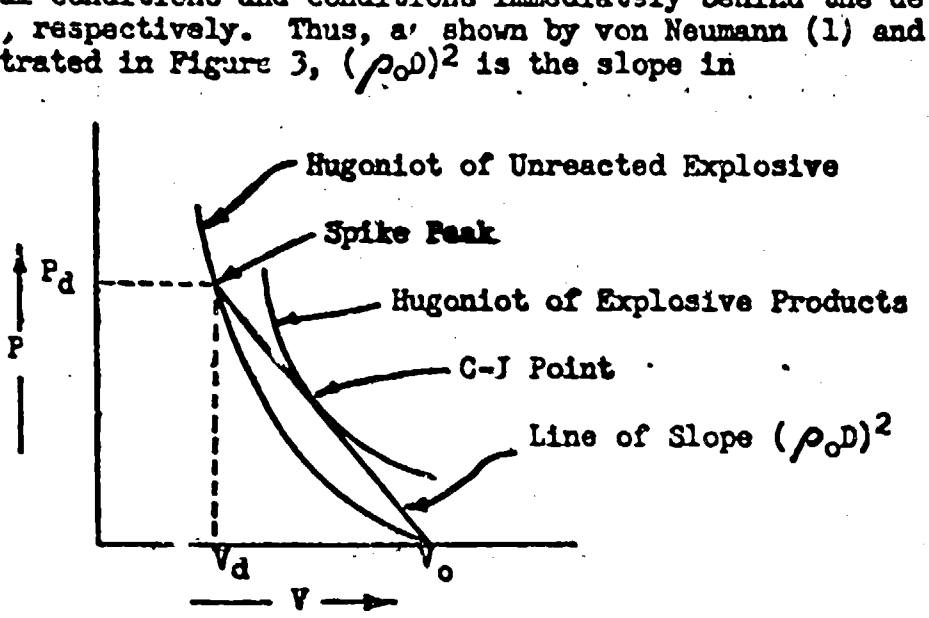


Figure 3 - The Detonation Process in the Pressure-Volume Plane

the pressure-volume plane of the line containing both the spike peak point and the C-J point. One may also write from the conservation equations:

$$\frac{P_d}{u_d} = \rho_o D$$

where u is the particle velocity behind a shock moving into a stationary medium. The straight line in the pressure-particle velocity plane passing thru the origin and of slope $\rho_o D$ must then also contain the C-J point. Hence, the intersection of the experimentally defined curve and the $\rho_o D$ line must be the C-J point.

## EXPERIMENTAL TECHNIQUE

The value of free-surface velocity corresponding to $P_m$ for a given explosive and material is established by measurement of free-surface velocity of an explosive-driven plate as a function of plate thickness. These velocities are measured photographically by the use of a rotating mirror smear camera with a writing speed of 3.2 mm/$\mu$sec. A Lucite block assembly like that of Figure 4 is placed with the

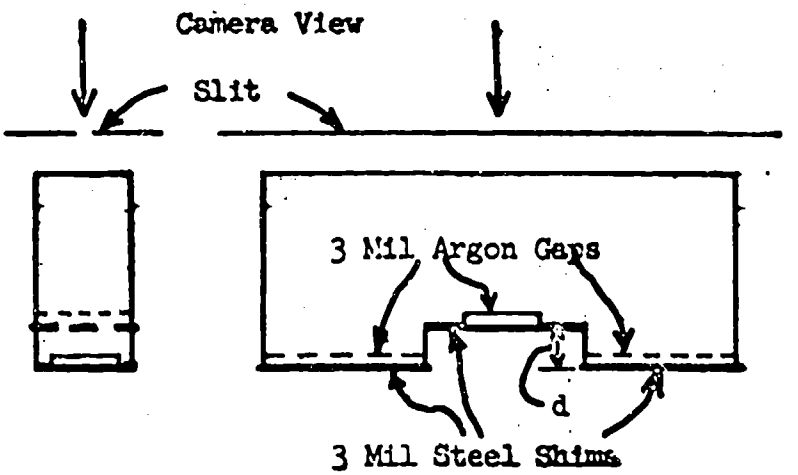


Figure 4 - Lucite Block Assembly

two outer shims adjacent to the surface to be studied. This is then viewed by the camera thru a slit parallel to the long axis of the Lucite piece and swept on the film in a direction perpendicular to the slit image. When the explosive-driven plate on which such an assembly is placed begins to move, the argon gaps near the surface are closed first and yield a brilliant flash of light of short duration. When the free surface moves the distance d, it closes the central gap and yields another flash of light. The gaps and shims are made as nearly identical as possible by machining with a single, shaped cutter and using pieces of shim cut from the same piece of stock. Good contact of shim and plate are assured by holding flatness tolerances over the contact surfaces to 0.0001". Identity of the central and side gaps closure times is readily established by a simple argument.

A print of a resulting camera record is shown as Figure 5.

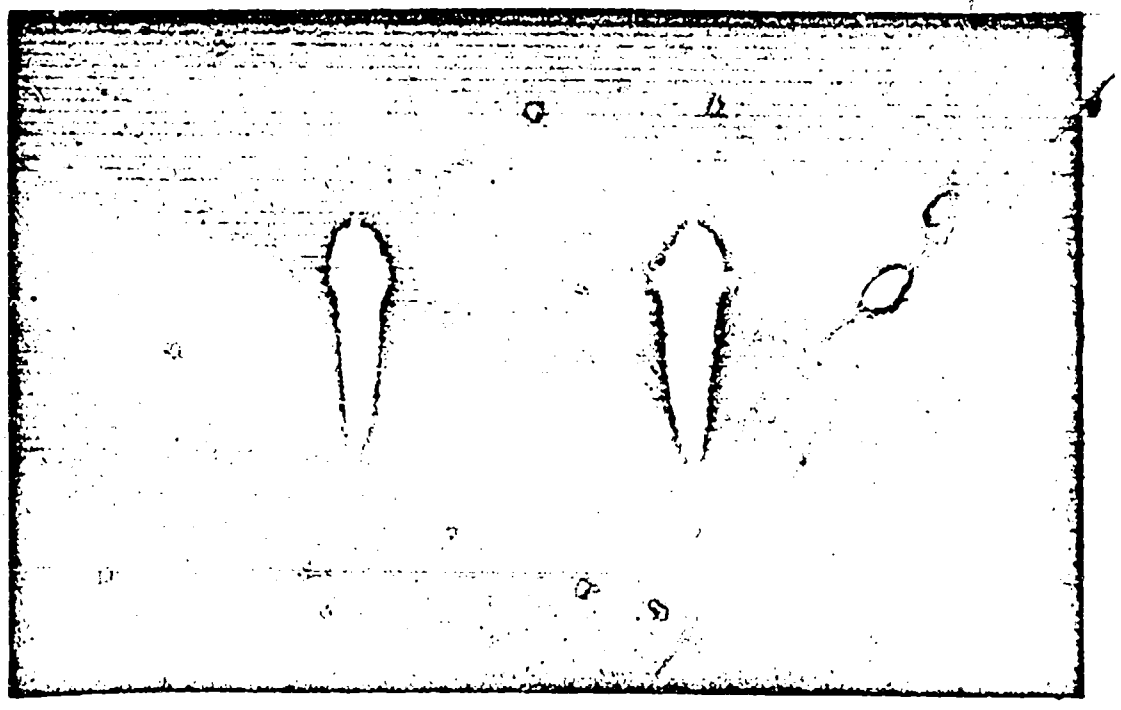

**Figure 5 - Smear Camera Record for a Lucite Block Assembly. Time Increases Downward.**

Such records are read with a comparator and plotted; interpolation of the two side traces yields a time of departure of the central free-surface which along with the central arrival trace gives a transit time and hence velocity thru the accurately measured depth of the step. Depths of steps in the Lucite blocks are chosen such that there is not time for the second shock arising from the rarefaction reflection at the explosive interface to return and affect the free-surface velocity. Also the step widths of Lucite blocks are chosen so that the central trace can not be affected by disturbances of the plate motion by parts of the block contacted earlier by the plate. Up to twelve such Lucite blocks $2\frac{1}{4}$" x 1" x $\frac{1}{2}$" may be placed on an appropriately machined plate to get free-surface velocities for twelve plate thicknesses from a single 10" diameter charge.

## DATA AND RESULTS

Charges of TNT, Composition B, 75/25 Cyclotol, and RDX were studied. The TNT charges were in the shape of truncated cones 8" thick with 8 3/8" diameter at the small end and 10.4" diameter at the large end. These were pressed without a binder to 99.1% of crystal density from a granular TNT of about 400 $\mu$ median particle size. The TNT charges were detonated on the small end. All charges were detonated by plane explosive lenses of 8" aperture. The opposite surfaces were placed against the test plates with a thin layer of mineral oil filling any gaps due to machining tolerances. The Composition B and 75/25 Cyclotol charges were 8" thick, each made up of two 10"x 10"x4" blocks of cast material. The Composition B was 64.7% RDX with a

spread of 1.5% within a piece. The 75/25 Cyclotol was 77.0% RDX with a spread of 1.5% within a piece. These compositions were based upon samples taken from similar castings. The RDX charges were 6" thick made up of two cylinders 6" in diameter and 3" thick pressed (6) without a binder to 97.7% of crystal density from a granular RDX of 100$\mu$ median particle size.

Tables I thru IV are listings of the free-surface velocity and thickness data. These are plotted on Figures 6 thru 9.

## Table I.
## Pressed TNT on Dural Plates

**Shot No. 1.**
charge density 1.640gm/cc.
plate density 2.793

| plate thickness | free-surface velocity |
|---|---|
| .069" | 2.473mm/$\mu$sec. |
| .094 | 2.454 |
| .119 | 2.421 |
| .144 | 2.419 |
| .194 | 2.372 |
| .244 | 2.365 |
| .294 | 2.360 |
| .344 | 2.348 |
| .394 | 2.350 |
| .444 | 2.334 |

**Shot No. 2**
charge density 1.639gm/cc.
plate density 2.793

| plate thickness | free-surface velocity |
|---|---|
| .069" | 2.494mm/$\mu$sec. |
| .094 | 2.466 |
| .119 | 2.414 |
| .144 | 2.407 |
| .194 | 2.373 |
| .244 | 2.339 |
| .294 | 2.340 |
| .344 | 2.309 |
| .394 | 2.298 |
| .444 | 2.310 |
| .469 | 2.309 |
| .493 | 2.319 |

Shot No. 3
charge density 1.639gm/cc.
plate density 2.793

| plate thickness | free-surface velocity |
|---|---|
| .074" | 2.444mm/$\mu$sec. |
| .099 | 2.436 |
| .124 | 2.417 |
| .149 | 2.400 |
| .199 | 2.362 |
| .249 | 2.344 |
| .299 | 2.307 |
| .349 | 2.319 |
| .399 | 2.319 |
| .449 | 2.317 |
| .474 | 2.308 |
| .493 | 2.324 |

Shot No. 4
charge density 1.640gm/cc.
plate density 2.788

| plate thickness | free-surface velocity |
|---|---|
| .979" | 2.287mm/$\mu$sec. |
| .979 | 2.311 |
| .979 | 2.273 |
| .979 | 2.285 |
| .979 | 2.284 |
| .979 | 2.287 |

## Table II
## Composition B on Dural Plates

**Shot No. 5**
charge density 1.711gm/cc.
plate density 2.793

| plate thickness | free-surface velocity |
|---|---|
| .073" | 3.389mm/μsec. |
| .100 | 3.362 |
| .123 | 3.358 |
| .150 | 3.332 |
| .197 | 3.359 |
| .199 | 3.320 |
| .249 | 3.343 |
| .300 | 3.324 |
| .399 | 3.293 |
| .400 | 3.304 |
| .500 | 3.245 |

**Shot No. 6**
charge density 1.712gm/cc.
plate density 2.793

| plate thickness | free-surface velocity |
|---|---|
| .071" | 3.411mm/μsec. |
| .096 | 3.418 |
| .125 | 3.382 |
| .151 | 3.366 |
| .200 | 3.346 |
| .200 | 3.322 |
| .249 | 3.299 |
| .299 | 3.273 |
| .400 | 3.254 |
| .401 | 3.253 |
| .450 | 3.229 |
| .482 | 3.226 |

**Shot No. 7**
charge density 1.711 gm/cc.
plate density 2.795

| plate thickness | free-surface velocity |
|---|---|
| .100" | 3.357mm/μsec. |
| .143 | 3.322 |
| .200 | 3.321 |
| .251 | 3.278 |
| .296 | 3.262 |
| .348 | 3.236 |
| .400 | 3.206 |
| .450 | 3.207 |
| .500 | 3.174 |

**Shot No. 8**
charge density 1.711 gm/cc.
plate density 2.793

| plate thickness | free-surface velocity |
|---|---|
| .075" | 3.443mm/μsec. |
| .100 | 3.411 |
| .125 | 3.393 |
| .150 | 3.352 |
| .200 | 3.324 |
| .250 | 3.295 |
| .300 | 3.292 |
| .350 | 3.265 |
| .400 | 3.267 |
| .450 | 3.263 |
| .475 | 3.229 |
| .495 | 3.247 |

**Shot No. 9**
charge density 1.713 gm/cc.
plate density 2.788

| plate thickness | free-surface velocity |
|---|---|
| .964" | 3.097mm/μsec. |
| .964 | 3.129 |
| .964 | 3.116 |
| .964 | 3.172 |
| .964 | 3.117 |
| .964 | 3.145 |
| .964 | 3.161 |
| .964 | 3.097 |

## Table III
## 75/25 Cyclotol on Dural Plates

Shot No. 10
charge density 1.742 gm/cc.
plate density 2.793

| plate thickness | free-surface velocity |
|---|---|
| .075" | 3.538mm/μsec. |
| .100 | 3.528 |
| .125 | 3.486 |
| .150 | 3.497 |
| .200 | 3.464 |
| .250 | 3.463 |
| .300 | 3.449 |
| .351 | 3.465 |
| .400 | 3.441 |
| .450 | 3.434 |

Shot No. 11
charge density 1.744 gm/cc.
plate density 2.793

| plate thickness | free-surface velocity |
|---|---|
| .074" | 3.558mm/μsec. |
| .099 | 3.546 |
| .124 | 3.513 |
| .149 | 3.517 |
| .199 | 3.449 |
| .249 | 3.437 |
| .299 | 3.422 |
| .349 | 3.389 |
| .399 | 3.390 |
| .449 | 3.425 |
| .474 | 3.343 |
| .491 | 3.354 |

Shot No. 12
charge density 1.743 gm/cc.
plate density 2.793

| plate thickness | free-surface velocity |
|---|---|
| .075" | 3.538mm/μsec. |
| .100 | 3.542 |
| .125 | 3.497 |
| .149 | 3.501 |
| .200 | 3.473 |
| .250 | 3.461 |
| .300 | 3.441 |
| .349 | 3.469 |
| .400 | 3.418 |
| .449 | 3.417 |
| .496 | 3.401 |

Shot No. 13
charge density 1.744 gm/cc.
plate density 2.793

| plate thickness | free-surface velocity |
|---|---|
| .100" | 3.496mm/μsec. |
| .150 | 3.462 |
| .250 | 3.433 |
| .350 | 3.399 |
| .450 | 3.421 |
| .496 | 3.379 |

Shot No. 14
charge density 1.744 gm/cc.
plate density 2.788

| plate thickness | free-surface velocity |
|---|---|
| .962" | 3.247mm/μsec. |
| .961 | 3.273 |
| .961 | 3.273 |
| .961 | 3.291 |
| .961 | 3.285 |
| .961 | 3.312 |

Table IV.
RDX on Dural Plates

Shot No. 15
charge density 1.762 gm/cc.
plate density 2.790

| plate thickness | free-surface velocity |
|---|---|
| .101" | 3.565mm/$\mu$sec. |
| .201 | 3.495 |
| .301 | 3.473 |
| .400 | 3.458 |

Shot No. 16
charge density 1.760 gm/cc.
plate density 2.790

| plate thickness | free-surface velocity |
|---|---|
| .100" | 3.610mm/$\mu$sec. |
| .201 | 3.489 |
| .300 | 3.454 |
| .401 | 3.469 |
| .493 | 3.487 |

Shot No. 17
charge density 1.764 gm/cc.
plate density 2.790

| plate thickness | free-surface velocity |
|---|---|
| .101" | 3.593mm/$\mu$sec. |
| .201 | 3.471 |
| .300 | 3.483 |
| .400 | 3.492 |
| .498 | 3.469 |

Shot No. 18
charge density 1.763 gm/cc.
plate density 2.790

| plate thickness | free-surface velocity |
|---|---|
| .100" | 3.578mm/$\mu$sec. |
| .201 | 3.481 |
| .300 | 3.468 |
| .400 | 3.463 |
| .498 | 3.449 |

Shot No. 19
charge density 1.759 gm/cc.
plate density 2.790

| plate thickness | free-surface velocity |
|---|---|
| .999" | 3.251mm/$\mu$sec. |
| .999 | 3.289 |
| .999 | 3.293 |
| .999 | 3.307 |
| .999 | 3.283 |

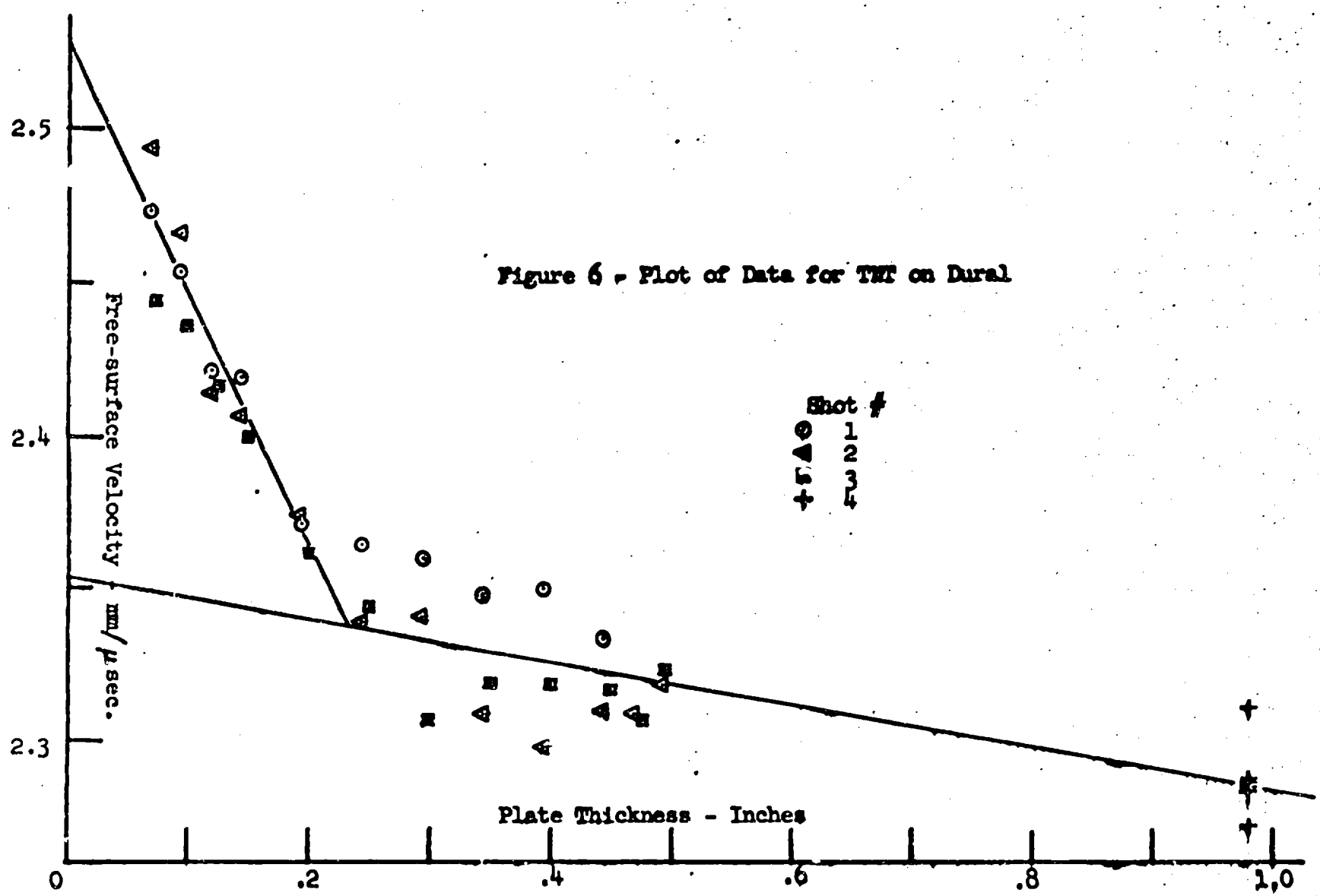


Figure 6 - Plot of Data for TNT on Dural

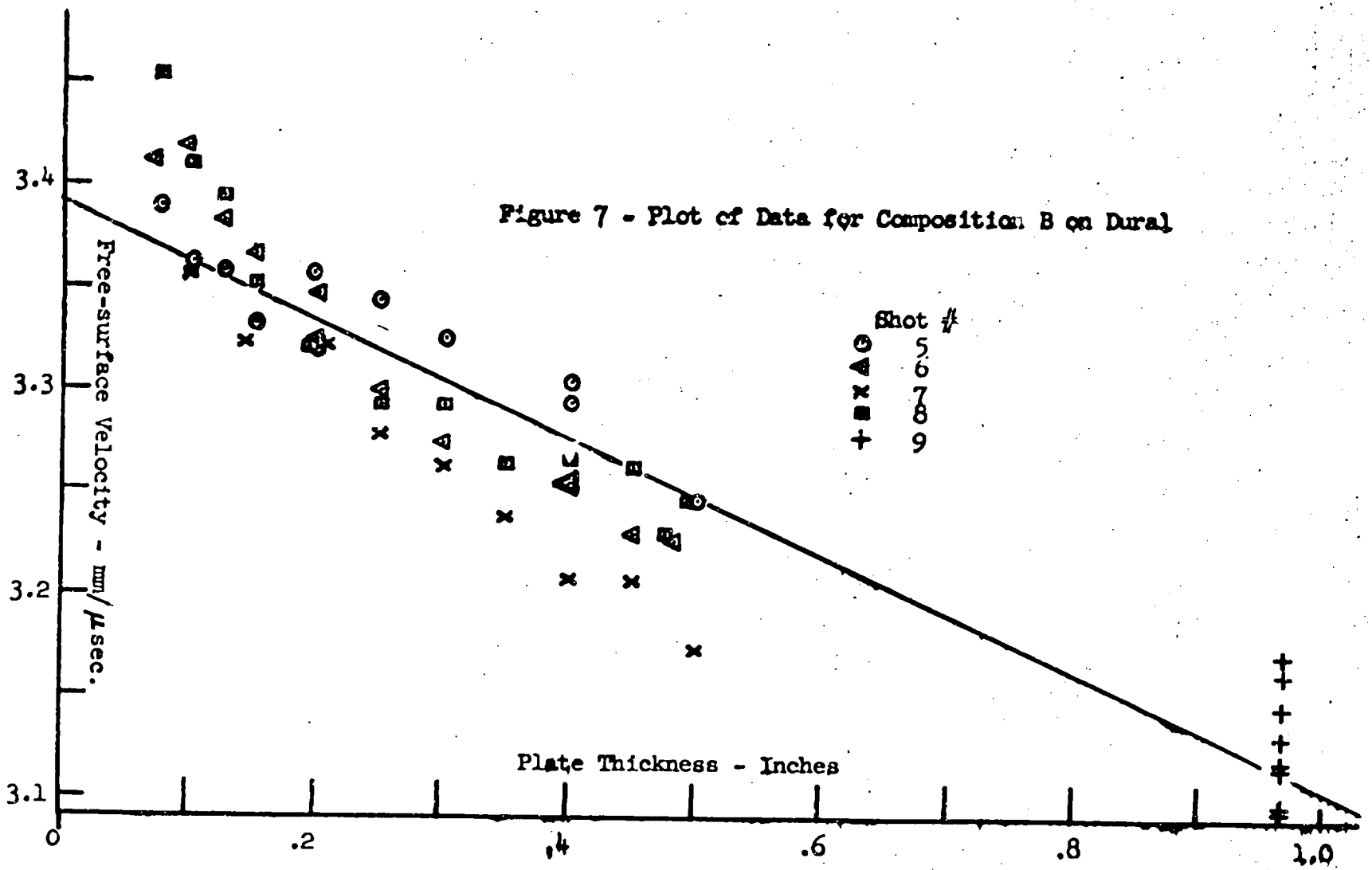


Figure 7 - Plot of Data for Composition B on Dural

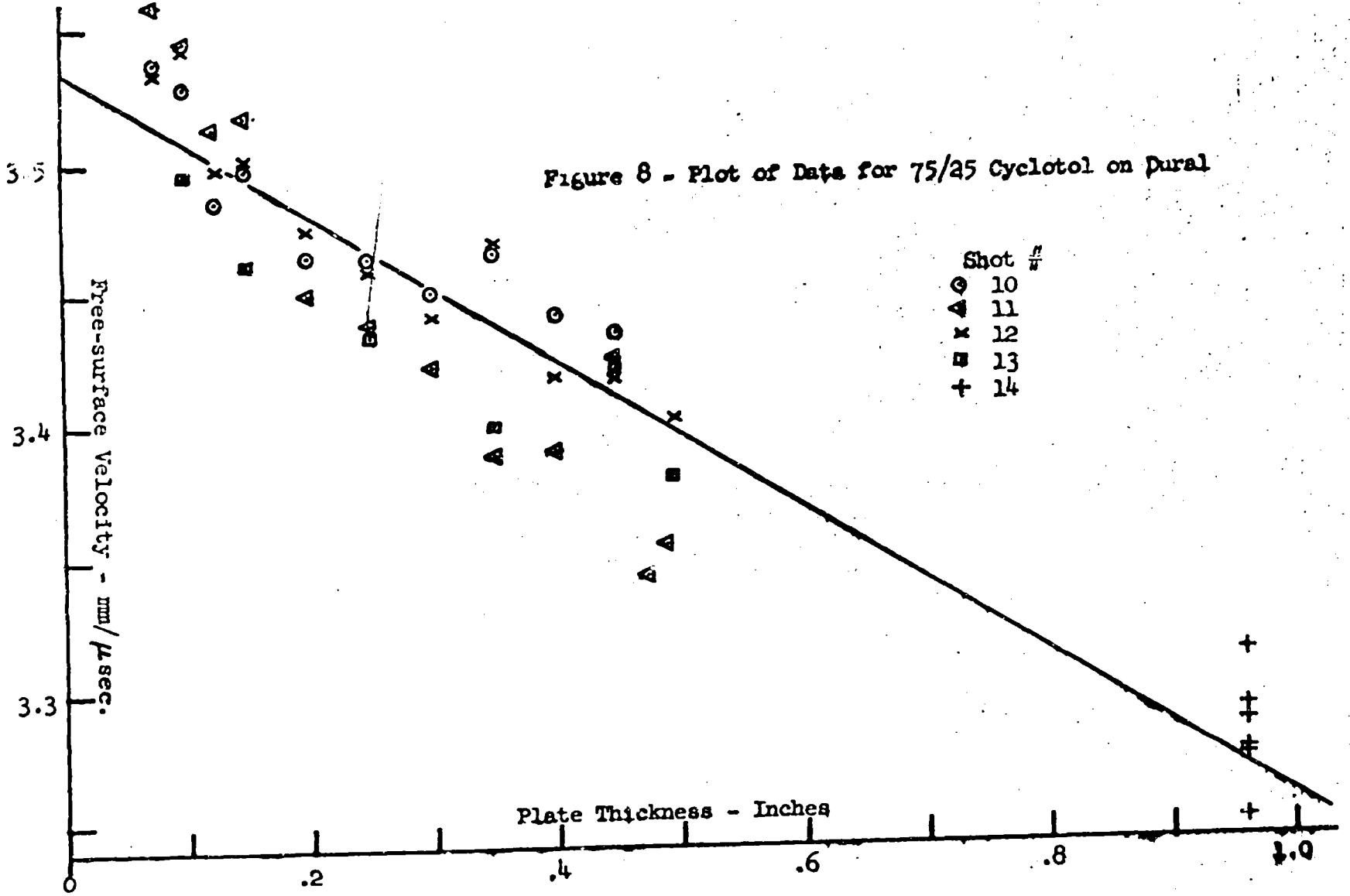


Figure 8 - Plot of Data for 75/25 Cyclotol on Dural

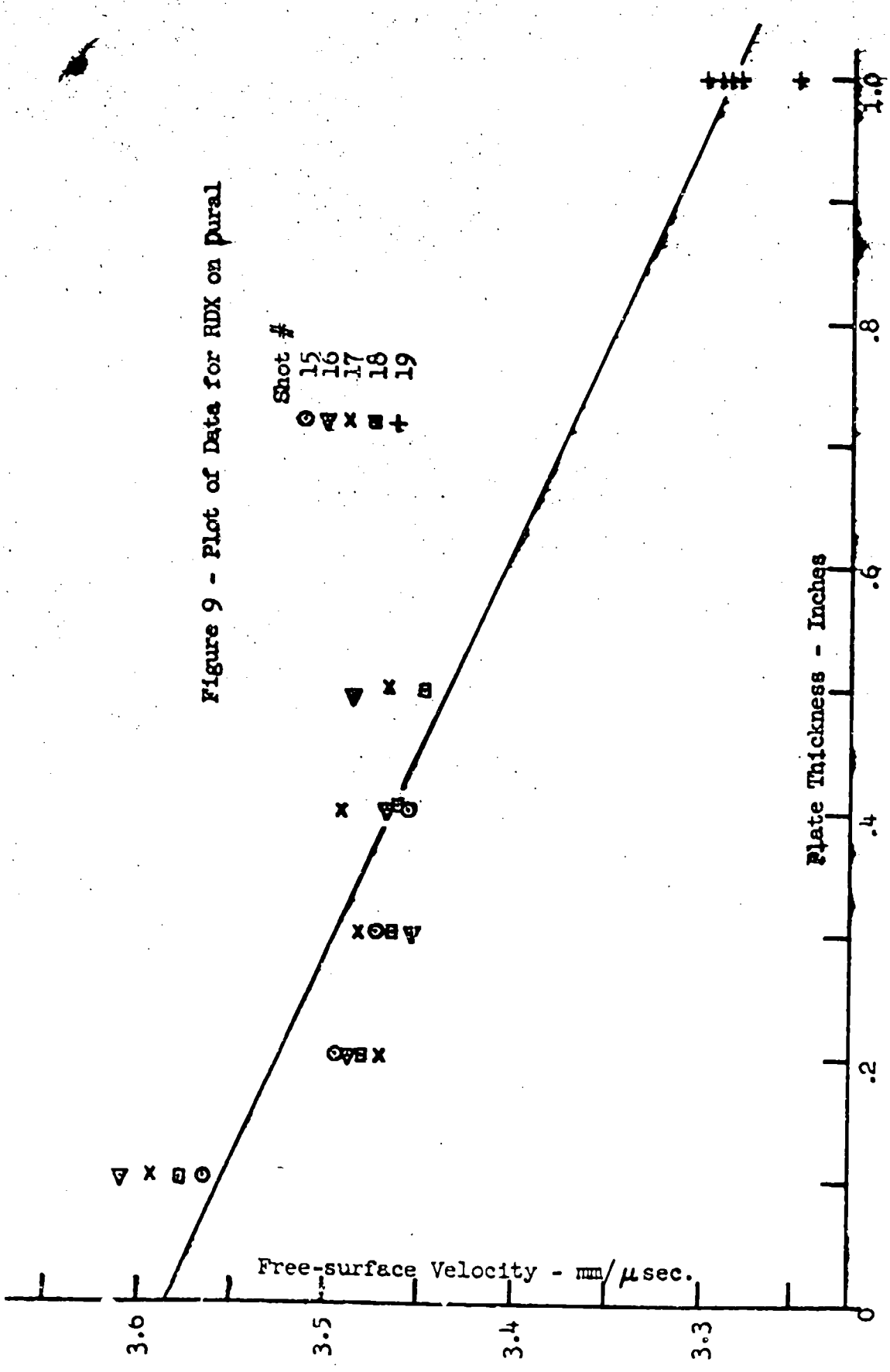


Figure 9 - Plot of Data for RDX on Dural

The TNT data show definite evidence of the presence of a spike in the explosive. Sufficiently thin plates were not used for the other explosives to show the spike. Linear least squares fits made to the data for plates thicker than 0.2" for TNT and for all data for the other explosives yield the slopes and intercepts of table five. The

Table V.

| Explosive | Intercept - mm/$\mu$sec. | Slope - mm/$\mu$sec.-inch |
|---|---|---|
| TNT | 2.354 ± 0.30% | 0.070 ± 17.3% |
| Composition B | 3.389 0.22% | 0.287 5.6% |
| 75/25 Cyclotol | 3.534 0.18% | 0.276 5.2% |
| RDX | 3.582 0.31% | 0.295 6.9% |

errors quoted are standard deviations. A linear least squares fit to the TNT data for plates thinner than 0.2" gives an intercept of 2.526 mm/$\mu$sec. and a slope of 0.819mm/$\mu$sec.-inch. This intercept corresponds to a spike pressure of 0.194 megabar. The intersection of the spike line and that of table five for TNT gives a free-surface velocity ($U_m$) from which $R_m$ can be deduced and C-J pressure calculated. The use of linear fits to the data is justified only by the relatively small deviations of the data (see Figures 7 and 8 ) from straight lines. The use of the extrapolated velocity to get spike peak pressure for TNT is, however, highly in question. Since the spike decay thickness for each of the explosives, exclusive of TNT, is certainly less than 0.1", less than 1% error is introduced by using the intercepts from Table V for the values of $U_m$. Thus the C-J pressures of Table VI follow from the interface equation. Velocities in the

Table VI.

| | TNT | Composition B | 75/25 Cyclotol | RDX |
|---|---|---|---|---|
| $U_m$ | 2.338 | 3.389 | 3.534 | 3.582 |
| $D_m$ | 6.961 | 7.646 | 7.733 | 7.762 |
| $P_m$ | 0.2244 | 0.3562 | 0.3753 | 0.3817 |
| $\rho_0$ | 2.792 | 2.792 | 2.792 | 2.790 |
| $\rho_0^o$ | 1.640 | 1.712 | 1.743 | 1.762 |
| $D_i$ | 6.951 | 8.022 | 8.252 | 8.622 |
| $P_{c-j}$ | 0.178 | 0.293 | 0.313 | 0.325 |

table are in mm/$\mu$sec. and pressures are in megabars. The metal pressures quoted are thought to be accurate to 1%.

Other work is in progress to obtain these C-J pressures using other materials so as to clear up the uncertainty regarding disturbances reflected back into the explosive.

## References

1. J. von Neumann, OSRD Report No. 549 (1942).

2. G. I. Taylor, Proc. Roy. Soc. A200, 235(1950).

3. R. E. Duff and E. Houston, Measurement of C-J Pressure and Reaction Zone Length in a Detonating High Explosive, reported at this meeting.

4. A. W. Campbell, M. E. Malin, T. J. Boyd, and J. A. Hull, Techniques for the Measurement of Detonation Velocity, reported at this meeting.

5. J. M. Walsh and R. H. Christian, Equation of State of Metals from Shock Wave Measurements, to be published in Phys. Rev.

6. E. James, Charge Preparation for Precise Detonation Velocity Studies, presented at this meeting.

# MEASUREMENT OF THE CHAPMAN-JOUGUET PRESSURE AND REACTION ZONE LENGTH IN A DETONATING HIGH EXPLOSIVE 16

Russell E. Duff and Edwin Houston
Los Alamos Scientific Laboratory
Los Alamos, New Mexico

## INTRODUCTION

In 1945 Goranson[1] suggested that the reaction zone of a detonating solid explosive could be investigated by determining the initial free surface velocity imparted to thin metal plates as a function of plate thickness. In particular he showed that reaction zone length and Chapman-Jouguet pressure could be estimated in this way. Unfortunately, the original results obtained by Goranson are available only in a classified report from this laboratory. This paper describes similar but improved theoretical and experimental results obtained during and since 1950.

## THEORY OF THE EXPERIMENT

The generally accepted picture of the structure of a steady state, plane detonation wave was proposed independently by Zeldovich[2], von Neumann[3] and Döring[4]. The wave is assumed to consist of a non-reactive shock followed by a steady state reaction zone which is terminated at the Chapman-Jouguet surface where the local flow velocity plus sound speed equals the detonation velocity. It can be shown that this condition is fulfilled at the point of tangency in the p-v plane of a straight line from the initial state to the final Hugoniot curve calculated for a fixed composition of the product gases. (More specifically, the C-J point is the tangent point on a Hugoniot curve for the product gases whose composition is assumed fixed at the equilibrium values appropriate for the tangent point. The relation of this statement of the Chapman-Jouguet condition to the usual statement, namely, that the C-J point is the tangent point on a Hugoniot every point of which is in chemical equilibrium, is not clear at the moment because of uncertainties in the equation of state

of the detonation products. The former statement can be derived from a recent theoretical investigation of the structure of a steady state, plane detonation wave by Kirkwood and Wood, J. Chem. Phys., (1954). It should be mentioned that this statement of the C-J condition has been shown to apply to all detonations which are not pathological in the von Neumann sense. Finally, no pathological detonation has yet been observed.) Figure 1 shows a representation of the detonation process in the p-v plane. Reference to the laws of conservation of mass and momentum shows immediately that if viscosity and heat conduction are neglected, the succession of state points assumed by the reacting explosive is represented by the straight line from $p_1v_1$ to the C-J point. The rate at which an element of explosive passes from $p_1v_1$ to the C-J state depends on the kinetics of the reactions involved and cannot be determined from hydrodynamic considerations. It follows, therefore, that the pressure-distance profile of a detonation wave consists most probably of a monotone but otherwise unspecified decrease in pressure from $p_1$ to $p_{C-J}$ in an unspecified distance. Two profiles often considered are shown qualitatively in Figure 2. They correspond to a reaction rate determined by grain burning and to a rate determined by a first or second order adiabatic reaction of the Arrhenius type. The unsteady flow behind the Chapman-Jouguet plane has been investigated by Taylor[5]. This flow may be simply described as a rarefaction wave ending either in cavitation or in a steady state region required to match boundary conditions at the back boundary of the explosive products.

When a plane detonation wave is incident normally on a metal plate, a shock wave is transmitted into the metal which is followed by a rarefaction wave corresponding to the pressure drop in the reaction zone of the explosive. The foot of this rarefaction wave will travel with a velocity equal to the sum of the local flow velocity and sound speed. It will overtake the shock in the metal after the shock has been attenuated by the rest of the rarefaction wave. The strength of the shock wave will decrease relatively quickly as this interaction proceeds because of the small thickness of the reaction zone. As a result, the velocity imparted to a thin metal plate, which depends directly on the strength of the shock in the plate, should change with plate thickness qualitatively as shown in Figure 3.

It has been shown that to a very good approximation the shock particle velocity of a metal in the high explosive pressure range is one-half of the free surface velocity[6]. This fact makes it possible to determine the Chapman-Jouguet pressure in the explosive from the free

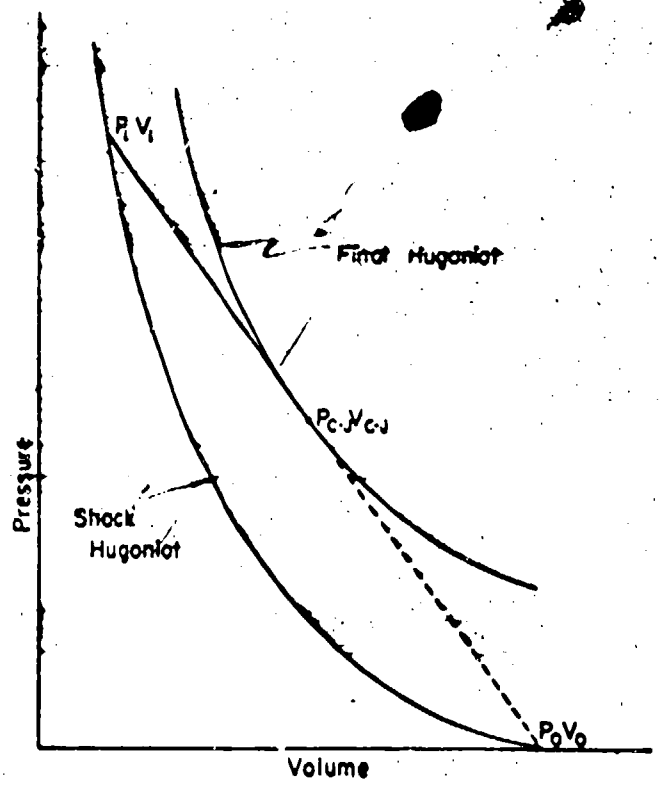


Fig. 1 - A representation of the detonation process in the pressure-volume plane.

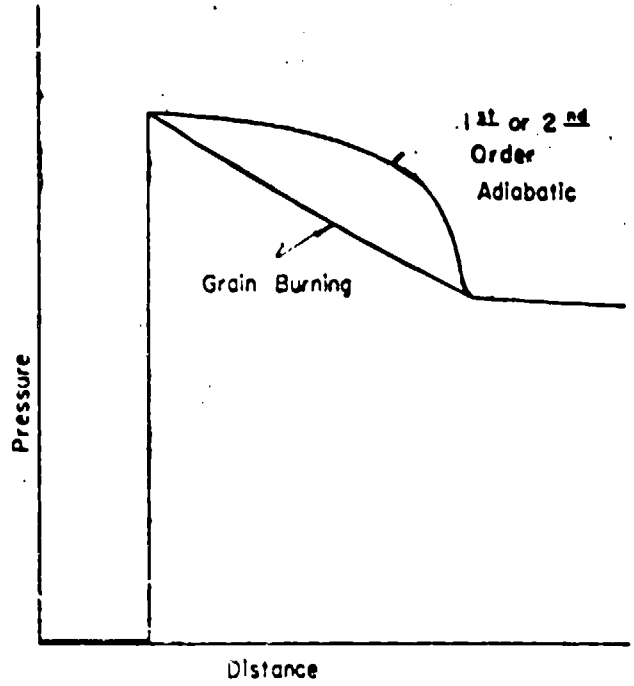


Fig. 2 - Two representative pressure profiles for the reaction zone of solid explosives.

surface velocity of a metal plate corresponding to the end of the interaction caused by the reaction zone. This velocity is v in Figure 3. An immediate consequence of the laws of conservation of mass and momentum is that the pressure behind a shock wave moving into a medium at rest is

$$p = \rho^{\circ} u D \qquad (1$$

where $\rho^{\circ}$ is the density of the unshocked material, u is the shock particle velocity, and D is the shock velocity. In all of the experiments discussed in the next section the metal used was aluminum or dural. For these materials Walsh[6] has determined experimentally a relation between shock velocity and free surface velocity in an investigation of the equation of state of the metals. The pressure in the metal can therefore be determined from the measured metal density, the free surface velocity, and this relation.

By applying the usual boundary corditions of equality of pressure and continuity of flow velocity at the interface between explosive and metal, the following expression can be developed relating incident pressure in the explosive to transmitted pressure in the metal.

$$\frac{p_m}{p_x} = \frac{\rho_t^{\circ} D_t}{\rho_i^{\circ} D_i} \left( \frac{\rho_i^{\circ} D_i + \rho_r^{\circ} D_r}{\rho_t^{\circ} D_t + \rho_r^{\circ} D_r} \right) \qquad (2$$

The subscripts i, t, and r refer to properties of the material in which the wave is respectively incident, transmitted, and reflected – in this case the undetonated explosive, the metal, and the explosive products. The superscript $^{\circ}$ refers to properties in front of a shock wave. D refers to shock velocity relative to the medium ahead of the wave. The pressure in the explosive, $p_x$, can now be calculated if $\rho_r^{\circ} D_r$ is known. An error analysis of this relation shows that

$$\frac{\delta p_x}{p_x} = \frac{(\rho_i^{\circ} D_i - \rho_t^{\circ} D_t)}{(\rho_i^{\circ} D_i + \rho_r^{\circ} D_r)} \frac{\rho_r^{\circ} D_r}{(\rho_t^{\circ} D_t + \rho_r^{\circ} D_r)} \frac{\delta(\rho_r^{\circ} D_r)}{\rho_r^{\circ} D_r}$$

If the acoustic approximation is made that $\rho_i^{\circ} D_i = \rho_r^{\circ} D_r$ and values appropriate for Composition B (nominally 60% RDX - 40% TNT) are inserted, then

$$\frac{\delta p_x}{p_x} = -.1 \frac{\delta(\rho_r^{\circ} D_r)}{\rho_r^{\circ} D_r}$$

Thus it is clear that the Chapman-Jouguet pressure is

quite insensitive to the value of $\rho_r^\circ D_r$ assumed. Furthermore, the acoustic approximation is correct insofar as the velocity of the reflected shock can be assumed equal to the velocity of a rarefaction wave in the product gases. Therefore, to a good approximation

$$\frac{p_m}{p_x} = \frac{\rho_t^\circ D_t}{(\rho_1^\circ D_1 + \rho_t^\circ D_t)} \qquad (3$$

An estimate of the reaction zone length can be made from a determination of the distance required for the end of the rarefaction corresponding to the Chapman-Jouguet plane to overtake the shock wave in the metal. This distance is b in Figure 3. If it is assumed that the metal is a perfect impedance match to the explosive so that no wave is reflected back into the explosive, an x-t representation of the interaction will be as shown in Figure 4. The interface is initially assumed to be at x = 0. A detonation wave comes in from the left with a velocity $D_1$. The reaction zone length is a. The velocity of the interface through the reaction zone is $\alpha D_1$, the shock velocity in the metal is $D_t$, and the velocity of the foot of the rarefaction wave is $u_t + c_t$. $D_t$ and $\alpha$ will vary as the interaction proceeds. The values used in the formula below and those indicated in Figure 4 are the appropriate average values. As long as the flow behind the shock can be considered isentropic (a good approximation), $u_t + c_t$ depends only on pressure and is the value corresponding to the C-J state transmitted into the metal. Simple analytical geometry leads to the following relation between the reaction zone length in the explosive and the interaction distance in the metal.

$$a = b\left[D_1(u_t + c_t - D_t)(1 - \alpha)\right]\left[D_t(u_t + c_t - \alpha D_1)\right]^{-1} \qquad (4$$

The appropriate average value of $D_t$ can be determined from the free-surface-velocity/plate-thickness relation since at every value of thickness this relation gives the corresponding shock velocity by using the equation of state. It can easily be seen that the appropriate average to be used in the above equation is the inverse average; i.e.

$$D_t = \left(\frac{1}{b}\int_0^b \frac{dx}{D(x)}\right)^{-1} \qquad (5$$

Likewise $\alpha$ should be determined from a similar inverse average of the interface velocity.

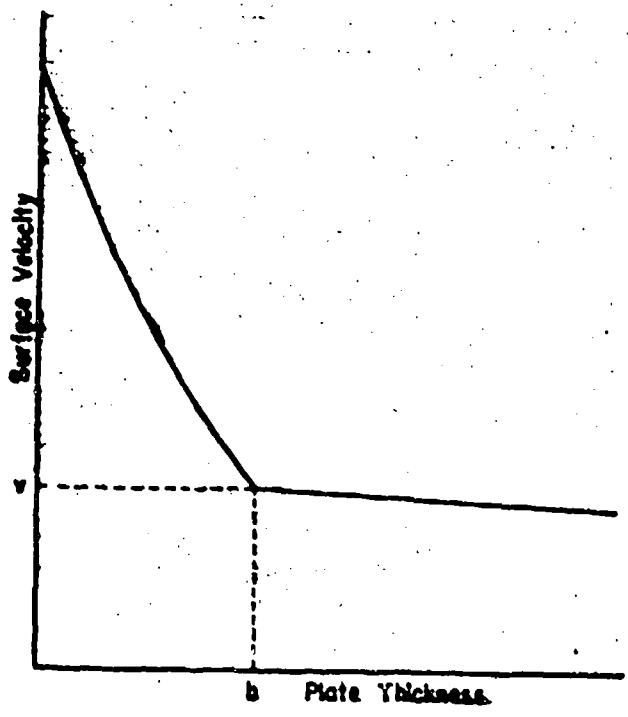


Fig. 3 - Free surface velocity of a metal plate as a function of plate thickness showing the high velocity produced in thin plates by the von Neumann spike in the explosive.

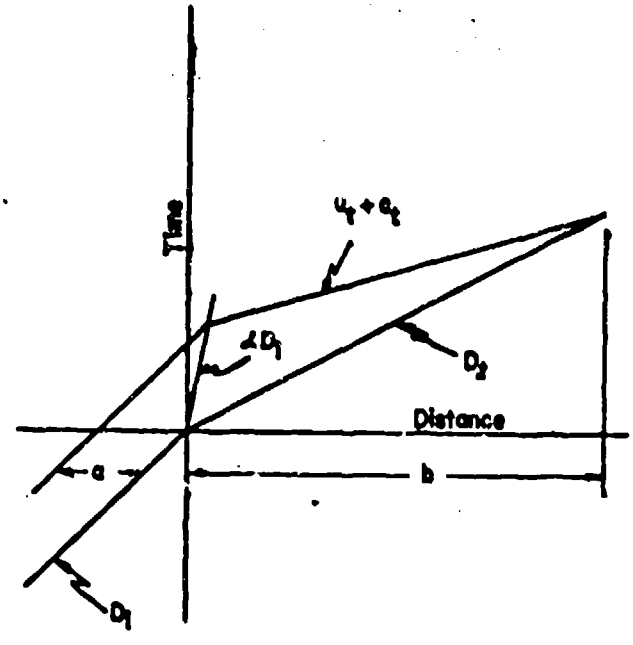


Fig. 4 - Distance-time representation of the interactions between the von Neumann spike in the explosive and the metal plate.

It is possible to calculate in detail the free surface velocity as a function of plate thickness by using the procedure outlined by Courant and Friedrichs[7] under the assumption mentioned above, namely, that the flow behind the shock can be considered isentropic. In particular, if the reaction zone rarefaction and the Taylor wave are both assumed to be centered rarefaction waves, and if a ratio of explosive charge length and reaction zone length is assumed, the ratio of slopes of the free-surface-velocity/thickness curve for the two waves at the point corresponding to the end of the reaction zone can be calculated. This ratio is about 25 if the charge length is 200 times the reaction zone length and if the spike pressure is 1.5 times the Chapman-Jouguet pressure. In practical cases the ratio of charge length to reaction zone length is much greater than 200 so the change of slope would be even larger than indicated above. This calculation justifies the sharp change in slope of the free-surface-velocity/plate-thickness curve shown in Figure 3.

It should be remembered that it was assumed in this calculation that the reaction zone rarefaction could be approximated by a centered rarefaction wave. However, most reaction rate expressions show that equilibrium is approached asymptotically in time. If such expressions are appropriate for solid explosives, and there is no experimental evidence that they are, the ratio of slopes could conceivably approach unity. However, the long reaction tail predicted by these kinetic expressions corresponds to a very small percentage of the total detonation reaction, and a rapid rate of change of slope would be expected not at a plate thickness corresponding to the C-J state but at a thinner one, corresponding to essentially complete reaction.

## EXPERIMENTAL TECHNIQUE

Free surface velocity was measured by recording the time of arrival of the metal surface at a series of metal contactors or pins. The technique used is identical with that described by Minshall[8]. In these experiments two or in some cases four velocity measurements were made in each experiment by using either two or four groups of pins each consisting of six pins set in a $\frac{1}{4}$ in. diameter circle. The spacing between pins measured perpendicular to the free surface was 0.003 in. for the thin plates 0.030 in. thick and under, and 0.006 in. for all thicker plates. A cross section through a thin foil experiment is shown in Figure 5.

The electronic circuitry used is indicated in Figure 6. As each pin is shorted to the moving plate, a condenser is discharged through the network producing a signal on the

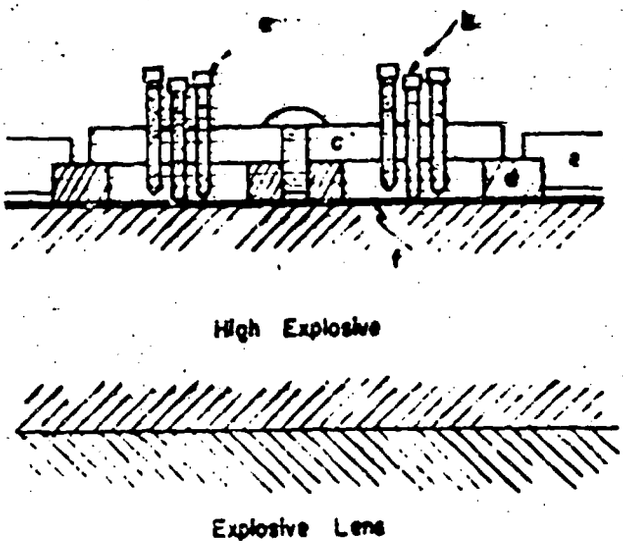


Fig. 5 - Cross-section of an experiment to determine the free surface velocity of a very thin plate or foil.

a. 0-80 pointed steel screws used as surface velocity pins.

b. Center ground contact pin also used to hold foil against the high explosive

c. Texalite pin mounting plate.

d. Aluminum backing plate $3\frac{1}{2}$ in. O.D., $\frac{1}{8}$ in. thick.

e. Blast shield 8 in. O.D., 3/8 in. thick.

f. Aluminum foil.

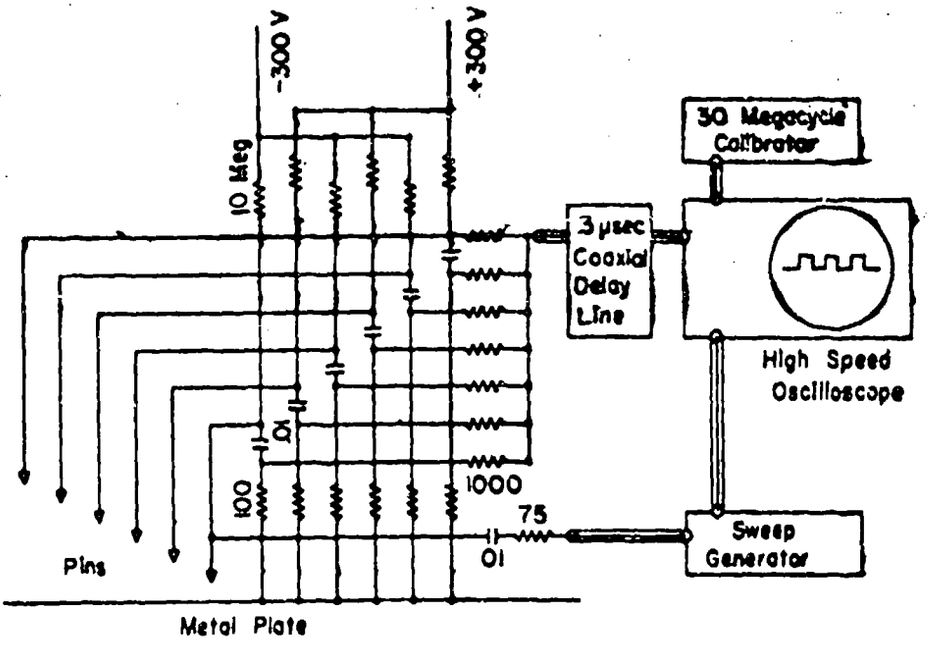


Fig. 6 - Electronic circuitry used to measure free surface velocity. The component values are the same for all circuits. Resistance values are ohms and capacitor values are ufd unless otherwise indicated.

oscilloscope. Successive pins have alternate polarities so that an ideal record would resemble the square wave indicated in the figure. A time base is provided by a trace from an accurately calibrated 30 megacycle crystal oscillator displaced slightly from the velocity record.

The high speed recording oscilloscopes used in these experiments were similar to the system described by the Radiation Laboratory[9]. A sweep speed of 10 in./μsec. was used and twenty thousand volts post acceleration was required in order to obtain single traces intense enough to photograph clearly at this high writing speed.

A photograph of a setup ready to be used is shown in Figure 7. The pulse-forming networks are sealed in the plastic blocks located near each pin group.

Precautions were necessary to eliminate two possible sources of error. The shock wave in air preceding the free surface was strong enough to discharge the pin circuits before the arrival of the surface. This difficulty was eliminated by maintaining a methane atmosphere around the pins. If velocity measurements were made on a machined and polished surface, the first several pins were often discharged prematurely by what appeared to be a fine spray of metal jetted out from the surface. This spray was eliminated by using unworked surfaces whenever possible and covering the surface with a very thin, almost invisible coating of light oil.

## EXPERIMENTAL RESULTS

### Experimental Data

Thirty-three separate experiments were performed in which eighty-seven measurements of free surface velocity were made. In the first twelve of the experiments the metal used was dural and in the remainder pure aluminum was used. Walsh[6] has shown that the particle velocity-shock velocity relationship is identical within experimental error for both metals. The explosive was Composition B which was cast into large blocks and then machined into pieces $5\frac{1}{2}$" x $5\frac{1}{2}$" x 3". The composition and density of the explosive varied by roughly 2 percent RDX and .01 gm/cc from charge to charge and within a given charge. These charges were prepared in 1950 and are not of as high a quality as those prepared currently.

All of the experimental results were corrected to the following standard conditions: metal density = 2.71 gm/cc; explosive density 1.67 gm/cc; explosive composition 63 per cent RDX; and detonation velocity 7.868 mm/μsec. The

following error expression was used in this correction:

$$\frac{\delta u_c}{u_c} = -0.861\,\delta\rho_i - 0.0023\,\delta\,\%_{RDX} + 0.192\,\delta\rho_t$$

In most cases the corrections made velocity changes of less than 1 percent. A random error of 1½ percent is caused by the composition and density fluctuations within a given charge. The average values of the velocities measured are presented in Table I.

TABLE I

Measured Free Surface Velocity as a Function of Plate Thickness

| Plate Thickness (in.) | Average Velocity (mm/μsec) | Standard Deviation of the mean (mm/μsec) | Number of Measurements |
|---|---|---|---|
| 0.0085 | 3.89 | 0.34 | 12 |
| 0.016 | 3.60 | 0.26 | 15 |
| 0.021 | 3.48 | 0.25 | 11 |
| 0.030 | 3.32 | 0.10 | 11 |
| 0.048 | 3.20 | 0.20 | 10 |
| 0.057 | 3.22 | 0.02 | 2 |
| 0.098 | 3.25 | 0.09 | 8 |
| 0.150 | 3.04 | 0.06 | 4 |
| 0.198 | 3.11 | 0.07 | 6 |
| 0.248 | 3.01 | 0.09 | 4 |
| 0.200 | 3.02 | 0.04 | 4 |

These data are also presented in Figure 8.

Two subjects deserve comment before conclusions are drawn from these data. First, the standard deviations reported in Table I are unfortunately large. However, this large standard deviation arises mainly from a systematic source. As discussed above, velocities are determined from measurements of position and time of the metal free surface by means of pins set in a circle. If the metal surface is not perfectly plane and if it does not move perfectly parallel to its initial position, a systematic error in the arrival time of the surface at each pin will be introduced which may be reflected into the surface velocity as determined by least squares techniques. It can be shown that the velocity calculated is related to the

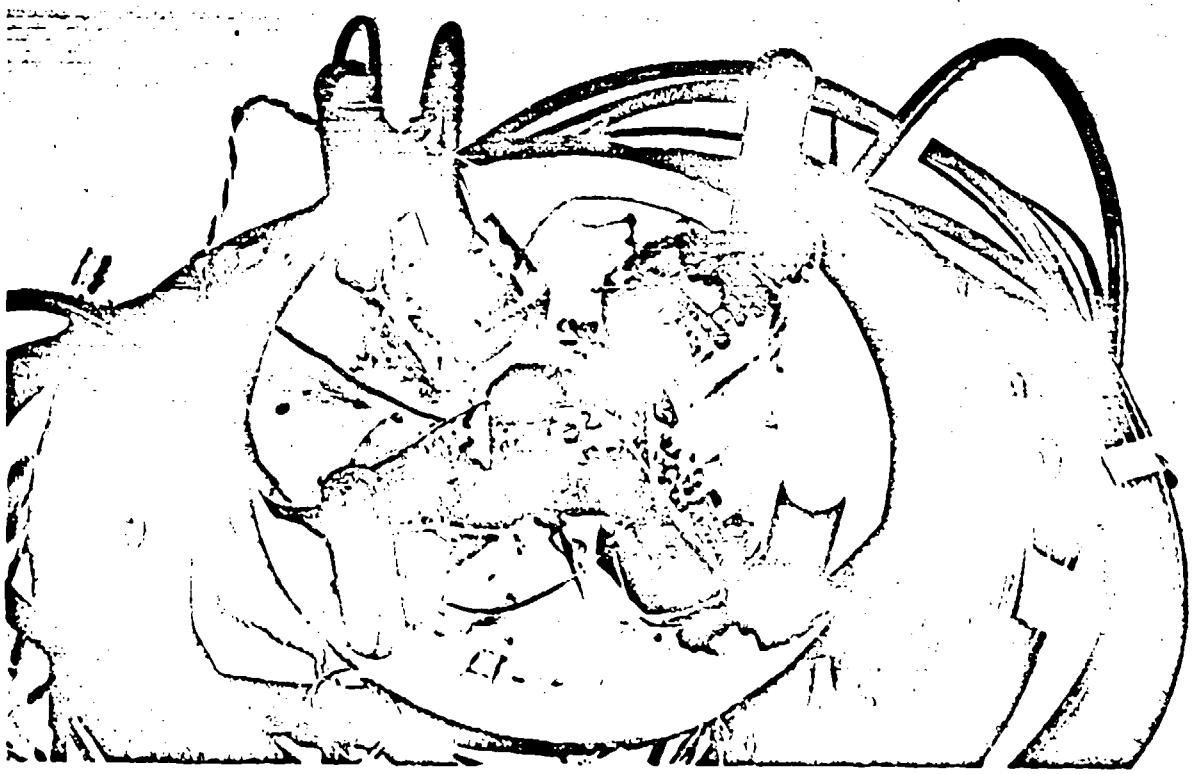

Fig. 7 - A photograph of an experiment ready to be fired.

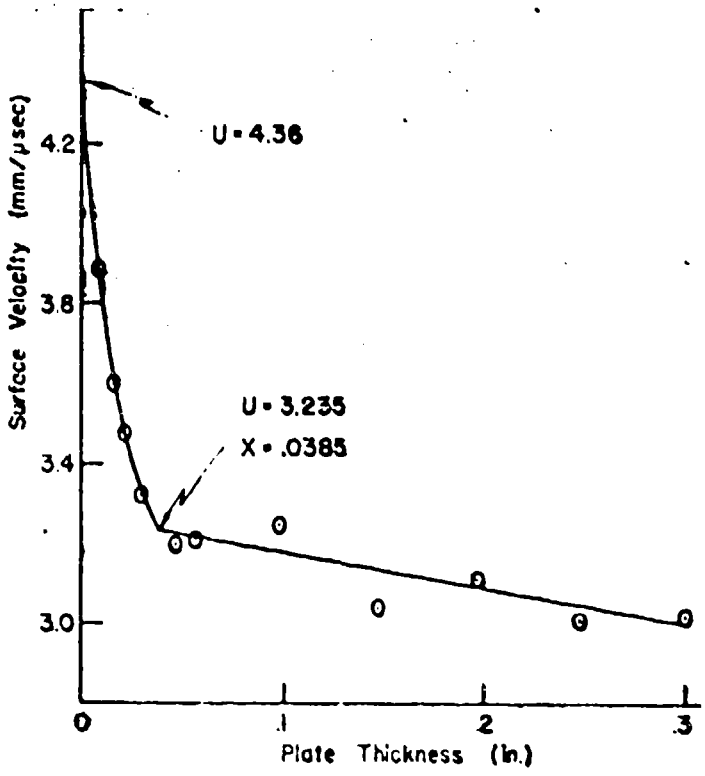


Fig. 8 - Measured free surface velocity as a function of plate thickness.

true velocity as follows:

$$V = V_{calc} \left(1 + \frac{R}{d} \epsilon \sin\theta\right)$$

where R is the radius of the pin circle, d is the incremental pin spacing, $\alpha'$ is the angle of tilt of the surface, $\epsilon$ is a constant = 0.11 for the pin geometry used in these experiments, and $\theta$ is an angle which describes the orientation of the pin circle with respect to the tilted wave. A wave tilt of as much as 0.03 radian was observed for some of the charges used. Therefore, this cause alone could produce a velocity error of 15 percent in plates 0.030 in. thick or thinner and 7½ percent for thicker plates. For this reason many measurements were made, especially on the thinner plates, so as to obtain a reliable value for the average velocity.

Second, it is desirable to place all of the pins close enough to the free surface so that the velocity measurement can be completed before a second disturbance arrives at the surface. This was done for all but the thinnest foil. One might expect a weak shock wave to be the second disturbance to arrive at the surface giving it a small increase in velocity at about the middle of the velocity measurement. Examination of the records does not indicate a noticeable increase in velocity. However, the velocity associated with the 0.0085 in. foil may be slightly high.

## Explosive Pressure

Two pressures in the explosive can be estimated from the surface velocity plot of Figure 8. A least squares straight line has been fitted to the experimental measurements at thicknesses greater than 0.030 in. Each of the average velocities was given a weight equal to the number of measurements included. A smooth curve was drawn through the remaining four measurements on thin plates. The Chapman-Jouguet pressure can be determined from the free surface velocity indicated by the intersection of these two lines, 3.235 mm/usec.

The equation of state data of Walsh[6] for aluminum has been analyzed by Fickett (unpublished communication). An analytic form of the equation of state was derived which agreed with Walsh's data at low pressures and with Fermi-Thomas-Dirac calculations at high pressures. The following fit of shock velocity as a function of free surface velocity is appropriate for the pressure range of interest in these experiments.

$$D = 4.8375 + 1.1235\, u - 0.1095\, u^2 + 0.0066\, u^3$$

Therefore, in the metal

$$p_m = {}_t u_t D_t$$

$$= 2.71 \times \frac{3.235}{2} \times 7.55 = 0.3309 \text{ megabar.}$$

In the explosive

$$p_{C\text{-}J} = \frac{p_m ( {}_i D_i + {}_t D_t)}{{}_t D_t} = 0.272 \text{ megabar.}$$

Thus the Chapman-Jouguet pressure in Composition B explosive containing 63 percent RDX at a density of 1.67 gm/cc is 0.272 megabar. This number is thought to be correct to within 2 percent.

The extrapolation of the free surface velocity to zero plate thickness in what is thought to be a reasonable manner gives a limiting velocity of 4.36 mm/μsec. From this number and the extrapolation of the equation of state data for aluminum made by Fickett, a peak pressure in the explosive of 0.385 megabar is estimated for the von Neumann spike. It is interesting to note that the spike pressure appears to be only 1.42 the Chapman-Jouguet pressure. It should be emphasized that the extrapolation to zero thickness is only what appears to be a reasonable one. There is no theoretical justification for the assumed form of the curve because the form depends on the details of the chemical kinetics of the detonation reaction about which essentially nothing is known.

## Reaction Zone Length

The reaction zone length was calculated from Eq. 4 using a value of $D_2$ determined from the experimental results as required by Eq. 5. $\alpha$ was determined from the two values of interface velocity which could be estimated from the experimental data, namely, the initial and final values. The assumption was made that the interface velocity changed with distance in the same way the shock velocity did. A value of $u_t + c_t$ was obtained from the equation of state calculation for aluminum made by Fickett. The actual numbers used are as follows: $D_i = 7.868$, $D_t = 7.771$, $u_t + c_t = 9.065$ mm/μsec. and $\alpha = 0.232$; giving $\frac{a}{b} = 0.139$. b was estimated to be 0.0385 in. Therefore, a = 0.005 in. or 0.13 mm. This estimate of reaction zone length of slightly greater than one tenth of a millimeter is probably accurate to within 20 percent except for the possible errors discussed below.

Two assumptions have been made in the estimation of reaction zone length. First, the shock wave reflected from the metal back into the explosive has been ignored. This assumption is questionable because the changes in temperature and pressure caused by the wave may decisively influence the kinetics in the as yet unreacted explosive into which it moves. Therefore, the value of reaction zone length determined is probably best described as a lower limit value.

The effect of this reflected shock wave on the detonation kinetics and reaction zone length could be investigated by varying the metal used in experiments of this type. In particular, the effect could be maximized by using a heavy material like brass which has a large acoustic impedance and minimized by using magnesium which is almost a perfect impedance match for Composition B.

The second assumption concerns the shape of the reaction zone. The experimental results have been represented by a profile similar to that of a rarefaction wave in an inert material. However, as discussed above, there could be a slow reaction tail which would cause the true reaction zone length to be somewhat longer than that indicated.

## CONCLUSIONS

A conclusion can be drawn from the data presented above which is fundamental to the understanding of the detonation phenomenon. Namely, the experimental results provide powerful confirmation for the hydrodynamic theory of the detonation process proposed by Zeldovich, von Neumann and Döring. In fact, this is thought to be the first experimental evidence published which directly verifies this theory which has, however, attained almost universal acceptance because of its hydrodynamic completeness.

The Chapman-Jouguet pressure in Composition B explosive containing 63 percent RDX at a density of 1.67 gm/cc was measured to be 0.272 megabar. The reaction zone length for the same explosive is 0.13 mm.

## ACKNOWLEDGEMENTS

The authors are indebted to many people for assistance in various phases of this work. In particular, we are happy to acknowledge the help of the following individuals: R. Holbrook, E. Gittings, R. E. Faudree and V. Thurlow for assistance in the actual performance of the

experiments; C. L. Miller for the preparation of the many explosive charges used; C. W. Mautz for the derivation of Equation 4; and W. W. Wood for many valuable discussions of the theoretical problems involved and also for making the detailed calculation of the attenuation of a shock wave in metal by a centered simple rarefaction wave.

## REFERENCES

1. R. W. Goranson, Classified Los Alamos Report LA-487.

2. Y. B. Zeldovich, J. Exptl. Theoret. Phys. (USSR) 10, 542 (1940).

3. J. von Neumann, O.S.R.D. Report No. 549, (1942).

4. W. Döring, Ann. Physik, 43, 421 (1943).

5. G. I. Taylor, Proc. Roy Soc. A200, 235 (1950).

6. J. M. Walsh, Phys. Rev. (in press).

7. R. Courant and K. O. Friedrichs, Supersonic Flow and Shock Waves, (Interscience Publishers, Inc., New York, 1948), p. 164.

8. R. S. Minshall, J. Appl. Phys. (in preparation).

9. M.I.T. Radiation Laboratory Report No. 1001, (1946).

# THE DETONATION ZONE IN CONDENSED EXPLOSIVES 17

H. Dean Mallory
S. J. Jacobs
U. S. Naval Ordnance Laboratory
White Oak, Maryland

## Introduction

The hydrodynamic concept of a steady state detonation with finite reaction time was independently proposed by Zeldovich[1], von Neumann[2] and Doring[3]. The theory describes a detonation wave as a non-reactive shock followed by a period of chemical reaction which ends in the well known and generally accepted Chapman-Jouguet condition. This theory shows the pressure level in the non-reactive shock to be higher than at the C-J point and has given rise to the concept of a pressure spike in the detonation head. From the hydrodynamic theory alone one can say only that the pressure decreases as reaction proceeds.

For detonation in gases, some few authors have insisted that reaction does not begin at the initial shock front but rather that it is preceded by a steady induction zone where little or no reaction occurs. Lewis and Von Elbe[4] state "If the reaction rate is exponentially accelerating, (the fraction of explosive reacted) changes initially very little and the pressure profile is very flat for some distance behind the shock front. In then drops sharply as the reaction goes to completion at a high rate." Finklestein and Gamow[5] and Kistiakowsky[6] present similar views. It is the purpose of this paper to present evidence that the steady state detonation of TNT at various bulk densities confirms the hydrodynamic picture given by Zeldovich, von Neumann and Doring, and that the views quoted above are applicable to condensed explosives also. Within the limitation of experiments to be described, the data show the detonation head to consist essentially of two separable zones, one of induction and one of chemical reaction.

Unclassified

The method employed in this paper is based on the hydrodynamic conditions which apply when a shock crosses a boundary between two media, and after propagating through the second media, causes the nearby free surface of the second to move in an ensuing rarefaction. The translational motions of shock propagation and free surface velocity of the second media are measured by a method now referred to as the pin technique. The observations made on the second medium can be made to yield pressure-density data for the explosive. An unexpected result, for low density charges, was that the explosive was not compressed to near crystal density by the shock front prior to reaction. Rather, the boundary conditions at the target interface required modest compression to a value far below crystal density.

## Experimental Details

In the fundamental experiments employed by us, the shock in the first medium is a detonation wave in TNT. Several bulk densities of explosive are used. The second medium is essentially pure (2S) aluminum. It can be shown that the free surface velocity set up in the aluminum is a function of the pressure level appearing at that free surface prior to rarefaction. A range of target thickness is a convenient method for sampling the pressure at given distances from the metal-explosive interface. Since reaction in the boundary layer of explosive is accompained by a pressure fall, a range of rarefaction waves spread from the boundary and overtake the pure shock front later in time. Knowledge of the wave velocities in the metal then permits a reconstruction of the pressure profile of the wave which struck the target. Data from this type of experiment can be interpreted as showing a well defined induction zone preceding the reaction in TNT.

In other experiments, an explosive was used to hurl a massive aluminum "driver" plate across an air gap where it impacted a target plate having one of several thicknesses. Since the first plate unloaded during its passage across the air gap, the shock wave induced in the target was free from reaction zone effects and the data obtained indicate only a smooth decrease in pressure at increasing distances from the impact boundary. The absence of the usual velocity plateau in this case, helps establish the reality of the plateau when TNT alone drives the target.

Yet a third series of experiments were performed in an attempt to produce a pressure spike as distinct

from the steady induction zone pressure observed in the first set. These experiments were identical with the aluminum-aluminum impact experiments except that a thin wafer of pressed TNT was centered on the target plate and initiated by impact of the driver plate after it crossed the air gap. The resulting free surface velocity data again show an initial steady induction zone followed by a sudden decrease in pressure, and demonstrate the effect of chemical reaction on the mass velocity transmitted to the target.

A schematic drawing of the aluminum-aluminum impact experiment with the included TNT wafer is shown in Figure 1. The TNT wafers were not used in the series of pure impact experiments. One set of experiments using TNT pressed to a bulk density of 1 g/cc was performed. In this set the "shock driver" was also removed, allowing the 3 inch diameter charge to rest on the target plate. These charges were 5 inches high.

A fourth series used cast TNT charges 6 inches square and 4 inches high. These also rested directly on the target plates. The fifth and last type described were made up of crystalline TNT at a bulk density of 0.624 g/cc (mean density of all those fired). These were our so-called "snow flake packed" charges which were made by first pinning a 6 inch I.D. aluminum tube to the target plate and sifting in the TNT at the firing site. The charge height was 5 3/4 inches. Over this charge was laid a 1 inch thick slab of cast TNT which rested on the rim of the tube and supported the plane wave booster. Most of the crystals passed a 50 but not a 70 mesh sieve.

The arrangement of the pin contactors for velocity measurements is shown in Figure 1. For the impact experiments, 16 contactors were used for each shot. Eight of these were insulated and set into holes drilled to various depths in the target to be shorted out on passage of the shock wave, while the remaining eight were spaced outside the target in such a manner that the moving free surface would contact each in turn. The pins were arranged in two concentric circles, one of 5/8 inches and the other 1 inch in diameter. A plane wave booster was used to initiate the main charge since the circular pin geometry required a plane impact in order to give meaningful data. Wave planeness is a difficult thing to control and for this reason a number of identical shots were made at each target thickness in order to obtain a statistically significant velocity.

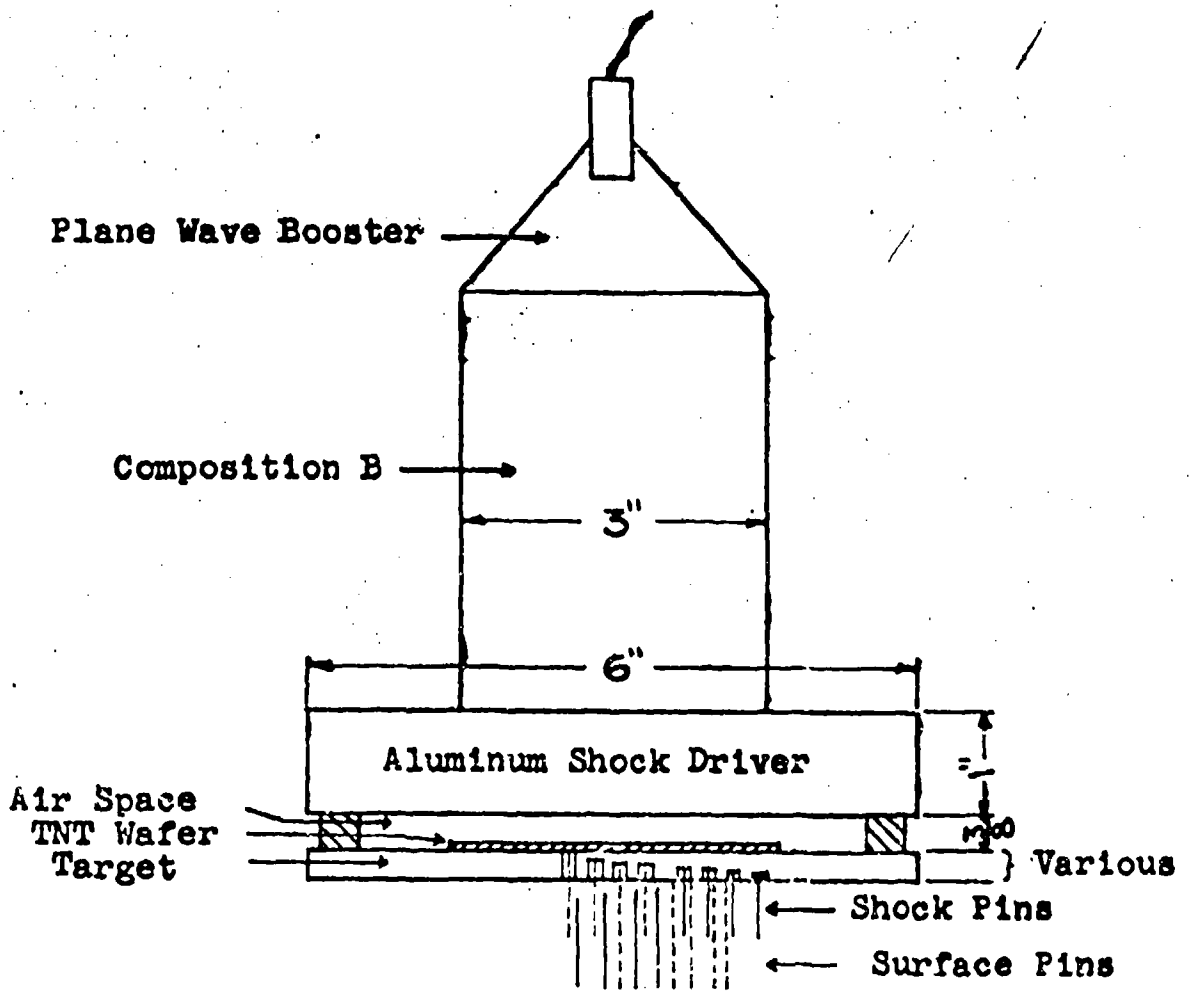


Figure 1. Experimental Arrangement for the Impact Experiments with Included TNT Wafer

Unclassified

Electrical pulses made by contact of the grounded moving target with the charged pins were led through 500 feet of coaxial cable to an oscilloscope where the scope beam deflections were photographed by a still camera. Synchronization with the oscilloscope was achieved by also sending the pulse from the first pin in a set through a second, shorter, piece of cable in a manner such that it started the scope beam in time to record itself and the others as they came through the long cable. The oscilloscope had a 5-10 mc frequency response and about a 2 microsecond time base, single sweep. The target plates were coated with a film of vasoline, insignificantly thick, to electrically separate the moving target from the charged pin contactors. External contactors were insulated along their shafts by glyptal resin and spaghetti tubing with their tips bare except for a film of vasoline similar to that on the target plate.

Accurate shock velocity measurements, for any except the impact experiments, were found to be virtually impossible due to violent pressure changes occurring in the detonation head. Free surface velocity measurements were relatively easy for all systems investigated and therefore these were measured while the corresponding shock velocities were computed from the equation of state for aluminum.

## The Measurement of Detonation Pressures

The well known hydrodynamic equation for the conservation of impulse in a shock wave is

$$1) \qquad p = \rho_o D u$$

in a coordinate system where $u_o = o$, and $p_o$ is neglected. The equation is general and applies to a detonating explosive or to an aluminum target being traversed by a shock. It has been shown[7] that u in aluminum is closely approximated by taking 1/2 the first order free surface velocity, $u_s$, of the targets and that shock velocity, D, and pressure, p, can both be calculated if $u_s$ is known.

From the conditions of equality of pressure and continuity of mass flow across a boundary between a detonating explosive and a metal target, an expression relating the incident particle velocity to that transmitted can be derived. The expression is

2) $$\frac{u_m}{u_e} = \frac{(\rho_o D)_e + (\rho D)_r}{(\rho_o D)_m + (\rho D)_r}$$

where subscripts e and m refer to explosive and metal respectively and r refers to the reflected wave sent back into the explosive by the metal interface. Thus if $(\rho D)_r$ can be approximated, the particle velocity, and therefore the pressure, in the explosive can be determined from the measured free surface velocities of metal targets. Ablard[8] has shown that

3) $$(\rho_o D)_e = (\rho D)_r$$

for cast Composition B and aluminum targets. His results are not restricted to a given explosive but are determined by the value of the product $(\rho_o D)_e$ which is only slightly higher than that for cast TNT reported on here. We have therefore assumed the relation 3) for our cast explosive and computed the peak pressure on this basis. However, this assumption is shown to be in gross error for the case of one of our lowest density explosives where the impedance of the explosive, $(\rho_o D)_e$, is much smaller than that of the aluminum targets, $(\rho_o D)_m$.

Impedance Mismatched Systems

The conservation of mass and momentum in a reflected wave can be used to establish limits for the reflected shock velocity. The following analysis, which applies to our low density charges describes the method.

Consider a piston driving a shock wave into a unit mass of explosive at pressure and volume $p_o$, $v_o$ before compression and $p_1$, $v_1$ after compression. Further, let the piston be the reaction products produced in a steady detonation wave. Since after establishment of the wave the pressure on the piston is $p_1$, the work done by the piston on the unit mass is $p_1(v_o - v_1)$. The work done goes to increase the internal energy by an amount of $\Delta E_1$ and also to give the unit mass a kinetic energy $\frac{1}{2} u_1^2$. Therefore

4) $$\Delta E_1 = p_1(v_o - v_1) - \frac{1}{2} u_1^2$$

The Hugoniot equation is

$$\Delta E_1 = 1/2\ (p_1+p_o)(v_o-v_1)$$

and if $p_o \doteq 0$, substitution into 4) gives

$$5) \qquad \Delta E_1 = 1/2\ p_1(v_o-v_1)$$
$$= 1/2\ u_1^2$$

If the shock wave with particle velocity $u_1$ strikes the boundary of a high impedance medium, a shock wave is reflected which propagates through the unit mass which has the pressure and volume $p_1$, $v_1$, after the first shock and $p_2$, $v_2$ after the second. As in equation 4) we may write

$$6) \qquad \Delta E_2 = p_2(v_1-v_2) - 1/2\ u_2^2$$
$$= 1/2\ (p_2+p_1)(v_1-v_2)$$

where $\Delta E_2$ is the change in internal energy due to the reflected wave and $u_2$ is the particle velocity in the wave referred to a coordinate system moving at velocity $u_1$.

The total internal energy change for material behind the reflected shock front is then

$$\Delta E_t = \Delta E_1 + \Delta E_2$$

which by substitution from 5) and 6) becomes

$$7) \quad \Delta E_t = 1/2\ [p_1(v_o-v_2) + p_2(v_1-v_2)].$$

But also

$$\Delta E_t = p_1(v_o-v_1) - \frac{u_1^2}{2} + p_2(v_1-v_2) - \frac{u_2^2}{2}$$

which becomes, on equating to 7) and substituting for $u_1^2$,

$$8) \qquad (p_2-p_1)(v_1-v_2) = u_2^2$$

The equation of state for aluminum(7) enables us to evaluate $p_2$ directly from the measured free surface velocity of aluminum targets since pressure is continuous across the metal-explosive interface. The equation just derived enable us to compute $v_2$ and $u_2$ $(= u_1-u_m)$.

For our lowest density explosive, crystalline TNT at a bulk density of 0.624 g/cc, the highest free surface velocity imparted to the aluminum targets was 1.08 mm/microsecond. This result, along with the corresponding shock velocity from the previously mentioned equation of state, determines the peak pressure in aluminum and therefore the reflected peak pressure in the explosive ($p_2$ in equation 8). We can choose arbitrary values for $u_1 (= u_e)$ and compute the corresponding values of $p_1$ from equation 1) since D is known for the explosive. The conservation of mass equation

$$9) \qquad \rho_0 D_e = \rho_1 (D-u)_e$$

then determines $v_1 = \frac{1}{\rho_1}$) for any $u_1$; since we have an experimentally determined value for $p_2$, equation 8) can be used to compute $v_2$. In this way we can examine the density behind the shock wave reflected from the metal interface. With values for $\rho_1, \rho_2$ and $u_2$ at hand, equation 9) can be applied to the reflected wave. The shock velocity so determined is then $D_r$, which when multiplied by $\rho_1$, is the impedance of the reflected wave, $(\rho D)_r$, as used in equation 2). Results of these calculations are set out in Table I.

Table I. Consistent Values of the Hydrodynamic Variables for TNT at a Loading Density of 0.624 g/cc Based on $u_m = 0.54$

| $u_e$ (mm/$\mu$sec) | $\rho_1$ (g/cc) | $\rho_2$ (g/cc) | $D_r$ (mm/$\mu$sec) | $p_1$ (dynes/cm$^2$ x $10^{10}$) | $\rho_1 D_r$ |
|---|---|---|---|---|---|
| 2.1 | 1.396 | 18.87 | 1.685 | 4.975 | 2.352 |
| 2.0 | 1.318 | 4.673 | 2.034 | 4.738 | 2.681 |
| 1.9 | 1.249 | 2.817 | 2.443 | 4.501 | 3.051 |
| 1.8 | 1.186 | 2.088 | 2.917 | 4.264 | 3.460 |
| 1.7 | 1.130 | 1.684 | 3.525 | 4.027 | 3.983 |
| 1.6 | 1.078 | 1.439 | 4.224 | 3.790 | 4.553 |
| 1.5 | 1.031 | 1.266 | 5.170 | 3.554 | 5.330 |
| 1.4 | 0.988 | 1.144 | 6.308 | 3.317 | 6.232 |
| 1.3 | 0.949 | 1.053 | 7.692 | 3.080 | 7.300 |
| 1.2 | 0.912 | 0.978 | 9.773 | 2.843 | 8.913 |

For our low density TNT, the acoustic approximation as given in equation 3), estimates $u_e (= u_1)$ to be 2.1 mm/microsecond. As can be seen from Table I, the corresponding value for $\rho_2$, the density behind the reflected wave, is impossibly high. Our best estimate for $u_e$ is 1.46 mm/microsecond as obtained in a

separate report[9]. As can be seen from the table, this choice of particle velocity implies that densities in both the reflected and incident waves are below crystal density. It can be seen that even if the reflected density were made to exceed crystal density by another choice of $u_e$, the incident density would still be less than crystal. Since these low density results are also interesting from the standpoint of the kinetics involved, the method used for estimating $u_e$ will be outlined after the experiment has been described.

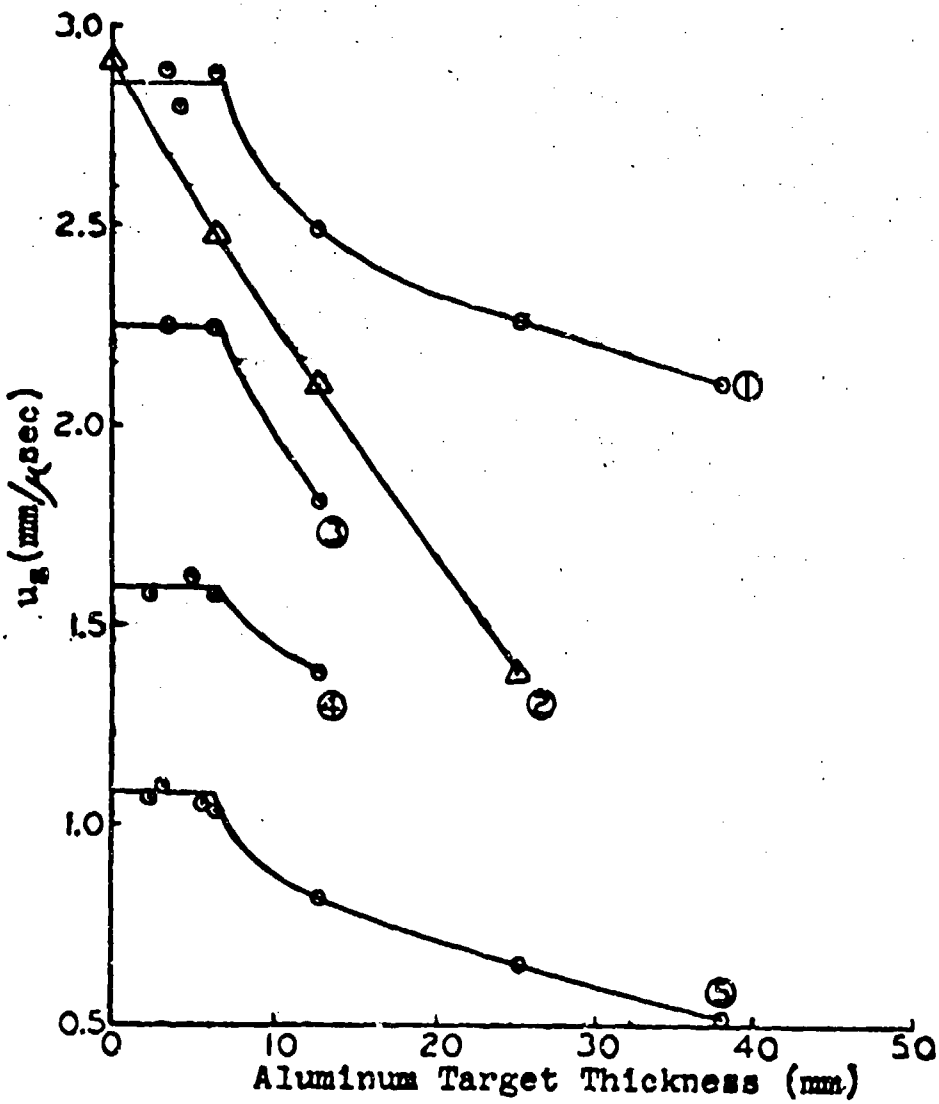


Figure 2. First Order Free Surface Velocities of 2S Aluminum Targets Driven by (1) cast TNT, $\rho_o$ = 1.58 g/cc, (2) aluminum plate impact, (3) pressed TNT wafers, 1/8 inch thick, $\rho_o$ = 1.55, (4) pressed TNT at $\rho_o$ = 1 g/cc (5) TNT at $\rho_o$ = 0.624 g/cc

## Experimental Results

The experimental results obtained for different density explosives in contact with the targets show striking similarities although the interpretations placed on the data must be very different. Figure 2 is a graph of the free surface velocities obtained in the various experiments, as a function of target thickness. These data are set out in tabular form in Table II.

Table II. Numerical Data for the Curves in Figure 2

| Curve No. | Target Thickness (in.) | $u_s$ ± P.E. (m/sec) | Number of Targets Fired |
|---|---|---|---|
| 1 | 1/8 | 2892 ± 70 | 6 |
| | 5/32 | 2795 ± 40 | 6 |
| | 1/4 | 2877 ± 72 | 3 |
| | 1/2 | 2497 ± 83 | 6 |
| | 1 | 2267 ± 37 | 3 |
| | 1 1/2 | 2114 ± 20 | 6 |
| 2 | 0 | 2908 ± 59 | 6 |
| | 1/4 | 2475 ± 8 | 8 |
| | 1/2 | 2103 ± 56 | 6 |
| | 1 | 1379 ± 40 | 6 |
| 3 | 1/8 | 2254 ± 56 | 4 |
| | 1/4 | 2234 ± 66 | 4 |
| | 1 | 1818 ± 30 | 4 |
| 4 | 3/32 | 1569 ± 64 | 4 |
| | 3/16 | 1619 ± 28 | 4 |
| | 1/4 | 1573 ± 20 | 4 |
| | 1/2 | 1385 ± 24 | 4 |
| 5 | 3/32 | 1072 ± 42 | 2 |
| | 1/8 | 1080 (est. from reverberation data) | |
| | 7/32 | 1058 ± 18 | 4 |
| | 1/4 | 1034 ± 22 | 6 |
| | 1/2 | 816 ± 6 | 7 |
| | 1 | 647 ± 3 | |
| | 1 1/2 | 513 ± 8 | 3 |

In order that the data be useable in the computation of explosion pressures, it is necessary that they be the free surface velocities present at the start of translational motion. When the unloading wave from the free boundary reaches the metal-explosive interface, a high pressure is still present in the explosion gases. This residual pressure can and does drive a second shock wave into the target. This second wave further increases the free surface velocity. Free surface measurements which include the second or later velocity orders will over estimate $u_s$ and therefore over estimate the pressure developed in the explosive.

Wave Reflections in the Target

Figure 3 shows the step wise accelerations which occur in targets of various thicknessess, explosion loaded by Composition B. These data are not to be discussed further in this paper and are included only to illustrate the process of momentum transfer from explosive to target which occurs later in time. They illustrate that the initial or "first order" free surface velocity is far from the terminal velocity which can be obtained. It is emphasized that the data presented in Figure 2 and Table II, are all first order velocities. Unpublished results show that experimental velocity jumps, shown in Figure 3, occur at about the times one would compute by use of the equation of state for aluminum.*

The velocity plateaus in the TNT data are intriguing since according to equation 1) they imply a steady initial pressure in the detonation head followed by a more or less sudden decrease in pressure level. We have interpreted this initial steady pressure to be an induction zone of finite width which precedes the zone of chemical reaction.

- - - - - - - - - - - - - -

*If the first order free surface velocities for Composition B driven aluminum targets are plotted as a function of target thickness, no plateau is observed as it is for TNT, but rather the curve continues to rise toward the zero target thickness axis. In view of the data obtained with TNT, we conclude that a flat top may be present in the Composition B data but that it occurs in such thin targets that we are unable to observe it with the pin technique.

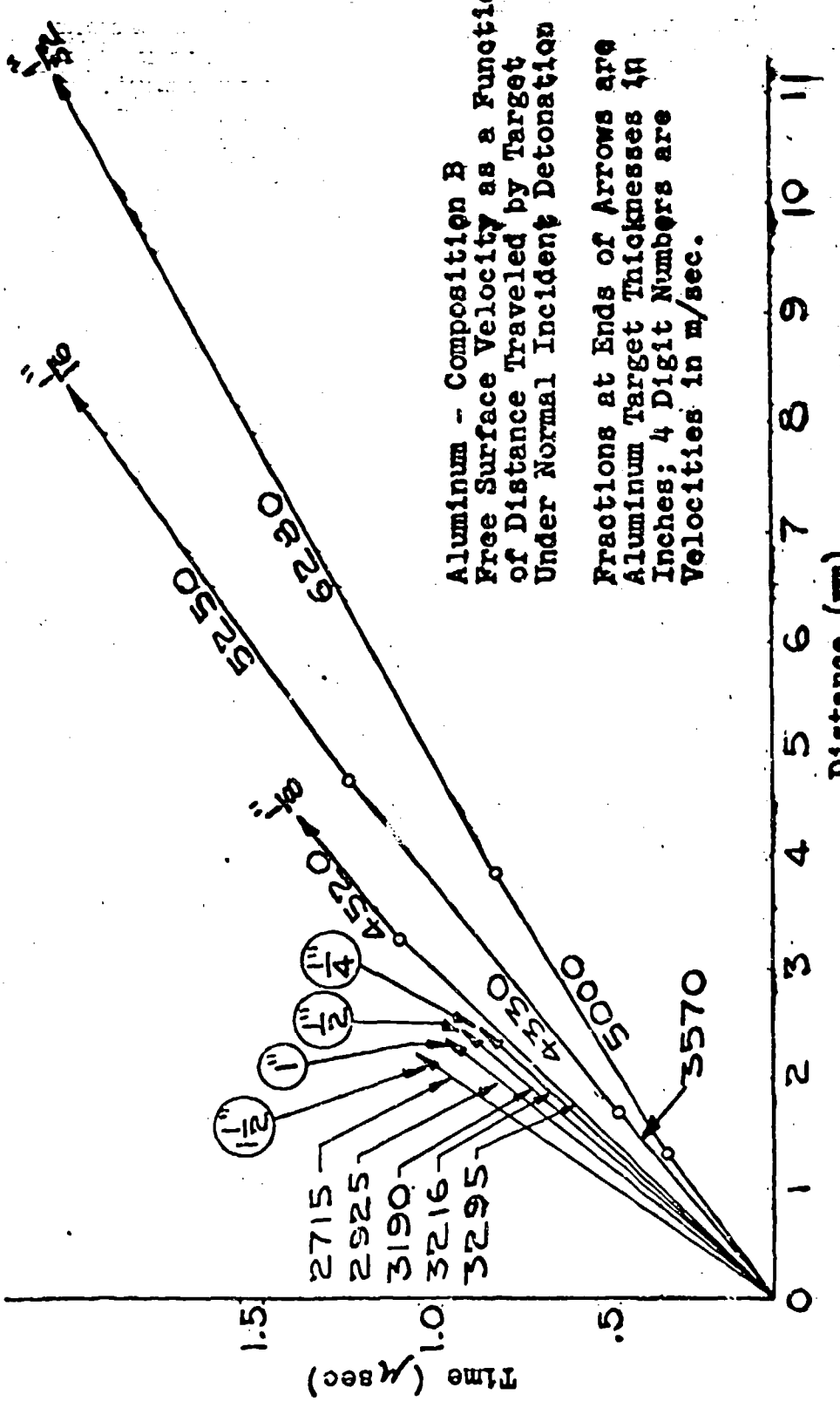
Aluminum - Composition B
Free Surface Velocity as a Function
of Distance Traveled by Target
Under Normal Incident Detonation
Fractions at Ends of Arrows are
Aluminum Target Thicknesses in
Inches; 4 Digit Numbers are
Velocities in m/sec.
Distance (mm)
Time (μsec)
0
1
2
3
4
5
6
7
8
9
10
11
.5
1.0
1.5
2715
2925
3190
3216
3295
3570
5005
4320
4520
5250
5290
1"
1/2"
1/4"
1-1/2"
1-1/4"

Figure 3.

## The Induction Zone in Cast TNT

Material in a detonation wave propagating through a homogeneous explosive has a high velocity in the direction of wave propagation. If the length of the induction zone is "a", the induction time can be obtained from

10) $$\Delta t = \frac{a}{D_e - u_e}$$

where $D_e$ is the steady state detonation rate (6880 meters/second) and $u_e$ is the particle velocity in the induction zone. By use of the acoustic approximation, equation 3) we can immediately obtain $u_e$ from equation 2) and the measured plateau velocity for cast TNT. The induction zone length, a, is approximately 0.216 (6.880-1.97) or 1.06 mm. This simple analysis does not apply to low density TNT.

## The Induction Zone in TNT at a Bulk Density of 0.624 g/cc

From equations 5) and 7) previously developed, one can compute changes of internal energy which occur behind the incident and reflected shock fronts at the target interface. By assuming the heat capacity at constant volume for the unreacted TNT to be approximately constant and equal to 1/3 cal/g., we can estimate the temperature behind the initial shock front from the expression

11) $$T_1 - 300 = \Delta E_1 / c_v \ .$$

Similarly, for the total change of internal energy due to the incident and reflected shock, we have

12) $$T_t - 300 = \Delta E_t / c_v \ .$$

The estimated temperatures which obtain in the explosive before reaction occurs are set down in Table III for arbitrary values of $u_e$. These computations show that, given an induction zone in the detonation wave, the temperature increase behind the reflected shock front may be adequate to initiate a secondary reaction at the metal interface. Despite such a possibility, curve 5 in Figure 2 shows an initial steady pressure extending to nearly the same target thickness as that for cast TNT. Accordingly we can compute the steady pressure time from

13) $$\Delta t_1 + \frac{\Delta \ell'_1 - u_1 \cdot \Delta t_1}{R_1} = \frac{\Delta \ell_1}{D_1}$$

Table III. Approximate Shock Temperatures in TNT vs. Initial Particle Velocity; $\rho_o$ = 0.624 g/cc

| $u_e$ (mm/$\mu$sec) | $\Delta E_1$ (ergs/gx10-10) | $\Delta E_t$ (ergs/gx10-10) | $T_1$ (°K) | $T_t$ (°K) |
|---|---|---|---|---|
| 2.1 | 2.205 | 6.718 | 1881 | 5118 |
| 2.0 | 2.000 | 5.646 | 1734 | 4349 |
| 1.9 | 1.805 | 4.736 | 1595 | 3697 |
| 1.8 | 1.620 | 3.960 | 1462 | 3140 |
| 1.7 | 1.445 | 3.292 | 1336 | 2661 |
| 1.6 | 1.280 | 2.721 | 1218 | 2252 |
| 1.5 | 1.125 | 2.228 | 1107 | 1898 |
| 1.4 | 0.980 | 1.757 | 1003 | 1560 |
| 1.3 | 0.845 | 1.456 | 906 | 1344 |
| 1.2 | 0.720 | 1.151 | 816 | 1125 |

and compare the results at the two density extremes. Equation 13) is obtained by equating two independent statements for the overtaking time in the metal target. The quantities used are obtained from Figure 4 where $R_1$ is the velocity of the first rarefaction increment and equals $u_1 + c_1$.

A comparison between the two TNT density extremes is given in Table IV.

Table IV. Properties of Shocked Aluminum and the Corresponding Steady Pressure Times for the Plateau Region of Figure 2

| Cast TNT | TNT at $\rho_o$ = 0.624 g/cc |
|---|---|
| $u_m$ = 1.43 mm/microsecond | $u_m$ = 0.54 mm/microsecond |
| $c_m$ = 7.45 " " | $c_m$ = 6.11 " " |
| $D_m$ = 7.12 " " | $D_m$ = 5.94 " " |
| $\Delta l_1$ = 6.5 mm | $\Delta l_1$ = 6 mm |
| $\Delta t_1$ = 0.216 microseconds | $\Delta t_1$ = 0.117 microseconds |

It can be seen that the steady pressure time for cast TNT is nearly double that for the low density explosive despite a higher temperature in the induction zone of the detonation wave in the cast material. This result makes an hypothesis of a secondary detonation reaction in the low density explosive quite plausible, for indeed if the induction zone were being burned by two distinct flame fronts, then material in the induction zone would be consumed at an extraordinary rate. On this basis, we postulate the sequence of events pictured

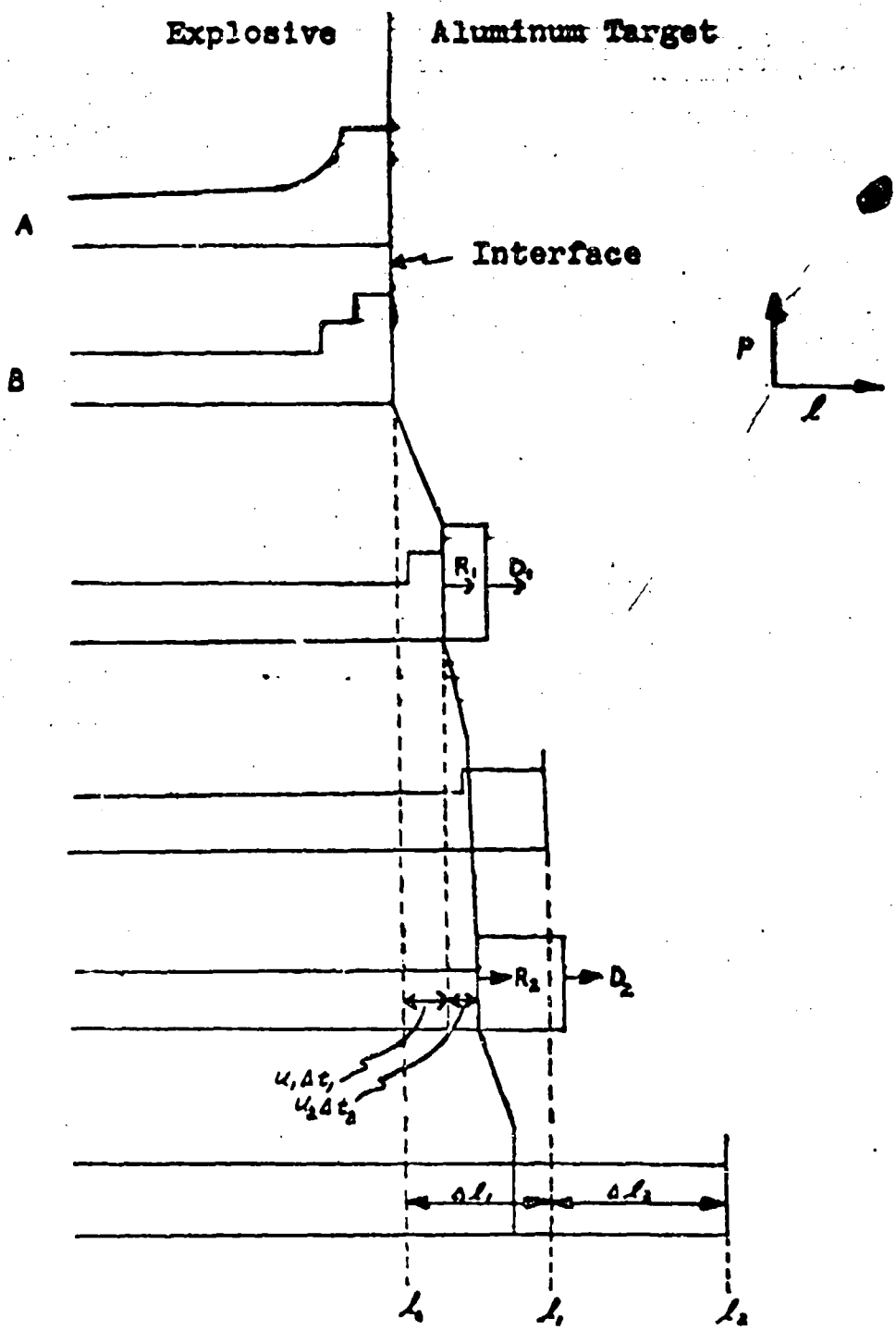


Figure 4. Instantaneous Pressure Profiles During The Impact of a Detonation Wave With a Stationary Aluminum Target. A (Probable True Wave Shape), B (Schematic Step Wave Used in Driving Equations 13 and 18). Reflected Waves Are Assumed to be Negligible

in Figure 5 as occurring at the metal explosive interface for low density TNT. From this figure it can be seen that the steady velocity plateau observed can be associated with a pseudo detonation pressure behind the secondary wave. The high pressure induction peak in the secondary wave would not be observed because its effects would be seen only in extremely thin targets. By assuming the thickness of the secondary induction zone to be negligible in comparison with the primary one, and also that a new C-J condition holds behind the secondary wave, it is possible to compute the length and time of an induction zone undisturbed by a reflected wave. The analysis is as follows:

Define

$D_d$ = velocity of the secondary detonation wave
$c_g$ = velocity of sound in the gaseous region burned by $D_d$
$t_c$ = time required for the two flame fronts to collide if time zero is the moment of contact of the primary induction zone with the metal surface
$t_r$ = time required for the rarefaction wave, following the primary induction zone, to cross the region burned by $D_d$ and reach the target metal
$u_e$ = particle velocity in the induction zone of the primary detonation wave
$u_d = u_e - u_m$ = particle velocity behind the secondary detonation wave. $D_m$, $D_e$ and $\Delta t$ have their usual meaning.

Let the primary induction zone be of length

$$x = a + b$$

where a is the distance traveled by the primary flame front at the velocity $(D_e - u_e)$ and b is the distance traveled by the secondary flame front at velocity $D_d$ during the time required for the flame fronts to collide. The steady pressure time is

$$\Delta t = t_c + t_r$$

Using a coordinate system traveling at the velocity $u_e$, one can quickly visualize the various waves since the induction zone stands still while the metal target impacts it and drives a shock wave into it at velocity $D_d$. We have then

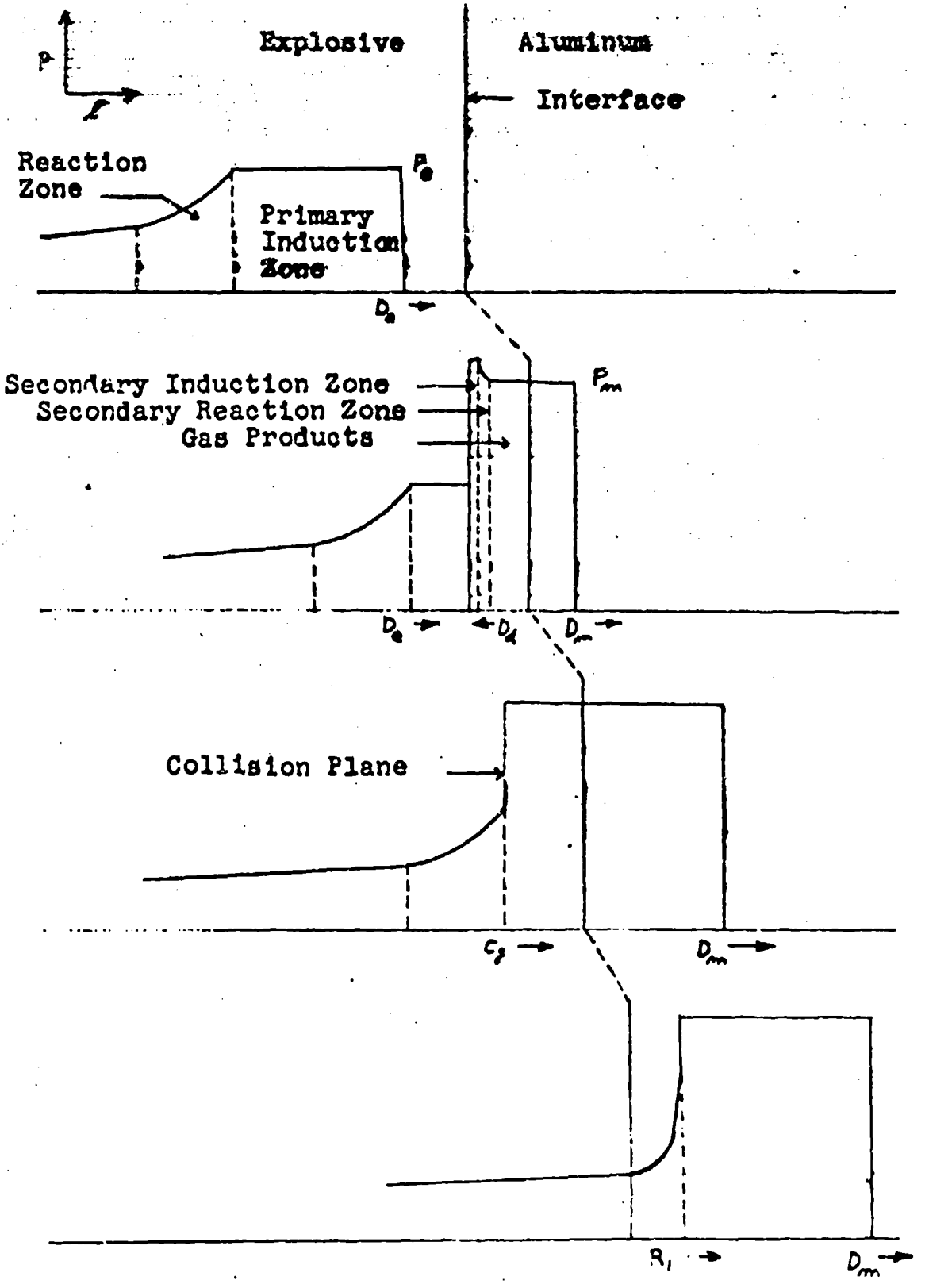


Figure 5. Instananeous Pressure Profiles During the Impact of a Detonation Wave on a High Impedance Metal Surface

$$14) \qquad t_e = \frac{b}{D_d} = \frac{a}{D_e - u_e}$$

$$t_r = \frac{b - u_d t_c}{c_g} = \frac{b\left(1 - \frac{u_d}{D_d}\right)}{c_g}$$

therefore

$$\Delta t = \frac{b}{D_1} + \frac{b\left(1 - \frac{u_d}{D_d}\right)}{c_g}$$

$$= b\left[\frac{c_g + D_d - u_d}{D_d\, c_g}\right]$$

If the C-J condition, $D_d = c_g + u_d$, approximately holds we obtain

$$15) \qquad \Delta t = \frac{2b}{D_d}$$

Solving equation 15) for b and substituting the result into equation 14) we have

$$16) \qquad b = \frac{(\Delta t)\, D_d}{2}$$

$$a = \frac{\Delta t}{2}\,(D_e - u_e)$$

From equations 16) we can compute the length of an undisturbed induction zone if values of $u_e$ and the velocity of the reflected detonation, $D_d$, can be estimated. According to Table I an upper limit for $u_e$ is probably about 1.7 mm/microseconds. The density behind the reflected wave is already greater than crystal density under these conditions and the corresponding velocity of a pure shock wave is 3.525 mm/microseconds. However, if the reflected wave went over into detonation, it would be feeding into material at density 1.130 grams/cc. At this loading density, the detonation velocity is greater than 5 mm/microseconds and therefore the pure shock front would be outrun by a detonation wave. Incoming mass at velocity $u_e$ would then meet a wave having a velocity higher than the 3.525 mm/microseconds consistent with a value of $u_e$ = 1.7 mm/microseconds.

It follows then that if a secondary detonation reaction occurs, a value of $u_e$ as high as 1.7 is not possible. Continuing in this manner, we have chosen that value of $u_e$ where the velocities $D_r$ of a reflected pure shock and $D_d$ of a detonation wave are equal. These values are graphed in Figure 6 and yield a value of $u_e$ = 1.46 mm/microsecond. Numerically we have

$$\Delta t = 0.117 \text{ microseconds}$$
$$D_d = 5.55 \text{ mm/microsecond}$$
$$D_e = 3.80 \text{ " "}$$
$$u_e = 1.46 \text{ " "}$$

and therefore the induction zone length for the steady state wave is

$$x = a + b = 0.325 + 0.137 = 0.46 \text{ millimeters}$$

and the induction time for an undisturbed detonation wave is

$$\tau = \frac{x}{D_e - u_e} = 0.20 \text{ microseconds}$$

The induction time computed for the low density TNT is very close to the steady pressure time obtained with cast TNT. Since in the later case we assume the acoustic approximation to hold, we then imply that the steady pressure time is approximately the induction time also. Having obtained the result that the induction times in the TNT density extremes are nearly identical, we conclude that an induction time in any intermediate density has a similar value. From equation 1) we can now compute the induction zone pressure in the low density TNT. Thus, p = 0.624 x 3.8 x 1.46 = 34.6 kilobars. If the postulates leading to equation 16) are correct, it is doubtful that C-J pressures can be obtained from our experimental data on low density TNT since the rarefaction, constituting the reaction zone, has propagated through a burned gas region and spread out to such an extent that the pressure corresponding to the end of the reaction is not clear cut. Fortunately this is not the case with cast TNT and the C-J plane probably arrives at the target interface relatively undisturbed by a reflected wave.

The Reaction Zone in Cast TNT

The reaction zone front in cast TNT has a rate of $(D_e - u_e)$ = 4.91 mm/microseconds relative to the moving particles. Considering the steady state detonation, the C-J plane approaches the metal interface at about this rate also.

Upon arrival a range of unloading waves will have already propagated into the target while the pressure at the interface fell during chemical reaction. Because each successive unloading increment propagates at a lower velocity than the one preceding, the entire range of pressure levels at the interface will propagate into the target and appear at a given distance from the interface.

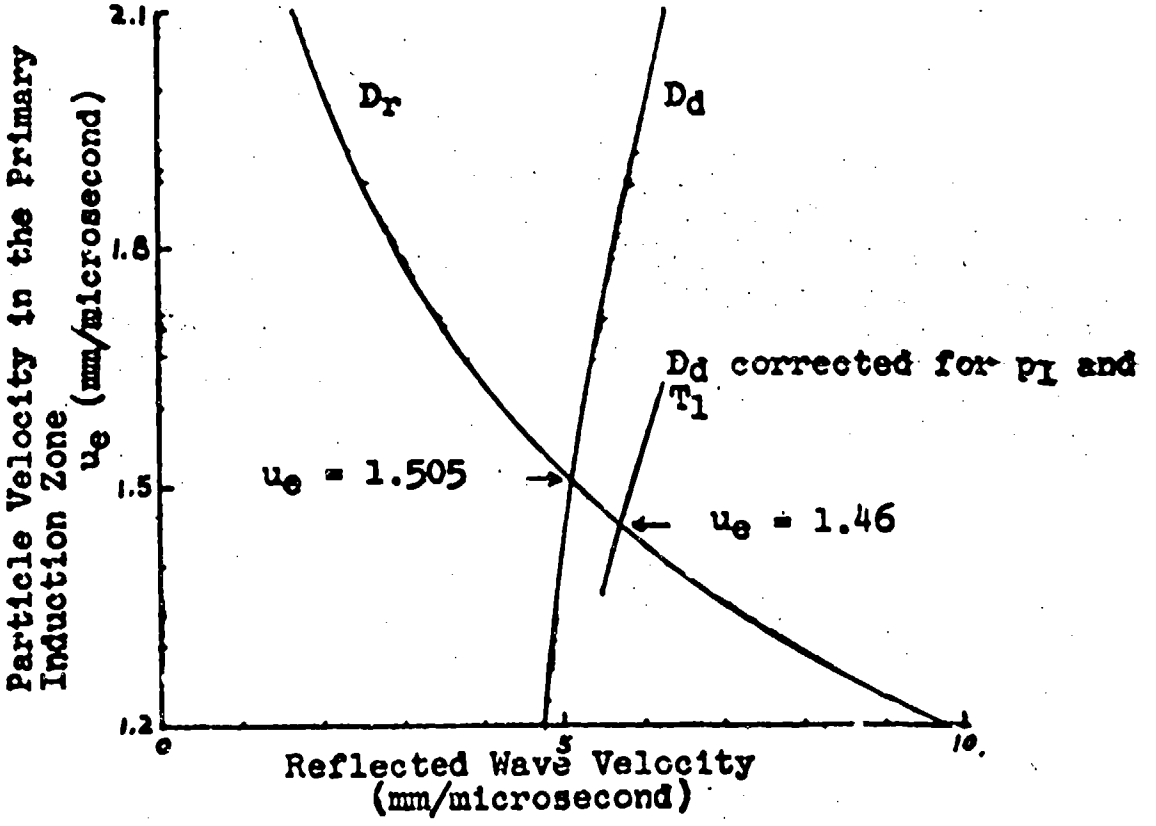


Figure 6. Reflected Wave Velocity as a Function of the Particle Velocity $u_e$, Striking the Aluminum Targets. Crystalline TNT at a Loading Density of 0.624 g/cc.

If we assume that reaction zone effects do not extend as far as 1 inch into the aluminum, then the last two data points (for 1 inch and 1 1/2 inch target thicknesses) are characteristic of a smoothly decreasing pressure behind the C-J plane. We can approximate this by assuming the pressure decrease to be of the same type observed in the aluminum-aluminum impact experiments. According to our equation of state for aluminum we can

write the equation $u = 0.7705\,D - 4.052$ over the range of aluminum densities from 3.1 to 3.5 grams/cc. This density range completely covers the data for cast TNT. The equation is consistent to within 10 meters/seconds in D over the restricted range. Since u changes but slowly over the post C-J part of the cast TNT curve in Figure 2, D can be described by a simple quadratic function of time and distance

$$t = b_0 + b_1 \ell + b_2 \ell^2$$

where $\ell$ is the thickness of aluminum penetrated by the shock wave. Therefore we can write

$$17) \qquad D = \frac{d\ell}{dt} = \frac{1}{b_1 + 2\,b_2 \ell}$$

Substituting the value of D from equation 17) into the linear relation between u and D and evaluating the constants from the experimental $u_s$ at the 1 and the 1 1/2 inch target thicknesses, we find for $\ell = 0$ that $D_o = 6.934$ and $u_s = 2.581$ mm/microseconds. The computed value of $u_s$ for zero target thickness is a point on an equation going through the data points for the 1 and 1 1/2 inch target thicknesses. At $\ell = 19.2$ mm the experimental velocity curve deviates from the theoretical curve through these three points. The corresponding free surface velocity, 2.350 mm/microsecond, is interpreted as that due to the C-J pressure in the explosive. The cast TNT curve in Figure 2 is therefore drawn in such a manner that it is somewhat flattened after the point $\ell = 19.2$ mm. Thus, the curve shows effects of reaction zone pressures extending from the target thickness $\ell = 6.5$ mm to the thickness $\ell = 19.2$ mm. Equation 13) can be extended to this portion of the curve by dividing the free surface velocity into equal increments. In general

$$18) \quad \Delta t_i + \sum_{k=1}^{m} \Delta t_k + \left[ \frac{\Delta \ell_i + \sum_{k=1}^{m} \Delta \ell_k - u_i \Delta t_i - \sum_{k=1}^{m} u_{k,k+1} \Delta t_k}{R_{m+1}} \right] = \frac{\Delta \ell_i}{D_i} + \sum_{k=1}^{m} \frac{\Delta \ell_k}{D_{k,k+1}}$$

In this equation, $u_{k,k+1}$ and $D_{k,k+1}$ are average slopes for discrete increments of shock front and target interface positions as shown in Figure 7.

In order to estimate the reaction time in cast TNT we have divided the free surface velocity curve

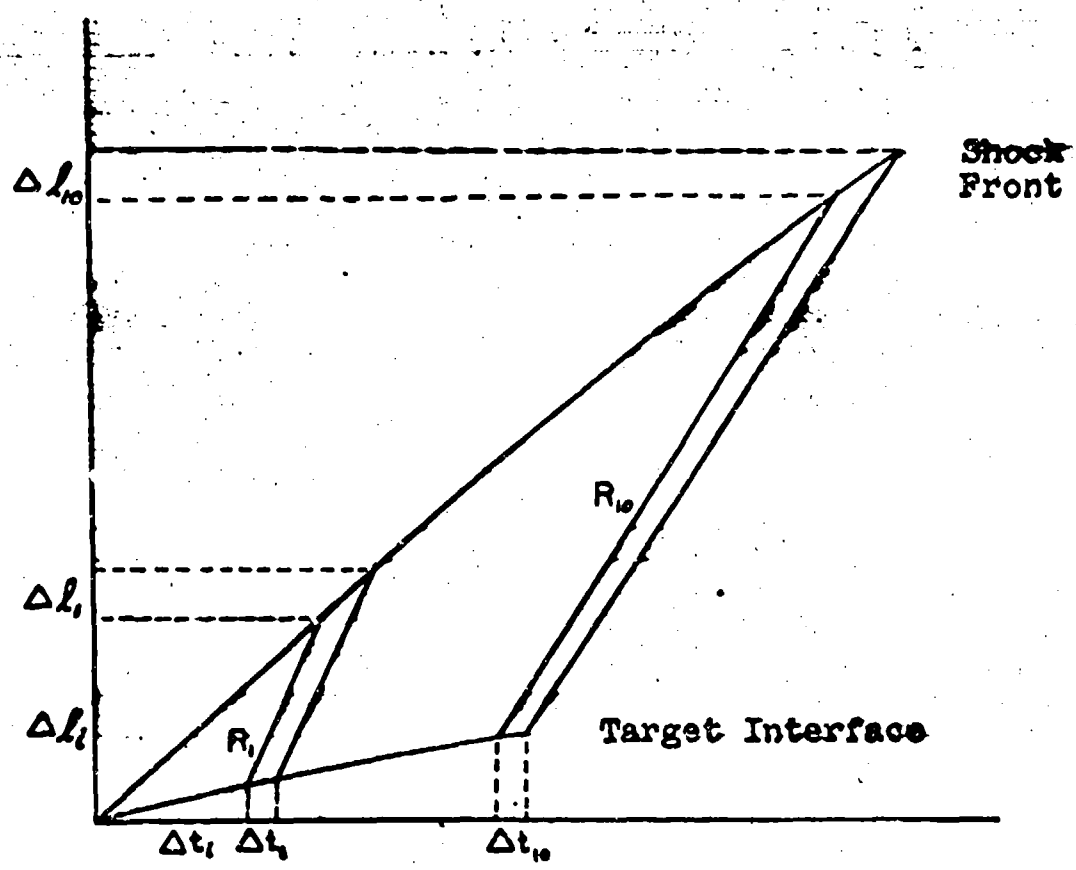


Figure 7. Overtaking of the Shock Front in Aluminum by Rarefactions from the Metal-Explosive Interface

between l = 6.5 and l = 19.2 mm/microsecond into 10 equal increments of $u_s$. Equation 18) was then evaluated by using the data shown in Table V. Our estimate of the reaction time is about 0.29 microseconds and the total time between the shock front and the C-J plane is about 0.51 microseconds. This time compares very favorably with a value obtained by Copp and Ubbelohde[10] by the method of case expansion. These authors have stated that their measured time is that to the "equilibrium of primary processes of explosive decomposition". By interpreting this to mean the induction plus reaction time, the data from the two different experimental methods are in good agreement.

| $\ell$ (mm) | $u_s/2$ (mm/μsec) | $R_k$ (mm/μsec) | $u_{k,k+1}$ (mm/μsec) | $D_{k,k+1}$ (mm/μsec) | $\Delta t_k$ (μsec) | $\Delta t_1 + \sum_{k=1}^{n} \Delta t_k$ (μsec) |
|---|---|---|---|---|---|---|
| 0 | 1.430 | | | | | |
| 6.50 | 1.430 | ($R_1$) 8.885 | | | 0.21335 | 0.21335 |
| 6.84 | 1.404 | ($R_2$) 8.823 | 1.417 | 7.098 | 0.00888 | 0.22223 |
| 7.26 | 1.379 | ($R_3$) 8.761 | 1.392 | 7.066 | 0.00747 | 0.22970 |
| 7.88 | 1.354 | 8.700 | 1.366 | 7.032 | 0.01338 | 0.24308 |
| 8.75 | 1.328 | 8.638 | 1.341 | 6.999 | 0.02059 | 0.26367 |
| 9.90 | 1.302 | 8.576 | 1.315 | 6.966 | 0.02835 | 0.29202 |
| 11.15 | 1.277 | 8.514 | 1.290 | 6.933 | 0.02999 | 0.32201 |
| 12.80 | 1.252 | 8.452 | 1.264 | 6.899 | 0.04089 | 0.36290 |
| 14.70 | 1.226 | 8.390 | 1.239 | 6.867 | 0.04637 | 0.40927 |
| 16.80 | 1.200 | 8.329 | 1.213 | 6.833 | 0.04996 | 0.45923 |
| 19.20 | 1.175 | 8.267 | 1.188 | 6.801 | 0.05611 | 0.51534 |

Induction time $\Delta t_1 = 0.213 \mu$sec.
Time length of detonation head $\Delta t_1 + \sum_{k=1}^{n} \Delta t_k = 0.515 \mu$sec

Reaction time $\sum_{k=1}^{n} \Delta t_k = 0.302 \mu$sec

Table V. Numerical Data for Figure 7

The Chapman-Jouguet Pressures

Since $u_s = 2.860$ at the peak and about 2.350/mm/microsecond for the C-J point, the corresponding particle velocities in cast TNT are 1.979 and 1.626 mm/microsecond respectively. Using a value of 6.880 mm/microsecond for the detonation velocity and 1.58 grams/cc for the density, we find from equation 1) that the pressure in cast TNT is 215 kilobars at the peak and 177 kilobars at the C-J point. Thus, the over-pressure in the induction zone is about 121% of the C-J pressure.

For the snow flaked packed TNT the C-J pressure can be estimated from the Jones equation(11).

$$19) \qquad \frac{D_e}{u_{C-J}} = (2 + \alpha)\left(1 + \frac{\rho_o}{D_e}\frac{dD_e}{d\rho_o}\right)$$

Assuming a value for the Jones constant, $\alpha = 0.25$ one computes $u_{C-J} = 1.1$ mm/microsecond and $p_{C-J} = 26.2$ kilobars. For the induction zone pressure we find p to be 34.6 kilobars and therefore the over-pressure in the induction zone is about 132% of C-J. In view of the approximations involved, the pressure ratios for the two extreme TNT densities can be considered to be essentially the same.

## Conclusions

Induction times have been shown to exist in the steady state detonation wave of TNT at various bulk densities. It is approximately the same for all densities, namely 0.2 to 0.25 microseconds. The reaction time has also been measured in cast TNT and amounts to approximately 0.29 microseconds. The total time from the shock front to the C-J plane is therefore 0.51 microseconds in the cast explosive.

The flat top observed in the free surface velocity of aluminum target is not to be interpreted as evidence of no reaction in the induction zone but rather that it is occuring at a negligible rate in comparison with the reaction zone proper. We have drawn the curves in the manner shown because we believe we are not justified in assuming a more detail contour from the data on hand.

The plateau is interpreted as due to a thermal induction period in the initiation of the explosive and is evidence that the reaction in TNT progresses by a thermal mechanism. Grain burning is not necessarily excluded by these results for the reason that time lags in building up to high rates of deflagration can still exist. Mathematically, the data has been treated as though the explosives were homogeneous fluids. This can be readily admitted in the detonation of gaseous and liquid systems, and may also be true for cast TNT. It should be pointed out that the percentage voids in the snow flaked packed TNT is quite large, and although the treatment appears straightforward, it is admittedly difficult to understand how material in the induction zone can be compressed to a value far below the crystal density while sustaining a pressure of at least 35 kilobars.

## Acknowledgements

The authors wish to express their appreciation to the following persons who contributed greatly to the success of these experiments: James Counihan, Halcom Curtis and Donald Danielson who carried out the firing program, Miss Mary Fix by whose considerable effort the results were computed and Keith Mason and Joseph Schleicher who constructed all the target assemblies.

REFERENCES

(1) Y. B. Zeldovich; J. Exptl. Theoret. Phys (USSR) 10 542 (1940)

(2) J. von Neumann; OSRD Report No. 549 (1942)

(3) W. Doring; Ann. Physik 43 421 (1943)

(4) B. Lewis and G. von Elbe; Combustion, Flames and Explosions of Gases, p. 604. Academic Press Inc. New York, 1951

(5) R. J. Finkelstein and G. Gamow, NavOrd Report 90-46, (1947) Confidential

(6) G. B. Kistiakowsky; Proceedings of the Conference on the Chemistry and Physics of Detonation, p. 39 (1951) Confidential

(7) H. Dean Mallory; The Propagation of Shook Waves in Aluminum, J. Appl. Phys. (In preparation)

(8) J. E. Ablard; ONR Report, Proceedings of the Conference on the Chemistry and Physics of Detonation, p. 82 (1951). Confidential

(9) H. Dean Mallory; On The Existance of a Binary Reaction Zone at a Metal-Explosive Boundary During Detonation. NavOrd Report 3772. July 1954.

(10) J. L. Capp and A. R. Ubbelohde; The Effect of Inert Components on Detonation, Trans. Faraday Soc. 44 658 (1948)

(11) H. Jones; The Properties of Gases at High Pressures Which Can be Deduced from Explosion Experiments, Third Symposium on Combustion, Flames and Explosion Phenomena p. 590 Williams and Wilkins Co. 1949

# CALCULATION OF THE DETONATION PROPERTIES OF SOLID EXPLOSIVES WITH THE KISTIAKOWSKY-WILSON EQUATION OF STATE

W. Fickett and R. D. Cowan
Los Alamos Scientific Laboratory
Los Alamos, New Mexico

## 1. INTRODUCTION

In an attempt to obtain a working equation of state for the gaseous products involved in the calculation of detonation phenomena, we have investigated a modification of an empirical equation of state first proposed by Halford, Kistiakowsky, and Wilson[1]:

$$\frac{PV_g}{RT} = F(x) = 1 + xe^{\beta x} \qquad (1.1)$$

$$x = \frac{k}{V_g(T + \theta)^{\alpha}} \qquad k = \chi \sum_i x_i k_i$$

Here $V_g$ is the molar gas volume, $x_i$ is the mole fraction of component i, and the sum extends over all chemical components of the gaseous mixture. The quantities $\alpha$, $\beta$, $\chi$, $\theta$, $k_i$ are empirical constants, the $k_i$ having the nature of covolumes. The values $\alpha = 0.25$ and $\beta = 0.30$, which were chosen originally to give agreement with experimental data[1], have been used in most of the previous work with this equation of state. However, different values of $\chi$ and several sets of $k_i$'s have been determined from experimental data (cf. references 1, 2, 3 and Table III). We have treated all of the parameters ($\alpha$, $\beta$, $\chi$, $k_i$'s) as adjustable in an effort to determine a set which would allow the calculations to reproduce a set of experimental data which includes both the variation of detonation velocity with loading density ($D - \rho_0$), and the Chapman-Jouguet pressure ($P_{C-J}$) at high loading density for a group of five related explosives (see Table II).

With the value $\theta = 0$ which has been previously used, it may easily be seen that the equation of state has a minimum in P vs. T (for constant $V_g$ and composition). With $\alpha = 0.25$ and with values of $V_g$ appropriate to the detonation region this minimum occurs near 0°K, but with $\alpha = 0.5$ it moves up to 2000 or 3000°K.

We have used the arbitrary value $\theta = 400$°K for all values of $\alpha$; this has proved to be large enough to eliminate the minimum throughout the volume region characteristic of plane detonations, and yet is small compared with the values of T encountered.

The calculations are complicated by the possible presence of solid carbon. We have assumed carbon to be present as graphite and treated its equation of state as known, using a form originated at this laboratory[4]:

$$P = P_1(V_s) + a(V_s)T + b(V_s)T^2 \qquad (1.2)$$

where, with P in megabars and T in volts (i.e., in units of 11,605.6°K),

$$P_1(V_s) = -2.467 + 6.769\eta - 6.956\eta^2 + 3.040\eta^3 - 0.3869\eta^4$$

$$a(V_s) = -0.2267 + .2712\eta$$

$$b(V_s) = 0.08316 - 0.07804\eta^{-1} + 0.03068\eta^{-2}$$

$$\eta = \frac{V_s^o(T^o)}{V_s} \; ; \; T^o = 25^oC$$

## 2. THEORY

If solid carbon is considered, expressions are needed for the thermodynamic functions of both gas and solid phases; these are summarized here:

For the gaseous component with equation of state (1.1):

$$E = \sum x_i (E^o - H_o^o)_i + \sum x_i (H_o^o)_i + RT\left[\frac{\alpha T}{T+\theta}(F-1)\right] \qquad (2.1a)$$

$$S = \sum x_i (S^o)_i - R\left[\sum x_i \ln x_i + \ln\left(\frac{P}{P^o}\right)\right] + R\left[\ln F - \frac{e^{\beta x}-1}{\beta} + \frac{\alpha T}{T+\theta}(F-1)\right] \qquad (2.1b)$$

$$\mu_i = (F^\circ - H_o^\circ)_i + (H_o)_i + RT \ln\left(\frac{x_i P}{P^\circ}\right) - RT\left[\ln F - \frac{e^{\beta x}-1}{\beta} - \frac{k_i}{k}(F-1)\right] \tag{2.1c}$$

where the gas imperfection factor F is defined in equation (1.1) and should not be confused with the free energies $F^\circ$ and $F_s'$.

For the solid with equation of state (1.2):

$$E = (H^\circ - H_o^\circ) + H_o^\circ - (PV_s)^\circ + \int_{V_s^\circ}^{V_s}\left\{b(V)T^2 - P_1(V)\right\}dV \tag{2.2a}$$

$$S = S^\circ + \int_{V_s^\circ}^{V_s}\left\{a(V) + 2b(V)\,T\right\}dV \tag{2.2b}$$

$$\mu = (F^\circ - H_o^\circ) + H_o^\circ + F_s' \tag{2.2c}$$

where

$$F_s' = PV_s - (PV_s)^\circ - \int_{V_s^\circ}^{V_s}\left\{P_1(V) + a(V)T + b(V)T^2\right\}dV$$

For chemical equilibrium:

$$\ln \Pi_g (n_i)^{\nu_i} = \ln K_p(T) - \left[\sum_g \nu_i\right]\left[\ln\left(\frac{P}{n_g P^\circ F}\right) + \frac{e^{\beta x}-1}{\beta}\right] - \left[\sum_g \nu_i k_i\right]\left[\frac{F-1}{k}\right] - \frac{\nu_s F_s'}{RT} \tag{2.3}$$

where

$$-RT \ln K_p(T) = -\sum \nu_i (F^\circ - H_o^\circ)_i - \sum \nu_i (H_o^\circ)_i$$

(one such equation for each independent chemical reaction).

In (2.1)-(2.3) E, S, and $\mu$ are internal energy, entropy, and chemical potential, respectively. A superscript o refers to the reference state (ideal gas or real

solid at pressure $P^o$ and temperature T)*, with $H_o^o$ being the enthalpy of formation from the elements; $x_i$ and $n_i$ are the mole fraction and number of moles of component i; $n_g = \sum_g n_i$. In (2.3) the $\nu_i$ are the coefficients of the chemical reaction, positive for products and negative for reactants, and the subscript g for a sum indicates it is for gaseous components only.

The thermodynamic state of the detonation products is defined by the Hugoniot equation[6]

$$h \equiv E - E_o - \tfrac{1}{2}(P + P_o)(V_o - V) = 0 \qquad (2.4)$$

and the Chapman-Jouguet condition**

$$\left(\frac{\partial P}{\partial V}\right)_S = -\frac{P - P_o}{V_o - V} \qquad (2.5)$$

In(2.4) the subscript o refers to the undetonated explosive, with $E_o$ given by

$$E_o = (\Delta H_f)_e + \sum_J N_J (H^o(T_o) - H_o^o)_J - P_o V_o \qquad (2.6)$$

where $(\Delta H_f)_e$ is the molar enthalpy of formation of the explosive at $T_o$ and $N_j$ is the number of moles of element J in one mole of explosive.

---

*In evaluating the thermodynamic functions for the solid we have neglected $(PV_s)^o$, and approximated $V_s^o$ by $V_s^o(T = 25^oC)$.

**In the usual statement of the C-J condition, $\left(\frac{\partial P}{\partial V}\right)_s$ is to be evaluated for equilibrium composition. However, Kirkwood and Wood, J. Chem. Phys., in press, have recently shown that this derivative should be evaluated with frozen composition. Our calculations have used the older statement of the C-J conditions, but there is very little difference between the two, at least for our equation of state. Check calculations showed that the use of the correct C-J condition would decrease $P_{C-J}$ by less than one percent at the lowest loading densities of interest ($\rho_o = 1.2$) and made almost no change at high loading density.

## 3. CALCULATIONS

The detonation products were assumed to be made up of the following chemical components:

$$1)H_2,\ 2)CO_2,\ 3)CO,\ 4)H_2O,\ 5)N_2,\ 6)NO,\ 7)C(\text{graphite}) \qquad (3.1)$$

Oxygen was not included, since none of the explosives considered were more oxygen rich than RDX, which balances to $N_2$, $H_2O$, and CO. In some preliminary calculations on IBM CPC equipment some of the components considered by Kirkwood, et al.,[5] viz. $NH_3$, $CH_4$, and OH were also included; these were found to be present in small though not negligible amounts.

For the final calculations, however, the set (3.1) was used in order to simplify the solution of the equilibrium equations and thereby reduce the machine time required. Although this set is rather restricted, components of differing size ($H_2$, $CO_2$) and with positive heat of formation (NC) are included.

It was found that with this set of components the determination of the equilibrium composition, given k, $n_g$, $V_g$, and T, could be reduced analytically to the solution of one equation in one unknown. With solid carbon present this unknown was $n_{CO}$; with carbon absent, $n_{H_2}$.

The reference-state thermodynamic functions and enthalpies of formation were taken from the tables published by the National Bureau of Standards.[7] The enthalpies of formation of the explosives are given in Table I.

The calculations were done on IBM 701 digital computers. It was found quite feasible to code a single problem to calculate adiabatic or Hugoniot curves, as well as detonation velocities. In order to produce points on these curves Eqs. (1.1), (1.2), and (2.1b), (2.2b) (for an adiabat) or (2.4) (for a Hugoniot) were solved by iteration to obtain values of V and T for the given S or h (=o), with the composition given by Eqs. (2.3) and the mass balance relations. The detonation velocity was determined by finding the point on the Hugoniot where

$$D = V_o \left[(P-P_o)/(V_o-V)\right]^{\frac{1}{2}} \qquad (3.2)$$

had its minimum value; this is equivalent to satisfying the C-J condition (2.5) with $(\partial P/\partial V)_s$ evaluated with

equilibrium composition.

TABLE I

Heats of Formation of the Explosives

| Explosive | $(\Delta H_f)_e$ kcal/mole at 25°C |
|---|---|
| RDX[a] | + 14.71 |
| TNT[b] | - 17.81 |
| $C_{3.3}H_{6.2}O_6N_{5.6}$[c,d] | + 0.49 |

[a] E. J. Prosen (NBS), private communication.

[b] G. Stegeman, NDRC Division-8 Interim Report PT-7 (1943).

[c] L. Sitney (LASL), unpublished communication.

[d] Explosive presently classified.

The time required for the calculation of one adiabat or Hugoniot point was about 20 sec.; for a detonation velocity, an average of about 140 seconds.

## 4. EFFECTS OF THE PARAMETERS

In order to determine the effects of the various parameters on the calculated D-$\rho_o$ curve and $P_{C-J}$, exploratory calculations were carried out for one explosive, 65/35 RDX/TNT. In order to save calculating time, these were carried out under the assumption of a fixed product composition resulting from the following decomposition equation

$$C_qH_rO_sN_t = \frac{r}{2} H_2O + (s - \frac{r}{2}) CO + (q - s + \frac{r}{2}) C + \frac{t}{2} N_2 \qquad (4.1)$$

A set of geometrical covolume values (Table III) was used, though with fixed composition the individual values of the $k_i$ are unimportant. The other parameters were varied from the values

$$\alpha = 0.6, \qquad \beta = 0.06, \qquad \chi = 30 \qquad (4.2)$$

which were found to give approximate agreement with the experimental D - $\rho_o$ and $P_{C-J}$. The results of the calculations are summarized in Figures 1 through 5.*

Viewed from the standpoint of attempting to reproduce experimental data, the effects of the parameters may be pictured as follows:

The value of $\chi$ may be changed to raise or lower the D - $\rho_o$ curve without greatly changing its shape (Fig. 1); $\beta$ may then be used to change its shape and slope while $\chi$ is varied so as to preserve a given value of D at one point (Fig. 2). Then the calculated C-J pressure may be changed by varying $\alpha - \beta$ and $\chi$ always being adjusted so as to best match D - $\rho_o$ (Figs. 3 and 4). Alpha also has a considerable effect on the C-J temperature (Fig. 3). There exist no accurate experimental data on $T_{C-J}$, but it is noteworthy that the T vs. $\rho_o$ curve for $\alpha = 0.45$ is similar to that obtained at this laboratory from preliminary calculations with the Lennard-Jones-Devonshire free-volume equation of state.(8)

In order to gain some idea of the effect of the carbon equation of state, calculations were made with the assumption that the carbon retained its normal volume, and also with the two equations of state for carbon mentioned in the footnote below. The results are shown in Figure 5.

## 5. RESULTS

By assuming a fixed product composition and varying the parameters as described above, a set of values for $\alpha$, $\beta$, and $\chi$ was found which gave results in good agreement

*These parameter studies differed from the final calculations in that they used a more incompressible equation of state for carbon than that which was finally adopted and used in the main calculations. The equation of state for carbon was first based on an interpolation between the static measurements of P. W. Bridgeman, Proc. Am. Acad. Sci., 76, 55-87 (1948), and Thomas-Fermi-Dirac calculations made by R. D. Cowan at this laboratory (unpublished communication). Recently, however, J. M. Walsh has obtained points on the shock Hugoniot of graphite (unpublished communication) by a dynamic method similar to that which he has used for aluminum, Phys. Rev. (in press). The carbon equation of state used in the final calculations, Eq. (1.2), was based on this work and was considerably more compressible than the one described above.

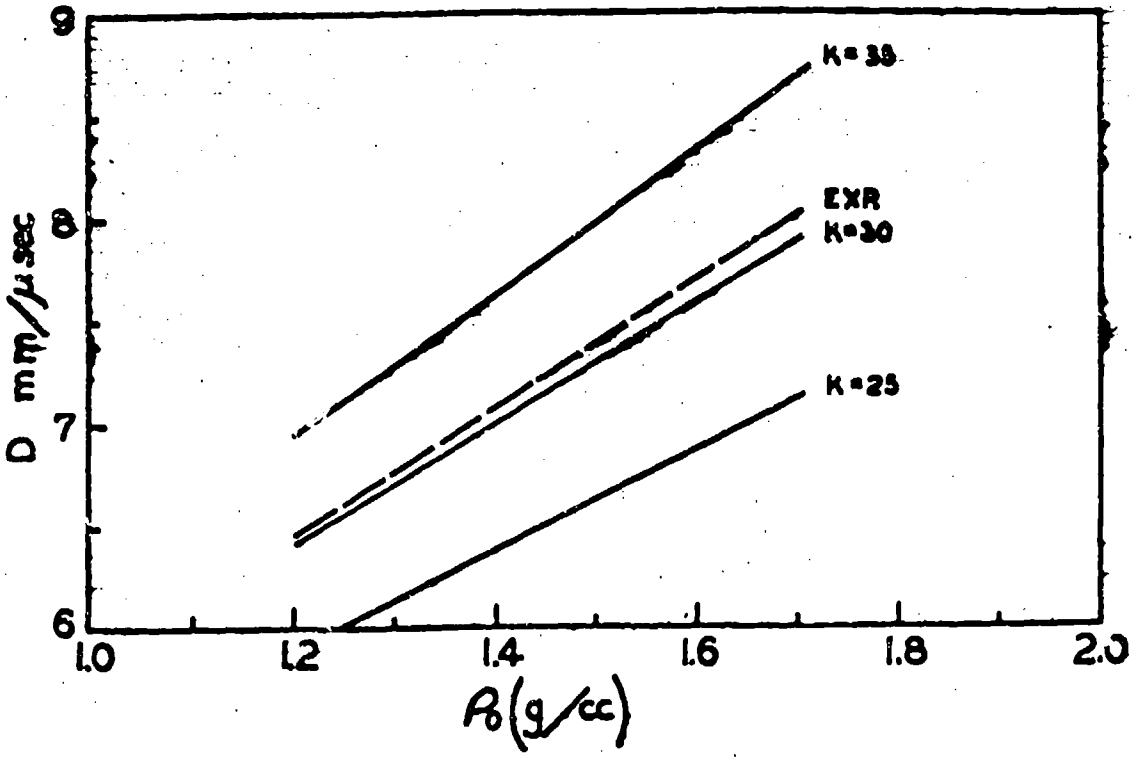


Fig. 1. The Effect of $\kappa$ on D – $\rho_0$.

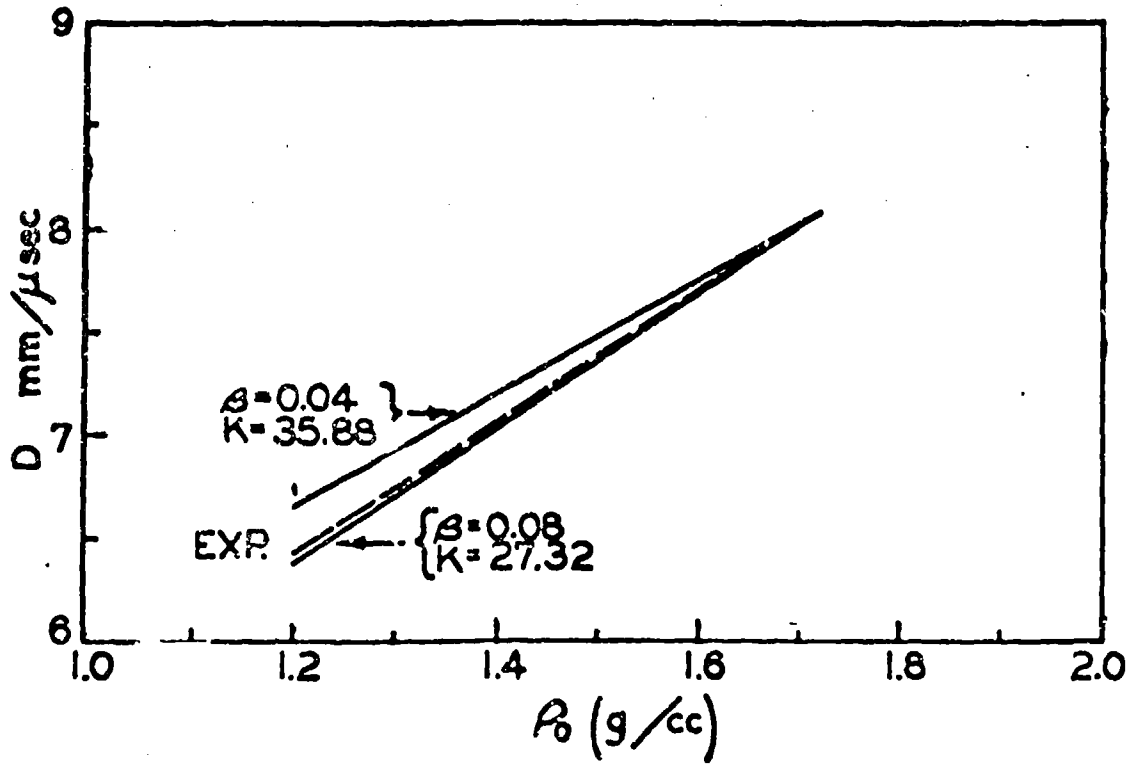


Fig. 2. The Effect of $\beta$ on D – $\rho_0$; $\kappa$ Chosen to Match Experimental D at One Point.

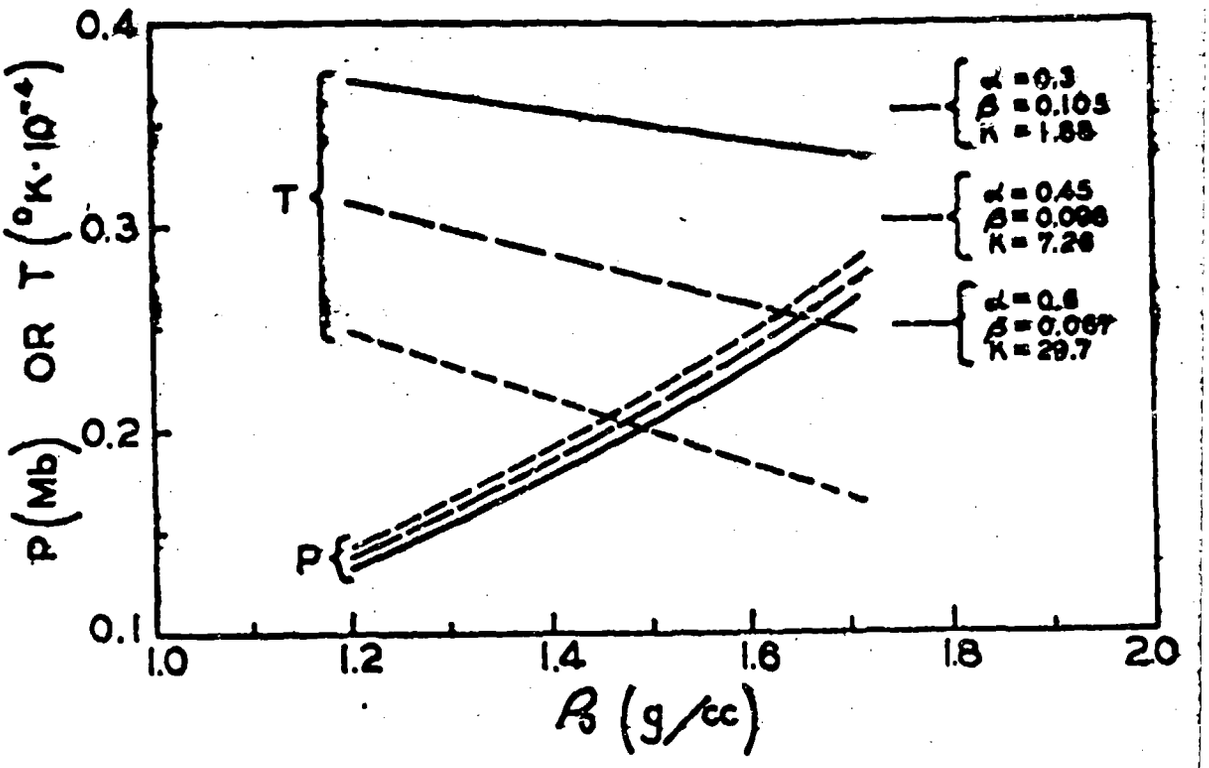


Fig. 3. The Effect of $\alpha$ on P vs. $\rho_o$ and T vs. $\rho_o$; $\beta$ and $\kappa$ Chosen to Match Experimental D – $\rho_o$.

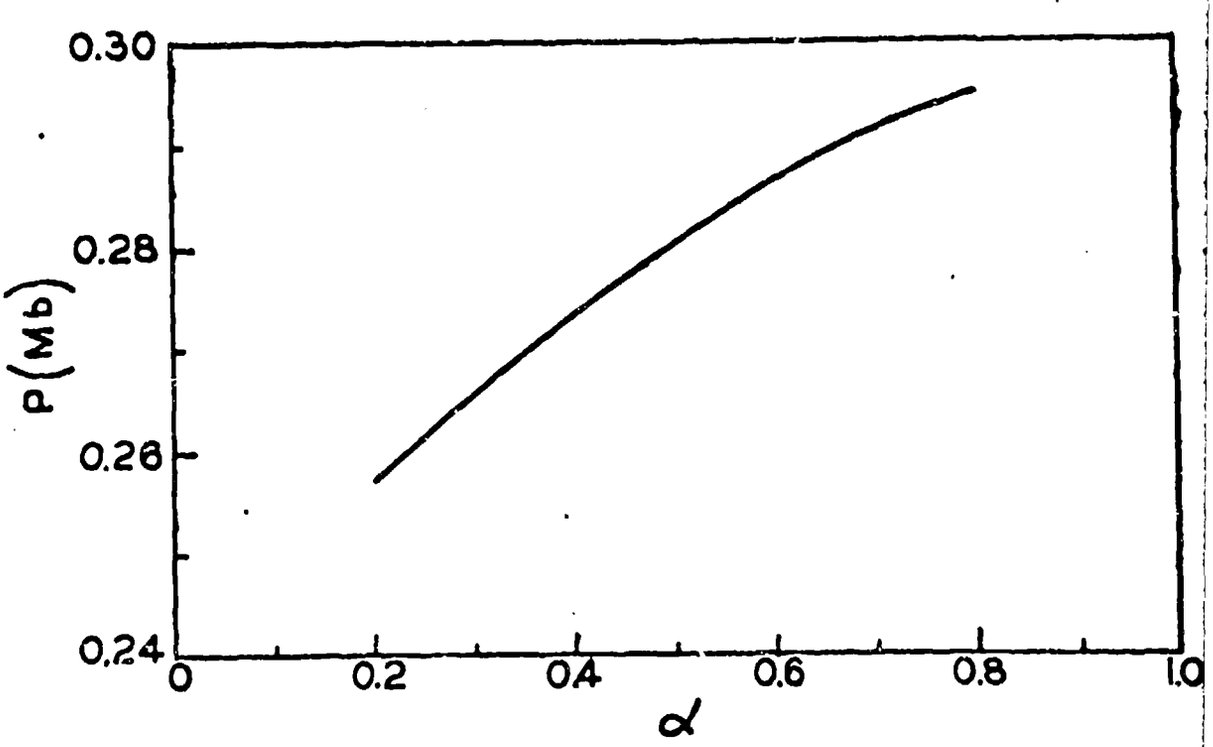


Fig. 4. The Effect of $\alpha$ on $P_{C-J}$ ($\rho_o = 1.715$); $\beta$ and $\kappa$ Chosen to Match Experimental D – $\rho_o$.

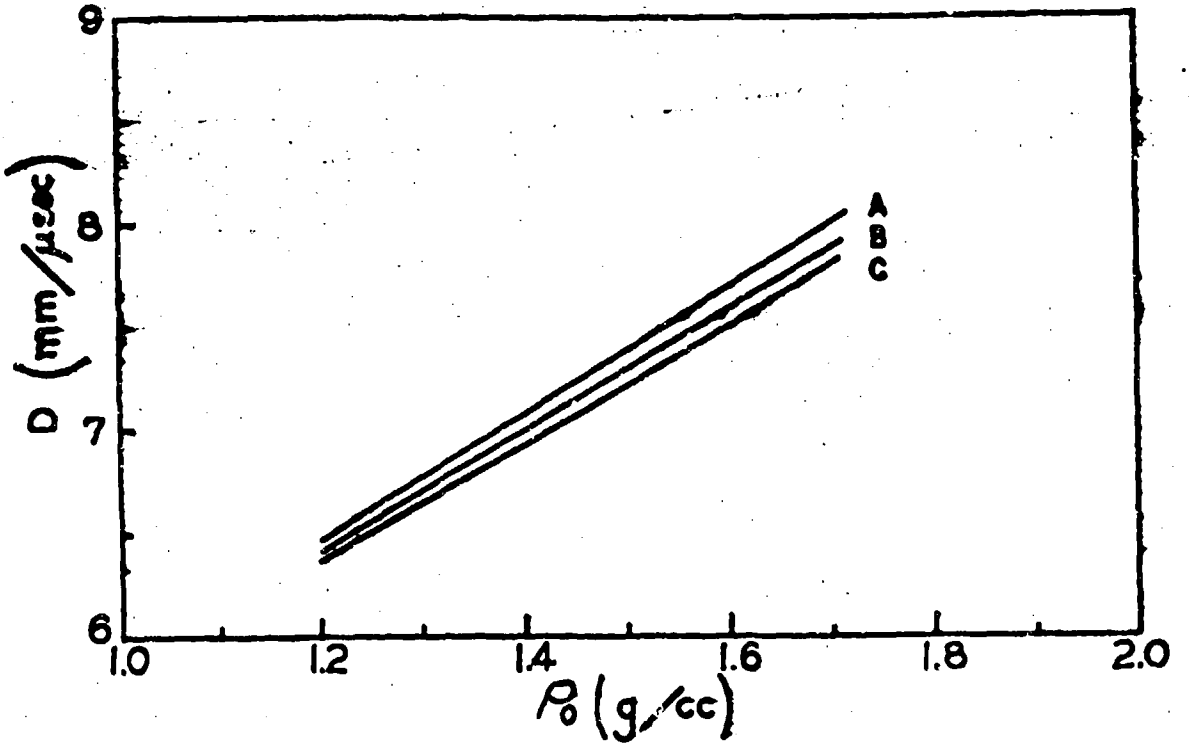


Fig. 5. Effect of the Graphite Equation of State on D – $\rho_o$: A - Incompressible, B - Graphite Equation of State used in the Parameter Studies, C - Graphite Equation of State used in the Final Calculations (see footnote on p. 271).

with experiment for 65/35 RDX/TNT. It was found that with equilibrium composition (and the "geometrical" $k_i$ discussed below) a not very different set also produced good agreement. The question of how well a single set of parameters could be made to serve for several explosives was then investigated.

The experimental data used were measurements of D - $\rho_o$ and $P_{C-J}$ at maximum loading density for a group of five related explosives.[9,10,11,12] These data are given in Table II and were obtained as follows:

Measurements of the detonation velocity for infinite diameter, $D_\infty$, were made for each explosive at two densities, $\rho_o$ = 1.2 and the highest $\rho_o$ obtainable by pressing or casting. (Values of $D_\infty$ were obtained by firing charges of different diameter d and extrapolating D vs. 1/d). It was assumed on the basis of previous work,

TABLE II

Experimental Data for Explosives

| Explosive and Density for $P_{C-J}$ | Detonation Velocity[a] $D = A\,\rho_o + B$, (m/sec) A | B | Dural Pressure[b] (Mb) | C-J Pressure[c] (Mb) Exp. | Calc. | Diff. |
|---|---|---|---|---|---|---|
| RDX | | | | | | |
| $\rho_c = 1.800$ | 3466 | 2515 | 0.398 | 0,341 | 0.3488 | + 2.2% |
| $C_{3.3}H_{6.2}O_6N_{5.6}$[d] | | | | | | |
| $\rho_o = 1.748$ | 3233 | 2785 | 0.378 | 0,316 | 0.3194 | + 1.1% |
| 78/22 RDX/TNT | | | | | | |
| $\rho_o = 1.755$ | 3193 | 2702 | 0.382 | 0,317 | 0.3106 | - 2.2% |
| 65/35 RDX/TNT | | | | (0,286)[f] | | |
| $\rho_o = 1.715$ | 3127 | 2673 | 0.358 | 0,292 | 0.2843 | - 2.8% |
| TNT[e] | | | | | | |
| $\rho_o = 1.640$ | 2799 | 2360 | 0.226 | 0,177 | 0.2066 | + 16.6% |

[a] Reference 9

[b] Reference 10

[c] See text

[d] Explosive presently classified

[e] More work on the TNT D - $\rho_o$ curve is in progress

[f] Reference 14

both at this laboratory and elsewhere[13] that over this range of loading density D *vs.* $\rho_o$ could be represented by a straight line within experimental error.

The dural pressures in Table II were obtained by measurements of shock and free-surface velocities in dural plates driven by the appropriate explosive.[16] The explosive C-J pressure $P_i$ is then given in terms of the metal pressure $P_t$ by the matching conditions at the H.E.-metal interface:[14]

$$\frac{P_i}{P_t} = \frac{1 + R\,(\rho_{oi}D_i/\rho_{ot}D_t)}{1 + R}\;;\quad R = \rho_{or}D_r/\rho_{oi}D_i \qquad (5.1)$$

where the subscripts i, r, and t refer to the incident, reflected, and transmitted shocks respectively, and the subscript o refers to material ahead of the shock. All velocities are referred to the material ahead of the shock in question. The value of R need not be known accurately,[14] the so-called "acoustic approximation" R = 1 giving results correct to within a percent or so. We have used values of R obtained by calculating shock curves for the detonation products (Table IV).

The measurements of $P_{C-J}$ and D - $\rho_o$ were taken on explosives of slightly differing composition and density, so all the data were corrected to the composition and density values in Table II by means of an error expression obtained by differential analysis of (5.1) with R = 1 and making use of the experimental dependence of D on composition and density:

$$\frac{\delta U_{fs}}{U_{fs}} = -0.86\,\delta\rho_o \;-0.0023\,\delta\,(\%\,\mathrm{RDX}) \qquad (5.2)$$

in which $U_{fs}$ is the experimentally measured free-surface velocity.

In attempting to determine a set of equation-of-state parameters from this experimental data, we started with a set of "geometrical" $k_i$ (Table III) based on molecular sizes estimated from both virial-coefficient data and spherical volumes from bond lengths and van der Waals radii. Using these $k_i$ in preliminary calculations it was found that $\alpha = 0.5$, $\beta = 0.09$, $\chi = 11.85$* would give D - $\rho_o$

---

*With the $k_i$ scaled so that $k_{H_2O}$ was about the same as that used by Brinkley and Wilson.[2]

and $P_{C-J}$ close to the experimental values for 65/35 RDX/TNT. However, the agreement for other explosives was rather poor (Fig. 6). A least-squares process was therefore carried out (with this same $\alpha$ and $\beta$) to determine a set of $k_i$ which would give the best agreement with all five explosives. The rather surprising result that the reaction

$$2\ CO \rightarrow CO_2 + C\ (\text{graphite})$$

shifts from far left to far right as $\rho_0$ is increased through the range of interest caused us to let points of different $\rho_0$ for the same explosive enter the least squaring on an equal weight with those from different explosives. Accordingly, the least squaring was carried out as follows:

Using a guessed set of $k_i$, a value of $k = \chi \sum x_i k_i$ was determined at four loading densities (1.2, 1.4, 1.6, and maximum) for each of the five explosives by adjusting $\chi$ in each case until the calculated D was equal to the experimental value. If we designate these values of k as $k_{obs}$ we then have a set of 20 linear equations for the set of $k_i$:

$$\sum_i (x_i)_r\ k_i = (k_{obs})_r,\ r = 1 \ldots 20 \qquad (5.3)$$

These were solved by least squares for a new set of $k_i$.*

*In a preliminary trial of the least-squaring process on three explosives with $\alpha = 0.6$ it was found that carrying out the entire least-squaring process a second time (starting with the $k_i$ produced from the first least squaring) produced almost no change in the $k_i$. It was also found that the rather sizeable change in $k_i$ from the initial geometrical set to the first least-square set produced composition changes of at most a few percent of the original mole fractions.

Since the determination of so many $k_{obs}$ is rather expensive in machine time, the final least squaring was started with the $k_i$ from the above trial run and was done only once.

The first result of this process was large negative values for $k_{H_2}$ and $k_{NO}$, probably because $H_2$ and NO were present in such small amounts. Therefore the equations were solved again with these two covolumes held constant at their original values (multiplied by the average $\chi$ from the determination of all of the $k_{obs}$). Table III contains the resulting $k_i$, together with our "geometrical" set and the values obtained by Brinkley and Wilson. The set obtained by Christian and Snay is rather different from any of these.[3]

TABLE III

Values of $k_i$

| Source | $k_i$ | | | | | |
|---|---|---|---|---|---|---|
| | $H_2$ | $CO_2$ | CO | $H_2O$ | $N_2$ | NO |
| Brinkley-Wilson[2] | 153 | 687 | 386 | 108 | 353 | 233 |
| "Geometrical" | [a]180 | 670 | 390 | 360 | 380 | 350 |
| | [b]2133 | 7940 | 4622 | 4267 | 4504 | 4148 |
| Least Square | 2133 | 6407 | 3585 | 3636 | 6267 | 4148 |

[a] Original set chosen so that $k_{CO}$ would be about the same as that used by Brinkley-Wilson.

[b] Scaled by the average $\chi$ (11.85) from the determination of all of the $k_{obs}$ (see text).

In Figures 6 and 7 the calculated results for D - $\rho_0$ are compared with experiment for both the geometrical and the least-square $k_i$. (To avoid confusion, results for only three explosives are shown; the others are qualitatively similar.) It can be seen that with the least-square $k_i$ fairly good agreement is obtained. The values of the parameters thus determined are

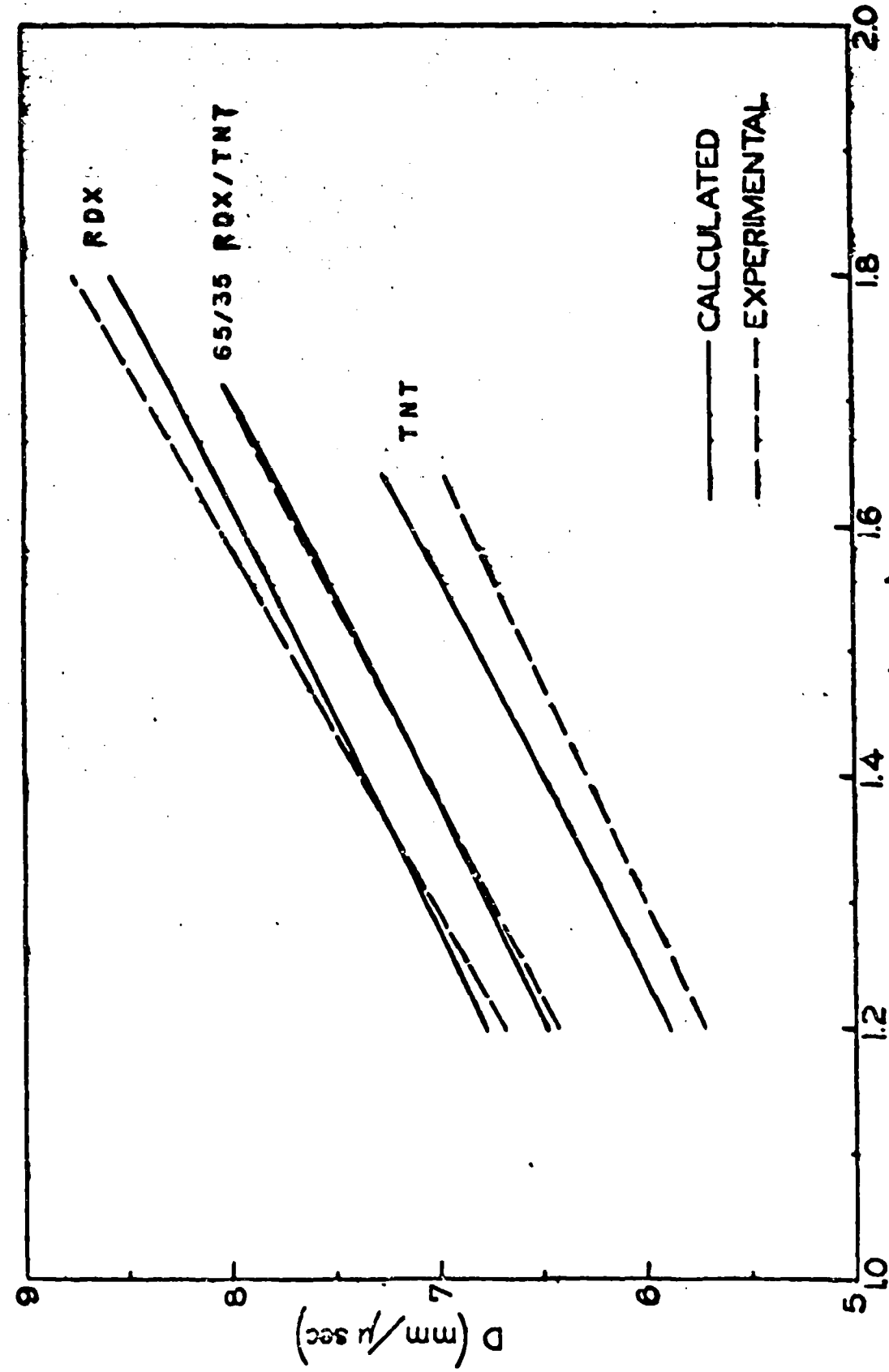


Fig. 6. Comparison of Calculated and Experimental D – $\rho_0$ Curves for "Geometrical" $k_1$.

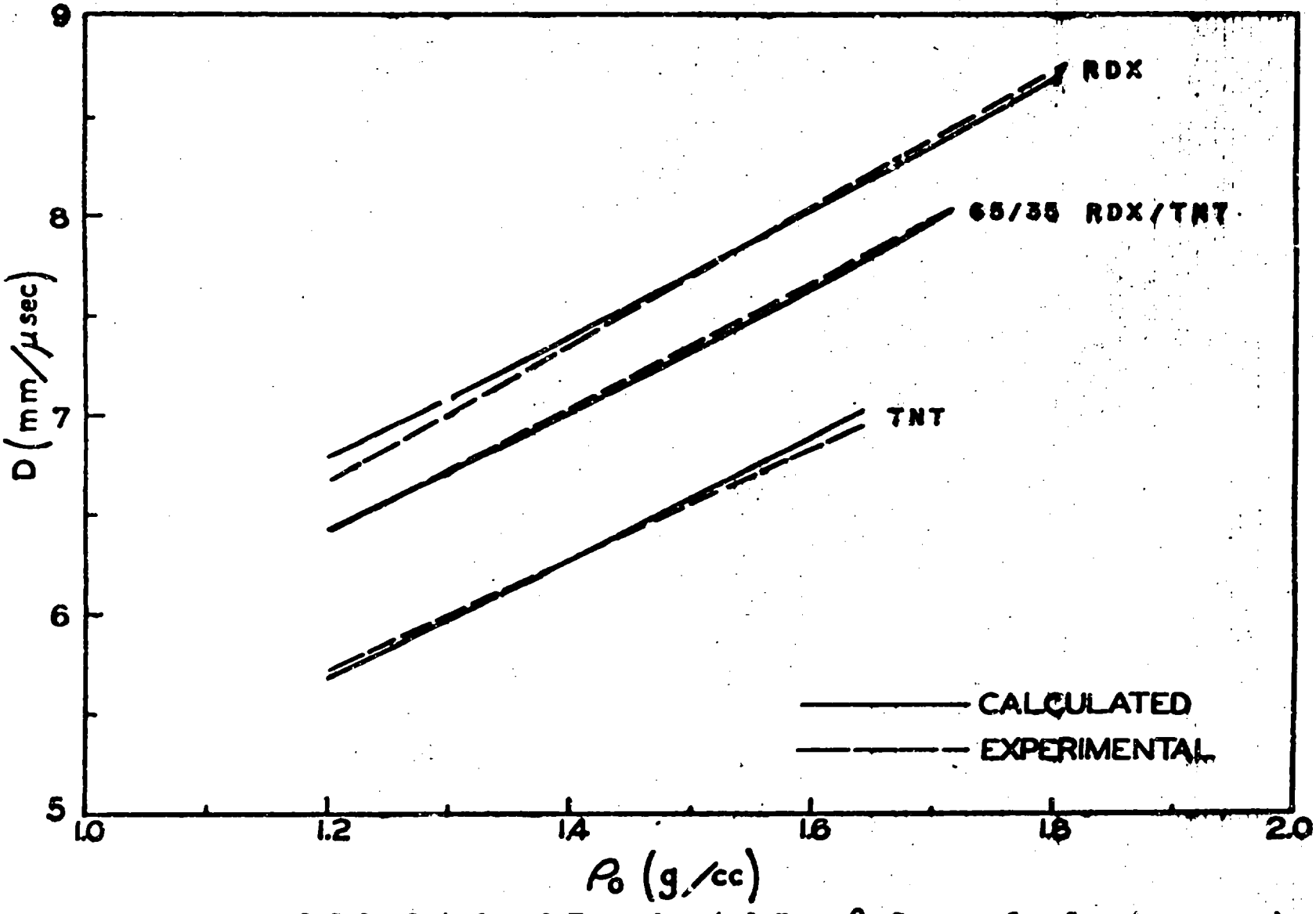


Fig. 7. Comparison of Calculated and Experimental D – $\rho_0$ Curves for Least-square $k_1$.

$$\alpha = 0.5$$
$$\beta = 0.09 \qquad (5.4)$$
$$\kappa = 1.0$$
$$k_i = \text{least-square set, Table III.}$$

The C-J pressures calculated with this set of parameters are compared with the experimental values in Table II.

The variation of C-J temperature and pressure with loading density for three explosives is shown in Figure 8. In Table IV are given (for 65/35 RDX/TNT) some points on the adiabat passing through the C-J point and also on the shock Hugoniot for the detonation products which originates at the C-J point. It can be seen that for all practical purposes these are identical over the region which can be studied by the interaction of plane detonation waves with stationary metal plates.

## 6. DISCUSSION

As can be seen from Figure 7 and Table II the agreement with experiment is good in the case of D vs. $\rho_o$, and, with the exception of TNT, fairly good in the case of $P_{C-J}$. The signs of the disagreement at both extremes of composition may be interesting: The calculated high-density D is low for RDX, high for TNT. For $P_{C-J}$, on the other hand, the calculated values are high for both RDX and TNT.

The disagreement of the calculated and experimental $P_{C-J}$ for TNT is rather large. Perhaps a more enlightening comparison of theory and experiment can be made with a quantity related to the adiabatic compressibility:

$$\gamma^*_{C-J} = -\frac{V}{P}\cdot\left(\frac{\partial P}{\partial V}\right)_S = \frac{\rho_o D^2}{P_{C-J}} - 1 \qquad (6.1)$$

This expression can be obtained from Eqs. (2.5) and (3.2) by neglecting $P_o$. The values of $\gamma^*$ obtained from the experimental $\rho_o$, D, and P, together with the calculated values of $\gamma^*$ and the fraction of total volume occupied by graphite are shown in Table V.

TABLE IV

Adiabat and Shock Hugoniot Through the C-J Point
65/35 RDX/TNT

| | Adiabat | | Shock Hugoniot | |
|---|---|---|---|---|
| $V/V_o$ | P | $\gamma^*$ | P | R(Eq.5.1) |
| 0.600 | 0.5320 | 2.98 | 0.5344 | 1.259 |
| 0.625 | 0.4713 | 2.96 | 0.4723 | 1.202 |
| 0.650 | 0.4198 | 2.94 | 0.4201 | 1.151 |
| 0.675 | 0.3757 | 2.93 | 0.3757 | 1.104 |
| 0.700 | 0.3378 | 2.91 | 0.3378 | 1.063 |
| 0.725 | 0.3050 | 2.90 | 0.3050 | 1.025 |
| 0.743(CJ) | 0.2843 | 2.89 | 0.2843 | 1.000 |
| 0.750 | 0.2765 | 2.89 | | |
| 0.800 | 0.2296 | 2.85 | | |
| 0.900 | 0.1643 | 2.81 | | |
| 1.000 | 0.1223 | 2.76 | | |
| 1.2 | 0.0743 | 2.69 | | |
| 1.4 | 0.0493 | 2.62 | | |
| 1.6 | 0.0349 | 2.55 | | |
| 1.8 | 0.0259 | 2.50 | | |
| 2.0 | 0.0200 | | | |

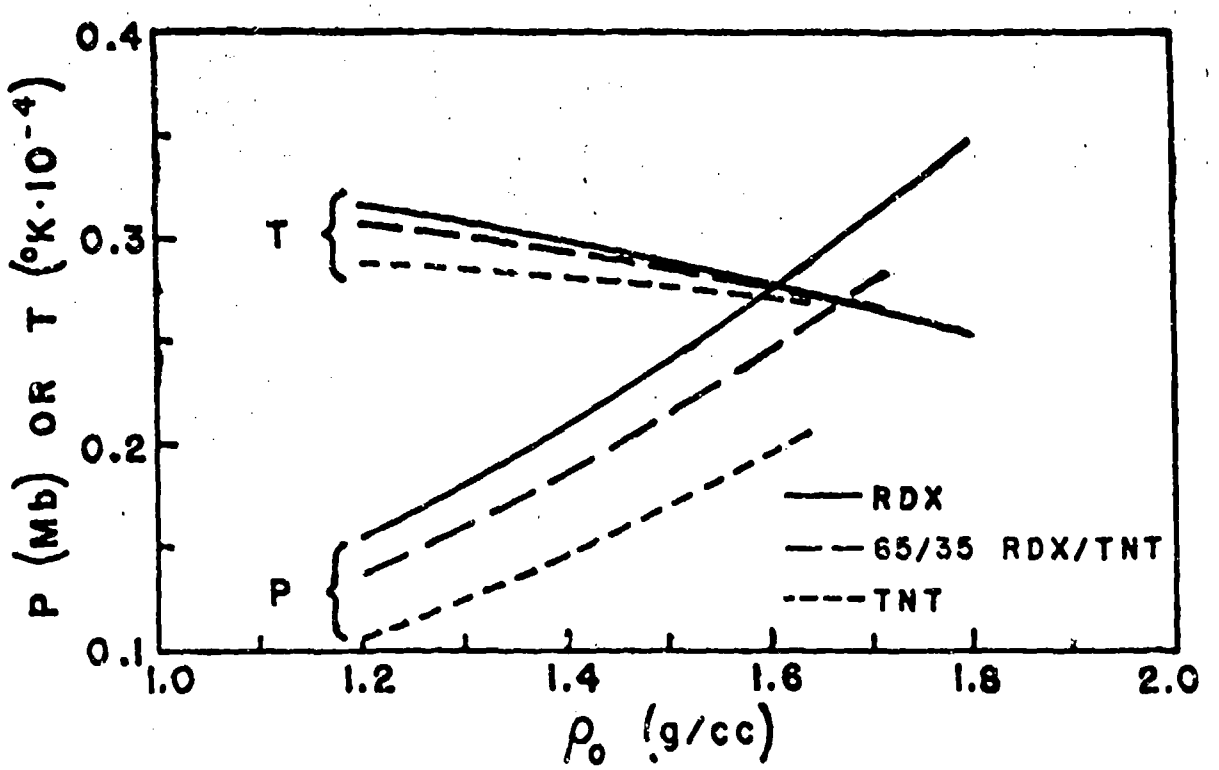


Fig. 8. Chapman-Jouguet Pressure and Temperature Calculated with the Final Set of Parameter Values (5.5).

TABLE V

| Explosive | $\gamma^*$ Experimental | $\gamma^*$ Calculated | $V_g/V$ |
|---|---|---|---|
| RDX | 3.04 | 2.908 | 0.0497 |
| $C_{3.3}H_{6.2}O_6N_{5.6}$ | 2.93 | 2.902 | 0.0633 |
| 78/22 RDX/TNT | 2.81 | 2.899 | 0.0785 |
| 65/35 RDX/TNT | 2.79 | 2.887 | 0.0945 |
| TNT | 3.47 | 2.912 | 0.1837 |

It can be seen that both calculated and experimental $\gamma^*$'s have a minimum as a function of % RDX. The former is undoubtedly due principally to the large $\gamma^*$ of graphite. (For our graphite equation of state at the TNT C-J point, $\gamma^* = 5.65$). Assuming that the usual equilibrium detonation theory applies, there are two possibilities which could explain our low $\gamma^*$ for TNT: a) the $\gamma^*$ for graphite is low, or there should be more graphite present; or b) the gas equation of state does not predict a sufficiently large change in $\gamma^*$ with changes in gas composition, or the gas composition should be different from what it is (probably in the direction of larger components).

In addition to this poor agreement with the experimental $P_{C-J}$ for TNT, the equation of state (1.1) has other unattractive features. The results obtained with the geometrical $k_i$ (Fig. 6) and the very different set of $k_i$ (Table III) required to give agreement with experiment indicate that a priori estimation of the covolumes is likely to be unsatisfactory, and extensive least squaring together with additional experimental data would be required for the introduction of any new chemical components into the detonation products. Also, analytical examination of Eq. (1.1) reveals that as Vg is decreased the minimum in P vs. T at constant Vg will again occur. This unphysical behavior reduces confidence in the equation of state, particularly if it is to be extended to smaller volumes.

This equation of state is probably fairly reliable if its use is restricted to explosives which are similar to those included in a determination of its parameters, and to pressures and volumes not too different from those existing at the Chapman-Jouguet point. There would seem

to be little justification for its use in an extended extrapolation of any sort.

No further work is planned on this equation of state; instead the Lennard-Jones-Devonshire free volume equation of state is being investigated for use along these same lines.

## 7. ACKNOWLEDGMENTS

The authors are indebted to Frederick R. Parker for help with the machine computations, and to W. W. Wood for several helpful discussions.

## REFERENCES

1. G. B. Kistiakowsky and E. B. Wilson, Jr., Final Report on the Hydrodynamic Theory of Detonation and Shock Waves, NDRC-Div. B, OSRD Report No. 114, June 1941.

2. S. R. Brinkley and E. B. Wilson, Jr., Report on Revised Method of Predicting the Detonation Velocities in Solid Explosives, NDRC-Div. B, OSRD Report No. 305, Sept., 1942; also NDRC-Div. 8, OSRD Report No. 1707, Aug., 1943.

3. E. A. Christian and H. G. Snay, Analysis of Experimental Data on Detonation Velocities, NAVORD Report No. 1508, Feb. 1, 1951.

4. J. Keller and N. Metropolis, unpublished communication, Los Alamos Scientific Laboratory.

5. J. G. Kirkwood, S. R. Brinkley, and J. M. Richardson, The Pressure Wave Produced by an Underwater Explosion, Part V, NDRC-Div. 8, OSRD Report No. 2022, Nov. 1943.

6. R. Courant and K. O. Friedrichs, Supersonic Flow and Shock Waves, (Interscience Publ., Inc., New York, 1948), p. 204.

7. U. S. National Bureau of Standards, Selected Values of Chemical Thermodynamic Properties, Series III (loose leaf).

8. W. W. Wood and W. Fickett, unpublished communication, Los Alamos Scientific Laboratory.

9. A. W. Campbell, E. James, M. Malin, C. W. Mautz, and M. J. Urizar, unpublished communication, Los Alamos Scientific Laboratory

10. W. E. Deal, The Measurement of C-J Pressure in Explosives, this conference.

11. A. W. Campbell, M. Malin, T. J. Boyd, and J. A. Hull, Techniques for the Measurement of Detonation Velocity, this conference.

12. A. W. Campbell, M. Malin, and T. Holland, Detonation in Homogeneous Explosives, this conference.

13. N. L. Coleburn and T. P. Liddiard, The Rates of Detonation of Several Pure and Mixed Explosives, NAVORD Report No. 2611, Sept. 22, 1952.

14. R. E. Duff and E. Houston, Measurement of C-J Pressure and Reaction Zone Length in a Detonating High Explosive, this conference.

# A SOLID-STATE MODEL FOR DETONATIONS 19

R. H. Parlin and J. C. Giddings
University of Utah
Salt Lake City, Utah

## INTRODUCTION

There are still two fundamental unsolved problems in the analysis of the ideal hydrodynamic-thermodynamic theory of detonation in condensed explosives. One of these is the choice of an equation of state from which to calculate, primarily, the mechanical work done in the Chapman-Jouguet compression. The other involves the question of determining the chemical composition at the Chapman-Jouguet point and from this the change in internal energy. The classical approach employs imperfect gas theory, using equilibrium constants extrapolated from relatively low temperatures, and assumes that the Chapman-Jouguet products are normal, stable molecules. While this is certainly correct for gaseous detonations and probably a good approximation for condensed explosives at very low densities (large void space) there is considerable doubt as to the truthfulness of the basic assumptions at the higher densities. Using an imperfect gas equation of state, for example, it is found necessary to make excessively large fugacity corrections in order to fit experimental detonation velocity data.

The equations of state that have been proposed to cover detonation phenomena are as varied in origin and purpose as in content. Much success has been found, especially in the last decade, in correlating experimental data of many explosives with a common theoretical treatment. The equations developed for this express purpose are capable of approximately predicting results for many explosives. Another line of attack however, has been directed towards predicting detonation velocities without the use of detonation data. The results of such equations do not completely agree with observed values (as might be expected, considering the difficulty of a rigorous derivation of such an equation of state) but they are sufficiently accurate to suggest the essential correctness of the usual thermodynamic-hydrodynamic approach to the detonation process.

In the first class, the methods of Cook[1], Halford, Kistiakowsky and Wilson[2] and others, have led to especially fruitful

results in predicting detonation velocities. An approach by Jones[3] has also been used, but not as extensively. Both Cook and Jones have used a modified Abel equation of state, Cook using the restrictive condition that $(\partial\alpha/\partial T)_V = 0$ (where $\alpha$ is the covolume), whereas Jones has used the condition that $(\partial\alpha/\partial V)_P = 0$. Previous to this the Abel type of equation was quite useful when $\alpha$ was regarded as a constant dependent upon initial loading density[4]. This form of the equation is, of course, convenient for its simplicity.

In the latter class, Jones[5] applied data from high-pressure measurements on nitrogen to a solid state model, and obtained values about 17 per cent above the observed detonation velocities. Kihara and Hikita[6] have derived a virial type of equation with the intermolecular forces assumed to be given by the repulsive term only of a Lennard-Jones type equation. The exponent of the distance was determined from detonation data, and was found to have the value of 9, which agrees quite well with kinetic theory measurements. Cottrell and Patterson[7] have used the values for the compression energy of a hydrogen molecule-ion that were obtained from quantum mechanical calculations. The detonation velocity predicted by their theory was in good agreement with experimental values. Both these workers, as well as Jones, fitted parameters to detonation velocity measurements for the final analysis, although this was not necessary to demonstrate a satisfactory agreement.

Andersen and Parlin[8] have recently derived equations based upon the concept that at high densities the Chapman-Jouguet (CJ) products form a lattice structure, and the corresponding degrees of freedom are vibrational. The primary contribution to their equation of state follows from a term expressing the change of vibrational frequency with volume. The value of a parameter used in their theory was determined from detonation data, and found to be in approximate agreement with solid state theory. The equations derived by these workers are exceedingly easy to apply in practical detonation velocity calculations.

In what follows, the lattice concept in[8] is retained. The equations are extended to include a very large range of loading densities by requiring the equation of state to reduce to the perfect gas equation at high volumes. Factors other than the equation of state may be expected to vitiate the treatment in the low density region, of course. All parameters are determined by physical data outside the field of detonations, and the results agree to within about 13 per cent with the experimental detonation velocities. The dependence of detonation velocity upon loading density is also in agreement with experimental findings. The equations derived lead very naturally to the concept of universal curves of the reduced variables, velocity, volume, temperature, pressure and material velocity vs. the reduced loading density. Such relationships are particularly simple in application since a single solution of the equation is sufficient for all different explosives under varying initial conditions. Finally the results

of calculations are applied to several actual explosives and the numerical correlation with measured velocities shown.

GENERAL CONSIDERATIONS

Since the various molecular fragments at the CJ surface are confined by extremely high pressures, they will occupy a volume comparable to that of the solid crystalline explosive itself at room temperature. This volume may reasonably be presumed to depend strongly upon the initial loading density; at maximum loading density the final CJ volume may be seventy-five per cent of the undetonated crystal volume, and as the initial explosive is made to occupy a larger volume, the CJ products also become more voluminous. A theoretical treatment of the detonation process must depend upon the theoretically predicted properties of these high-density CJ products. The properties that are so derived depend upon the model used for interatomic and intermolecular potentials, and the simplifications that are made in the evaluation of the configurational partition function. An exacting semiempirical approach (the empiricism of which should not depend upon detonation data per se) would employ experimental data from kinetic theory, solid state physics, etc. From the above the form of the partition function is obtainable in principle, but not without considerable difficulty.

Somewhat simplified models may be assumed however, and some of these lead to a prediction of the detonation velocity with considerable accuracy. Thus the Abel equation of state can be derived from the hard-sphere model of a gas; this equation is most successful at low loading densities. However, the correct results for detonation velocities are obtained only if the size of the hard spheres is made dependent upon the initial loading density of the explosive.

The Andersen-Parlin equation of state is derived from a solid state, harmonic-oscillator model, the frequency of which increases as the -nth power of the volume. This equation is successful in the high-loading density region with reasonable values of n. However, n must be made to depend upon the initial loading density in order to predict detonation velocities.

In this region of high loading densities, there is doubtless an advantage in comparing the CJ products to a solid. Certainly the thermal motion of a given molecule will be a periodic vibration within a small confinement space, and not a translation along a path of uniform potential (which latter assumption leads both to the perfect gas and the Abel equations of state). As the loading density is greatly decreased, however, the perfect gas law must certainly eventually become applicable.

In this paper a simplified model of a vibrating solid leads to a partition function, from which the equation of state is derived. In this partition function are three fundamental parameters. At very low specific volumes the only important forces are repulsive, and the value of one parameter is determined by the exponent of the repulsive term in a Lennard-Jones

type of potential equation. The condition that the perfect gas equation of state is adequate at large specific volumes fixes the second parameter. The obvious condition that the repulsive and attractive forces must equilibrate at some density fixes the last of these parameters. The partition function that we intend to use is, as in the previous discussion, that of a harmonic oscillator model. At high temperatures the oscillators are classically excited, and the partition function goes over into the form:

$$f = \left(\frac{kT}{h\nu}\right)^{3N} \cdot e^{\varepsilon/kT}$$

$$\varepsilon = \varepsilon(V) \ , \ \nu = \nu(V). \qquad (1)$$

The Einstein vibrational frequency is made to depend upon the volume, and this dependence is chosen such that the perfect gas law results at high volumes. Since it has been the object to choose a highly simplified partition function, there are a number of shortcomings which must be corrected for in a more elaborate theory. It is proposed to discuss these now:

i) At low volumes and high temperatures, an anharmonic correction may add important terms to Eq. 1. The potential energy of a vibrating molecule is usually expanded in a power series about the point of minimum energy. Only the quadratic term is retained for low amplitude vibrations, and this term leads to the factor kT/hν of Eq. 1. In the high temperature region, the higher order terms of the expansion should be kept (because of the large average amplitudes) and the configurational integral re-evaluated.

ii) Although the frequency, ν, depends upon volume in such a way that the perfect gas law results at large volumes, the partition function above is obviously not correct at the higher volumes. It is important to note that Eq. 1 predicts a specific heat of k for every degree of freedom for all volumes. At large volumes many degrees of freedom will actually be translational and rotational and thus will contribute only 1/2 k to the specific heat At intermediate volumes, some intermediate specific heat will result. Because of this dependence of specific heat upon volume, the temperature dependence predicted by Eq. 1 will necessarily be unreliable.

iii) The equation of state at low volumes is that obtained by assuming repulsion energy between atoms that varies as some inverse power of the distance between the atoms, where this power is probably something of the order of from nine to twelve. On the other hand, the equation of state at high volumes is just that of a perfect gas. The region between these extremes is joined smoothly but in a somewhat arbitrary way. There is not a

definite, well established model used for this "imperfect gas" region. Among other factors is the communal entropy contribution, which would increase from zero to R as the volume increases. The proper correction would add this contribution in the region in which the non-localization of molecules becomes important, but the partition function would otherwise be unaffected.

That these and other difficulties exist is a primary reason for the difficulty experienced in predicting detonation parameters on a purely theoretical basis. It is likely that all of the corrections demanded by the remarks above would be insurmountably difficult to formulate at the present time, and it is equally probable that any such formalism would be so cumbersome that it would demand extremely laborious methods to solve for final detonation properties. Thus we propose Eq. 1 for its simplicity, and it is of interest that both the detonation velocity and its dependence upon loading density are found to be predictable within reasonable limits without the use of detonation data as such.

THEORY

In the following discussion we will use as the partition function Eq. 1, for the species characteristic of the CJ plane or surface. The equation of state and the thermal equation which follow from this partition function are then given as

$$p = kT\left(\frac{\partial \ln F}{\partial V}\right)_T = -3RT\ \frac{d \ln v}{dV} - \frac{d\varepsilon}{dV} \qquad (2)$$

$$E = kT^2\left(\frac{\partial \ln F}{\partial T}\right)_V = 3RT + \varepsilon(v) \qquad (3)$$

As usual we assume the customary hydrodynamic-thermodynamic conditions: the thermodynamic properties of the system are determined by the partition function above. The nature of the thermodynamic quantity $(E-E_0)$ in the Hugoniot equation,

$$E - E_0 = \tfrac{1}{2} p\ (V_0 - V) \qquad (4)^*$$

must be discussed from the point of view of the particular model chosen. Since energy is a property of a system's state, and is independent of the path through the reaction zone, the energy difference in Eq. 4 will be a function of the initial state and the Chapman-Jouguet state of the explosive, and we may choose any convenient path between these. We have considered the final state as a lattice structure with each atom confined by its neighbors to a certain small region in which it may move. The composition of a substance is usually described by stating the number of atoms of a particular type that are bonded to each of the other types of atoms. (thus the composition is specified when we know how many oxygen atoms are free, and how many are bonded to another oxygen atom, how many to a carbon to form CO, etc.). In the case of a lattice

* We neglect $p_0$ in comparison with p, as we deal only with condensed explosives.

structure, the composition is determined by the number and type of nearest (to a first approximation) neighbors for any representative atom. In both cases the composition is determined by temperature and volume. In particular, at high temperatures a given atom may roam to a position of higher energy with a corresponding increase of entropy. Thus with a free gas as a model, a certain atom will be found dissociated for a fraction of the time. At very high temperatures there will be a large concentration of free atoms. The lattice model is exactly analogous: at high temperatures an atom may be found in a lattice site of high energy (perhaps surrounded by atoms whose valenses are completely saturated). No matter what its position, the atom will still undergo periodic vibrations around a point of minimum energy.

The composition that we are interested in is that appropriate to the final CJ temperature and volume. Now let the following process take place: the initial explosive is transformed into the CJ composition at constant volume and temperature. The energy of the CJ composition is an amount $\Delta Q$ below the energy of the initial explosive; thus an amount of energy $\Delta Q$ is released in this process. We write

$$E_o - E_i = \Delta Q \qquad (5)$$

where $E_i$ is the energy of the CJ composition at the initial temperature and density. Next the substance is compressed and heated to the final CJ temperature and volume. This brings us to the final state of energy, E. Equations 4 and 5 can be combined to eliminate $E_o$:

$$E - E_i = \Delta Q + p(V_c - V) \qquad (6)$$

Inasmuch as the CJ composition depends upon the CJ volume and temperature, and the CJ volume and temperature depend upon $\Delta Q$, and $\Delta Q$ depends upon final composition, normally one requires iterative methods to obtain any of these variables. Of course they will depend upon initial density, temperature, etc., as well. Application of such methods using imperfect gas model seems to indicate, however, that $\Delta Q$ varies only a few per cent with rather wide changes in loading density, in most cases. As a first approximation, we will therefore assume in the following $\Delta Q$ is constant for a given explosive.

From Eqs. 3 and 6 we obtain

$$3R(T - T_o) + \varepsilon - \varepsilon_o = \Delta Q + p(V_o - V) \qquad (6)$$

since $T_i = T_o$ and $\varepsilon_o(V_o) = \varepsilon_o(V_i)$. The equation of state Eq. 2, can be arranged into the form,

$$3RT = A + Bp$$

$$A(V) = -(d\varepsilon/dV)(dV/d \ln v), \quad B(V) = -(dV/d \ln v) \qquad (8)$$

from Eqs. 7 and 8, solving for the pressure, we obtain:

$$p = \frac{\Phi - \Psi(v)}{\left[\frac{1}{2}(V-V_0)+B\right]}$$

$$\Phi = \Delta Q + \tfrac{3}{2}RT_0 + \epsilon_0, \Psi = A + \epsilon \qquad (9)$$

This can be combined with the equations of momentum and matter conservation in the usual way and lead to the following expression for the detonation velocity:

$$D^2 = \frac{\Phi - \Psi(v)}{\Theta(V)}$$

$$\Theta = \left(1 - \frac{V}{V_0}\right)\left(\frac{B}{V_0} - \frac{1}{2} + \frac{1}{2}\frac{V}{V_0}\right) \qquad (10)$$

Now there is a value of the variable v such that the detonation velocity is a minimum, and for which the actual detonation velocity is given. This is a form of the Chapman-Jouget condition, and is the most convenient way to determine the stable detonation velocity from our equations. For certain combinations of the functions $B(V)$, $\epsilon(V)$ and $A(V)$, the detonation volume and velocity can be easily determined, but these rather special situations will not be discussed now. Suffice it to say that if $\epsilon(V)$ is taken proportional to $\gamma(V)$, the function $\Psi(V)$ must vanish and the resulting algebra is greatly simplified.

Taking $\gamma = aV^{-n}$ and consequently $\epsilon = (3/2)NahV^{-n}$, it has already been shown[8] that one is led to the result

$$D^2 = n(n+2)\Phi \qquad (11)$$

and

$$V = (n+2)/(n+1) \cdot V_c \qquad (12)$$

We now consider the general case, using the equation of state given in Eq. 2. The detonation velocity will depend upon the initial loading density according as the average frequency depends upon the volume V. The latter dependence we take as

$$\nu = (a/V^m) + (b/V^n) \qquad (13)$$

for the following reasons. If the detonation products were compressed from some greater volume the molecular vibrational frequency would at first depend very little upon the volume. At a volume $V^*$, the specific volume of the molecules (without void space) a given atom will be in "contact" position with its neighbors. At a volume slightly smaller than $V^*$ the rapidly mounting repulsive forces will determine the nature of each atom's motion. With increase of repulsion, there is an increase of force constant, and of average vibrational frequency.

The pressure of a confined substance is the outwardly directed momentum transferred to a unit of area per unit time. At high specific volumes, when groups of atoms tend to have an independent existence, the interatomic vibrations are not important in determining the pressure, since these vibrations tend to cancel out in the average, as regards their contribution to a directed

momentum. In this region of densities, translations are all-important: a translating group transfers net outwardly-directed momentum to its neighboring molecules. As soon as the C-J products are confined to a volume less than $V^*$, however, all degrees of freedom are vibrational, and since the important forces are repulsive there will be a net outward momentum transfer. Another way of stating the same principle is to remark that molecular rotations tend to disapear at about the same time that molecular translations do, namely when molecular identities become submerged into a general lattice. Since frequency is an inverse function of volume (cf. Eq. 13 above), pressure likewise will be an inverse function, as will be shown when we write the equation of state.

It has been shown previously[8] that if the potential energy between atoms depends upon the distance separating them as an inverse power, $c/r^a$, the low amplitude (harmonic) frequency depends upon volume as $c'/V^{(a+2)/6}$. The best fit to kinetic data is found for a value of the exponential parameter of a 12. Thus the larger exponential in Eq. 10 will be approximately m=7/3. To determine a value of n, we must examine the thermal equation. It may be mentioned that if every atom acted as a free translator at high volumes $\nu$ could be considered as the number of collisions with a containing wall, and would be proportional to the reciprocal of the translation length, or the reciprocal one-third power of volume. In that case, our value of n would equal 1/3.

Before writing the equation of state we will determine the values of a and b. When $V=V^*$, the vibrational frequency $\nu^*$ will be something like a normal solid vibrational frequency which may be assumed to be known. Since at volumes less than $V^*$ the first term on the right of Eq. 10 will be important, and for greater volumes the second term will predominate, we will let these terms equal one another at $V=V^*$. These conditions determine a and b:

$$a = \nu^* V^{*m}/2, \qquad b = \nu^* V^{*n} \tag{14}$$

As a close approximation to $\nu^*$ and $V^*$, we will let these be the Einstein vibrational frequency and the specific volume of the undetonated crystal explosive, respectively.

Defining $y = V/V^*$ as the reduced volume, Eq. 13 becomes

$$\nu = \nu^* V^{*m}/yV^{*m} + \nu^* V^{*n}/yV^{*n} = \frac{\nu^*}{2y^m}\left(1 + y^{m-n}\right) \tag{15}$$

The equation of state, Eq. 2, becomes

$$p = -(3RT/V^*)\frac{d\ln\nu}{dy} - (1/V^*)\frac{d\varepsilon}{dy}$$
$$\frac{d\ln\nu}{dV} = -\frac{1}{V^* y}\cdot\frac{m + ny^{m-n}}{1 + y^{m-n}} \tag{16}$$
$$\frac{d\varepsilon}{dV} = -\frac{Ch\nu_*}{2V_* y^{m+1}}\left(m + ny^{m-n}\right)$$

The last equation is the result of assuming the proportionality,

$$\epsilon(V) = Nch\,\nu(V) \tag{17}$$

Finally, the equation of state is written in terms of the compressibility:

$$pV/RT = \frac{c}{2y^m}\left(\frac{h\nu^*}{RT}\right)(m+ny^{m-n}) + \frac{3(m+ny^{m-n})}{1+y^{m-n}} \tag{18}$$

At very large volumes, Eq. 15 becomes

$$pV/RT = 3m \tag{19}$$

In this region the ideal gas law approximately holds and we have

$$pV/R'T = 1, \tag{20}$$

where $R' = N'k$ and $R = Nk$, and

$N'$ = number of translating groups per gram at low density, and
$N$ = number of atoms per gram of explosive.

If the arbitrary decomposition scheme used previously[8] is followed to obtain the number of translating groups (molecules) divided by the number of atoms, an average fraction equal to $N'/N$ 0.457 is obtained and hence $n = N'/3N = 0.152$. If $N'$ equaled $N$ then, as shown previously, $n$ would be 1/3.

As a final result of using the frequency dependence of Eq. 15, we substitute it into the detonation equation, Eq. 10. Defining $g$ as $V/V_0$ whence $gy = V/V_0$, and using the definition of $B(y)$ one obtains the result

$$D^2 = \frac{2\phi}{(1-gy)\left[gy(2f(y)+1)-1\right]} \tag{21}$$

where

$$f(y) = \frac{1+y^{m-n}}{m+ny^{m-n}} \tag{22}$$

To find the hydrodynamic velocity, we differentiate and set the derivative of the detonation velocity with respect to the volume equal to zero. This gives

$$\frac{dD}{dy} = -\frac{\phi}{2D\theta^2}\frac{d\theta}{dy} = 0 \tag{23}$$

The quantities $\phi$, D and $\theta(y)$ must be finite if the detonation velocity is to be finite so that we must have

$$\frac{d\theta}{dy} = 0$$

$$= \frac{(1-2g\gamma)(1+\gamma^{m-n})}{m+n\gamma^{m-n}} + \frac{(1-g\gamma)(m-n)\gamma^{m-n}}{(m+n\gamma^{m-n})^2} + (1-g\gamma) \qquad (24)'$$

Since we have fixed the values of m and n, the reduced volume y depends only upon the reduced loading density, g. For a given value of g, Eq. 24 is solved by graphical methods to obtain a value of y. Values of gy as a function of g are given in Fig. 1.

Values of D are obtained from Eq. 21 when a value of $\phi$ is known. $\phi$ depends upon $\epsilon_o$ and thus on the value of c of Eq. 17. We shall rather arbitrarily give c the value of ½ so that $\epsilon(V)$ is the zero-point vibrational energy. This latter could be made larger to correspond to a higher potential energy at low volumes but the average potential energy is a function of temperature as well as volume; hence this procedure would not be consistent with the model demanded by the partition function itself and the results would be doubtful value. It has been shown that none of the CJ properties would be changed more than about five per cent by changing c from zero to one half. Thus a new condition is introduced that will simplify the calculations of all of the CJ properties. To facilitate this procedure we abreviate Eq. 9

$$\phi = \Delta Q + 3RT_o + \epsilon_o = \gamma + \epsilon_o \qquad (25)$$

and then assume that $\epsilon^*$, the vibrational zero point energy at y=1 is equal to

$$\epsilon^* = K\gamma \qquad (26)$$

where K is a constant, equal for all explosives. If K is set equal to 0.1, c equal to ½ and N, the number of atoms per gram equal to $6.03 \times 10^{22}$, then $\nu^* = 2.73 \times 10^{13}$ ($\omega = 910$) when $\gamma$ is taken to be 1300 cal/g. The values of $\gamma$ and $\nu^*$ are about what one might expect for an average explosive. Now by combining Eqs. 14, 22, and 23, we obtain the important result

$$\phi = \gamma\left(1 + K\frac{\gamma_2}{\gamma_{\infty}}\right) \qquad (27)$$

Every property of the CJ surface depends in some way upon parameters which characterize the explosive and upon the initial conditions. The parameters that we consider to be important are $\Delta Q$, N and $V^*$ (properties of the explosive) and $T_o$ and $V_o$ (initial thermodynamic conditions). The quantities m, n and K are assumed to be approximately independent of explosive type and of the initial conditions, and $p_o$ is neglected. The parameter g, of course, is a useful combination of $V_o$ and $V^*$. Now if a particular quantity is dependent upon a number of these parameters, such parameters will be designated in parentheses after the quantities symbol. Thus in Eq. 24, $\gamma \equiv \gamma(Q, T_o, N)$. The quantity $\theta$, which before has

been explicitly designated as a function of the variable y, will now be considered as a function of g alone, since y is determined as a function of g through Eq. 24. Two other quantities along with their parametric dependence are now defined.

$$F(g) = \left(1 + k\frac{\gamma}{\gamma_0}\right) \tag{28a}$$

$$\sigma(g) = \frac{(1-g\gamma)g}{\theta(g)} \tag{28b}$$

We now examine the dependence of detonation velocity upon these parameters. From Eq. 21 we obtain

$$D^2 = \phi(\Delta Q, N, T_0, g)\,\theta(g)$$
$$= \gamma(\Delta Q, N, T_0)\,F(g)\,\theta(g) \tag{29}$$

The reduced detonation velocity becomes

$$\left(\frac{D}{\bar{D}}\right)^2 = \frac{F(g)\bar{\theta}}{\theta(g)\bar{F}} = \delta^2(g) \tag{30}$$

where $\bar{D}$ (and all other barred quantities) refers to the resulting value of that variable when $g = 1$. The reduced detonation velocity is seen to be a function of the reduced loading density only. The value of $\bar{D}$ is, of course,

$$\bar{D}^2 = \gamma(\Delta Q, N, T_0)\frac{\bar{F}}{\bar{\sigma}} = \bar{D}^2(\Delta Q, N, T_0) \tag{31}$$

Equation 30 specifies a universal detonation curve (against loading density reduced by the parameter $V^*$) independent of the nature of the explosive or the initial conditions. It was to obtain the result, Eq. 30, that the condition Eq 26 was introduced.

The pressure is a detonation property amenable to similar treatment. Solution of the hydrodynamic-thermodynamic equations leads to the expression,

$$P = \frac{\gamma(\Delta Q, T_0, N)F(g)\sigma(g)}{V^*} \tag{32}$$

$$\frac{P}{\bar{P}} = \frac{F(g)\sigma(g)}{\bar{F}\,\bar{\sigma}} = \pi(g) \tag{33}$$

$$\bar{P} = \frac{\gamma(\Delta Q, T_0, N)\bar{F}\,\bar{\sigma}}{V^*} = \bar{P}(\Delta Q, T_0, N, V^*) \tag{34}$$

Substituting into the equation of state, Eq. 8, and using Eqs. 15 and 17 we get an expression for temperature,

$$T = (pV - e)/3R \tag{35}$$

but, from Eq. 32, we must have

$$pV = \frac{V\phi\sigma}{V^*} = y\phi\sigma \tag{36}$$

Also, from Eqs. 17 and 26,

$$e = \frac{v}{v^*} K\gamma \tag{37}$$

whence, finally, we obtain for the temperature the expression,

$$T = \frac{\gamma(\Delta Q, T_0, N)}{3NR}\left[\gamma(g) f(g)\sigma(g) - K\gamma\frac{v}{v^*}\right] \tag{38}$$

or, in reduced form,

$$\frac{T}{\bar{T}} = \frac{\left[\gamma(g) f(g)\sigma(g) - K\gamma(g)/v^*\right]}{\left[\bar{\gamma}\bar{f}\bar{\sigma} - K\bar{\gamma}/v^*\right]} = \tau(g) \tag{39}$$

where

$$\bar{T} = \frac{\gamma(\Delta Q, N, T_0)}{3NR}\left[\bar{\gamma}\bar{f}\bar{\sigma} - K\bar{\gamma}/v^*\right] \tag{40}$$

Volume could be treated just as detonation velocity, pressure and temperature, but it is more convenient to express gy as a function of g, (since gy does dot differ from unity by a large amount at any value of g, while the reduced volume goes to infinity as g approaches zero). Likewise, the material velocity, W, can be treated as those above: the pertinent equations follow.

$$\left(\frac{W}{\bar{W}}\right)^2 = \frac{F(g)\,\theta(g)\left[1 - g\gamma(g)\right]}{\bar{F}\,\bar{\theta}\,(1 - g\bar{\gamma})} = \omega^2(g) \tag{41}$$

$$\bar{W}^2 = \gamma(\Delta Q, N, T_0)\,\bar{F}\,\bar{\theta}(1 - g\bar{\gamma}) \tag{42}$$

The above treatment leads to the formulation of universal loading density curves for all detonation properties. We do not imply that our particular dependence upon loading density provides the best possible reduced curves (since we have fitted no parameters), nor does it imply that such curves are a rigorous consequence of detonation theory. However it is shown that to a good approximation such curves can be derived. A more exact dependence on loading density can be obtained by considering m , n, $V^*$, and K as free parameters, rather than as quantities previously determined from physical data.

RESULTS

Figures 2 and 3 give a representation of the various detonation properties discussed above as functions of the quantity g, which is essentially the loading density. It will be noticed from Figure 2 that the detonation velocity according to this treatment is essentially linear in low g density over a wide range of the latter. The pressure increases fairly rapidly with density as is the case in most treatments. The temperature appears nearly independent of density in the high density region, but is an increasing function over most of the range. The fall in temperature at low values of g probably occurs in a region of density in which the theory is not applicable, for reasons discussed above.

The equation of state and the consequent detonation properties depend upon the quantities m, n, $V^*$ and K. The detonation velocity is sensitive to these quantities to the following approximate extent. Increasing m by unity, in the range in which we are working increases D by about thirty per cent. The reduced detonation velocity of g = .5 will decrease by about sever per cent (thus a change in m affects the magnitude of the detonation velocity more strongly than it does the shape of the detonation curve). An increase in n by one-tenth increases D by about one to two per cent, and increases $\delta$ at g = .5 by about 3 or 4 per cent. A given increase in $V^*$ causes about the same percentage decrease in D at any velocity. Of course the ratio of A to D at g = ½ . remains unchanged. It has been previously mentioned that K does not affect the detonation velocity strongly in the region of interest.

Calculations have been made for the following five explosives - - TNT, tetryl, picric acid, PETN, and RDX. The results of the calculations are shown in Table I. The difference between theory and experiment amounts to about 13 per cent as an average for all compounds. The agreement is seen to be particularly satisfactory for RDX and PETN. The oxygen negative compounds especially TNT, lead to a predicted detonation velocity much too high. This is a consequence of the choice of $\Delta Q_v$ which was taken as the high density value 1296 cal/gm in the case of TNT[4].

In Figure 4 are plotted the experimental points for velocity over a wide range of loading density for PETN. It is seen that the calculated values run generally above the experimental velocities at high loading densities. However if the density, $\rho^*$, is taken to be 2.00, instead of the crystal density 1.77, the agreement is found to be good at all loading densities. Likewise, calculated velocities for other explosives agree quite closely with experimental values when $P^*$ is taken as slightly larger than the crystal density (except for RDX, for which the crystal density appears to be a very good approximation to $P^*$). The value of $P^* = 2$ was selected for PETN in such a way that the linear D vs. $P_o$ equation: $D = D(P_o - 1) + M(P_o - 1)$, passed through the point $\delta = 1$, $\alpha = 1$. For PETN, $D(P_o - 1) = 5620$, and $M = 5500$[1]. This

straight line is also shown in Figure 4.

Table II presents a comparison of several well known treatments of the detonation process with that of this paper, using the pressure as a typical variable. It will be noted that in general the present treatment and that of Ref.(8) give somewhat higher pressure values at high densities, falling off somewhat at the lower densities. However, Cottrell and Patterson as well as Jones also tend to calculate rather higher pressures than are obtained from the conventional thermodynamic treatment.

Finally it may be mentioned that $\gamma$, $V^*$, and N must be known to obtain $\overline{D}$, $\overline{P}$, $\overline{T}$, and $\overline{W}$. The numerical values that we have obtained are $\overline{D} = 3.53\sqrt{\gamma}$, $\overline{P}\,V^* = 2.91$, $3\overline{RT} = 1.16\gamma$, and $\overline{W} = .826\sqrt{\gamma}$.

TABLE I

The calculated and observed (ρ) detonation velocities of Picric acid, PETN, TNT, tetryl, and RDX. (m/sec)

| EXPLOSIVE | ρ | D(calc) | D(obs) |
|---|---|---|---|
| Picric Acid | 1.50 | 7970 | 6900 |
| | 1.00 | 6090 | 5100 |
| D = 8710 | .50 | 3700 | 3350 |
| PETN | 1.50 | 8290 | 7600 |
| | 1.00 | 6360 | 5500 |
| D = 9100 | .50 | 3850 | 3850 |
| TNT | 1.50 | 8320 | 6700 |
| | 1.00 | 6430 | 4900 |
| D = 8760 | .50 | 3900 | 3200 |
| Tetryl | 1.50 | 8350 | 7300 |
| | 1.00 | 6420 | 5500 |
| D = 9040 | .50 | 3890 | 3850 |
| RDX | 1.60 | 8080 | 8042 |
| | 1.20 | 6750 | 6614 |
| D = 8760 | .80 | 5050 | 5186 |

TABLE II

Chapman-Jouguet Pressure for PETN obtained by present Theory compared with that of Jones ( 3 ), Cook ( 1 ), Brinkley and Wilson ( 2 ), Cottrell and Patterson ( 7 ), Anderson and Parlin ( 8 ), and Kihara and Hikita ( 6 ).

$P \times 10^{-3}$ atm.

| P | This Paper | Jones | Cook | B-W | C-P | A-P | K-H |
|---|---|---|---|---|---|---|---|
| 1.727 | 286 | | | | 285 | | |
| 1.69 | 273 | | 255 | | | | |
| 1.6 | 243 | | 225 | 218 | | 282 | 239 |
| 1.5 | 210 | | | | | | |
| 1.4 | 179 | | | | 186 | | |
| 1.25 | 139 | 136 | | | | | 131 |
| 1.2 | 126 | | 125 | 117 | | 155 | 118 |
| 1.15 | 114 | 114 | | | | | |
| 1.0 | 82 | 86 | 85 | 83 | 88 | | 83 |
| .85 | 52 | 62 | | | | | |
| .8 | 50 | | | | | 68 | |
| .75 | 42 | 50 | | | 53 | | 47 |
| .65 | 31 | 39 | | | | | |
| .50 | 18 | 25 | | | | | |
| .40 | 11 | | | | 19 | | |
| .35 | 9 | 15 | | | | | |
| .25 | 5 | 10 | | | | | |

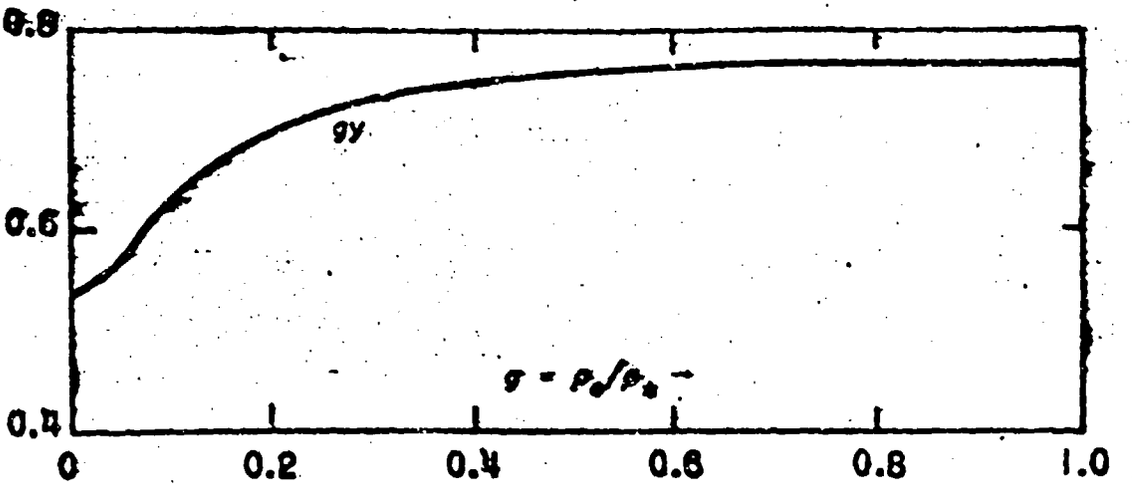


FIGURE 1

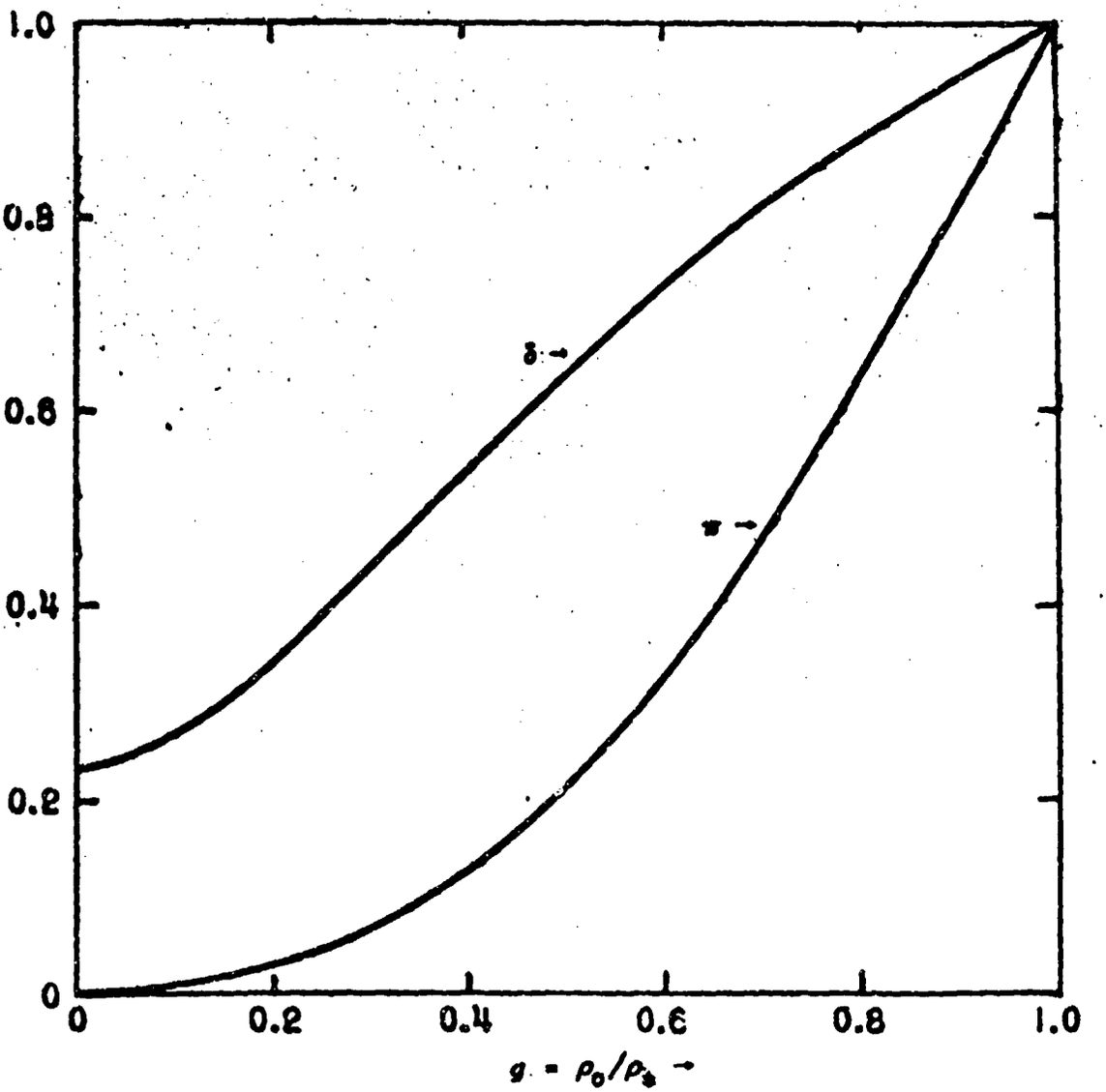


FIGURE 2

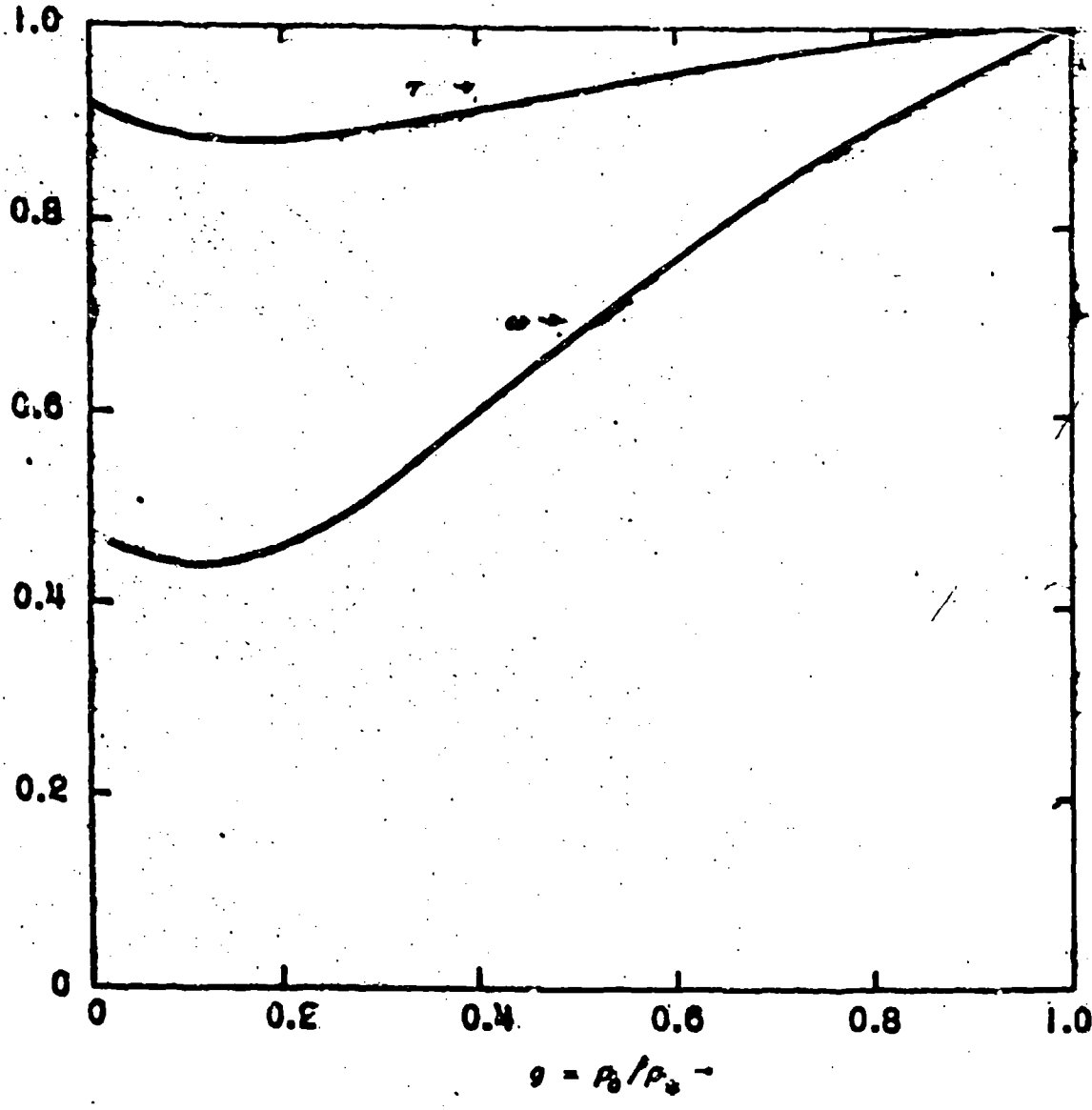


FIGURE 3

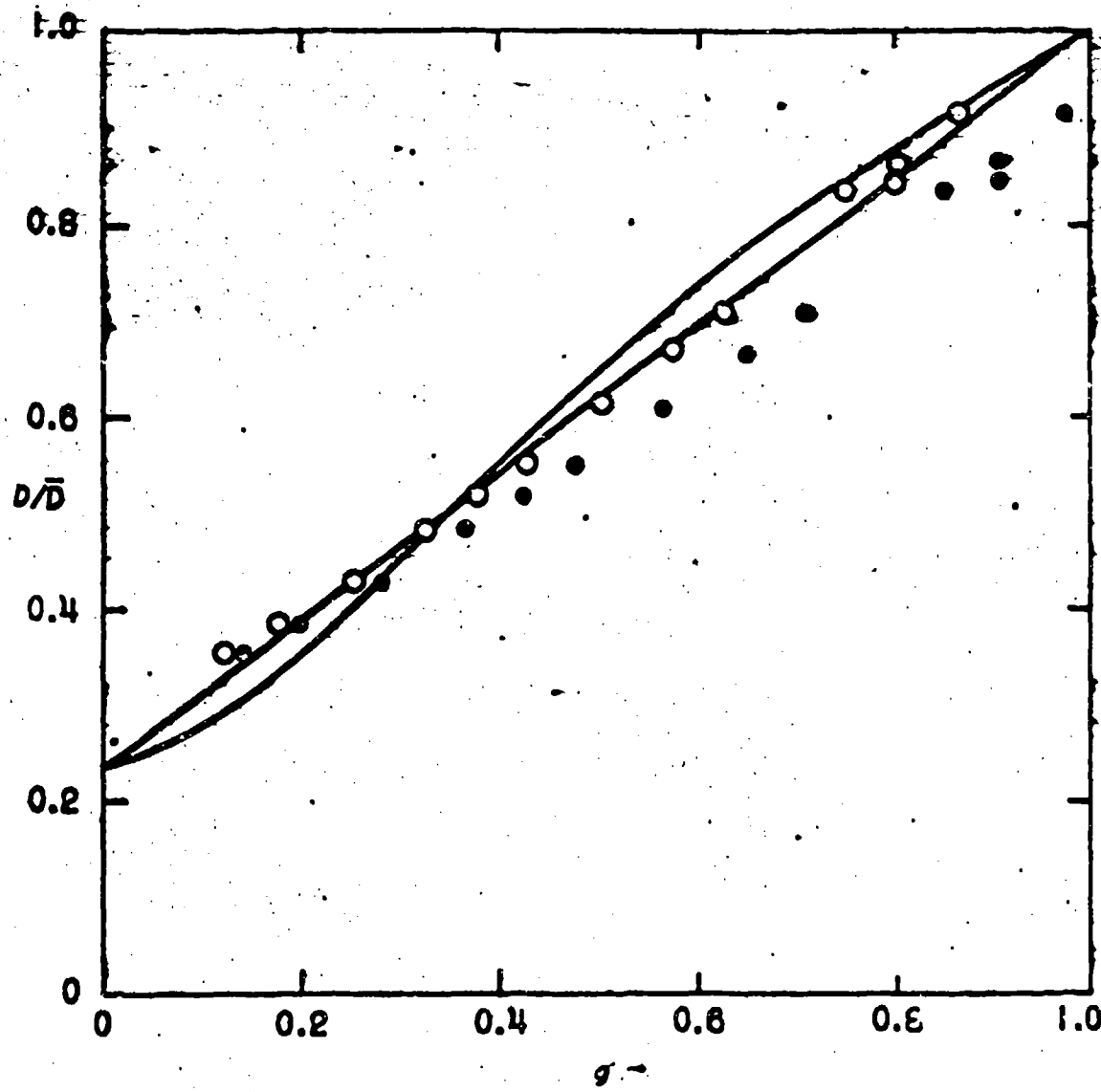


FIGURE 4

THE REDUCED DETONATION VELOCITY OF PETN.

● EXPERIMENTAL POINTS WITH $\rho^o$ = 1.77

○ EXPERIMENTAL POINTS WITH $\rho^o$ = 2.00

## BIBLIOGRAPHY

1. Cook, M. A., J. Chem. Phys., 15, 518 (1947).

2. Kistiakowsky, G. B., and Wilson, E. B., O SRD Report 114 (1941).

3. Jones, H., Third Symposium on Combustion and Flame and Explosion Phenomena, p. 590, (Williams and Wilkins Co., Baltimore, 1949).

4. Taylor, J., Detonation in Condensed Explosives, (Oxford University Press, London, 1952).

5. Jones, H., 1941. See Cole, R. H., Underwater Explosions, p. 81, (Princeton Univ. Press, 1948).

6. Kihara, T. and Kikita, T., Fourth Symposium on Combustion, Flame and Explosion Phenomena, (Williams and Wilkins Co., Baltimore, 1949)

7. Cottrell, T. L., and Paterson, S., Proc. Roy. Soc. A213, 214 (1952).

8. Anderson, W. H., and Parlin, R. B., Technical Report 28, Institute for the Study of Rate Processes, University of Utah, Salt Lake City, Utah, (1953).

# DIAMETER EFFECT IN CONDENSED EXPLOSIVES. THE RELATION BETWEEN VELOCITY AND RADIUS OF CURVATURE OF THE DETONATION WAVE 20

William W. Wood
Los Alamos Scientific Laboratory
Los Alamos, New Mexico

and

John G. Kirkwood
Sterling Chemical Laboratory
Yale University
New Haven, Connecticut

## ARSTRACT

The limiting slope of the detonation velocity-wave front curvature locus for small velocity deficits is obtained under an assumption concerning the "reaction zone length" as related to the charge diameter and the radius of curvature of the wave front. The model is an extension to two dimensions of von Neumann's classical theory of the plane wave detonation.

## I

The relationship between the velocity with which a detonation wave propagates axially along a cylindrical charge and the finite radius of the charge has been studied theoretically by Eyring, Powell, Duffey and Parlin[1] and by Jones[2]. Our objective in the present work is somewhat different, namely, to give an account of the relation between velocity and radius of curvature of the wave front, rather than the charge radius. It happens that it is possible to derive such a relation under considerably more straightforward assumptions than have been needed by the investigators mentioned. The theory of Eyring, et al, is commonly called the curved front theory; the present work is closely related to it in many of its details, although the basic model, as well as the

objective, is considerably different. In the following we will use certain results from the preceding paper on the structure of the steady-state plane detonation wave, which we shall abbreviate as SSPD.

## II

Our model is once again a compressible, non-dissipative, adiabatic, reactive medium into which a detonation wave is propagating in steady-state. Here, however, the medium is a cylinder of indefinite length, but finite radius. We introduce a system of cylindrical coordinates with z-axis along the charge axis in the direction of propagation, and with r denoting the radial distance from this axis. The origin of z is conveniently taken as the position of the intersection of the wave front and z axis at time t = o. We assume cylindrical symmetry throughout, so that none of the variables depend on azimuthal angle, and all velocities lie in planes containing the z-axis. Under these conditions the equations of hydrodynamics, including the first law and the reaction rate law, become

$$\frac{d\rho}{dt} + \rho\left(\frac{\partial u}{\partial z} + \frac{\partial w}{\partial r}\right) + \rho\,\frac{w}{r} = 0, \tag{1a}$$

$$\rho\,\frac{du}{dt} + \frac{\partial p}{\partial z} = 0, \tag{1b}$$

$$\rho\,\frac{dw}{dt} + \frac{\partial p}{\partial r} = 0, \tag{1c}$$

$$\frac{dE}{dt} + p\,\frac{dv}{dt} = 0, \tag{1d}$$

$$\frac{d\lambda}{dt} = R, \tag{1e}$$

$$\frac{d}{dt} = \frac{\partial}{\partial t} + u\,\frac{\partial}{\partial z} + w\,\frac{\partial}{\partial r}. \tag{1f}$$

The notation is the same as in SSPD, except that u now denotes the axial component of mass velocity, $\omega$ the radial component, and R the rate function. For simplicity in notation we consider here the case of a single reaction; there is no difficulty in extending the argument to the case of several reactions.

As in SSPD we suppose the reaction zone to be preceded by a (curved) shock, across which we apply the (vector) Rankine-Hugoniot conditions. We assume the medium ahead of the detonation front to be at rest. With $\underset{\sim}{D}$ denoting the detonation velocity along the z-axis, $\underset{\sim}{U}$ the vector mass velocity at any point on the back side of the shock, $\underset{\sim}{n}$ the unit normal to the shock at the same point drawn in the forward direction, $\underset{\sim}{\ell}$ any unit vector perpendicular to $\underset{\sim}{n}$, variables behind the shock by unsubscripted symbols, and zero subscripts for values in the medium ahead of the shock, the Rankine-Hugoniot conditions are

$$\rho(\underset{\sim}{D}-\underset{\sim}{U})\cdot\underset{\sim}{n} = \rho_0 \underset{\sim}{D}\cdot\underset{\sim}{n}, \tag{2a}$$

$$(p-p_0)/(v_0-v) = \rho_0^2 D^2, \tag{2b}$$

$$E-E_0 = \tfrac{1}{2}(p+p_0)(v_0-v), \tag{2c}$$

$$\underset{\sim}{U}\cdot\underset{\sim}{\ell} = 0, \tag{2d}$$

$$\lambda = 0. \tag{2e}$$

For any assumed initial shape and velocity for the leading shock the preceding equations determine the state immediately behind the shock. Thereafter the differential equations (1, coupled with the jump conditions determine the flow, which would not be steady in general. Our next step is to ascertain what shock front shapes and detonation velocities are compatible with the steady-state assumption. According to the latter, the flow region behind the shock should be steady when viewed

from a coordinate system moving with velocity $D$. Introducing such a coordinate system by the transformatio

$$\xi = Dt - x, \tag{3}$$

$\xi$ being the axial distance measured backwards from the shock, and putting derivatives with respect to t at constant $\xi$ and r equal to zero, we obtain

$$(D-u)\rho_\xi - \rho u_\xi + \omega \rho_r + \rho(\omega_r + \omega/r) = 0, \tag{4a}$$

$$\rho(D-u)u_\xi - p_\xi + \rho\omega u_r = 0, \tag{4b}$$

$$\rho(D-u)\omega_\xi + p_r + \rho\omega\omega_\xi = 0, \tag{4c}$$

$$\frac{dE}{dt} + p\frac{dV}{dt} = 0 \tag{4d}$$

$$\frac{d\lambda}{dt} = R, \tag{4e}$$

$$\frac{d}{dt} = (D-u)\frac{\partial}{\partial\xi} + \omega\frac{\partial}{\partial r}; \tag{4f}$$

$$u_\xi = \left(\frac{\partial u}{\partial \xi}\right)_r, \quad u_r = \left(\frac{\partial u}{\partial r}\right)_\xi, \text{ etc.}$$

To eliminate the derivatives of $\rho$ from these equations we use equation (9 from SSPD,

$$\frac{d\rho}{dt} = \frac{1}{c_0^2}\frac{dp}{dt} - \sigma\rho R, \tag{5}$$

where the thermodynamic parameter $\sigma$ is defined in SSPD, equations (10a. Use of (5 in (4 then gives

$$-\rho c_0^2 u_z + (D-u) p_z = \rho c_0^2 \phi, \tag{6a}$$

$$\phi = \sigma R - \omega_r - \frac{\omega_z}{\rho c_0^2} p_r - \omega/r, \tag{6b}$$

$$\rho (D-u) u_z - p_z = -\rho \omega u_r, \tag{6c}$$

$$(D-u)\, \omega_z + \omega\, \omega_r = -\frac{1}{\rho} p_r, \tag{6d}$$

$$(D-u)\, \dot{\lambda}_z + \omega \lambda_r = R, \tag{6e}$$

$$(D-u)(E_z + p V_z) + \omega (E_r + p V_r) = 0. \tag{6f}$$

## III

The explicit solution of the set of partial differential equations (6 would be an extremely difficult task. Here we follow a different procedure, and begin by specializing them to the axis.* From obvious conditions

---

*In the following we designate equations valid only on the axis with an asterisk.

---

of symmetry the radial component of velocity $\omega$ vanishes on the axis:

$$\omega (\xi, r = 0) = 0, \tag{7a*}$$

$$u(\xi, 0) = U(\xi, 0). \tag{7b*}$$

Equations (6 specialized to the axis give

$$-\rho c_0^2 U_\xi + (D-U)p_\xi = \rho c_0^2 (\sigma R - 2\omega_r), \tag{8a*}$$

$$\rho (D-U) U_\xi - p_\xi = 0, \tag{8b*}$$

$$p_r = 0, \tag{8c*}$$

$$(D-U)\lambda_\xi = R, \tag{8d*}$$

$$E_\xi + pV_\xi = 0, \tag{8e*}$$

where all variables are to be evaluated at any $\xi$ with $r = o$. Solving (8a and (8b as linear equations for $u_\xi$ and $p_\xi$ we obtain

$$u_\xi = -\frac{1}{\eta}(\sigma R - 2\omega_r), \tag{9a*}$$

$$p_\xi = -\frac{\rho(D-U)}{\eta}(\sigma R - 2\omega_r), \tag{9b*}$$

$$\eta = 1 - (D-u)^2/c_0^2. \tag{9c}$$

Since the flow behind a shock propagating in the direction normal to itself is subsonic (the curved shock in question clearly satisfying this condition because of symmetry), it is clear that $\eta\,(\xi = 0,\ r = 0) > 0$. Furthermore, it is clear that in steady state the flow behind the shock must be similar to that of Prandtl-Meyer steady state expansion, in which the flow becomes supersonic (see ref. 2). Consequently we expect $\eta$ to vanish at some point in the steady zone, and therefore the numerators in (9a and (9b must vanish at the same point. Thus we obtain a generalized "Chapman-Jouguet condition" for detonation in a finite stick:

$$D = u + c_0 \ , \tag{10a*}$$

$$\sigma R - 2\omega_r = 0 \tag{10b*}$$

This result is similar to that of Eyring, et al, equation B-12, which is attributed by them to Devonshire[3]. Equation (10b may be interpreted as relating the degree of reaction at the sonic point to the radial flow divergence at this point.

In the plane wave theory, the Rankine-Hugoniot relations are integrals of the differential equations of steady-state motion. We now proceed to derive analogous relations for the steady zone of the present theory, where, however, the flow divergence introduces certain correction terms.

For this purpose we return to equation (4a, specializing it to the axis, obtaining

$$(D-u)\rho_\xi - \rho u_\xi = -2\rho\omega_r . \tag{11*}$$

This may be integrated immediately, with use of the Rankine-Hugoniot condition (2a at $\xi = 0$ to give

$$\frac{\rho}{\rho_0}\left(1-\frac{u}{D}\right) = 1 - 2L(\xi) \ , \tag{12a*}$$

$$L(\xi) = \int_0^{\xi} \frac{\rho(\xi')}{\rho_a} \frac{\omega_r(\xi')}{D} d\xi' \qquad (12b^*$$

It will be noted immediately that this is the usual plane wave relation for mass conservation with the divergence perturbation given by (12b added.

In a similar way, (8b may be integrated with use of (12a and (2b to give**

$$p = \rho_0 DU \left\{ 1 - \varepsilon \int_0^{\xi} \left(1 - \frac{u(\xi')}{u(\xi)}\right) \frac{\rho(\xi')}{\rho_0} \frac{\omega_r(\xi')}{D} d\xi' \right\} . \qquad (13^*$$

---

**We have neglected $p_0$ in the customary fashion.

---

With neglect of terms in $\omega_r^2$, this may be reduced to

$$p = \rho_0 D^2 (1 - v/v_0) \left\{ 1 + \varepsilon \frac{v/v_0}{1 - v/v_0} \cdot \left( \varepsilon L(\xi) - \frac{\rho}{\rho_0} \Omega(\xi) \right) \right\} , \qquad (14a^*$$

$$\Omega(\xi) = \int_0^{\xi} \frac{\omega_r(\xi')}{D} d\xi' . \qquad (14b$$

We again obtain a plane wave relation with added perturbation. In similar fashion, equation (4d, specialized to steady-state flow on the axis, may be integrated to

$$E - E_0 - \tfrac{1}{2} p (v_0 - v) = D^2 \left\{ (1 + v/v_0) \Omega(\xi) - \varepsilon \frac{v}{v_0} L(\xi) \right\} , \qquad (15^*$$

again with neglect of terms in $\omega_r^2$. With the equation of state, (10a, (10b, (12a, (14a, and (15 constitute a sufficient number of equations to determine D and also the axial values of $p$ $U$, $\rho$, and $\lambda$ throughout the steady zone, providing we are able to determine $\omega_r(\xi)$. In the

following we designate the C-J point by $\xi = \xi^*$, which is determined by

$$\xi = \int_0^{\lambda} \frac{D-U(\lambda')}{R(\lambda')}\, d\lambda' \qquad (16^*$$

obtained from (8d.

IV

In order to determine $\omega_r(\xi)$ we first return to (6d, differentiate it with respect to r, and then specialize to the axis, obtaining

$$(D-U)\frac{\partial \omega_r}{\partial \xi} + \omega_r^2 = -V p_{rr} \,. \qquad (17^*$$

With neglect of $\omega_r^2$ and use of (12a this may be integrated to give

$$\omega_r(\xi) = \omega_r(0) - \frac{1}{\rho_0 D}\int_0^{\xi} p_{rr}(\xi')\, d\xi' \,. \qquad (18^*$$

The value of $\omega_r$ at $\xi = 0$ can be obtained from the Rankine-Hugoniot conditions, in terms of the radius of curvature S of the shock front at its intersection with the axis:

$$\omega_r(0) = U(0)/S \,. \qquad (19^*$$

It remains to estimate $p_{rr}(\xi)$. For this purpose we introduce an assumption concerning the geometry of the reaction zone. We assume the plane $\xi = \xi^*$ intersects the shock front in the explosive, and that the portion of the shock front for $\xi < \xi^*$ can be adequately represented by a sphere of radius S; i.e. we neglect the variation of radius of curvature over this part of the shock wave; see Fig. 1. Our procedure is to use the shock relations to

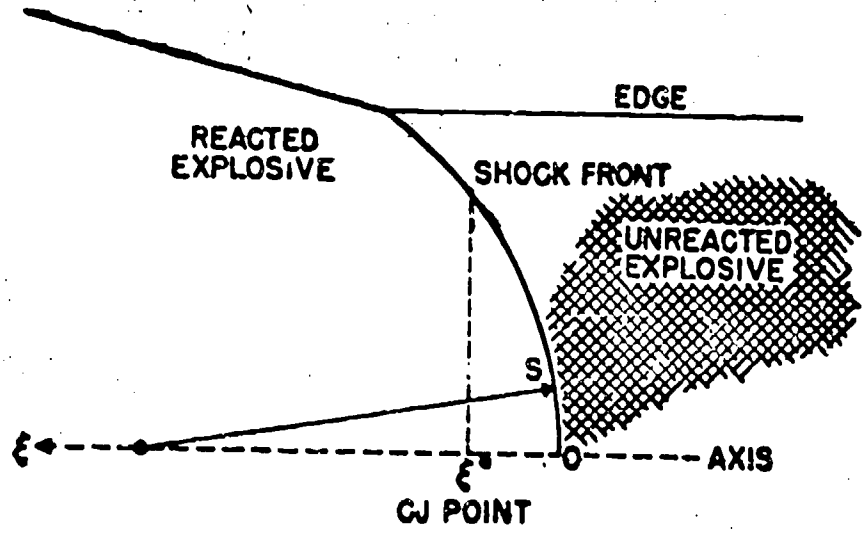


FIG. 1

obtain the pressure at any point on the shock front for $\xi < 0$*. Then expanding the pressure into a power series in r for fixed $\xi$, and retaining only the quadratic term (the linear term vanishes because of (8c) we obtain an approximation to the second radial derivative of p,

$$p_{rr}(\xi) = \left(p_s(\xi) - p(\xi)\right)/s\xi , \qquad (20*$$

where $p_s(\xi)$ denotes the pressure at the point $\xi$ on the shock front. In (20 we have approximated the equation of the spherical front as

$$r^2 = \epsilon s \xi . \qquad (21$$

Furthermore, with neglect of terms of order 1/S, $p_s(\xi)$ is equal to p(o), the axial shock pressure. Thus we finally obtain an expression for $p_{rr}(\xi)$ correct to terms of order 1/S,

$$p_{rr}(\xi) = \frac{p(o)}{s\xi}\left(1 - \frac{p(\xi)}{p(o)}\right). \qquad (22*$$

Substitution of (22 and (19 into (18, with use of (12a, yields

$$\frac{\omega_T(\xi)}{D} = \frac{U(0)}{D}\,\frac{1}{S}\,b(\xi)\,, \tag{23a*}$$

$$b(\xi) = 1 - \int_0^{\xi}\left(1 - \frac{\rho(\xi')}{\rho(0)}\right)\frac{d\xi'}{\xi'}\,. \tag{23b*}$$

With the preceding expression for $\omega_T$, we may summarize the important equations as follows:

$$\frac{\rho}{\rho_0}\left(1 - \frac{U}{D}\right) = 1 - \alpha(\xi)/S\,, \tag{24a*}$$

$$\alpha(\xi) = 2\,\frac{U(0)}{D}\int_0^{\xi}\frac{\rho(\xi')}{\rho_0}\,b(\xi')\,d\xi'\,, \tag{24b*}$$

$$p = \rho_0 D^2(1 - V/V_0)(1 + \beta(\xi)/S)\,, \tag{25a*}$$

$$\beta(\xi) = 2\,\frac{V/V_0}{1 - V/V_0}\,\frac{U(0)}{D}\left\{2\int_0^{\xi}\frac{\rho(\xi')}{\rho_0}\,b(\xi')\,d\xi' - \frac{\rho}{\rho_0}\int_0^{\xi} b(\xi')\,d\xi'\right\}; \tag{25b*}$$

$$E - E_0 - \tfrac{1}{2}p(V_0 - V) = D^2\,S(\xi)/S\,, \tag{26a*}$$

$$\delta(\xi) = \left(1 + \frac{V}{V_0}\right)\int_0^{\xi} b(\xi')\,d\xi' - 2\,\frac{V}{V_0}\int_0^{\xi}\frac{\rho(\xi')}{\rho_0}\,b(\xi')\,d\xi'\,, \tag{26b*}$$

$$\sigma(\xi^*)\,R(\xi^*) = 2\,U(0)\,b(\xi^*)/S\,, \tag{27a*}$$

$$(D-U(\xi^*))^2 = G(\xi^*) \,, \tag{27b*}$$

$$G \equiv C_*^2 \,; \tag{27c*}$$

$$\lambda = \int_0^{\xi^*} \frac{R(\xi')}{D-U(\xi')}\, d\xi' \,. \tag{28}$$

Equations (24, (25, (26, and (28 hold throughout the steady zone; equations (27 hold only at the C-J point. Equations (24a, (25a, and (27b may be manipulated to obtain

$$\frac{pV^2}{V_0-V}\left(1-\frac{2\alpha+\beta}{S}\right) = G^* \,, \tag{29a*}$$

$$D^2 = \frac{V_0^2 p}{V_0-V}\left(1-\beta/S\right). \tag{29b*}$$

We may conveniently regard (26a, (27a, (28, and (29a as determining the C-J values of p, $V$, and $\lambda$, with (29b then determining D.

## V

The theory at this point is formally complete, since the solution of the above equations will yield the desired relation between D and S, correct to order 1/S. To actually proceed further we require explicit information concerning a), the equation of state in the reaction zone and b), the rate function R. Here we shall limit ourselves to a very brief and preliminary discussion which may be appropriate to the detonation of liquid explosives.

With respect to the chemical kinetics problem, a model often used is that of a homogeneous, self-heating

reaction with a rate

$$R \sim f(\lambda)\, e^{-\Delta E/RT} \qquad (30$$

where $f(\lambda) \sim (1-\lambda)^n$ with n a number of order of magnitude one or two; $\Delta E$ is a molar activation energy. The appearance of the temperature in the exponential results in a rate of reaction which is initially small behind the shock front (assuming the temperature at this point to be appreciably lower than that near complete reaction, as is almost surely the case), at first increases very slowly, rises to a sharp maximum very close to complete reaction, then falls to zero (asymptotically, for most $f(\lambda)$). If this be true, it is plausible to expect the von Neumann pressure spike to be quite flat-topped during the induction period, then fall rather rapidly to its C-J value. In the following we idealize this pressure spike into a square wave:

$$p(\xi) = \begin{cases} p^{(o)}, & \xi < \xi^*, \\ p(\xi^*), & \xi \geq \xi^*. \end{cases} \qquad (31$$

Furthermore, the above discussion suggests that the rate R will be very large for some $\lambda$ close to complete reaction, then will decrease as $\lambda$ increases. This suggests that for large radii of curvature the value of $\lambda$ obtained from (27a will be very close to its plane wave C-J value. In the following we assume this to be true. The same assumption has been made in other discussions of diameter effect[1, 2].

We now perform a simple perturbation calculation on equations (26a and (29a to obtain the increments

$$\Delta v = v(\xi^*) - v^{(o)}, \qquad (32a$$

$$\Delta p = p(\xi^*) - p^{(o)}, \qquad (32b$$

where $v^*$ and $p^*$ denote the plane wave C-J values. The

result is two linear equations for the determination of $\Delta p$ and $\Delta v$,

$$\left\{\frac{pE_p}{D^2}-\frac{1}{2}\left(1-\frac{V}{V_0}\right)^2\right\}\frac{\Delta p}{p}+\left\{\frac{VE_V}{D^2}+\frac{1}{2}\frac{V}{V_0}\left(1-\frac{V}{V_0}\right)\right\}\frac{\Delta V}{V}=\frac{\delta}{S}\,. \qquad (33a$$

$$\left(1-\frac{pG_p}{G}\right)\frac{\Delta p}{p}+\left(\frac{2-\frac{V}{V_0}}{1-\frac{V}{V_0}}-\frac{VG_V}{G}\right)\frac{\Delta V}{V}=\frac{2\alpha+\beta}{S} \qquad (33b$$

where $E_p=\left(\frac{\partial E}{\partial p}\right)_V$, $\quad E_V=\left(\frac{\partial E}{\partial V}\right)_p$ , etc.

From (29b we obtain the detonation velocity deficit

$$\frac{D^{(s)}-D}{D^{(s)}}=\frac{1}{2}\left(\frac{\beta}{S}-\frac{\Delta p}{p}-\frac{1}{\frac{V_0}{V}-1}\,\frac{\Delta V}{V}\right). \qquad (34$$

We have used (31 to estimate the plane wave values of the quantities $\alpha$ , $\beta$ , and $\delta$ , and a free volume equation of state* to estimate the values of the various thermodynamic

---

*The equation of state is based on an intermolecular potential energy of the Buckingham type.

---

variables under conditions which may be representative for the C-J point of liquid explosives. We assumed $V/V_0=.7$ at the C-J point, $V/V_0=.55$ at the shock. The result for velocity deficit is

$$\frac{D^{(s)}-D}{D^{(s)}}=3.5\,\delta^*/S \qquad (35$$

The exact value of the coefficient is quite sensitive to the C-J and spike compressions, especially the former, as well as depending also on the equation of state. The above value should be regarded as only approximate. We hope in the near future to apply the present theory to specific explosives.

## REFERENCES

1. H. Eyring, R. E. Powell, G. H. Duffey, and R. B. Parlin, Chem. Revs. 45, 69 (1949; see also R. B. Parlin, C. J. Thorne, and D. W. Robinson, Tech. Report No. 1, Institute for the Study of Rate Processes, University of Utah, Salt Lake City, Utah.

2. H. Jones, Proc. Roy. Soc. (London) A189, 415 (1947).

3. A. F. Devonshire, Theoretical Research Report No. 3/43.

E. A. Igel and L. B. Seely, Jr.
Los Alamos Scientific Laboratory
Los Alamos, New Mexico

Early results on the detonation characteristics of nitromethane by Campbell et al (1) showed a number of unusual phenomena which led to the work on liquid TNT reported here. TNT above its melting point (about 80° C) is a liquid less sensitive (2) than nitromethane, with a presumably longer reaction zone, in which the same peculiarities of behavior exhibit themselves.

## Materials

Triple-recrystallized TNT with a melting point of 80.75 ±0.02°C and light transmission of 65%/cm relative to distilled water* was used for all the work reported here. This material was specially prepared at Picatinny Arsenal as Lot PA-48-1-3 by treatment of USA Grade 1 TNT with sodium sulfite, followed by recrystallizations from alcohol and from an ethylene dichloride-carbon tetrachloride mixture, with appropriate washing after each step.

The liquid TNT was fired in glass tubes which were made of Pyrex brand glass with walls 0.1 inch thick. This thickness was believed to constitute "infinite" confinement as far as Pyrex was concerned, a belief which was consistent with the results of others (1) (2) on confinement in other liquid explosives. It was further supported by several shots at 0.31 inch wall thickness which showed a behavior consistent with other shots at 0.1 inch wall thickness.

Samples of the Pyrex tubes were tested by immersion and the density was found to be 2.212 gm/cm$^3$. Individual tubes were measured for wall thickness and diameter. The wall thickness ranged on each tube from a maximum of 0.10" to some lower extreme depending on the tube, but always above 0.08" for these firings. Since both these thickness values were believed to be "infinite", no attempt was made to achieve better control.

*Melting points and transmission values were obtained with the aid of A. Popolato and W. Barry.

The diameters of the tubes varied slightly from tube to tube, along each tube and with the orientation of the diameter being measured. All these variations, however, were limited to ±0.01". Since the detonation velocity of liquid TNT was found to be insensitive to diameter, these variations did not produce detectable velocity variations.

Detonations were also studied in Dural tubes (24ST). Dimensions were much more closely controlled than for glass, and the effect on the velocity of such variations as existed must have been entirely negligible.

Method of Velocity Measurement

The liquid TNT problem puts high requirements on the accuracy of detonation velocity measurement. Early in the work it became clear that the total velocity decrement in glass tubes was quite small. It was necessary to keep the error to a few percent of the decrement (rather than of the velocity itself) in order to be able to determine the detailed dependence of the decrement on charge radius.

In the case of liquid TNT the problem of measuring detonation rates by optical means is more than ordinarily difficult, because of low light intensities. Therefore it was decided to use the pin method for velocity determinations. The camera method was used for diagnostic work. The camera was also used for measurements of the radius of curvature of the detonation wave. Here extreme accuracy was not necessary, because the detonation velocity of TNT is not extremely sensitive to the radius of curvature of the wave front.

Pin Method

The so-called "pin" method of velocity determination consists of recording the time of arrival of a shock or detonation wave at two precisely determined points by means of the electrical conductivity of the wave (3). When the detonation wave reaches a conductivity probe a small condenser discharges to ground through the detonation wave by means of a ground probe with which the wave has made contact earlier. In general it is not clear what part of the detonation wave causes the signal. The situation is particularly questionable in the case of a shocked homogeneous material, for which the temperature is much lower than in the interstices of a particulate explosive. In liquid TNT we do not know whether the original shock front triggers the probe or whether a certain amount of chemical reaction is necessary before the discharge can be started. From the point of view of obtaining measurements all that is necessary is that the wave trip the pins in the same manner at both ends of the measurement interval. One can perhaps believe that this is so if a truly steady wave has first been developed. The final consistency of the data is a fairly good indication that the method of triggering was always the same.

The pin signals were recorded on the "Cable Delay Timing System". This is a system by which signals generated early in the travel of the wave are delayed and presented on the same fast oscilloscope sweep with the later signals. Readings can be made quite accurately because of the speed of the sweep. To the time differences as seen on the sweep must be added the times spent by the delayed signals in traveling through the delay cables.

The delay cables were RG-18/U of various lengths up to 10 microseconds which could be connected together by lengths of more flexible cable at a connection panel. We believe the system would be practical for delays up to about 15 microseconds. At some time beyond this the signals would become degraded and reading accuracy would fall off. The advantages of the cable method are ruggedness and electronic simplicity. The cable transit times do not vary with aging or external conditions, but depend only on the dielectric constant of the insulating material. On the other hand the cable delay system is inferior to a raster scope system in flexibility and simplicity in forming the signals.

The results of cable calibrations are shown in Table I. Short cables were calibrated by presenting test pulses on a calibrated sweep before and after travel through the cable in question. Long cables were calibrated by comparing a signal through the cable in question with a simultaneous signal, either direct or reflected, through a previously calibrated cable or collection of cables. This led to a somewhat complicated multiplication of errors for the longer cables, as can be seen from the trend of the standard deviations in Table I.

## Absolute Accuracy

The cable calibration values given in Table I are the predominant factor in determining the absolute error of the liquid TNT measurements. We have calculated the 95% confidence limits for these values and prefer to use these as an index of absolute accuracy. In the arrangement of cables used for the liquid TNT studies the accuracy of the longest cables was most important so that the absolute accuracy of the final results was about ±0.1%.

## Relative Accuracy

The relative accuracy was something quite different. In the liquid TNT work reported here the cable arrangement was the same for all shots, and under these conditions the relative accuracy was considerably better than the absolute accuracy. The random scatter of the final data results from reading and instrumental errors, from errors in placement of the pins, variations in the explosives and poor control of conditions. As will be seen later in this paper the final velocity results are characterized by a population RMS deviation, $\sigma_p = 0.1\%$. Thus by using a sample size of 10, the $\sigma$ for the average can be reduced to 0.03%.

TABLE I

SUMMARY OF CABLE CALIBRATIONS

| Cable Designation | No. Samples N | Mean Time usec. | $\sigma_p$ (population) | $\sigma_t$ (of Mean) | 95% Confidence |
|---|---|---|---|---|---|
| | | | microseconds x $10^{-3}$ | | |
| 0.1 | 14 | 0.1268 | .54 | .14 | ± 0.30 |
| 0.2B | 10 | 0.2019 | 1.06 | .36 | ± 0.38 |
| 0.2A | 11 | 0.1968 | 1.00 | .30 | ± 0.33 |
| 0.5 | 10 | 0.4948 | 1.75 | .55 | ± 1.24 |
| 0.6 | 10 | 0.6179 | 1.20 | .38 | ± 0.86 |
| 1.0 | 11 | 0.9702 | 1.60 | .48 | ± 1.07 |
| 2.0A | 8 | 2.0033 | 3.30 | .97 | ± 2.3 |
| 2.0B | 11 | 2.0544 | 3.26 | .93 | ± 2.1 |
| 5.0 | 10 | 4.9521 | 7.56 | 2.27 | ± 5.1 |
| 10.0 | 10 | 9.9441 | 15.20 | 4.58 | ±10.4 |

Temperature Control

The first attempts to obtain detonation velocities for this program yielded spreads much too large to define the details of the velocity decrement. Studies of the detonation wave shape with the camera showed great variability as well. Therefore, a number of investigations were made at that time to study various possible reasons for this instability. The measurement system, explosives purity, presence of dissolved or dispersed gases and other factors were looked into. No positive evidence was encountered to indicate that these particular factors were responsible for velocity variations of the size observed.

The detonation velocity dependence on density for solid TNT is about 350 m/sec. per 0.1 gm/cm$^3$ according to OSRD 5611 (4). The variation of the density of liquid TNT with temperature is approximately linear with a slope of 0.001 gm/cm$^3$ per degree C.* Thus the detonation velocity varies about 3.5 meters/sec. per degree C. On this basis one would not expect that uniform deviation of the temperature from charge to charge was responsible for the spreads observed, since the temperature could be controlled to within a few tenths of a degree from charge to charge. However, the variable wave shapes that were observed suggested that there may have been temperature gradients within each charge.

In order to develop satisfactory control, measurements of the temperature were made in twelve positions in the charge by means of thermocouples monitored by a Leeds and Northrup automatic recorder. With the original techniques of cooling and stirring by bubbling nitrogen through the liquid, differences in temperature of as much as a 3°C were observed at firing time. By means of such tests several tech-

* Variation of density of liquid TNT with temperature was measured by W. H. Stein, LASL.

niques were developed for holding the temperature constant throughout the charge. Two of these have been used for the shots reported here.

Apparently the key to maintaining uniform temperature was to circulate the liquid, either by means of a twisted-blade stirrer or an exterior circulating pump. This was effective with both a heated-sand jacket and with a pre-heated-circulating-air jacket. When stirring was stopped, before firing, it took several minutes for the gradients to become apparent--long enough for preparations to be made for firing.

Probe Arrangement

Conductivity probes should be rugged enough to hold their position but yet small enough to avoid perturbing the detonation wave. For work in glass tubes and large diameter metal tubes, .030" tungsten rods were chosen, since they were quite rigid for the diameter. It was also believed that high density would be advantageous in avoiding perturbations. There were, however, serious reservations about their use near failure diameter where the introduction of this foreign material might be expected to affect propagation of the wave. The probes were glued with plastic cement in Micarta caps as shown in Fig. 1.

To test the suitability of this style probe assembly, a number of caps were mechanically vibrated to simulate possible abuse prior to shot time. Measurements of the inter-probe-point distance were also made in water at 93° C behind plate glass windows. These tests showed no effect of vibration or temperature provided strains were first relieved by holding the probes in an oxygen-butane flame for two minutes. Repeated cathetometer readings of the distance between a pair of probes to be used for firing showed a range of ±0.01%.

For metal tubes smaller than 2" in diameter the 0.030" probe was thought to be too large. Instead a 0.005" tungsten wire was strung across a diameter of the tube. This required mounting in 1/8" diameter plastic plugs for insulation in the metal wall. Furthermore close-fitting removable plugs of metal had to be made in the wall at right angles to each wire so that the position of the wires could be measured by means of a cathetometer after installation.

Method of Wave Curvature Measurement

Two closely related techniques were developed for observing the shape of the detonation waves. In the first the wave was allowed to collide with a thin aluminum foil against a ground plate of glass. This assembly was held perpendicular to the axis of the tube by the fit of the glass against the tube end, which was ground accurately perpendicular. The aluminum was flat because it was held against the glass by the liquid TNT. In order to increase the light intensity, the small spaces between the ground glass and the aluminum were flushed with argon. The Rotating Mirror Camera then viewed the light through the unground side of the glass.

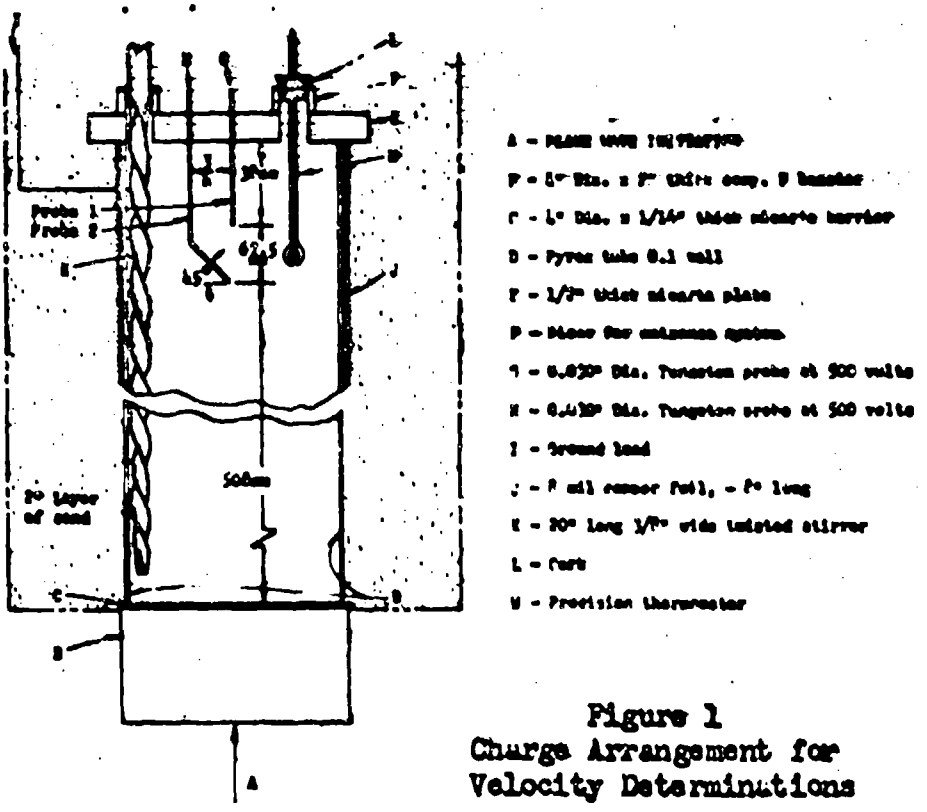


Figure 1
Charge Arrangement for
Velocity Determinations

There was some difficulty with this technique in reproducing intensities, probably because of variations in sand-blasting the glass. Further irregularities in the trace were produced by wrinkling in the foil at 100° C., caused by the difference in the coefficient of expansion between glass and aluminum.

In order to overcome these difficulties, the tube-end was constructd of brass and the joint to the glass made with a circumferential "O"-ring seal. A piece of .005" thick brass shimstock could then be firmly fastened to the brass tube-end, and difficulties caused by differential expansion avoided. A smooth piece of plate glass was held .005" above the brass shimstock by soft aluminum shims, providing a narrow space for argon.

## The Charges

A number of charge designs were tried in the preliminary shots without any definite specification of the optimum length or mode of initiation. One would like to keep charge weight at large diameters as low as possible and yet it is clear that the detonation must be positively initiated and reach a steady state before measurements are made. The final charge design is shown in Figure 1. The liquid TNT was over-driven by the Comp. B with only 1/16" Micarta between the two explosives. A plane wave generator was used because it was thought better always to have an initiating wave curvature less than the final stable one. By this means some of the possible

initiation trouble at diameters near failure could be avoided.

It was never shown in this work just what the minimum satisfactory charge length was. In all velocity measurements in glass tubes we allowed 20" of free run in liquid TNT before starting the measurement. This gave somewhat over three diameters of length at the largest diameter studied (where, incidentally, the least alteration from the original plane wave shape was necessary) and a more generous situation in the small diameters. For other shots in metal tubes involving determination of wave shapes we allowed always more than four diameters of free run before starting measurements.

With either sand jacket or air jacket the total charge assembly was quite bulky. In both cases the signal forming components were mounted as close to the probes as possible and connections made in such a way as to form as small loops as possible. The metal tubes themselves served as electrical grounds. In the case of glass tubes the electrical ground at the charge was an 8 mil copper sheath surrounding the tube in the vicinity of the probes. It was found that this sheath (instead of a simple wire) increased the sharpness of the signal making reading of the films easier.

## Data Analysis

Velocity Data. A typical velocity data film, reproduced in Figure 2, shows five traces. The first two are marked calibration sweeps which were recorded after an hour's warm-up for the scope and as close to firing time as possible. The last two traces are also calibrations, but taken immediately after firing. The middle trace is the data trace taken with no markers. All four calibration traces were read on the comparator and the sweep curve plotted. The data trace was then read and the sweep speed corresponding to the signal interval applied to reducing the data.

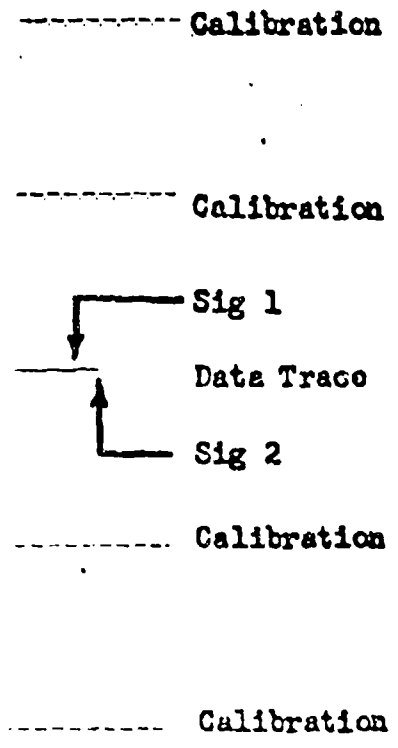


Figure 2
Cable Delay Timing Film

Wave Curvature Data. A wave trace of the type shown in Figure 3 was produced when glass tubes were used. The film was placed on the comparator and the stage rotated until the static image of the slit and the horizontal traverse of the comparator agreed. Thus we at this point assumed that the camera slit was truly perpendicular to the direction of writing, in practice an extremely difficult adjustment to make accurately.

By means of the edges of the trace, or markers, if provided, the magnification factor could be computed and the center of the charge determined. Five sets of readings were made of the time displacements relative to the position of the center of the wave at intervals across the face of the trace.

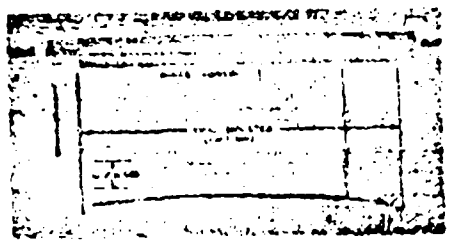

Figure 3
Typical
Wave-Curvature Film

The data were reduced by fitting an ellipse to all but the lagging outer edges of the trace. The central curvatures of these ellipses have been reported as the pertinent data. We are indebted to W. W. Wood for devising this scheme and adapting it for the IBM 701 Computer, and to F. R. Parker for coding and machine operation. The method assumed that an axis of the ellipse fell on a line parallel to the camera slit. In some of the earliest work this introduced a slight error, since the camera slit was not quite perpendicular to the direction of writing. However, comparison with hand calculations in which radii of curvature were computed for various groups of three points on the wave trace showed that the skewness was very small and that the error thus introduced in the radius of curvature was negligible.

## Results

Velocities. Shots at various diameters in glass and aluminum were fired over a period of months. The individual results with averages and RMS deviations are shown in Tables II and III. From the results in glass tubes for which a large number of shots were made under identical conditions it is concluded that the population RMS deviation, $\sigma_p$, is about 6 m/sec.

The point at the largest diameter ($1/R = 0.132$) for glass is the average of only three shots. We believe that these shots are part of a population which has the same characteristics as those revealed by the larger number of shots made at other diameters. On this basis we have conservatively assumed that the true $\sigma_p$ is 6 m/sec. Clearly then the $\sigma$ for the average of three shots is 3.5 m/sec. rather than the smaller value which can be calculated from the variations of the three shots themselves.

These results for glass tubes, with the proper $\sigma$'s indicated, are shown plotted against $1/R$ in Figure 4. It is seen that the data are adequately satisfied by a straight line with intercept at $R = \infty$ of 6574 m/sec. Failures occurred invariably at $R = 3.0$ cm. Thus the lowest point at which measurements were made was $R = 3.25$ cm, where the velocity was 6515 m/sec. The decrement in velocity, from the extrapolation at infinite diameter to the point nearest failure was 60 m/sec.

TABLE II

Detonation Velocity of Liquid TNT
100° C  Pyrex Glass Tubes

| Film No. | Detonation Velocity D, m/sec. | Average Detonation Velocity $\bar{D}$, m/sec. | Standard Deviation of Mean $\sigma_{\bar{D}}$, m/sec. |
|---|---|---|---|
| Radius = 3.25 cm. (1/R = 0.308) | | | |
| 15-399 | 6521 | | |
| 15-402 | 6508 | | |
| 15-403 | 6516 | | |
| 15-404 | 6512 | | |
| 15-405 | 6516 | 6515 | 1.6 |
| 15-408 | 6515 | | |
| 15-409 | 6516 | | |
| 15-410 | 6522 | | |
| 15-411 | 6509 | | |
| Radius = 3.50 cm. (1/R = 0.286) | | | |
| 15-382 | 6529 | | |
| 15-383 | 6528 | | |
| 15-413 | 6515 | | |
| 15-414 | 6511 | | |
| 15-415 | 6521 | 6520 | 2.0 |
| 15-416 | 6515 | | |
| 15-427 | 6525 | | |
| 15-428 | 6520 | | |
| 15-429 | 6513 | | |
| 15-430 | 6524 | | |
| Radius = 4.75 cm. (1/R = 0.210) | | | |
| 15-346 | 6537 | | |
| 15-348 | 6541 | | |
| 15-350 | 6535 | | |
| 15-352 | 6531 | | |
| 15-354 | 6534 | 6534 | 1.3 |
| 15-356 | 6531 | | |
| 15-360 | 6534 | | |
| 15-361 | 6539 | | |
| 15-379 | 6528 | | |
| Radius = 7.56 cm. (1/R = 0.132) | | | |
| 15-449 | 6553 | | |
| 15-450 | 6549 | 6549 | 3.5 |
| 15-451 | 6547 | | |

($\sigma_p$ assumed 6)

TABLE III

Detonation Velocity of Liquid TNT

100° C  Dural (24ST) Tubes

| Film No. | Detonation Velocity $D_i$ m/sec. | Average Detonation Velocity $\bar{D}$, m/sec. | Standard Deviation of Mean $\sigma_{\bar{D}}$, m/sec. |
|---|---|---|---|
| Radius = 3.18 cm. ($1/R = 0.315$ cm$^{-1}$) | | | |
| 15-458 | 6543 | | |
| 15-459 | (6500) | 6537 | 3.6 |
| 15-460 | 6534 | | |
| 15-461 | 6533 | | |
| Radius = 1.59 cm. ($1/R = 0.630$ cm$^{-1}$) | | | |
| 15-485 | 6515 | | |
| 15-486 | 6515 | 6515 | 4.3 ($\sigma_D$ assumed 6) |
| Radius = 0.95 cm. ($1/R = 1.05$ cm$^{-1}$) | | | |
| 15-492 | 6462 | — | — |

The velocity data presently available for aluminum confinement are listed in Table III. Although the number of shots is less the accessible range in $1/R$ is greater than for glass, and the (presumed) straight line can be adequately determined, using, as seems reasonable, an extrapolation point common with that for the glass curve.

There is one shot at the largest diameter among the data for aluminum which is apparently subject to a large error. This point has not been averaged with the others.

The data for aluminum confinement are plotted in Figure 5. In the large-diameter region the data can be represented by a straight line of smaller slope than the line for glass, as one might expect for the denser material. The data are not complete enough to show the form of the curve as failure diameter is approached. However, it appears that the maximum velocity decrement for aluminum is about three times that for glass.

Wave Curvatures

The wave curvatures obtained from the IBM 701 Computer are listed in Table IV. At the largest diameter in glass there are enough determinations so that a reasonable estimate of the experimental error can be made. For the other conditions there is really no basis for assigning an estimate of accuracy but we have nevertheless tried to assign one. This should be considered not so much as a guarantee of accuracy as a warning lest the data be used for more than they are worth.

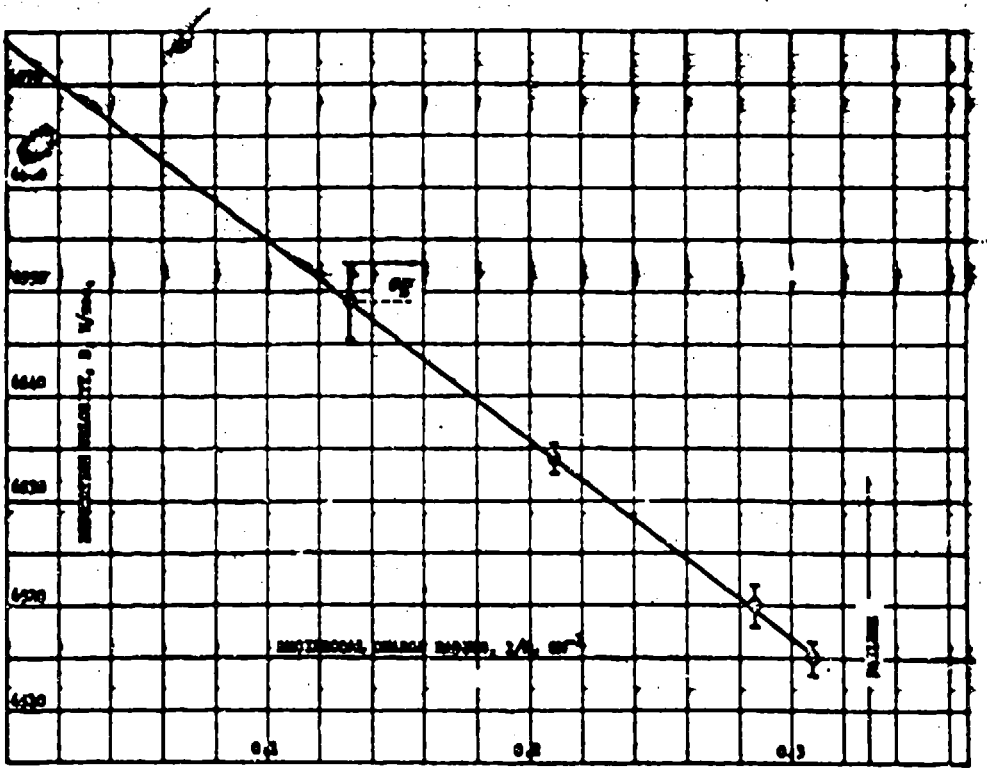

Figure 4
Diameter Effect in Liquid TNT
100°C Pyrex Confinement

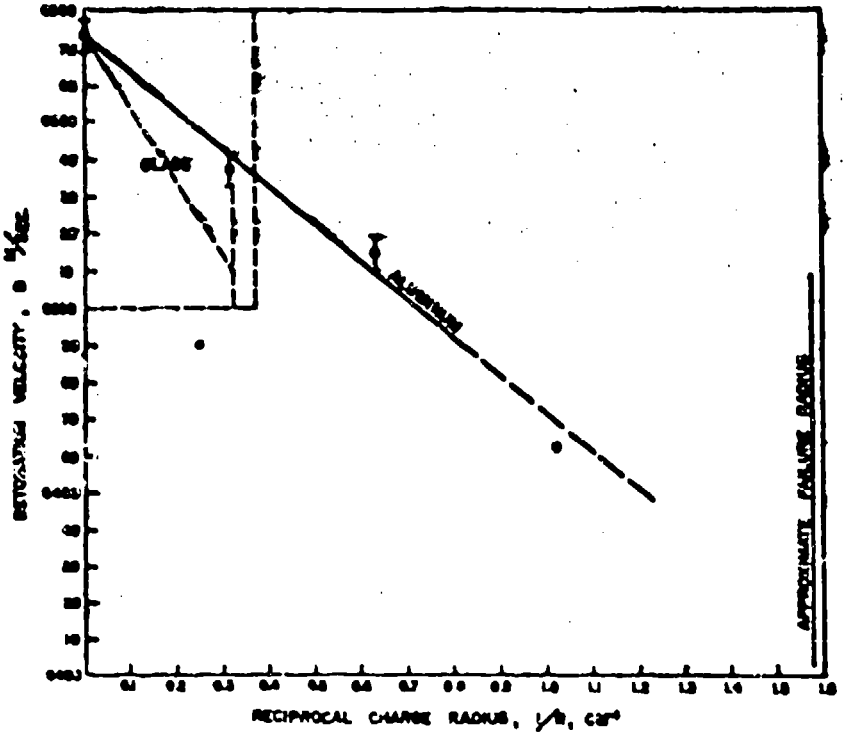

Figure 5
Diameter Effect in Liquid TNT
100°C Dural Confinement

TABLE IV

Radius of Curvature of Detonation Waves in Liquid TNT at 100° C

| Film No. | Tube Dia.,mm | Detonation Velocity | Rad.Curv. S,mm | $\sigma'_s$ % | S mm | Error mm |
|---|---|---|---|---|---|---|
| Glass: | | | | | | |
| 448 | 151.2 | 6548 | 1253 | | | |
| 448 | 151.2 | 6549 | 1221 | | | |
| | 151.2 | 6549 | 1203 | | 1255 | 40* |
| | 151.2 | 6549 | 1272 | | | |
| | 151.2 | 6549 | 1314 | | | |
| | 79.8 | 6526 | 546 | 1.4 | -- | 55 |
| 422 | 65.0 | 6515 | 308 | 2.2 | -- | 40 |
| Aluminum: | | | | | | |
| 430 | 63.5 | 6537 | 575 | | 506 | 70 |
| 429 | 63.5 | 6537 | 437 | | | |
| 485 | 31.8 | 6503 | 306 | 3.8 | -- | 40 |

*R.M.S between determinations.

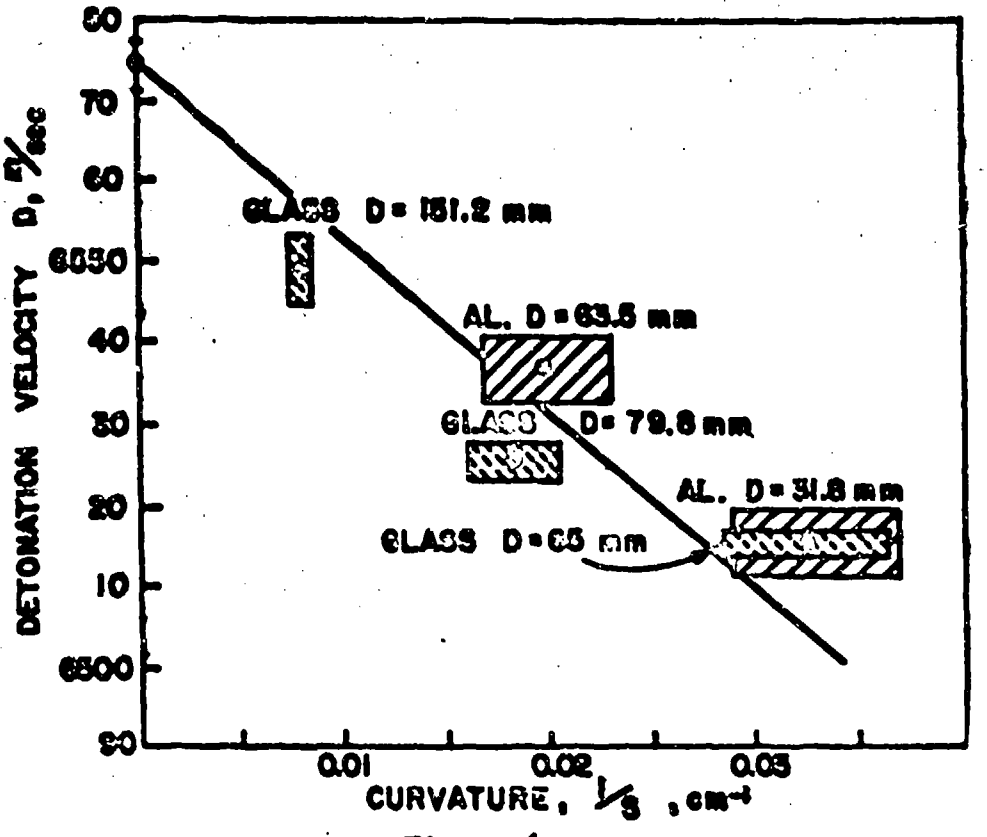


Figure 6

Effect of Wave Curvature
on Detonation Velocity of Liquid TNT

Some of the radius of curvature values have associated $\sigma$'s quoted in per cent. These $\sigma$'s express the uncertainty in the radius of curvature resulting from the scatter of the experimental readings and the failure of the series of points to fit the ellipse perfectly. It is believed that the experimental accuracy is better indicated by the variation in the radius of curvature from shot to shot, since there are a number of factors which can affect the shot-to-shot scatter, and not be evident in any one shot.

The velocity data of the preceding section are shown plotted against the reciprocal of the radius of curvature in Figure 6. According to the Wood-Kirkwood theory all the points, whether with glass or aluminum confinement, should lie on the same straight line. Within the limits set by the rather large experimental error this is the case. At the same time it is possible that more extensive and more accurate data will indicate shortcomings of the theory.

## Discussion

The small velocity decrement of liquid TNT in glass confinement is unexplained. No theory in its present form treats the mechanism of failure, and it is perhaps unjustified to consider failure as a case in which the divergence of material postulated in theories of the diameter effect is carried to its ultimate. As the wave curvature plot now stands, failure occurs in glass and aluminum at different degrees of divergence. The shape of the wave front in glass, characterized by a rapid increase in curvature as the wall of the tube is approached, (see Fig. 3) is not duplicated in the same diameters for metals (very small diameters in metals have not been investigated). For metals the wave front intersects the tube wall with a smooth curvature, almost unchanging. The wave front with magnesium ($\rho = 1.7$ gm/cm$^3$) confinement is of the typical metal type. The failure diameter in cellulose-filled plastic ($\rho = 1.35$ gm/cm$^3$) is approximately that in glass ($\rho = 2.2$ gms/cm$^3$). All this tends to suggest that failure in glass is governed by a unique property of the glass, perhaps its inability to withstand circumferential tension without cracking.

In attempting to treat the data according to earlier theories such as those of Jones and of Eyring et al., one is confronted with immediate experimental contradiction of the theories. As far as the Jones theory (8) is concerned there are two contradictions. First, Jones has ignored the presence of wave-front curvature. Second, the wave shapes observed in glass suggest that flow is not normal at the boundary as assumed by Jones.

In spite of this, one can go ahead, ignore the contradictions, use the angle of expansion calculated by Jones and Strickland for TNT in glass together with charge-radius versus detonation-velocity data reported here, and calculate a reaction zone length. The answer thus obtained is a reaction zone length 0.9 mm.

A similar calculation for the aluminum data gives a value of 1.1 mm for the reaction zone length, the difference between the two calculations probably being due to inconsistency in estimation of the expansion angle.

Eyring's theory assumes a curved detonation wave front with which our experimental findings are more nearly in agreement. However, the wave shape in glass has not been found to agree with the spherical surface assumed by Eyring, but has been found to curve sharply at the edges. The Eyring theory for "infinite" confinement calls for an angle $\xi$ which the wave makes with the confining wall. We have assumed that the most sensible angle to take is not the actual angle but the angle that the "normal" central part of the wave would make with the case if extended to it. On this basis the results in glass give a reaction zone length of 0.3 mm. The aluminum results indicate a reaction zone length of 0.25 mm.

Finally, the Wood-Kirkwood theory relates the radius of curvature of the detonation wave to the detonation velocity. Our data present no obvious contradictions with the assumptions in this theory. The theory assumes a spherical wave in the center, and this is approximately true. According to the theory this constant curvature should extend radially at least to a point where the wave front has dropped one reaction zone length behind its position at the center of the charge, and this also seems to be approximately true at least at the large diameters. In small diameter metal tubes it is clear that it is not true. There are in the theory certain assumptions necessary for mathematical tractability or concerning the equation of state which have to be put up with. In no case do these appear unreasonable, but in no case do we have an experimental check. Accepting them, we have calculated a reaction zone length of 1.2 mm.

It is probably fruitless to speculate as to which value of the calculated reaction zone lengths lies nearest the actual one. However, by obtaining additional information on the properties of liquid TNT and on the products of its detonation the theoretical idealizations in the Wood-Kirkwood theory can be made more realistic. There is some hope that the detonation process can in this manner be taken apart and described in greater detail than now possible. As a check on these possibilities great interest is focused on experimental techniques for studying the details of the reaction region.

## REFERENCES

(1) T. P. Cotter, A. W. Campbell, T. E. Holland, M. E. Malin and H. W. Schmitt, unpublished communications, December 20, 1950, August 20, 1951. More exact and complete data are given in "Detonation in Homogeneous Explosives", this conference.

(2) L. C. Smith, E. James, Jr., M. J. Urizar, unpublished communication, August 15, 1951, giving approximate failure diameters for liquid TNT.

(3) James L. Tuck, Private communication.

(4) D. P. MacDougall, G. E. Messerly, et al, OSRD 5611.

(5) H. Eyring, R. E. Powell, G. H. Duffey and R. B. Parlin, Chem. Rev. 45, 69-181 (1949).

(6) S. J. Jacobs, paper presented at 1st ONR Conference on Detonation.

(7) W. W. Wood and J. G. Kirkwood, Jour. Chem. Phys. in press, also presented at 2nd ONR Conference on Detonation.

(8) H. Jones, Proc. Roy. Soc. A-189, 415-426 (1947). Additional work of Jones is quoted in Ref. 5.

# DETONATION IN HOMOGENEOUS EXPLOSIVES

A. W. Campbell, M. E. Malin, and T. E. Holland
Los Alamos Scientific Laboratory
Los Alamos, New Mexico

## INTRODUCTION

The work to be discussed in this paper began as an attempt to obtain precise data for comparison with the predictions of the Eyring[1] and the Jones[2] theories of the diameter effect. The use of liquid explosives seemed to offer a ready means of preparing homogeneous charges. Of the many liquid explosives known, Nitromethane seemed the most desirable for many reasons, among which were its ready availability, cheapness, low toxicity and low sensitivity. Soon after the work was begun on measuring detonation velocities and failure diameters, scatter appeared in the data to a degree which was not explainable on the basis of measuring error. Further investigation, aided by high-performance optical and electronic equipment, revealed several new aspects of the detonation process, some of which appear to be peculiar to liquids, others to homogeneous explosives whether liquid or solid.

## MATERIALS

The Nitromethane used in this work was obtained in 55 gal drums from Commercial Solvents Corporation. It was specified as having the following composition:

| | |
|---|---|
| Nitromethane, % by weight, minimum | 95 |
| Nitroparaffin, total, % by weight, minimum | 99 |
| Specific gravity, 25/25°C | 1.1283 |
| Acidity as acetic acid, % by weight, maximum | 0.01 |
| Water, % by weight | 0.052 |

To further guard against the presence of alkaline materials which might act as sensitizers, the Nitromethane was redistilled at reduced pressure from sulfuric acid and stored in glass bottles.

The Ethyl Nitrate used was White Label grade obtained from Distillation Products Industries. The PETN used was obtained from the Hercules Powder Company.

## EFFECT OF TEMPERATURE ON DETONATION VELOCITY OF NITROMETHANE

The first experiments on the effect of confinement on the detonation velocity of Nitromethane were done in dural and steel tubes at constant charge-weight/casing-weight ratio. Subsequent observations on the effect of metal confinement on Nitromethane have led us to regard the confinement employed here as equivalent to infinite confinement. The detonation velocities were measured using the pin technique[3] and are shown plotted in Fig. 1. These results indicated that very little diameter effect was to be expected from Nitromethane in metal tubes, and that some uncontrolled factor was causing bad scatter in the observed velocities. Temperature variations in the explosive at the time of firing were suspected. Such variations could have two effects: raising the temperature of a liquid explosive tends to increase the detonation velocity; the accompanying decrease in density tends to lower the velocity.

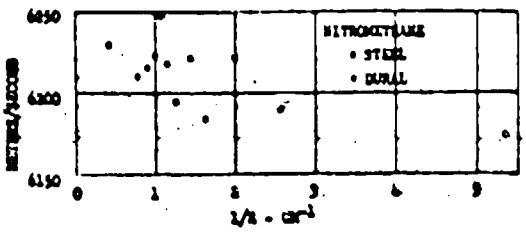


Fig. 1. Detonation velocity of Nitromethane confined in metal tube. No temperature control.

The second of these two effects is the easier to examine. The temperature dependence of the density is given for Nitromethane by the following[4]:

$$d_T = 1.1645 - 1.337\ 10^{-3}\ T - 1.15\ 10^{-6} T^2 + 3.8\ 10^{-9} T^3$$

where $d_T$ is the density at T °C.
Since the Nitromethane used in these experiments contained some impurities, as shown in the above analysis, a set of temperature-density data was taken on it with the result as shown in Fig. 2. The temperature coefficient was found to be $1.33\ 10^{-3}$ g/cc/°C, in good agreement with the value given in the above equation. Since the velocity dependence on density for most solid explosives, where the density can be varied independently of the temperature, lies in the range 3000 - 4000 m/sec/g/cc, one might expect Nitromethane to show a velocity dependence on temperature of approximately -4.7 m/sec/°C due to the change in density alone.

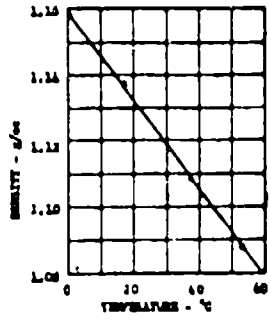

Fig. 2. Density-temperature plot for commercial grade Nitromethane

To determine whether Nitromethane did, indeed, show such a temperature effect, a series of six rate measurements was made

including two at ambient temperature, two just above the freezing point and two at as high a temperature as was deemed safe with our equipment. The experimental arrangement is shown in Fig. 3.

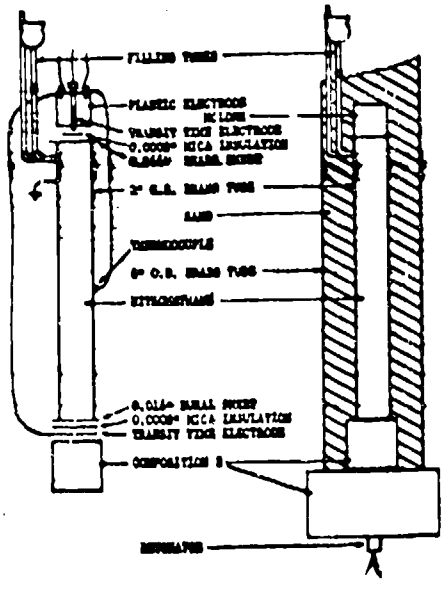

Fig. 3. Charge arrangement used to determine the effect of temperature on the detonation velocity of Nitromethane

The explosive was contained in a brass tube 2.000 in. o.d. with 0.125 in. wall. The tube was sealed at the top by a 0.066-in. brass plate which was soldered into place. The tube was sealed at the bottom with a 0.016-in. dural plate after experiments had shown that adequate initiation could be obtained through such a plate. Two holes were drilled through the container near the top and two copper tubes were soldered into position. A thistle tube was cemented onto one of these tubes using Armstrong cement*, which was found to be one of the few plastic materials not attacked by Nitromethane. The thistle tube served as a funnel during the filling operation and as a reservoir in the heating or cooling process.

After assembly, but before the top and bottom plates were attached, the height of the container was measured with a vernier height gauge which could be read directly to 1 mil. The thicknesses of the brass and dural plates were measured with a micrometer.

Detonation velocities were determined, as before, with the pin technique. The lower pin switch was made of a copper strip, 2 mils thick, insulated with a thin sheet of mica as shown in Fig. 3. The upper switch was a 10-24 brass screw the end of which was turned to a point with a very small flat left at the tip. This was threaded into a Lucite block which was cemented into place with Armstrong cement. The signal circuit ground was formed by a wire soldered to one of the copper filling tubes.

Temperature measurements were made by means of an iron-constantan thermocouple. Two 12-mil holes were drilled near the center of the container part way through the wall, and the thermocouple leads were peened into them. A Leeds-Northrup Portable Indicator Millivolt Potentiometer, Model 8662, was used on which voltage could be read directly to one hundredth of a millivolt and estimated to a thousandth. In the range used, the sensitivity of the iron-constantan thermocouple is about 0.03 millivolt per degree F so that temperature

*Adhesive type A - 1 manufactured by Armstrong Products Company, Warsaw, Indiana.

could be read to one-third degree F.

Since there was an appreciable time lapse between the removal of a charge from the thermostat and the firing instant, it was desirable to use a setup with a large heat capacity to minimize temperature changes. For this purpose a brass container, 6 in. o.d., 1/16 in. wall, 18 in. height, was used as an outside container for the charge, and the space between the two was filled with sand. High temperatures were obtained with an oven, low temperatures with a deep-freeze unit. In the heating and cooling processes, the temperature of the sand alone was adjusted to approximately the value desired and the sand was then poured into the container. The temperature was followed until it became reasonably constant, and the shot was then fired. It was assumed that by the time the temperature appeared to be constant the conductivity of the walls of the charge container and convection currents in the Nitromethane would have served to produce a satisfactorily uniform temperature throughout the charge. In the first shot there was a 22-minute wait before the shot was fired, with the temperature being constant for the last 4 minutes. Other charges behaved in a similar manner. All of the six charges were completed within a period of five days, using Nitromethane taken from a single lot so as to ensure uniformity in the explosive.

Experimental results are given in Table I and are presented in Fig. 4.

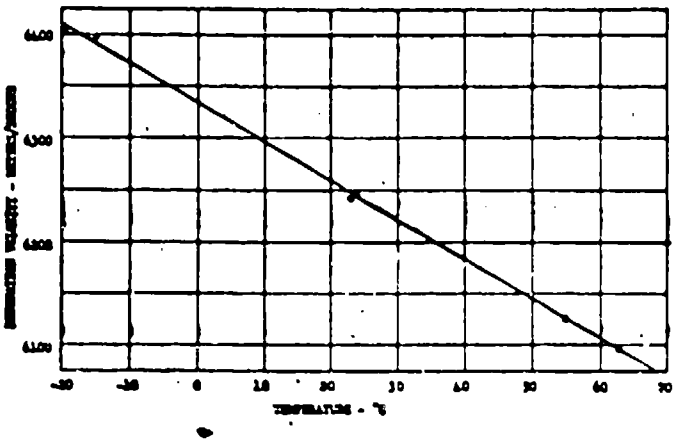

Fig. 4. Effect of temperature on detonation velocity of Nitromethane in brass tubes. 0.125-in. wall, 1.75 in. i.d.

An examination of the data shows that under the conditions of the experiment, Nitromethane exhibits a velocity dependence on temperature of - 3.7 m/sec/°C. This is smaller than might be expected from the density effect produced by temperature change as mentioned earlier. A part of this discrepancy results from the tendency for the detonation velocity to increase with an increase in the initial temperature, density held constant; another part is due to the finite diameter of the test charges, as will be shown in the next section.

## THE DIAMETER EFFECT IN NITROMETHANE AS AFFECTED BY TEMPERATURE

After determining the effect of temperature on the detonation velocity of Nitromethane, experiments were performed to measure the diameter effect in glass tubes. The results of this series of shots and also of observations made during a study of "failures"

Table I

| Shot Number | 2736 | 2737 | 2738 | 2739 | 2740 | 2741 |
|---|---|---|---|---|---|---|
| Overall Length (in.) | 12.072 | 12.070 | 12.044 | 11.939 | 12.011 | 12.079 |
| Thickness of Tube Caps (in.) | 0.066 Brass; 0.016 Aluminum - same for all guns. | | | | | |
| Nitromethane Path Length (in. mm.) | 11.990" 304.546 | 11.988" 304.495 | 11.962" 303.835 | 11.857" 301.168 | 11.929" 302.997 | 11.997" 304.724 |
| Transit Time Overall (μsec) | 49.159 | 49.130 | 50.000 | 49.812 | 47.708 | 47.946 |
| Time through Al. and Brass Caps (μsec) * | 0.377 | 0.377 | 0.377 | 0.377 | 0.377 | 0.377 |
| Transit Time for Nitromethane (μsec) | 48.782 | 48.753 | 49.623 | 49.435 | 47.331 | 47.569 |
| Correction for Brass Expansion ** (mm.) | No correction | | +.164 | +.205 | -.218 | -.244 |
| Corrected Velocity | 6.2429 | 6.2456 | 6.1262 | 6.0963 | 6.3971 | 6.4008 |
| Temperature (°C) | 23.09 | 24.09 | 55.04 | 62.80 | -15.01 | -19.42 |
| Density | 1.1283 | 1.1270 | 1.0862 | 1.0757 | 1.1788 | 1.1848 |

* Shock wave velocity in Al. taken as 7.1 mm/μsec. (0.016" = 0.056 μsec).
Shock wave velocity in Brass taken as 5.3 mm/μsec. (0.066" = 0.321 μsec).

** Taking $1.8 \times 10^{-5}$/°C as linear coefficient of expansion of Brass

(to be discussed later) suggested that the diameter effect might be a function of temperature. Consequently, another set of experiments was designed to investigate this point.

The experimental arrangement used is shown in Fig. 5.

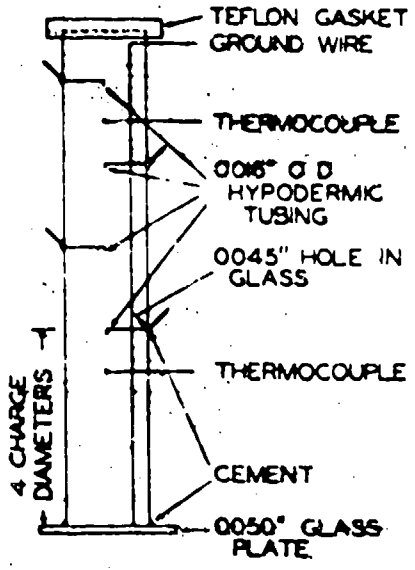


Fig. 5. Charge arrangement for measuring detonation velocity as a function of charge diameter

The containers were made of standard-wall Pyrex brand glass tubing. Holes for pin switches were made in the glass at 5-in. intervals using a hot tungsten wire technique. The tubes were then ground flat on each end, and glass plates were sealed on with Armstrong cement. The pin switches were made with steel hypodermic tubing 16 mils o.d., 4 mils wall, this material being used because of its stiffness. The lower end of each piece of tubing was collapsed and ground flat. After the probes had been inserted and cemented in place with Armstrong cement, the spacing of the probe tips was measured with a cathetometer to an accuracy of about 1 mil.

After each glass tube was assembled and filled with Nitromethane, it was placed in a wooden box and insulated with vermiculite. This assembly was then placed in an oven or a deep-freeze and brought to the desired temperature. The temperature of the Nitromethane was assumed to correspond with the temperature of a piece of brass shim stock taped to the middle of the charge tube and monitored by means of a thermocouple. After the charge had come to the desired temperature it was removed from the thermostat and fired within ten minutes.

Following the above procedure for charge preparation and firing, two sets of diameter-velocity data were obtained — one at 22.5°F and one at 91.3°F. Each series contained four shots, and each shot contained three rate intervals. Between the booster and the first rate interval, a minimum of four diameters of charge was allowed for stabilization of the detonation process. The resulting data are given in Table II and are plotted in Fig. 6.

The straight line drawn through the data taken at 91.3°F was obtained by the method of least squares; the straight line at 22.5°F was simply drawn through the points and found to be adequate. The equations of the two curves are:

$$(22.5^{\circ}F) \qquad D = 6374.5 - 170.5\ (1/d)$$

$$(91.3^{\circ}F) \qquad D = 6212.5 - 51.7\ (1/d)$$

In these equations D is the detonation velocity, expressed in meters per second, at a stick diameter of d cm.

Because the slope of the diameter-effect curve at the lower

## Table II

### Firing temperature approximately 91.3°F

| Lot Number | I.D. Average (inches) | O.D. Average (inches) | 1/I.D. ($cm^{-1}$) | Velocity Uncorrected (m/sec) | Average Velocity Corrected to 91.3°F. (m/sec) |
|---|---|---|---|---|---|
| B-3261 | 0.974 | 1.097 | 0.404 | 6192<br>6194<br>6195 | 6194 |
| B-3265 | 1.247 | 1.415 | 0.316 | 6192<br>6198<br>6193 | 6194 |
| B-3266 | 1.749 | 1.900 | 0.225 | 6199<br>6200<br>6201 | 6199 |
| B-3267 | 4.055 | 4.289 | 0.0971 | 6203<br>6218<br>6207 | 6209 |

### Firing temperature approximately 22.5°F.

| | | | | | Average Velocity Corrected to 22.5°F. (m/sec) |
|---|---|---|---|---|---|
| D-4723 | 1.330 | 1.460 | 0.296 | | Failed |
| D-4741 | 1.742 | 1.890 | 0.226 | 6335<br>6334<br>6337 | 6336 |
| D-4748 | 2.571 | 2.769 | 0.153 | 6346<br>6348<br>6349 | 6348 |
| D-4750 | 4.059 | 4.295 | 0.0970 | 6361<br>6363<br>6354 | 6358 |

temperature is steeper (with relatively little change in the infinite medium velocity), it may be assumed that the decrease in the initial temperature has caused an increase in the reaction zone thickness. The thickness of this zone at each of the two temperatures in the experiment may be estimated by applying the Eyring equation for unconfined charges (which should be a good approximation for Nitromethane in glass tubes):

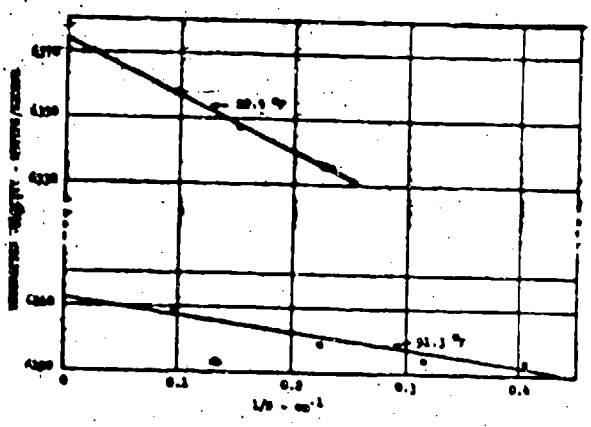

Fig. 6. Effect of temperature on the diameter effect. Nitromethane confined in glass tubes.

$$D/D_i = 1 - 0.5\,(a/R)$$

D: detonation velocity of stick with diameter R.
$D_i$: detonation velocity in infinite medium.
a: reaction zone length.

The results of the calculations are:

(22.5°F) a = 0.08 mm

(91.3°F) a = 0.27 mm

The value of a obtained at 91.3°F corresponds closely to that obtained by Cotter[5] at approximately 75°F using a streak camera technique.

It is also of interest to note that the temperature coefficient of the detonation velocity is greater for infinite medium than it is for small diameters. Using the two infinite medium extrapolations given above, a value of -4.2 m/sec/°C is obtained. At a charge diameter of 1.75 in. the value of the temperature coefficient of the detonation velocity is found to be -3.5 m/sec/°C. This is in good agreement with the value -3.7 m/sec/°C found for brass confinement at this diameter, reported in the preceeding section.

## EFFECT OF TEMPERATURE ON FAILURE DIAMETER

The effect of temperature on the failure diameter of Nitromethane was determined with the use of the charge arrangement shown in Fig. 7. The charge of Nitromethane was contained in a Pyrex brand glass tube approximately 12 diameters long. It was poured into the tube through a small hole in a thick dural plate; damage to the latter was used as a criterion for deciding whether detonation or failure had occurred (Fig. 8). Initiation of the Nitromethane was accomplished by use of a heavy booster of Composition B acting through a 50-mil glass plate, this combination resulting in slight overboosting. As in the previous set of experiments, the temperature of the charge was

maintained constant by means of substantial insulation.

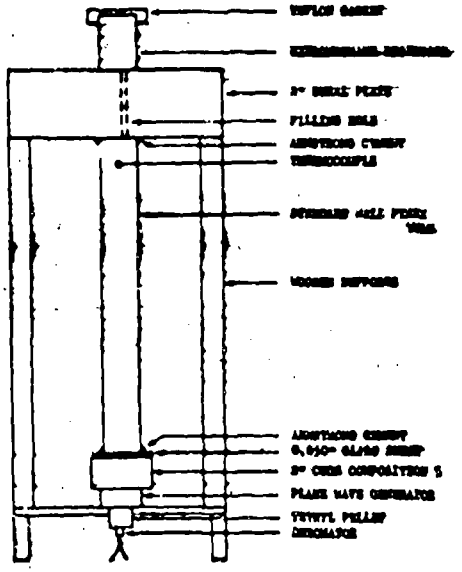

Fig. 7. Charge arrangement used to determine failure diameter

The results obtained at three temperatures are shown in Fig. 9 and are listed in Table III. While there is some overlap apparent at a given temperature, the failure diameter is defined to about 2-3 mm. Over the temperature range covered in these experiments the failure diameter varied from approximately 15 mm to 35 mm, increasing as the initial temperature was lowered.

## FAILURE PROCESS IN LIQUID EXPLOSIVES

Early work on the diameter effect in Nitromethane was directed to finding the failure diameter of this explosive in tubes of glass and various metals. Plastic tubes were not used because of the possibility of contamination of the explosive by solvent action. It soon became evident that Nitromethane would propagate (at about 75°F) in brass tubes of 3 mm i.d. and 1.6 mm wall and in dural tubes of 4.8 mm i.d. and 1.6 mm wall, but would fail in glass tubes below 17 mm i.d. Subsequent examination of the process

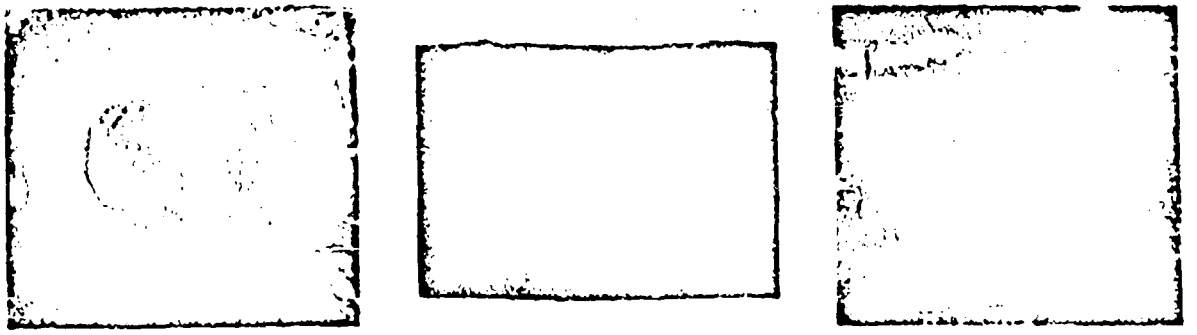

Fig. 8. Photographs A, B show the damage to dural plates resulting from propagation of detonation in charges as sketched in Fig. 7. Photograph C shows the result of detonation failure.

of failure using a streak camera showed non-luminous areas spreading inward from the confining walls and choking off the detonation process. These "failures", first observed in connection with other experiments by T. P. Cotter[5], appear to be characteristic of homogeneous explosives.

A rotating-mirror camera record of the failure of detonation in Nitromethane is shown in Fig. 10. In this figure and in Figs. 11-19 the camera has been directed to look along the axis of the charge. Time proceeds to the right at the rate of 0.39 μsec/mm. In

Table III

| I. D. Average (millimeters) | Tube Length (inches) | Temperature (degrees F) | Result* |
|---|---|---|---|
| 30.9 | 18 | -8.5 | F |
| 33.9 | 17 | -9.0 | F |
| 33.5 | 16 | -10.5 | F |
| 34.5 | 17.5 | -6.5 | F |
| 36.5 | 17.5 | -7.0 | P |
| 38.4 | 18 | -12.0 | P |
| 40.4 | 18 | -9.8 | P |
| 22.3 | 12 | 17.0 | F |
| 27.3 | 14 | 17.0 | P |
| 31.0 | 15 | 20.0 | P |
| 40.5 | 17.8 | 30.0 | P |
| 23.9 | 12 | 19.9 | F |
| 26.0 | 15 | 19.5 | F |
| 27.2 | 16 | 20.0 | F |
| 28.2 | 15.8 | 18.5 | F |
| 28.8 | 16 | 19.3 | P |
| 30.9 | 16 | 21.8 | P |
| 31.3 | 16 | 17.5 | P |
| 33.4 | 16 | 19.8 | P |
| 12.7 | 12 | 96.7 | F |
| 14.9 | 12 | 98.0 | P |
| 15.5 | 12 | 90.4 | F |
| 16.7 | 11.8 | 95.9 | P |
| 17.5 | 12 | 92.2 | P |

*F-Failure
P-Propagation

Note: All tubing was standard wall Pyrex glass tubing.

Fig. 10 the explosive was contained in a glass tube 17 mm i.d. Detonation ceased after a travel of approximately 50 mm in the Nitromethane. Similar behavior was also observed for Ethyl Nitrate (Fig. 19) and for large single crystals of PETN as will be described in a later section of this report.

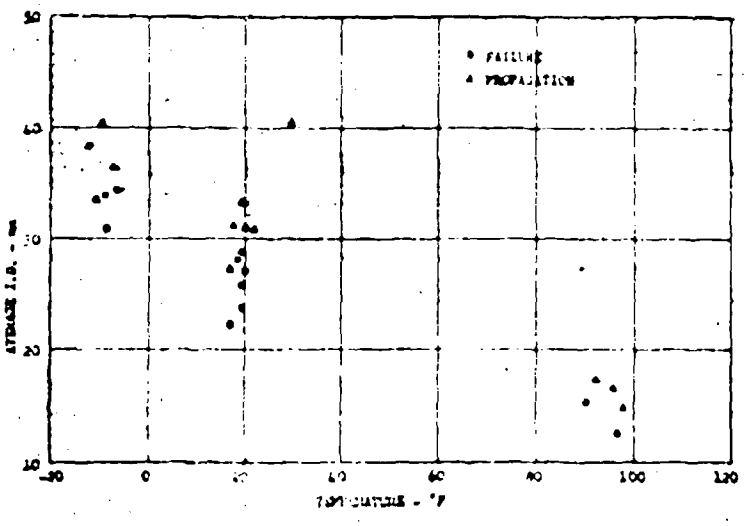

Fig. 9. Effect of temperature on the failure diameter of Nitromethane confined in glass tubes

Figure 11 shows the streak record from a charge similar to that which produced the record in Fig. 10, except that the glass was replaced by dural. No failures are evident. This difference in the effects of glass and dural on the occurrence of failures was at first quite puzzling. Since the charge-weight/casing-weight ratios for the two charges were essentially the same, and since the densities of the two materials were nearly equal, the intuitive feeling arose that the observed difference was, perhaps, not

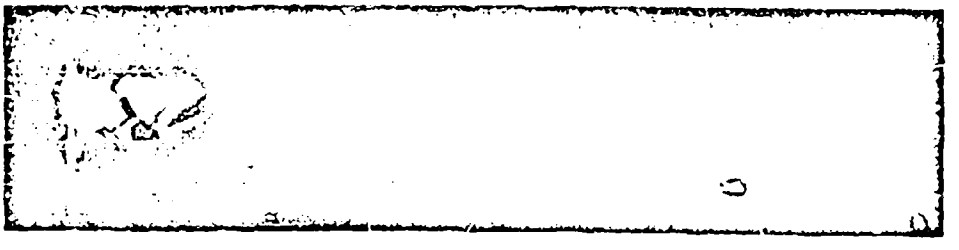

Fig. 10. Nitromethane in glass tubing. Booster flash at left end of trace. Tube i.d.: 17 mm. Time increases to the right at 0.39 μsec/mm.

the result of confinement in the usual sense, but came about through some difference in surface effects. This feeling was strengthened by the shot record shown in Fig. 12. This was produced by Nitromethane detonated in a glass tube close to failure diameter. The wall thickness of the tube was about 1 mm. Lead tape was wrapped to a thickness of 1/8 in. about the first two inches of the tube. The second two inches were lined loosely with one layer of 2-mil aluminum foil. Thus, the mass of the first part of the tube was increased substantially over that of the glass alone; the mass of the second part was essentially unchanged, but the inner surface was now aluminum. From the camera record it is evident that the increased confining mass in the first interval was relatively ineffective in eliminating failures

when compared to the action of the aluminum foil.

Referring again to Fig. 12, it should be noted that the detonation process appears to cease abruptly after reaching the end of the aluminum foil. A more direct illustration of the action of failures to choke-off the detonation is presented in Fig. 14. This is a

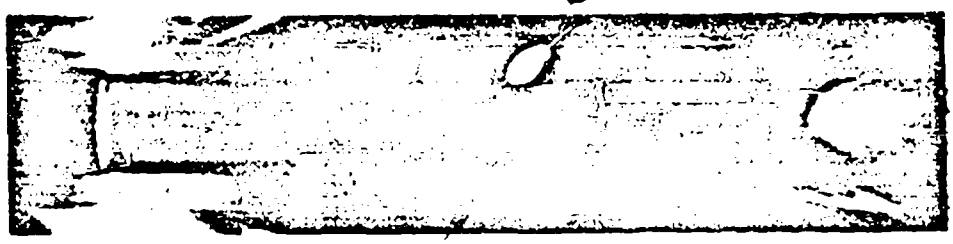

Fig. 11. Nitromethane in dural tubing. Time scale: 0.39 μsec/mm.

succession of pictures of a single charge undergoing failure. The experimental arrangement is diagrammed in Fig. 13. A glass tube filled with Nitromethane was arranged to extend into a small glass-walled box, also filled with Nitromethane. The diameter of the glass tube was chosen to be considerably below failure diameter at the temperature of firing. Propagation of detonation in the glass tube was made possible by a lining of 2-mil stainless steel foil. During detonation, the box was illuminated from the rear with argon shock light.

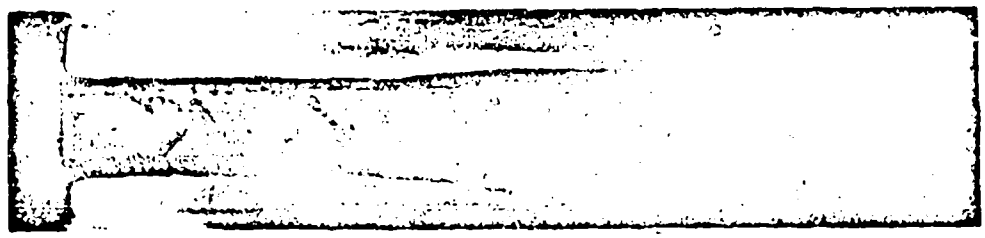


Fig. 12. Nitromethane in glass tubing. Lead foil wrapped outside tube over first 2 in. of tube length; 2 mil aluminum foil used to line tube for second 2 in. of length

Picture frames were taken with exposures of 0.3 μsec and were spaced at intervals of 1.5 μsec.

In Fig. 14, the approach of the detonation wave to the upper end of the tube is shown first in frame No. 2. As the wave emerges from the end of the tube, a rarefaction spreads inward from the periphery, giving the wave the appearance of a truncated cone. (Frame No. 3). In frame No. 4 the detonation process has ceased, and a simple shock wave is passing out into the Nitromethane filling the box.

Reverting to the thought that the effectiveness of aluminum foil in suppressing failures might be due to some surface character-

istic not possessed by glass, three experiments were tried to investigate obvious differences. These tests did not constitute an exhaustive examination of the problem, but were performed in the hope of uncovering clues which might suggest more detailed experiments. Although the results were negative, they are offered here because they contribute to limiting the possible explanations of the effect of metal foils in repressing failures.

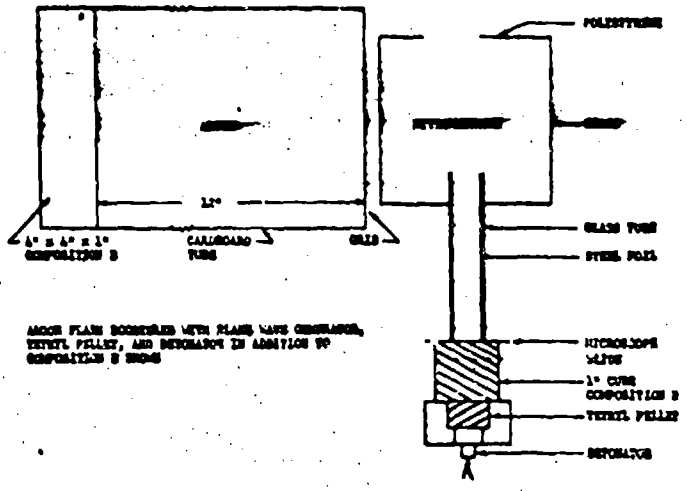

Fig. 13. Charge arrangement used to illustrate failure of detonation in Nitromethane

The first surface effect tested was that of smoothness. The glass tubing used had always had a fire-polished inner surface, whereas the metal foil had been ralatively rough. To exaggerate this difference in smoothness, a 35 mm i.d. glass tube was prepared with the latter half of the inner surface roughened with No. 54 Carborundum. The firing trace, Fig. 15, shows little or no difference between the effects of the smooth and the roughened portions. In passing, it should be noted that increase of the tube diameter resulted in the production of smaller failures than those in Fig. 10.

The next surface effect investigated was that of chemical reaction. It was argued that, contrary to the action of glass, the aluminum might react with the Nitromethane to produce decomposition products of the latter which would sensitize the explosive near the confining walls. To test this possibility, aluminum foil was immersed in Nitromethane for 19 hours. The explosive was then decanted into a glass tube. For purposes of reference the first inch of the tube was lined with 2-mil aluminum foil. The firing record, Fig. 16, shows that the Nitromethane was not sensitized to any appreciable extent.

The third surface effect to be studied was that of catalytic activity by the metal foil. A 2-mil platinum foil was poisoned with hydrogen sulfide. This was then used to line a portion of a glass tube, the remainder of which was lined with untreated platinum foil. The firing test showed the two foils to be indistinguishable in regard to the repression of failures.

In the hope of finding some difference between various metals which might furnish a hint of the mode of action of the aluminum in repressing failures, several metals were tried as foils in glass tubes. Because of ready availability, the metals tested included steel, copper, tungsten and platinum. All proved effective in thicknesses of a few mils.

One of the first clues to the true mode of action of foils was obtained in the firing record presented in Fig. 17. In this shot the diameter of the glass tube was less than failure diameter. The

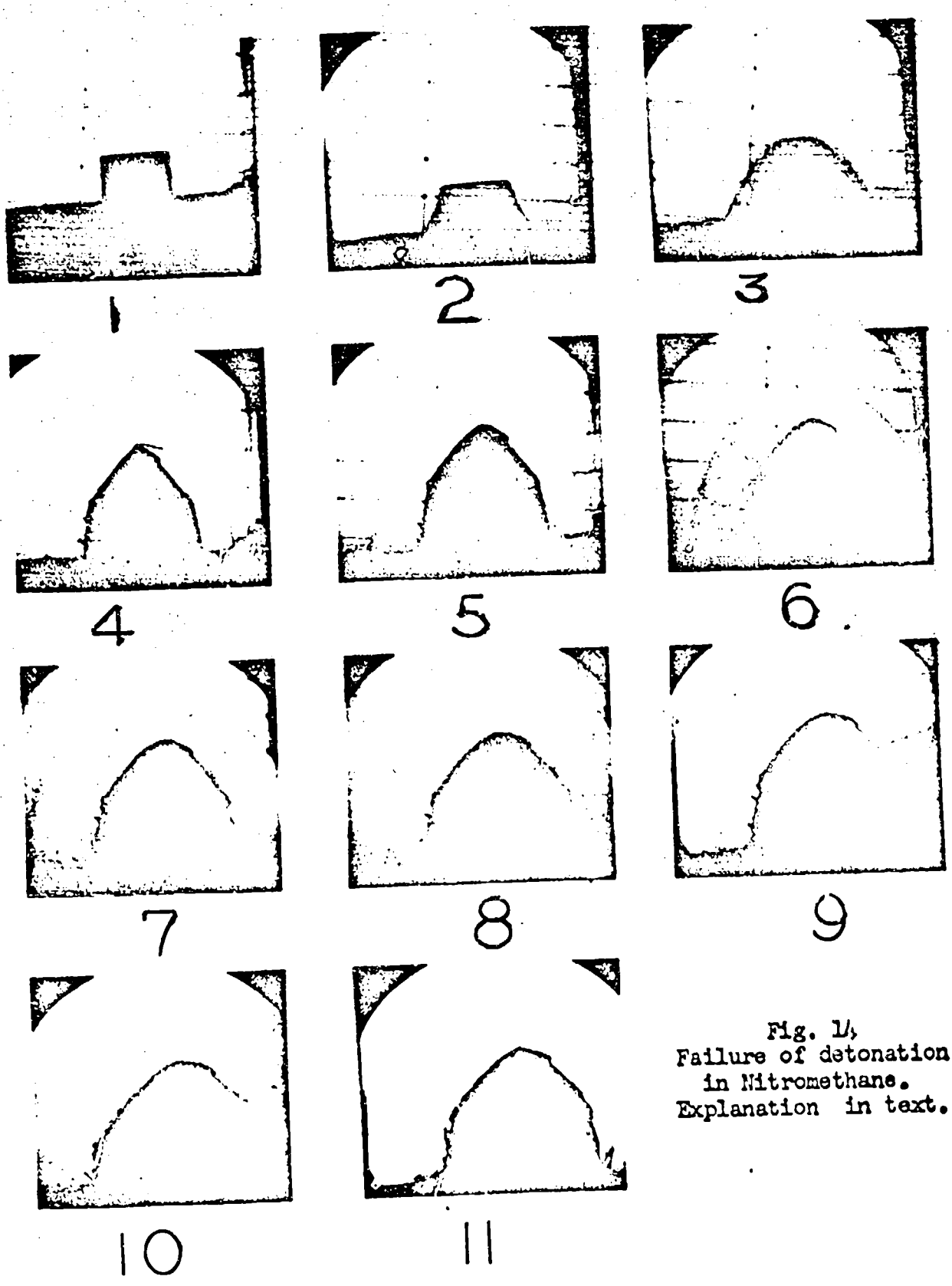


Fig. 14
Failure of detonation in Nitromethane.
Explanation in text.

first two inches were lined with 2-mil aluminum and the second two inches were lined with 1/4-mil copper. The firing record shows that

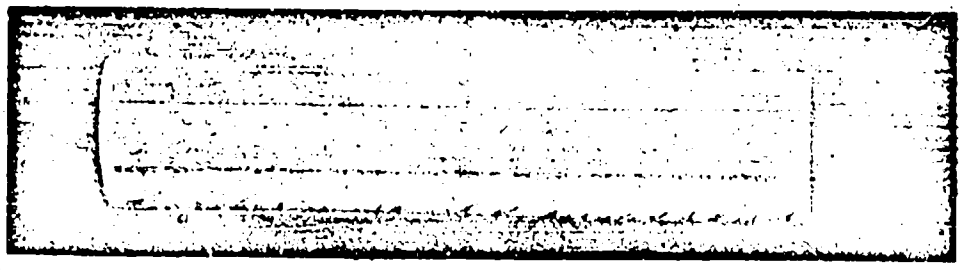

Fig. 15. Nitromethane in glass tubing. Right half of tube ground with Carborundum on inner surface. Time scale: 0.39 μsec/mm.

the detonation failed on reaching the copper foil. Since thicker copper foil had been found to be effective in preventing failures, it was suggested here that the thickness of the foil was important.

To investigate further the effect of foil thickness a glass tube with a diameter less than failure diameter for unlined glass was lined with three platinum foils of differing thicknesses. The first foil encountered by the detonation wave was 1 mil thick, the next was 1/2 mil thick and the third was 1/5 mil thick. Each foil occupied two inches of the length of the tube. The firing trace, Fig. 18, shows that only the 1/5-mil foil was ineffective in preventing failure. A

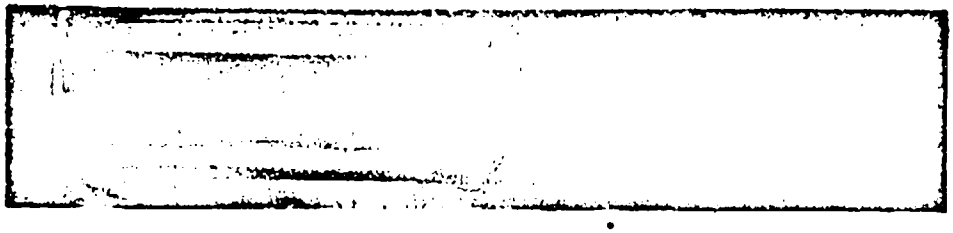

Fig. 16. Nitromethane in glass tubing. The explosive was maintained in contact with aluminum for 19 hours prior to firing. First 2 inches of tube lined with 2-mil aluminum foil. Time scale: 0.39 μsec/mm.

similar shot in which the foils were made of copper gave a similar result. Here, then, was a method of differentiating the action of foils which differed by only 0.3 mil in thickness. Additional experiments suggested that for a given foil thickness, steel was more effective a confining material than aluminum, and tungsten was more effective than steel. The effectiveness was evidenced by the minimum diameter glass tube in which propagation was made possible by the presence of the foil.

On the basis of the experimental evidence presented above and from the results of other similar experiments, it may be concluded that the action of metal foils in repressing failures in Nitromethane

is one of confinement of the detonation wave. Such parameters as the density, compressibility and thickness of the confining material are the important ones, and the specific nature of the surface seems to be without effect. Glass may be anomalous, but not enough is known about

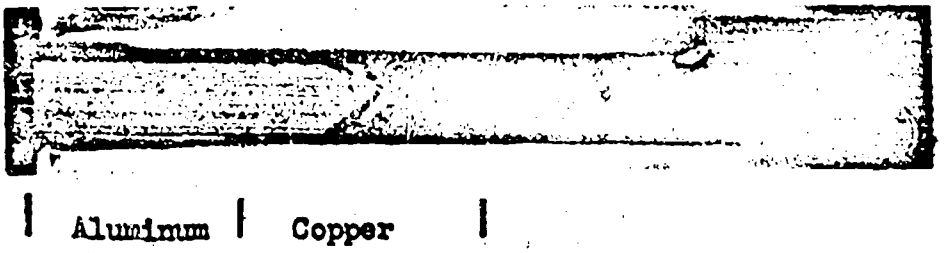


Fig. 17. Nitromethane in glass tubing. First two inches of tube lined with 2-mil aluminum foil; second two inches lined with 1/4-mil copper foil. Detonation failed before reaching end of copper foil. Time scale: 0.39 μsec/mm.

shock processes in this material to be certain of this. Because of the surprisingly thin layers of metals which are effective, it may be that confinement of the reaction zone until some initial stage of the reaction is completed is sufficient to prevent the occurrence of failures.

## DETONATION PHENOMENA IN LARGE CRYSTALS

Work on large, single crystals of high explosive was begun partly because so little was known about the behavior of such crystals and partly because of some unique properties which had been suggested

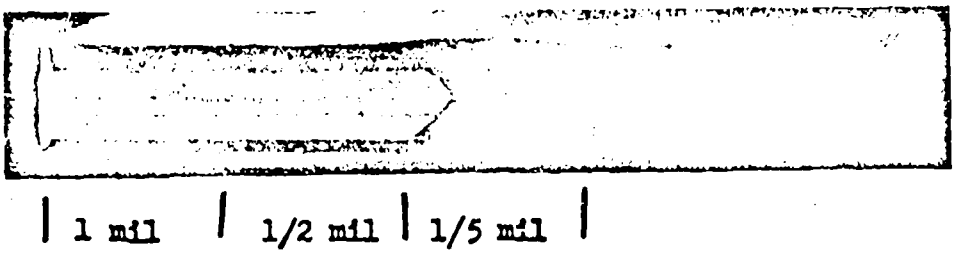


Fig. 18. Nitromethane in glass tubing. Tubing lined with three 2-in. platinum foils in series. Foil thickness: 1 mil, 1/2 mil and 1/5 mil. Detonation failed on encountering the 1/5-mil foil. Time scale: 0.39 μsec/mm.

for them. There are those who are of the opinion that it is not possible to produce a stable detonation in a single large crystal. This view follows from the belief that the compressional heating in the shock front, in the absence of air voids, is insufficient to account for the rapid rate of reaction associated with detonation. On the other hand, there is a commonly-held view that large crystals of explosive may be much more sensitive to mechanical shock

than the smaller crystals normally encountered.

These questions have been investigated for such different materials as PETN, Tetryl, RDX and TNT. Large crystals of any given explosive studied have been found to be markedly less sensitive to initiation by mechanical shock than the powdered form. However, under

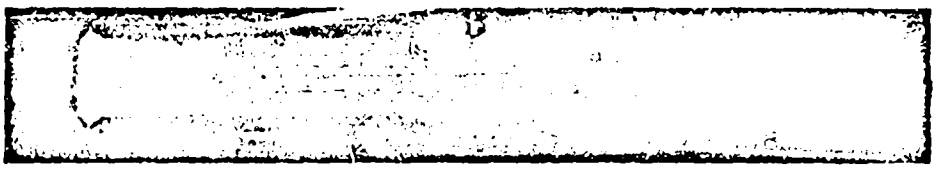

Fig. 19. Ethyl Nitrate in glass tubing 27.2 mm i.d. Tubing lined with 2.5-mil stainless steel foil. Time scale: 0.17 μsec/mm.

suitable conditions of boosting, large single crystals may be caused to detonate. It is important to note that the crystals used for detonation studies were in most cases optically clear and free from visible defects, but there was always the possibility that small-scale lattice defects throughout each crystal may have served as centers of reaction, fulfilling the requirements of the "hot spot" theory. Although this possibility may have obscured the main issue here, other equally interesting phenomena have been observed which relate the behavior of large, single crystals to that of liquids.

## Preparation of Crystals

The crystals used were grown from saturated solutions by two methods: by evaporation of solvent, and by lowering the temperature of the solution. In both methods, seed crystals were used. The solvent principally employed was acetone.

Many difficulties were encountered in growing flawless crystals to a size of one inch or larger. PETN crystals in particular, but all of them to some extent, were found to be extremely fragile when exposed to thermal shock. Merely touching the crystal with the fingers was sufficient to produce cracking which was both visible and audible. Evaporation of solvent from the crystal surface when the crystal was removed from the growing solution produced disastrous effects on the clarity of the crystal. This sensitivity to thermal shock increased rapidly with crystal size.

The quality of the crystals was quite variable. Some crystals were grown which were almost optically clear, while others had clear sections which were cut out for use in the experiments to be described below (Fig. 20). The very large crystals used in the rifle bullet tests were quite cloudy. An index of the quality of the better crystals is furnished by the data in the following table.

| Explosive | Appearance of Crystal | Density Observed g/cc (25°C) | Density Reported in Literature g/cc |
|---|---|---|---|
| PETN | Clear | 1.777 | 1.773 (6) |
| TNT | Cloudy | 1.653 | 1.654 (7) |
| Tetryl | Clear | 1.734 | 1.73 (8) |
| RDX | Cloudy | 1.802 | 1.82 (9) |

The observed density values reported above were determined by preparing a zinc chloride solution in which the crystal could be suspended. The density of the solution was then measured with a hydrometer which had been calibrated with a pycnometer.

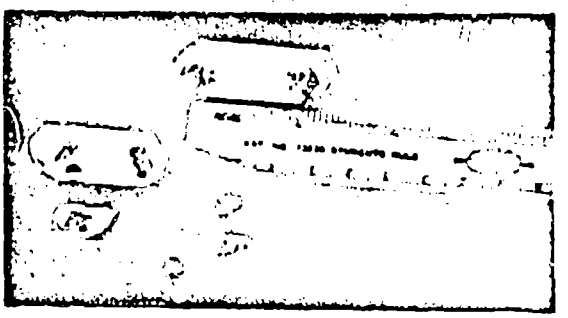

Fig. 20. Unpolished crystals of PETN

Crystals were found to be much easier to cut and shape than to grow. They could be chipped to shape with a razor blade and polished in a manner reminiscent of optical polishing methods. A more elegant way of shaping them was that of grinding with high speed grinding equipment, using kerosene as a coolant and dust allayer. The process of fabricating a cylinder from a PETN crystal was as follows: the rough crystal was cemented to a short section of wood dowel, using Armstrong cement. Only a thin layer of the cement was used because of the heat evolved in the polymerization process. When the cement had set, the dowel was mounted in a lathe and rotated slowly. The cylinder was formed by taking fine cuts with a 5-in. Alundum wheel (Norton No. 38 A 120 LV) mounted in a tool post grinder and rotated at 5000 RPM. When the cylinder had been ground to the correct diameter, the ends were cut off (Fig. 21) using a rubber-bonded Alundum wheel 4 inches in diameter and 8 mils thick (Norton No. A-240-x-10R30), also rotated at 5000 RPM.

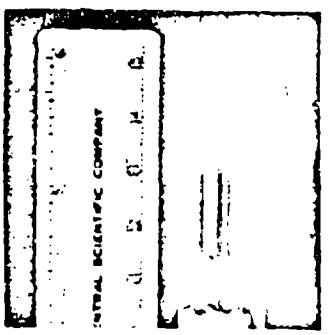

Fig. 21. Cylinder ground from PETN crystal

## Rifle Tests

At the time work was begun on crystals, there seemed to exist a widespread apprehension that large crystals of explosives were more sensitive than the same materials in any other physical state. This apprehension may have originated from a knowledge of

the great sensitivity of large grains of lead azide. Crystals of this explosive 1 mm in length have been reported to explode spontaneously (10). It was desirable, therefore, to obtain some information on the sensitivity of the large crystals of PETN being grown.

The test decided upon was a rifle test. A rifle chambered for the .220 Swift cartridge was employed; the type of bullet used in the tests was a soft-point one weighing 48 grains. It had a muzzle velocity of 4000 ft/sec and a muzzle energy of 1800 ft-lbs. In each test, with the exception of one, the crystal was mounted on plywood or corrugated paper board at a distance of 50 ft from the muzzle of the gun. The crystal was oriented with the minimum dimension in a direction parallel to the path of the bullet.

The result of each rifle test was determined from the damage to the crystal support and from the manner in which the crystal disintegrated. In all, 25 tests were made with crystals varying in thickness from 3/4 in. to 3 1/4 in. It was found that PETN crystals less than 1 1/4 in. thick did not detonate to any detectable extent; crystals approximately 1 3/8 in. thick sometimes detonated partially; and crystals more than 1 3/8 in. thick always detonated with accompanying loud noise, bright flash and thorough destruction of the backing and supporting stand.

Figure 22-A shows a PETN crystal mounted for testing on a sheet of plywood, and the damage to the backing as a result of the disintegration of the crystal is shown in Fig. 22-B. In Fig. 23-A, a 3/4 in. thick PETN crystal is shown mounted on a steel plate. The only damage to the plate as a result of the rifle test was a pit due to the impact of the bullet. Later, a similar crystal was mounted on the same plate at the lower right corner and was initiated with an electric detonator to produce damage for comparison with the result of the rifle bullet test. It is apparent that the crystal struck by the bullet did not detonate.

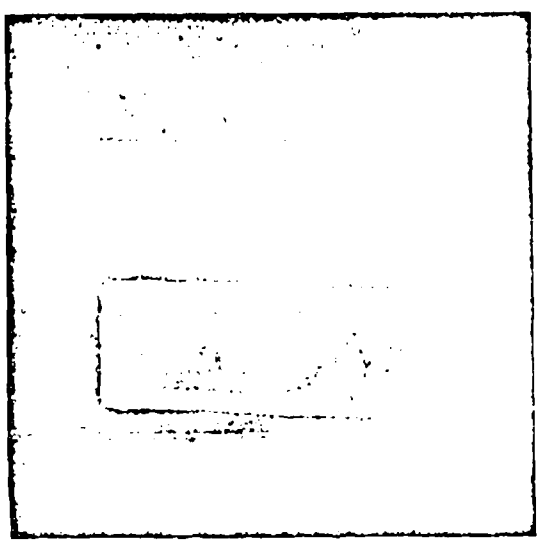

Fig. 22A. PETN crystal mounted on plywood for rifle test

The relative sensitivity of powdered PETN was illustrated by the results of thirteen additional rifle tests. In each of these tests, the powdered material was poured onto a sheet of cardboard to form a thin, uniform layer of explosive. Thin strips of wood were used to support the edges of the layer, and a thin cellophane sheet was placed over the top to hold the explosive in place when the assembly was turned on edge. The thickness of the PETN layer was 0.148 in. in the first test. Since this charge detonated, the thickness was reduced in each of the succeeding tests until on the last test a

thickness of 0.092 in. was reached. All tests resulted in detonation. Thus, it became apparent that powdered PETN was much more sensitive than large crystals of the same explosive.

Fig. 22B. Damage caused by disintegration of crystal under bullet impact

## Detonation of Single Crystals

Observations on the detonation of single crystals were made both with rotating mirror cameras and with the pin technique. Unfortunately, the work on the measurement of detonation velocity was interrupted before satisfactory data could be obtained. Nevertheless, many interesting qualitative details of the detonation process were discovered and these will be discussed here.

In Fig. 24-A, a PETN crystal .616 in. thick is shown mounted above a plane wave generator. A flat face was ground on one side of the crystal, making an angle of 45° with the base. The crystal was separated from a Composition B booster by a distance of 0.3 in. When the charge was fired a plane detonation wave was produced in the plate of Composition B. This in turn produced a plane shock wave in the air space above the plate, which initiated the PETN crystal weakly. The detonation wave proceeding up the crystal gave evidence of its position by a luminous shock in the narrow air space under the plastic cover.

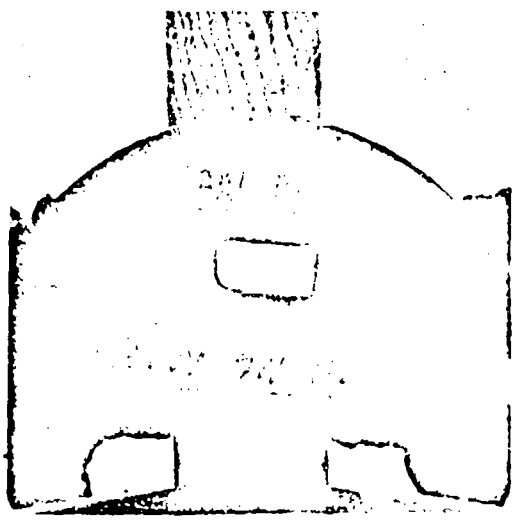

Fig. 23A. PETN crystal mounted on steel plate for rifle test

The firing trace from this shot is shown in Fig. 24-B and is explained by means of the sketch in Fig. 24-C. In the latter figure, interval I shows the shock traversing the air space between the Composition B and the crystal. In interval II, a detonation wave proceeds at low velocity and with low luminosity through the crystal. At the beginning of interval III, the detonation wave undergoes an abrupt increase in velocity and brightness. The velocity actually exceeds the steady-state value for a short space, then drops to that value. In interval IV, the shock wave in air

beyond the crystal is evident. The details of this record were found to be repeated in many similar experiments. Besides the interesting phenomenon of overshoot in the velocity, which has also been observed for detonation in gases[11], the experiment shows that with underboosting, the detonation rate increases to the final, steady-state condition, proving that stable detonation in single crystals is possible.

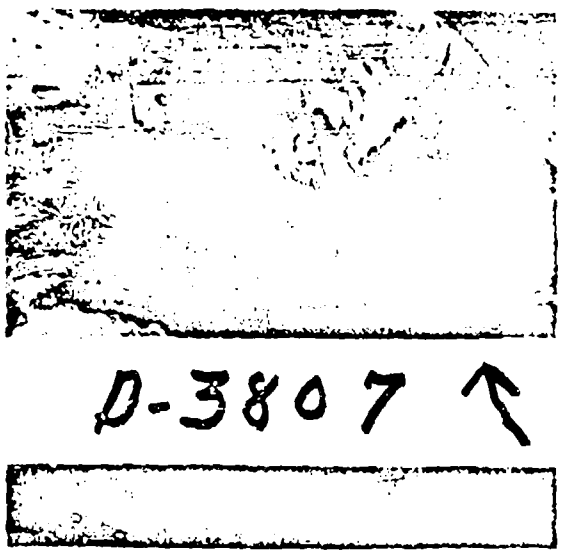


Fig. 23B. Circular pit at left is due to bullet impact in rifle test of crystal shown in Fig. 23A. Rectangular pit at right is damage which resulted from the initiation of a similar crystal with an electric detonator.

Actual detonation velocities in the above experiment were difficult to measure with accuracy, because of the problem of accurate space measurement. The estimated values of the detonation velocity were 5560 m/sec for the initial phase, 11,120 m/sec for the overshoot and 7240 m/sec for the final state.

In another type of experiment, crystals were ground into rods and stacked to make rate sticks as shown in Fig. 25. The purpose of the two experiments of this type which were completed was to estimate the failure diameter, and to measure the detonation rate, if detonation occurred, using the pin technique. In the first shot, the crystals were ground to a diameter of 1/4 in. and a length of approximately 1 in. Boosted with a cube of Composition B 1/2 in. on a side, this charge failed to detonate. In the second experiment, the crystal diameter was 1/3 in. and the lengths of the two sections were 0.929 in. and 0.763 in. Measured velocities were 7973 m/sec over the first piece beyond the booster, and 6083 m/sec over the second piece. Since the diameter of the stick may still have been near the failure value, failure might have occurred in the second interval and the final pin signal could have been due to closure of the pin switch by air blast.

## Failures and the Foil Effect for Crystals

The fact that crystals exhibit "failures" and the foil confinement effect is demonstrated in Fig. 26. This is the record obtained from a PETN crystal cut in the form of a parallelepiped measuring 0.25 x 0.25 x 0.40 in. A 2-mil copper foil was glued around the crystal, extending 0.2 inch in the long direction. The end of the crystal which was thus wrapped with foil was initiated with a 1/2-in. cube of Composition B. A rotating mirror camera was directed to look down the long axis of the crystal. From the firing record, Fig. 26,

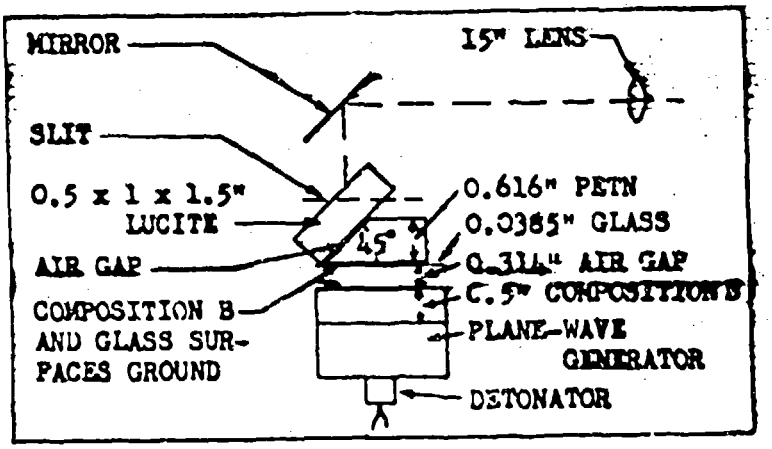


Fig. 24A. Charge arrangement for shot to measure detonation velocity in a single crystal of PETN

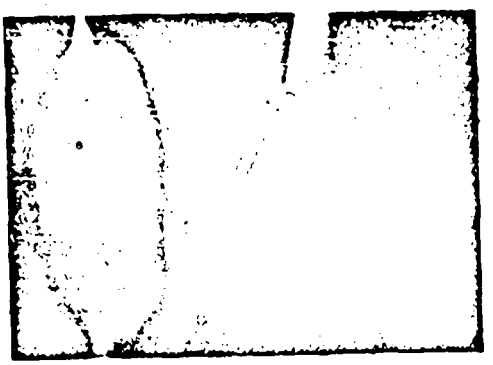

Fig. 24B. Firing trace

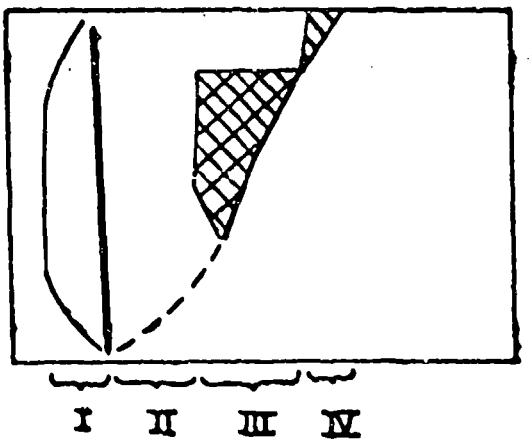


Fig. 24C. Sketch of firing trace

it is evident that while the cross section of the crystal was quite small, no failures occurred until the detonation wave passed beyond the copper foil confinement, at which time failures appeared and rapidly choked off the detonation. Many similar records were obtained in other experiments.

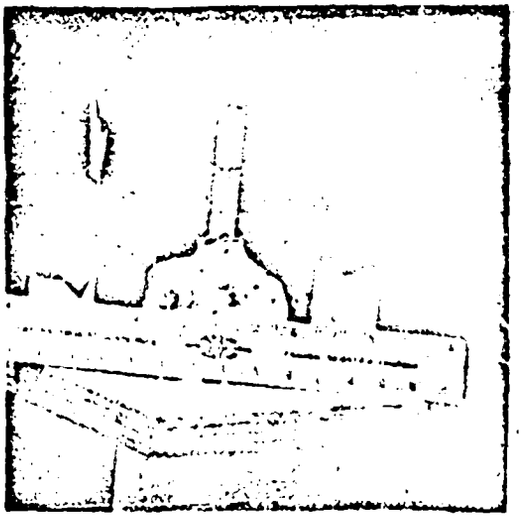

Fig. 25. Rate stick made of PETN crystals ground to cylindrical shape. Putty was placed over the booster to hold back air blast.

## CONCLUSION

In the foregoing sections, data have been presented to show that initial temperature has a pronounced effect on the detonation velocity of Nitromethane. The velocity was found to increase with decrease in temperature, as was also the diameter effect and the failure diameter. The curves of detonation velocity as a function of the diameter were, for Nitromethane lightly confined in glass, essentially straight lines out to failure diameter.

When detonation failure occurs in liquid explosives and single crystals, the failure process begins abruptly at the periphery of the detonation wave and spreads inward to engulf the entire wave. For glass confinement above failure diameter, small failures were shown to occur at the walls with high frequency, but each of these persisted for only a brief time.

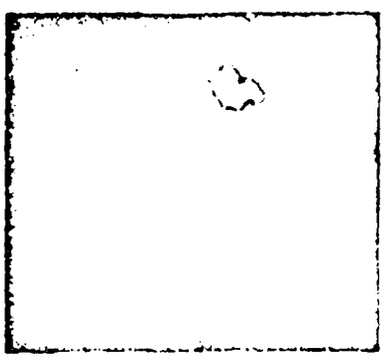

Fig. 26. Single crystal of PETN showing failures. Time increases to the right.

For explosives in the form of liquids and single crystals, thin metal foils were shown to be effective in suppressing failures and in reducing the failure diameter substantially. The density and the thickness were of importance in determining the confining effect exerted by a foil.

Lastly, work on the growth and fabrication of large crystals of various explosives was reported. Crystals of PETN were tested with rifle bullets and found to be relatively insensitive when compared to powdered PETN. Incomplete experimental work on measuring detonation velocities in single crystals was described to show that detonation will propagate under the conditions prevailing in these crystals.

## REFERENCES


1. H. Eyring, R. E. Powell, G. H. Duffey and R. B. Parlin, Chem. Revs., 45, 69(1949).

2. H. Jones, Proc. Roy. Soc. (London), A189, 415(1947).

3. K. W. Campbell, M. E. Malin, T. J. Boyd, Jr. and J. A. Hull, "Technique for the Measurement of Detonation Velocity". (This Conference).

4. International Critical Tables (McGraw-Hill Book Company, Inc., New York, 1928), first edition, Vol. III, p. 28.

5. T. P. Cotter, Jr., "The Structure of Detonation in Some Liquid Explosives". (Dissertation, Cornell University, 1953).

6. C. D. Hodgman, Handbook of Chemistry and Physics (Chemical Rubber Publishing Company, Cleveland, O., 1951). 33rd edition, p. 1150.

7. N. A. Lange, Handbook of Chemistry (Handbook Publishers, Inc., Sandusky, O., 1952), eighth edition, p. 693.

8. I. M. Heilbron, Dictionary of Organic Compounds (Oxford University Press, New York, 1943), Vol. III, p. 740.

9. W. C. McCrone, Analy. Chem., 22, p. 954(1950).

10. T. L. Davis, The Chemistry of Powder and Explosives (John Wiley and Sons, Inc., New York, 1943), p. 425.

11. D. J. Berets, E. F. Greene and G. B. Kistiakowsky, J. Am. Chem. Soc., 72, 1086(1950).

# PARTICLE SIZE EFFECTS IN ONE- AND TWO-COMPONENT EXPLOSIVES 23

M. E. Malin, A. W. Campbell and C. W. Mauts
Los Alamos Scientific Laboratory
Los Alamos, New Mexico

## INTRODUCTION

The subject of particle size effects is an important one in many military and commercial explosives. With the exception of liquid explosives and the blasting gelatins, every explosive in common use is composed of material whose state of subdivision has a bearing on its detonation properties. From a practical viewpoint, then, particle size effects warrant attention.

Aside from practical consideration, it appears that those theories which do not inquire into the details of the reaction kinetics, e.g., early diameter effect theories, do not correctly predict the behavior of at least some heterogeneous explosives at finite diameters. Further, the apparent persistence of particle size effects to infinite diameter opens speculation concerning the location of the Chapman-Jouguet surface under infinite-medium conditions. It seems, therefore, that a better understanding of these effects will require additional theoretical and experimental inquiry into reaction zone structure and also into the mechanism of detonation propagation under conditions of varying particle size and geometry; reaction rate considerations have been introduced by Kirkwood and Wood[1] into their theory of the structure of a plane detonation wave, and this theory does indeed offer possible explanations for certain of the observed infinite diameter effects, as will be seen later in the paper.

The importance of particle size effects in one-component explosives has been well-demonstrated by various workers. MacDougall, Martin, Boggs and Messerly[2] have shown that in low density ammonium picrate charges the addition of a small percentage of coarse material to fine particles markedly lowers the detonation velocity (all charges corrected to the same density). More surprisingly, in their experiments the addition of a small amount of fine material to coarse particles also lowers the velocity, while mixtures in the vicinity of 70% coarse, 30% fine (under their conditions of particle size, charge diameter and confinement), could not be detonated. Explanations for this

behavior have been offered by Gamow[3] in terms of numbers of load-bearing contact points, but the effect is still not completely understood.

Jones and Mitchell[4] have shown that, within certain particle size ranges, low-order detonation is possible in low density TNT charges and in Tetryl charges.

Tranter[5] and others have shown that particle size effects are also important in high density, cast explosives. In their experiments, they demonstrate a marked effect of the rate of cooling of cast TNT charges on the detonation velocity.

Although the above is far from being a complete survey of the particle size effect literature, it indicates that in the past much attention has been devoted to one-component systems, and understandably so, since these are already sufficiently complex. Nevertheless, there are many two-component heterogeneous explosives in use in which particle size effects appear to be important, in a manner perhaps different from the case of one-component systems, and this paper is primarily concerned with a discussion of such two-component systems.

The work described here has been done principally with Composition B, a cast explosive containing approximately 60% RDX and 40% TNT. In the casting of this material, the temperature is raised sufficiently to melt the TNT, the RDX is then added, and the TNT is allowed to slowly solidify to form a continuous matrix in which the RDX particles are embedded. Under these casting conditions there is some solubility of RDX in TNT (4 to 8% by weight), the dissolved RDX precipitating as the TNT solidifies. The size of these precipitated RDX particles is not known and probably varies with casting conditions.

The reasons for the choice of Composition B for this work can be stated briefly: Composition B is a relatively inexpensive and available material of intermediate sensitivity and high energy. It is characterized by a short reaction zone length and an accompanying convenient range of working diameters. The failure diameter is approximately 1/6", and sticks 1 1/2" in diameter have a detonation velocity which is lower than infinite medium velocity by about 40 m/sec. Perhaps most important, it is a high density explosive, readily machinable to tolerances of 0.001".

Along with other two-component cast explosives, charges of Composition B have the disadvantage of particle size, density and composition segregation. These are compensated for, to some extent, by well-developed sampling and analytical techniques. Composition B also contains a variable amount of wax and other additives (1 to 1.5%), and for precise work these must be quantitatively determined.

The paper will be divided into two parts; Sections I - III will be concerned with particle-size effects at finite diameter and IV - V with particle-size effects at infinite diameter.

## EXPERIMENTAL I

The detonation velocity of a species of Composition B, which

will be called Type I, was determined as a function of diameter. The general technique of charge assembly is discussed in another paper[6], so that only the more important details need be given here. The charges were assembled vertically with 0.0002" aluminum ionization foils inserted between sticks. Duco cement was used to keep the sticks in place, and care was taken in the cementing process to avoid introducing any glue between the joints. In each case, before velocity measurements were taken, the detonation wave ran at least four charge diameters in a section of the booster which was the same diameter as the rate stick. The rate sticks were each approximately 2" long. Plate 1 shows a typical charge assembly.

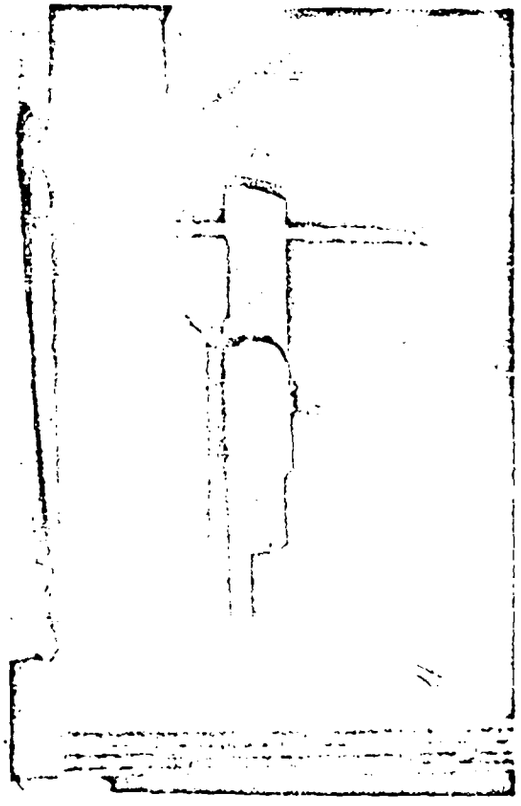

Plate 1. Composition _ Charge Assembly

The charges fired were of two types: those including only one rate stick section and those including three rate stick sections. The velocities obtained in a three-rate-stick charge are designated in Table 1, below, as A, B and C.

The casting from which these charges were obtained had been sampled and analyzed throughout for composition and density. It was therefore possible to correct the velocity of each rate stick to a common composition and density, 63.00% RDX and 1.700 g/cc. The correction factors used were +32 m/sec for +0.01 density unit and +13.4 m/sec for +1.00% RDX. These numbers have been obtained from other experiments, involving pressings and castings, in which the density and composition were varied separately.

## DISCUSSION I

The data given in Table 1 are shown plotted in Figure 1. A plot of detonation velocity versus the reciprocal of charge radius (hereafter referred to as D versus 1/R) is a significant one for comparison with theory.

According to the general diameter effect theory developed by Eyring et. al.[7], which includes certain specific assumptions to extend the theory to the range of small radii of curvature, the D versus 1/R plot for values of a/R from 0 to 0.5 should be very similar to a straight line of the form:

## Table 1

### Type 1 Composition B

| Charge Diameter (inches) | 1/Radius ($cm^{-1}$) | Length (cm) | Transit Time (microseconds) | Experimental Velocity (m/sec) | Corrected Velocity (m/sec) |
|---|---|---|---|---|---|
| 1.003 | 0.785 | 5.088 | 6.466 | 7869 | 7851 |
| 1.002 | 0.786 | 5.086 | 6.449 | 7886 | 7869 |
| 0.975 A | 0.808 | 5.066 | 6.438 | 7869 | 7858 |
| 0.975 B | 0.808 | 5.057 | 6.431 | 7863 | 7858 |
| 0.975 C | 0.808 | 5.064 | 6.453 | 7848 | 7852 |
| 0.500 | 1.58 | 5.059 | 6.473 | 7816 | 7805 |
| 0.500 | 1.58 | 5.078 | 6.494 | 7820 | 7810 |
| 0.395 A | 1.99 | 5.027 | 6.455 | 7788 | 7777 |
| 0.394 B | 2.00 | 5.074 | 6.512 | 7792 | 7789 |
| 0.394 C | 2.00 | 5.069 | 6.537 | 7754 | 7751 |
| 0.313 A | 2.52 | 5.060 | 6.539 | 7738 | 7725 |
| 0.313 B | 2.52 | 5.090 | 6.589 | 7725 | 7712 |
| 0.313 C | 2.52 | 5.060 | 6.532 | 7746 | 7733 |
| 0.334 | 2.36 | 5.036 | 6.508 | 7738 | 7725 |
| 0.333 | 2.37 | 5.050 | 6.522 | 7743 | 7719 |
| 0.251 | 3.14 | 6.612 | 8.645 | 7648 | 7639 |
| 0.250 | 3.15 | 5.060 | 6.614 | 7650 | 7650 |
| 0.221 | 3.56 | 5.071 | 6.697 | 7572 | 7553 |
| 0.221 | 3.56 | 4.959 | 6.559 | 7561 | 7542 |
| 0.201 | 3.92 | 4.694 | 6.280 | 7475 | 7459 |
| 0.200 | 3.94 | 5.046 | 6.749 | 7477 | 7461 |
| 0.183 | 4.30 | 5.069 | 6.920 | 7325 | 7317 |
| 0.181 | 4.35 | 5.070 | 6.938 | 7308 | 7291 |
| 0.182 | 4.33 | 5.075 | 6.865 | 7393 | 7377 |
| 0.175 | 4.50 | 5.075 | 7.156 | 7092 | 7088 |
| 0.175 | 4.50 | 5.076 | 7.184 | 7066 | 7058 |
| 0.168 | 4.69 | 5.034 | Failed, only first signal obtained. | | |
| 0.168 | 4.69 | 3.369 | 5.014 | 6719 | 6703 |

$$\frac{D}{D_i} = 1 - 0.5\, a/R, \qquad (1)$$

where D = detonation velocity,

$D_i$ = infinite medium detonation velocity,

a = reaction zone length, (assumed constant),

R = charge radius.

It is clear from Figure 1 that this equation does not represent the experimental data over the entire range covered, although at diameters above 0.25" a straight line fits the data well. Below 0.25", the detonation velocity falls markedly with decreasing charge diameter, the slope reaching a value as high as 50 m/sec velocity decrease per 0.001" diameter decrease. The Eyring theory as given in (7) does indeed predict that the D versus 1/R plot will deviate from a straight line at values of a/R above 0.5. It is thought, however, that in the experimental data presented a/R is below 0.5. Further, the deviations from a straight line that we observe at small diameters are in the opposite direction to those predicted by the theory.

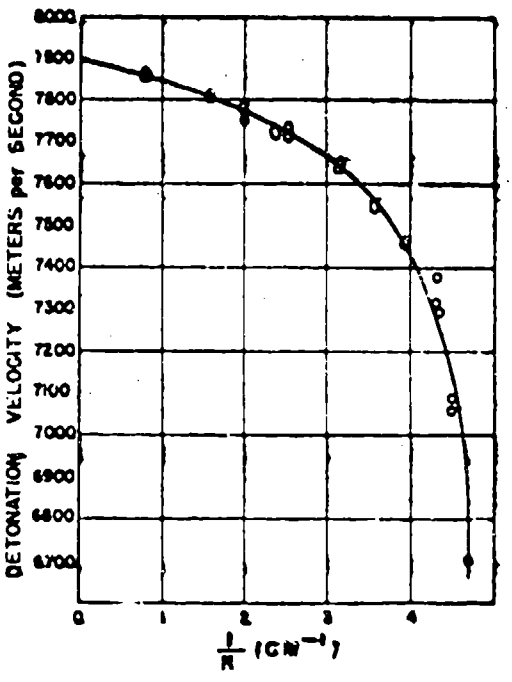


Fig. 1. Detonation velocity versus reciprocal of charge radius, Type 1 Composition B.

If the Eyring theory is applied to the section of this graph above 0.25" one obtains a value of 0.2 mm for the reaction zone length.

An extension to this diameter effect theory has been proposed by Parlin, Thorne and Robinson[8] which gives somewhat different conclusions. This extension still does not allow for the sharp drop in velocity at the smaller diameters, but, in general, is more successful in predicting the overall shape of the D versus 1/R plot.

To compare the diameter effect theory of Jones[9] with the experimental data, a more complicated procedure is necessary. From the Jones theory one obtains the equations:

$$\frac{D_i}{D^2} = 1 + c(r^4 - 1) \qquad (2)$$

$$r = 1.85(1 - a/R \cot \theta) \qquad (3)$$

$$a/R = 0.919 \frac{\sin \theta}{1 + \cos \sqrt{2}\ \theta}, \qquad (4)$$

where D = the detonation velocity at charge radius R,

$D_i$ = the detonation velocity at infinite charge radius,

a = the reaction zone length (assumed constant as the radius is varied),

r = the relative expansion of the stream tube at a distance equal to the length of the reaction zone,

(90 - θ) = the angle between two lines drawn from the inner Meyer streamline, a reaction zone length behind the edge of unreacted explosive, one parallel to the charge axis, and the other drawn to the outer edge of the unreacted explosive,

c is a constant, taken to be 2.0 for many cast explosives.

To obtain D/Di for values of a/R smaller than those calculated by Jones (so as to be in our working range), the following was done: an assumed value of a/R was placed in equation (4), and the equation solved for θ; this value of θ was placed in equation (3), which was solved for the value of r. This value of r was then placed in equation (2), and the process was repeated for each value of a/R. The results are given below in Table 2.

Table 2

Jones Nozzle Theory for Unconfined Explosives

| a/R | r | D/Di |
|---|---|---|
| 0.1 | 1.0003 | 0.9987 |
| 0.2 | 1.0011 | 0.9956 |
| 0.3 | 1.0044 | 0.9827 |
| 0.4 | 1.0120 | 0.9545 |
| 0.5 | 1.0245 | 0.9116 |
| 0.6 | 1.0418 | 0.8587 |
| 0.7 | 1.0626 | 0.8032 |
| 0.8 | 1.0869 | 0.7474 |
| 0.9 | 1.1192 | 0.6840 |

From Table 2, we obtain a plot of D/Di versus a/R, according to the Jones theory. Next, by taking the experimentally extrapolated value of Di (7895 m/sec), we can plot our experimental data in the form of D/Di versus 1/R as shown in Figure 2. If we then take one value of D/Di on this experimental curve, we obtain a corresponding value of 1/R. If we take the same value of D/Di on a plot of the data of Table 2, shown as a solid curve in Figure 3, we obtain a corresponding value of a/R, thus leading to a value of a for this value of D/Di. Next, taking another value of D/Di and repeating this process, another corresponding value of a is obtained, and so on. Since the Jones theory postulates a constant value of a, this procedure is a test for the applicability of the theory. Using this method of comparison, the results obtained were:

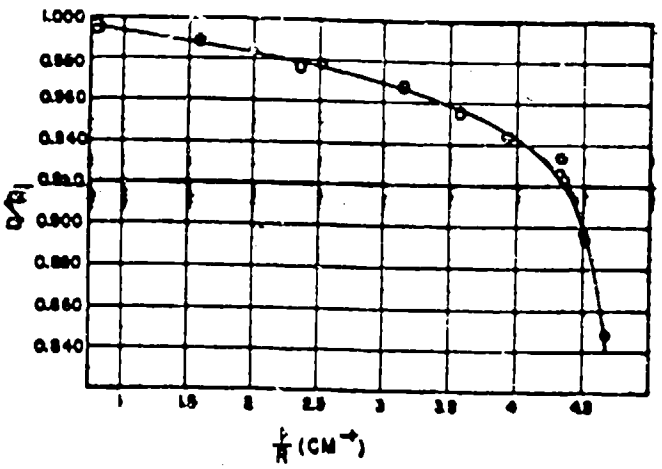


Fig. 2. Experimental velocity/infinite medium velocity versus reciprocal of charge radius. Type 1 Composition B.

| D/Di | a (in mm) |
|---|---|
| 0.990 | 1.79 |
| 0.970 | 1.20 |
| 0.950 | 1.09 |
| 0.930 | 1.08 |
| 0.910 | 1.13 |
| 0.890 | 1.19 |
| 0.870 | 1.24 |
| 0.850 | 1.31 |

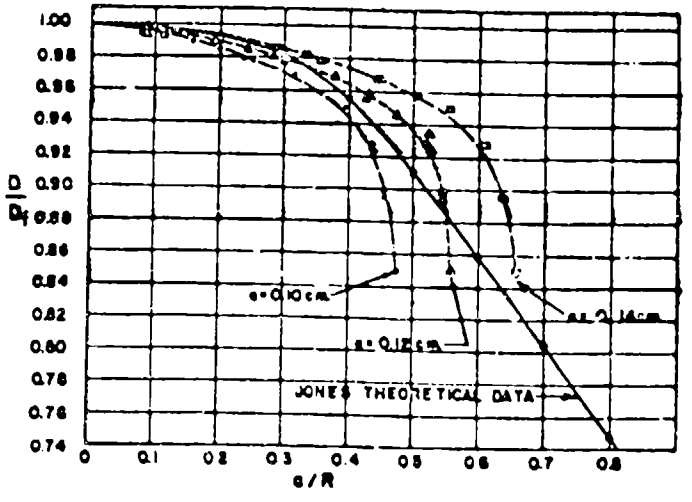


Fig. 3. Experimental and theoretical plots according to the Jones theory.

The value of a obtained here is greater by a factor of 5 or 10 than the value obtained by applying the Eyring theory at the larger diameters.

Next, assuming respectively values of a = 1.0 mm, 1.2 mm, 1.4 mm, a plot of the experimental data in the form of D/Di versus a/R is obtained. These are shown as the dotted curves in Fig. 3.

It appears that the Jones theory at least predicts the general shape of the experimental curve, although the agreement is not exact over the entire experimental range.

## EXPERIMENTAL II

Having established a reference curve for a particular type of Composition B, i.e., a particular RDX particle size distribution, the next point of interest is the effect of a change in the particle size on the D vs 1/R relationship. In Type 1 Composition B, 80% of the RDX particles were less than 400 microns and 20% were 400 microns or greater. The first alteration introduced was an increase in the RDX particle size: a Composition B casting was prepared using spherical grain RDX of particle sizes ranging from 20 to 35 mesh (833 microns to 417 microns). Since this RDX of large particle size had a tendency to segregate in the bottom of the melt, it was necessary to add the RDX when the TNT was quite viscous. This resulted in the entrapping of air bubbles, so that the casting was not as free from voids as was the Type 1 casting.

The casting was sectioned into five slabs, the top, bottom and center sections being used for analyses and the two remaining sections for the experimental work.

The charge assembly technique was the same as that described in connection with Type 1 Composition B. The experimental results are given in Table 3, in which this Composition B of large RDX particle size is designated as Type 2. The velocities have been corrected again to 63.00% RDX and 1.700 g/cc.

## DISCUSSION II

The data obtained in this experiment are neither so consistent nor so reliable as the Type 1 data because of the lack of uniformity of the casting previously discussed. It can be observed in Table 3 that two sticks of the same diameter may differ in velocity by as much as 100 m/sec. In spite of this large scatter at several diameters, the trend remains clear.

The experimental results are shown in Figure 4, where the circles indicate the mean of the velocities obtained at each diameter for Type 2 Composition B. Also shown in the same figure for comparison is the curve obtained for Type 1 Composition B. The curve for the Type 2 material is similar in form to that for Type 1, a relatively straight line section at the smaller values of 1/R, followed by a sharp decrease in velocity at larger 1/R. If the Eyring theory for unconfined charges (equation 1) is applied to the straight line portion of the Type 2 curve, one obtains a value of 0.4 mm for the reaction zone length, compared with the 0.2 mm obtained in the same way for Type 1.

The value of 1/R above which the rapid decrease in velocity occurs is smaller for the Type 2 material than for the Type 1. The failure diameter of Type 2 Composition B is also significantly greater than that of Type 1.

Table 3
Type 2 Composition B

| Charge Diameter (inches) | 1/Radius ($cm^{-1}$) | Length (cm) | Transit Time (microseconds) | Experimental Velocity (m/sec) | Corrected Velocity (m/sec) | Average Corrected Velocity |
|---|---|---|---|---|---|---|
| 0.980 | 0.803 | 6.617 | 8.541 | 7747 | 7743 | |
| 0.979 | 0.805 | 5.586 | 8.451 | 7793 | 7789 | 7773 |
| 0.980 | 0.803 | 6.541 | 8.376 | 7809 | 7787 | |
| 0.501 | 1.57 | 6.565 | 8.621 | 7615 | 7631 | |
| 0.501 | 1.57 | 6.588 | 8.616 | 7646 | 7643 | 7646 |
| 0.500 | 1.57 | 6.537 | 8.547 | 7648 | 7664 | |
| 0.333 | 2.36 | 6.591 | 8.833 | 7462 | 7503 | |
| 0.334 | 2.36 | 6.565 | 8.709 | 7538 | 7516 | 7501 |
| 0.334 | 2.38 | 6.620 | 8.878 | 7457 | 7485 | |
| 0.308 | 2.56 | 6.597 | 8.949 | 7372 | 7394 | 7438 |
| 0.308 | 2.56 | 6.629 | 8.887 | 7459 | 7481 | |
| 0.295 | 2.67 | 4.580 | 6.236 | 7344 | 7372 | 7415 |
| 0.295 | 2.67 | 4.587 | 6.174 | 7430 | 7458 | |
| 0.282 | 2.79 | 6.577 | 9.903 | 7233 | 7233 | |
| 0.283 | 2.78 | 6.617 | 9.135 | 7244 | 7268 | 7263 |
| 0.280 | 2.81 | 6.605 | 9.001 | 7338 | 7369 | 7321 |
| 0.280 | 2.81 | 6.593 | 9.104 | 7242 | 7273 | |
| 0.274 | 2.87 | 6.603 | Failed | | | |
| 0.265 | 2.97 | 6.602 | Failed | | | |
| 0.202 | 3.90 | 4.816 | Failed | | | |
| 0.201 | 3.92 | 4.811 | Failed | | | |
| 0.192 | 4.10 | 4.098 | Failed | | | |

The difference in detonation velocity between these two materials is greater the smaller the diameter.

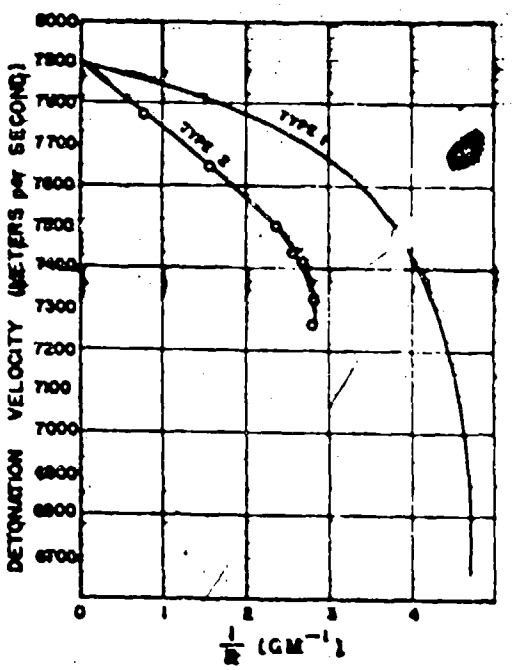


Fig. 4. Detonation velocity versus reciprocal of charge radius, Types 1 and 2 Composition B.

## EXPERIMENTAL III

Since it has been shown that in Composition B variations in the RDX particle size distribution influenced the detonation velocity at finite diameters, it was thought interesting to inquire into the effects of variations in the TNT crystal size. For a preliminary investigation, the simplest method of introducing variations in the TNT crystal size is by preparing several castings which differ only in cooling time.

Two cylindrical castings were prepared using Type 1 Composition B. These castings were 12" in diameter and 20" high. One of these castings, designated "fast-cooled", was allowed to settle for five hours so that no further settling would take place during the cooling period, and then cooled using circulating water at 30° C. The cooling was from the bottom and from the sides half way up to the top. The top section was insulated to prevent air-cooling. It is estimated that the time required for the entire casting to solidify was 5 to 6 hours.

The other casting, designated "slow-cooled", was allowed to settle for 3 hours and then cooled, using water at 70° C. It is estimated that the total cooling time for this casting was at least twice as long as for the fast-cooled, possibly as long as 14 hours.

The bottom section of each charge was then sectioned into rectangular pieces, density and composition analyses spotted through the sections, and the remainder used for rate sticks.

The shots were assembled and fired, using the same method described in connection with Type 1 Composition B. Each shot consisted of a booster, machined to the same diameter as the rate sticks, and two rate sticks. The booster section had a minimum length of five charge diameters.

In Tables 4 and 5, the detonation velocities for each of the two rate sticks in each charge are given. The velocity of the lower rate stick is given first in each case. The velocities have been corrected to 69.00% RDX and 1.700 g/cc.

Type 3 is the fast-cooled Composition B, and Type 4 is the slow-cooled.

Table 4
Type 3 Composition B

| Charge Diameter (inches) | 1/Radius ($cm^{-1}$) | Length (cm) | Transit Time (microseconds) | Experimental Velocity (m/sec) | Corrected Velocity (m/sec) |
|---|---|---|---|---|---|
| 0.499 | 1.58 | 7.160 | 9.018 | 7940 | 7914 |
| 0.499 | 1.58 | 6.359 | 8.015 | 7934 | 7908 |
| 0.334 | 2.36 | 5.260 | 6.716 | 7832 | 7806 |
| 0.334 | 2.36 | 5.249 | 6.694 | 7841 | 7815 |
| 0.250 | 3.15 | 3.310 | 4.268 | 7755 | 7717 |
| 0.250 | 3.15 | 3.959 | 5.141 | 7701 | 7684 |
| 0.220 | 3.58 | 3.396 | 4.473 | 7592 | 7566 |
| 0.223 | 3.53 | 2.787 | 3.657 | 7621 | 7583 |
| 0.201 | 3.92 | 3.264 | 4.335 | 7529 | 7503 |
| 0.200 | 3.94 | 4.021 | 5.313 | 7568 | 7542 |
| 0.185 | 4.26 | 3.095 | 4.192 | 7383 | 7357 |
| 0.185 | 4.26 | 3.048 | 4.108 | 7420 | 7394 |
| 0.167 | 4.71 | Failed | | | |

Table 5
Type 4 Composition B

| | | | | | |
|---|---|---|---|---|---|
| 0.499 | 1.58 | 5.151 | 6.607 | 7796 | 7883 |
| 0.499 | 1.58 | 5.123 | 6.578 | 7788 | 7875 |
| 0.334 | 2.36 | 6.339 | 8.232 | 7700 | 7775 |
| 0.334 | 2.36 | 5.876 | 7.659 | 7672 | 7747 |
| 0.251 | 3.14 | 3.971 | 5.304 | 7487 | 7562 |
| 0.250 | 3.15 | 2.668 | 3.541 | 7535 | 7610 |
| 0.223 | 3.53 | 3.800 | 5.110 | 7436 | 7511 |
| 0.222 | 3.55 | 2.624 | 2.532 | 7429 | 7516 |
| 0.201 | 3.92 | 3.526 | 4.785 | 7369 | 7444 |
| 0.202 | 3.90 | 3.533 | 4.783 | 7387 | 7462 |
| 0.186 | 4.23 | Failed | | | |
| 0.168 | 4.69 | Failed | | | |

## DISCUSSION III

The experimental data are shown plotted in Figure 5, again as D vs 1/R. As is anticipated with any preliminary casting in which unusual requirements of particle size or cooling procedure are imposed, the points at any one diameter and among the several diameters show a certain lack of uniformity.

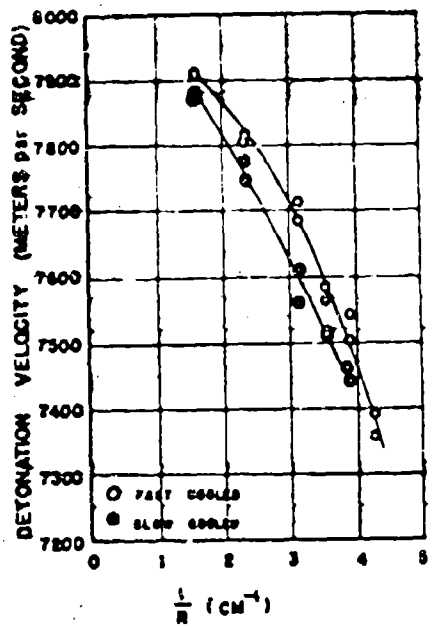


Fig. 5. Detonation velocity versus reciprocal of charge radius, Types 3 and 4 Composition B.

It can be seen in Figure 5 that at every diameter fired, the fast-cooled material has a higher velocity than the slow-cooled, so that there is clearly an effect of cooling rate on detonation velocity. Also, the fast-cooled material (on the basis of only a few shots) has a smaller failure diameter than the slow-cooled. We did not have enough material to complete the curve at the larger diameters; and, indeed, if the velocity difference becomes smaller at larger diameters the effect might have been masked by the lack of uniformity of the castings.

One can safely say that there is an effect demonstrated here, but the data are not sufficiently precise (in relation to the extent of the effect) to specify, for example, the dependence of the velocity difference on charge diameter.

In addition to the effect of cooling time on TNT crystal size, there is also the 4 to 8% RDX dissolved in the TNT, whose final particle size very likely depends on the cooling time, and may contribute to the effect observed here.

In spite of the advantages of Composition B discussed before, this experiment clearly indicates the need for a more precise method of controlling and varying the RDX and TNT particle sizes than is attainable in a casting.

## EXPERIMENTAL IV

Although in Figure 4 the curves for Type 1 and Type 2 Composition B are shown extrapolated to the same infinite diameter velocity (for want of conclusive evidence indicating otherwise), the data could be so interpreted as to indicate that Type 1 actually extrapolated to a slightly higher velocity than Type 2. To inquire further into this point, a diameter effect experiment was designed to determine

the infinite diameter detonation velocities of three types of Composition B with sufficient precision (in terms of the expected effect) to draw conclusions.

Our previous data indicated that if we fired of the order of ten 2" long rate sticks at each diameter, the average deviation would be approximately 10 m/sec, which was thought to be adequate. The diameters selected were 0.500", 0.645", 0.902", 1.500", which are equally spaced on a reciprocal radius plot.

The data previously given for Composition B, as described above, had been obtained from sticks which were placed vertically on top of each other with only a thin ring of cement at the joints for rigidity. Since this is a slow and laborious assembly procedure, we decided in this experiment to use a pair of thin angle-iron rails and place the charge horizontally on these rails (the rails having been ground previously, so as to give a minimum of contact), using Scotch tape to fasten the sticks in place. Later in the experiment, the rails were replaced with the V-notch assembly shown in Plate 2, which can be more economically machined.

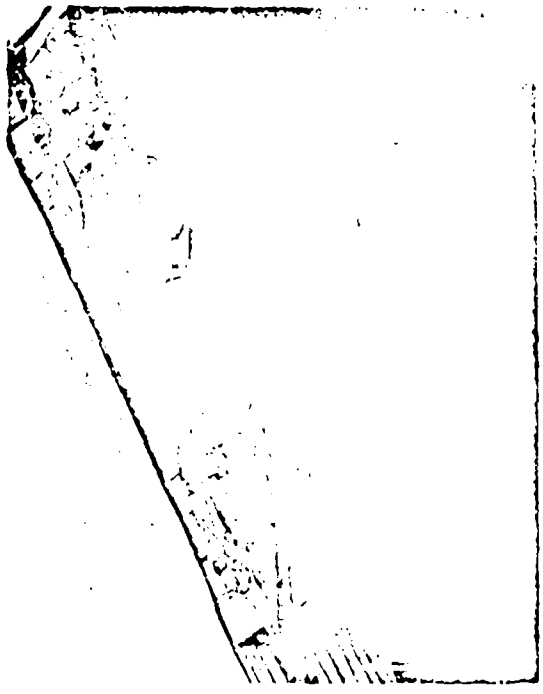

Plate 2. Improved Composition B Charge Assembly.

As described in another paper[6], precautions must be taken with the use of Scotch tape to avoid jetting which can cause premature tripping of the ionization foils. As can be seen in Plate 2, the tape is always placed posterior to a stick junction (where the foils are located), never immediately anterior.

The castings used were well analyzed throughout, and they were of uniformly high quality.

As in previous experiments, a minimum of four charge diameters was allowed for booster run-up.

The three species of Composition B investigated will be designated respectively as Type 5, Type 6, and Type 7. The results from a typical charge are given in Table 6. The velocities have been corrected to 63.00% RDX and 1.715 g/cc.

## Table 6

Type 5 Composition B, Diameter = 1.500"

| Stick Number | Length (cm) | Transit Time (microseconds) | Uncorrected Velocity (m/sec) | Corrected Velocity (m/sec) |
|---|---|---|---|---|
| 1 | 4.798 | 6.050 | 7931 | 7947 |
| 2 | 5.032 | 6.362 | 7909 | 7925 |
| 3 | 5.067 | 6.396 | 7921 | 7937 |
| 4 | 5.077 | 6.409 | 7922 | 7937 |
| 5 | 5.004 | 6.303 | 7939 | 7939 |
| 6 | 5.047 | 6.343 | 7957 | 7965 |
| 7 | 5.014 | 6.325 | 7927 | 7937 |
| 8 | 4.973 | 6.252 | 7954 | 7968 |
| 9 | 4.902 | 6.184 | 7927 | 7937 |
| 10 | 5.075 | 6.405 | 7923 | 7939 |
| 11 | 5.050 | 6.354 | 7947 | 7948 |

Mean = 7943 m/sec

Standard Deviation = 13.1 m/sec

The summarized results are given in Table 7 where the velocities are corrected to 63.00% RDX and 1.715 g/cc.

## Table 7

Types 5, 6, 7, Composition B

| Stick Diameter (inches) | Mean Corrected Velocity (m/sec) | Number of Observations | Standard Deviation (m/sec) |
|---|---|---|---|
| **Type 5 Composition B** | | | |
| 1.500 | 7943 | 11 | 13.1 |
| 0.902 | 7928 | 8 | 8.3 |
| 0.645 | 7902 | 8 | 9.6 |
| 0.500 | 7884 | 10 | 12.0 |
| **Type 6 Composition B** | | | |
| 1.500 | 7970 | 10 | 17.9 |
| 0.902 | 7941 | 10 | 14.7 |
| 0.645 | 7917 | 10 | 12.2 |
| 0.500 | 7890 | 9 | 17.8 |
| **Type 7 Composition B** | | | |
| 1.500 | 7936 | 10 | 10.0 |
| 0.902 | 7918 | 10 | 6.7 |
| 0.645 | 7904 | 9 | 11.8 |
| 0.561 | 7874 | 11 | 10.6 |
| 0.500 | 7854 | 9 | 11.8 |
| 0.250 | 7620 | 8 | 8.0 |

These data are shown plotted in Figure 6.

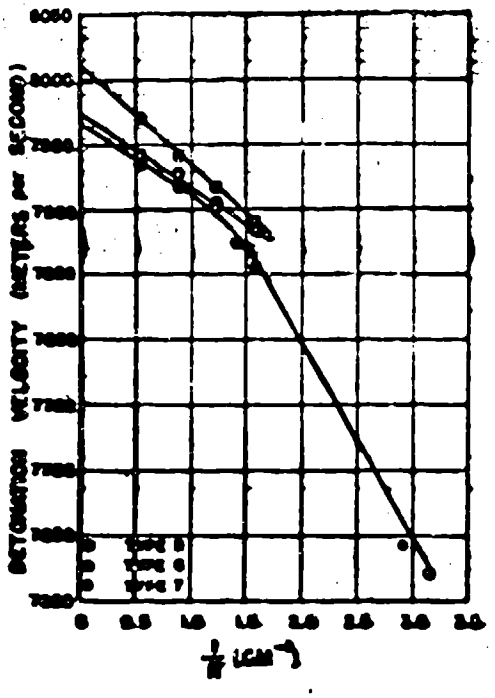

Fig. 6. Detonation velocity versus reciprocal of charge radius. Types 5, 6, and 7 Composition B.

## DISCUSSION IV

Types 5 and 6 Composition B differ in RDX particle size as indicated in Figure 7. Shown in this bar diagram is the weight percent of RDX as a function of RDX particle size. For example, 3% by weight of the RDX particles in Type 5 Composition B are between 350 and 500 microns in size. This particle size analysis was reproducible to about 1.5%.

Least-squared lines have been obtained for the Types 5 and 6 data and are given below:

Type 5 $D = 7975.1 - 57.99\ 1/R$ (5)

Type 6 $D = 8008.6 - 75.42\ 1/R$ (6)

where: D is the detonation velocity in m/sec.

1/R is the reciprocal of charge radius in $cm^{-1}$.

The fit of these equations to the experimental data is displayed in Table 8, where the entries show the m/sec difference obtained by subtracting the experimental point from the calculated point at each diameter.

Table 8

Types 5 and 6 Composition B

| Diameter (inches) | 1.500 | 0.902 | 0.645 | 0.500 |
|---|---|---|---|---|
| Type 5 | 1.7 | -3.7 | 2.1 | -0.2 |
| Type 6 | -1.0 | 1.6 | -0.7 | -0.1 |

In equations (5) and (6) the infinite medium extrapolated velocity is, of course, the constant immediately to the right of the equality sign. The difference, then, in the infinite-medium velocities for these two types of Composition B is 33 m/sec.

An estimate of the 95% confidence interval for the difference between the two infinite-medium extrapolations is ± 15 m/sec. This estimate was obtained by doubling the interval obtained from the

following equation:

$$\mu_1 - \mu_2 = A_1 - A_2 \pm 2\sqrt{\frac{\sigma_1^2 + \sigma_2^2}{N}} \qquad (7)$$

Here, $\mu_1$ and $\mu_2$ are the true extrapolations, $A_1$ and $A_2$ are the experimental extrapolations, $\sigma_1$ and $\sigma_2$ are the standard deviations of the two sample populations, and N is the number of observations in each sample. Since, strictly speaking, this equation applies to sample means and not to extrapolations, the result calculated from it is an underestimate of the width of the confidence interval. It is believed, however, that doubling the width gives a conservative estimate.

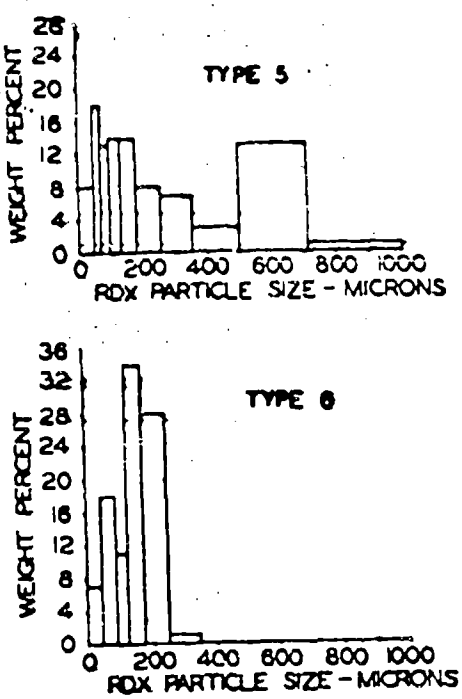


Fig. 7. RDX particle size analysis, Types 5 and 6 Composition B.

Referring to Figure 7, it can be seen that the Type 5 material is characterized by a bimodal weight distribution of RDX particles while the Type 6 material contains essentially all fine particles. It is not yet clear in detail why such a difference in particle sizes should lead to a difference in infinite medium velocities, but the Kirkwood-Wood theory, referred to before, offers the following interesting possible explanation for this type of behavior.

From this theory one obtains the following important generalized statement of the Chapman-Jouguet condition for the case of a plane detonation wave:

$$D = u + c_o, \qquad (8)$$

$$\sum_j \sigma^j r^j = 0, \qquad (9)$$

where: D = detonation velocity,

u = mass motion velocity,

$c_o$ = sound speed with the composition frozen at the values characteristic of the end of the steady state region,

$r^j = \frac{d\lambda^j}{dt}$, where j indicates a particular chemical reaction,

$\lambda^j$ is a progress variable, indicating the extent of a particular reaction j,

t = time,

$$\sigma^j = -\frac{\rho \beta_o}{c_\rho^o}\left(\frac{\partial E}{\partial \lambda^j}\right)_{\rho,v},$$

$\rho$ = density,

$$\beta_o = \left(\frac{\partial v}{\partial T}\right)_{\rho,\lambda},$$

E = specific internal energy (so defined that for an endothermic reaction $\left(\frac{\partial E}{\partial \lambda}\right)_{\rho,v} > 0$,

v = specific volume,

$c_\rho^o = \left(\frac{\partial H}{\partial T}\right)_{\rho,\lambda}$, i.e., the frozen heat capacity.

If one now thinks of the condition for the Chapman-Jouguet surface at infinite diameter for a two-component explosive as being that given by equation (9), namely:

$$\sigma^1 r^1 + \sigma^2 r^2 + \ldots + \sigma^n r^n = 0 \qquad (10)$$

where: 1, 2, ... n indicate specific chemical reactions postulated as occurring in the reaction zone and the normal Chapman-Jouguet condition occurs when $r^j = 0$, j = 1, 2, ... n. (i.e., the point of chemical equilibrium),

then this condition, contrary to the diameter effect theories of Jones and Eyring, does allow for the possibility of particle size effects persisting to infinite diameter. For example, Kirkwood and Wood (and also G. B. Kistiakowsky in a qualitative plausibility argument) have suggested that the normal exothermic reaction might be followed by an endothermic one. In such a case the $\sigma$ for that reaction would become negative and the $r^j$'s might not be zero at the Chapman-Jouguet surface. If one further postulates that in at least one of the n reactions above the rate is dependent upon the initial state of subdivision of at least one of the explosive components, then a difference in infinite diameter velocities would be expected for two such explosives differing only in particle size. The important point here is that Equation (10) shows that the location of the C-J surface can be influenced by the rates of reaction, even at infinite diameter.

Although the above is offered as a possible explanation, there is no evidence that such is the case. Further conclusions must await detailed calculations involving reaction mechanisms and reaction rates for the particular explosives and these will be made difficult by the lack of sufficient data.

Considering next Type 7 Composition B, particle-size analyses of the type shown in Figure 7 indicate no detectable difference between Types 6 and 7 Composition B, in spite of the 40 m/sec difference in infinite diameter velocity indicated by the data in Figure 6. Also indicated in the plot in Figure 6 is the fact that the Type 7 Composition B material shows curvature at diameters above 1/2", unlike the Types 5 and 6 materials.

As a possible explanation of the different infinite diameter velocities of Types 6 and 7 Composition B, we inquired in detail into the nature of the small amounts of additives in the castings. The data are given below in Table 9.

Table 9

Chemical Analysis of Types 5, 6, and 7 Composition B

| | Type 5 | Type 6 | Type 7 |
|---|---|---|---|
| TNT | 33.87% | 35.82% | 33.79% |
| RDX | 64.87% | 62.89% | 64.79% |
| Wax | 0.96% | 0.99% | 0.92% |
| Casting Additive 1 | 0.30% | 0.30% | |
| Casting Additive 2 | | | 0.50% |

In the above table, the RDX and wax were determined directly and the remaining components obtained either from a knowledge of casting additives or by subtraction. These analytical results are precise to about 0.1% in each case.

Heats of combustion were also experimentally measured for these three types of Composition B, and the agreement on the basis of compositions indicated by Table 9 is within the combined experimental calorimetric and analytical errors.

Considering Types 5 and 6 Composition B, Table 9 indicates that the additives to each are almost identical. (The difference in TNT and RDX composition is corrected in Table 7.)

Considering Types 6 and 7, the two types which have similar RDX particle sizes and yet an infinite diameter detonation velocity difference of 40 m/sec, it can be seen in Table 9 that the additives are somewhat different. However, a detonation velocity calculation made according to the Kistiakowsky-Wilson equation of state indicated that these differences in additives could amount to no more than 2 - 3 m/sec difference in velocities.

On the bases of chemical analysis for additives, heats of

combustion and detonation velocity calculations, it is felt that the difference in infinite medium velocity is not due to the effects of additives but is actually a result of particle-size effects persisting to infinite diameter.

Considering Types 6 and 7, there were differences in the casting procedures used, involving different settling times and a different cooling procedure, but these differences do not enable one to predict the final effect on the TNT crystal size. Here again the difficulties involved in the use of cast explosives become evident.

It may also be that the very small particles, i.e., those of the order of microns are of some importance. Since the particle-size analyses shown in Figure 7 only go down to 44 microns, a difference between Types 6 and 7 Composition B may exist without having been shown.

These difficulties which occur with the use of cast explosives have led us to search for a two-component explosive in which the particle size of each component can be varied more systematically and precisely. Pressing techniques have been developed to the point where it is possible to produce charges which are lower than crystal density by only 1 or 2%, thereby retaining the machinability and other advantages of high density material. The use of pressed material for experiments investigating particle size effects in two-component systems introduces additional problems involving segregation of particles and alteration of particle sizes during pressing. Nevertheless, at the moment, this seems the most fruitful method for further investigations.

## EXPERIMENTAL V

Another interesting case of particle-size effects persisting to infinite diameter has been demonstrated. Bagley[10] investigated the relation between detonation velocity and charge diameter for different sieve cuts of spherical-grain RDX, at a density of 1.200 g/cc. The separate cuts used were: 1190 to 840 microns; 840 to 710 microns; 710 to 590 microns, 500 to 350 microns. The straight line relationships obtained (on a D versus 1/R plot) for each of these cuts all extrapolated to a detonation velocity of 6850 m/sec at infinite diameter, at density 1.200 g/cc.

Urizar[11] established the D versus 1/R relationship for a single type of RDX, considerably finer than the above. This RDX was ball-milled and varied in size from 5 to 40 microns. The infinite diameter velocity at a density of 1.200 g/cc obtained from an extrapolation of this relationship, is approximately 100 m/sec below the value obtained by Bagley in his experiments.

This difference in infinite diameter velocities of 100 m/sec is thought to be considerably larger than the combined experimental errors, so that here again, particle-size effects exist at infinite diameter. It is thought, however, that the effect here is of a different nature from that previously observed in Composition B.

An experiment which may shed some light on the situation in

the RDX experiments has been done using spheres of Composition B. Spheres of two sizes were used, 5/8" and 1/4" diameters. The spheres were prepared from rough-sawed cubes by means of a device which abraded the corners off the cubes in a random manner. The device consisted of a hollow cone, attached with its apex downward to the shaft of an electrical motor, rotating inside a stationary, vertical, hollow cylinder. Both cone and cylinder were lined with a coarse abrasive cloth, so that cubes of explosive placed in the rotating cone were thrown violently and randomly about, from the cone to the cylinder and back, being quickly reduced to near spheres. This operation was carried on outdoors with a large centrifugal blower continually removing the dust. Plate 3 shows samples of both sizes of spheres.

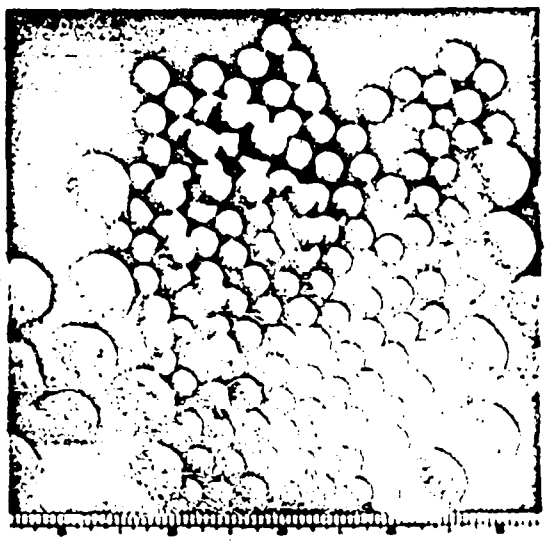

Plate 3. Composition B Spheres Diameters Approximately 1/4" and 5/8".

Three shots were fired which will be discussed in the following order:

Shot No. 1 consisted of 5/8" spheres fired in an octagonal wooden tube 36" long and 7-1/2" in diameter (across flats). Ionization pins were supported by four 1/8" brass rods spaced at 10" intervals, beginning 4" from the booster end. Each rod was drilled with four holes 1" apart, which carried the pin wires. Plate 4 shows this charge assembled.

Shot No. 2 consisted of a single row of 5/8" spheres held directly one above the other in a paper tube.

Shot No. 3 consisted of 1/4" spheres in a tube 24" long and 3-1/4" in diameter (across flats). The ionization pins consisted of 0.040" o.d. hypodermic tubing inserted 4" apart, starting 4" from the bottom, with a common ground wire running the length of the charge.

## DISCUSSION V

The overall density of Shot No. 1 was 1.0 g/cc. Its detonation velocity was 7050 ± 100 m/sec. According to the usual ideas about the dependence of detonation rate on charge density mentioned in Experimental I, an infinite diameter Composition B stick of density 1.0 g/cc should detonate at about 5600 m/sec. It is thought that in Shot No. 1 the detonation wave traveled at a velocity close to that characteristic of casting density from contact point to contact point, with perhaps some initiation delay at each junction.

Shot No. 2 gave a detonation velocity of 7520 ± 31 m/sec.

This stacked single-row shot therefore, gave an increase in velocity over Shot No. 1 of 470 m/sec. This appears to be in accordance with the hypothesis given above since there are fewer contact points and a more direct path is available when the balls are stacked as in Shot No. 2, compared with Shot No. 1.

Plate 4. "Composition B Spheres" Charge-Assembled.

Shot No. 3 had an overall density of 1.0 g/cc and detonated at a velocity of 6020 ± 100 m/sec. In this shot the number of contact points per unit length is greater than in Shot No. 1 and it also seems probable that the initiation delay at each contact point increases somewhat as the sphere diameter is decreased.

On the basis of our present knowledge, it would appear that the large sphere Composition B shots are an extreme case of the effect mentioned before. It is not clear whether jetting was important in the large RDX particle shots (as it might be for a sensitive material) or whether the detonation proceeded in a manner analagous to that postulated in the case of the Composition B spheres.

## SUMMARY

It has been shown in Discussions I, II, and III that particle-size effects are important in two-component explosives at finite diameters. Variations in the RDX particle sizes in Composition B greatly alter the shape of the D versus 1/R curve and also the failure diameter of the material. Variations in the cooling pattern of the casting, through a mechanism not yet completely understood, also affect the detonation properties of Composition B.

It has been shown in Discussion IV that particle-size effects appear to lead to different infinite diameter velocities for materials otherwise chemically similar. A plausibility argument, in terms of the Kirkwood-Wood theory, is offered.

It has been shown in Discussion V that even at infinite diameter the presence of large crystals in low density, sensitive explosives may lead to velocities greater than those characteristic of fine

crystalline material. An experiment has been performed using large spheres of Composition B, which may represent an extreme case of these effects.

Further work is planned on these particle-size effects, using pressed materials which may offer greater opportunities for particle-size control and variations than have cast material.

We would like to acknowledge our gratitude to following members of the Los Alamos Scientific Laboratory for assistance in these experiments:

M. J. Urizar, who prepared the Types 2, 3 and 4 Composition B castings.

A. Popolato, who directed the particle size, composition and density analyses for Types 5, 6 and 7 Composition B castings.

L. R. Sitney, who performed the heats of combustion experiments.

W. Fickett, who performed the detonation velocity calculations for Types 6 and 7 Composition B.

F. W. Kramer, for assistance in the preparation of graphs.

## REFERENCES

(1) Kirkwood, J. G. and W. W. Wood, "The Structure of a Steady-State Plane Detonation Wave with Finite Reaction Rate". (This conference).
(2) MacDougall, D. P., F. J. Martin, E. Boggs and G. H. Messerly-work described in Reference (7) below, pages 154-156.
(3) Gamow, G.-work described in Reference (7) below, page 155.
(4) Jones, E. and D. Mitchell, Nature, 162, 98(1948).
(5) Tranter, T. C., Nature, 174, 81(1954).
(6) Campbell, A. W., M. E. Malin, T. J. Boyd, Jr. and J. A. Hull, "Technique for the Measurement of Detonation Velocity". (This conference).
(7) Eyring, H., R. E. Powell, G. H. Duffey and R. B. Parlin, Chemical Reviews, 45, 69(1949).
(8) Parlin, R. B., C. J. Thorne and D. W. Robinson, Technical Report Number 1, Institute for the Study of Rate Processes, University of Utah (1952).
(9) Jones, H., Proc. Roy. Soc. (London) A189, 415(1947).
(10) Bagley, C. H., Unpublished Report.
(11) Urizar, M. J., Unpublished Report.

# DETONATION WAVE FRONTS IN IDEAL AND NON-IDEAL DETONATION 24

Melvin A. Cook
University of Utah
Salt Lake City, Utah

## ABSTRACT

The experimental wave shape measurements for a number of ideal and non-ideal explosives in cylindrical charges at various charge lengths L and diameters d are summarized. These results show the followings

(1) The wave fronts are in general spherical.

(2) The radius of curvature R increases at first directly as L (R = L), but at a value of L between 0.5 d and 3.5 d depending on the explosive it suddenly becomes constant at a value $R_m$ which maintains for all larger values of L.

(3) The steady state value of wave curvature $R_m$ varies with diameter and density from a minimum value of 0.5 d at the critical diameter to a maximum value never exceeding 3.5 d - 4.0 d in large diameters.

(4) Values of $R_m/d$ less than 3.5 - 4.0 appear to be determined simply by finite reaction zone lengths. The maximum value of 3.5 - 4.0 maintains in explosives in which the reaction zone length is negligible in comparison with the charge diameter.

The experimental results show that wave curvature is not associated with pressure gradients across the front of the detonation wave. Instead, they are apparently determined simply by the geometry of the detonation head and the tendency for pressure to remain substantially constant in the detonation head. The wave shape results are not only explicable in terms of detonation head concepts but appear to provide strong evidence for this theory.

## INTRODUCTION

Aside from the extensive wave shape studies conducted in this laboratory, very little data have been published concerning the characteristic features of the fronts of detonation waves. One reason for the previous lack of information on wave shape was the lack of suitable methods for accurate measurement of wave shape. Developments of high speed rotating mirror cameras which have taken place at an accelerated pace during the past ten years, however, have placed into availability excellent precision methods for wave shape study. In spite of the availability of high speed cameras, wave shape studies are still beset with some difficulties, especially as a result of restrictions as to total charge size. Restrictions in charge size are particularly troublesome in studies of cast and pressed explosives of small reaction zone length $a_o$ where the difference in time of arrival of the wave front at the end of the charge on its central axis and at the periphery of the charge is exceedingly small in small diameter charges. Indeed any laboratory restricted to the use of small size charges and concerning itself only with cast and pressed ideal explosives might easily fail to observe many important characteristic features of the wave front even with the use of the best modern rotating mirror streak cameras owing to the high resolution and charge reproducibility required in studies with small diameter charges. Large diameter shots with low-density, ideal, and non-ideal explosives, however, may be used without difficulty in wave shape studies.

Eyring and co-workers[1] called attention in their development of the "curved front" theory to the possibility that reaction rate and wave shape may be intimately related. In addition, wave shape is important in the design of many devices. A systematic study of the characteristics of the detonation wave fronts for various types of explosives were therefore undertaken here both in ideal (detonation velocity D equal to the theoretical maximum or hydrodynamic velocity D*) and non-ideal ($D < D^*$) detonation. The location and laboratory facilities developed proved to be ideal for the study of wave shape. An excellent high speed, rotating mirror camera was constructed with film writing speeds up to 5 mm/μsec. By use of this camera in an inside-out bombproof (camera and investigators inside, explosive outside) in a remote area, it was possible to study charges of almost any desired diameter (d) and length (L). Indeed charges of $L/d \geq 6$ have been fired in diameters up to 25 cm in many cases, and in one explosive a diameter as high as 46 cm was used. With this instrumentation and by use of explosives of various types and under various physical conditions, many of the characteristic features of the detonation wave front have been elucidated. This paper summarizes the extensive experimental data obtained in these wave shape studies. Also presented is a discussion of the results from a largely geometrical viewpoint employing the concepts of the detonation head model.

## EXPERIMENTAL

Three types of charges were used in this study, namely loose packed, pressed, and cast charges. Finished charges were either bare charges (in some cast explosives) or were contained in thin-walled paper, cellophane, or plastic tubes. Except perhaps for measurements made in diameters of 5 cm or less where measurements were unreliable anyway, the confinement provided by these tubes was probably quite negligible. Except for determinations of the influence of charge length, photographs of the detonation wave front were made for the most part at $L/d \geq 6.0$. To conserve explosive, shots of DNT at d = 25 cm and ammonium nitrate at d = 46.0 cm were made at L/d = 4.0 to 4.5. Since, as will be shown later, the wave shape became steady at $L/d < 3.5$ in all cases studied, the shots at L/d = 4.0 to 4.5 gave the steady state curvature. Pressed tetryl or cast pentolite boosters having preformed axially centered cap wells were used to detonate the charges requiring boosters. In measurements of the influence of charge length the booster was one inch in thickness with a preformed cap well 3/4" deep. Less care was needed in regulation of the exact position of the cap in steady state wave shape measurements. For cap sensitive explosives the charges were fired directly by caps axially centered at one end of the charge by means of wooden forms placed on this end of the charge. In measurements of the influence of charge length the cap was butted against but not inserted into the end of the charge.

The loose-packed charges were all vibrated to provide density uniformity. In some of the loose mixtures studied such as RDX-salt, RDX-glass beads, etc., however, vibration of the charges may have caused some segregation as indicated by some poorly reproducible results obtained for these mixtures. Cast charges were poured in lengths enough greater than the desired one to provide a 6 to 10 inch head to minimize cavitation in the finished charge. This head was then removed and only the bottom part of the charge used in the test. The pressed charges were made in 1 inch thick wafers, and the charge was made up by placing enough wafers end to end to give the desired length.

The wave was photographed in each case as it emerged from the end of the charge. This end of the charge was made perfectly perpendicular to the charge axis by cutting the tube on a lathe and covering the end with a flat piece of wood during charge preparation. Just before firing, this wooden form was removed and either replaced by a glass plate, or the charge end was left bare depending on the nature of the explosive. The slit of the camera was focussed on the end of the charge across a diameter after a suitable static image of the charge, and a 10 cm grid was taken for determination of the magnification factor. A static image with the slit in was also taken defining the line of view of the camera to show that the slit actually crossed a diameter of the charge. In some of the lowest velocity, non-ideal explosives it was necessary to use a thin (about 1 mm) layer of tetryl at the end of the charge along the line viewed by the camera through the slit in order to produce enough luminosity to observe the emerging wave.

The mirror of the camera was usually operated at or near maximum speed (600-700 r.p.s.) in wave shape measurements in order to reduce errors in measurement of the trace to a minimum. All traces were read on a Cambridge Universal Measuring Machine with a least count of 0.01 mm. The distance across the charge diameter was determined from the measured distance (x') multiplyed by the magnification factor M obtained from the static image. The y component parallel to the charge axis was obtained by measuring the perpendicular (y') distance from an arbitrary x'-axis to the trace and multiplying the measured value by the factor $D/W_s$ where D is the velocity at the terminal end of the charge and $W_s$ is writing speed of the camera. Thus the measured coordinates were converted to real coordinates by the relations

$$x = M x'$$
$$y = y' D/W_s \qquad (1)$$

where x' and y' are the values measured with respect to a given set of coordinates on the film itself, and x and y are the actual distances (with respect to the coordinate system) defining wave shape. The velocity D was generally measured on the same charge as was used to measure wave shape for charges long enough that this could be done by means of a pin-oscillograph.(2) In cases where this was not possible and where velocities were not known, velocities at the end of the charge needed in this study were obtained from measurements made in systematic studies of the variation of velocity with charge diameter and length.

Much of the data obtained in the wave shape studies in this laboratory have been presented in various previous technical reports on this project. Additional data used here not previously reported are available upon request. The data are plotted as average values with smooth curves drawn through these average value data. Each point in each of the graphs of Figs. 1 to 9 inclusive, represents usually an average of two or more shots. Sometimes a given point is an average of as many as ten shots. In a few cases, however, a point may represent only one shot. The reproducibility of data in wave shape studies depended on the type of explosive involved and the diameter. Loose-packed shots of pure granular explosives usually gave R/d values reproducible within about 10 percent in diameters above 5 cm. With present techniques this is true also of pressed charges, although in early studies less reproducibility was obtained owing possibly to small air gaps between individual wafers of 1 inch thickness used in making up the charge. In some cast explosives reproducibility has not been as satisfactory, the scatter of results indicating a spread of about 30 percent. Cast mixtures of amatol, baratol, and sodatol, however, have given excellent reproducibility. The difficulty in the reproducibility of measurements of R/d in some cast charges is the tendency toward cavitation and small density fluctuations both of which show up in exaggerated form in wave shape studies. Further work on cast charges is in progress. Other studies will include a plastic, a liquid, and a gaseous explosive.

## RESULTS

### Spherical Wave Fronts

A very striking result of the wave shape studies carried out in this laboratory is the fact that the wave fronts showed a constant radius of curvature (spherical) across practically the entire wave front. In some cases something similar to the edge effect anticipated from shaped charge studies could be seen as a sharp increase in curvature on the outer edges of the trace. However, in no case did this edge effect amount to as much as expected, namely 3 mm, the maximum observed edge effect not exceeding 2 mm in any case. In many cases, however, the wave remained spherical right out to the edge of the charge. In some cases wave irregularities, usually tipped or asymmetrical wave fronts were observed. These were traced to density and sometimes compositions fluctuations in the charge. When results were repeated with more accurately controlled charges, spherical waves were found. Cavitation near the end of the charge in cast explosives always distorts the wave. Cast charges in which density along the axis is reduced by poor casting tend to give excessive curvature, or if exaggerated, inverted waves. These effects are, however, not reproducible. The wave shape, except for the edge effect, may be expressed in each case except for these irregularities by a single value R, the radius of curvature of the wave front. All wave shape data in this paper are presented in this manner.

### Influence of Charge Length

Fig. 1 shows results of measurements of the radius of curvature of the wave front as a function of charge length in some ideal explosives ($D = D^*$). For $L/d < 3$ in low density TNT, R increased almost directly with L until a value of 1.8 d was reached after which it settled down quickly to the constant value $R_m/d = 1.8$ and remained at this value up to the maximum length studied ($L/d = 18.5$). In EDNA a similar situation prevailed; R/d increasing almost directly with L/d to $L/d = 2.5$ after which it remained constant at $R_m/d = 2.6$. Wave shape with pure granular RDX, 40/60 RDX-salt, and cast pentolite was also studied (as a function of charge length) and the results showed that the wave in these cases expanded geometrically ($R = L$) for values of $L < 3.5$ d, but at $L > 3.5$ d, R remained constant at $R_m/d = 3.5$.

Striking results were obtained in studies of wave shape at large L/d using various types of initiators. It was found that the same steady state wave shape maintained at large L/d independent of the mode of initiation of the charge. In these studies plane wave initiation, peripheral initiation, irregular wave shape initiation, and inverted wave initiation were used. In all cases the same steady state wave shape resulted as was found in the R vs. L/d studies showing that steady state wave shape is a function only of the explosive and its physical state and not of conditions of initiation.

Fig. 2 shows the results obtained with two non-ideal explosives for which $D/D^*$ was appreciably less than unity in the particular diameters studied. These explosives were coarse (-6 + 8 mesh) TNT in diameters of 5 and 10 cm, and a simple mechanical mixture of 50/50 TNT-sodium nitrate (SN) employing -28 + 48 mesh SN in diameters of 5 and 10 cm. Measurements were made at charge lengths ranging from 1 d to 6 d. They showed that R/d increased directly as L/d for L/d not exceeding $R_m/d$. Significantly the steady state value $R_m/d$ in these non-ideal explosives was established at smaller values of L/d than in the ideal explosives shown in Fig. 1. In fact, the wave appeared to change suddenly from geometrical expansion (R = L) to steady state wave shape ($R = R_m$) at $L = R_m$. The establishment of a steady state wave front of $R_m/d \leq 3.5$ even in ideal explosives of very short reaction zone length shows that other factors besides reaction rate influence wave shape. However, the lower values of $R_m/d$ found for non-ideal explosives show that reaction rate influences wave shape at least to some extent in accord with the suggestion of Eyring. Other factors not taken into account are of sufficient importance, however, to require modifications of the "curved front" theory.

Influence of Diameter on Wave Shape in Ideal Explosives

Since the results shown in Fig. 1 and 2 show that steady state curvature is established at $L/d \gtrsim 3.5$, values of $R_m/d$ as a function of d and $\rho_1$ were measured in a number of ideal and non-ideal explosives at $L/d \geq 6.0$ except as indicated above for DNT and AN where L/d was 4.0 to 4.5 at maximum d. The results are shown in Figs. 3 to 9, inclusive. Results for cast TNT, 50/50 pentolite, and composition B at $L/d \geq 6.0$ are shown in Fig. 3. As mentioned above, wave shape is extremely sensitive to slight charge fluctuations. Unfortunately cast charges are difficult to prepare without such fluctuations. Hence $R_m/d$ values were reproducible only to within about $\pm$ 0.5 in these three explosives. Within these limits the results shown in Fig. 3 show that the upper limit of $R_m/d$ found at large diameters in these ideal explosives was about 3.5 to 4.0. It is significant that the maximum effective charge length in shaped charge phenomena and other phenomena employing "end effect" such as lead block compression and sympathetic detonation is also about 3.5 d to 4.0 d. While R/d and the total end impulse increase uniformly with charge length for values of L/d between zero and 3.5 to 4.0 results for these explosives showed that D did not vary appreciably with charge length in the region $0 < L/d < 3.5$. It appears, in fact, that velocity in ideal explosives at diameters well above $d_m^*$ (minimum diameter for ideal detonation) is independent of wave shape. In non-ideal explosives, however, velocity transients have been observed to occur over the entire range $0 < L/d < 3.5$, but $D/D^*$ is constant at less than unity for $L/d > 3.5$. Similar transients have been observed in ideal explosives in diameters near $d_m^*$.

Fig. 4 shows plots of $R_m/d$ vs. d for some loose-packed, granular ideal explosives including TNT, EDNA, tetryl, RDX, and coarse 50/50 pentolite, all at $L/d \geq 6.0$. These results showed $R_m/d$ to increase with diameter for $R_m/d < 3.5$ although only quite slowly for 50/50 pentolite.

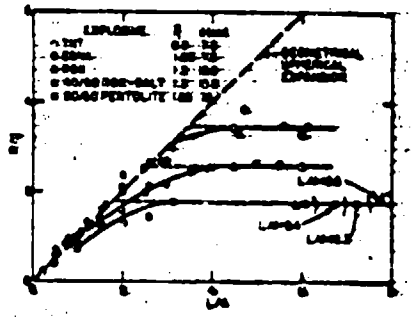

Fig. 1 - Variation of Wave Shape with Charge in Ideal Detonation

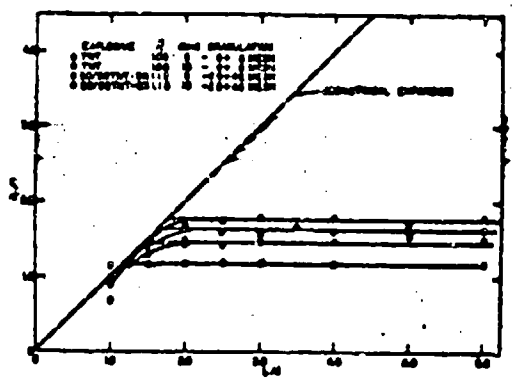

Fig. 2 - Variation of Wave Shape with Charge Length in Non-Ideal Detonation

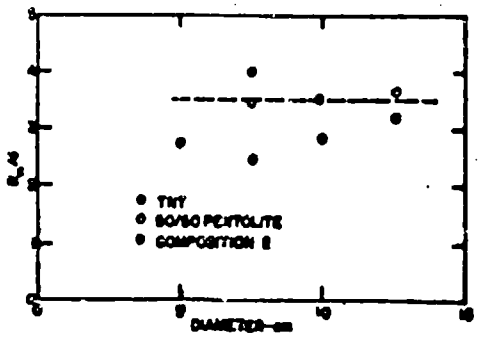


Fig. 3 - $R_m/d$ vs. d in Some Cast, Ideal Explosives

Only in the cases of RDX and EDNA did the value of $R_m/d$ reach the limiting value 3.5. These results might indicate that the maximum value of $R_m/d$ even at large diameter may be lower than 3.5 for explosives of sufficiently low density, indicating possibly a purely density effect on curvature. However, it is more probable that this effect is simply a reaction rate effect and that $R_m/d$ would approach 3.5 at large enough d. While these explosives were ideal, it is possible (as predicted by the detonation head model) that the reaction zone length may still be appreciable and that this may be responsible for the low $R_m/d$ values in low density, ideal explosives. It has been shown that $z_o$ is much longer for a given explosive at low density than at high density apparently simply because the temperature increases quite markedly with density (e.g., at least as rapidly as that predicted by the $\alpha(v)$ equation of state).(3)

## Influence of Density on $R_m/d$ in Ideal Explosives

Numerous measurements of $R_m/d$ were made as a function of density with fine-grained TNT, EDNA, 50/50 pentolite, and various pentolite-salt and TNT-salt mixtures in a diameter of 5.2 cm and with tetryl in 2.5, 5.0, 8.5, and 10.4 cm diameter charges all at $L/d \geq 6.0$. These results are shown in Fig. 5. They show that $R_m/d$ increased with density $\rho_1$ in all cases as long as $R_m/d$ was less than 3.5 to 4.0. (In the initial series of $R_m/d$ vs. $\rho_1$ measurements made with TNT a maximum value of 4.5 for $R_m/d$ was obtained at $\rho_1 = 1.51$. It was suspected that this high value might be associated with small air gaps between the individual 1 inch thick wafer used in these charges. Hence in later work care was exercised to avoid an air gap by dusting off each pellet carefully and making sure that good contact was obtained between them.) The maximum value of $R_m/d$ did not exceed 4.0 with the explosives tetryl, EDNA, and 50/50 pentolite, all of which would be expected to give at least as large maximum values of $R_m/d$ as TNT. The fact that the maximum value obtained for $R_m/d$ with cast TNT at $\rho_1 = 1.59$ was between 2.5 and 3.9 in all cases at diameters between 5 and 12.7 gives further evidence that the true limiting value of $R_m/d$ may not exceed 3.5 to 4.0 in this as well as other explosives.

## Influence of Inert Additives on $R_m/d$ in Ideal Detonation

Since low density ideal explosives were shown to give $R_m/d$ values below 3.5 at least at the maximum diameters studied, questions arose regarding $R_m/d$ in explosives with inert additives. Theoretically the temperature would be higher for a given explosive if the voids were filled with inert solid than if these voids were filled with air because of the covolume effect on temperature shown in previous studies. Assuming therefore that the explanation of low $R_m/d$ values in low density, ideal explosives is an appreciable reaction zone length, measurements of $R_m/d$ were made in various loose-packed pressed and cast TNT-salt, pentolite-salt, and RDX-salt mixtures. The results are shown in Fig. 6. In loose-packed TNT-salt mixtures at d = 10 cm, $R_m/d$ decreased appreciably with salt content from 2.1 at zero percent salt to 1.3 at 60 percent salt. This suggested that the density effect

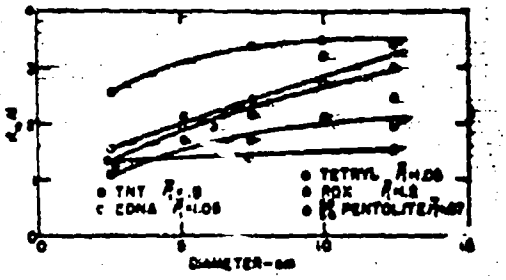

Fig. 4 - $R_m/d$ vs. d for Some Loose-Packed, Ideal Explosives

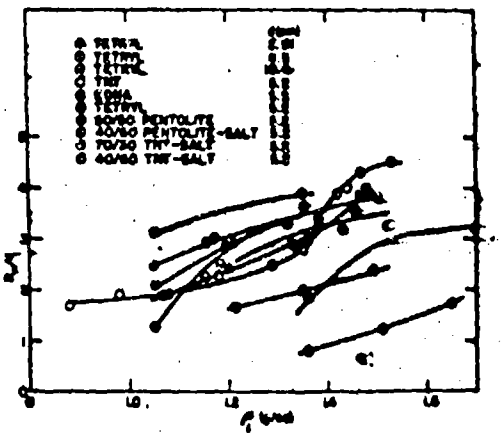

Fig. 5 - Variation of $R_m/d$ with Density in Some Ideal Explosives

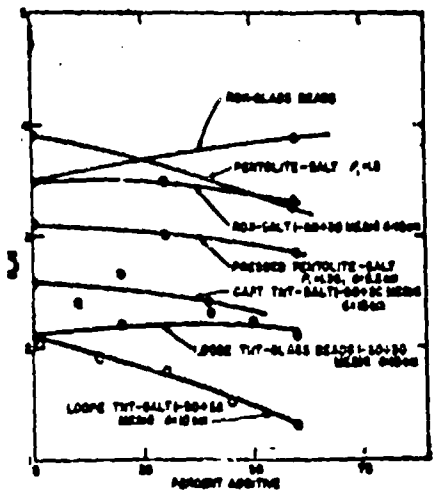

Fig. 6 - Influence of Inert Additives on Wave Shape

described above might not be a reaction zone length effect, although the possibility remained that some of the salt might have vaporized to cause lower temperature and longer $a_0$. Hence measurements were repeated using glass beads of -20 + 30 mesh. In this case the influences of inert additive disappeared completely lending credence to the suggestion that the effect is actually a reaction zone length effect.

Cast TNT-salt mixtures showed very little effect of salt on curvature, the $R_m/d$ values decreasing only from 2.6 at zero percent salt to about 2.2 at 50 percent salt. The smaller effect of salt on $R_m/d$ in cast compared with loose TNT may be associated with the fact that the exposure time of salt to the detonation head in the cast charge is only about half that of the low density mixture so that less vaporization occurred in the reaction zone. It is clear that vaporization of salt in the reaction zone was not large in either case, since vaporization of only a small percentage of the salt would quench detonation in cast and loose-packed TNT. Powdered salt in small amounts quenches detonation even in very sensitive dynamites.

Results obtained with RDX-salt and RDX-glass bead mixtures showed very little change of $R_m/d$ with percent inert. This may be simply the result of the fact that $R_m/d$ was already at 3.5.

In the RDX-inert and TNT-inert mixtures the density increased with inert content because of the higher density of the inert. To determine the influence of inert at constant density, pressed charges of 50/50 pentolite and salt were prepared in a diameter of 5.2 cm. These results are also given in Fig. 6 and show that the salt additive influenced $R_m/d$ very little at $\rho_1$ = constant. The conclusions to be drawn from these studies therefore appear to be (1) that additives which are strictly inert do not influence wave shape appreciably for a constant free space inside the charge and (2) that the density effect noted in Fig. 5 may be simply a reaction zone length effect.

## Influence of Reaction Zone Length on $R_m/d$ in Ideal Explosives

Some additional studies were carried out to provide evidence for the suggestion that only reaction zone length influences wave curvature in ideal and non-ideal explosives when $R_m/d < 3.5$. One will note that cast TNT at d = 5 to 7.5 cm showed a relatively low $R_m/d$, whereas the pressed charges at d = 5 cm showed normal (or slightly too large) $R_m/d$ values at densities from 1.38 to 1.5. Moreover, there was a rather rapid increase in $R_m/d$ with density in pressed TNT between $\rho_1$ = 1.35 and 1.40 g/cc. In the first place cast TNT is coarser than the fine pressed TNT, and at the same density its reaction zone length should therefore be greater. This would explain the higher $R_m/d$ for the pressed compared with the cast TNT. On the assumption that the density effect in the pressed TNT is a reaction zone length effect, there are two factors to consider, namely (1) the increase in the detonation temperature $T_2$ with density, and (2) the fact that pressing breaks down the particles and should therefore decrease the reaction zone length. The temperature effect would be expected to be continuous

with increasing $\rho_1$ with no abrupt change in the slope of the $R_m/d$ vs. $\rho_1$ curve. However, the particle size effect would produce a sudden change at the density where the particles are crushed by pressing. Particle size studies of pressed TNT charges showed that the particles did not crush appreciably due to pressing until a density of 1.35 is reached. But between $\rho_1$ = 1.35 and $\rho_1$ = 1.40 g/cc considerable particle breakdown was found. This is precisely the density range at which a sharp increase in $R_m/d$ was encountered.

Average wave shape vs. diameter measurements of loose-packed tetryl and PETN of particle sizes -20 + 28 mesh and -35 + 48 mesh for tetryl and -35 + 48 mesh and -65 + 100 mesh for PETN made in plastic tubing of 1.6 mm wall thickness are plotted in Fig. 7. These measurements were made at diameters at and above $d_m$*, the minimum diameter at which D/D* = 1.0. While results in such small diameters are questionable owing to poor reproducibility, one will note that $R_m/d$ not only continued to increase with d in the ideal detonation region, but that an apparently definite particle size effect also occurred, the values of $R_m/d$ for the finer tetryl and PETN always being greater than those of the coarser granulation of tetryl and PETN. The fact that particle size effects on wave shape are pronounced in the ideal detonation region near $d_m$* as well as in the non-ideal detonation region seems clearly to show that $a_o/d$ is appreciable in the ideal detonation region near $d_m$*.

It is concluded from density and diameter studies in ideal explosives with and without inert additives that values of $R_m/d$ lower than 3.5 are associated with reaction zone lengths of appreciable magnitude but not long enough to reduce D/D* below unity. According to the detonation head model D/D* will not drop below unity until $a_o/d$ (the reaction zone length/diameter ratio) is greater than about unity. However, it appears obvious that $R_m/d$ will be lower than the maximum value 3.5 as long as the ratio $a_o/d$ is appreciable. Apparently only when $a_o/d$ approaches zero will $R_m/d$ attain the maximum value of 3.5. The above evidence thus substantiates the detonation head model in this regard.

## $R_m/d$ vs. Diameter in Non-Ideal Detonation

Fig. 8 presents plots of $R_m/d$ vs. d for several loose-packed, non-ideal explosives. In all cases except ammonium nitrate (AN) $R_m/d$ increased with diameter but was considerably below the limiting value of 3.5 to 4.0 at the maximum diameters used. With the -4 + 6 mesh TNT product the velocity was at the maximum value D* at the largest diameter studied. However, $R_m/d$ was still only 1.9. D/D* was just slightly below unity, but $R_m/d$ was only 1.6 for DNT. In both 50/50 TNT-SN and 50/50 TNT-AN D/D* was still considerably lower than unity at d = 25 cm, where $R_m/d$ was 2.5 and 1.6, respectively. $R_m/d$ was very low for AN (about 0.8 to 1.2) but did not increase appreciably with d even up to d = 46 cm. This is probably simply because D/D* was considerably lower than unity (theoretically about 0.45 at d = 17.5 cm and 0.65 at d = 46.0 cm) over the range of diameters studied. Except possibly for

the relatively high value for the TNT-Si mixture these results are consistent with the concept that $R_m/d$ is a function of reaction zone length at values of $R_m/d < 3.5$. Even in coarse TNT and fine DNT at d = 25 cm, $a_o/d \sim 1.0$ according to the detonation head model. Hence, in accord with observations, $R_m/d$ should be appreciably lower than the limiting value of about 3.5 attained for $a_o/d \ll 1.0$.

Results of $R_m/d$ vs. d for some cast explosives, non-ideal in small diameters and ideal in some cases and non-ideal in others in large diameter are shown in Fig. 9. Only in the composition B-AN cast charges did $R_m/d$ reach the approximate limiting value (3.8 in this case). This explosive, however, was ideal under conditions at which $R_m/d = 3.8$. In all the others except cast amatol, $R_m/d$ seemed to attain approximately a constant or slowly rising value at $d \geq 10$ cm.

All of these explosives except the baratols were ideal at the maximum diameter studied. Even the milled barium nitrate product, however, was non-ideal at d = 25 cm. Of particular interest is the fact that 70.7/29.3 cast composition B-AN exhibited an $R_m/d$ vs. d curve which reached the maximum value (3.8) at about the same diameter at which D/D* became unity. This is probably associated with the small percentage of the slowly reacting component, AN, and a very short reaction zone for the faster one, composition B.

## THEORETICAL CONSIDERATIONS

Phenomenology allows one to write the following equations pertaining to wave shape:

$$R_i\ (y_i) = \text{constant};\ y < y' \tag{2}$$

$R_i$ = radius of curvature of the wave at a particular charge length and at a point on the wave front a distance $y_i$ perpendicular to the charge axis, y' is the effective radius of the charge, defining effective radius to exclude the slight edge effect which did not exceed 2 mm in any case. Equation (2) simply expresses the experimental fact that the wave front is in general spherical in shape.

$$\begin{aligned} R &\cong L;\ L < R_m \\ R &= R_m = \text{constant};\ L > R_m \end{aligned} \tag{3}$$

Equation (3) expresses the facts shown in Figs. 1 and 2 that the spherical wave front expands geometrically for a length nearly up to $R_m$ and then settles down rather suddenly to the steady state value $R_m$. For theoretical purposes it is evident that the assumption of a sharp, discontinuous change from spherical expansion (R = L) to the steady state wave front ($R = R_m$) is reliable almost within experimental error as indicated by the dotted horizontal lines in Figs. 1 and 2.

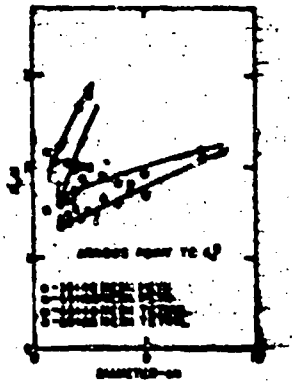

Fig. 7 – Wave Shape vs. Particle Size in Tetryl and PETN at Diameters near $d_m$*

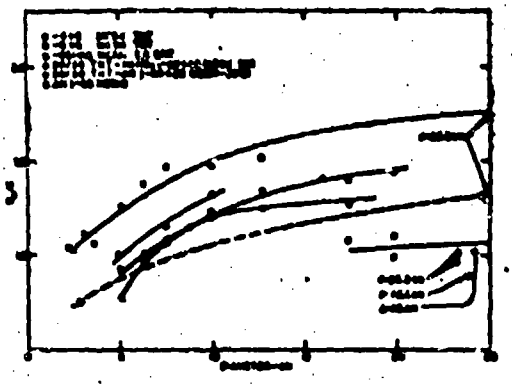

Fig. 8 – $R_m/d$ vs. d for Some Loose-Packed, Non-Ideal Explosives

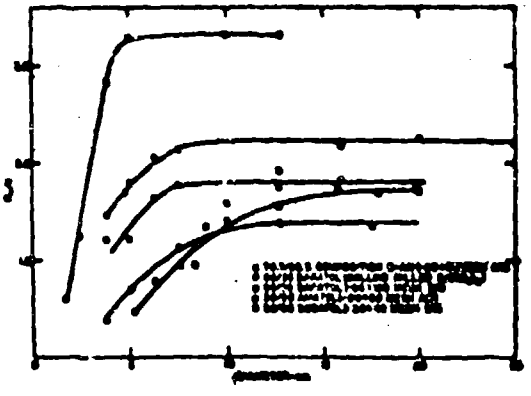

Fig. 9 – $R_m/d$ vs. d for Some Cast, Non-Ideal Explosives

$$R_m/d \neq 3.5;\ a_o/d \ll 1$$
$$R_m/d = f(a_o/d,\ X);\ a_o/d \text{ finite} \qquad (4)$$

Here X represents a yet unknown factor determining wave shape in the region of finite $a_o$ possibly involving detonation pressure $p_2$ and perhaps also D. Equation (4) expresses the extensive $R_m/d$ vs. d results obtained in the studies in this laboratory, evidence that $R_m/d$ is not the same in all cases at a given $a_o/d$ being ample. The problem in the interpretation of wave shape results thus involves (1) the elucidation of the factors included in X and (2) the determination of the function f. These functions have not yet been formulated. However, the nature of the unknown variable X may perhaps be implied from the following considerations.

In the geometrical expansion stages of the wave during which R = L, one has no indication that the edge of the charge or the reaction zone length $a_o$ influences wave shape at all. Moreover, in this region all explosives seem to be alike as to wave shape, whether ideal or non-ideal even though they exhibit widely different velocities or velocity transients as the case may be. One might interpret this result therefore to indicate that nothing occurring at the edge of the charge or in the reaction zone influences conditions determining wave shape in region of geometrical expansion. The only alternative explanation of this fact is that edge effects influence all explosives in exactly the same way in this region of wave propagation. This explanation, however, seems heavily strained, particularly in view of the observed spherical wave fronts.

The influence of explosive characteristics suddenly come into play at the limit of geometrical expansion, $L = R_m$. At this limit the only effect of explosive characteristics is apparently simply to prevent any further change in wave shape; the differences between explosives regarding wave shape reside simply in the value of L at which steady state conditions are established. Values of $R_m/d$ and therefore also L/d at the (apparent) discontinuity in transfer from spherical expansion to steady state wave propagation fall in the range $0.5 < R_m/d < 3.5$. The lower limit corresponds to the critical diameter $d_c$; the wave front is a hemisphere at $d_c$. $R_m/d$ obviously cannot be less than 0.5. From the geometrical arguments presented here, the facts seem quite significant that values of $R_m/d$ approaching 0.5 have been observed quite frequently as one approaches $d_c$, although no values of $R_m/d$ less than 0.5 have been observed. On the other hand, the upper limit of 3.5 is precisely the value of L/d at which the detonation head attains in unconfined charges its maximum size or that end impulse is optimum as shown, for example, by extensive shaped charge and other studies. The maximum effective length $L_m$ for optimum end impulse is approximately the same in non-ideal detonation as in ideal detonation, namely 3-4. This may be shown, for example, by determinations of "end effect" by means of the lead block compression method using a non-ideal explosive. One finds that the compression of the block for a charge of constant composition, density, and diameter continues to

increase with charge length up to L/d = 3 to 4 about which it remains constant. Moreover, when plotted in reduced units ($\delta/\delta_o$ vs. L/d, where $\delta$ is the compression at length L and $\delta_o$ is that at L/d > 3 to 4), all curves of this sort may be approximately superimposed; they would all apparently superimpose at least within experimental error except for the effect of the small "edge effect" mentioned above which is approximately a constant and therefore causes deviations at small L which increase as d is reduced. Wave shape in non-ideal explosives is thus not determined by the total end impulse. However, when $a_o/d$ is negligible, the same factor or factors which limit end impulse also limit R so that $L_m$ and $R_m$ then and only then coincide.

The detonation head model gives a ready explanation for the upper limit value $R_m = 3.5$ d, as well as a quantitative explanation of the $\delta/\delta_o$ vs. L/d curves obtained in end impulse studies. Rarefactions from the sides reach the charge axis (at a distance about d behind the wave front) only after the wave has traveled the length $L_m = 3.5$ d. For L/d > 3.5 the detonation head propagates in steady state. Wave shape is also steady in all cases at L/d > 3.5 simply because at $L > L_m$ all effects of the point of initiation have been erased by the influence of lateral rarefactions.

Possibility of Pressure Gradients Across Wave Front

The fact that detonation wave fronts propagate in steady state in all cases with appreciable curvature would seem to imply a pressure gradient across the detonation wave front. However, simple arguments based on the experimental facts show that this is not the case, but that the pressure at the wave front is always approximately constant over the entire front except in the region of the edge effect mentioned above which does not exceed 2 mm.

During geometrical expansion (R = L) it is obvious that no pressure gradient exists across the wave front; otherwise expansion would not be geometrical. It follows that at the limit of geometrical expansion ($L = R_m$) no pressure gradient should exist across the wave front. But wave shape remains unchanged for $L > R_m$; it maintains the same spherical shape for $L > R_m$ that it had at $L = R_m$. Hence no appreciable pressure gradient occurs across the wave front at any stage of propagation since the appearance of a pressure gradient beyond $L = R_m$ would obviously change the wave shape. This conclusion is in accord with the detonation head model for explosives of $a_o/d \ll 1.0$; as mentioned, this model shows a rarefaction front which moves in from the sides at lower velocity than the wave front velocity D and such rarefactions cannot, therefore, influence the pressure at the front. The pressure all across the front will, therefore, be determined by the C-J condition which occurs (for $a_o \ll d$) a distance small with respect to d behind the wave front.

That no pressure gradient exists across the wave front when $a_o/d$ is appreciable is not a priori as obvious as it is when $a_o/d \ll 1$. However, the experimental fact is still the same, namely that the wave

front is spherical at $L > R_m$ with the same radius of curvature that it had at the limit of geometrical expansion ($L = R_m$) at which point there could have been no pressure gradient. This fact still seems to require that no pressure gradient exists across the wave front at $L > R_m$. Again if a pressure gradient were to develop as L increases above $R_m$, the wave would change shape and would hardly remain spherical in all cases since this pressure gradient if it were to develop would be a function of $a_o/d$, the total pressure, and other factors the combination of which could hardly produce invariably spherical wave fronts.

Qualitative Interpretation of Wave Shape by Detonation Head Model

The mere fact that detonation with finite $a_o/d$ values is possible shows that there is a strong tendency for microscopic shocklets carrying the energy and impulse generated by chemical reaction to move forward more rapidly than the wave front itself. In ordinary shock waves this effect causes the rarefactions that move forward from behind to eat into the wave front. A normal shock wave exhibits, therefore, rapidly decreasing density-distance ($\rho(x)$) and particle velocity-distance ($W(x)$) characteristics from the wave front backward. Detonation waves are apparently, however, not simple shock waves. They differ from simple shock waves at least in the one important respect that they are supported continuously by chemical reaction whereas simple shock waves are not. Conventional theoretical discussions of detonation waves (4,5) have assumed that this effect of chemical reaction in the detonation wave is simply to cause the wave to grow in such a way that $\rho(x/x_o)$ and $W(x/x_o)$ remain constant ($x_o$ the distance from the point of initiation to the wave front and x the distance from the point of initiation to a particular characteristic $\rho$ and W plane behind the wave front). One may, however, question this hypothesis at least in cases where $a_o \ll d$, and chemical reaction appears at the front instead of at the rear of the wave. In this case impulse generated by chemical reaction would not only be sent forward but also to an equal extent backward into the rarefaction region. This effect should surely modify the shape of the $\rho(x)$ and $W(x)$ curves; it would tend to flatten them. This should be true also in the cases where $a_o/d$ is appreciable, since at least part of the chemical reaction will appear at the wave front.

The experimental evidence of reaction rate studies shows that reaction zone lengths are much longer than can be accounted for by $\rho(x)$ and $W(x)$ contours which commence to decline immediately behind the wave front. A $\rho(x)$ contour flat at the front and for a distance (for $L \geq L_m$) about d behind the front, and showing rarefaction or a declining $\rho(x)$ contour for $x = x_o - d$ seems to be required to account for observed reaction rates. Fig. 10 shows a comparison between the $\rho(x)$ contour observed by Kistiakowsky and Kydd(5) and the theoretical one of the detonation head model which on the charge axis has a $\rho(x)$ flat for a distance d followed by a normal rarefaction. The experimental $\rho(x)$ contours of Fig. 10, however, have been questioned by the authors on the basis of a possible excessive time constant in the electronic equipment used to measure them. Still, other evidences for a $\rho(x)$ flat region have been found, some of which are discussed by the author. (6)

The detonation head model assumes a steady state flat $\rho(x)$ region varying in length from zero at the edge to about d on the charge axis in unconfined cylindrical charges of $L \geq L_m$. The $\rho$-flat region of the detonation head model undergoes change only in the region $0 < L < L_m$. Fig. 11 indicates the development of the detonation head in a cylindrical unconfined charge for $a_o \ll d$.

In the detonation head model rarefactions from the sides and the rear have rather definite fronts of the type indicated in Fig. 11. For $L < 0.5$ d, there is a tendency only for the wave to remain spherical since no lateral rarefaction occurs in this region, and the effective reaction zone length supporting each element of the wave front is the same for all elements. For $L > 0.5$ d, however, the region of the wave front falling in the annulus of the charge of thickness about $a_o/2$ (which for $a_o > d$ would be the entire charge), in which the lateral rarefaction cuts into the reaction zone, there is a tendency toward weakening of the detonation head and perhaps curvature also, owing to the fact that the energy developed by reaction behind the rarefaction front cannot be fed into this region because of the sharpness of the pressure and density gradient at the rarefaction front. The effective reaction zone length will thus fall below $a_o$ (or d, whichever is smaller) starting at the inside of the annulus and finally reaching zero at the edge. This effect, however, does not at first ($L = 0.5$ d) influence the curvature of the wave front because of the tendency for energy and impulse to move forward from the rear of the detonation wave. The tendency toward pressure loss in the annulus is thus quickly overcome simply by drawing momentum from the rear of the wave and the effect is merely to increase the ratio $V_{l.r.}/D$ where $V_{l.r.}$ is the lateral rarefaction velocity. In other words, the loss in energy and pressure due to incomplete reaction in the annulus (or over the entire wave front if $a_o > d$) may be offset by impulse being fed into the region of the detonation head falling inside this annulus from the rear of the head itself both inside and outside the annulus if $a_o < d$ and only inside if $a_o > d$. Assuming that this momentum transfer is fast enough (which it must be since the wave remains spherical) the pressure in the entire head may then be held at the same value as that on the charge axis as long as the angle $\alpha$ (Fig. 5) between the charge axis and the lateral rarefaction front (determined by the curvature of the wave at the edge) remains sufficiently large. The angle $\alpha$ is determined by the angle $\varphi = \alpha + \theta$ between the wave front and the side of the charge. But $\varphi$ decreases from $180^\circ$ at $L = 0.5$ d to a minimum value of $90^\circ + \sin^{-1} y'/R_m$. However, $\theta$ might be expected to remain approximately constant being determined solely by the hydrodynamics at the wave front near the edge of the charge which should be approximately constant in geometrical expansion. The angle $\alpha$ is thus at the maximum value (greater than $90^\circ$) at $L = 0.5$ d and decreases steadily as L increases reaching a minimum value at $L = R_m$. While $\alpha$ continues to decrease until $L = 3.5$ d for $a_o \ll d$, for finite values of the ratio $a_o/d$ the critical value of $\alpha$ is reached at $L = R_m < 3.5$ d. Apparently for values of $\alpha$ less than $\sin^{-1} y'/R_m$ impulse cannot be fed into the annulus from the rear of the wave as rapidly as it is needed to maintain approximately a constant pressure within the detonation head. The angle $\alpha$ is thus critical at

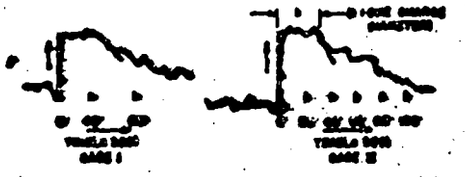

Fig. 10 - Density Distance (or Time) Contours in the Detonation Wave of a Gaseous Explosive (Solid Line Measurements by Kistiakowsky and Kydd, Dotted Line Detonation Head Model)

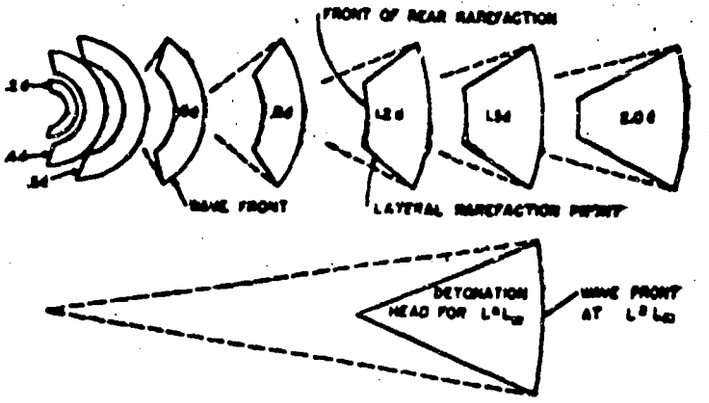


Fig. 11 - Development of Detonation Head in an Ideal Detonation with $a_o/d << 1.0$ (Dotted lines extend point of initiation for $L < L_m$ and to apparent initiation point for $L \geq L_m$.)

$L = R_m$. Since the tendency for the head to remain isobaric is (experimentally) greater than the tendency for wave shape to continue to increase, a steady state wave front is established at this critical value of $\alpha_y$ and $\epsilon$ as well as wave curvature then becomes steady.

A complete description of wave shape would provide a description of factors determining the minimum value of $\alpha$ (or $\alpha_m$) or the dependence of $R_m/d$ upon these factors through the functions $\chi$ and $f$ in equation (4). This problem is a difficult one and has not yet been solved. The experimental evidence appears to be of such a nature, however, to require theoretical concepts of the type employed in the detonation head model as indicated above.

## ACKNOWLEDGMENT

This work was supported by Office of Naval Research, Contract Number N7-onr-45107, Project Number 357 239, and was carried out by the Explosives Research Group. The excellent work of Dr. G. Smoot Horsley, Dr. William S. Partridge, and Mr. Wayne O. Ursenbach, together with other members of the Explosives Research staff is gratefully acknowledged.

## BIBLIOGRAPHY

(1) H. Eyring, R. E. Powell, G. H. Duffey, R. B. Parlin, Chem. Rev. 45, 1 (1949).

(2) M. A. Cook and E. F. Pound, "'Pin Oscillograph' for Measurement of Detonation Velocity", Technical Report No. XXXIII, May 4, 1954, ERG, Utah University.

(3) M. A. Cook and W. O. Ursenbach, "Velocity-Diameter and Wave Shape Studies in Low Density 50/50 TNT-SN Mixtures", Technical Report No. XXXVI, July 30, 1954, ERG, Utah University.

(4) G. I. Taylor, Proc. Roy. Soc. A200, 235 (1940).

(5) G. B. Kistiakowsky and P. H. Kydd, "The Rarefaction Wave Following a Gaseous Detonation", Report submitted under Contract N5-ori-76, T. O. XIX, NR-053-094, Office of Naval Research.

(6) M. A. Cook, "Detonation Head Model and Chemical Reaction Rates in Detonation" (submitted for publication).

# DETERMINATION OF REACTION RATE OF SODIUM NITRATE AND THE EQUATION OF STATE OF 50/50 TNT-$NaNO_3$

25

Melvin A. Cook and Wayne O. Ursenbach
University of Utah
Salt Lake City, Utah

## ABSTRACT

Reaction rates of sodium nitrate (SN) in low density mechanical and high density cast mixtures of 50/50 TNT-SN were determined by each of the three theories extant (nozzle, curved front, and detonation head) using the experimental velocity (D) vs. diameter (d) curves measured over a broad range of diameters from the critical diameter $d_c$ up to 25 cm. The total reaction times found for SN may be expressed by the equations

$$\tau_2 = 6.8 \times 10^{-4}\, \bar{R}_g \cdot f \; ; \; (\bar{\rho}_1 = 1.83)$$

$$\tau_2 = 2.1 \times 10^{-3}\, \bar{R}_g \cdot f \; ; \; (\bar{\rho}_1 = 1.15)$$

where $\tau_2$ = reaction time of SN in seconds, $\bar{R}_g$ = grain radius of SN in centimeters, and f = 1.0 for the detonation head model, 0.07 to 0.09 for the nozzle theory, and 0.03 to 0.04 for the curved front theory.

The approximately three times greater total reaction time or slower reaction rate of SN in the explosive at $\bar{\rho}_1 = 1.15$ than in that at $\bar{\rho}_1 = 1.83$ (irrespective of the theory used to determin) it) implies a temperature difference $T_2$ ($\rho_1 = 1.83$) - $T_2$ ($\rho_1 = 1.15$) of about 600° C in agreement with the $\alpha(v)$ equation of state which leads also to a value of 600°C for this difference.

## INTRODUCTION

Cook, Mayfield, and Partridge (1) determined the velocity-diameter D(d) curves for ammonium nitrate (AN) in 50/50 TNT-AN at $\bar{\rho}_1 = 1.55$ (cast) and $\bar{\rho}_1 = 0.9$ (loose-packed), 70.7/29.3 composition B-AN (cast $\bar{\rho}_1 = 1.59$) and pure AN ($\bar{\rho}_1 = 1.04$). They found that the reaction time ($\tau_2$) of AN in the detonation of these widely different

explosives followed in all cases (within a factor of 1.5) the equation

$$\tau_2 = 1.7 \times 10^7 \bar{R}_g/k' \qquad (1)$$

where k', the specific gas constant, is given by

$$k' = 4 \times 10^9 T_2 \exp -38{,}300/RT_2 \qquad (2)$$

Here $\tau_2$ (in seconds) was determined by the detonation head model, (2) equation (2) was determined in this laboratory in isothermal decomposition studies; $\bar{R}_g$ is the average radius of the AN in centimeters and $T_2$ is the detonation temperature computed by the $\alpha(v)$ equation of state, calculated temperatures for the above four explosives being $T_2$ = 3510, 3300, 4150, and 1720°K, respectively. The nozzle theory (3) gave reaction times ranging from 0.04 to 0.12 times as long as those given by equations (1) and (2) and the curved front theory (4) gave values of $\tau_2$ ranging from 0.025 to 0.085 times those computed by these equations. Hence the correlation between the $\tau_2$'s themselves as well as with isothermal decomposition studies was much better in these studies with the detonation head model than with the latter two theories. Moreover, the fit of the experimental D(d) curves by the detonation head model was consistently better than by the nozzle theory which in turn was better than by the curved front theory. The constant factor in k' would necessarily be in the range from 8 to 60 times greater than the value found in isothermal decomposition studies to agree with the $\tau_2$ results found by the latter two theories. Factors ranging only from 0.7 to 1.5 are required, however, to bring the results for the detonation head model into agreement with equations (1) and (2). Note that the theoretical Eyring equation for k'

$$k' = kT/h\, e^{\Delta S^{\neq}/R}\, e^{-\Delta H^{\neq}/RT} \qquad (3)$$

gives for this constant the value $2 \times 10^{10}\, e^{\Delta S^{\neq}/R}$. The values of the constant factor obtained in the nozzle and curved front theories for AN were even larger than k/h (k and h are the Boltzmann and Planck constants) by a factor ranging from 4 to 20. This gave $\Delta S^{\neq}$ values ranging from 2.8 to 6.0 E.U. The factor $4 \times 10^9$ in equation (2) which was the isothermal decomposition value gave $\Delta S$ = -3.2 e.u.

Direct comparison of the reaction rates of AN in 50/50 TNT-AN at $\rho_1$ = 0.9 and 1.55 showed that the reaction rate was about 3.5 times faster at the high density than at the low one. This requires a temperature about 500°C higher at 1.55 than at 0.9 g/cm. The calculated difference by the $\alpha(v)$ equation of state was 240°C if the molecules $CH_2OH$ and $CH_2O_2$ are assumed to form making use of the equilibrium constants determined by statistical mechanics. However, by omitting the equilibrium equations for the molecules $CH_3OH$ and $CH_2O_2$ the computed equilibrium constants for which were somewhat doubtful, the computed temperature difference was about 500°C in agreement with that required by the observed reaction rates. The Kistiakowsky-Wilson-Brinkley equation of state leads to about -400°C for this temperature difference and it was

therefore concluded that the α(v) equation of state is much better than the K-W-B equation of state for 50/50 TNT-AN.

SN lends itself well to a study of the type carried out for AN. The two systems, in fact, are much alike not only in the nature of the mixtures but also in the shapes of the D(d) curves. This article presents the experimental velocity-diameter (D(d)) curves for cast and loose-packed 50/50 TNT-SN mixtures measured over the diameter range from the critical diameter $d_c$ to diameters up to 25.2 cm.

Measurements of the shape of the front of the detonation wave were also carried out for the TNT-SN mixtures and are described in a separate paper in this symposium. (5) They showed spherical wave fronts throughout (aside from a few scattered non-reproducible traces of slightly tipped or asymmetrical wave fronts). The radius of curvature R of the spherical wave for a given set of conditions was reproducible within ± 10 percent for both the cast and loose-packed products in this case. The radius of curvature/diameter ratios (R/d) in diameters of 5 and 10 cm and $\rho_1 \sim 1.15$ g/cc increased at first geometrically (R = L) with length L but changed abruptly to the steady state wave shape of $R = R_m$ at $L = R_m$ remaining at this value for $L > R_m$. Values of $R_m/d$ were 1.45 at d = 5 cm and 1.8 at d = 10 cm. The $R_m/d$ curves increased from unity near the critical diameter to about 2.5 at d = 25.2 cm. The significance of these data are discussed in terms of reaction rates in reference (5).

## EXPERIMENTAL METHODS AND RESULTS

The SN used in the loose-packed TNT-SN mixtures was screened through 28 on 48 mesh standard Tyler screens. Closer screen cuts were taken for the cast charges. While the effect of particle size was clearly evident and seemed to follow the Eyring surface burning law, it was too small in this case owing to the small range of sizes available for quantitative study of the Eyring surface burning model other than by the D(d) curve itself. The TNT used was the regular fine-grained product. The loose-packed charges were vibrator packed in manila paper tubes and densities determined by total weight/total volume measurements. Cast charges were poured also in manila paper tubes using 6-8" "heads" which were removed and only the bottom portion of length $L \geq 6d$ was used. Velocities were measured primarily by a pin oscillograph (6) although a high speed, rotating mirror camera was used to measure velocity in the smallest diameter charges. Pin oscillograph measurements were made in all cases at $L > 3d$.

In initial studies (7) with 50/50 TNT-SN, the ideal velocity-density ($D^*(\rho_1)$) curve was calculated from the α(v) equation of state and the 'universal' α(v) curve established primarily with C-H-N-O explosives. The D(d) curve at d = 25.2 cm for the low density product was only 20 m/sec lower than the calculated ideal velocity, and this curve appeared still to be increasing at d = 25.2 cm. The D(d) curve for the cast product was flat for diameters above d = 12.7 cm and the

observed velocity was 250 m/sec higher than the calculated value. To determine D* at the low end of the $D^*(\rho_1)$ curve, therefore, two charges of 50/50 TNT-SN at d = 20 cm were prepared using ball-milled SN. These results (with corrections for density) checked very closely the values found at d = 25.2 cm with the -28 + 48 mesh SN indicating that the velocity had reached the hydrodynamic one (D*) at d = 25.2 cm. Assuming a linear $D^*(\rho_1)$ curve this result together with the large diameter values for the cast product established the experimental $D^*(\rho_1)$ curve for 50/50 TNT-SN shown in Fig. 1. The equation for D* was

$$D^* = 4100 + 2580\ (\rho_1 - 1.0) \qquad (4)$$

Using the slope 2580 m/sec/g/cc to correct the velocities of the cast product to $\bar{\rho}_1 = 1.83$ and those of the loose-packed one to $\bar{\rho}_1 = 1.15$, the velocity-diameter curves given in Fig. 2 were obtained.

## THERMO-HYDRODYNAMIC PROPERTIES OF 50/50 TNT-SN

Thermo-hydrodynamic properties were computed by the inverse method using the equation of state (8)

$$pv = nRT\ e^x;\ x = K(v)/v \qquad (5)$$

and the observed $D^*(\rho_1)$ data (equation (4)). In these calculations the molecules $CH_3OH$ and $CH_2O_2$ were neglected even though the calculated equilibrium constants indicated that they should be appreciable at high fugacity. The reason for neglecting these molecules as mentioned previously was the uncertainty in the theoretically computed equilibrium constants. The results of these calculations are given in Table I together with a comparison of the calculated $\alpha(v)$ curve and the 'universal' one [9] equation (5) being identical with the $\alpha(v)$ equation of state

$$pv = nRT + \alpha(v)\ p$$

with $e^x = v/(v - \alpha)$. The maximum difference was 0.02 l/kg in $\alpha$ and occurred on the low density side. The difference corresponds to a velocity difference of about 200 m/sec, which is just outside the range of experimental error in velocity determinations at low density owing to density and composition fluctuations.

## REACTION RATE DETERMINATIONS

Using the values D*(1.83) = 6240 m/sec and D*(1.15) = 4390 m/sec, the experimental D(d) curves were analysed by the nozzle, curved front and detonation head theories. Although a careful study of the nozzle theory shows that such is not necessarily the case, Taylor (10) states that a plot of $(D^*/D)^2$ against $1/R^2$ should give a straight line. Also the initial curved front theory indicated that a plot of D vs. 1/d should give a straight line although the more recent formulation of the

curved front theory [17] shows that this too is not the case. Accordingly the data obtained here are plotted both as $1/D^2$ vs. $1/d^2$ and as D vs. 1/d in Fig. 3. One will note that the Taylor condition is approximately satisfied for cast sodatol, but for the loose-packed product the curve differs widely from a straight line both at small and large diameters. The curve at low density, however, does not agree in shape with the nozzle theory.

Using the nozzle theory directly and the most recent formulation of the curved front theory the following values of the reaction zone length $a_o$ were obtained from computations at various values of $D/D^*$ across the D(d) curves.

| Nozzle | | | | Curved Front | | | |
|---|---|---|---|---|---|---|---|
| $\rho_1 = 1.83$ | | $\rho_1 = 1.15$ | | $\rho_1 = 1.83$ | | $\rho_1 = 1.15$ | |
| d(cm) | $a_o$(cm) | d(cm) | $a_o$(cm) | d(cm) | $a_o$(cm) | d(cm) | $a_o$(cm) |
| 3.8 | 1.25 | 3.8 | 1.2 | 3.2 | 0.6 | 3.2 | 0.67 |
| 5.0 | 1.32 | 4.45 | 1.4 | 4.3 | 0.6 | 4.65 | 0.73 |
| 7.5 | 1.42 | 6.38 | 1.7 | 6.65 | 0.51 | 9.1 | 0.78 |
| 10.0 | 1.50 | 8.4 | 1.9 | 9.15 | 0.39 | 15.0 | 1.20 |
| $\bar{a}_o = 1.4$ | | 12.5 | 2.4 | 10.2 | 0.36 | $\bar{a}_o = 0.8$ | |
| | | 15.7 | 2.5 | 12.0 | 0.15 | | |
| | | 17.0 | 2.2 | $\bar{a}_o = 0.4$ | | | |
| | | $\bar{a}_o = 1.9$ | | | | | |

The detonation head model leads generally to a better fit of the D(d) curves than either of the above theories. However, in this case the shape of the curve is such that the reaction time $\tau_2$ for SN in the case of the low-density mixture is very sensitive to the particular value one selects for D*. For the cast sodatol $\tau_2$ was not as sensitive to the value one chooses for D* and moreover D* in this case could be readily established without ambiguity. Using D* (1.15) = 4700 m/sec (computed from the $\alpha(v)$ curve), for example, $\tau_2$ was about 180 μsec, and the general fit of the D(d) curve was excellent for d > 3 cm. However, using the experimental value D*(1.15) = 4390 m/sec one obtains $\tau_2$ = 60 μsec. Despite this relatively large difference the computed D(d) curve for $\tau_2$ = 60 μsec was still within experimental error of the observed data for d > 3.0 cm (Fig. 4).

While the fit by the detonation head model at small diameters was not perfect, the $\tau_1$ (for TNT) values obtained were consistent for both sodatol and amatol. In both cases $\tau_1$ was 8.5 μsec in the cast products and increased to 20 μsec and 26.5 μsec in the loose-packed amatol and sodatol, respectively. This increase was about the same relative amount as for $\tau_2$ (for AN and SN) in going from the cast to the low density mixtures.

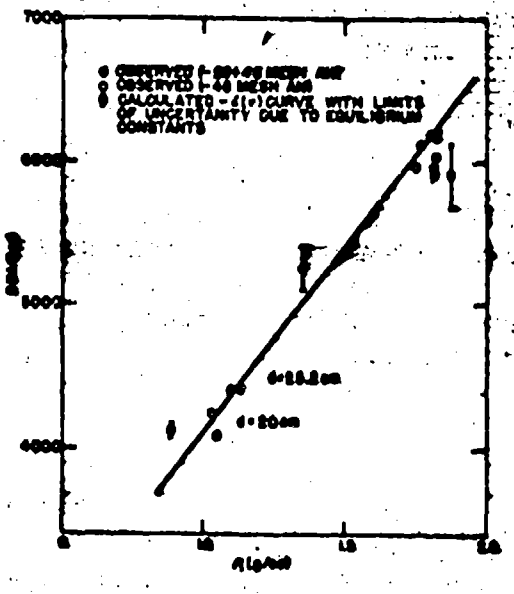

Fig. 1 – Maximum or Hydrodynamic Velocity-Density Curve for 50/50 TNT-SN

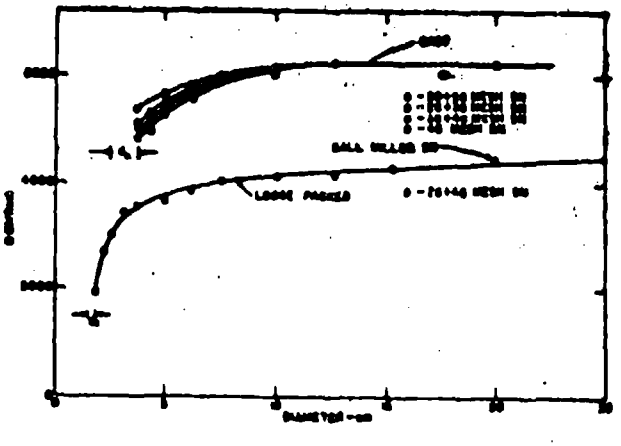

Fig. 2 – Velocity-Diameter Curves for 50/50 TNT-SN. (Each Point is an Average of 2-5 Measurements.)

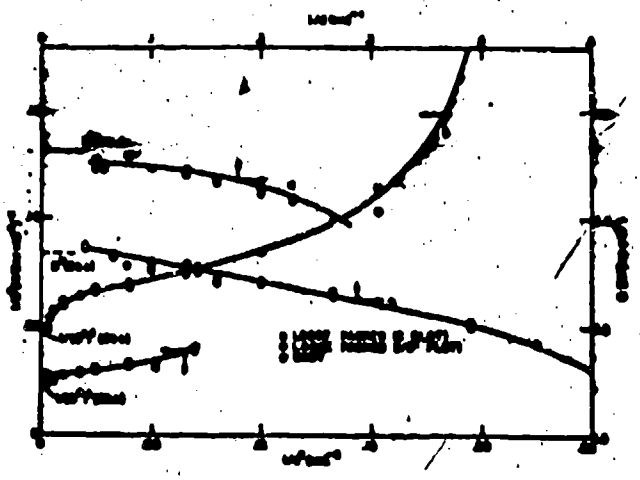

Fig. 3 - $1/D^2$ vs. $1/d^2$ for 50/50 TNT-RDX

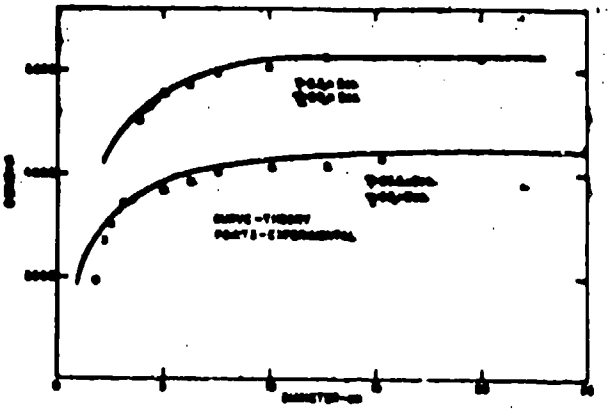

Fig. 4 - Comparison of Theoretical D(d) Curves (Detonation Head Theory) with Experimental Results

The total reaction times may be expressed in terms of the Eyring surface burning equation

$$\tau = \bar{R}_g / \lambda k' \qquad (6)$$

which may be shown to be consistent with results obtained in this study and has been verified quantitatively in previous studies. The results of these studies may therefore be summarized by the equations

$$\tau_2 = 2.1 \times 10^{-7} \bar{R}_g \cdot f \ (\rho_1 = 1.15) \qquad (7)$$

$$\tau_2 = 6.8 \times 10^{-4} \bar{R}_g \cdot f \ (\rho_1 = 1.83) \qquad (8)$$

where $f = 1.0$ in both equations for the detonation head model (from the average $a_o$), $f = 0.09$ and 0.07 in equations (7) and (8), respectively for the nozzle theory, and (from the average $a_o$) $f = 0.04$ and $f = 0.03$ for equation (7) and (8), respectively, for the curved front theory.

As in the case of AN in amatol, the reaction time of SN in sodatol increased by a factor of about three in decreasing the density from $\bar{\rho}_1 = 1.83$ to $\bar{\rho}_1 = 1.15$. This shows that the detonation temperature increased with density. If one assumes (1) that the activation energy of SN is the same as for decomposition of SN (61 kcal/mol), (2) the temperatures in Table I, and (3) the equation

$$k' = AT\, e^{-61{,}000/RT} \qquad (9)$$

of absolute reaction rate theory, the ratio $\tau_2(1.15)/\tau_2(1.83)$ turns out to be 3.0 in agreement with the value found by the detonation head model and (within the limits of uncertainty) with the values found by either the nozzle or curved front theory. This shows, as in the case of amatol, that the $\alpha(v)$ equation of state is essentially correct. The Kistiakowsky-Wilson-Brinkley equation of state

$$pv = nRT\,(1 + x\, e^{x}); \quad x = KT^{-1/4}/v$$

gives for $T_2(1.83) - T(1.15)$ a value of about -500°. This would require by equation (9) a ratio $\tau_2(1.15)/\tau_2(1.83)$ of about 0.3 which is too low by a factor of about ten.

The remarkable consistency of the detonation head model may be shown also by noting the absolute values of k' found in this investigation in comparison with those for AN, TNT, and others found in previous studies. Values of k' for SN computed from equation (6) were $10^{9.93}$ for the low density product and $10^{10.4}$ for the cast product. Equation (9) with $\Delta H = 61$ kcal/mole requires $\Delta S^{\neq} = -2.0$ E.U. to give these values of k'. This value is practically the same as that found for AN. Again values of $\Delta S^{\neq}$ from +3 to +6 E.U. are required to give the values of k' one computes through equations (6) and (9). Positive values of $\Delta S^{\neq}$, however, seem highly improbably for a process such as this. While autocatalysis leads to positive values of $\Delta S^{\neq}$, autocatalysis can hardly come into play in a surface burning reaction of the type involved in detonation.

Table I: Thermo-Hydrodynamic Properties of Cast and Loose-Packed 50/50 TNT-[redacted]

| $\rho_1$ (g/cc) | $D^*$(obs) (m/sec) | $T_2$(°K) | n (mol/kg) | Q (kcal/mol) | $\bar{C}_v$ (kcal/kg/deg) | $v_2$ (g/cc) | W (m/sec) | $P_2$ (atm) |
|---|---|---|---|---|---|---|---|---|
| 1.15 | 4490 | 3750 | 26.0 | 850 | 0.287 | 0.646 | 1155 | 59,000 |
| 1.83 | 6240 | 4350 | 23.0 | 940 | 0.307 | 0.424 | 1395 | 158,000 |

Calculated $\alpha(v)$ Curve

| | | | | | | |
|---|---|---|---|---|---|---|
| $\rho_1$ | 1.0 | 1.2 | 1.4 | 1.6 | 1.8 | 2.0 |
| $\alpha$ | 0.543 | 0.491 | 0.447 | 0.409 | 0.377 | 0.348 |
| $v_2$ | 0.723 | 0.620 | 0.540 | 0.479 | 0.431 | 0.391 |

(Universal Curve)

| | | | | | | |
|---|---|---|---|---|---|---|
| $\alpha$ | 0.565 | 0.510 | 0.460 | 0.420 | 0.375 | 0.340 |
| $v_2$ | 0.723 | 0.620 | 0.540 | 0.479 | 0.431 | 0.391 |

Products of Detonation (mols/kg)

| | $H_2$ | $N_2$ | $CO_2$ | CO | $H_2O$ | $NH_3$ | $CH_4$ | $Na_2O$ |
|---|---|---|---|---|---|---|---|---|
| $\rho_1$ = 1.15 | 0.3 | 6.2 | 10.0 | 5.3 | 3.5 | 0.6 | 0.1 | 8.94 |
| $\rho_1$ = 1.83 | — | 5.5 | 12.9 | 1.4 | 0.6 | 1.4 | 1.2 | 8.94 |

Unclassified

Cook and Urtiew

ACKNOWLEDGMENT

This work was supported by Office of Naval Research, Contract Number N7-onr-45107, Project Number 357 239, and was carried out by the Explosives Research Group, Utah University.

BIBLIOGRAPHY

(1) M. A. Cook, E. B. Mayfield, and W. S. Partridge, "Reaction Rates of Ammonium Nitrate in Detonation" (submitted for publication).

(2) M. A. Cook, "Detonation Head Model and Reaction Rates in Detonation" (submitted for publication).

(3) H. Jones, Proc. Roy. Soc. (London) A189, 415 (1947).

(4) H. Eyring, R. E. Powell, G. H. Duffey, and R. B. Parlin, Chem. Rev. 45, 1 (1949).

(5) M. A. Cook, "Detonation Wave Fronts in Ideal and Non-Ideal Detonation", This Symposium.

(6) M. A. Cook and E. F. Pound, "'Pin Oscillograph' for Measurement of Detonation Velocity", Technical Report No. XXXIII, May 4, 1954, ERG, Utah University.

(7) M. A. Cook and W. O. Ursenbach, "Velocity-Diameter and Wave Shape Studies for Low Density 50/50 TNT-Sodium Nitrate Mixtures", Technical Report No. XXXVI, July 30, 1954, ERG, Utah University.

(8) M. A. Cook, R. T. Keyes, G. S. Horsley, and A. S. Filler, "A Study of the Equation of State for EDNA", Accepted for Publication, J. Phys. Chem.

(9) M. A. Cook, J. Chem. Phys. 15, 518 (1947).

(10) J. Taylor, "Detonation in Condensed Explosives", Oxford Press, (1952).

(11) R. B. Parlin and D. W. Robinson, "Effect of Charge Radius on Detonation Velocity", Technical Report No. VII, October 3, 1952, ERG, Utah University.

# THE DECOMPOSITION OF ALPHA-LEAD AZIDE

J. M. Grocock
C.S.A.R., Ministry of Supply
Great Britain

## General Introduction

Detonation, from a chemical viewpoint, is essentially an extremely rapid exothermal reaction, but there is little certain evidence to show that this reaction for any given initiator is simply the thermal decomposition reaction greatly accelerated by extreme physical conditions. However, it would seem that a clear understanding of the kinetics of the low-rate decomposition of initiators and of the decomposition that, under suitable conditions, can be observed prior to detonation is a necessary precursor of an understanding of the chemistry of detonation. A study of the reaction kinetics of the decomposition of lead azide is therefore being made at the Armament Research Establishment in Great Britain. So far, work has been completed on the photolysis and electron bombardment decomposition under vacuum of pure alpha lead azide and this paper will deal mainly with these. Reference will also be made to a study of the thermal decomposition of lead azide at moderate temperatures, which experimentally has reached a fairly advanced stage and to some preliminary results obtained at higher temperatures, where the decomposition passes into detonation.

## Decomposition of Azides

The study of solid reactions has made rapid progress in recent years since the importance of lattice defects was pointed out by Frenkel (1) and Wagner and Schottky (2) and further impetus was given by the development of the theory of electrons in solids (3 and 4). The first detailed elucidation of a solid reaction using these ideas was given by Gurney and Mott (5) for the photochemical process taking place in silver bromide. In recent years considerable attention has been given to the metallic azides (6 to 17). There is a series of these of the general formula $MN_3$ for monovalent, $MN_6$ for divalent metals, and they all decompose stoichiometrically under suitable conditions according to the equation:

$$2MN_3 \rightarrow 2M + 3N_2$$

The reaction can be studied by measuring the build up of the pressure of nitrogen in a vacuum system. Thermochemical data shows that the decomposition of one azide radical to give a nitrogen molecule plus a nitrogen atom is endothermic, i.e.

$$N_3 \rightarrow N_2 + N - 37 \text{ k.cals.}$$

whereas the decomposition of two azide radicals to give three nitrogen molecules is exothermic,

$$2N_3 \rightarrow 3N_2 + 151 \text{ k.cals.}$$

and most methods of decomposition involve the latter. In the crystal there is some stabilisation by resonance but this is low for metals with high ionisation potentials.

The kinetics of the thermal decompositions of lead, sodium and potassium, calcium, strontium and barium azides have been studied (6 to 15) but these will not be discussed here. The photochemical decompositions of barium and potassium azides (11, 14, 15) and the electron bombardment decomposition of sodium and barium azides (16 and 18) have also been studied.

The Photolysis of Barium and Potassium Azides

The reflection spectra of barium, potassium and sodium azides have been measured by Jacobs and Tompkins (15) and it was found that absorption of wavelengths shorter than 2700 to 2800 Å took place. They found no evidence of photoconductance in these salts. The photolysis of barium azide has been investigated by Garner and Maggs (11) and in more detail by Thomas and Tompkins (14). The latter found that on irradiation with light of wavelength 2537Å, nitrogen is evolved and the rate becomes linear with time. In fresh unirradiated barium azide there is an initial fast rate of decomposition which gradually decays to a constant value. Between -106° and 40°C the rate is proportional to the square of the intensity. Between -106° and -52° the activation energy is 200 cals., between -52° and -10° 1700 cals., and between -10° and 40° the activation energy is 4,500 cals. Similar results have been obtained by Jacobs and Tompkins (15) for potassium azide. An immediate emission of nitrogen occurs at a rate which increases slightly for the first five minutes and then becomes constant, at a rate proportional to $I^2$. Activation energies of 700 cals. below 1°C, and 2,700 cals. above 1°C were obtained and slow decomposition was found to continue after switching off the light source.

According to Thomas and Tompkins, absorption of a quantum of light must excite an electron either into the exciton level or the conduction band. They then consider that it is likely that

decomposition involves two positive holes or excitons which must be trapped at adjacent sites. Positive holes in the lattice will be held apart by their charges, and reaction with the low activation energy found experimentally will be possible only if the centre as a whole is uncharged; i.e. the trap is a doubly charged vacant cation site. The rate of decomposition is constant and thus the number of these centres must be independent of time and reaction must therefore regenerate a trapping centre. Thomas and Tompkins first consider the rate of decomposition as proportional to the rate at which traps containing two positive holes are formed. The formation of traps containing one positive hole is proportional to the concentration of free positive holes, while they can be destroyed in three ways; by trapping an electron, by thermal liberation of the hole, and by reaction with a neighbouring positive hole giving the measured reaction rate. By means of a detailed analysis of such factors Thomas and Tompkins obtained an expression for the rate of formation of traps containing two positive holes and then showed that if the traps are deep, the rate of decomposition is proportional to I rather than $I^2$ as found experimentally. If the traps are shallow, however, the temperature dependence is incorrect and the mobility of the positive holes should give photoconductivity. Thomas and Tompkins suggest that the mechanism involved two excitons and show by a treatment similar to that outlined above that the experimental facts can be explained in terms of this. The difference is that excitons having no net charge can be trapped at any discontinuity in the lattice. The temperature dependence found is explained in terms of two possible processes for the reaction together of the excitons, one utilising the energy released by the trapping of one of the excitons, and the other requiring thermal energy from the lattice.

The Electron Bombardment Decomposition of Barium and Sodium Azides

The electron bombardment decomposition of sodium azide has been studied by Müller and Brous (18), and Groocock and Tompkins (16) who also investigated barium azide by this technique. They found that on bombardment of both compounds with electrons of constant velocity and intensity there was an immediate evolution of gas and that the decomposition rate rose quickly to a maximum and then slowly decayed approximately exponentially finally to approach a constant rate after long periods of bombardment. If now bombardment was stopped and the salt was left under high vacuum for some hours, on recommencing bombardment the rate of decomposition was found to have recovered completely and the first curve could be repeated exactly. Detailed investigation showed that the recovery process had first order kinetics. No colour change was produced by the bombardment. The variation in the decomposition rate with the intensity of bombardment was complex but all the results could be adequately explained in terms of a theory which postulated that the action of the electron beam was to produce positive holes and conduction band electrons in a relatively thick layer. Decomposition to give nitrogen occurred whenever two positive holes were produced in adjacent positions in

the surface; therefore the reaction was controlled by the number of single surface positive holes present. This in turn was determined by the concentration of azide ions in the deeper layer penetrated by the electron beam but where decomposition did not take place. The recovery process was seen in terms of the recombination of positive holes and conduction band electrons in this lower layer.

## The Photolysis of α-Lead Azide

### Experimental details

The apparatus consisted of the reaction cell A (Fig.1) connected to a high vacuum system comprising a Pirani gauge P, a liquid nitrogen trap, a mercury cut-off and a mercury diffusion pump with a rotary oil pump. The azide was contained in a flat tray of pyrex glass 12 mm's. in diameter and the junction of a copper constantan thermo-couple was sealed with Araldite into a groove ground into the face of the tray. Using this the temperature of the azide could be measured and the values are accurate to ± 0.2°C. The Pirani gauge had a sensitivity such that pressure differencies of $1 \times 10^{-5}$ mms. could be detected easily. The ultra-violet light was obtained using a low pressure mercury vapour lamp having 90 per cent of its total radiation in the 2537 Å line. A calibration of intensity of radiation against current through the lamp was obtained with excellent reproducibility, using a zirconium cathode photocell sensitive in the ultra-violet only.

FIG. 1

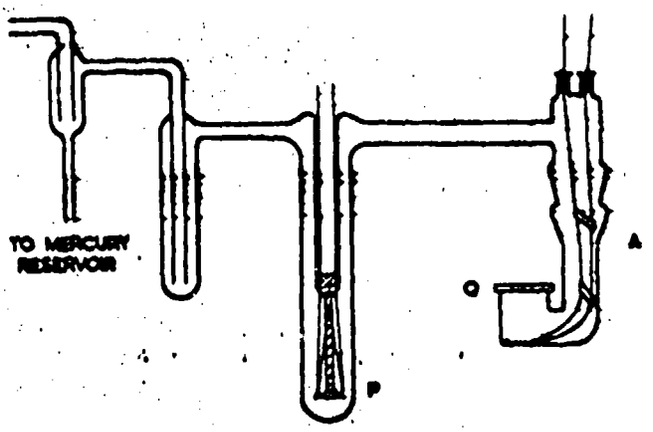


DIAGRAM OF REACTION UNIT

Measurements of rate of decomposition against time were obtained as follows: The time Δt1, for a small pressure increase in the system closed by the cut-off was measured; this part of the apparatus was then quickly pumped out and the time Δt2 for the same small pressure increase measured again. As Δt is small $\frac{1}{\Delta t}$ is proportional to the rate of decomposition at time t, and from a series of values of Δt, a plot of rate of decomposition against time can be obtained for any period of decomposition, while the pressure within the cut-off system varies between small limits only. This technique has the further advantages that measurements are independent of the shape of the Pirani gauge calibration curve and that the resulting rate of change of pressure/time curves are more useful theoretically

than the more usual pressure/time curves.

## Results

### Photolysis at constant intensity

Fig.2 shows the plot of rate of decomposition against time for the photolysis of 40 mg. of α-lead azide. The temperature of the azide rose from 3.6°C to 7.0 ± 0.2°C during the first ten minutes of the photolysis due to the heating effect of the beam, but in view of the low activation energy of the reaction (reported later) this would increase the rate by only 2 per cent and no correction is therefore made. Gas is evolved immediately on commencing the irradiation and the rate reaches a maximum within a few minutes and then falls approaching a constant value after some hours. Mathematical analysis of this and other decomposition curves shows that the final decay in rate is exponential in form:

$$\text{i.e. } R - R_\infty = (Ro - R_\infty) \exp(-kt)$$

where R is the rate of decomposition at time t, Ro is the rate extrapolated to zero time and $R_\infty$ is the rate approached after prolonged photolysis.

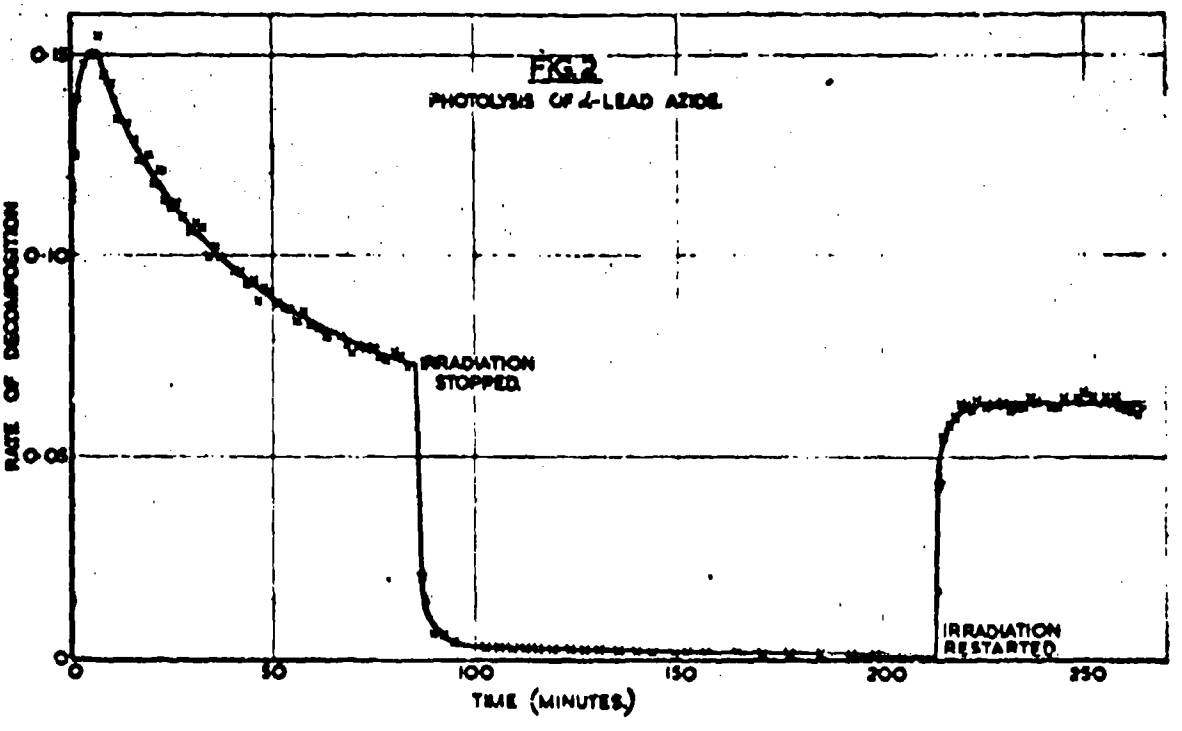


This exponential decay in rate is held fairly closely for the later stages of the photolysis, but in all cases in the region immediately following the maximum the rate was too high to accord with an exponential decay. As the temperature is low at this time

and the effect of the initial rise will still be tending to reduce the rate, this result is unexpected. Within a few minutes of the commencement of the photolysis, the surface of the azide had become noticeably yellow, and the colour rapidly darkened through orange to brown, and finally black.

After 85 minutes the irradiation was stopped but gas continued to be evolved although at a much reduced rate. This "dark rate" decayed rapidly and after about an hour was 1/50 x $R_\infty$. On recommencing irradiation there was again an immediate evolution of gas at a rate which increased rapidly to a constant value, but lower than the rate at which irradiation had been stopped. The dark rate was checked after allowing the azide to stand unirradiated in high vacuum overnight, and then had a very low value probably accounted for by the outgassing of the apparatus.

Re-irradiation again showed a rise to a constant value lower than the rate at which the previous irradiation had been stopped.

Variation of photolysis rate with temperature

The rate of decomposition at constant intensity of illumination was measured at several temperatures in the range - 117°C to + 171°C, and in all cases the general form of the rate/time curve was the same as that outlined above. Values of $R_\infty$ were selected such that plots of log $(R - R_\infty)$ against time gave the best possible straight lines and these values of $R_\infty$ were then plotted in a conventional activation energy curve. (Fig.3). This graph of log $R_\infty$ against $1/T°K$ has three straight regions of different slopes: above 121°C there is an activation energy of 5,300 cals; between 121°C and some temperature below -60°C it is 1,000 cals, and at very low temperatures the reaction has an activation energy of less than 350 cals.

FIG 3. — ACTIVATION ENERGY OF PHOTOLYSIS OF LEAD AZIDE.

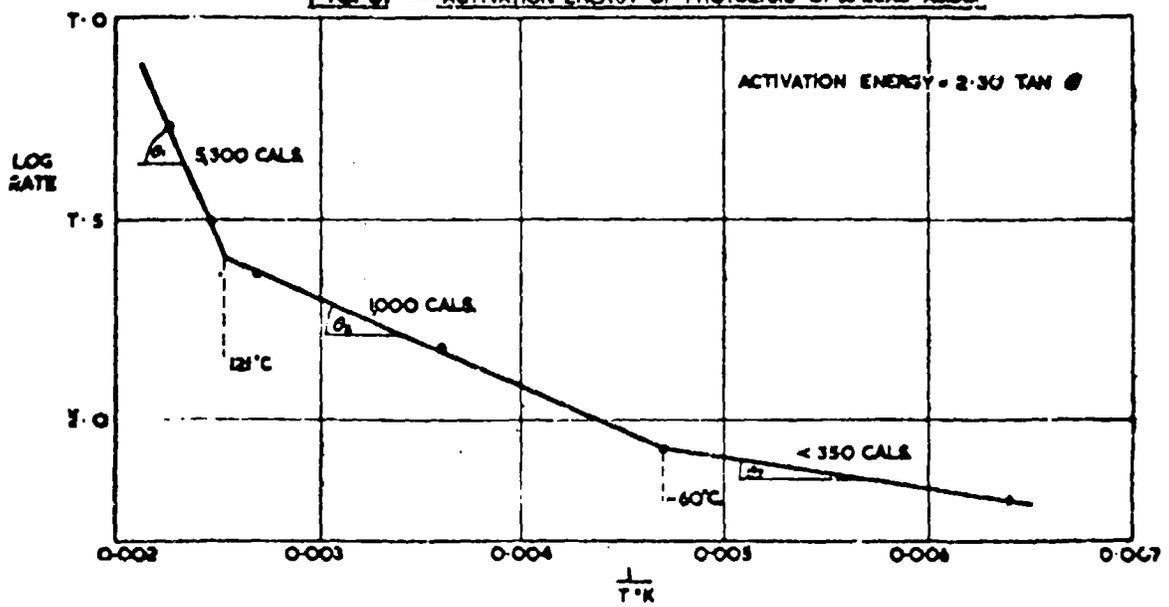

## Variation of photolysis rate with intensity

The intensity of irradiation was varied by altering the current passing through the mercury vapour lamp to correspond with the photocell calibration curve, as noted above. Two temperatures, 7.5°C and 102.5°C were used for these experiments; at lower temperatures, except at maximum intensity of irradiation, the rates of decomposition were too low to be measured with sufficient accuracy. The procedure adopted was to irradiate a fresh sample of the azide at the maximum intensity until the rate was falling only very slowly. The intensity was then reduced by a known amount and irradiation continued while 12 readings of rate were taken, these in general showing merely a scatter about a constant value. Their mean could therefore be taken as the decomposition rate for this intensity. By successively reducing the current (lamp) through fixed amounts a series of readings of rate against intensity were obtained. Although the bath temperature was kept constant throughout a run, the varying intensities of illumination used affected the actual temperature of the azide; the temperature of the salt at maximum illumination was up to 5°C higher than that of the unilluminated salt. However, this corresponded to a rate change of only 3 per cent and was not therefore corrected for. The results obtained at the two temperatures are shown graphed in Fig.4. In both cases the plot of rate against intensity is a good straight line passing through the origin. The rate of decomposition is therefore proportional to the intensity.

FIG. 4.

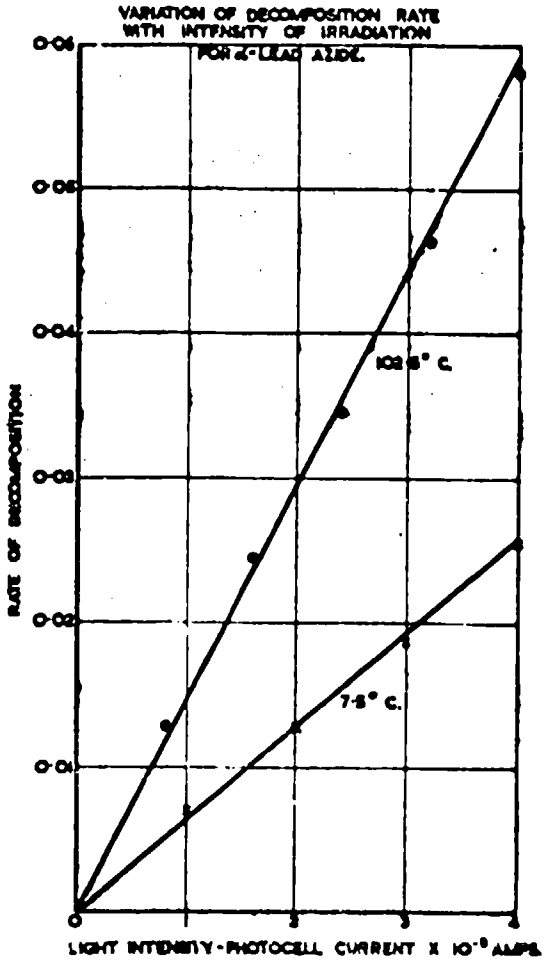

Discussion of results

For the photolysis of α-lead azide the main experimental facts which must be explained are as follows:-

(i) At constant intensity of irradiation and constant temperature, the rate of decomposition rises first to a maximum and then decays probably exponentially to a constant value.

(ii) There is an immediate colour change followed by blackening.

(iii) On ceasing irradiation there is a slow "dark rate" which decays to zero.

(iv) Re-irradiation produces a rapid rise to a constant value which is lower than the final value of the previous irradiation.

(v) The $R_\infty$ value varies as the first power of the intensity.

(vi) The temperature dependence is complex, but is very similar to that of barium and potassium azides.

Theoretical treatments of the results obtained for the photolysis of barium and potassium azides have been given by Thomas and Tompkins (14) and Jacobs and Tompkins (15) and as noted in the introduction they postulate a mechanism involving the reaction together of two excitons produced by the radiation. Similar assumptions applied to lead azide demand that the rate of decomposition shall be proportional to the square of the intensity of illumination rather than the first power, as found experimentally. A theory based on reaction of positive holes however overcomes this difficulty. Although the direct excitation of an electron into the conduction band by absorption of a quantum of light is thought to be a forbidden transition, if the exciton level is very near to the conduction band most electrons which reach the exciton level will then be thermally excited into the conduction band. For lead azide it is therefore a reasonable assumption that absorption of a quantum of light excites an azide ion giving a conduction band electron and a positive hole. It is now assumed that whenever two positive holes are trapped at adjacent positions in the lattice reaction can then occur to give three molecules of nitrogen. The number of effective traps is taken as constant because an equilibrium rate of decomposition is soon reached and this implies that reaction of a trap releases it for further trapping. Let there be N traps of which n are empty, $n_1$ contains one positive hole and $n_2$ two. let the probability of trapping a positive hole be $P_+$ and of trapping a free electron (destroying a positive hole) be $P_-$.

In addition centres containing one and two positive holes may thermally dissociate, but if reaction takes place at cation vacancies which are deep traps this effect should be negligible. Finally $km_2$ is the decomposition rate to give gaseous nitrogen. At equilibrium, i.e. when the rate has fallen to $R_\infty$

$$\frac{dn}{dt} = km_2 + p_- n_1 - p_+ n = 0$$

$$\frac{dn_2}{dt} = p_+ n_1 - p_- n_2 - km_2 = 0$$

and as the number of traps remain constant $N = n + n_1 + n_2$. Now $p_+$ and $p_-$ are proportional to the intensity of irradiation, i.e. $p_+ = C_+ I$ and $p_- = C_- I$. Solution of these equations gives the following expression for the measured rate:

$$\text{Rate} = \frac{kC_+^2 N I}{\left[C_+^2 + C_-^2 + C_+ C_-\right] I + k\left[2C_+ + C_-\right]}$$

If now $$\left[C_+^2 + C_-^2 + C_+ C_-\right] I \ll \left[2C_+ + C_-\right] k$$

the rate will be proportional to I. $C_+$ and $C_-$ must be less than unity and are likely to be small as most of the electrons and positive holes will not be trapped before recombining. The lifetime of a cation vacancy containing two positive holes must be short in view of the low activation energy of the overall process so k must be large; therefore unless I is large the rate should be proportional to I. At very high intensities the rate should become independent of the intensity. Although the above mechanism utilises positive holes and conduction band electrons it does not necessarily demand a high photoconductivity, for the reacting positive holes are immobilised in deep traps and reaction produces many anion vacancies which are deep electron traps. The absorption bands associated with the resulting F centres undoubtedly give rise to the colour changes observed during decomposition. The blackening observed after further decomposition indicates that coalescence of n $Pb^{++}$ ions with 2n F-centres is taking place, the azide lattice is collapsing and particles of colloidal metallic lead are being produced.

Analysis of the initial stages of the decomposition curves, i.e. before the rate has become constant $R_\infty$, requires solution of the initial differential equations for non-equilibrium conditions. The following expression then results:

$$\frac{\text{Rate}}{k} = S\left\{1 - \exp.\tfrac{1}{2}\left[-(k + 2p_+ + 2p_-) - \sqrt{\ }\right]t\right\}$$

$$+ T \left\{ \exp.\tfrac{1}{2}\left[-(k + 2p_+ + 2p_-) + \sqrt{}\right]t - 1 \right\}$$

where $\sqrt{} = \sqrt{k^2 - 4\,p_+\,(k - p_-)}$

and $-S + T = -R_\infty$

i.e. an equation of the form.

$$\frac{R}{R_\infty} = S\left[1 - \exp.(-\alpha t)\right] + T\left[\exp.(-\beta t) - 1\right]$$

This equation is the sum of two exponential terms the first of which is zero at $t = 0$ and rises to a maximum $R_\infty^1$ when $t \to \infty$, and the second of which is zero at $t = 0$ and then falls to a minimum $R_\infty^{11} = -T$ when $T \to \infty$. It gives a very good qualitative representation of the experimental curve provided certain conditions, such as that both $\alpha$ and $\beta$ are positive, are satisfied. Further examination shows in general that these conditions are fulfilled.

A "dark rate" is logically predicted by the above theory. When the irradiation is stopped production of positive holes and free electrons will cease and a source of energy will be removed, but double positive holes trapped at cation vacancies will continue to decompose unimolecularly. Furthermore free positive holes and those released from shallow traps will continue to be trapped at cation vacancies and there decompose, this being a much slower bimolecular process. Combination with F-centres and conduction band electrons will also destroy positive holes and when all have been destroyed or immobilised singly the rate will become zero. From this it would be expected that on stopping the irradiation the decomposition rate would first fall very rapidly and then finally approach zero at a much slower rate, as found experimentally.

If irradiation is now restarted after a waiting period the initial rate should be low while the number of traps containing double positive holes builds up to its equilibrium value. This build up as found experimentally should however be more rapid than the build up that takes place on first irradiating a sample of the salt, for many of the cation vacancies will already contain a single positive hole. During the waiting period it is possible that in the absence of a large excess of positive holes, some of the cation vacancies might trap two anion vacancies produced during the irradiation, this giving effective destruction of the trap. This would explain the lower equilibrium reaction rate after a waiting period.

The activation energy values are very similar to those found for the photolysis of barium and potassium azides and the explanation is the same; the final reaction to give nitrogen can take place in two ways, either with zero activation energy, all the energy being supplied by the radiation, or with the addition of a thermal activation energy. These two result in the temperature dependence found. (This point is discussed in detail by Thomas and Tompkins).

As noted above the colour changes produced by the irradiation are due to the production of additional adsorption bands, probably F-bands, and the blackening is due to the production of metallic lead. In the thermal decomposition of barium azide the presence of nuclei of barium metal has the effect of greatly catalysing the decomposition and the same is true to a lesser degree in the thermal decomposition of α-lead azide. There is no experimental indication that this is so, for the photolysis of α-lead azide and no modification of the theory is thus needed.

## Electron Bombardment Decomposition of α-Lead Azide

### Experimental details

The apparatus was identical with that described above for the photolysis experiments except that the irradiation cell was replaced by a bombardment cell. This reaction cell was fundamentally a simple diode electronic valve in which the cathode and anode were supported in glass cones so that the whole cell could be easily dismantled.

The technique used was to place a weighed sample of the finely powdered azide on the anode and to flatten and smooth this to give complete coverage of the metal. After pumping overnight, a known A.C. potential was applied to the anode. The temperature of the directly heated cathode, which was a short length of electric light filament, was then adjusted to give the desired electron current and the rate of decomposition of the azide measured using the method described above for the photolysis experiments. The number of electrons reaching the anode in unit time was measured using a D.C. micro-ammeter (the reaction cell behaved as a half-wave rectifier) and kept constant by adjusting the cathode temperature. The earlier work of Grocock and Tompkins had shown that serious irregularities of behaviour were found if a D.C. potential was used, because of the build up and discharge of space-charges in the cell. It had also shown that it was experimentally impossible to work at very low potentials and that above 50 volts, variations in potential had little effect on the reaction rate. Therefore, so long as the conditions remained constant, there was little disadvantage in using an A.C. potential. All experiments were carried out at room temperature.

Experimentally it is difficult to get satisfactory results from the electron bombardment method. It is necessary to have an electrode system that allows insertion of the azide on the anode and gives sufficient cathode anode separation to ensure that the azide is not thermally effected by heat from the cathode. High voltages are undesirable because the electrons then have sufficient energy to produce multiple effects in the azide, making interpretation of the results more difficult. Consequently high electron currents giving easily measurable decomposition rates cannot be obtained. Electron space charges form about the relatively non-conducting azide layer covering the anode and produce further difficulties. Neutralisation of the space charges is aided by allowing the gas pressure to rise when positive ions are formed, but these in turn have their own complicating effects. The best compromise found was to use a cathode anode separation of 2.5 cms, a potential difference by 200 volts A.C. and a gas pressure of about $3 \times 10^{-3}$ mms. 15 mg. of azide was spread on the anode which was 1 sq.cm. in area.

## Results

### Decomposition at constant electron current

Fig.5 shows a typical decomposition curve at constant electron current and applied voltage. It is very similar to the curves found for sodium and barium azide by Crocecock and Tompkins. With lead azide however there was no recovery of rate after standing unbombarded under vacuum. In fact as in the photolysis work the rate

FIG. 5 — ELECTRON BOMBARDMENT OF α - LEAD AZIDE

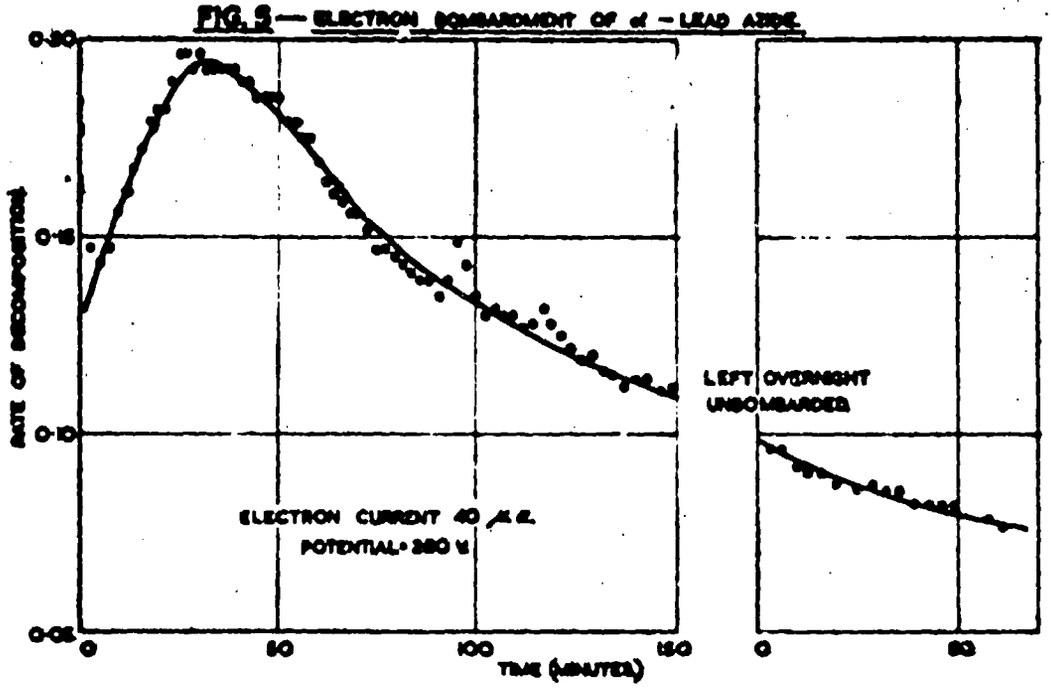

was lower on re-bombarding. Experimentally this meant that the sample of lead azide had to be changed after each run. With sodium and barium azides which "recovered" completely on standing it was possible to adopt the much more satisfactory procedure of doing a whole series of runs on the same sample. Electron bombardment of lead azide produced the same permanent colour changes as shown in the photolysis experiments.

**Thin azide layers**

Because of the quantitatively irreproducible results a different method of applying the azide to the anode was tried. A particularly fine sample of the azide was sieved into the top of a long glass tube and fell onto the anode at the bottom. Complete coverage was thus obtained with only 1 mg. of azide. The results were now markedly different from those obtained with the thicker layers. The shape of the decomposition curves at constant electron current showed an immediate evolution of gas which stayed constant for an hour or more (Fig.6). There followed a fairly sharp fall in rate and this was associated with a considerable fall in conductivity. At higher electron currents (50 to 80 $\mu$a) the region of

FIG. 6.—ELECTRON BOMBARDMENT OF THIN FILMS OF LEAD AZIDE.

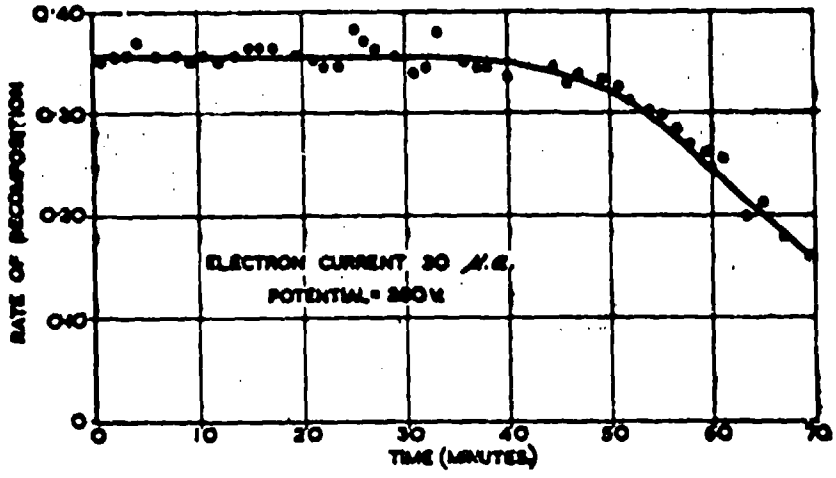


constant decomposition was comparatively short, the fall in rate occuring when relatively little of the azide had decomposed. With lower electron currents (10 to 20 $\mu$a) a much larger proportion of the azide could be decomposed before the fall in conductivity made the continuation of the run impossible.

With a 1 mg. sample of azide a few minutes bombardment caused darkening of a well defined but irregular shaped patch of the azide, the remainder staying white. As bombardment continued this patch darkened, the remainder of the surface still being unaffected.

With an azide sample of only 0.7 mg the whole of the azide surface rapidly discoloured on bombardment while with 1.5 mg there was no rapid discolouration, the whole of the surface darkening after an hour or more. The conductivity variations noted above were also affected by the layer thickness. The 1.5 mg samples showed the sudden fall in conductivity after 1 to 2 hours bombardment, but the 0.7 mg samples did not show this fall in rate and conductivity till after 10 to 20 hours bombardment, if at all.

Variation of decomposition rate with electron current

The effect of variations in the electron current on the rate was determined both by varying the electron current during a run and also by varying the current from run to run. Similar results were obtained and these resembled those found for sodium and barium azides, in that the rate was roughly proportional to the current at low electron currents and approached a maximum as the current increased (Fig.7). At low electron currents for these thin azide samples, the ratio of the number of azide radicals decomposed to the number of incident electrons was about 0.75; the energy of the electrons was probably about 280 ev. For the earlier work using thicker azide samples there was no long period of constant decomposition rate, but even the highest rates reached during the course of the runs corresponded to an electron yield value lower (0.3 to 0.75 ev) than that found for the thinner samples. These electron yields are of the same order as those found for sodium and barium azides.

FIG 7—RATE OF DECOMPOSITION OF A LEAD AZIDE AGAINST ELECTRON CURRENT

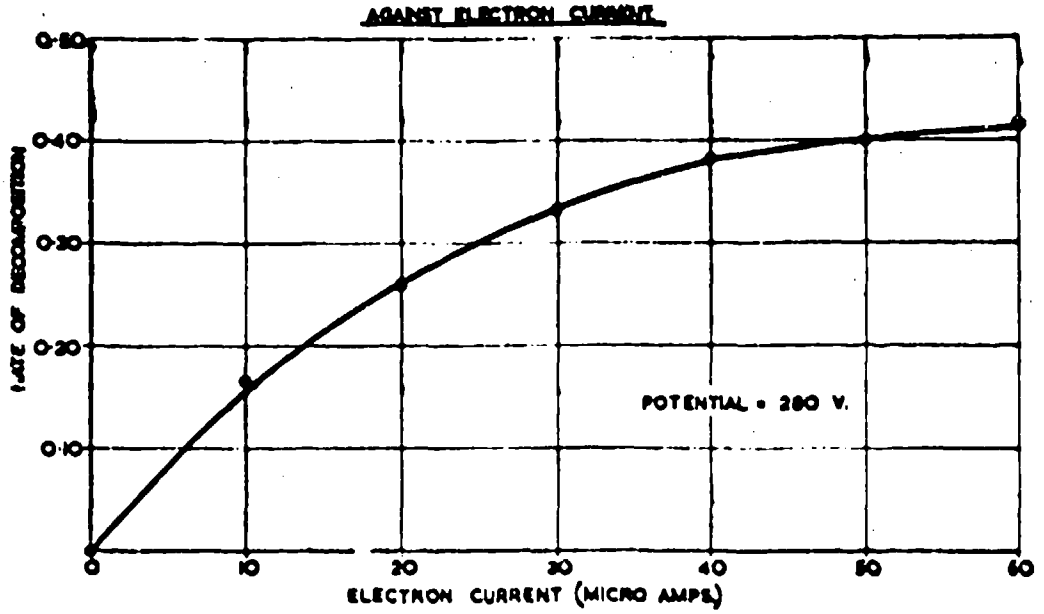

## Discussion of results

For the electron bombardment decomposition of α-lead azide the main experimental facts which must be explained are as follows:-

(i) At constant bombardment flux the rate of decomposition rises first to a maximum and then decays probably exponentially to a constant value.

(ii) There is an immediate colour change followed by blackening.

(iii) There is no "dark-rate" on stopping bombardment.

(iv) Re-bombardment after a waiting period shows no "recovery process"; the rate rises rapidly to a constant value which is lower than the final value of the previous bombardment.

(v) The variation of the rate with the electron flux is complex but appears to be the same as that for barium and sodium azides.

(vi) Finally the special phenomena associated with very thin azide layers need explanation.

Groocock and Tompkins (16) have discussed the electron bombardment decomposition of sodium and barium azides in terms of a theory which has several major differences from that applied by Thomas and Tompkins (14) to the photolysis results. It was thought unlikely that the electrons used, which had an energy roughly 50 times that of light of wavelength 2537Å, would produce excitons. Ample energy is available to give decomposition of single azide ions, but the very simple kinetics which would result from a mechanism of this kind do not accord with experiment. A further difference from the photolysis theory is that a mechanism depending upon a thermal activation energy is thought unlikely. Experimentally the absence of a "dark rate" indicates a different mechanism. They therefore postulated that decomposition occurs instantaneously without further activation energy when an azide ion adjacent to a surface hole is excited by an electron of the primary beam. Positive holes formed at a deeper level in the azide do not decompose to give nitrogen. The recovery in decomposition rate on re-bombardment after a waiting period is due to the regeneration in the bulk layer of azide ions from positive holes by the trapping of conduction electrons. A mathematical treatment based on these postulates gave quantitative agreement with the experimentally found curves for the rate of decomposition against time at constant electron current, for the variation of the rate with electron current and for the recovery in rate with time of standing.

The above arguments which were formulated for barium and sodium azides apply also to lead azide. While the lead azide results are not sufficiently reproducible to give the quantitative correspondence with the theory that the sodium and barium azide results gave, qualitatively the agreement is good. Two points need further explanation: the colour changes produced in lead azide, and the absence of a recovery process. The former, which are also produced by ultra-violet irradiation are readily explained. In all three azides large number of F-centres must be produced during bombardment and the absence of colour in barium and sodium azides, as suggested by Thomas and Tompkins is probably due to their F-bands being in the near ultra-violet rather than the visible part of the spectrum. The blackening of α-lead azide shows the presence of colloidal metallic lead produced by the reaction: $Pb^{++}$ + 2F-centres → Pb + 2 vacant anion sites, followed by collapse of the lattice. Experimentally however there is no indication that the electron bombardment decomposition (or the photolysis) is catalysed by metallic lead, nor do F-centres or metallic nuclei play any important part in the mechanism postulated by Crocoock and Tompkins. These special effects in α-lead azide do not therefore call for any important change in the mechanism. That there is no recovery process in α-lead azide implies that the regeneration of azide ions from positive holes does not take place in the absence of the electron beam probably because the conduction electrons are preferentially trapped at some other type of trap e.g. anion vacancies or metallic particles or possibly at a deeper level in the azide beyond the region where positive holes are formed.

The special effects found with very thin layers of α-lead are probably electrical rather than chemical in nature. The bombarding electrons penetrate into the solid and lose energy by collision with the lattice electrons, exciting these into the conduction band and leaving behind positive holes. Finally the electrons and positive holes will tend to be trapped at suitable lattice imperfections or to recombine and it is during these transitions that they may take part in chemical reactions. Under the conditions used for electron bombardment decomposition studies, there will be a potential gradient across the solid and consequently there will be a directional motion superimposed upon the random thermal motion of the conduction electrons and positive holes. As a result the trapping of the positive holes and electrons will tend to take place respectively near and far from the bombarded surface. It can be seen that when the above factors are considered together with the actual chemical reactions taking place in the decomposition the overall picture must be complex, but some explanation of the observed effects can be given in terms of the strong internal space-charges formed in the solid.

Thermal Decomposition of α-Lead Azide

A study is being made of the thermal decomposition of α-lead azide under vacuum. While this work is not yet complete it has already shown that the kinetics of the decomposition are more

complex than earlier workers believed. Experimentally the azide (c.1 mg.) contained in a platinum bucket is lowered under vacuum by means of a magnetic device into a furnace chamber maintained at the desired temperature (to $\pm$ 0.1°C) by an electric furnace. Decomposition rates are then measured by the method used for the photolysis experiments. The most fruitful work has been done on good crystals of pure α-lead azide, sieved to give particles of roughly constant size. Fig.6 shows the rate of decomposition of

FIG. 6—THERMAL DECOMPOSITION OF α-LEAD AZIDE.

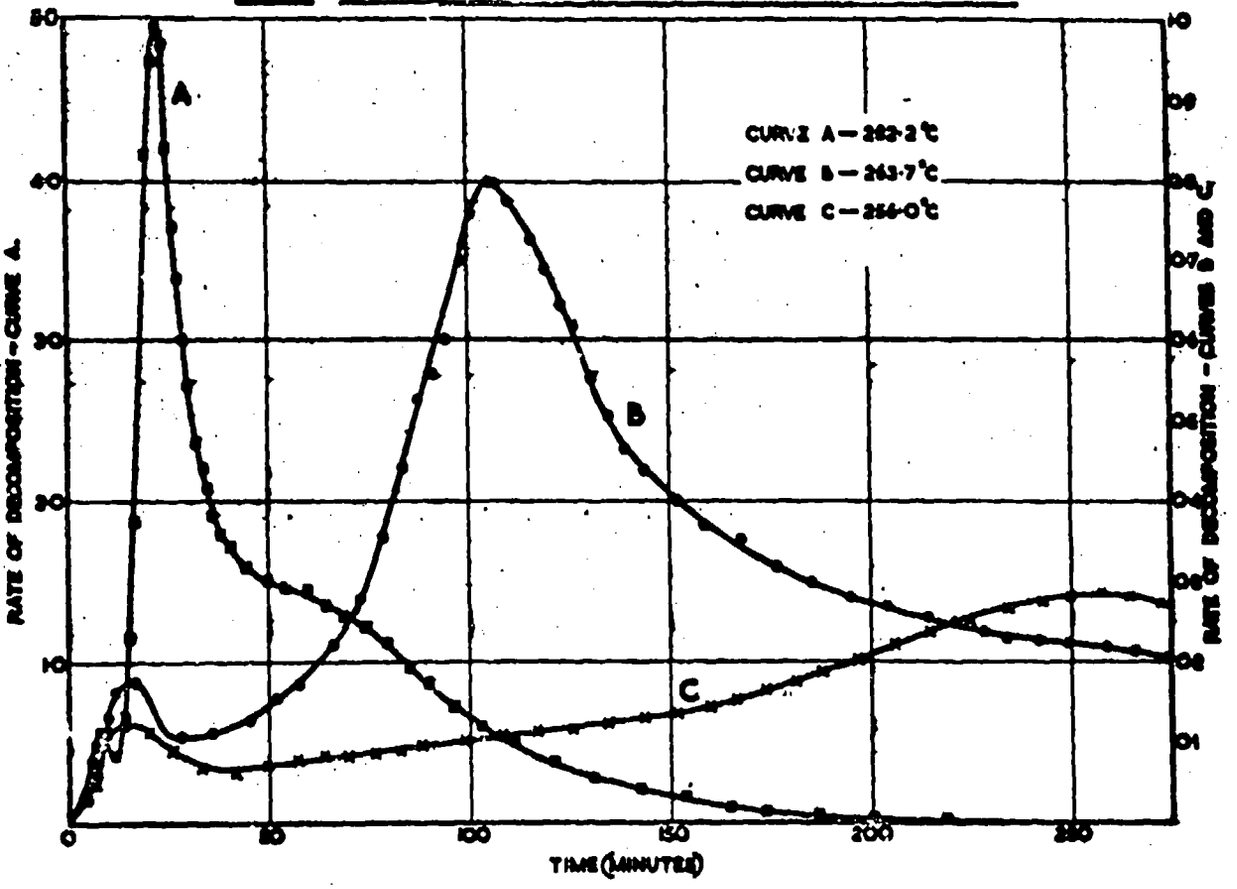


lead azide sieved between 150 and 200 mesh at temperatures of 256.0°C, 263.7°C and 282.2°C. Features to be noticed are the region in the lowest temperature curve, where the rate increases linearly and the very sharp peak in the highest temperature curve. The very rapid decay after the peak cannot be explained in terms of destruction of material or reduction of the area of the reaction interface. Work with other sieve fractions has shown that the height of this peak is proportional to the surface area of the crystals.

In the experiments being carried out at the higher temperatures above 300°C the azide is tipped under vacuum by a magnetic device onto a copper block heated in a furnace and the reaction rates prior

FIG. 9 — DETONATION OF β-LEAD AZIDE

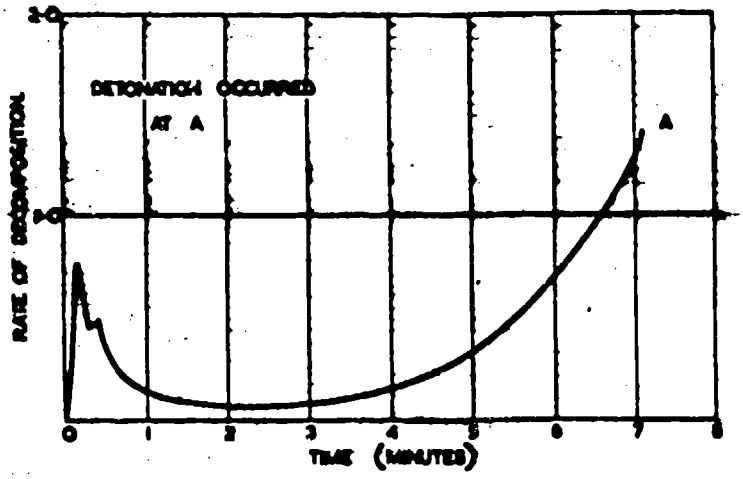


to detonation are recorded automatically. Using this system with small crystals, isothermal conditions are established very quickly and self-heating is minimised. Fig.9 shows a typical trace obtained from 2 mg. of crystalline β-lead azide (120 - 200 mesh) at 304.5°C. The initial peak is probably outgassing and detonation occurred at A on the curve.

Work on the thermal decomposition of lead azide is being continued and a more comprehensive report will be prepared later.

## Bibliography


1. Frenkel: Zeits. f. Physik. (1926) 35,652.
2. Wagner and Schottky: Z.Phys. Chem. B. (1930) 11,163.
3. Mott and Gurney: "Electronic Processes in Ionic Crystals". O.U.P. (1948)
4. Seitz: "Modern Theory of Solids" McGraw Hill (1940).
5. Gurney and Mott: Proc. Roy. Soc. A. (1938) 164,151.
6. Garner and Gomm: J.C.S. (1931) 2123.
7. Harvey - Trans. Far. Soc. (1933) 29,653.
8. Garner and Hoon: J.C.S. (1933) 1398.
9. Garner and Marke: J.C.S. (1936) 657.
10. Maggs: Trans. Far. Soc. (1939) 35,433
11. Garner and Maggs: Proc. Roy. Soc. A(1939) 172,299
12. Wischin: Proc. Roy. Soc. A (1939) 172,314.
13. Audubert and Roberts: J.Chem.Phys. (1946) 43,127.
14. Thomas and Tompkins: Proc.Roy.Soc. A. (1951) 209,550. (1951) 210,111.
15. Jacobs and Tompkins: Proc.Roy.Soc. A. (1952) 215,254,265.
16. Groocock and Tompkins: Proc.Roy.Soc. A. (1954) 223,267
17. Mott: Proc.Roy.Soc. A. (1939) 172,325.
18. Muller and Brous: J. Chem. Phys. (1933) 1,482


## Acknowledgments

Acknowledgment is made to the Chief Scientist, British Ministry of Supply, for permission to publish this paper for this symposium.

British Crown Copyright reserved. Reproduced with the permission of the Controller, H.B.M.S.O.

# THE DETONATION OF AZY AS BY LIGHT

J.S. Courtney-Pratt, B.E. Ph.D. and G.T. Rogers, M.A.
Research Laboratory for the Physics & Chemistry of Surfaces,
Department of Physical Chemistry,
Cambridge, England.

## Introduction.

It is well known that crystalline azides decompose slowly when irradiated with ultra violet light of normal intensity(1,2,3). The present work shows that if the intensity is raised sufficiently the detonation of silver azide can be initiated. Besides its intrinsic interest, this result provides a useful approach to a more fundamental study of the processes leading to stable detonation in these compounds.

In many experiments on initiation it is very difficult to obtain an estimate of the amount of energy actually received in the explosive since this often depends on a number of unknown factors. With initiation by light absorption this difficulty is largely overcome as the amount and initial distribution of energy within the crystal can be obtained from absorption spectrum and actinometric measurements. Further a light source which will both provide illumination and initiate explosion in what might be expected to be a reproducible manner, will be of considerable

advantage for high speed photographic studies of these reactions. Eggert[4] has investigated the initiation of nitrogen iodide by the light from a flash lamp. More recently Berchtold and Eggert[5] have initiated explosion in a variety of sensitive substances. They interpret their results as indicating a thermal mechanism. Work by Bowden et. al.[6] has shown that the initiation of explosion by friction and impact proceeds through the formation of a small thermally hot region. This work shows that the overall description of initiation by light is beyond reasonable doubt a thermal one. The absorbed light is degraded to heat forming a hot surface layer on the crystal. This layer is responsible for setting up the detonation.

Experimental

Silver azide has been used for all the experiments described in this paper. Pure and fairly perfect crystals of silver azide were prepared by crystallisation from an aqueous ammonia solution in the dark and irradiated with ultraviolet light of high intensity in the apparatus shown in Figure 1.

A crystal of silver azide is placed in the stainless steel spoon S mounted in the quartz cell C. The cell is evacuated. The crystal is irradiated with a high intensity flash from the krypton filled flash tube F of the shape shown in Figure 1. This design was employed to give the maximum useful efficiency. The flash tube has a quartz envelope and is filled with 18 cms. of pure krypton. A bank of condensers of 30 $\mu$ F which can be charged to any voltages V between 2.0 and 4.0 Kv is connected between the main

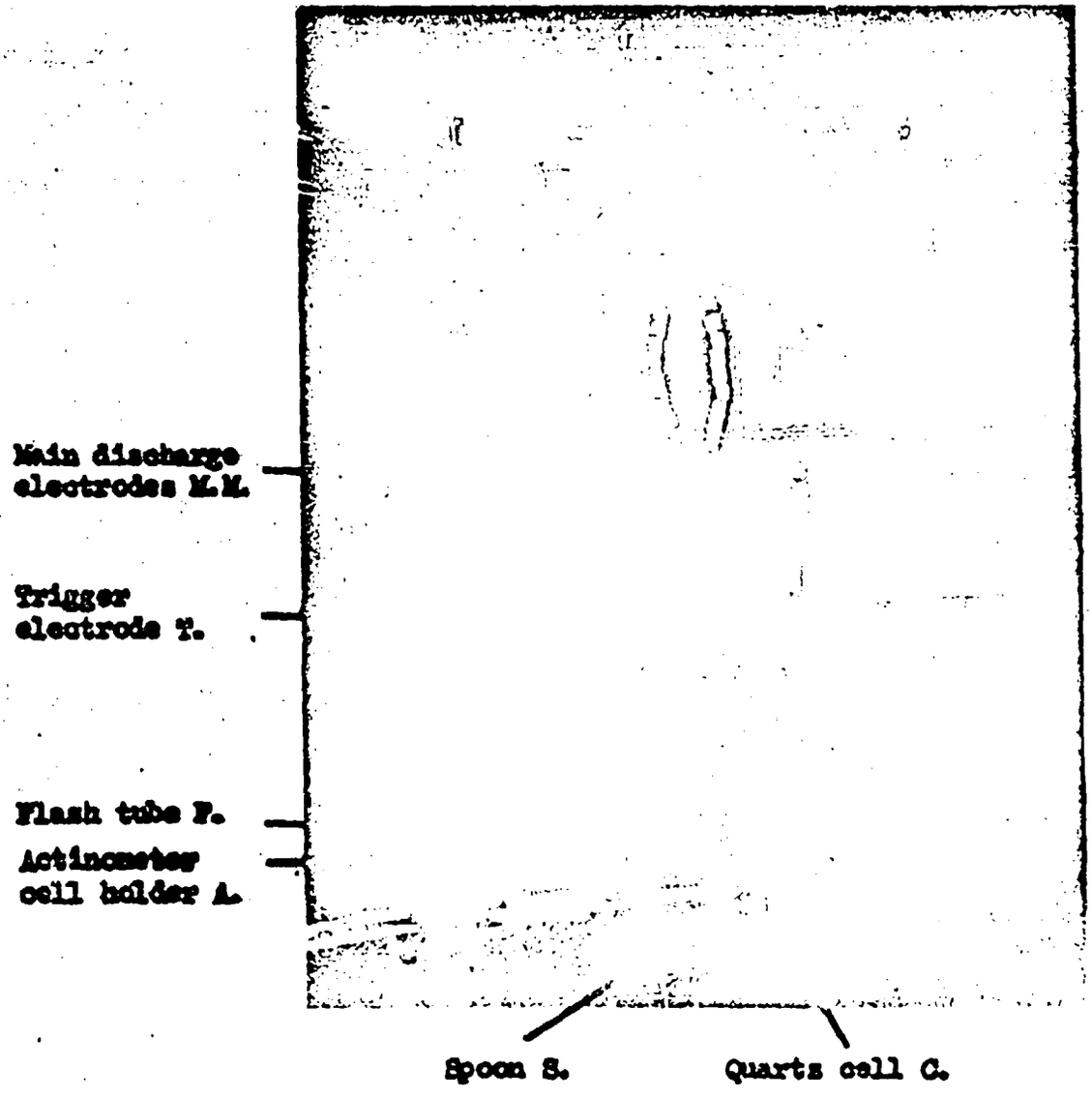


Figure 1. Apparatus for irradiating crystals of silver azide with high intensity ultra violet light. The crystal is placed on the spoon S in vacuum and is irradiated with light from the quarts flash tube F.



Unclassified

electrodes M. M. The lamp is fired by applying a high voltage trigger pulse to the third electrode T.

In all experiments the horizontal positioning of the spoon relative to the basal plane of the flash tube was unchanged. The vertical distance between the spoon and the basal plane of the lamp was adjusted to 1.0 ± 0.1 cm. for each experiment; this represents a variability of ± 5% in the light received on the spoon.

The perspex rod A holds a small liquid irradiation cell used for calibrating the photometer described in the next section.

Characteristics of the flash and measurement of the integrated absorption Q.

The intensity versus time curves for flashes at various voltages were measured using a photocell and cathode ray tube. A typical curve shown in Figure 2. These curves show that over the range in which the lamp is used the peak intensity increases with the voltage while the time integrated intensity is proportional to the square of the voltage. For flashes at greater than 2.5 Kv the duration* of the flash is sensibly constant at 61 ± 2 μ secs.

Results are expressed in terms of the integrated specific absorption Q defined as the total number of quanta per flash falling on one square millimetre of surface at the position of the crystal in the wavelength step 2000 - 3600 Å.

---

* The flash has a low intensity "tail" lasting some 40 μsec. As the integrated output of the tail is small the flash duration is taken as the time between the start of the initial rise and the point where the intensity has fallen to 1/10 peak intensity.

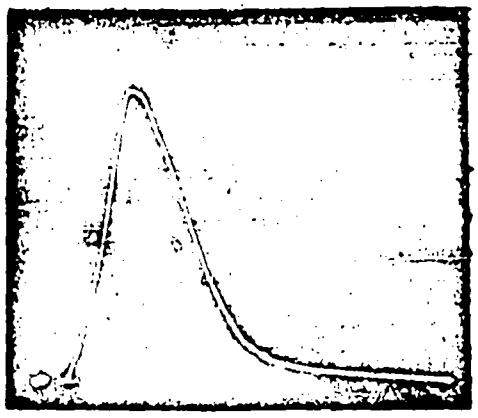

Figure 2. Light output versus time curve for a flash using 80 μ F capacity at 2.5 Kilovolts.

This quantity was measured for each flash using an integrating photoelectric photometer calibrated against the uranyl oxalate actinometer[7] an accuracy of ± 10% is possible for comparing results obtained in the same apparatus. Light losses due to reflection and scattering at the various quartz-air interfaces make less certain the absolute accuracy of Q but it is reliable within a factor of two.

The spectral distribution of the light from flash tubes with similar characteristics to the one used here has been investigated by Christie and Porter.[8]

The visible and ultraviolet absorption spectrum of silver azide was measured using a Unicam ultraviolet spectrophotometer. Transparent platelike crystals of about 0.06 mm thickness were prepared for these measurements.

Results.

Values of the absorption coefficient for thin plates of

silver azide are given in Table I.

TABLE I.

| wavelength in Å | absorption coefficient in $k.cm^{-1}$ |
|---|---|
| 4000 | 103 |
| 3800 | ??? |
| 3700 | 183 |
| 3600 | 920 |
| 3550 | $10^5$ |

These show that for the thicknesses of crystal used in these experiments all light of wavelength less than 3600 A entering a crystal would be completely absorbed. Below 2000 A quartz absorbs a large part of the radiation. The azide therefore absorbs energy in the same range as the uranyl oxalate. Q is then a measure of the total ultraviolet energy absorbed by the crystal. The crystalline azides absorb in the infra red(9,10). Quartz does not transmit wavelengths > 35,000 A so that any effects produced by infra red absorption must be confined to absorption at wavelengths shorter than this. The only band reported is at 29,000 A. With a water filter, which removes all radiation > 10,000, explosion was still obtained though absorption of the infrared does make a contribution to initiation. Experimentally it has been more convenient not to filter out the infrared in most cases.

When small crystals of silver azide were irradiated with single flashes such that Q progressively increased very little decomposition occurred until a critical value $Q_{crit}$ was reached when explosion occurred.

The value of $Q_{crit}$ does not depend on the mass of the crystal in the range 0.2 to 1.5 milligrams, the projected area of the crystal facing the lamp in the range 0.3 to 2.0 $mm^2$, or the area per unit mass. A sample of silver azide powder particle size ca $10^{-3}$ cms diameter had the same sensitivity as individual crystals.

TABLE II.

The critical integrated specific absorption for silver azide.

| Range of Q quanta/$mm^2$ | Number of experiments | Number of explosions | % explosions |
|---|---|---|---|
| $< 4.6 \times 10^{15}$ | 12 | 1 | 8 |
| $4.6$ to $4.8 \times 10^{15}$ | 9 | 2 | 22 |
| $4.8$ to $5.0 \times 10^{15}$ | 8 | 5 | 63 |
| $5.0$ to $5.2 \times 10^{15}$ | 6 | 4 | 67 |
| $> 5.2 \times 10^{15}$ | All explode | | 100 |

The results in Table II. show that the value of Q needed to give 50% probability of explosion lies between 4.8 and $5.2 \times 10^{15}$ quanta/$mm^2$ in the wavelength range 2000 - 3600 Å. The range of $Q_{crit}$ is probably much narrower than this since the two values of Q bounding $Q_{crit}$ differ by only 10% which is the same as the error in the measurement of Q. Because the effects of preirradiation on $Q_{crit}$ are not quite clear a fresh crystal was used for every determination. No appreciable amount of decomposition was ever detected when the crystal did not explode. However, if by chance a crystal was flashed at a value of Q very close to but below $Q_{crit}$, the crystal, which is always heavily darkened, usually broke up into a number of

quite large fragments. This effect is particularly striking if thin flat crystals are used when the pieces are seen to have straight sides generally at right angles to each other, and fit together exactly, on a microscopic scale, to reform the crystal.

Preirradiation with ultra violet light is known to modify the kinetics of subsequent thermal decomposition of solid azides. Preliminary experiments on the effects of preirradiation on Q suggest that if there is any increase in sensitivity it is small < 10%.

A preliminary study of the times involved in the photochemical initiation has been made. A two beam cathode ray oscillascope was used to record the light intensity time curve of the flash on one beam while the moment of explosion was detected on the other by the ion current flowing between the spoon S and a small ring electrode mounted ca 2 mm. above the azide crystal. The results indicate strongly that the moment of explosion is connected with the integrated light intensity rather than with the peak intensity.

Silver azide may be markedly sensitised to photochemically initiated explosion by colouring it with an adsorption indicator. Samples of powder coloured by precipitating 0.1 gms $AgN_3$ in the presence of 0.010 gms of erythrosin and excess silver ions had a value of $Q_{crit}$ $2.1 \times 10^{15}$ quanta/mm$^2$. Control experiments showed that this increase in sensitivity was due to the presence of the dye and not to adsorbed silver ions or the physical form of the precipitate. It must be remembered that Q refers only to light absorbed in the wavelength range 2000 - 3600 Å. Erythrosin dyed

silver azide also absorbs light in the region 3600 - 5500 Å so that if the coloured and normal azides are compared in terms of total energy absorbed at all wavelengths the sensitivity of the two may be identical. That the absorption of visible light makes a definite contribution is shown by the fact that erythrosin dyed azide may be detonated with the light from a medium sized photographic flash bulb while the largest flash bulbs do not even produce darkening of normal silver azide.

Discussion.

These results show clearly that the absorption of sufficient ultra violet light can initiate the explosion of silver azide.

Consider a square millimetre of the face of a silver azide crystal uniformily illuminated by a flash so that it explodes. The absorption coefficient is very high ca $10^3$ at 3600 Å so that the light is absorbed close to the surface. Although the light initially causes electronic excitation this energy is very rapidly degraded to heat and this will raise a surface layer to a high temperature which may be calculated in the normal way.

The energy equivalent to an integrated specific absorption of Q quanta $mm^{-2}$ in the range 2000 - 3600 Å is easily shown to be given by

$$\text{Total energy} = 7.0 \times 10^{-12} Q \text{ ergs/mm}^2$$
$$= 1.6 \times 10^{-19} Q \text{ cals/mm}^2$$

The absorption coefficient increases very rapidly with decreasing wavelength around 3600 Å Table I. Taking the absorption

coefficient as $10^4$ cm$^{-1}$ between 3600 Å and 3550 Å 95% of the incident radiation is absorbed in $3 \times 10^{-4}$ cms. The density of silver azide is 4.8 gm/cm$^3$ (11,12) and its specific heat 0.12 cals/grm.(13) The critical value of Q for explosion of pure silver azide is $5 \times 10^{15}$ quanta/mm$^2$, the energy absorbed from the flash $Q_{crit}$ is therefore $8 \times 10^{-4}$ cals/mm$^2$. If no energy losses from the surface layer occurred in the time of the light pulse or during the time taken for all the energy absorbed to be degraded to heat, whichever is the longer, this surface layer $3 \times 10^{-4}$ cms thick would be raised 480° i.e. to about 500°C by that amount of light energy. This is well above the ignition temperature of silver azide, 273°C(14) or 380°C(13).

Considering the surface layer as the explosion nucleus its volume and the amount of heat in it are proportional to the projected area. Since the results show that $Q_{crit}$ is independent of the projected area it seems likely that the thickness and temperature are the two important parameters determining the onset of explosion.

It has been shown(6) that the explosion nucleus must exceed a critical size before for it to result in explosion. This work suggests that the smallest dimension, here the thickness of the explosion nucleus, is a critical factor.

So far heat losses from the surface have been neglected. The main source of heat loss will probably be by conduction through the azide. The temperature of the surface layer will not be uniform throughout its thickness and, if heat losses are appreciable

during the flash duration this temperature distribution will also vary with time depending on the shape of the light intensity versus time curve of the flash tube. One advantage of this method of studying the initiation of explosion is that this variation of temperature with time and distance from the surface can be obtained explicitly from experimental data. At the present time not all the data has been obtained but an estimate of the order of magnitude of the heat losses can be obtained by considering the surface layer as at a uniform steady temperature of 500°C and calculating how much heat is lost through a square millimetre of surface in the duration of the flash which is 60 μsec. This shows that about $4 \times 10^{-5}$ cals is lost i.e. about 1/20 the energy input $Q_{crit}$ over the same area.

The absorption of ultra violet light produces initially electronic excitation; electrons being raised to exciton or conduction levels. Estimates of the life time of these excited states indicate that the time for the degradation of electronic excitation to heat is probably very short compared with the 60 μsec duration of the flash. Hence both photochemical and thermal decomposition will occur in this period at a high temperature. It is not possible to make any quantitative estimate of the amount of heat liberated under these conditions. We may expect it to be somewhat greater than the amount of heat lost but still small compared with the incident energy. The incident energy is then the critical factor.

Providing no appreciable decomposition occurs during the time of the flash the thickness of the surface layer and relative variation of temperature with distance perpendicular to the surface would depend only on the absorption coefficient, and would therefore be constant for a given wavelength range. The temperature at a given distance increases with increasing time integrated intensity unless the thermal conductivity were exceptionally high.

The rates of heat loss and generation will depend on the temperature so that the critical value of Q, table II required to produce explosion may reasonably be associated with a minimum temperature requirement.

Erythrosin alters the absorption spectrum and the nature of the surface of silver azide.

It is not possible to draw any fundamental conclusions from the results for coloured azide but the results are compatible with the proposed thermal mechanism and support Berchtold and Eggert[5] who also found that the more highly coloured compounds were the more sensitive.

In conclusion the results so far obtained indicate that the photochemical initiation of the explosion of silver azide involves the creation of a hot surface layer by the degradation of the energy of the absorbed light. For successful initiation a minimum thickness and temperature of the layer are required.

Bowden and Singh[15,16] have found a similar temperature thickness relation for thermally initiated explosion. The minimum thicknesses and temperatures found by them are of the same

order of magnitude as those deduced here.

The investigation provides further evidence that the setting up of an explosive reaction which will lead to detonation involves energy considerations on a scale which is very large measured on a molecular scale.

Acknowledgements.

We wish to express our thanks to Dr. F.P. Bowden for his interest in the work, to the Ramsay Memorial Fellowship for an award to one of us (G.T.R.), the Ministry of Supply (Air) for a grant to the Laboratory, and the Royal Society for a grant for equipment.

Unclassified

References.


1. Garner, W.E. and Maggs, J. Proc. Roy. Soc. A172, 299, (1939).

2. Thomas, J.G.N. and Tompkins, F.C. Proc. Roy. Soc. A209, 550, (1951).

3. Jacobs, P.W.M. and Tompkins, F.C. Proc. Roy. Soc. A215, 254, (1952).

4. Eggert, J. Fundamental Mechanisms of Photographic Sensitivity. Butterworth (1951) p.94.

5. Berchtold, J. and Eggert, J. Naturwissenschaften 40, 55, (1953).

6. Bowden, F.P. and Yoffe, A.D. The initiation and Growth of Explosions in liquids and solids. Cambridge Monographs on Physics (1952).

7. Leighton, W.G. and Forbes, G.S. J.A.C.S. 52, 3139, (1930).

8. Christie, M.I. and Porter, G. Proc. Roy. Soc. A212, 398 (1952).

9. Garner, W.E. and Gomm, A.S. J. Chem. Soc. 2123, (1931).

10. Delay, A., Duval, C and Lecomte, J. Bull. Soc. Chim. 12, 581, (1945).

11. Bassiere, M. Compt. Rend. 201, 735, (1935).

12. Hughes, E.W. Thesis Cornell University (1935).

13. Yuill, A.M. Thesis, Cambridge University (1954).

14. Taylor, C.A. and Rinkenback, W.H. J. Franklin Inst. 204, 369, (1927).

15. Bowden, F.P. and Singh, K. Nature 172, 378, (1953).

16. Bowden, F.P. and Singh, K. Proc. Roy. Soc. (to be published).

# DETONATION IN AZIDES WHEN THE DIMENSIONS ARE COMPARABLE WITH THE LENGTH OF THE REACTION ZONE

F.P. Bowden F.R.S. and A.C. McLaren
Research Laboratory for the Physics and Chemistry of Surfaces,
Department of Physical Chemistry,
Cambridge, England.

## Introduction.

We now have a good deal of evidence that the initiation of explosives by impact and by friction is generally thermal in origin. The mechanical energy of the blow or of rubbing is degraded into heat and concentrated to form a "hot spot". These hot spots are readily formed in two main ways: 1. By the adiabatic compression of small included gas bubbles. 2. By friction on the confined surfaces, on grit particles or on crystals of the explosive itself. Under very extreme conditions a sufficient temperature rise can be produced by viscous heating of the rapidly flowing explosive. For a general survey of this see Bowden and Yoffe (1).

More recently Dr. A.M. Yuill (2) has been investigating a new type of hot spot formed by the impact of a sharp point on a hard surface. The work done in plastically deforming a pointed metal striker causes its temperature to rise to a value of several hundred degrees. This temperature rise is proportional to the hardness of the striker and inversely proportional to the heat capacity of the metal. These hot spots caused by plastic deformation can initiate explosion. (See Figure 1.).

The actual value of the hot spot temperature necessary to initiate explosion varies but there is evidence that for a wide range of explosives it is in the vicinity of 400 - 500°C, when the duration is of the order of about $10^{-5}$ sec. There is also strong evidence that the hot spots must be much larger than molecular dimensions if they are to lead to explosion. Again the limiting size depends upon the explosive and upon its temperature but experiments show that the size may vary from $10^{-3}$ to $10^{-5}$ cms. in diameter.

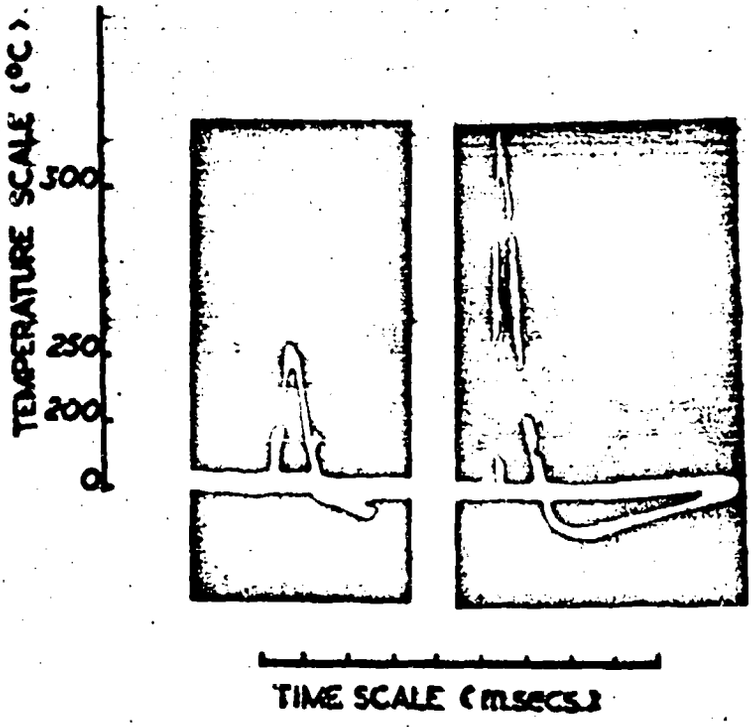


**Figure 1 :** Cathode ray oscilloscope traces of the high temperature pulses obtained with tungsten needle strikers on a steel anvil. The first trace, for a 1,100 g.cm. impact, gives a maximum temperature rise of 250°C and is not sufficient to initiate cyanuric triazide at 95°C. The second trace gives a peak temperature of 315°C, with a 3,300 g.cm. impact, an energy sufficient to cause 100% initiation.

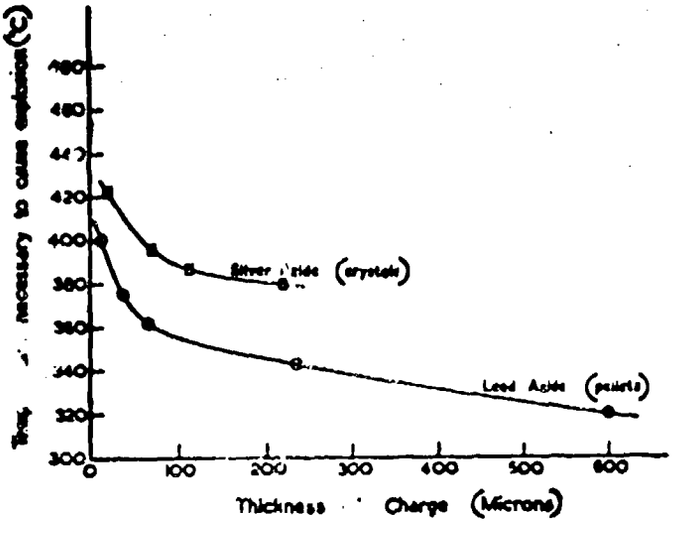


**Figure 2 :** Curves showing the increase in temperature necessary to cause explosion of thin charges of lead azide.

There is strong evidence that in most explosives, both liquid and solid, the reaction begins at the hot spot as a comparatively gentle burning which accelerates to a speed of a few hundred meters per second before passing over into a constant velocity detonation which may be of the order of 2 km/sec. Finally, if the conditions and dimensions of the charge are suitable it will accelerate to the normal high velocity detonation of about 5 to 7 km/sec. Under appropriate conditions the process may be considered as a four stage one:- (i) Initiation ——→ (ii) Burning which accelerates ——→ (iii) Low velocity detonation ——→ (iv) High velocity detonation.

The existence of the burning stage means that there may, in initiation by impact, friction or shock, be an appreciable time delay before detonation occurs. This can vary from a few to several hundred microseconds (3). It should be emphasised that the failure of an explosive to detonate is frequently due to a failure in this burning stage rather than to a failure in stage (i).

With simple metallic azides such as those of lead and silver, this burning stage, if it exists at all, is very short. With the more complex azides, such as cyanuric triazide, the burning stage is, however, observed. This is associated with the fact that in a complex molecule the decomposition can occur in more than one way. Experiments show that the products of decomposition during the burning stage are quite different from those obtained during detonation (4).

Size effects in the initiation and growth of an explosion.

The growth of a thermal explosion from a small nucleus is governed by simple physical considerations. A theoretical treatment of the factors involved in this simple thermal theory for gaseous systems was first given by van't Hoff (5) and has been re-examined by Frank-Kamenetzki (6), Rice (7) and also Dainton (8). It has been applied by Rideal and Robertson (9) to condensed high explosives and their calculations indicate that for hot spot temperatures of 400 - 500°C the minimum size is in the range mentioned above.

A series of experiments has been performed to study the effect of crystal size on the explosive decomposition of metallic azides. The thermal theory of explosion, outlined above, suggests that if we take crystals of smaller and smaller size and heat them at a fixed temperature we should find a size limit below which explosion does not occur.

The critical size appears to be determined by the smallest dimension of the crystal, its thickness if it has a plate-like structure. Experiments (10) with small crystals of lead and cadmium azide show, as we should expect, that the

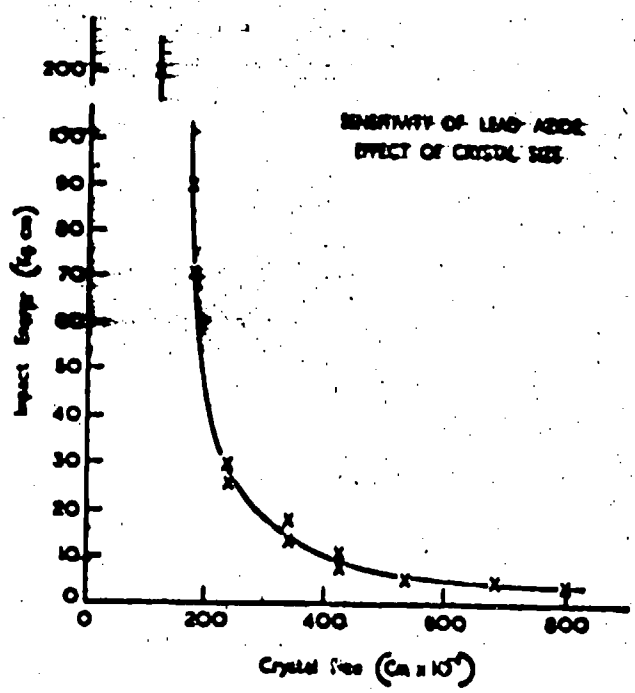


Figure 3 : Curves showing the increase in impact energy necessary to cause the explosion of very small crystals of lead azide.

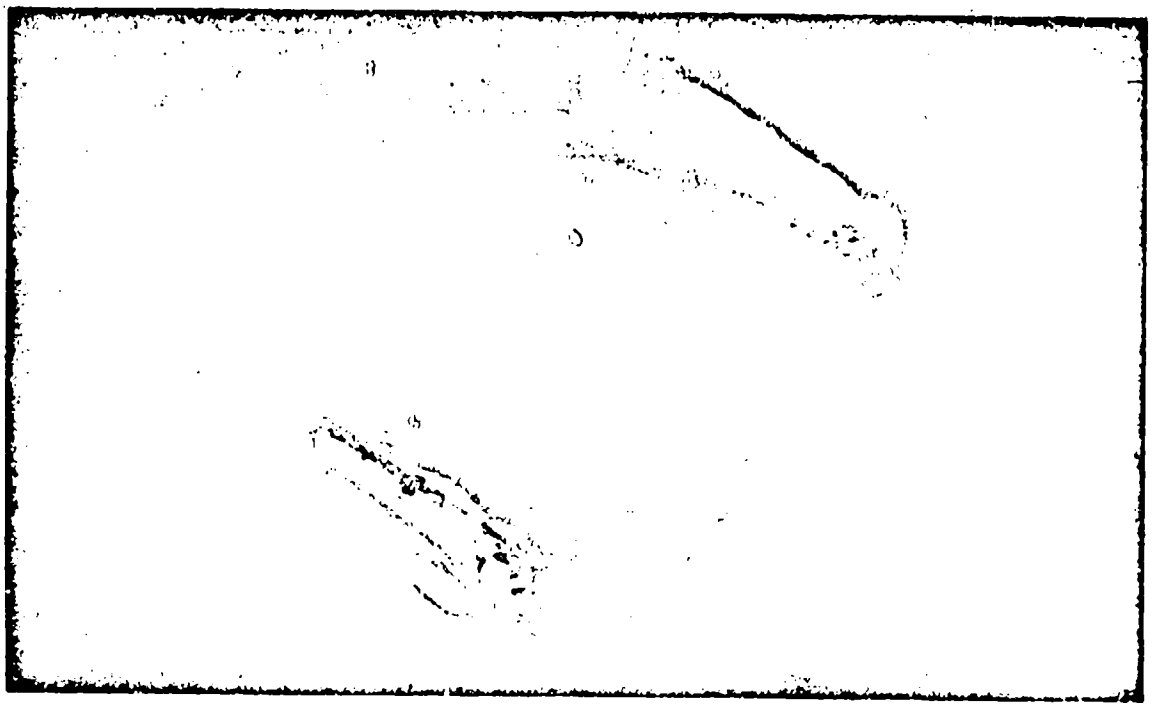

Figure 4. : A crystal of cadmium azide after heating at 317°C, showing the cracking and breaking up along crystallographic planes. X400.

critical size depends on the temperature and with cadmium azide, for example, it is about 24 microns at 320°C.

In a further series of experiments, thin compressed sheets of lead azide and single crystals of silver azide of thicknesses varying from 10 to 600 microns were placed on a mica hot plate in a small electrically heated oven, the temperature of which was indicated by a thermocouple. The results are shown in Figure 2, where it will be seen that as the thickness of the pellet is decreased the temperature necessary to cause explosion increases. If we extrapolate these results to a temperature of 500°C the critical thickness is about a micron which is of the same order of magnitude as the critical hot spot size for the same temperature, estimated by the earlier methods. It is interesting to note that this limiting size of a few microns is similar to the thickness of the "hot layer" obtained by Dr. Courtney-Pratt and Dr. Rogers in their recent experiments of the explosion of azides by light. (See paper in this symposium).

From similar considerations we may expect the impact sensitivity of a crystal to be dependent upon its size. Dr. A.M. Yuill (2) has recently investigated the effect of crystal size on the impact sensitivity of lead azide. His results are illustrated in Figure 3. It will be seen that the impact energy necessary to cause explosion increases as the size of the crystal is reduced in a manner similar to that observed when the crystals were heated. It should be noted that under impact, the crystals are crushed and flow plastically to form a pellet the thickness of which is about one-tenth to one-quarter that of the original crystal, suggesting that if the explosion starts at a late stage of the impact, the thickness may be the limiting factor.

Initiation of explosion with high speed particles. The effect of irradiating a number of sensitive explosive crystals (such as lead azide, silver azide, cadmium azide and nitrogen iodide and silver acetylide) with high speed particles has been studied by Bowden and Singh (10). They were subjected to irradiation by electrons, by neutrons, by fission products and by X-rays. All these substances were exploded by an intense electron stream but experiment showed that this is a thermal effect and is due to a bulk heating of the crystal. Nitrogen iodide is exploded by fission products but this substance is anomalous. With other substances interesting changes within the crystal are observed and these affect the subsequent thermal decomposition but no explosion results. The experiments show that, in general, the activation of a small group of adjacent molecules is not enough to cause explosion and support the view that the necessary "hot spot" size is large on a molecular scale (ca. $10^{-6}$ cms in diameter).

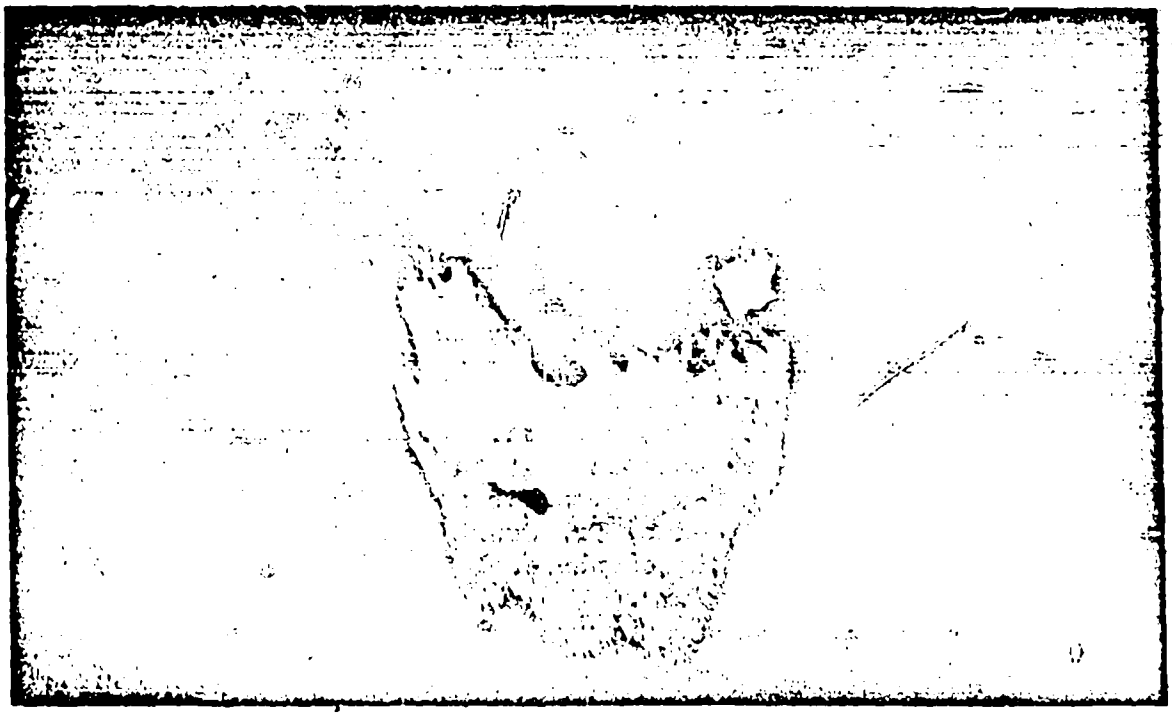

Figure 5 : Electron microscope picture (X50,000) of a partially decomposed lead azide crystal. The crystal is apparently breaking up into tiny blocklets about $10^{-5}$cm. across.

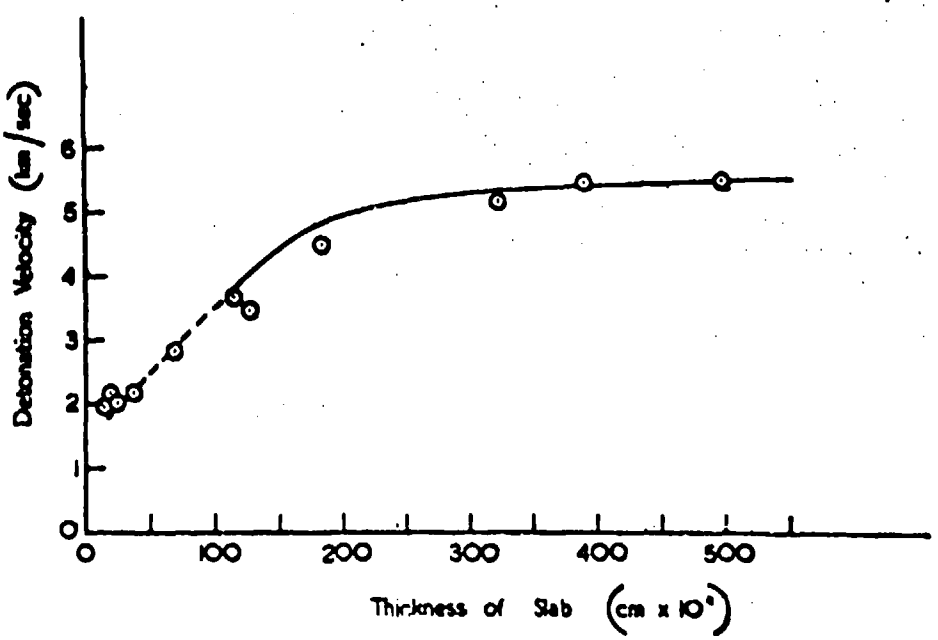


Figure 6 : The relation between the thickness of a sheet of lead azide and the detonation velocity. The continuous curve is the relation to be expected from the modified Jones' theory taking the length of the reaction zone as 75 microns.

Changes within the crystal. If the crystals are below the critical size or if larger crystals are heated at a lower temperature so that only thermal decomposition takes place, the crystals split and break up along crystallographic planes(10). This is illustrated in Figure 4, for cadmium azide. This suggests that the rate of decomposition may be a maximum along preferred directions within the crystal. The decomposition involves the formation of metallic nuclei and the evolution of gaseous nitrogen, accompanied by a large amount of heat, and this may easily lead to a splitting of the crystal. This splitting can occur with violence. The spreading of the defects and cracks through the crystal may play a part in the propagation process. It will also influence the rate of thermal decomposition by exposing a large amount of fresh surface. In addition to the development of cracks a darkening of the crystal takes place showing that nuclei are being formed within the crystal.

The electron micrograph (Figure 5) of a small partially decomposed crystal of lead azide is of particular interest. The photograph which is taken at high magnification (50,000) shows that during decomposition the crystal appears to break up into very small blocks about $10^{-5}$cms. across indicating that preferential decomposition occurs at the surface of these blocks. These may correspond to the elementary mosaic structure of the crystal. Since we would expect decomposition to occur preferentially at the crystal defects these elementary blocks may be more resistant to reaction and require a higher temperature to decompose them. These small crystal fragments can detach themselves from the parent crystal and quite frequently this happens with explosive violence. These flying fragments may play a part in propagating the explosion from crystal to crystal.

## Size effects in the detonation of azides.

We have, up till the present, been considering the influence of size on the initiation or the growth of explosion - that is on stages (i) and (ii). It is of interest to consider the influence of physical dimensions on the last stage of the explosion, that is on the stable detonation - stage (iv) - in azides.

The effect of charge diameter on the detonation velocity of a high explosive has been studied by a number of workers (e.g. Bichel, Mettegang, Dautriche, Kast, Hiscock, E. Jones, Paterson and Ford) and the results have been summarized by J. Taylor (11). The experiments have been almost exclusively concerned with high explosives such as TNT and complex nitroglycerine explosives, and in all cases the diameters were large (of the order of 1-20 cm) compared with the lengths of the reaction-zones. The estimated length of the reaction zone of finely powdered TNT is, for example, about 0.3 cm. and that of

liquid nitroglycerine is 0.04 cm. It was observed that the detonation velocity increased with the diameter of the explosive charge, approaching a maximum asymptotically. The results may be explained in terms of the hydrodynamic theory.

Little work seems to have been done with the initiating explosives and recently experiments have been made to analyse the effect of change of thickness on the detonation velocity of lead azide when pressed into thin sheets or slabs. The thickness of these was comparable with the length of the reaction zone and varied from about 20 to 500 microns. The sheets were 1.3 cm. long and 0.5 cm. wide and were made in a device which ensured that the density did not vary by more than a few percent from one sheet to another. The mean density of the sheets was 3.14 gm.cm$^{-3}$ compared with the crystal density of about 4.60 gm.cm$^{-3}$. "Pure" lead azide from a single batch was used throughout.

The detonation velocity was determined by means of a simple drum camera. A sheet of known thickness was placed at the end of a trail (about 2 cm long) of powdered lead azide on a glass plate over a slit, and the explosion initiated by means of an electrically heated wire in the powder. The results are plotted in Figure 6. It will be seen that for sheets of thickness of 400 microns and greater the detonation velocity is constant at approximately 5.5 km/sec, and decreases steadily to about 2 km/sec for a thickness of about 20 microns.

An attempt has been made to explain these results in terms of the expanding jet theory of J. Jones (12), itself an extension of the hydrodynamic theory, modified to apply to the present experimental conditions. The theory is based upon the fact that in solid explosives a certain lateral expansion of the decomposing materials will always take place with any practical degree of confinement. If this expansion within the reaction zone takes place before the reaction is complete, part of the explosive decomposes at a lower effective loading density, and hence, a lower detonation velocity than that which would occur if no lateral expansion took place, is to be expected. Jones' calculations were made for cylindrical charges where the constraint is symmetrical about the axis.

In our experiments, with very thin sheets of explosive, this was not the case since the width of the charge is so much greater than the thickness. We have assumed that the expansion is symmetrical in a vertical direction about the axis of the charge and that no lateral expansion takes place horizontally. We should thus expect the detonation velocity to decrease more slowly with decreasing thickness than in the case of a cylindrical charge where expansion in two dimensions will take place. The reaction is initiated at the shock-wave front and develops over a certain distance, X; - the reaction zone.

The theory provides an expression for the detonation velocity V, for any thickness of charge in terms of the maximum stable velocity $V_o$ and the ratio of the length of the reaction zone (X) to the thickness of the charge. From the thickness for which $V = V_o$ we can calculate X. We see from Figure 6 that for lead azide the critical thickness lies between 400 and 600 microns. This gives a value for X of approximately 75 microns. The theoretical relationship between the detonation velocity and the thickness of the charge is plotted (continuous curve) in Figure 6, where it may be compared with the experimental results. Fairly good agreement between experiment and theory is obtained over the range of thicknesses for which the theory is valid, i.e. for thicknesses greater than the length of the reaction zone. Below 100 microns the curve (dotted) joining the experimental points is a smooth continuation of the theoretical curve.

We may conclude, therefore, that the variation of detonation velocity with thickness of charge for azides is analogous , though on a very different scale, from that observed for high explosives and can be explained reasonably well in terms of the hydrodynamic theory. The calculated length of the reaction zone for lead azide is from these experiments approximately 75 microns.

## Influence of prior-heating on the detonation velocity.

Some experiments have also been carried out to investigate the effect of heating on the subsequent detonation of lead azide. Compressed sheets of the explosive were heated in an oven to a fixed temperature lying between 200° and 300°C. The heating was carried out for periods of five minutes or longer. The explosive was then allowed to cool and the detonation velocity determined. It was found that a comparatively gentle heating of the explosive could cause a marked diminution in the detonation velocity.

In a parallel series of experiments, the explosive was heated in vacuo under identical conditions and the pressure of gas evolved measured as a function of time; it was found that the decomposition was small. The mechanism of this retardation is not yet clear and further work is in progress.

## Acknowledgements.

We thank the Ministry of Supply (Air) for a grant to the Laboratory, and the Royal Society for a grant for apparatus.

## References

(1) Bowden, F.P. and Yoffe, A.D. (1952); Initiation and Growth of Explosion in Liquids and Solids (Cambridge Univ. Press).

(2) Yuill, A.M. Ph.D. Thesis, Cambridge. - See also (10).

(3) Bowden, F.P. and Gurton, O.A. (1949) Proc. Roy. Soc. A198, 337.

(4) Robertson, A.J.B. and Yoffe, A.D. (1948) Nature, 161, 806.

(5) van't Hoff, J.H. (1884) Etudes de Dynamique Chimique.

(6) Frank-Kamenetski, D.A. (1939) Acta Phys-Chim U.R.S.S. 10, 565.

(7) Rice, O.K. (1940) J. Phys. Chem. 8, 727.

(8) Dainton, F.S. (1942) Trans. Faraday Soc. 38, 227.

(9) Rideal, E.K. and Robertson, A.J.B. (1948) Proc. Roy. Soc. A195, 135.

(10) Bowden, F.P. and Singh, K. (1953) Nature, 173, 378.

(11) Taylor, J. (1952) Detonation in Condensed Explosives (Oxford University Press).

(12) Jones, H. (1947) Proc. Roy. Soc. A189, 415.

Elwyn Jones
Imperial Chemical Industries Limited,
Nobel Division,
Stevenston, Ayrshire, Scotland

When Mallard and Le Chatelier(1) first used a rotating-drum camera to study detonation in explosive gases, it was at once apparent that the luminosity of the phenomenon varied according to the chemical nature of the medium, being much brighter in some gases than in others. Such photographs normally show an initial bright line or "streak", coinciding with the passage of the "detonation-wave", and a residual glow which may be traversed by similar streaks representing the passage of "shock-waves"(2). The residual glow often shows striations, commonly attributed to mass movement of incandescent matter, and sometimes alternating bright and dark bands, supposed by some to indicate the helical progression of the "detonation head"(3). Thus, the luminous effects accompanying detonation in gases reflect the train of chemical and physical events occurring in the medium following the initiation of the explosive reaction.

The flames of condensed explosives appear to be equally complex and have attracted considerable attention, particularly where photography has been used in the development of "flameless" explosives for use in fiery coal mines. Three different kinds of flame have been noted in condensed explosives and, according to Lemaire(4), these represent three distinct chemical stages in the detonation process, namely, the fast "primary reaction", in which the condensed explosive is suddenly converted into gas at high temperature and pressure, the slower "secondary reactions" which take place among the products of the primary reaction and the "tertiary reaction" in which the hot secondary products combine with atmospheric oxygen. Thus, Lemaire attributes all detonation luminosity to chemical action.

On the other hand, Moraour(5) asserts that most, if not all, of the light accompanying detonation arises from the physical impact of the detonation-wave on the ambient medium, this type of luminosity being strikingly demonstrated in the "argon photographic flash"(6).

According to this view, the light emanates from sources entirely outside both the explosive and its detonation products, and so would appear to be only remotely connected with the chemistry of detonation. Thus, the two current views on this matter appear to be contradictory.

It will be seen from this short review that detonation flames make an interesting study and, if the sources of these transient luminosities can be identified, information may be obtained on the chemical and physical behaviour of matter under the influence of detonation-waves and shock-waves.

## Analysis of Detonation Flames

The flames from condensed explosives may be conveniently illustrated by means of photographs taken in the dark with an ordinary camera with its shutter open. With powerful explosive compounds, in contrast with weak explosive mixtures, a "still" photograph obtained in this way usually shows little more than an illuminated cloud. This is evident in the photographs of Will(7), Hiscock(8) and others, and is illustrated in Fig. 1, which was obtained with a small pellet of tetryl, $(NO_2)_3C_6H_2N(NO_2)CH_3$. Anything which may have happened in the immediate vicinity of the cartridge is obscured by this highly luminous cloud and the first task is to remove this obstacle.

One way in which this may be done is by reducing both the oxygen deficiency of the explosive and the size of the charge. The photograph reproduced in Fig. 2 shows simultaneously the position, size and shape of each flame relative to the cartridge and to each other for a particular explosive. Like Fig. 1, this is an ordinary still photograph, taken in the dark, of a small cylindrical cartridge, 1 in. long by 0.5 in. diameter, of granular explosive wrapped in cellophane and fired vertically downwards. In this case, however, the explosive used was pentaerythritol tetranitrate, $C(CH_2NO_3)_4$.

Reading from the cartridge outwards or, in other words, taking the flames in chronological order, we have first the "primary flame" which seems to fill the cartridge but keeps rigidly inside it, then the "secondary flame" characterised by luminous streamers issuing from the explosive and, finally, the "tertiary flame" which, in this instance, is somewhat attenuated and has risen just enough to let the primary and secondary flames be seen. The buoyancy of the detonation products and the appreciable delay before the cloud burst into flame are interesting to note.

Our identification of the three flames of detonation in condensed explosives is confirmed in Fig. 3 and 4, where the tertiary and secondary flames of nitroglycerine, $[C_3H_5(NO_3)_3]$ have been extinguished in that order by adding increasing proportions of inert matter, this being the traditional method of producing "flameless" explosives for use in coal mines(9). Here, the cartridges were much larger and the photographs illustrate the effect of cartridge size and shape on these flames. In conjunction with Fig. 1 and 2, these photographs show certain characteristics of high explosive flames which are very suggestive, namely:-

The primary flame takes its size, shape and even its texture from the unexploded material; it illuminates the stationary matter and goes out again before movement begins or, at least, before it becomes noticeable.

The secondary flame consists of luminous streamers which travel mainly in straight lines and diminish in width with increasing distance from the cartridge; the incandescent material behaves more like projected matter than an expanding gas.

The tertiary flame increases in size and intensity with increasing oxygen deficiency of the explosive, c.f. Fig. 1 and 2. It appears, therefore, that this flame represents the deflagration of a cloud of combustible residues and, further, that ignition occurs spontaneously after an appreciable delay in an upward-moving cloud which, until then, is invisible.

These inferences tend to support a chemical interpretation of the origin of detonation luminosity and, so far, give little evidence of shock-wave luminosity. Nevertheless, there are certain features of the primary and secondary flames which suggest that the explanation offered by Lemaire is not wholly acceptable. Moreover, the apparent absence of shock-wave luminosity is rather surprising in view of Muraour's experiments and it seems desirable to take a closer look at the primary and secondary flames.

Primary Flame

To study the primary flame, it is convenient to use a "streak" camera which provides a time scale whereby the speed and duration of the flame may be estimated. The photographs which we shall reproduce were obtained with a rotating-mirror camera capable of writing speeds up to 400 m. per sec., the optical system comprising two lenses with the conventional "slit" located between them. This arrangement is not recommended.

As illustrated in Fig. 5, the photograph of the primary flame takes the form of an inclined streak which plots its progress along the cartridge against a vertical time scale. The explosive cartridges

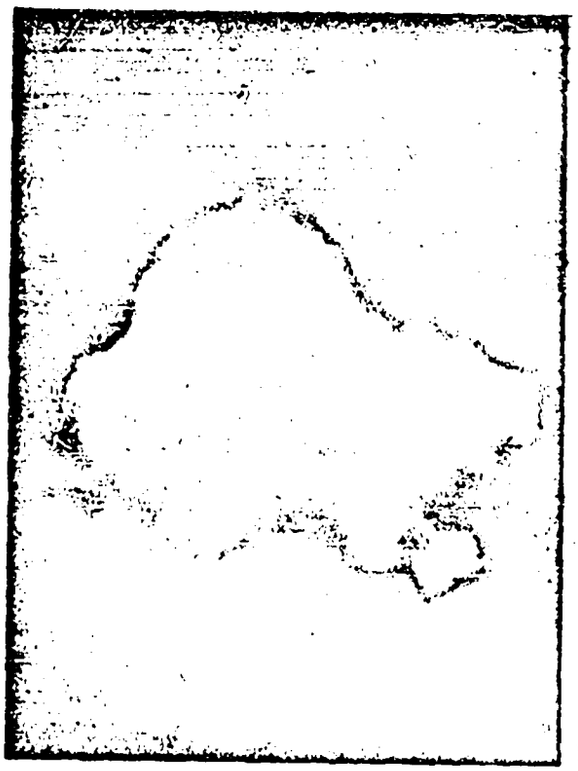

FIG. 1

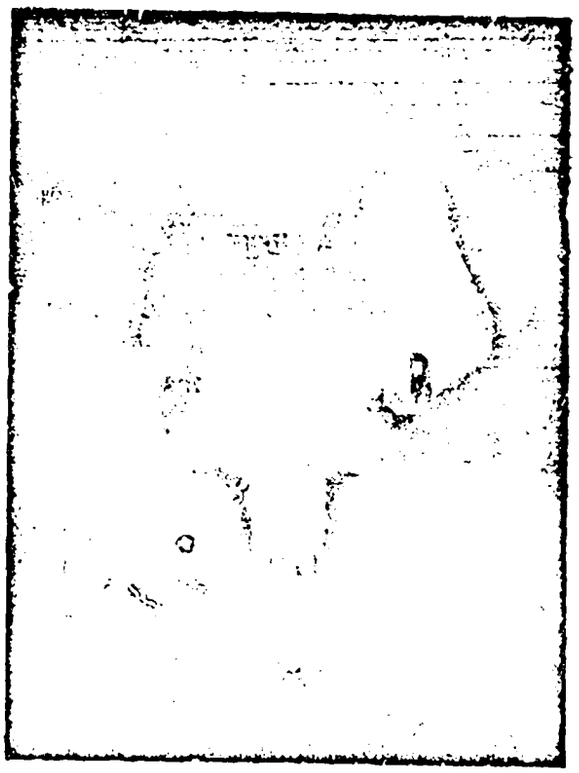

FIG. 2

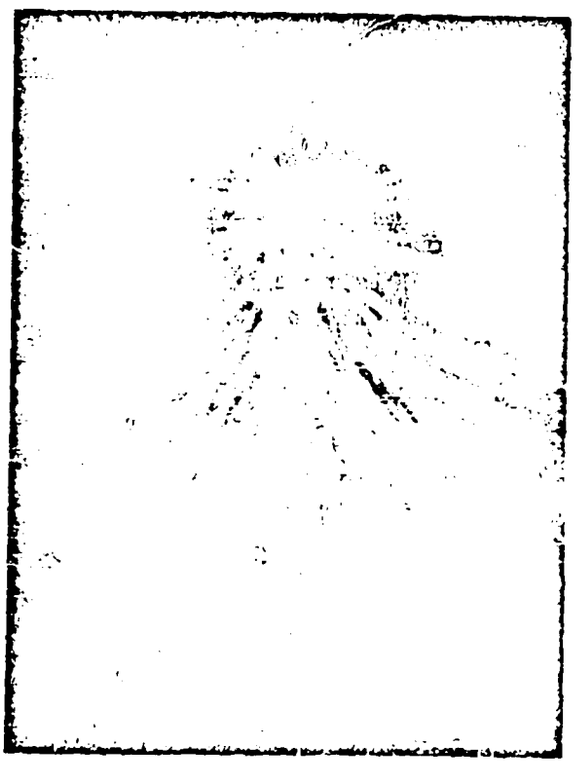

FIG. 3

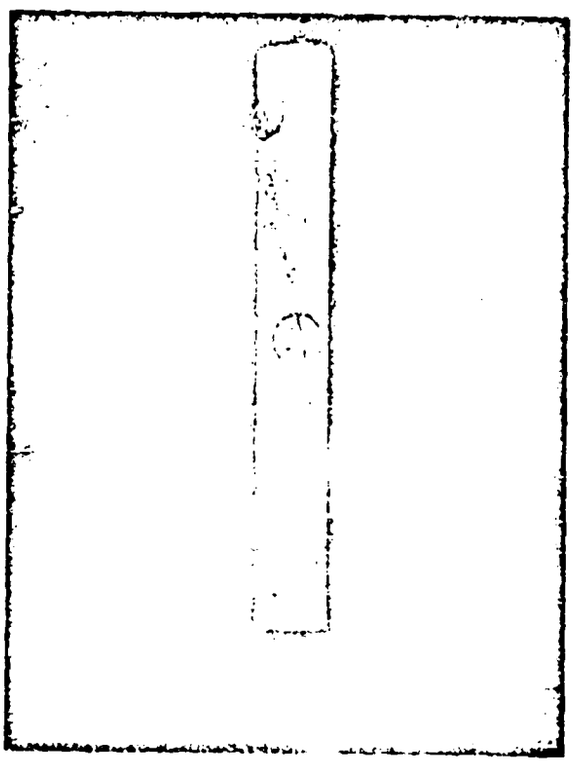

FIG. 4

were usually around 1¼ inch in diameter and up to a foot in length. In the present context, numerical details are unimportant because our analysis is qualitative rather than quantitative.

Fig. 5 was obtained with a cartridge of granular pentaerythritol tetranitrate, and it should be remarked that the lens aperture was adjusted to avoid recording the less luminous secondary flame. It would be incorrect, therefore, to assume that the absence of secondary and tertiary flames in detonation photographs signifies that none existed. On the contrary, Fig. 2 shows that even small charges of this explosive produce both secondary and tertiary flames. Although this point is often overlooked, this situation is inevitable because, even with a constant aperture, the apparent intensity of the light would still depend on other factors such as, for example, the speed of the flame. Comparison of luminous intensities should therefore be made with some caution, especially when one photograph is compared with another. On the other hand, since Fig. 2 and 5 both agree on this point, it seems reasonable to conclude that the primary flame in granular pentaerythritol tetranitrate is much more vivid than either the secondary or tertiary flames.

The most remarkable feature of this photograph, a feature common to all primary flame photographs, is the extremely short duration of the primary luminosity. Measurements of such photographs suggest that the emitters are active for probably less than one microsecond. They seem to appear abruptly and to disappear with the same abruptness, which suggests that they may be atoms or free radicals, their brief period of activity being a measure of their limited life.

The photograph reproduced in Fig. 6 was obtained with the same explosive as before, but on this occasion half of the cartridge was infused with argon and the other half with butane. Where the intergranular spaces were filled with the monatomic gas argon, the primary flame is much more luminous than where the interstices were filled with the complex gas butane. This leads to two interesting inferences, namely, that the emitters are probably atoms and that they derive, at least partly, from the interstitial gas.

The latter inference is borne out by the remarkable fact that pure explosive compounds in the form of cast or highly compressed pellets give surprisingly little primary luminosity, the same being true of liquid and gelatinous explosives. A striking demonstration of this fact is given by Taylor(10) who reproduces a streak photograph of a composite charge made up of alternate layers of a high density explosive and an inert salt. In these circumstances, the primary luminosity is very intense in the granular salt, but is hardly visible in the explosive. Moreover, in mixtures of nitroglycerine and common salt, the intensity of the primary flame seems to increase with decreasing proportion of nitroglycerine. In other words, the presence of chemically inert matter tends to intensify the primary flame.

These apparently irrational facts admit of a very simple explanation, namely, that the initial products of detonation possess kinetic energy rather than heat. It may be recalled that Berthelot's(11) theory of detonation implies that the energy released in an explosive reaction appears first as kinetic energy of the newly-created molecules and that the fundamental difference between deflagration and detonation resides in the fact that the motion of the molecules is random in the former case, but unidirectional in the latter. It follows from this that collisions occur immediately in deflagration and similar slow reactions, giving the spontaneous effect of heat, but, because the molecules are travelling in the same direction in detonation, collisions are fewer and less energetic with the result that there is little heat as ordinarily understood. To produce collisions, the molecules must encounter resistance.

This inference suggests that confinement should increase the luminosity of the primary flame and Fig. 7 demonstrates the effect of removing the cellophane wrapper from part of an explosive cartridge, the brighter portion corresponding to the wrapped explosive. As Bowden(12) and his collaborators have shown, thin films of explosive caught between impacting surfaces give out a surprising amount of light. Again, if a high density explosive is fired in a vacuum and an obstacle is placed in the way of the expanding products, the sudden conversion of their kinetic energy into "heat" produces a brilliance far transcending the light from the primary flame. As a vacuum can neither support a shock-wave nor emit light, this incandescence must occur in the products of detonation. Ratner(13) seeks to explain this effect, which is also apparent in air, by assuming that the outer skin of explosive escapes decomposition in the primary flame but is overtaken at an obstacle. Even this explanation associates the light with the explosive rather than the ambient medium.

Thus the evidence suggests that the energy released in the primary reaction is contained in the products largely in the form of kinetic energy in the direction of propagation and that any resistance they meet causes kinetic energy to be converted into the equivalent of heat and so leads to incandescence. If the resistance is offered by a gas, incandescence may be induced in the gas, provided not too much energy is absorbed in its chemical dissociation.

Shock-wave Luminosity

The reality of shock-wave luminosity is demonstrated in a very convincing manner by Muracur(14) who produced incandescence at the meeting point of two non-luminous shock-waves. It may be deduced from this experiment that before a shock-wave can become self-luminous, it would have to travel at a speed approximating to the relative velocity of Muracur's shock-waves, which would suggest a figure of the order of 5 km. per sec.

It has been demonstrated(15), however, that when an explosive is fired in or into the air, the shock-wave does not separate from the expanding products until the speed of the combined disturbance has fallen to about 2 km. per sec., at which speed the shock-wave is quite definitely non-luminous. It appears, therefore, that shock-wave luminosity is likely to appear only with high velocity explosives and, when it does appear, it will be difficult to distinguish it from product luminosity or, in other words, Lemaire's secondary flame.

It has been said already that the primary flame is rather feeble in a homogeneous explosive so that this type of explosive might be very suitable for studying shock-wave luminosity. By directing the disturbance from the end of such a cartridge into a close-fitting tube, lateral expansion is prevented and the high velocity is maintained over greater distances. Moreover, lateral losses being small, the "wave" may be expected to assume a plane front so that, by viewing it from the side, some idea of the depth of the luminous zone may be obtained. This technique was used by Laffitte(16) but, being handicapped by the low resolving power of his camera, he was unable to disclose the fine structure of the "wave". We therefore reproduce in Fig. 8 a high-speed camera photograph of the luminous effects produced in an air-filled tube on firing a charge of compressed pentaerythritol tetranitrate at one end. Fig. 9 shows the same shot fired into argon but with a considerably reduced aperture. Except for the fact that the disturbance is very much more luminous in argon than in air, the two photographs are almost identical. It may be added that, on replacing the air by butane, the luminosity is markedly decreased.

These results agree with those of other observers and confirm that the luminosity of the disturbance varies according to the nature of the surrounding gas, but whether the ambient medium contributes to the emission or interferes with it is open to question. It is well-known that the secondary flame can be suppressed by firing the explosive in an atmosphere of butane or some other complex organic vapour and it seems likely in this case that the kinetic energy is absorbed in dissociating the vapour. In other words, if the chemical energy of the explosive can be given out as kinetic energy of the products, it is equally possible for the kinetic energy of the products to be absorbed in the chemical dissociation of the medium. Moreover, if the emitters are atoms, the difficulty of producing luminosity in complex organic vapours is explained.

On this view, the heavy monatomic gas, argon, is a major contributor to this type of luminosity but, since action and reaction are equal but opposite, the product molecules involved in these collisions are also liable to be dissociated and contribute to the luminosity, as they do on striking a rigid obstacle. Thus, the difficulty in separating shock-wave luminosity from product luminosity still persists.

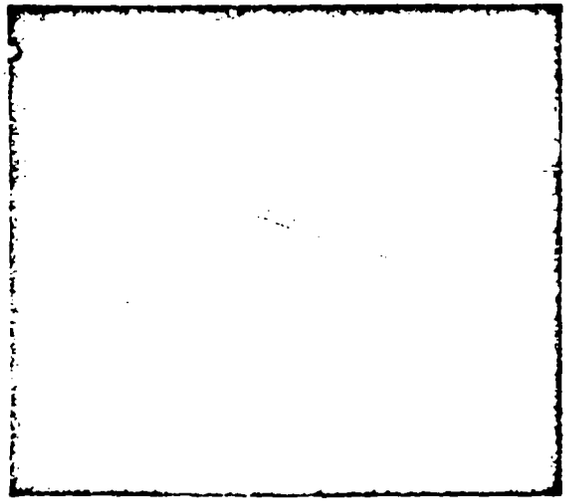

FIG. 5

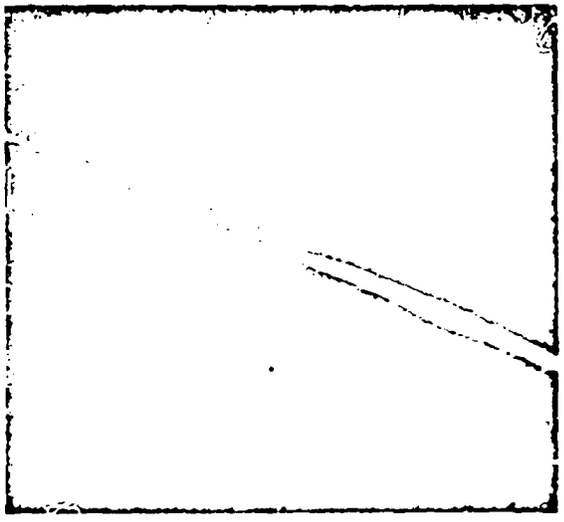

FIG. 6

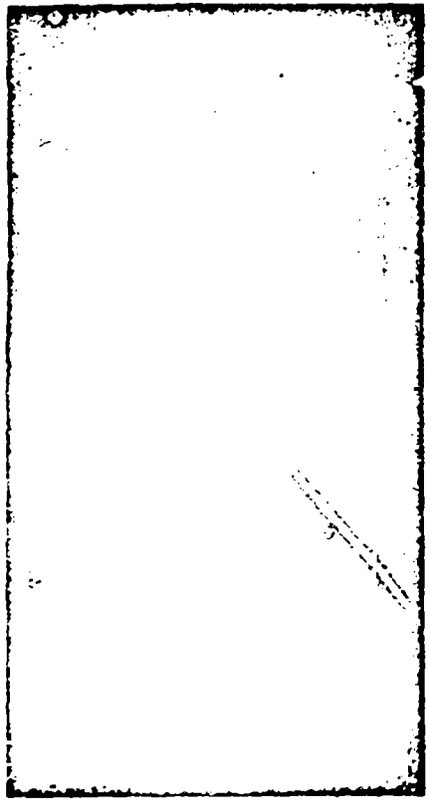

FIG. 7

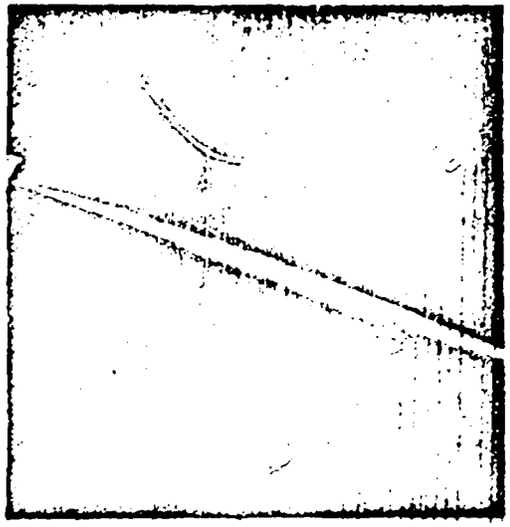

FIG. 8

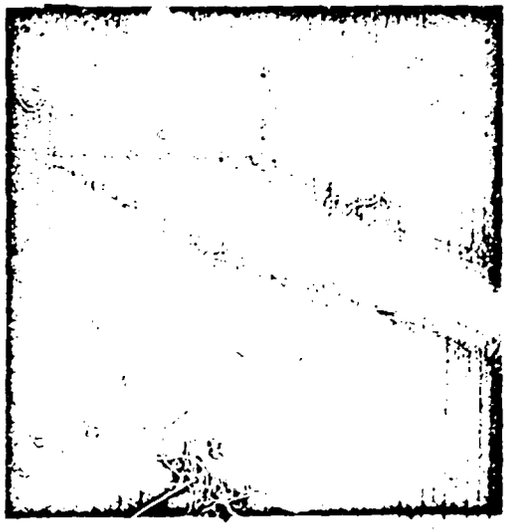

FIG. 9

460

James

On examining the detailed structure of the two photographs, it will be seen that the evidence is consistent with this mechanism of light emission. The products of detonation are relatively non-luminous to begin with and their first encounter with the ambient medium is at a surface. This surface approximates to a plane which is viewed from the side and so appears, at first, very thin. As the products advance into the gas, the collision zone increases in depth according to the time and space required for the alien particles to accommodate themselves to the movement of the medium they have entered. Once they fall into step, order is restored and the luminosity ceases.

Secondary Flame

It appears from the foregoing that the distinction is difficult to draw between shock-wave luminosity and product luminosity due to collision, both of which may be regarded as representing the type of luminosity which Muraour describes. This part of the secondary flame arises from physical causes, but, if emission is due to atoms, their presence is indicative of chemical change. The chemical changes which may be initiated depend on the nature of the explosive and here it is necessary to distinguish between explosive compounds and explosive mixtures. Most military high explosives are substantially pure chemicals but commercial explosives are often heterogeneous mixtures of different explosives, with or without inert diluents. In this way, the characteristics of an explosive are adapted to the purpose for which it is intended. Coal mining explosives, in particular, contain flame-suppressing ingredients so that it would be wrong to judge all explosives by the amount of flame produced by these explosives. By the same token, photographic techniques, like flashlight and Schlieren photography, which are effective only with substantially flameless explosives, are open to the same criticism. On the other hand, military high explosives, which by virtue of their high rates of detonation exaggerate the importance of shock-wave luminosity, present an equally one-sided picture of high explosive flame. To obtain a comprehensive view, due regard should be given to both types of explosive, but they should be considered spearately.

Fig. 3 is typical of the kind of photograph obtained with some of the British coal mining explosives in present use, and it is worth noting that the shock-wave velocity in this case is too low to produce luminosity due to collision. Nevertheless, the secondary flame is still in evidence and the origin of this luminosity must be sought in the explosive itself. Besides nitroglycerine, these explosives contain such combinations as ammonium nitrate and woodmeal which react much slower than nitroglycerine. It is understandable, therefore, that anyone working with this class of explosive should attribute the secondary luminosity to chemical reactions initiated by the primary detonation reaction.

It will be apparent that the picture of the detonation process presented here differs from that normally assumed for theoretical purposes, but it is felt that any theory which ignores the activation energy of the reaction, and so fails to take cognisance of the sensitivity factor, can not be complete. The emphasis here is on the energy absorbed in the dissociation of the explosive molecule and, indeed, of any unstable complex molecule which may become entrained in a high velocity shock-wave.

The author is indebted to Messrs. T.A. Brown and L.G. Cumming for supplying the photographs from which the accompanying illustrations were selected.

## REFERENCES


1. Mallard, E. and Le Chatelier, H.L. Ann. Mines, Ser. 8; 4, 296, 1883
2. Dixon, H.B. Phil. Trans., A, 184, 97, 1893
3. Campbell, C. and Finch, A.C. J. Chem. Soc., 8, 2094, 1928
4. Lemaire, E. Ann. Mines. de Belg., 19, 37, 1914
5. Muraour, H. and Michel-Levy, A. Mem. des Poudres, 26, 171, 1934-5
6. Grimshaw, H.C. and Hardy, V.O. Safety in Mines Res. Est. Rept. No. 32, 1951
7. Will, W. Schiess-und Spreng., 323, 343, 1909
8. Hiscock, W.G. Iron and Coal Trades Rev., 1, 18, 1924
9. Marshall, A. "Explosives", London, 1915
10. Taylor, J. "Detonation in Condensed Explosives", Oxford, 1952
11. Berthelot, M. Compt. rend. 94, 149, 1882; 96, 672, 1883
12. Bowden, F.P., and Yoffe, A.D. "Initiation and Growth of Explosion in Liquids and Solids", Cambridge 1952
13. Ratner, S.B. J. Tech. Phys. USSR, 20, 1422, 1951
14. Muraour, H. Compt. rend. 198, 1499, 1934
15. Laffitte, P. and Patry, M. Compt. rend., 191, 1335, 1930
    Payman, W. and Woodhead, D.W. Proc. Roy. Soc., A. 163, 575 1937
16. Laffitte, P. Ann. de Phys. 4, 587, 1925

# THE ROLE OF GAS POCKETS IN THE PROPAGATION OF LOW VELOCITY DETONATION

30

Owen A.J. Gurton
I.C.I. (Nobel Division)
Stevenston
Ayrshire, Scotland.

For many years it has been known that nitroglycerine and explosives based on nitroglycerine detonate at either of two velocities. If the explosive receives a heavy shock from a priming charge it will detonate at a rate approaching the maximum or hydrodynamic velocity, but if it receives a weaker shock (such as the blow from a detonator) it may detonate at a much slower rate. Thus, nitroglycerine may detonate at about 8,000 m. per sec., or at about 1,000 to 2,000 m. per sec. High velocity detonation of liquid nitroglycerine is very constant in character. The detonation front seems to advance at a steady rate through the explosive and the detonation velocity does not vary from experiment to experiment. This is not true of low velocity detonation which does not propagate with a very steady front, in the pure liquid(1).

However, nitroglycerine is not usually used commercially in a pure condition, but is mixed with other materials which remove its obvious fluid properties. The simplest admixture, and the one which leads to the least change in thermochemical properties, is the addition of small quantities of nitrocellulose. H.C. Clapham 1930 showed that this addition had a profound effect on the ease with which low velocity detonation would propagate. He showed that if nitrocotton was allowed to gel in nitroglycerine without stirring, the resultant mixture would detonate at high velocity if adequately primed, but either failed to detonate or gave rise to a very low velocity propagation if an attempt was made to set up normal low velocity detonation. When one of these gels was aerated by stirring, the propagation of low velocity detonation in liquid nitroglycerine again became possible. In fact, low velocity detonation in liquid nitroglycerine is much less steady than low velocity detonation in an aerated gel(1). Thus, the aeration of an explosive gelatine was in some way related to the ease with which low velocity detonation would propagate in it.

The phenomenon of dual velocity of detonation has been

observed not only in other liquid explosives(2), but also in granular solid explosives including T.N.T. and tetryl(3). To achieve a steady low velocity detonation in solid explosives two requirements had to be met. Firstly, the grain size of the explosive had to be moderately coarse, and secondly, the cartridge density had to be fairly low, (about 1 g. per c.c.). In other words, the explosive had to contain gas pockets.

Bowden, Mulcahy, Vines and Yoffe(4), showed that the inclusion of small bubbles of air in nitroglycerine and in other liquid explosives increased their sensitivities to initiation by impact. The reason for the high sensitivity of the aerated liquid was traced to the high temperatures which were attained in the gas pockets when they were suddenly compressed. Yoffe(5) replaced the air by other gases and vapours and also by gases at higher pressure. He showed that as the ratio of the specific heats of the gases increased, the sensitivity of the explosive appeared to increase, but that as the pressure of gas increased the sensitivity decreased. This second effect was observed in solid explosives as well as liquids.

Ratner(6), calculated the temperature to which the shock wave accompanying detonation would raise liquids like nitroglycerine, etc., and concluded that if high velocity detonation occurred, the temperatures would be about 3,000°C. However, in low velocity detonation, the temperature rise of a liquid or solid due to compression in the shock front would be insignificant. Bowden and Gurton(7), pointed out that if gas bubbles were present the temperatures produced in the bubbles would be very high, and the hot spots at the bubbles would become new explosion centres. Consequently, low velocity detonation in an aerated explosive was probably maintained by these hotspots.

Evidence in support of this has been obtained with small scale experiments by Bowden & Williams(8).

In this paper direct experimental evidence will be brought forward to indicate that these views are substantially correct for large charges, at least in the low velocity detonation of solids, but that some other mechanism is probably operative in the low velocity detonation of nitroglycerine.

The methods employed were similar in principal to those used on a smaller scale by Yoffe(5), and Bowden and Williams(8), but since larger quantities of explosives were being detonated, the apparatus used was of a different form.

## I. EXPLOSIVES CONTAINING VARIOUS GASES

In the adiabatic compression of an ideal gas

$$T_2 = T_1\left(\frac{p_2}{p_1}\right)^{\frac{\gamma - 1}{\gamma}} \qquad (1)$$

where $T_1$ and $T_2$ are the initial and final temperatures, $p_1$ and $p_2$ the initial and final pressures, and $\gamma$ the ratio of the specific heats of the gas at constant pressure, and constant volume. If one were to replace the gas by one of lower $\gamma$ value, provided the initial temperature and the compression ratio were constant, the final temperature would be decreased. The effect of this change on the initiation of explosives has been fully discussed by Bowden & Yoffe(9).

Experiments were carried out with three solid explosives, namely, granulated tetryl, flake T.N.T., and nitroguanidine. The nitroguanidine was obtained in the form of fine crystals, and had a very low natural bulk density. The tetryl and the T.N.T. were packed loosely in thin paper or celluloid wrappers to form cylinders ¼" in diameter and 5" long. The packing density aimed at was 0.9 g. per c.c. for tetryl and 0.8 g. per c.c. for T.N.T. Nitroguanidine was packed in increments into cylindrical paper or celluloid wrappers 7/16" in diameter, and was compressed to a bulk density of 0.5 g. per c.c.

The paper or celluloid wrappers were thoroughly perforated and the cartridges inserted in wide bore glass tubes. The assemblies were primed with detonators and evacuated. Since the wrappers were perforated, the gas between the grains of explosive was removed. Ether vapour or pentane were then introduced until the saturation vapour pressure was reached. The velocities of detonation were then measured photographically (See E. Jones(10)), and compared with the detonation velocities measured in air. In some cases the detonation velocities of the explosives were measured by the Dautriche method using the system which will be described in the next section. The results which have been arranged in Table 1 gave little indication that replacing air by ether or pentane vapour has any effect on the detonation velocities. In the course of this work several failures were obtained when pentane vapour had been introduced into T.N.T. cartridges, but in those cartridges which did detonate the velocity of detonation was never much less than the velocity of detonation in a similar cartridge of T.N.T. interspersed with air.

Table 1

Velocity of detonation of granular explosives set off by a No. 6 A.S.A.T. copper detonator

| Explosive | Diameter: inches | Density: g./c.c. | Gas contained in explosive | Method of measurement | Velocity of detonation m. per sec. | | |
|---|---|---|---|---|---|---|---|
| Nitroguanidine 1st batch | ¾ | 0.5 | Air | Dautriche | 2,500 | | |
| | | | Ether | " | 2,500 | 2,630 | |
| | | | Pentane | " | 2,230 | 2,380 | 2,500 |
| Nitroguanidine 2nd batch | 7/16 | 0.5 | Air | High speed camera | 2,680 | 2,700 | |
| | | | Ether | | 2,620 | | |
| | | | Pentane | | 2,600 | 2,620 | |
| Tetryl | ¾ | 0.9 | Air | Dautriche | 1,700 | 2,080 | |
| | | | Ether | " | 1,700 | 1,725 | |
| | | | Pentane | " | 1,818 | 2,080 | |
| | 7/16 | 0.9 | Air | High speed camera | 1,430 | 1,540 | |
| | | | Pentane | | 1,460 | | |
| T.N.T. | ¾ | 0.8 | Air | Dautriche | 1,750 | 2,040 | |
| | | | Ether | " | 1,700 | | |
| | | | Pentane | " | 1,725 | 1,818 | |

## II. EXPLOSIVES CONTAINING GAS UNDER HIGH PRESSURE

Since a change of gas from air to a vapour of low $\gamma$ value (like ether and pentane) at a low pressure did not effect any marked change in the properties of the detonating explosives, experiments were carried out with methane ($\gamma = 1.31$) at high pressure. According to equation 1 an increase in the initial gas pressure would reduce the compression ratio and, therefore, reduce the maximum temperature to which the gas would be raised, provided that the maximum pressure was not increased. In fact, the final pressure in detonation is increased by an increase in the initial pressure, but it was found that for the initial pressure range used in these experiments, the change in the detonation pressure was insignificant.

### Experimental Method

The experiments were carried out in a gas tight vessel of 15 litres capacity. The vessel had very thick walls and was built to stand pressure up to several thousands of atmospheres. Cylindrical cartridges of explosives were prepared in waxed paper wrappers which were thoroughly perforated. Figure 1 shows how the cartridge was set up so that its velocity of detonation could be measured by the Dautriche method. In order to avoid damage to the vessel the length of detonating fuse employed was cut to a minimum which was usually 25 cm. Plastic covered Cordtex fuse with a core of PETN was used.

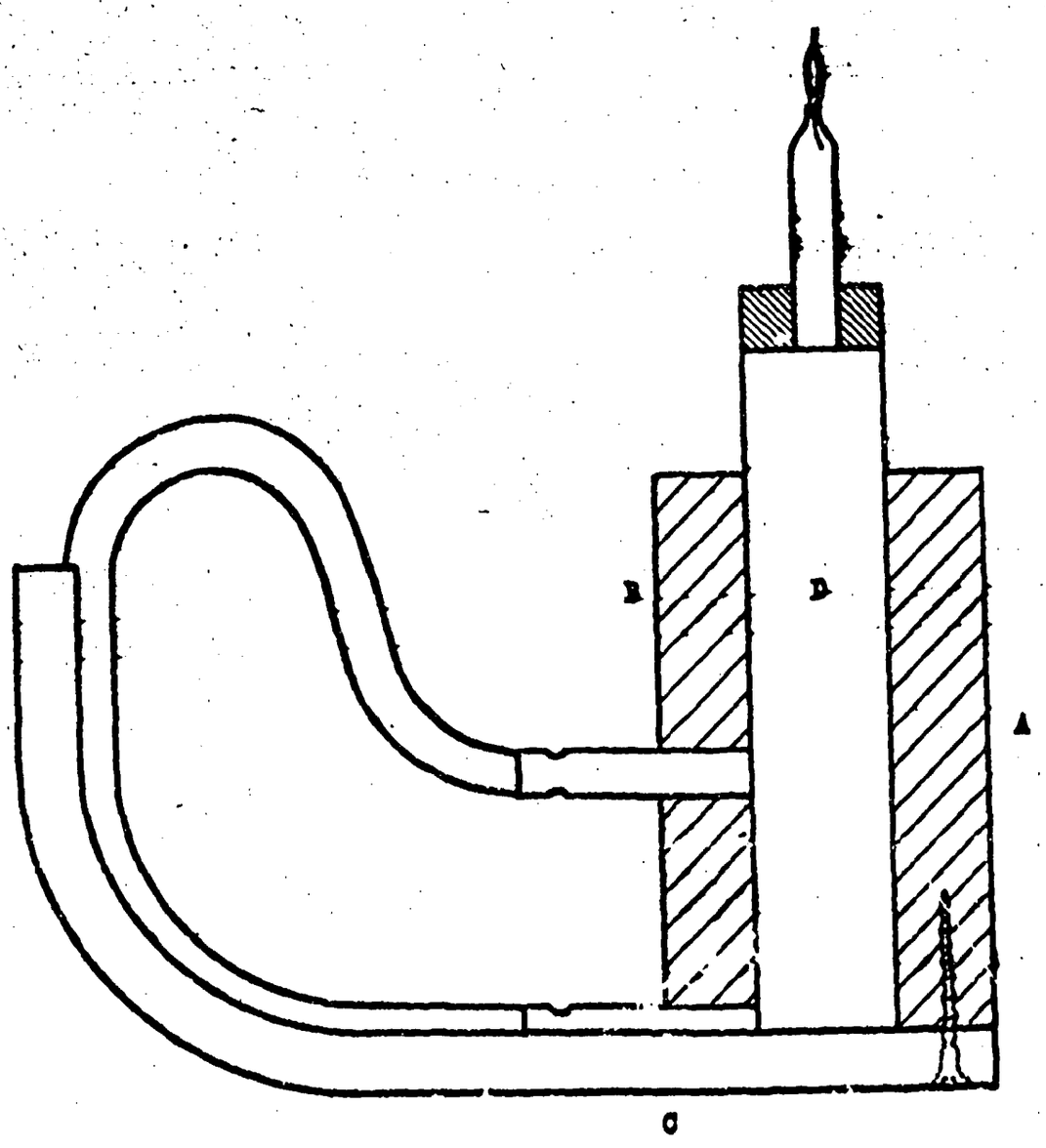


FIG. 1.

Arrangement of explosive and detonating fuse for the measurement of detonation velocity by the Dautriche method.

This had a detonation velocity of 6,600 m. per sec. The fuse was capped with No.6 fulminate detonators. A small strip of wood, A, was screwed to a curved lead plate, C. The cartridge of explosive, B, was strapped to this strip of wood. Another piece of wood, B, had a ¼" diameter hole drilled in it 3 cm. from its edge, where a ¼" diameter groove of semicircular cross section had been cut parallel to the hole. This piece of wood was strapped to the cartridge and its support. The detonators capping the fuse were inserted in the two holes, one in the wooden block, B, and the other in the hole formed by the adjacent grooves in the wooden block, B, and the lead plate, C. The lead plate was bent so that the fuse rested in the groove. The plate was marked at the position where the mid-point of the fuse rested against it. A detonator was inserted in the cartridge, and the whole assembly was lowered into the gas tight vessel. The complete assembly is shown in Figure 2. This vessel was closed and evacuated. Gas was then injected until the required pressure was reached, and the detonator fired electrically. In these experiments the gas used was methane so that the combined effect of low γ value and high initial pressure would be exerted. Since the cartridge wrappers were thoroughly perforated, the injected gas was able to enter the spaces between the grains of explosive in the cartridge without compressing the whole charge. The loading density of the explosive was, therefore, unaltered, except for the insignificant increase in the mass of the gas pockets. When the detonator was fired, detonation was set up in the cartridge and a wave of explosion travelled down to the first detonator capping the detonating fuse. A new detonation wave was then initiated in the first arm of the fuse, while the original wave continued to the second detonator where another detonation wave was initiated in the second arm of the fuse. By this time the wave in the first arm had travelled a distance $2\ell = dt$ where d is the detonation velocity of the fuse and t the time taken for the detonation wave in the cartridge to travel 7 cm. (the distance between the detonators). This interval is, of course, 3/D where D is the detonation velocity of the cartridge. The two waves in the fuse would meet at the mid-point of the fuse if both arms had been set off instantaneously, but since the first arm had a lead $2\ell$ over the second arm they met at a distance $\ell$ from the mid-point and made a mark on the lead plate.

$$\text{But } D = \frac{3d}{2\ell}$$

A measurement of $\ell$ therefore gave a measure of the unknown detonation velocity D.

Experiment with Grained Tetryl

Grained tetryl was loosely packed into cartridge wrappers 7/16", ½", and 15/16" diameter at a loading density of 0.9 g./c.c. and each cartridge set up as shown in Figures 1 and 2. The vessel was evacuated and then filled with gas. The pressure was measured by a Bourdon gauge, and then the cartridge was set off by a No.6 A.S.A.T. copper detonator.

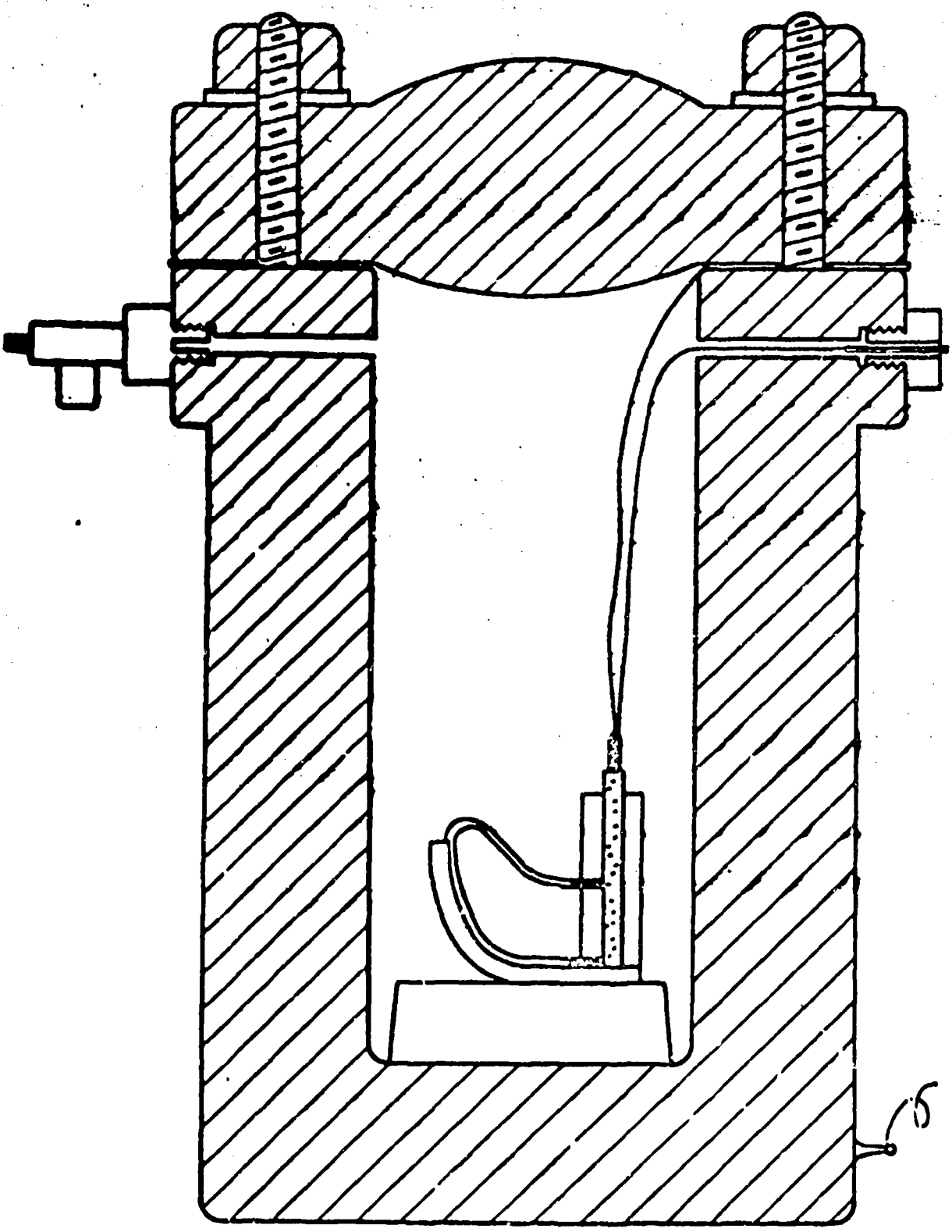

FIG. 2.

Arrangement for firing an explosive charge under pressure.

It was found that as the gas pressure increased, the detonation velocity became progressively slower, and above a threshold pressure the explosion did not propagate. Some typical results are given in Table 2. Some results obtained by the high speed camera method described in part 1 are included to show that the Dautriche method was not highly inaccurate.

Table 2

Effect of pressure on the velocity of detonation of grained tetryl density 0.9 g./c.c. set off by a No.6 A.S.A.T. copper detonator

| Diameter: inches | Pressure: atmospheres | Gas filling: voids | Velocity of detonation m./sec. |
|---|---|---|---|
| 7/16 | 0.03 | Air | 1460* |
| " | 1.0 | Air | 1,480, 1,300, 1,330 1,430*, 1,540* |
| " | 14.3 | Methane | 910 |
| " | 27.7 | " | Failed |
| ¾ | 1.0 | Air | 1,700 |
| " | 14.3 | Methane | 1,890 |
| " | 21 | " | 1,450 |
| " | 27.7 | " | 1,330 |
| " | 47.7 | " | Failed |
| 15/16 | 1.0 | Air | 2,860 |
| " | 14.3 | Methane | 2,330 |
| " | 17.6 | " | 2,085 |
| " | 21.0 | " | 1,695 |
| " | 41.0 | " | Failed |

* Determined by high speed camera method.

In all these experiments the distance from the initiating detonator to the first pick-up detonator, the "run-up", was kept constant at 6 cm. and it might be argued that the average velocity between the pick-ups appeared to fall as the pressure increased because the acceleration to maximum velocity was being slowed. A few experiments were, therefore, carried out in which the "run-up" was varied. For these experiments some ¾" diameter cartridges were used. In Table 3 results obtained at one atmosphere in air are compared with those obtained at 14.3 atmospheres in methane.

Table 3

Velocity of detonation of grained tetryl density 0.9 g./c.c. ½" diam. fired by a No.6 A.S.A.T. copper detonator

| Length of run up: cm. | Gas pressure: atmospheres | Velocity of detonation: m./sec. |
|---|---|---|
| 1 | 1 atm. of air | 1,670 |
| 4 | " | 1,[illegible] |
| 7 | " | 2,440 |
| 10 | " | 2,380 |
| 1 | 14.3 atm. of methane | 1,515 |
| 4 | " | 1,515 |
| 7 | " | 1,515 |
| 10 | " | 1,500 |

These results showed a definite tendency for acceleration of the detonation wave to a steady velocity of about 2,400 m./sec. at 1 atmosphere pressure of air, but an apparent deceleration of the velocity to about 1,500 m./sec. if the intergranular spaces were filled with methane at 14.3 atmospheres. This suggests that high pressure reduced the final steady velocity of detonation.

In all these experiments only velocities between 900 and 2,500 m./sec. were recorded, but if the explosive was sufficiently primed it would detonate at a much higher velocity. Sufficient priming was obtained when 2 g. of fine PETN was put on top of the cartridge of tetryl, and was set off by a No.6 A.S.A.T. copper detonator. When 7/16" diameter cartridges were set off by this means the following velocity records were obtained:-

1. At one atmosphere pressure in air, run up 6 cm. 4,550 m./sec.
2. At 67.7 " " in methane, run up 6 cm. 4,550 m./sec.
3. At 64.3 " " " " " " 25 cm. 4,550 "

Obviously the high velocity detonation of this explosive was unaffected by a change in the pressure of the gas in the intergranular spaces up to 67.7 atmospheres.

Experiments with Flake T.N.T.

The low velocity regime of a batch of flake T.N.T. was studied in experiments essentially similar to those carried out with grained tetryl. Only two cartridge diameters were investigated, ½" and 15/16" and the results have been set out in Table 4.

Table 4

Velocity of detonation of T.N.T. flake density 0.8 g./c.c. fired by a No.6 A.S.A.T. copper cased detonator

| Diameter inches | Pressure atmospheres | Gas present | Velocity of detonation m./sec. | |
|---|---|---|---|---|
| 1/2 | 0.05 | Air | 2020* | 2020* |
| | 0.12 | " | 1754 | 1818 |
| | 1.0 | " | 1750 | 2040 |
| | 21 | Methane | 2080 | |
| | 24.3 | " | No reading obtained | |
| | 27.7 | " | Some T.N.T. left | |
| | 41 | " | Failed completely | |
| 15/16 | 1.0 | Air | 2,380 | |
| | 9.3 | Methane | 2,330 | |
| | 11.0 | " | 1,020 | |
| | 14.3 | " | 2,000 | |
| | 26 | " | 1,820 | |
| | 41 | " | Failed completely | |

The velocities recorded in these experiments were not as regular as those recorded in the experiments with grained tetryl, but the continual propagation of low velocity detonation was prevented if the gas pressure between the grains of explosive was above a critical value.

It was found that high velocity detonation could be initiated in ¾" diameter cartridges of this flake T.N.T. if a primer of 5 g. of powdered PETN was placed on top of the charge. The primer was then set off by a No.6 A.S.A.T. electric detonator. High velocity detonation was observed when pressures of one atmosphere of air or 67.7 atmospheres of methane were applied in the gas spaces, and no drop in detonation velocity occurred.

Experiments with Nitroguanidine

Very fine nitroguanidine was stemmed in increments into paper shells to form cartridges of bulk density 0.5 g. per c.c. The wrappers were perforated and the cartridges set up in the arrangement shown in Figures 1 and 2. The explosive was quite porous in spite of the stemming, and gases at low pressure could be swept through the cartridges with ease. The experimental procedure followed was essentially similar to that employed in the experiments with tetryl and T.N.T. described above. The vessel was evacuated and the gas injected to the required pressure. The charge was fired, and the lead plate recovered. The detonation velocity was then calculated from a measurement of the distance between the zero mark on the plate and the mark due to the collision of the two approaching waves in the fuse. Typical results have been set out in Table 5.

## Table 5

### Detonation velocity of nitroguanidine density 0.5 g./c.c. set off by a No.6 A.S.A.T. copper cased detonator

| Diameter of cartridge inches | Pressure atmospheres | Gas injected | Velocity of detonation m./sec. |
|---|---|---|---|
| 7/16 | 0.05 | Air | 2650* |
| | 1.0 | " | 2750 2680* 2700* |
| | 6.0 | Methane | 2500 |
| | 7.0 | " | 1490 |
| | 11.0 | " | 2170 |
| | 17.7 | " | Failed |
| ¼ | 1.0 | Air | 3150 |
| | 6.7 | Methane | 3220 |
| | 11.0 | " | 3090 |
| | 14.3 | " | Failed |

* Determined by high speed camera methods.

Once again there was a tendency for the detonation velocity to fall as the pressure increased, and if the pressure exceeded about 11 to 15 atmospheres the propagation did not continue.

In the experiments with coarse tetryl and T.N.T. heavier priming caused a marked increase in the velocity of detonation. There were two distinct velocities at which detonation could propagate. However, fine nitroguanidine detonated at its maximum velocity when set off by a weak detonator, and no amount of priming could establish a steady propagation at a higher rate. It might be argued that the effect of pressure on the results obtained with tetryl and T.N.T. was merely to reduce the effectiveness of the detonator, for, if heavier priming was employed (and high velocity established) pressures of methane up to 67.7 atmospheres had no effect. Experiments were, therefore, carried out with cartridges of nitroguanidine 7/16" diameter primed with 2 g. of fine PETN powder. Table 6 shows the results. They showed that there was a marked effect due to increasing the gas pressure, and the continued propagation of detonation was eventually stopped.

Table 6

Velocity of detonation of nitroguanidine density 0.5 g./c.c. diameter 7/16", primed with 2 g. of PETN and set off by a No.6 "Briska" type detonator

| Pressure atmospheres | Gas injected | Velocity of detonation m./sec. |
|---|---|---|
| 1.0 | Air | 2,000 |
| 14.0 | Methane | 1,750 |
| 14.3 | " | 2,130 |
| 16.7 | " | 2,330 |
| 17.7 | " | Failed |
| 19.3 | " | " |
| 27.7 | " | " |
| 41.0 | " | " |

Further proof that the propagation of explosion rather than the initiation process was being modified by the increase in pressure was provided by some experiments in which the length of "run-up" between the initiating detonator and the first pick-up was changed. 7/16" diameter cartridges of various lengths were set up in the system shown in Figures 1 and 2. A series of velocity determinations over the last three centimetres of cartridges of increasing length provided a picture of the way in which the velocity of detonation increased along the length of a single cartridge. Experiments were performed with the gas spaces filled with air at one atmosphere, methane at 7.7 atmospheres, and methane at 17.7 atmospheres, and the results are set out in Table 7. The cartridges fired at 17.7 atmospheres pressure were primed with 2 g. of PETN and a No.6 Briska detonator.

Table 7

Velocity of detonation of nitroguanidine density 0.5 g./c.c. 7/16" diam.

| Initiator | Run up cm. | Pressure atmospheres | Gas injected | Velocity of detonation m./sec. |
|---|---|---|---|---|
| No.6 A.S.A.T. | 1 | 1.0 | Air | 1670 |
| | 3 | 1.0 | " | 2330 |
| | 6 | 1.0 | " | 2130 |
| | 9 | 1.0 | " | 2380 |
| " " | 1 | 7.7 | Methane | 1725 |
| | 3 | 7.7 | " | 1820 |
| | 6 | 7.7 | " | 1700 |
| | 9 | 7.7 | " | 2040 |
| 2 g. PETN + a | 1 | 17.7 | " | 1930 |
| No.6 Briska | 3 | 17.7 | " | 1330 |
| | 6 | 17.7 | " | Failed |
| | 9 | 17.7 | " | Failed |

These results may be translated into the distance time curves shown in Figure 3.

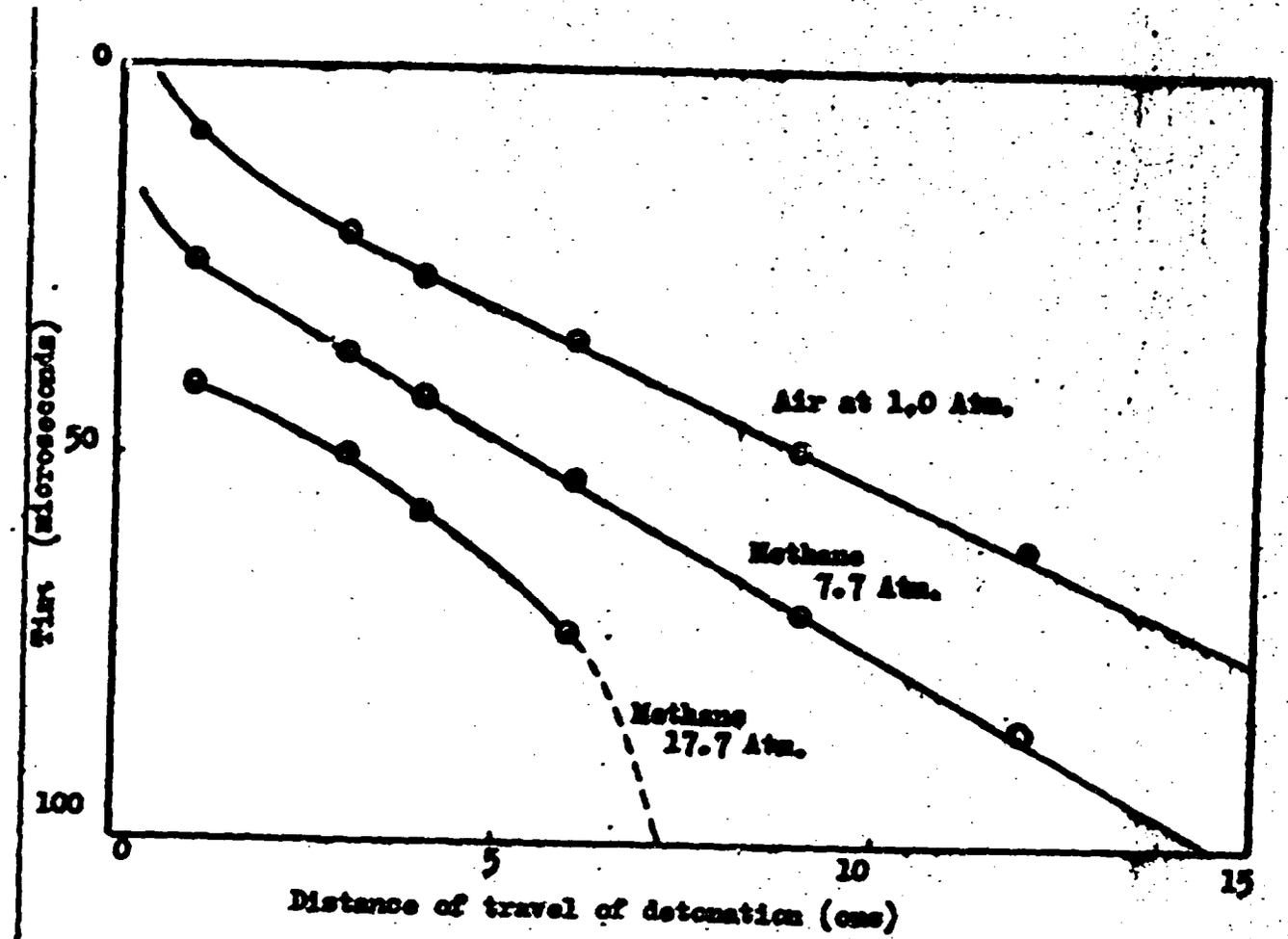


FIG. 3.

Relationship between the length of cartridge of nitroguanidine and the time taken for detonation under various gas pressures. The velocity of detonation falls as the pressure is increased and above a certain value propagation is not maintained.

It can be seen that the detonation velocity as measured by the slope of these lines rapidly settled to a steady value when the cartridges were fired in air at one atmosphere. If the cartridges were fired in 7.7 atmospheres of methane the same thing happened, but the steady value reached was somewhat lower. When the cartridges were fired with a pressure of 17.7 atmospheres of methane in the intergranular spaces, the velocity fell rapidly and with cartridges over 6 cm. in length complete consumption of the explosive did not occur.

Experiments with Liquid Nitroglycerine

The experiments with tetryl, T.N.T., and nitroguanidine showed that low velocity detonation could be prevented by increasing the included gas pressure. High velocity detonation of tetryl and T.N.T. was unaffected by a pressure of 67.7 atmospheres. Since liquid nitroglycerine was known to detonate at two discrete velocities it was of interest to study the effect of pressure on the propagation of explosion in this substance.

Nitroglycerine was poured into thin walled shells made of cellophane. It was found that low velocity detonation would not propagate in charges of ¼" diameter or less, and so for all experiments the lowest practicable diameter 7/16" was used. The cartridges were set up in the same way as those of T.N.T. tetryl and nitroguanidine (as shown in Figures 1 and 2) but the cartridge wrapper was not, of course, perforated.

It has already been mentioned that low velocity detonation in liquid nitroglycerine is an irregular propagation differing markedly from the steady low velocity detonations observed in aerated gelatines or coarse powders. It is not surprising, therefore, that the low velocities recorded at atmospheric pressure varied from 1410 to 950 m. per sec. Velocities below about 900 m. per sec. were often not recorded by the Dautriche method because the fulminate detonators capping the fuse were not sensitive enough to be set off by such weak explosion waves.

In the first series of experiments the initiator used was a No.1 fulminate detonator, the weakest detonator available. When the pressure was increased to 11.3 atmospheres no velocity readings were obtained, although the fuse detonated, and the lead was dented by the explosion when it reached the end of the cartridge. It is probable that only one of the detonators capping the fuse was set off by the explosion, consequently there was no mark due to the meeting of two waves. At higher pressures the complete fuse with detonators was often recovered, but even when the pressure was 71 atmospheres the explosion of the liquid was complete, for its "brisance" caused a dent to be punched in the lead plate. This dent did not appear to grow smaller as the pressure increased. The experiments were repeated with a heavier initiator, a No.4 fulminate detonator. Occasionally this initiated high velocity propagation.

However, as the pressure increased, the incidence of high velocity detonation became less frequent and there was a definite tendency for the low velocity records to be reduced in value, although no complete failure was observed. The results have been set out in Table 8.

Table 8

Velocity of detonation of liquid nitroglycerine
7/16" diameter

| Initiator | Pressure atmospheres | Gas used | Velocity of detonation m. per sec. | Remarks |
|---|---|---|---|---|
| No.1 detonator | 1.0 | Air | 1410, 1160, 950 | |
| | 11.3 | Methane | No reading | Fuse detonated |
| | 30.3 | " | " " | Fuse recovered |
| | 71.0 | " | " " | " " |
| No.4 detonator | 1.0 | Air | 1250 | |
| | 1.0 | " | 7690 | |
| | 14.3 | Methane | 6670 | |
| | 17.7 | " | 1205 | |
| | 20.5 | " | 1040 | |
| | 32.7 | " | 1010 | |
| | 44.3 | " | 807 | |
| | 67.7 | " | 909 | |

If the propagation depended on the presence of small bubbles one might expect this result. A number of attempts were made to remove all gas bubbles from the liquid before firing by leaving the cartridges several hours before firing them, and by storing the cartridges under vacuum, but low velocity propagation was still possible. Finally, small quantities of nitroglycerine were outgassed under a vacuum of $10^{-2}$ mm. of mercury, and then poured into the cartridge shells. The cartridges were returned to the vacuum chamber which was opened just before the cartridge was inserted in the assembly shown in Figure 1. A cartridge so assembled was set off by a No.1 detonator at one atmosphere air pressure and detonated at high velocity. It gave a reading of 6670 m. per sec. Two other cartridges were removed in turn from vacuum chambers, and rapidly arranged in the Dautriche assembly (Figure 1) inserted in the pressure vessel (Figure 2) and rapidly raised to a high pressure. It was very unlikely that any air bubble could remain in the liquid after outgassing, but if any invisible one was left it was compressed by the applied pressure to an insignificant volume. Pressures of 47.7 atmospheres and 64.3 atmospheres were used and the initiator was a No.1 detonator. In both cases complete low velocity propagation occurred. No explosive was left, a distinct dent was made in the lead plate, and the fuse detonated. Although no velocity records were obtained, it was clear that low velocity detonation had propagated in liquid nitroglycerine when gas bubbles were completely excluded.

## Discussion

These experimental results reveal a striking similarity between the initiation of explosion by the impact of a hard body, and the propagation of explosion by the impact of a low velocity detonation wave. In order to initiate explosion by impact it is apparently necessary to have within the explosive something which will provide a local high temperature or hot spot. The most effective hot spot source is a small bubble of gas. During impact this bubble is rapidly compressed, and reaches a high temperature. The explosion is then initiated at the hot spot. If no bubbles are present it is very difficult to start an explosion.

## Low Velocity Detonation in Solid Explosives

In order to maintain low velocity detonation in solid explosives like T.N.T. or tetryl, or in gelatinous mixtures containing nitroglycerine it is again of great advantage, if not essential, that gas pockets should be present. In the experiments with tetryl, T.N.T., and nitroguanidine subjected to increasing gas pressure, it was clear that as the gas pressure increased, the ease of propagation of low order detonation was reduced, and above a threshold pressure, which varied with the explosive and with the cartridge diameter, ceased to maintain a steady rate.

This effect cannot be explained by hydrodynamic considerations of the explosive as a homogeneous body, for the pressures used in these experiments were insignificant in comparison with the detonation pressures. We must, therefore, look at the mechanism of detonation for an explanation. Detonation waves which all travel at supersonic velocities are really shock waves maintained by chemical reactions. The front of the shock wave on meeting a new layer of explosive compresses it very rapidly and thereafter the chemical reaction begins in that layer. Bridgeman(11), has shown that static pressures of the same order as detonation pressures do not initiate explosion in solid explosives, and it seems reasonable to attribute initiation to the suddenness of the pressure rise. Such compressions bring about a rapid increase in temperature and since the shock wave also brings about a change in the kinetic energy of the material, the temperature attained is even higher than the temperature in adiabatic compression over the same pressure range. During the high velocity detonation of nitroglycerine the compression of the liquid phase may bring about temperature rises of 3,000°C.(6), but in low velocity detonations the pressure changes cannot be great enough to raise the temperature of a liquid or solid phase more than a few tens of degrees. The much more compressible gas pockets would, however, be raised to very high temperatures. Hot spots would be formed at the gas bubbles and these would initiate explosion in their vicinity immediately a shock wave encountered them. Thus a low velocity detonation in a granular solid would appear to be a shock wave supported by a chemical reaction which is initiated at the gas bubbles encountered by the shock wave.

Support for this view has been obtained in the study of the light emitted in explosions.

A considerable amount of study has been given to the origin of the luminosity near detonating explosives and Muraour(12) has shown that the majority of the light comes from the surrounding gas which is raised to a very high temperature by the compression it suffers in the passage of a shock wave (Michael Levy and Muraour(13)) showed that if grains of lead azide were separated by 3 mm. gaps, an explosion would propagate from grain to grain in air, but if the air was replaced by carbon dioxide at 22 atmospheres pressure, the luminosity was reduced, and propagation of the explosion was incomplete. Paterson(14) has obtained evidence that luminosity may be produced within a granular material by the passage of a shock wave, and since this may be brighter than the luminosity of an explosion supported by a shock wave of greater intensity, it is reasonable to suppose that the luminosity comes from the compressional heating of the small gas pockets. This may be regarded as evidence that the gas pockets within a granular explosive do become very hot when a detonation wave passes over them, and we would expect that these hot spots would act as centres of explosion. Now if the initial pressure of the gas in the pockets were increased, the compression ratio in the detonation wave would be reduced, and so the maximum temperature in the gas pockets would be reduced. Eventually, if the compression ratio were sufficiently reduced the hot spot temperatures would not be high enough to initiate local explosions. Thereafter the detonation would not propagate. On this view of the mechanism of initiation of explosion in the wave front we would expect that there would be a threshold pressure in the gas pockets above which low velocity detonation would no longer be possible. The experiments with tetryl, T.N.T. and nitroguanidine confirm that there is such a threshold pressure.

If air was replaced by other gases of lower $\gamma$ value at low pressures there was no substantial drop in the velocity of detonation of the granular solids. At first sight a drop in velocity, or complete failure in the propagation might have been expected, but several factors have to be remembered. Firstly, the gases of lower $\gamma$ value cannot be considered to behave as ideal gases during such large compressions, and the temperatures produced by adiabatic compression would be higher than those predicted by the ideal equation(1). Secondly, since it is a shock wave compression rather than an adiabatic compression, the effect of $\gamma$ variations would be considerably less than the effect in adiabatic compression. It is more likely however that the change in the specific heat of the gas pockets brought about by the replacement of air by pentane or ether vapour was not sufficient for it to have a distinctly measurable effect on the properties of the explosive. Some cartridges of T.N.T. failed to detonate when they contained pentane vapour, whilst similar cartridges containing air detonated completely, but this occurred only when the diameter was near the minimum diameter for

propagation, and it would be unwise to base any conclusions on these results alone.

Low Velocity Detonation in Liquid Nitroglycerine

In the introduction to this paper it was pointed out that the low velocity detonation of nitroglycerine is more irregular than the low velocity detonation of granular solids or aerated gelatines. This suggests that low velocity detonation of liquid nitroglycerine may differ in mechanism from low velocity detonation in granular solids. The experiments described above have shown that the complete absence of gas bubbles in the liquid does not prevent the propagation of low velocity detonation. An increase in the external pressure does seem to reduce the velocity of detonation, but pressures up to 71 atmospheres failed to prevent propagation of the explosion. The only reasonable explanation would appear to be the one previously offered for the detonation of thin films of nitroglycerine (Bowden and Gurton(7)) that the mechanical effects of the detonation wave rapidly broke up the explosive to provide a large burning surface which was ignited by conduction of heat from the reacting material. There is no obvious explanation for the apparent drop in velocity with pressure, but since the variation in records obtained at atmospheric pressure covered almost the whole range observed under pressure, this drop in velocity may not have any significance.

In general it may, therefore, be concluded that in most explosives the chemical reaction responsible for the propagation of low velocity detonation of solids is continuously initiated in the shock front of the detonation wave by the hot spots formed in the compression of gas pockets. There is no evidence that the presence of gas pockets is essential for the maintenance of high velocity detonation in solids, or low velocity detonation in liquid nitroglycerine.

This work followed logically from the study of detonation in thin films which the author carried out in conjunction with Dr. F.P. Bowden, F.R.S., and I thank him for suggesting the investigation. The author also wishes to thank Dr. J. Taylor, M.B.E. for his constant encouragement, and Messrs. G. Boyd and I.G. Cumming who helped to carry out the experimental work.

## REFERENCES


(1) Taylor, J., 1952 — Detonation in condensed explosives. Oxford University Press

(2) Ratner, S., 1944 — C.R. Acad.Sci. U.R.S.S., 42, 265

(3) Jones, E. and Mitchell, D., 1948 — Nature 161, 98

(4) Bowden, F.P., Mulcahy, M.F.R., Vines, R.G. and Yoffe, A., 1947 — Proc.Roy.Soc. (A) 188, 241, 311

(5) Yoffe, A., 1949 — Proc.Roy.Soc. (A) 198, 373

(6) Ratner, S., 1947 — Acta Physicochemica U.R.S.S., 22, 357

(7) Bowden, F.P. and Gurton, O.A., 1949 — Proc.Roy.Soc. (A) 198, 350

(8) Bowden, F.P. and William, H.T., 1951 — Research 4, 1951

(9) Bowden, F.P. and Yoffe A., 1952 — Initiation and growth of explosion in liquids and solids. The University Press, Cambridge

(10) Jones, E., 1928 — Proc.Roy.Soc. (A), 120, 603

(11) Bridgeman, P., 1947 — J.Chem.Phys. 15, 311

(12) Muraour, H., 1942 — Chemie et Industrie, 47, 3

(13) Michael-Levy, A. and Muraour, H., 1936 — Comptes Rendues, 202, 755

(14) Paterson, S., 1951 — Nature 167, 479

Rhys Jones and Ian G. Cumming
I.C.I. (Nobel Division)
Stevenston,
Ayrshire, Scotland.

A sensitive explosive is one which needs little encouragement to induce it to explode or, at least, to undergo chemical changes leading to explosion. The necessary stimulus may come from any one of a number of sources, such as friction, impact, flame, electric sparks and so on, and since explosives vary in their reactions to different stimuli, it is desirable in discussing sensitiveness to specify the kind of initiating agency in mind. Thus, one explosive may be very sensitive to ignition by an electric spark whereas another may be more susceptible to impact or friction. In fact, the same explosive can be made sensitive to electrical discharges or to friction merely by introducing a little graphite in the one case and a few particles of grit in the other.

In some explosives the explosive reaction, however initiated, inevitably builds up to detonation, sometimes with astonishing rapidity. Other high explosives require a "detonator", or even a "booster" or "primer", to initiate reaction; in these cases, if the initiating device does its work, detonation sets in immediately. It is necessary, therefore, to distinguish between the direct initiation of detonation and its initiation through an intermediary. In other words, the sensitiveness of an explosive to detonation is not to be confused with its sensitiveness to ignition.

As its name implies, sensitiveness to detonation is an exclusive property of the so-called high explosives. There are circumstances, however, where a high explosive may lose its ability to detonate as, for example, when spread in a thin layer on an anvil. It appears, therefore, that sensitiveness to detonation is a property, not of the explosive substance, but of the explosive system. In other words, the geometry of the explosive charge and its environment are factors which must be

taken into account both in defining sensitiveness to detonation and in developing methods for its measurement.

Sensitiveness Tests

It has been indicated that direct initiation of detonation, particularly in condensed explosives, normally requires a detonator or primer. Hence, sensitiveness to detonation may be measured by the weakest detonator or primer capable of initiating detonation in the explosive charge in question(1). For reasons of symmetry, the explosive charge is usually prepared in the form of a cylindrical cartridge and, for convenience, the cartridge is fired in the open. Thus the conditions of test are arbitrarily chosen, but experience has shown that initiators which function satisfactorily under these conditions perform equally well, if not better, under field conditions as, for example, in borehole charges or high explosive bombs.

The almost universal use of detonators for initiation in practice makes a minimum detonator test very attractive from the practical point of view, but the geometry of this system is unnecessarily complicated for initial study, see Fig. 1 (a). A primer, on the other hand, can be made to match the shape of the receptor and its strength varied without necessarily affecting the geometrical requirements of the test. Primer and receptor cartridges placed in line would appear to offer the simplest and most convenient arrangement for experimental purposes. It may be worth noting here that the geometrical basis of this model is a straight line, namely, the axis of symmetry.

To measure the sensitiveness to detonation of the receptor cartridge, it is necessary to be able not only to vary the strength, or "initiating power", of the primer but also to express this property in terms of some numerical quantity. This is usually done by separating the primer and receptor cartridges and increasing the intervening gap in successive experiments until the point is reached at which, on firing the primer, the receptor just fails to detonate, the critical distance being taken as an arbitrary measure of the sensitiveness of the receptor. The space between the cartridges may be filled with any homogeneous medium but it is convenient in practice to use air. The arrangement of the gap test is illustrated in Fig. 1 (b).

The presence of a gap in the explosive column is a complication which, as will be seen shortly, is not altogether desirable and the alternative may be suggested of varying the initiating power of the primer by diluting it with inert material and, this time, taking the critical amount of diluent required to cause failure as a measure of sensitiveness. This is essentially the same test only that in this version the receptor cartridge is initiated by a true "detonation-wave" in an explosive rather than by the "shock-

(a) MINIMUM DETONATOR TEST
(ILLUSTRATING CHANGING SHAPE OF DETONATION FRONT)

(b) GAP TEST

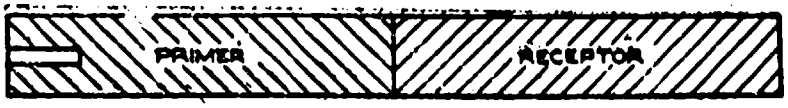


(c) CONTACT TEST

FIG. 1 SENSITIVENESS TO DETONATION TESTS

wave" set up in the medium separating the two cartridges, see Fig. 1(c). Whether or not there is any real difference between a detonation-wave and a shock-wave as regards initiating power is a matter which need not concern the present discussion because the work to be described was done with explosives in intimate contact.

The gap test, however, will serve to illustrate a point of some significance which may be conveniently considered at this stage. If the test is carried out with a constant primer, the critical gap at which detonation is just transmitted to each of a series of different receptors will, as already seen, arrange these receptors in order of their sensitiveness to detonation. Conversely, if a standard receptor is used with a range of primers, the critical gap now arranges the primers in order of initiating power. Actually, the converse is not strictly true because it depends on the doubtful hypothesis that the decay of initiating power with distance is the same for all explosives; this is why a contact test presents fewer complications than a gap test.

If, as is more usual in carrying out the gap test, the same explosive is used as primer and receptor, explosives are again arranged in a definite order of sensitiveness to detonation but this arrangement is not necessarily the same as that obtained with a standard primer. It appears, therefore, that there are two kinds of sensitiveness to detonation and, since one is measured by the maximum gap over which transmission occurs in a given explosive, this is called "sensitiveness to propagation" and the other "sensitiveness to initiation". There are, therefore, three primary factors concerned in the double cartridge test, namely, initiating power, sensitiveness to initiation and sensitiveness to propagation.

An elementary relation between these quantities may now be noted. To measure the sensitiveness to initiation of a receptor, the initiating power of the primer must be reduced until it just fails to initiate the receptor. In other words, the sensitiveness to initiation equals the minimum effective initiating power. Again, the sensitiveness to propagation is the margin by which the actual initiating power exceeds the minimum effective value, or sensitiveness to initiation. At the limit for propagation the initiating power of an explosive cartridge coincides with its sensitiveness to initiation and the sensitiveness to propagation vanishes. These statements reduce to the following equality:-

Initiating power - sensitiveness to initiation

= sensitiveness to propagation.

This relationship derives from our definitions of these quantities and must now await experimental verification. Nevertheless, it is interesting to note that, if this relation holds, these three quantities have the same dimensions in the mathematical

sense and so can be measured in the same units, an encouraging prospect.

## Experimental

As already indicated, the experimental procedure for carrying out the preferred form of the double-cartridge test is to join the primer and receptor cartridges end to end in the same straight line and to vary one or other in a systematic way until the point is reached when, on firing the primer, the receptor just fails to detonate. If the cartridges are carefully made and are long enough to ensure steady detonation, the end-point is usually remarkably sharp. By varying the primer and receptor in turn, results will be obtained showing how the sensitiveness to initiation on the one hand, and the initiating power on the other, vary with certain physical and chemical properties of the explosives.

For example, a series of receptor cartridges might be prepared to cover a certain range of sensitiveness to initiation; these could be a series of trinitrotoluene/ammonium nitrate mixtures cartridged at a constant density or, alternatively, a particular trinitrotoluene/ammonium nitrate mixture cartridged at different densities. In these cases the sensitiveness to initiation might be expected to increase with increasing proportion of trinitrotoluene in the mixture and to decrease with increasing density. The primer for either or both series of constant receptors could be nitroglycerine absorbed in kieselguhr, the proportion of nitroglycerine to kieselguhr being varied for each test until the point of failure is established. The proportion of nitroglycerine in the critical mixture is taken to represent the sensitiveness to initiation of the particular receptor concerned and, when this has been done for all the receptors, the combined results show how the sensitiveness to initiation varies with the composition of the trinitrotoluene/ammonium nitrate mixture in the one case and with cartridging density in the other. The complementary process, of course, provides similar information about the initiating power.

Such experiments can be made with almost any explosive or explosive/inert combination but it is not the intention here to compare explosives but rather to illustrate certain general principles. It is proposed, therefore, to describe an experiment involving a receptor cartridge having two stable rates of detonation and so combining two explosives in one. Such a cartridge may be expected to show two levels of initiating power, sensitiveness to initiation and sensitiveness to propagation. The particular explosive chosen for this experiment was flaked trinitrotoluene, size 20 x 30 B.S.S. cartridged at a density of 1.0 g./c.c. A 3 cm. diameter cartridge of this explosive, for example, detonates at 1900 or 4100 m./sec. depending on the strength of

the initiator. The problem is, as before, to determine the minimum primer required to initiate each of these detonation regimes.

Even with two rates of detonation, one cartridge can only give two results and, since this is not enough to solve a problem involving three variables, it becomes necessary to vary the detonating properties of the cartridge in a way which will not alter the explosive or disturb the basic model. This may be done quite simply by varying the diameter of the cartridge, which is obviously an arbitrary factor. Thus it becomes possible, at least in theory, to produce two infinite series of results from one explosive of one grain size at one density. By varying the size and density, the results may, if necessary, be multiplied without end.

It remains now to find a common unit for measuring the explosive properties of the cartridge. If, as seems likely, the initiating power is a function of the velocity of detonation, a weak primer may be expected to initiate detonation in the receptor at a lower rate than a strong one and we can therefore measure the strength of a primer by the magnitude of the initial velocity induced in the receptor. On this view, the minimum initiating power needed to ensure complete detonation of a receptor, i.e. the sensitiveness to initiation of the receptor, is measured by the minimum initial rate of detonation which ensures complete propagation. Similarly, the sensitiveness to propagation is represented by the margin between the stable value of the detonation velocity and this critical initial value. Thus, by photographing the double-cartridge test on a moving film and measuring the initial and final rates of detonation in the receptor, it should be possible to obtain quantitative measurements of the initiating power, sensitiveness to initiation and sensitiveness to propagation. This assumes, of course, that all three quantities are functions of the rate of detonation and that the process of attaining stable detonation is sufficiently gradual to be observable.

As will be seen from the specimen photographs reproduced in Fig. 3, the explosive chosen for the experiment does in fact lend itself to this technique and it was found possible, by examining the photographs with a comparator and measuring the tangents to the trace at various points, to plot the rate of detonation against distance along the receptor cartridge. By extrapolating to the point where primer and receptor meet, the starting rate in the receptor was obtained. The method is not very accurate but by using different sets of primers, several values for the same result were obtained and an average taken.

The primers used were in two groups, (a) picrite, nitrated cotton wool and a commercial explosive (Glasgow Dynamite), all cartridged at varying densities and (b) nitroglycerine/kieselguhr, pentaerythritol tetranitrate/common salt and trinitrotoluene/common salt mixtures of varying proportions. The primer cartridges were usually 6 in. long, which is normally sufficient to establish stable detonation. By varying the density in group (a) and the composition in group (b), the critical conditions for initiation were established for the trinitrotoluene receptor cartridge in different diameters.

Results

In ¾ in. diameter cartridges, flaked trinitrotoluene, size 20 x 30 B.S.S., cartridged at a density of 1.0 g./c.c. did not propagate detonation, however well primed.

In 1 in. diameter cartridges, this explosive, if initiated at any speed between about 1,600 and 3,200 m./sec., accelerated or decelerated until the rate of detonation reached a figure of approximately 1,700 m./sec., after which it remained steady. If initiated at anything below 1,600 m./sec., detonation died out and, if initiated at anything above 3,200 m./sec., the rate of detonation became steady at approximately 3,400 m./sec.

In 1 3/16 in. diameter cartridges, the same explosive, if initiated at speeds between about 1,400 and 2,400 m./sec., settled down to a stable regime at approximately 1,900 m./sec., whereas if initiated at speeds exceeding 2,400 m./sec., its final velocity of detonation was approximately 4,100 m./sec.

In 1¾ in. diameter cartridges, this explosive had only one stable velocity of detonation which was approximately 4,400 m./sec. This required a minimum initiating speed of about 1,200 m./sec.

Difficulty was experienced in producing primers which were too weak to initiate this explosive so that the minimum initiating velocities for the low velocity regime are a little uncertain.

The results are reproduced graphically in Fig. 2 and it will be seen that they form two pairs of intersecting lines, the upper line of each pair representing the stable velocity of detonation, or initiating power, of the regime concerned and the lower representing the minimum effective initiating rate, or sensitiveness to initiation. Thus, AB represents the initiating power of the high velocity regime, BC the sensitiveness to high velocity initiation, CD the initiating power of the low velocity regime and DE the sensitiveness to low velocity initiation.

FIG. 2 RELATION BETWEEN INITIATING POWER AND SENSITIVENESS TO INITIATION (TWO-VELOCITY EXPLOSIVE)

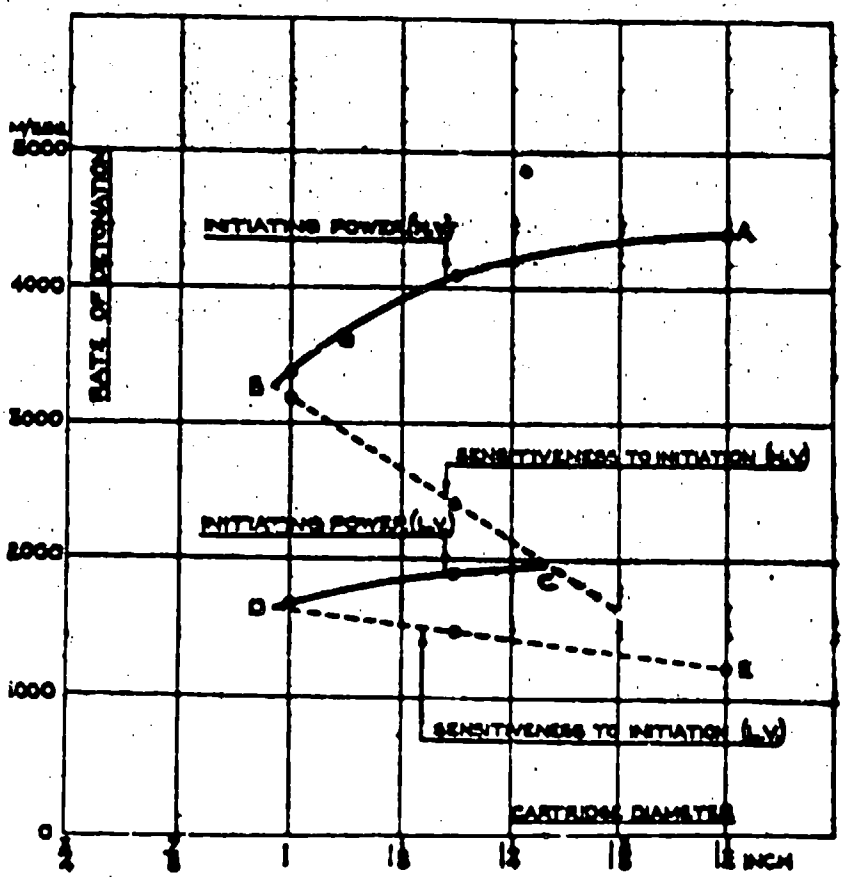

At the points of intersection B and D, the initiating power equals the sensitiveness to initiation and, by definition, this distinguishes the limiting diameter for propagation. The fact that cartridges of slightly lower diameter could not be made to detonate completely, even with the heaviest priming, thus confirms expectations. Moreover, as the cartridge diameter increases above the limiting value, the lines are seen to diverge, showing that the sensitiveness to propagation increases with cartridge diameter. This is also a well-established experimental fact.

At C the initiating power of the stabilised low velocity regime equals the sensitiveness to initiation of the high velocity regime, with the result that the one leads to the other. If, as seems likely, the build-up of detonation occurs at different rates under the two regimes, the velocity curve would suffer an abrupt change of slope at this point. For example, if a cartridge of the critical diameter were to be initiated at the minimum effective rate, which according to Fig. 2 is approximately 1,400 m./sec., detonation accelerates at the characteristic "low velocity" rate up to about 2,000 m./sec., at which point the change-over occurs and, thereafter, acceleration proceeds at the "high velocity" rate. It may be further anticipated that the line BC continues beyond C and that, above the critical diameter, the low velocity regime gradually disappears. Photographs taken in this region bear out these inferences, at least in a qualitative way. In fact, this phenomenon has been observed and commented on before(2) but no adequate explanation of the mechanism of the change-over has previously been offered.

Another interesting feature of the results is the indication that the sensitiveness to initiation of a given explosive varies with cartridge diameter, the smaller diameter cartridges being more difficult to initiate. This confirms the earlier inference, based on other evidence, that sensitiveness to detonation is a property of the explosive cartridge or charge rather than that of the explosive substance.

The fact that the minimum diameter for propagation of detonation is the same for both high and low velocities of detonation may be fortuitous because there is evidence that this is not the case with other two-velocity explosives. Thus Blasting Gelatine detonates at the high velocity in diameters too small to propagate low velocity detonation whereas the opposite is true for Polar Saxonite No. 3.

It may be said in conclusion that the results of the experiments described above confirm predictions relating to the behaviour of detonation in a two-velocity explosive which were based on the assumptions that initiating power, sensitiveness to initiation and sensitiveness to propagation are inter-related and can be defined in terms of the rate of detonation.

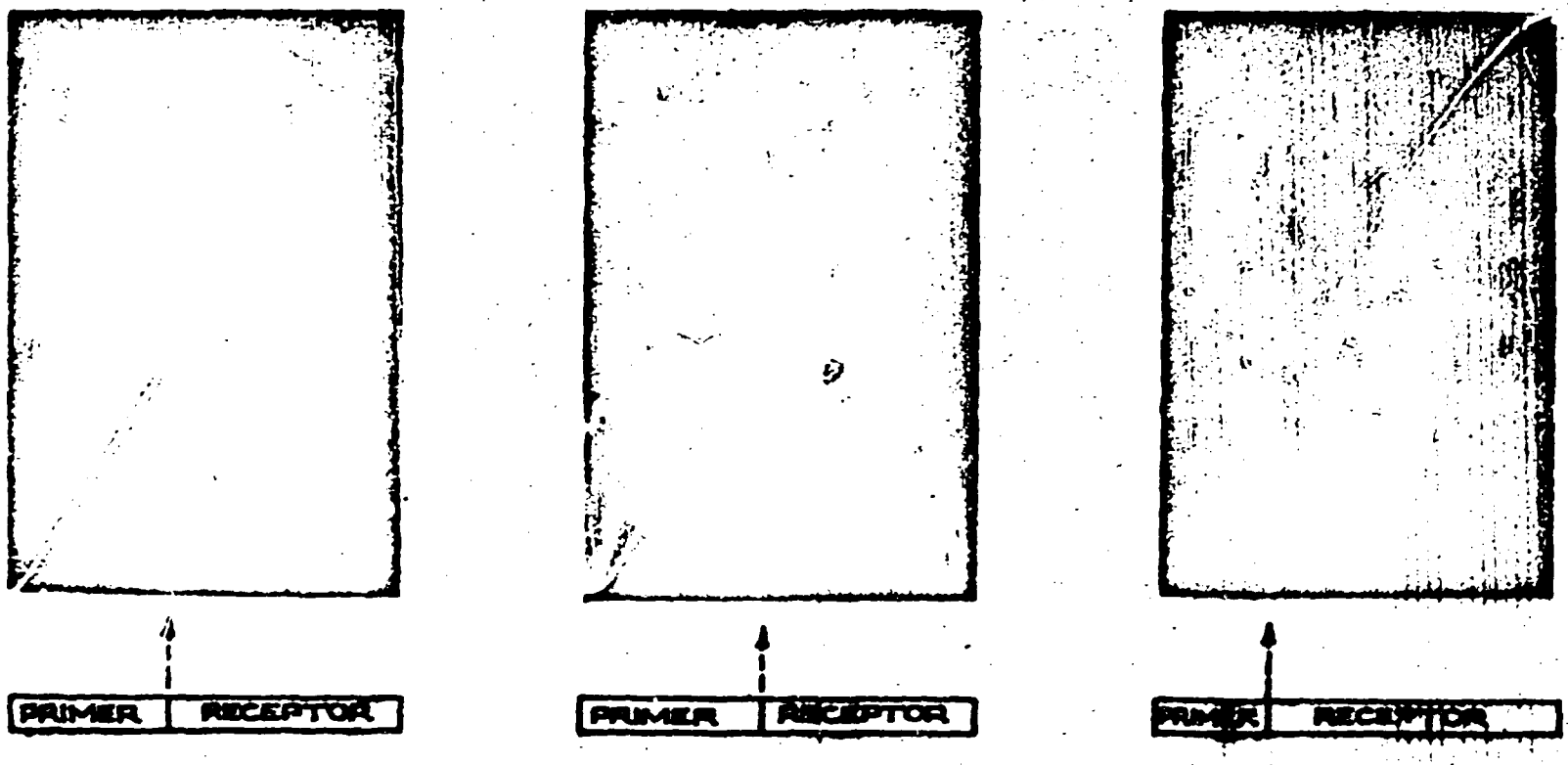


Fig. 3

Transmission of Detonation - High Speed Camera Photography

## References

(1) A. Marshall "Explosives" Vol. 2, p. 429. London, 1917.

(2) E. Jones, D. Mitchell Nature, 161, 1948, 98.

# INITIATION OF MILITARY EXPLOSIVES BY PROJECTILE IMPACT

J. M. Dewey
Ballistic Research Laboratories
Aberdeen Proving Ground, Md.

## INTRODUCTION

An experimental study of the factors controlling initiation of detonation in impact of high speed fragments has been undertaken. The first phase has been aimed at an understanding of the many discrepancies in the literature.[1] Tetryl was used because of the convenience of its relatively high sensitivity, with Composition B (60/40 cyclonite TNT) for comparison.

## RESULTS AND DISCUSSION

It was found that detonation was initiated, if at all, either at the surface of impact or where explosive was trapped between a projectile and a backing plate. Neither a backing plate nor the thickness of the explosive (above the critical diameter) affected the first process. No burning starting at the initial impact of the projectile has been observed. Ignition frequently results from flash of the projectile against a backstop, following break-up of the charge by the projectile, as seen in Figure 1. In one case a 2-1/2" x 1" Composition B disc struck by a Caliber .50 flat-ended steel slug spalled, apparently in powdered form, and the spall was ignited or detonated at impact on the metal backstop, giving a bright flash. Tetryl pellets (density 1.48 ± 0.04 g/cc) 1/2" thick burned, under the conditions of these experiments, when struck by Caliber .30 carbine ball (which has an approximately hemispherical nose) at velocities above 700 m/s, while a velocity of 900 m/s was required with 1" thick pellets. At velocities up to 1000 m/s neither Caliber .30 nor Caliber .50 standard ball, which have streamlined contours, caused burning or detonation of an unbacked charge. The charge, whether of cast or pressed explosive, simply broke up under impact. As Kouba[2] reported in 1947, shape, size, and velocity, not mass and velocity, of the projectile determine the result. Charges backed by metal detonated within the hole in the back plate, as could be seen by observation of the plate.

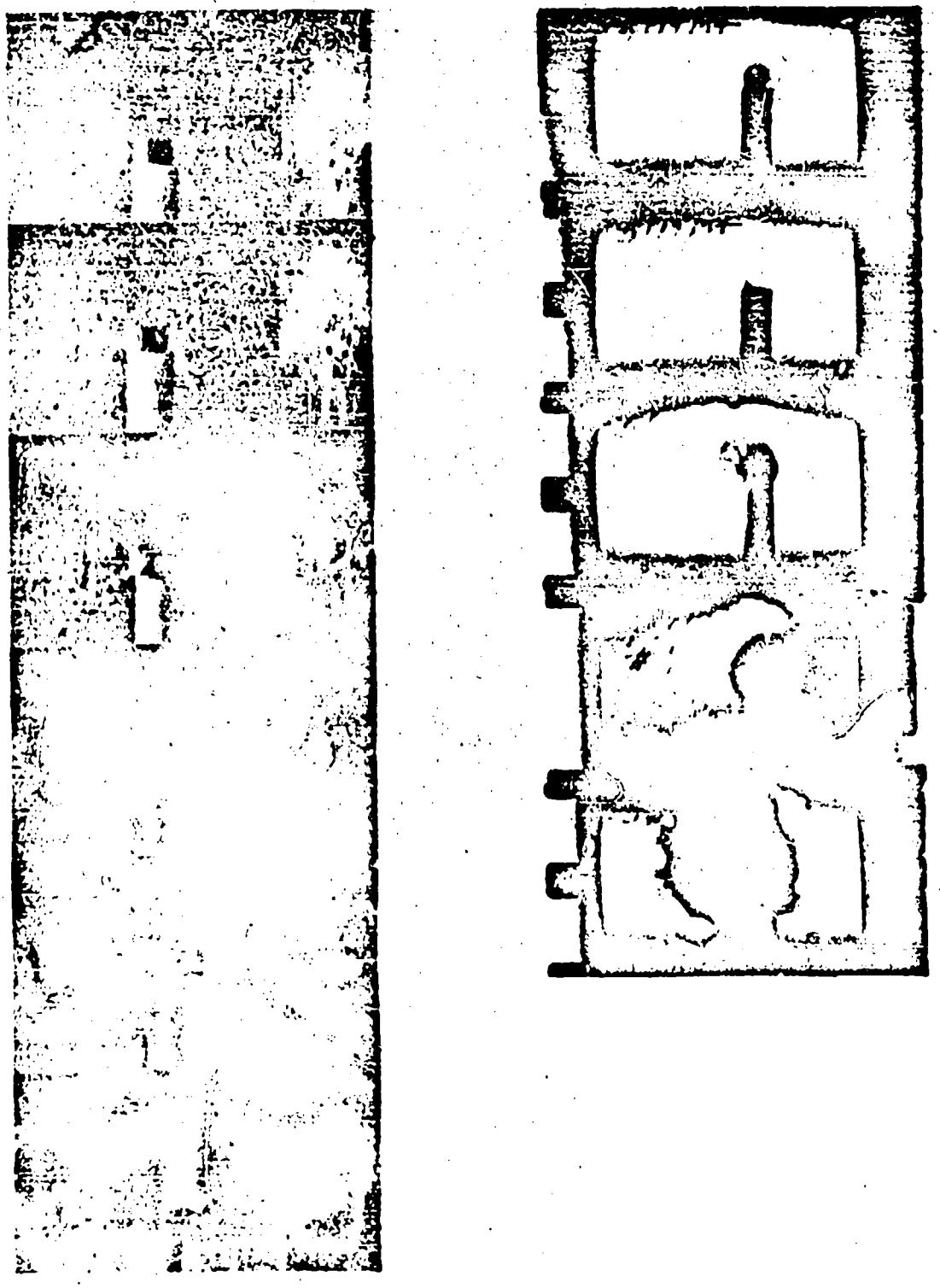

Figure 1 - Ignition of Comp. B Discs by Flash at Backstop, about 5000 Frames/Sec.

Flat-ended brass cylinders of various lengths were fired against Tetryl and cast Composition B. As far as possible in rapid setting up of charges, impact was normal. The results on the effect of the shape of the impacting surface of the projectile lead to the conclusion that small variations from normal would have little effect, since a small area of contact is ineffective at the velocities used. No effect of mass was observed with differing lengths. The lowest velocity at which a projectile caused detonation was sensitive to the diameter of the projectile but not to its length. Caliber .30 cylinders do not detonate Comp B at velocities up to 1000 m/sec. Figure 2 gives results with Caliber .50 cylinders. Figure 3 gives results with Caliber .30 cylinders fired against Tetryl, plotted against velocity and against kinetic energy. It is seen that the slight correlation with kinetic energy results only from the small range of masses used. "Partial detonation" means that detonation was followed by burning. This is shown by the jagged irregularities in the luminosity seen in frames of the high-speed motion pictures following the single frame overexposed by the luminous airshock resulting from detonation, as well as by very assymetric shock fronts in one-half microsecond single frame photographs. Figure 4 gives examples, while Figure 5 shows detonations believed to be complete. The term "low order detonation" has been avoided because it appears to have as many meanings as there are authors in the literature of initiation. Incomplete detonation can also be detected by the apparent duration of the luminosity. With the 22g to 45g Tetryl pellets used, film blackening followed detonation for 3 to 12 milliseconds. When burning but no detonation occurred, the apparent luminosity persisted for 30 to 80 milliseconds. The particular values are, of course, without significance, since they depend on the photographic method and on the size of the charge, but the absence of overlap suggests that a practical field test for complete detonation could be developed from observations of times of luminosity with particular charges and cameras. Probably the longer times of luminosity observed following detonations result from burning following incomplete detonation. The data reported here are not suited to a statistical test of the reliability of this method of identifying complete high order detonations, as most of them were obtained in the course of experimentation with the instrumentation.

## INTERPRETATION IN PHYSICAL TERMS

All of the results are consistent with the idea that impact is effective in initiating detonation when it produces a high gradient of compression and therefore of temperature. In backed explosives, this may occur in a layer trapped between projectile and backing. With a bare free charge struck by a blunt-ended projectile a strong compression shock is propogated, while with a streamlined projectile the pressure is relieved by the motion of the explosive sidewise. Hot spots, which Bowden and co-workers[1] have found so important in thin films, may be essential also in initiating detonation in bulk

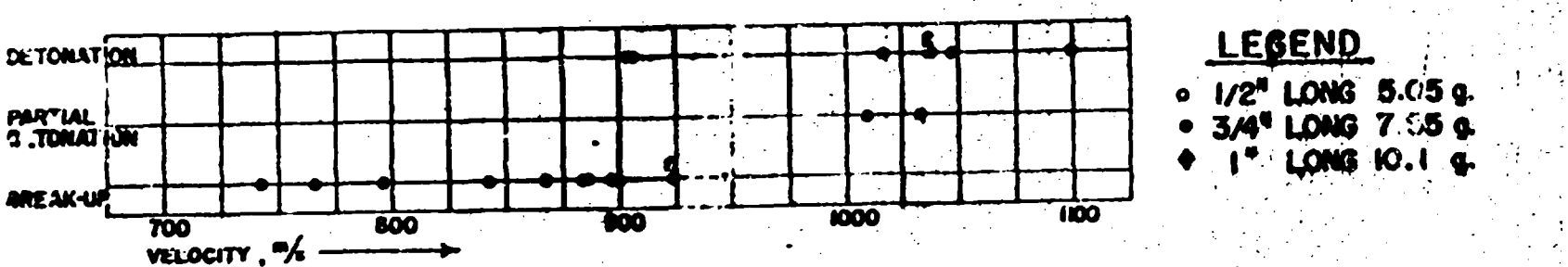


Figure 2 – Partial and Apparently Complete Detonation of Composition 'B' by Impact of .50 Caliber 21g. Cylinders (3/4" long) vs Velocity of Cylinders

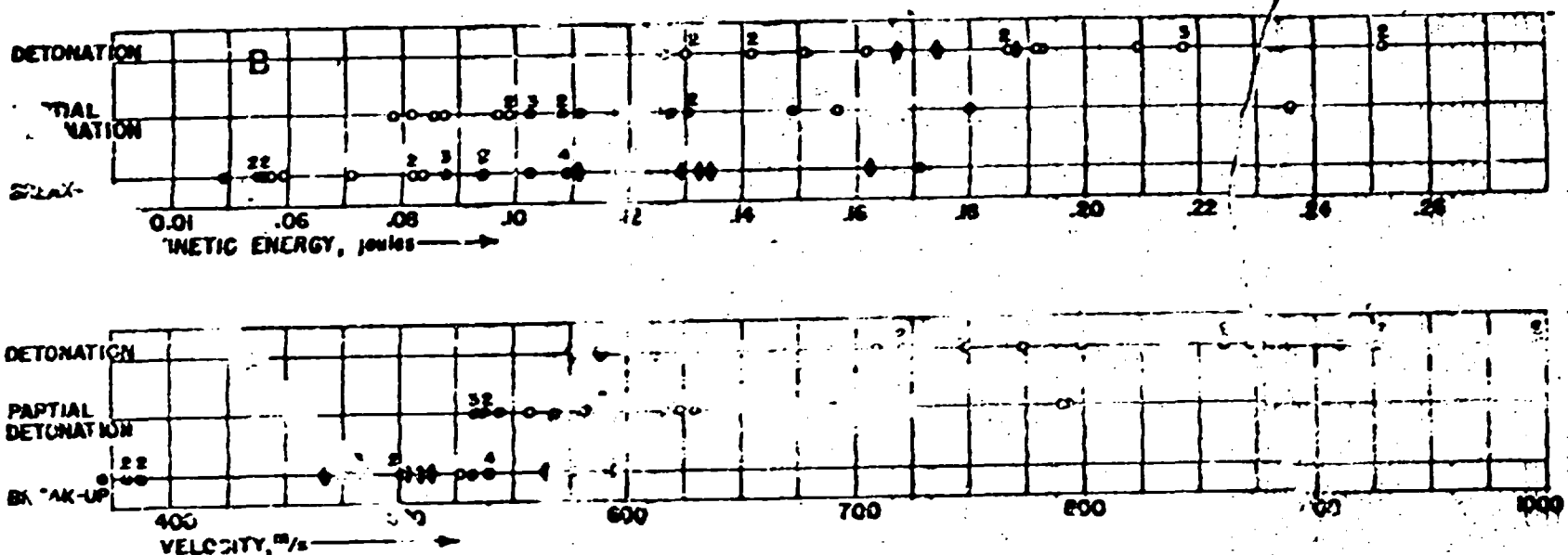


Figure 3 – Partial and Apparently Complete Detonation of Tetryl by Normal Impacting Flat-ended .30 Caliber Cylinders: A, vs Velocity of Cylinders; B, Kinetic Energy of Cylinders

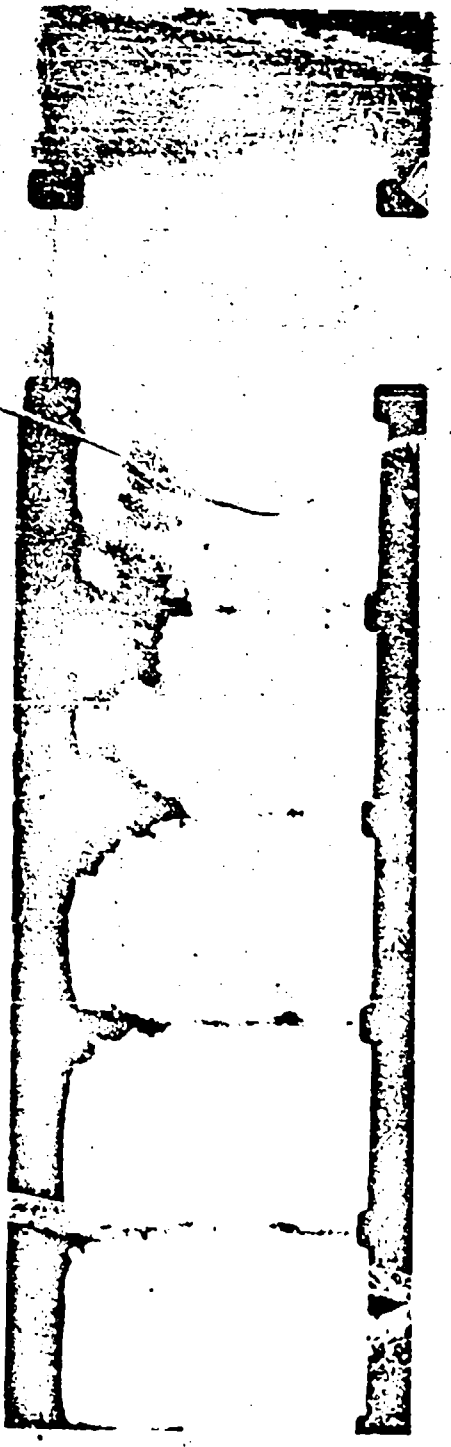

COMP. B

TETRYL

Figur - Partial Deto ions. Single Repatronic Frame at Uppe ight of Same De ation as Fastax Frames

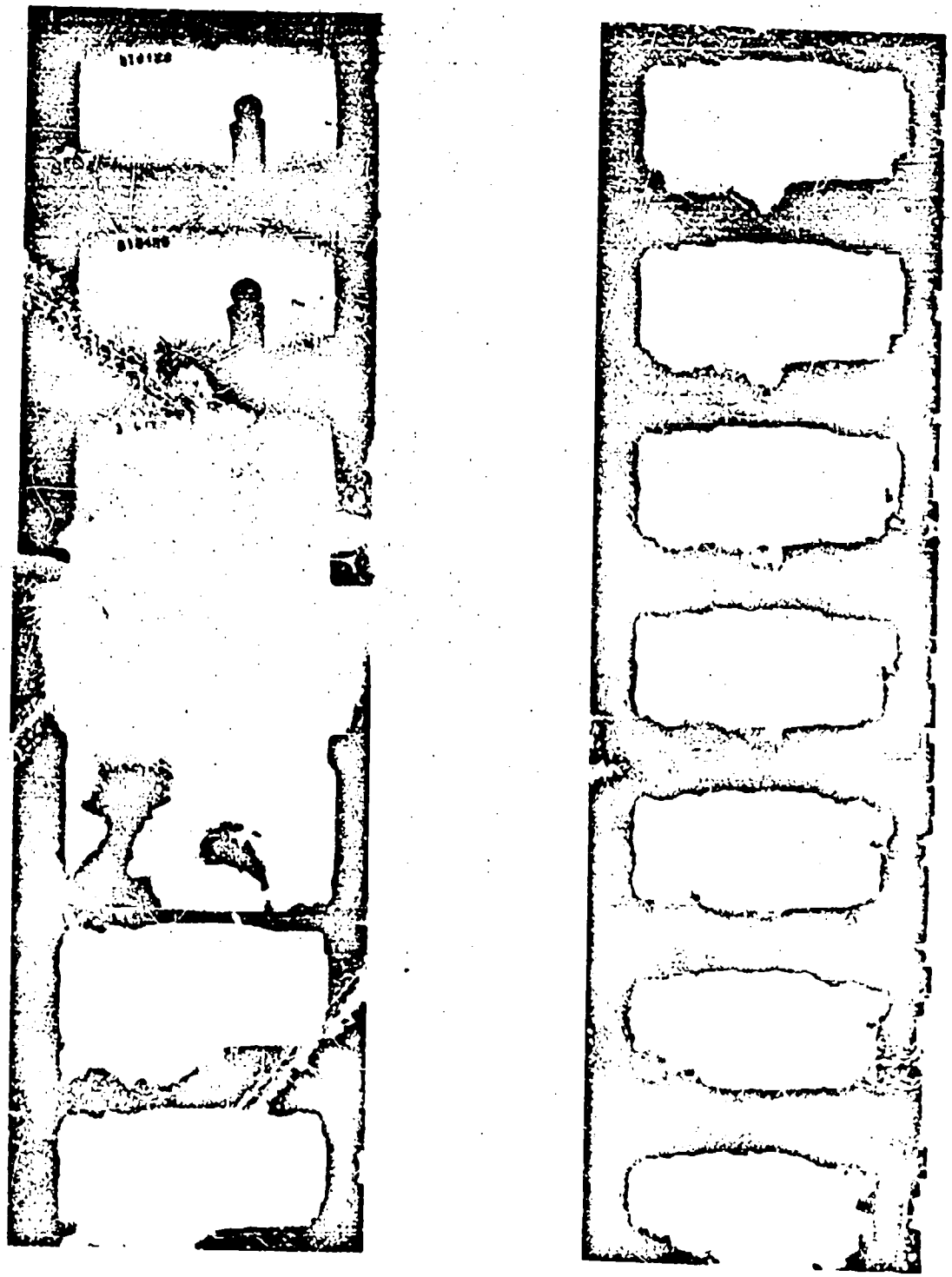

Figure 5 - Apparently Complete Detonation

explosives. They will always be provided by the granular nature of military explosives, even in the absence of the foreign material usually present. A gradual rise in temperature is ineffective because the explosive decomposes thermally or burns before the temperature required for detonation is reached, while a shock or entrapment of a thin layer raises the temperature too rapidly for the slow reaction to occur before the more rapid one. If a shock mechanism is the effective one, no effect of the mass per unit area of projectiles impacting on a bare charge should be observable, since the detonation occurs within a few microseconds after impact. An extremely short projectile would be required to show a mass effect in this short time. Nor should the material of the projectile be of importance. Only a material softer than the explosive would be sufficiently easily deformed to reduce the shock strength appreciably.

The effectiveness of backing a thin layer of explosive may under some circumstances result from the increase in shock strength occurring at reflection. In thicker layers decay would prevent initiation at the surface of reflection by shocks too weak to be effective at the surface of impact.

It is planned to check these points and to greatly extend the range of projectile masses used in order to distinguish more positively between area and mass effects.

## INSTRUMENTATION

Projectiles are fired from a modified machine gun or a Mann barrel, varying the velocity by changing the powder load. The velocity of each round is measured by foil screens triggering 1.6 megacycle Potter counters through a simple pulse shaping and lock-out circuit. Three screens are used in a distance of I meter.

Observations are made with Kodak or Fastax high-speed cameras and with Model No. 2208-1 (one-half microsecond exposure) Rapatronic cameras.(2) The photoelectric trigger circuit of the latter camera furnished with the Faraday shutter is not satisfactory for initiation work as the delay varies with light intensity, usually exceeding 20 microseconds from the time of impact. Thus, the air shock following complete detonation is all that is seen. As it would be excessively inconvenient to use any other type of triggering, a circuit with a smaller delay was substituted. Triggering on the initial flash is still not obtained and further work is required to give a reliable interpretation of all the results. It is hoped to improve this part of the instrumentation and use two Faraday cameras with a known interval between exposures to observe separately the first stage of initiation and the airshock formed when detonation is complete. The photoelectric trigger does not operate unless some detonation occurs. Each round which triggers the Faraday camera gives a single over-exposed frame on the Fastax followed by a short period of luminosity. In spite of the close agreement of results of the two types of cameras

on the occurrence of detonation, the use of two types of camera should lead to a better understanding of the partial detonations by giving an extended view and one rapid enough to show the form of the airshock. A Polaroid-Land back on the Rapatronic camera makes immediate observation of the result of each round possible, a great convenience in field firings.

Little reliance can be placed on direct observation. With bare charges the sound correlates with the occurrence of detonation but gives no indication of its extent. With backed charges even this cannot be said. Some effort was made in the first firings to improve the estimates made without instrumentation by the use of witness plates, viewing in a mirror, etc. The reliability of such estimates remained so low that they were abandoned.

As hits near the edge of a charge are relatively ineffective, the high-speed camera record was used to determine the point of impact. Rounds on which neither the projectile nor the point of impact could be seen were discarded. The cast charges were X-rayed for uniformity but only those with gross defects, such as cavities, were discarded. They were prepared by cutting from a carefully cast cylinder and are considerably more uniform than service rounds. Nine Tetryl pellets had densities ranging from 1.45 to 1.55, suggesting a lower degree of uniformity. As sensitivity is known to vary with density, this variability may account for much of the variation in results seen in Figure 4A.

Future work will be directed toward a better understanding of results of practical weapons tests, so that reliable predictions can be made of the results of new conditions.

REFERENCES

1. Most of the literature is confidential. Important exceptions include:

E. K. Rideal and J. B. Robertson, Proc Roy Soc A195, 135, (1948).

G. B. Kistiakowsi, Third Symposium on Combustion and Flame, The Williams and Williams Co., Baltimore (1949) p. 560.

F. P. Bowden and A. D. Yoffe, The Initiation and Growth of Explosions in Liquids and Solids. Cambridge Monographs on Physics, Cambridge University Press (1952). The Fourth Symposium on Combustion, The Williams and Wilkins Company (1953) p. 161.

2. NOrd Contract with Hercules Powder Company.

3. M. Sultanoff and R. A. Bailey, The Application of the Faraday Magneto-Optic Effect, etc., BRL 791, (1951).

## INDEX TO AUTHORS


Bennett, A. L. - 133
Bowden, F. P. - 443
Bonnar, M. - 38
Boyd, T. J., Jr. - 18, 33
Campbell, A. W. - 18, 336, 360
Cook, M. A. - 382, 401
Cooper, J. C. - 39
Courtney-Pratt, J. S. - 50, 429
Cowan, R. D. - 265
Cullen, R. E. - 148
Cumming, I. G. - 483
Davidson, N. - 98
Deal, W. E., Jr. - 209
Dewey, J. M. - 494
Duff, R. E. - 225
Fagan, P. - 33
Fickett, W. - 265
Gibson, F. C. - 39, 163
Giddings, J. C. - 286
Gilkerson, W. R. - 98
Greifer, B. - 163
Groocock, J. M. - 411
Gurton, O. A. J. - 464
Heybey, W. H. - 177
Holland, T. E. - 336
Houston, E. - 225
Hull, J. A. - 18
Igel, E. A. - 321
Jacobs, S. J. - 240
James, E., Jr. - 1
Jones, E. - 453, 483
Kirkwood, J. G. - 194, 306
Kistiakowsky, G. B. - 69, 80
Kydd, P. H. - 69
Malin, M. E. - 18, 336, 360
Mallory, F. B. - 240
Mason, C. M. - 39, 163
Mautz, C. W. - 360
McLaren, A. C. - 443
Morrison, R. B. - 148
Nicholls, J. A. - 148
Parlin, R. B. - 286
Peek, H. M. - 113
Reed, S. G., Jr. - 177
Rogers, G. T. - 429
Scott, F. - 39
Seely, L. B., Jr. - 321
Summers, C. R. - 39
Thrap, R. G. - 113
Ursenbach, W. O. - 401
Wedra, H. W. - 133
Wood, W. W. - 194, 306
Zinman, W. G. - 80




AD59930

Received 3/10/2000

DEPARTMENT OF THE NAVY
OFFICE OF NAVAL RESEARCH
800 NORTH QUINCY STREET
ARLINGTON, VA 22217-5660

IN REPLY REFER TO
5510/1
Ser 43/190
7 Mar 00

From: Chief of Naval Research
To: Defense Technical Information Center
(DTIC-BCS)
8725 John J Kingman Road Suite 0944
Ft Belvoir VA 22060-6218

Subj: DISTRIBUTION STATEMENT CHANGE

1. **AD 052 144** (Second ONR Symposium on Detonation) has been reviewed for public release by this Command. This document should be remarked Distribution **Statement A: Distribution Unlimited.**

2. Questions may be directed to the undersigned on (703) 696-4619.

Peggy Lambert

PEGGY LAMBERT
By direction